PROCEEDINGS OF THE FOURTH WORKSHOP ON GENERAL RELATIVITY AND GRAVITATION

Yukawa Institute for Theoretical Physics, Kyoto University,
November 28th - December 1st, 1994

edited by

K.Nakao(Secretary of this workshop), T.Nakamura, K.Maeda,
M.Shibata, H.Ishihara, Y.Eriguchi, T.Futamase, Y.Kojima

PREFACE

The Fourth Workshop on General Relativity and Gravitation was held in the week 28th November - 1st December, 1994 in the Yukawa Institute for Theoretical Physics at Kyoto University, Japan. A purpose of this workshop is to review the latest works in all fields relating to the gravity.

At present, there are many branches in issues on the gravity and there are so many researchers in Japan that it seems to be possible to construct a small society of gravitation if they hope. However, in a workshop restricted on ordinary scale, it seems to be impossible to cover all such fields even if it is important in order to get activities and to search for new research directions by stimulating interaction there. This is just a further purpose of this series of workshops.

105 researchers participated and 56 speakers gave 13 invited talks and 43 short contributions. In reality, they came from various fields: the classical gravity, or equivalently, the space-time structure from a point of view of the mathematical science; the observations of astrophysical and cosmological systems in which the gravity plays an important role, and the theoretical research deeply related to that; the quantum field theory in curved space-times and the early stage of the universe in which the dynamics of quantum fields is highly influenced by the gravity; the quantum nature of the gravitational interaction and the application for the very early stage of the universe. We believe that there were many useful discussions and interactions between the participants.

This workshop supported by a Grant-in-Aid for Scientific Research on Priority Areas (No.04234104) from the Japanese Ministry of Education, Science and Culture. This proceedings volume was also partially supported by Grant-in-Aid for Scientific Research on Priority Areas "Gravitational Wave Astronomy"(No.04234105), and Grant-in-Aid for Cooperative Research (No.06302021) from the Japanese Ministry of Education, Science and Culture, which were the financial base of this workshop.

K. Nakao (*Secretary of this workshop*)	(Kyoto University)
T. Nakamura	(YITP),
K. Maeda	(Waseda University)
M. Shibata	(Osaka University)
H. Ishihara	(Kyoto University)
Y. Eriguchi	(University of Tokyo)
T. Futamase	(Hirosaki University)
Y. Kojima	(Tokyo Metropolitan University)

PROGRAM (TABLE OF CONTENTS)

PREFACE iii

MONDAY, 28th NOVEMBER

AFTERNOON SESSION

Chairperson: *T. Nakamura*

New Cosmic Landscapes Viewed by the Hubble Space Telescope 1

S. Ikeuchi

Anisotropy of Cosmic Microwave Background 3

- Overview of the Recent Results -

N. Gouda

Variable Cosmological Term and Age of the Universe 20

T. Fukui

Hot MHD Flows in a Black Hole Magnetosphere 24

M. Takahasi

Cold MHD Black Hole Magnetosphere Near Force-Free Limit 31

T. Uchida

(Coffee Break)

Chairperson: *Y. Kojima*

Gamma Ray Burst

T. Murakami

Large Hysteretic Behavior of Stellar Black Hole Candidate X-ray Binaries 38

S. Miyamoto, S. Kitamoto, K. Hayashida and W. Egoshi

Gamma Ray Bursts; Relativistic Astrophysical Objects? 48

H. Hanami

What Cavities? 54

Y. Okuda and J. Katz

MONDAY, 29th NOVEMBER

MORNING SESSION

Chairperson: *A. Hosoya*

Fractal Structure of 2-Dimensional Quantum Gravity

N. Kawamoto

Analysis of the Wheeler-De Witt Equation

beyond Planck Scale and Dimensional Reduction 64

K. Maeda

Entropies of Scalar Fields on Three-Dimensional

Black Holes 68

I. Ichinose and Y. Satoh

Supersymmetry and general Killing-Yano Tensors 76

M. Tanimoto

Brans-Dicke Theory in Non-Commutative Geometry 86

G. Konishi, T. Saito and K. Wu

(Coffee Break)

Chairperson: *H. Ishihara*

Quantum Smearing of Spacetime Singularity 96

A. Hosoya

Wave Function of Black Hole Decay 107

A. Tomimatsu

Four Dimensional Quantum Topology Changes 112

M. Siino

AFTERNOON SESSION

Chairperson: K. Oohara

Equation of Motion in the Slow-Motion Approximation in General Relativity 120

T. Futamase

Post-Newtonian Approximation in (3+1) Formalism and the Quadrupole Radiation-Reaction 130

H. Asada, M. Shibata and T. Futamase

Post-Newtonian Expansion of Gravitational Waves from a Particle Orbiting around a Rotating Black Hole 140

H. Tagoshi

Radiative Reaction in Kerr Geometry 161

Y. Mino

(Coffee Break)

Chairperson: *T. Futamase*

Review and Comment on Critical Behavior in Gravitational Collapse 170

Y. Fujiwara

Critical Behavior in Scalar Wave Collapse 176

Y. Oshiro, K. Nakamura and A. Tomimatsu

Critical Phenomena in Gravitational Collapse 183

T. Koike and T. Mishima

Einstein-Scalar Spacetime with Local Symmetry 192

K. Nakamura

MONDAY, 30th NOVEMBER

MORNING SESSION

Chairperson: *Y. Eriguchi*

Exotic Black Holes

K. Maeda

Cosmic Colored Black Holes 200

T. Torii, K. Maeda and T. Tachizawa

Evolution of Dilatonic Black Holes by Hawking Radiation 209

J. Koga and K. Maeda

On the Phase Transition of Kerr-Newman Black Holes 219

O. Kaburaki

(Coffee Break)

Chairperson: *K. Maeda*

Ergoregion and Preferred Time 228

S.A. Hayward

Chaos in Axisymmetric Static Vacuum Spacetime II 234

S. Suzuki, Y. Sato and K. Maeda

Quantum "De"coherence and Real Time Quantum Tunneling 239

M. Morikawa

AFTERNOON SESSION

Chairperson: A. Tomimatsu

Project of Gravitational Wave Detection

K. Tsubono

Coalescence of Affine Star Binary

Y. Ogawaguchi and Y. Kojima

Gravitational Waves from Boson Stars 250

S. Yoshida, Y. Eriguchi and T. Futamase

Non-Radial Oscillations of Ultra Compact Stars 260

Y. Kojima

Pulsar Timing as an Experimental Tool of Relativistic Gravity

S. Kopeikin

(Coffee Break)

Chairperson: *K. Nakao*

Evolution of Pure Gravitational Waves in 3D Numerical Relativity 266

M. Shibata

Fully Relativistic 3D Numerical Simulations

of Coalescing Binary Neutron Star 302

T. Nakamura

Numerical Relativity with Help of Ashtekar's Formulation 323

H. Shinkai and G. Yoneda

Ashtekar Variables and Matter Coupling 333

M. Tsuda, T. Shirafuji and H. Xie

MONDAY, 1st DECEMBER

MORNING SESSION

Chairperson: *J. Soda*

How to Make a Open FRW Universe; One Bubble Inflationary Model 342

T. Tanaka, K. Yamamoto and M. Sasaki

Excitation by the Self Interaction in the False Vacuum Decay 372

T. Hamazaki, M. Sasaki, T. Tanaka and K. Yamamoto

Density Fluctuation in Brans-Dicke Inflation 381

A.A. Starobinsky and J. Yokoyama

(Coffee Break)

Chairperson: *M. Sasaki*

Numerical Analysis of Topological Inflation 391

N. Sakai, H. Shinkai, T. Tachizawa and K. Maeda

Exponential Potentials and Scalar Field Inflation 400

R. Easther

Lorentzian Topology Changing Cosmology 410

A. Ishibashi, T. Koike and M. Siino

Can Quantum Matter be an Energy Source to Make a Visible Change in the Classical Geometry? 419

S. Konno

AFTERNOON SESSION

Chairperson: J. Yokoyama

CP Violation and Physics in B-Factory

M. Kobayashi

Subcritical Bubbles and Electroweak Phase Transition 423

T. Shiromizu, M. Morikawa and J. Yokoyama

(Coffee Break)

Chairperson: *M. Shibata*

General-Relativistic Second-Order Gravitational Instability and Inhomogeneous Cosmological Models 431

K. Tomita

Gradient Expansion in Ashtekar Formalism 439

A. Nakamichi and H. Ishihara

The Relation of Gradient Expansion Method to the Linear Perturbation Theory 446

O. Iguchi, H. Ishihara and J. Soda

Solving the Hamilton-Jacobi Equation
for General Relativity with Perfect Fluid 452
T. Chiba

Silent Universe Damaged by Gravito-Magnetic Part 462
Y. Kojima

Gradient Expansion in Brans-Dicke Theory 470
J. Soda

New Cosmic Landscapes Viewed by the Hubble Space Telescope

Satoru IKEUCHI
Department of Earth and Space Science
Faculty of Science
Osaka University

One year has passed after the successful repairing mission of the Hubble Space Telescope (HST). The new repaired HST is showing its powerful abilities of observations in the ultraviolet wavelength, the high spatial resolution and the deep survey. Here, I summarize briefly several important results by the HST.

The key projects of the HST are the following three: (1) The distance scale by observing the Cepheid variables of the Virgo galaxies. (2) The medium deep survey in the blank sky for detecting faint galaxies till the redshifts $z \sim 0.5$. (3) Absorption systems of quasars in the UV wavelength. Interesting results for each project are reported as summarized in the followings.

(1) *Distance scale*

By resolving the 20 Cepheid variables in M100 in the Virgo cluster and utylizing the period-luminosity relation, the distance to the Virgo center is determined accurately as R=17.1+-1.8 Mpc. Since the distance ratio of the Virgo to the Coma cluster is decided by the Tully-Fisher relation, the Type I supernovae and others, the Hubble constant is reduced from the Coma's redshift as H_0=80+-17 $kms^{-1}Mpc^{-1}$ (Freeman et al 1994). This value seems to contradict with the age of globular clusters. We are confronted the age problem of the Universe.

(2) *Medium deep survey*

For the blank sky of 0.1 square degrees, the HST observed 30 minutes for detecting galaxies and clusters of galaxies till the redshifts $z \sim 0.5$. The first results are presented in the special issue of Ap.J.Letters Nov. 20. As is seen, many irregular and interacting galaxies are discovered. It is highly probable that galaxies had experienced mutural interactions before they settled to present states. When this survey finished for 50 fields, we can discuss the statictics of interacting galaxies quantitatively.

(3) *QSO absorption systems*

The most important discovery of the UV spectroscopy of a QSO by the HST

is the positive detection of the intergalactic medium by the HeII Gunn-Peterson test(Jacobsen et al 1994). After the proposal by Gunn and Peterson(1965) for probing the intergalactic medium by the continuum depression at the short-wavelength side of the HI emission line of a QSO, there has been no positive detection of this Gunn-Peterson test. Finally, the HST has succeeded in the probable detection of the continuum depression at the HeII Lyman alpha emission line of Q0302-003. Although it can not be denied this absorption may occur by a Lyman α cloud, it is natural to consider this the HeII absorption of ionized intergalactic medium. If so, we can use three conditions(the upper limit of the HI Gunn-Peterson test, the upper limit of the y-parameter of CMB and the HeII optical depth) for constraining the physical properties of the IGM(Ikeuchi 1994) and the diffuse ionizing UV flux(Sasaki and Takahara 1994). More definite observations are necessary to confirm the physical state of the IGM.

Other projects such as Deep Survey, Gravitational Lensing, QSO Environments, AGN, Protogalaxies and so on are planned to devote much observing time of the HST. We may expect fruitful information from the new HST in coming years.

References

Freeman,W., et. al.(1994) *Nature* **371**, 757.
Gunn,J.E., and Peterson,B.A.(1965) *Ap.J.* **142**,1633.
Ikeuchi,S.(1994) Submitted to *Ap.J.Lett.*
Jacobsen,P., et. al.(1994) *Nature* **370**,35.
Sasaki,S., and Takahara,F.(1995) *Ap.J.* in press.

Anisotropy of Cosmic Microwave Background
-Overview of the Recent Results-

NAOTERU GOUDA

Department of Earth and Space Science, Faculty of Science, Osaka University, Toyonaka, Osaka 560, Japan
E-mail: gouda@vega.ess.sci.osaka-u.ac.jp

ABSTRACT

The first detection of the anisotropy of cosmic microwave background(CMB) by COBE certainly opend the new door in the obseravtional cosmology. Furthermore there appear recently many observational results of the CMB anisotropy by other measurements after the first detection of the anisotropy by COBE. Hence it becomes more and more important to analyze the CMB anisotropy. Here the base of the theoretical estimate of the CMB anisotropy is briefly reviewed. Moreover the recent results of the analyses of the measured anisotropies are reviewed including the analysis of COBE two-years sky map.

I.INTRODUCTION

The first detection of the CMB(Cosmic Microwave Background) anisotropy by COBE certainly promotes the progress in the observational cosmology. Some detections of the CMB anisotropies on a few degree angular scales by the observations on the ground or by using balloon have been reported after the first detection by COBE. Moreover the analysis of COBE two-years data has been reported.

These results severely constrain the cosmological models for the large-scale structure formations. In. the observational cosmology, it is very important to understand the distributions of the gravitational matters including dark matters. However the distribution of the luminous matters(*i.e.*galaxies) are not believed to the distribution of the gravitational matters due to the bias effect. On the other hand, th CMB anisotropy is directly related to the gravitational matters. So it is very important to use the CMB anisotropy in order to get the informations of the distribution of the gravitational matters, which implies the primordial density fluctuations, and constrain the cosmological models. Furthermore we can get the informations about the density fields on various scales by changing the angular scale of the CMB anisotropy in the measurements. Hence we can conclude that it is very important to measure the CMB anisotropy and its anisotropy informs us the primordial density fluctuations in principle while we have problem that it is difficult to get the effective physical informations from those measurements in practice("cosmic confusion", see to §IV).

In this paper, we briefly review the method of the theoretical analysis of the CMB anisotropy and the recent observational results. In §I, I show the method of the theoretical analysis of the CMB anisotropy based on the standard scenario by the gravitational instability. In §III, I show the recent observational results by COBE including the COBE two-years data and theoretical estimate. The recent observational measurements on the medium and small angular scales and the theoretical estimates on the cosmological models are shown in §IV. Finally,

§V is devoted to the conclusions and discussions.

II.THEORETICAL ANALYSIS OF THE CMB ANISOTROPY

Here I briefly comment on the procedure of the theoretical analysis of the CMB anisotropy based on the standard scenario for the large-scale structure formations due to the gravitational instability. Please refer to N.Sugiyama and N.Gouda(1992) [1] about the detailed explanations.

In the standard scenario of the large-scale structures, it is generally believed that the present structures such as galaxies, clusters of galaxies and super-clusters are resulted from the growth of the small density fluctuations originated at the very early universe due to the gravitational instability[2]. However we do not know the exact conditions of the initial density fluctuation. Then we usually assume that the initial density fluctuations obey the random Gaussian distribution with the power spectrum $P(k) \equiv |\delta_k|^2 \propto k^n$, where n is the initial power index. The inflation universe with the exponential expansion predicts $n = 1$, which is called Harrison-Zel'dovich spectrum. The other some inflationary models predict $n \lesssim 1$[3] Furthermore we consider two cases which are the adiabatic perturbation (curvature perturbation) and the entropy perturbation(isocurvature perturbation)[4] as for the initial conditions of the density fluctuations.

The evolutions of density fluctuations are calculated by the linear analysis of the perturbed Einstein equations before the decoupling era[1]. In this period, baryons and photons strongly couple with each other due to Thomson scattering. Then the shape of the power spectrum of baryon and photon density fluctuations change as time goes through the increase of the Jeans scale(and Silk damping scale for the adiabatic case)[2]. Jeans scale and the Silk damping scale depend on the cosmic parameters(Ω_0, Ω_b, h) and then their power spectra depned on the cosmic parameters and also the initial conditions (adiabatic or isocurvature and the initial power index n)[1]. When we consider the dark matters, the power spectrum of the dark matter depends on the kind of the dark matter, that is, cold or hot one.

After the decoupling era, baryon density fluctuations grow freely without the pressure of the photons. The smaller baryon density fluctuations on large scales grow linearly. The growth rate depends on Ω_0 and Λ. On the other hand, the larger fluctuations on small sales go into the stage of the non- linear growth and the growth rate depends the wavenumber and the shape of the power spectrum besides the cosmic parameters in the complicated way.

As for the photon fluctuations, their evolution obeys the perturbed relativistic collisionless Boltzmann equation from the decoupling time to the present time. The present photon fluctuation is the solution of that equation at the present time. That solution consists of three effects which are the intrinsic term, the Sachs-Wolfe term and the integrated Sachs-Wolfe term[5] The intrinsic term is the contribution of the photon fluctuation at the decoupling time to the present one. The Sachs-Wolfe and the integrated Sachs-Wolfe effect are resulted from the fluctuation of the gravitational potential between the decoupling time and the present time. The integrated Sachs-Wolfe term vanishes in the case that $\Omega_0 = 1$ and $\Lambda = 0$. As for the adiabatic case, we find that the Sachs-Wolfe effect dominates for $\Omega_0 = 1$ and the integrated Sachs-Wolfe effect dominates for $\Omega_0 < 1$ on large scales[5, 6]. On the other hand, as for the isocurvature case, the intrinsic term dominates for $\Omega_0 = 1$ and the integrated Sachs-Wolfe term dominates for $\Omega_0 < 1$ on large scales. On small scales, the intrinsic term dominates both for adiabatic and isocurvature cases. Furthermore it is suggested that in some inflation models the tensor mode of the metric fluctuations gives rise to the CMB anisotropy by the Sachs-Wolfe effect in addition to the CMB anisotropy due to the scalar modes associated with the density fluctuations[3]. In some models, we must take into account this contribution.

Using the above procedure, we theoretically estimate the CMB anisotropy in the cosmological models. Then in comparison of the theoretical estimates of the CMB anisotropy in the cosmological models with the measured anisotropy, we can constrain the models. However we can not directly compare the theoretical estimates and the measured one: we can measure the only sky temperature in

our universe. On the other hand, we can not know the exact initial phase of the initial density fluctuation and then we can not theoretically estimate the real sky map. Hence we must use the statistical quantities as follows:

(i)Angular two-point correlation function

The angular two-point correlation function is defined by

$$C(\theta) = \langle \delta T(\mathbf{x}, \hat{\gamma}_1) \cdot \delta T(\mathbf{x}, \hat{\gamma}_2) \rangle_{\mathbf{x}}$$

where $\delta T(\mathbf{x}, \hat{\gamma})$ is the temperature fluctuations at the direction of the unit vector $\hat{\gamma} : \delta T(\hat{\gamma}) = T(\hat{\gamma}) - T_0$($T_0$ is the mean temperature) and $\hat{\gamma}_1 \cdot \hat{\gamma}_2 = \cos\theta$. In the real observations, we must take into account the smoothing of the temperature fluctuations due to the finite antenna beam. Then the modified angular correlation function is given by

$$C(|\gamma_1 - \gamma_2|; \sigma) = \int d\Omega_1' d\Omega_2' f(|\gamma_1 - \gamma_1'|; \sigma) f(|\gamma_2 - \gamma_2'|; \sigma) C(|\gamma_1' - \gamma_2'|).$$

where f is the function of the beam profile. If the profile is approximated by the Gaussian distribution function with the antenna beam width σ, f is given as follows:

$$f(|\gamma_1 - \gamma_2|; \sigma) = \frac{1}{2\pi\sigma^2} \exp(-\frac{1}{2\sigma^2} |\gamma_1 - \gamma_2|^2),$$

where γ_1 and γ_2 are direction cosines. Here it must be noticed that the Gaussian beam size σ of an antenna is related to the beam size defined by FWHM, σ_{FWHM} as follows:

$$\sigma_{FWHM} = 2\sqrt{2\ln 2}\sigma.$$

(ii)Angular power spectrum

The temperature fluctuation on the sky, $\frac{\delta T}{T}(\theta,\phi)$, is expanded by the spherical harmonics, Y_ℓ^m:

$$\frac{\delta T}{T}(\theta,\phi) = \sum_{l=0} \sum_{m=-\ell}^{\ell} a_\ell^m Y_\ell^m(\theta,\phi).$$

Then the modified angular correlation function can be represented by

$$\begin{aligned}\frac{C(\theta,\sigma)}{T_0^2} &= \langle \frac{\delta T}{T}(\gamma_1) \cdot \frac{\delta T}{T}(\gamma_2) \rangle \\ &= \frac{1}{4\pi} \sum_\ell (2\ell+1) C_\ell P_\ell(\cos\theta) B_\ell\end{aligned}$$

where $C_\ell \equiv \langle |a_\ell^m|^2 \rangle$ and B_ℓ is the smoothing function due to the beam profile. If the beam profile is approximated by the Gaussian distribution, B_ℓ is given by $e^{-(\ell+\frac{1}{2})^2\sigma^2}$. As for the flat($\Omega_0 = 1$ and $\Lambda = 0$) and adiabatic case with the initial power index n, C_ℓ is analytically estimated for $n > -3$ as follows:

$$C_\ell = C_2 \frac{\Gamma[\ell + (n-1)/2] \cdot \Gamma[(9-n)/2]}{\Gamma[\ell + (5-n)/2] \cdot \Gamma[(3+n/2)]}.$$

Especially, $C_\ell = 6C_2/\ell(\ell+1)$ for $n = 1$ [7].

We use the above statistical quantities such as the angular correlation function $C(\theta,\sigma)$ and/or the angular power spectrum C_ℓ in comparing the theoretical estimated CMB anisotropy with the measured one.

III. COBE RESULTS

As known well, COBE DMR instrument detected the CMB anisotropy on large angular scales at first[8]. The FWHM beam width of COBE DMR is 7° if the beam profile is fitted by the Gaussian profile. They observed CMB anisotropies at31.5, 53 and 90GHz. Last year, the COBE team shows the observational results including the 2-year data[9]

Here I show the recent results of COBE DMR[9]. The dipole anisotropy is 3.363±0.024mK and the direction is $\ell = 264.°4 \pm 0.°2, b = 48.°1 \pm 0.°4$. This result

is consistent with the 1-year data analysis. The rms temperature fluctuation at 10° degree, which is defined by

$$\delta T_{rms}(10^\circ) \equiv C(\theta = 0^\circ, \sigma_{FWHM} = \sqrt{7^{\circ 2} + 7^{\circ 2}} \sim 10^\circ),$$

is $30.5 \pm 2.7\mu$K. Here the first 7° in the square root is the beam FWHM width of COBE DMR and the second one is the smoothing angular scale of the temperature fluctuation on the sky map by the Gaussian window function. This result is also consistent with the 1-year data analysis while the error reduces in using the 2-years data (1 and 2-year data). However the rms quadrupole anisotropy, Q_{rms}, are reduced to $6 \pm 3\mu$K(68% C.L.) though the Q_{rms} was $13 \pm 4\mu$K in the 1-year analysis. The reason might be effects of some noises, but it is not certain.

If we assume that the power spectrum on large scales obeys the power law with the power index n, we can determine the most expected rms quadrupole anisotropy, Q_{rms-ps}, and n by analyzing the angular correlation function or the angular power spectrum. In these analysis, the maximum likelihood function is used[10]. Bennet *et al.*[9] analyzed the angular correlation function. They conclude that $Q_{rms-ps} = 14.3^{+5.2}_{-3.3}\mu$K, $n = 1.42^{+0.49}_{-0.55}$(68%C.L.) if the measured Q_{rms} is included. If the measured Q_{rms} is excluded, $Q_{rms-ps} = 17.4^{+7.5}_{-5.2}$, $n = 1.1^{+0.60}_{-0.55}$(68% C.L.). In analyzing the angular power spectrum, we must be careful about the effect of the cut off galactic plane($|b| < 20^\circ$) in the sky temperature map. Then Górski *et al.*[11] used the angular power spectrum defined by using the orthogonal polynomial on the galactic cut sphere($|b| \geq 20^\circ$). Their results are $Q_{rms} = 17.0^{+7.6}_{-4.6}$, $n = 1.22^{+0.43}_{-0.52}$ if the observed Q_{rms} is included and $Q_{rms-ps} = 20.0^{+10.5}_{-6.5}$, $n = 1.02^{+0.53}_{-0.59}$ if the measured Q_{rms} is excluded. Wright *et al.*[12] used the angular power spectrum defined by using the modified spherical harmonic function. They concluded that $n = 1.25^{+0.4}_{-0.45}$ and $Q_{rms-ps} = 19.8 \pm 2.0$ if $n = 1$. Smoot *et al.*[8] in the 1-year data analysis used the least-square fit for the analysis of Q_{rms-ps} and n instead of use of the maximum-likelihood function. So they did not take into account of the bias due to the cosmic variance and alias due

to the cut sphere. The difference between the Q_{rms-ps} expected by the analysis including the measured Q_{rms} and excluding the measured Q_{rms} suggest that in our universe there might appear the Q_{rms} which is lower than the true rms quadrupole due to the cosmic variance[13]

In the above analyses for Q_{rms-ps} and n, they considered the simple case that the fluctuation is adiabatic and the universe is flat($\Omega_0 = 1, \Lambda = 0$). Then only the Sachs-Wolfe effect is considered on large angular scales. As for open and/or isocurvature cases, we must take into account the integrated Sachs-Wolfe effect and/or the intrinsic fluctuations. Then it is found that in these cases it remians possibilty that the COBE result suggests $0 \lesssim n \lesssim 2$ in fact[14]. In all analyses, the assumption that the temperature fluctuation obeys the Gaussian distribution is essential. This assumption is not strongly denied by the analysis of the topology("genus") of the sky map[15].

IV. OBSERBATIONAL RESULTS ON MEDIUM AND SMALL ANGULAR SCALES

Many experiments on the medium and small angular scales are being done from the ground and using balloons. Most of these observations report the detections of the CMB anisotropy at $\sim 10^{-5}$ level. These experiments are called as follows: FIRS[16], MSAM[17], MAX[18], ACME South Pole[19], ULISSE[20], ARGO[21], Big Plate[22], Tenerife[23], Python[24], White Dish[25], OVRO[26] and ACTA[27].

Recently the observational results are shown by the conventional form, that is, the broad band power spectrum[28, 29]: the observed rms temperature fluctuation on the medium or small angular scale, θ_s, is given by

$$[\frac{\delta T}{T}(\theta_s)]^2_{rms} = \frac{1}{4\pi}\sum_{\ell}(2\ell+1)C_\ell W_\ell(\theta_s, \sigma)$$

Here W_ℓ is a window(filter) function which depends on the beam profile and the procedure of the beam switching. If we consider the beam profile of the Gaussian

form with the beam width σ and two-beam switching,

$$W_\ell = 2[1 - P_\ell(\cos\theta_s)]e^{-(\ell+\frac{1}{2})\sigma^2}.$$

On the other hand, if we consider the triple-beam switching,

$$W_\ell = [\frac{3}{2} - 2P_\ell(\cos\theta_s) + \frac{1}{2}P_\ell(\cos 2\theta_s)]e^{-(\ell+\frac{1}{2})\sigma^2}.$$

[28]. The W_ℓ used in the experiments group are shown in Fig.1[29]. Then the broad band power spectrum is defined by

$$\langle C_\ell \rangle_W \equiv I[\ell(\ell+1)C_\ell W_\ell]/I[W_\ell]$$
$$I[f_\ell] \equiv \sum_\ell \frac{(2\ell+1)}{4\pi\ell(\ell+1)} f_\ell.$$

The all observational results of the broad band power spectrum are shown in Figs.2(a) and 2(b)[28]. Some results are not consistent with each othe now.

These observational results on medium and small angular scales with the COBE results constrain the cosmological models with the cosmic parameters such as $C_2^{(S,T,I_s)}, n_{(s,t,is)}, h, \Omega_b, \Omega_\Lambda, \Omega_{CDM}, \Omega_{HDM}$, etc. [30, 31]. Here $C_2^{(S,T,I_s)}$ and $n_{(s,t,is)}$ are the amplitude of the angular power spectrum at $\ell = 2$ and the initial power index for adiabatic scalar modes, tensor modes, isocurvature scalar modes, respectively. $\Omega_{b,\Lambda,CDM,HDM}$ are the density parameters for baryon, Λ term, CDM and HDM, respectively. However it is suggested that the cosmic parameters in the models can not be determined separately by only using the constraint from the CMB measurements[30, 31]. In order to restrict the large spaces of the cosmic parameters, J.R.Bond *et al.*[30, 31] considered only the case in which the universe is geometrically flat$(\Omega_0 + \Lambda = 1), \Omega_{HDM} = 0, \Omega_b h^2 = 0.0125, n_t \sim n_s - 1, r \equiv C_2^{(T)}/C_2^{(S)} \sim 7(1 - n_s)$ and $C_2^I = 0$. Their results are shown in Figs.3(a)~(d)[31]. They found that even in this restricted space of the cosmic parameters we can not discriminate the cosmological models with the

same $\bar{n}_s \sim n_s - 0.28\log(1+0.8r) - 0.52[(1-\Omega_\Lambda)h^2]^{\frac{1}{2}} - 0.00036 z_R^{3/2} + 0.26$, where z_R is the redshift at the late ionization. This is called "cosmic confusion". Then we need also other constraints on the models besides the constraint from the CMB anisotropy.

V. CONCLUSIONS AND DISCUSSIONS

The analysis of the 2-years COBE DMR data suggests that the results including the 2-year data are almost consistent with that including only the 1-year data. Some statistical analyses show that $n \sim 1[0 \lesssim n \lesssim 2]$ and $Q_{rms} \sim 18\mu$K. And $C(10°) \sim 30\mu$K. As for the medium and small angular scales, the most of the experiment group using the telescopes on the ground or balloons report the detections of the CMB anisotropy. However their results are not consistent with each other now. We need the further measurements on these scales with better accuracy. Furthermore the measured anisotropy can not discriminate the cosmological models with the same $\bar{n}_s$: this is called "comic confusion". So we need some other approaches in order to determine the cosmic parameters, such as the constraint from the cosmic age, the observation of the Hubble constant, two-body correlation functions of galaxies and clusters of galaxies and the velocity fields of galaxies etc.

As for the observations of the CMB anisotropy, COBE will report the results including the 3 and 4-years data in the near future, which will give us C_ℓ at lower ℓ with better accuracy. Moreover we need the more exact measurement of C_ℓ with higher ℓ by the observations on the medium and small angular scales. The measurements on the medium and small scales by the satellite is now planed. One of them is called COBRAS/SAMBA by ESA. Then we can expect the more exact measurements of the CMB anisotropy in the near future. As for the theoretical estimate, we need the more accurate estimate of the anisotropy on the medium and small scales in taking into account the effects of reionization, gravitational lens and the non-linear growth of density fluctuations. Although it remain still now problems for the accuracy of the measured anisotropies and the theoretical estimates, I believe that the CMB anisotropywill give us more

important informations about our universe.

REFERENCES

1. N.Sugiyama and N.Gouda, Prog.Theor.Phys. **88**, 803 (1992).
2. P.J.E.Peebles, The Large-Scale Structure of the Universe (Princeton University Press, 1980.
   P.J.E.Peebles, Principles of Physical Cosmology(Princeton University Press, 1993).
3. R.L.Davis *et al.*, Phys.Rev.Lett. **69**, 1856 (1992).
4. H.Kodama and M.Sasaki, Int.J.Mod.Phys. **A1**, 265 (1986).
5. N.Gouda, N.Sugiyama and M.Sasaki, Prog.Theor.Phys. **85**, 1023 (1991).
6. W.Hu and N.Sugiyama, preprint(1994), CfPA-94-Th-55, UTAP-193.
7. J.R.Bond and G.F.Efstathiou, Mon.Not.R.Astron.Soc. **226**, 655 (1987).
8. G.F.Smoot *et al.*, Astrophys.J.Lett. **396**, L1 (1992).
9. C.L.Bennet *et al.*, Astrophys.J. **436**, 423 (1994).
10. U.Seljak and E.Bertschinger, Astrophys.J.Lett. **417**, L9 (1993).
11. K.M.Górski *et al.*, Astrophys.J.Lett. **430**, L1 (1994).
12. E.L.Wright*et al.*, Astrophys.J. **436**, 443 (1994).
13. A.J.Banday *et al.*, preprint(1994).
14. N.Sugiyama and J.Silk, Phys.Rev.Lett. **93**, 509 (1994).
15. G.F.Smoot *et al.*, preprint(1994).
16. S.S.Meyer, L.Page and E.S.Cheng, Astrophys.J.Lett. **371**, L7 (1991).
    K.Ganga, L.Page, E.Cheng and S.Meyer Astrophys.J.(1994) in press.
    L.A.Page, E.S.Cheng and S.S.Meyer, Astrophys.J.Lett. **355**, L1 (1990).
17. E.S.Cheng *et al.*, Astrophys.J.Lett. **422**, L37 (1994).

18. M.L.Fisher *et al.*, Astrophys.J. **388**, 242 (1992).
D.C.Alsop *et al.*, Astrophys.J. **395**, 317 (1992).
P.Meinhold *et al.*, Astrophys.J.Lett. **409**, L1 (1993).
A.C.Clapp *et al.* Astrophys.J.(1994) in press.

19. T.Gaier *et al.*, Astrophys.J.Lett. **398**, L1 (1992).
J.Schuster *et al.*, Astrophys.J.Lett. **412**, L47 (1993).

20. P.de Bernardis*et al.*, Astrophys.J.Lett. **396**, L57 (1992).

21. P.de Bernardis *et al.*, Astrophys.J.Lett. **422**, L33 (1994).

22. E.J.Wollack *et al.*, Astrophys.J.Lett. **419**, L49 (1993).

23. S.Hancock *et al.*, Nature. **367**, 333 (1994).

24. M.Dragovan *et al.* preprint(1993)

25. G.S.Tucker *et al.*, Astrophys.J.Lett. **419**, L45 (1993).

26. S.T.Myers *et al.*, Astrophys.J. **405**, 8 (1993).

27. R.Subrahmayan, R.D.Ekers, M.Sinclair and J.Silk, Mon.Not.R.Astro.Soc. **263**, 416 (1993).

28. J.R.Bond, preprint(1994), CITA-94-5

29. J.R.Bond, in the proceedings of the 8-th Nishinomiya-Yukawa Memorial Symposium(1994)

30. J.R.Bond *et al*, Phys.Rev.Lett. **72**, 13 (1994).

31. J.R.Bond, R.L.Davis and P.J.Steinhardt, preprint(1994)

FIGURE CAPTIONS

Fig.1. Window(filter) functions for some experiment groups[29].

Figs.2(a) and (b). The measured broad band power spectrum by the experiment groups. Refer to [28] about the detailed explanations.

Figs.3(a), (b), (c), (d). The theoretically estimated broad band spectrum for some combinations of the cosmic parameters. Refer to [31] about the detailed explanations.

Fig.1

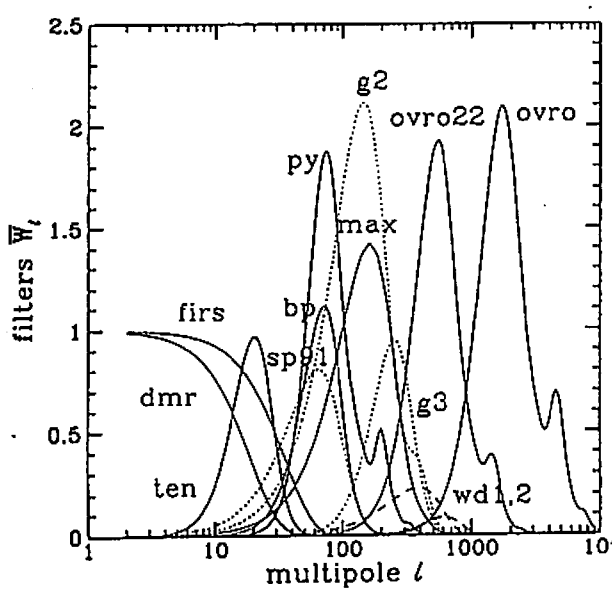
filters $\overline{W}_l$
multipole l
g2
ovro22
ovro
py
max
firs
bp
sp91
dmr
g3
ten
wd1,2

Fig.2(a)

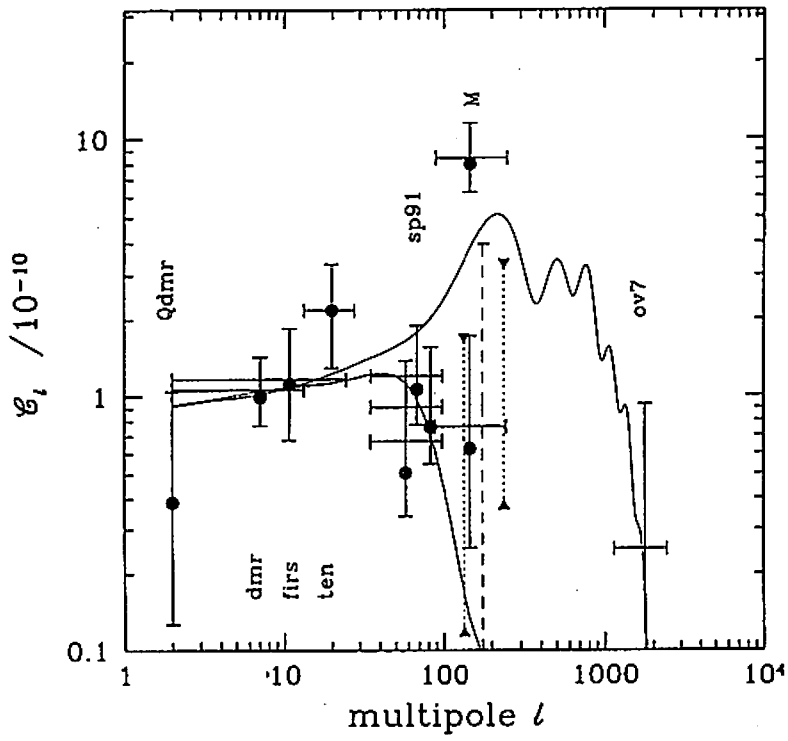
$\mathcal{C}_l$ /10^{-10}
multipole l
M
sp91
Qdmr
ov7
dmr
firs
ten

Fig.2(b)

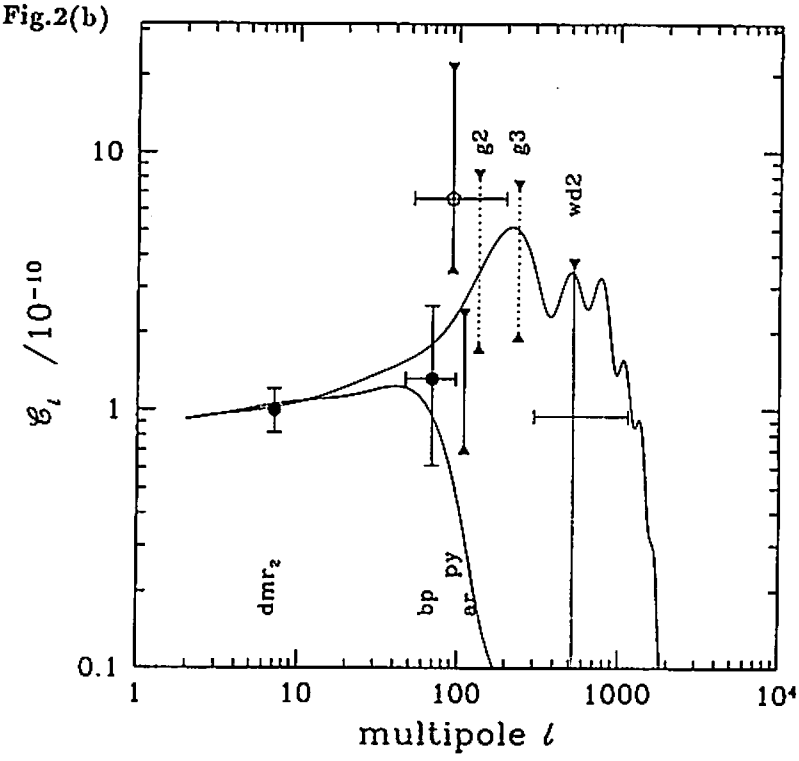
10
1
0.1
1
10
100
1000
10^4
$\mathscr{C}_l$ /10^{-10}
multipole l
g2
g3
wd2
dmr2
bp
py
ar

Fig.3(a)

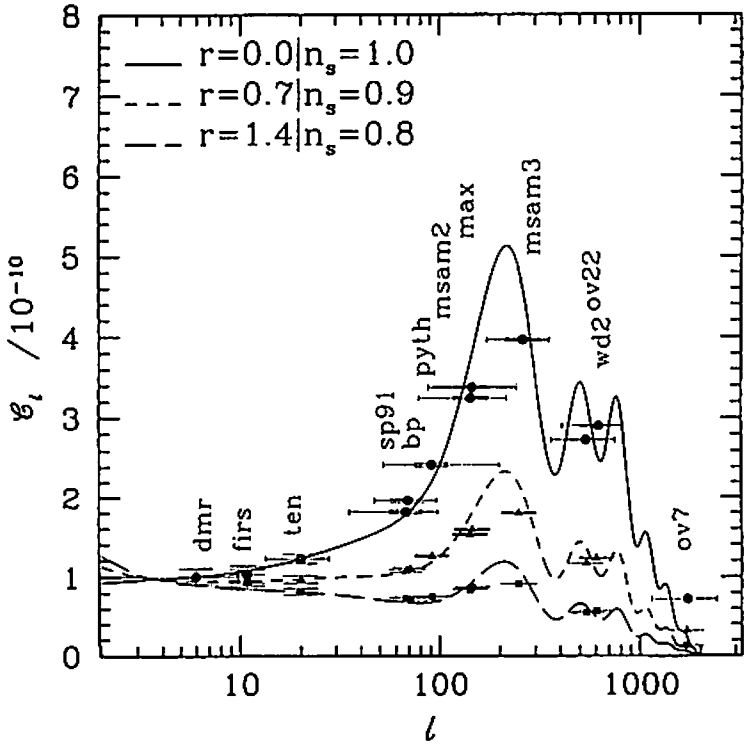
r=0.0|n_s=1.0
r=0.7|n_s=0.9
r=1.4|n_s=0.8
8
7
6
5
4
3
2
1
0
10
100
1000
$\mathscr{C}_l$ /10^{-10}
l
dmr
firs
ten
sp91
bp
pyth
msam2
max
msam3
wd2
ov22
ov7

Fig.3(b)

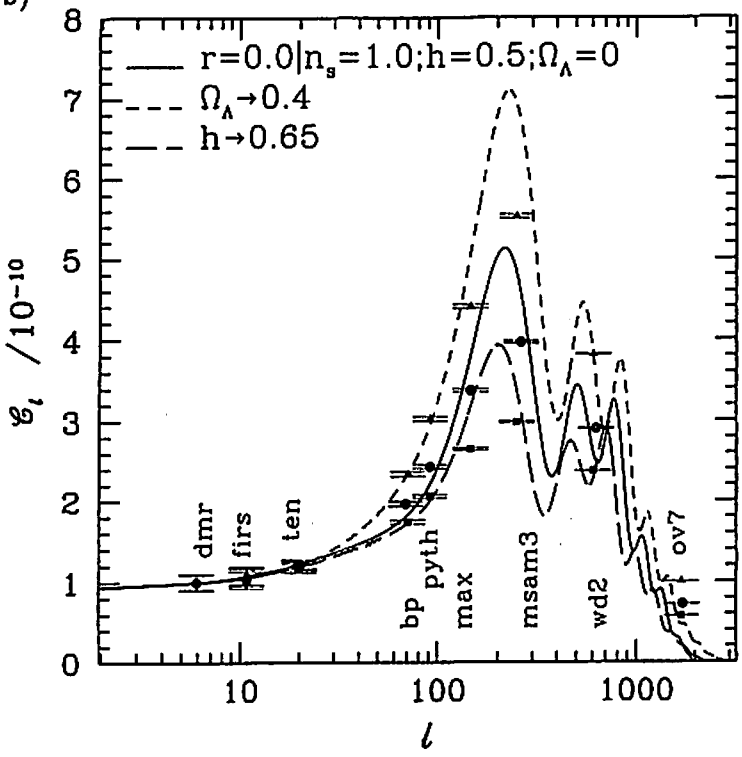
r=0.0|n_s=1.0;h=0.5;Ω_Λ=0
Ω_Λ→0.4
h→0.65
dmr
firs
ten
bp
pyth
max
msam3
wd2
ov7
ℓ(ℓ+1)C_ℓ /10^-10
ℓ

Fig.3(c)

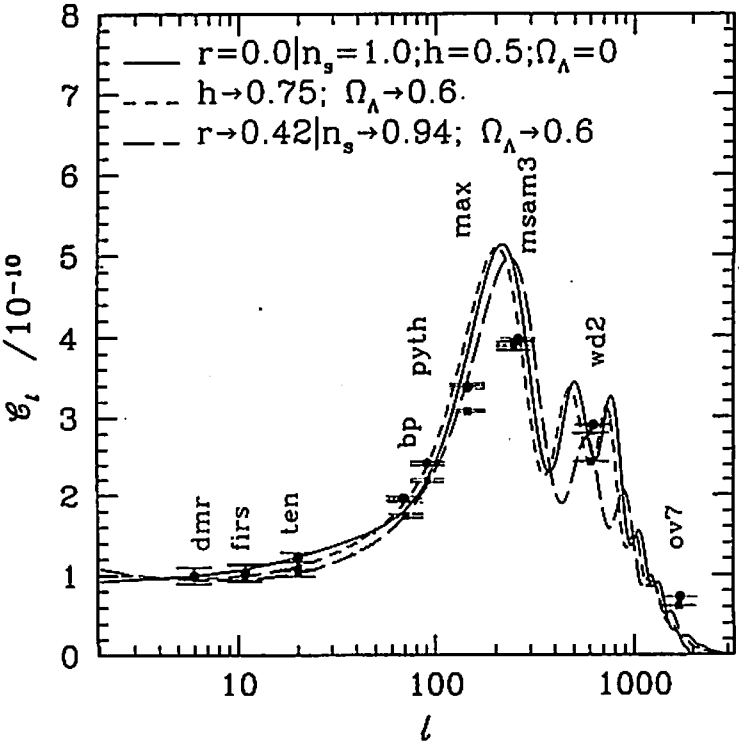
r=0.0|n_s=1.0;h=0.5;Ω_Λ=0
h→0.75; Ω_Λ→0.6
r→0.42|n_s→0.94; Ω_Λ→0.6
dmr
firs
ten
bp
pyth
max
msam3
wd2
ov7
ℓ(ℓ+1)C_ℓ /10^-10
ℓ

Fig.3(d)

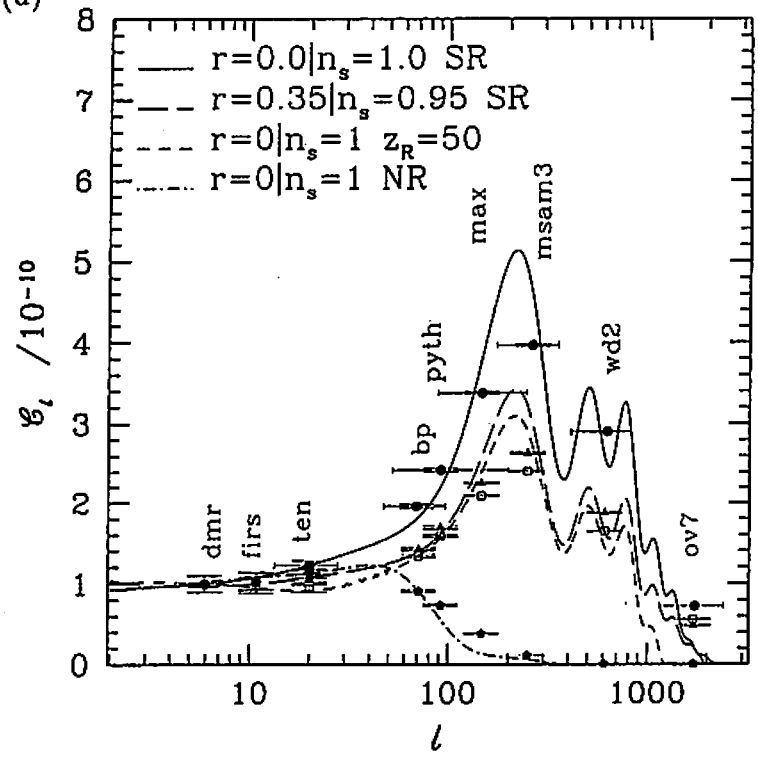
r=0.0|n_s=1.0 SR
r=0.35|n_s=0.95 SR
r=0|n_s=1 z_R=50
r=0|n_s=1 NR
max
msam3
pyth
wd2
bp
dmr
firs
ten
ov7
ℓ(ℓ+1)C_ℓ /10^-10
ℓ
0
1
2
3
4
5
6
7
8
10
100
1000

Variable Cosmological Term and Age of the Universe

Takao Fukui

Liberal Arts, Dokkyo University, Soka, Saitama, Japan

Abstract. The age of the Universe is studied in the framework of the generalized scalar-tensor theory. It depends on a constant μ which leads to a variable cosmological term in the case of $\mu \neq 1$.

1. Field Equations

The Lagrangian L for a generalized scalar-tensor theory is given here as

$$L = \phi[R-2\Lambda(\phi)] + 16\pi L_m/c^4 - \omega(\phi)\phi_{,l}\phi^{,l}/\phi,$$

where $\Lambda(\phi)$ is the cosmological term and $\omega(\phi)$ the Brans-Dicke coupling "constant". Then the field equation for metric field and the wave equation for ϕ are obtained by requiring that the action be stationary under variation of the tensor field and the scalar field respectively.

2. Cosmological Problem

The field equations are applied to the homogeneous and isotropic Universe where the Robertson-Walker metric and the energy-momentum tensor of a perfect fluid can be employed. All the equations in detail can be referred to the previous work[1]. Since it is suggested that our Universe experienced a stiff matter state in the very early epoch[2], here we regard the Universe as that evolving from a stiff matter state ($p_s = \varepsilon_s$, $\varepsilon_s x^6 = \varepsilon_{s0}$)

through a radiation state ($p_r=\varepsilon_r/3$, $\varepsilon_r x^4=\varepsilon_{r0}$) to a matter state ($p_m=0$, $\varepsilon_m x^3=\varepsilon_{m0}$). p and ε are the pressure and the energy density respectively. x is a scale factor normalized to that of the present time.

3.Assumptions

The following three assumptions are made on the grounds explained in the previous work[1].

(a)[3] $\omega = \omega_* \phi^n$,
(b)[4] $\dot{\phi} x^3 = K\phi^m$,
(c)[5] $[(2+n/m)\omega+3]\Box\phi = 8\pi\mu T/c^4$,

where positive n and K, and negative m are constants.

4.Age of the Universe

The equations shown in the previous work[1] are applied to the age of the Universe. Of the three typical cases listed there, however, we take here the case n=-2m where the quantities don't depend on ω, because the case bridges the gap in the values of ω between observation and theory.

Then the followings are the equations to be employed,

$$G = 4/(3\phi),$$
$$\Lambda = 4\pi(1-\mu)(2\varepsilon_{s0}x^{-6}-\varepsilon_{m0}x^{-3})/(3c^4\phi),$$
$$\phi = \{8\pi\mu(-2\varepsilon_{s0}+\varepsilon_{m0}x^3)/(3c^2K^2m)\}^{1/(2m-1)},$$
$$3K\phi^m + 16\pi\mu\varepsilon_{s0}/\{c^2K\phi^{m-1}(1-m)\} = (8\pi\mu\varepsilon_{m0}/c^2)t + B, \quad (1)$$
$$(\dot{G}/G)x^3 = -(\dot{\phi}/\phi)x^3 = -K\phi^{m-1}.$$

By putting $x_0=1$ for the present time in the equations above, the age of the Universe is obtained from Eq.(1) as,

$$t_0 = 3\phi_0 K\phi_0^{m-1}(1-2m)/\{8\pi\mu(\varepsilon_{m0}/c^2)(1-m)\} + $$
$$+ 1/\{K\phi_0^{m-1}(1-m)\} - Bc^2/(8\pi\mu\varepsilon_{m0}).$$

Here we take the following observational data,

$$\varepsilon_{m0}/c^2 = 10^{-26} \quad [kg/m^3],$$
$$\Lambda_0 = -(1-\mu)m(K\phi_0^{m-1})^2/(2\mu c^2),$$
$$= 4\pi G_0\varepsilon_{m0}/c^4 = 9\times10^{-53} \quad [m^{-2}]^{(6)},$$
$$\phi_0 = 4/(3G_0) = \{8\pi\mu(-2\varepsilon_{s0}+\varepsilon_{m0})/(3c^2K^2m)\}^{1/(2m-1)},$$
$$= 2\times10^{10} \quad [kg^2/(N\cdot m^2)],$$
$$H_0 = 80 \quad [km/s/Mpc],$$
$$|(\dot{G}/G)_0| = K\phi_0^{m-1},$$
$$= |\sigma| H_0 < 0.6H_0 = 1.6\times10^{-18} \quad [s^{-1}]^{(7)}.$$

With the data, $\Lambda_0 = 9\times10^{-53} < 2.8\times10^{-53}(-m)(1-\mu)/\mu$. For $m<0$, we get a constraint for μ, $0<\mu<1$, which makes the assumption (c) be reasonable. This constraint can be obtained regardless of the factor in the value of Λ_0. A vanishing cosmological term is achieved in the case of $\mu=1$, which is not concerned in the present work. $\mu\neq1$ means that the cosmological term is variable.

Adopting B=0 which is sensible for an initial condition of ϕ at t=0, the first term in Eq.(1) will significantly contribute to the age, because the second term works just to lengthen the age for negative m. Therefore we study here only the first term. By taking the data into account, the first term is

$$t_0 = 6.5\times10^{17}|\sigma|(1-2m)/\{(1-m)\mu\}$$
$$< 3.9\times10^{17}(1-2m)/\{(1-m)\mu\} \quad [s^{-1}].$$

For $m<0$, $6.5\times10^{17}|\sigma|/\mu < t_0 < 13.0\times10^{17}|\sigma|/\mu$. The constraint, $0<\mu<1$, lengthens the age old enough to be

consistent with the ages of astronomical objects.

In conclusion, the variable cosmological term can contribute to an older age of the Universe, and it is worth while studying the generalized scalar-tensor theory to solve the age problem and the cosmological term problem as well.

References

(1)Fukui,T.,and Arai,K.:1994,Proceeding of the Third Workshop on "General Relativity and Gravitation" (held at the University of Tokyo)274.

(2)Fukui,T.:1992,Astron.Astrophys.,253,1.

(3)Van den Bergh,N.:1982,Gen.Rel.Grav.,14,17.
Burd,A.,and Coley,A.A.:1992,Proceeding of the 6th Marcel Grossmann Meeting (World Scientific)678.

(4)Brans,C.,and Dicke,R.H.:1961,Phys.Rev.,124,925.
Schwinger,J.:1970,*Particles,Sources and Fields*,vol.1 (Addison-Wesley,Massachusetts).

(5)Arai,K.,Hashimoto,M.,and Fukui,T.:1987, Astron.Astrophys.,179,17.

(6)Peebles,P.J.E.:1993,*Priciples of Physical Cosmology* (PRINCETON UNIV.PRESS).

(7)Will,C.M.,1993,*Theory and experiment in gravitational physics*,REVISED EDITION (CAMBRIDGE UNIV.PRESS).

Hot MHD Flows in a Black Hole Magnetosphere

Masaaki TAKAHASHI

Department of Physics and Astronomy, Aichi University of Education

Hirosawa, Igaya-cho, Kariya 448, Japan

ABSTRACT

We present the critical conditions of hot trans-fast magnetohydrodynamical (MHD) flows in a stationary and axisymmetric black-hole magnetosphere. For an accretion onto the black hole or a highly accelerated wind/jet, the MHD flow injected from plasma sources with low-velocity must pass through the slow magnetosonic point, the Alfvén point and the fast magnetosonic point in order, and then the MHD flow falls into the black hole or blows away to far distant region. To pass through smoothly these critical points, the MHD flow's five parameters are restricted by the critical conditions. We consider the thermal effects on hot MHD flows and evaluate the energy flux of the trans-fast MHD flows as functions of the fast magnetosonic radius, the Alfvén radius, the light radius and the location of plasma injection point, and we argue that the trans-fast MHD accretion solution can be broken by highly thermal effects.

1. INTRODUCTION

To explain the activity of active galactic nuclei or compact X-ray sources, we consider a black hole magnetosphere in the center of these objects. The considering black hole magnetosphere is composed of a massive black hole with surrounding fluids and magnetic fields. In this magnetosphere, both an accretion and a highly accelerated wind/jet would be created. The outgoing MHD flow carries the angular momentum effectively, and then the accretion would go on stationary, releasing its gravitational energy. These MHD flows are ejected from plasma sources (e.g., an accretion disk and its corona) with low-velocities, which are at least less than the slow magnetosinic wave speed. The ejected flow passes through the slow magnetosonic point, the Alfvén point and the fast magnetosonic point in order, and then accretes onto the

black hole or goes to far disant region. In cold plasma limit, the critical condition of the trans-fast MHD flows was discussed by Takahashi (1994), while the trans-Alfvén condition was discussed by Takahashi (1990). For hot MHD plasma, the slow magnetosonic point appears in the wind and accretion solutions. The significance of the slow magnetosonic point condition is similar to that of a Newtonian wind and accretion model by Bondi (1952).

2. Basic Equations for Hot MHD Flows

We present the basic equations of a stationary and axisymmetric hot ideal MHD flow, which accretes onto the black hole or blows away to far distant region. These flows stream along magnetic field lines in the black hole magnetosphere. To determine the magnetosphere's structure: configuration of the magnetic field lines and poloidal velocity of the MHD flows, we must solve what is called the Bernoulli equation along magnetic field lines and the force-balance equation self-consistently. These equations are derived from the equation of motion for MHD plasma

$$T^{\mu\nu}_{;\nu} = \left[(\rho + P)u^\mu u^\nu - Pg^{\mu\nu} + \frac{1}{4\pi}\left(F^{\mu\delta}F_\delta{}^\nu + \frac{1}{4}g^{\mu\nu}F^2\right)\right]_{;\nu} = 0 \ , \qquad (1)$$

the conservation law of particle number $(nu^\mu)_{;\mu} = 0$, the ideal MHD condition $u^\mu F_{\mu\nu} = 0$ and Maxwell's equations. Here, ρ, P and n are the total energy density, the pressure of plasma and the proper particle density. The electromagnetic field tensor $F^{\mu\nu}$ satisfies Maxwell equations and u^μ is the four-velocity of plasma. The background metric is written by the Boyer-Lindquest coordinate with $c = G = 1$ and signature -2. The flow with the above assumptions streams along a magnetic field line $\Psi(r, \theta) =$ constant. We should solve both the relativistic Bernoulli equation and the magnetic force-balance equation. However, it is too difficult to solve these equations self-consistently. So, to obtain the critical conditions, we only discuss the relativistic Beunoulli equation with a given magnetic field line.

Stationary and axisymmetry require the existance of four constants of motion (e.g., Camenzind 1986a,1986b). These conserved quantities are the total energy $E(\Psi)$, the total angular momentum $L(\Psi)$, the angular velocity of the field line $\Omega_F(\Psi)$ and the particle flux through a flux tube $\eta(\Psi)$, which are given by

$$E = \mu u_t - \frac{\Omega_F}{4\pi\eta} B_\phi \ , \tag{2}$$

$$L = -\mu u_\phi - \frac{1}{4\pi\eta} B_\phi \ , \tag{3}$$

$$\Omega_F = -\frac{F_{tr}}{F_{\phi r}} = -\frac{F_{t\theta}}{F_{\phi\theta}} \ , \tag{4}$$

$$\eta = \frac{n u_p}{B_p} \ , \tag{5}$$

where $\Psi = A_\phi(r,\theta)$ is the magnetic stream function, B_ϕ is the toroidal magnetic field, u_p is the poloidal velocity defined by $u_p^2 \equiv -u_A u^A$ $(A = r,\ \theta)$, B_p is the poloidal magnetic field seen by a lab-frame observer

$$B_p^2 \equiv -\frac{1}{\rho_w^2}[g^{rr}(\partial_r\Psi)^2 + g^{\theta\theta}(\partial_\theta\Psi)^2] \ , \tag{6}$$

and $\rho_w^2 \equiv g_{t\phi}^2 - g_{tt}g_{\phi\phi}$. For a polytropic equation of state, the relativistic specific entalpy μ is written by (see Camenzind 1987),

$$\mu = mc^2 \left\{ 1 + \frac{\Gamma}{\Gamma - 1} \frac{P_{\rm inj}}{n_{\rm inj} mc^2} \left(\frac{n}{n_{\rm inj}} \right)^{\Gamma-1} \right\} \tag{7}$$

$$= mc^2 \left\{ 1 + \frac{\Gamma}{\Gamma - 1} \frac{P_{\rm inj}}{n_{\rm inj} mc^2} \left(\frac{u_{\rm inj} B_p}{u_p B_p^{\rm inj}} \right)^{\Gamma-1} \right\} \ , \tag{8}$$

where m is the rest mass of the particle and the subscript 'inj' means the quantities at the injection point. Now we require the specification of an additional constant of motion, $P_{\rm inj}/n_{\rm inj}$, at the injection point. (For cold limit, $P_{\rm inj}/n_{\rm inj} \to 0$, and then $\mu = mc^2$.)

The poloidal equation (relativistic Bernoulli equation) can be written as (Takahashi et.al. 1990)

$$\mu^2(1 + u_p^2) = E^2[(k_0 - 2M^2)f^2 - k_4] \ , \tag{9}$$

where

$$f \equiv \frac{(g_{t\phi} + g_{\phi\phi}\Omega_F) + (g_{tt} + g_{t\phi}\Omega_F)L/E}{\rho_w(M^2 - k_0)} , \tag{10}$$

$$k_0 \equiv g_{tt} + 2g_{t\phi}\Omega_F + g_{\phi\phi}\Omega_F^2 , \tag{11}$$

$$k_4 \equiv g^{tt} - 2g^{t\phi}(L/E) + g^{\phi\phi}(L/E)^2 , \tag{12}$$

and M is the relativistic Mach-number defined as

$$M^2 \equiv \frac{4\pi\mu n u_p^2}{B_p^2} = \frac{4\pi\mu\eta u_p}{B_p} . \tag{13}$$

When the poloidal field geometry $\Psi(r,\theta)$ is known and the various conserved quantities are specified at the injection point (as boundary conditions), the Mach-number (13) used togeter with (8) in the poloidal equation (9) determines a complicated equation for u_p as a function of r.

The differential form of the above poloidal equation is written by

$$(\ln u_p)' = \frac{N}{D} , \tag{14}$$

where

$$N = (M^2 - k_0)^2 \left[(1 + u_p^2)(M^2 - k_0)\frac{a_s^2}{1 - a_s^2} + \left(\frac{E}{\mu}\right)^2 M^4 f^2 \right] (\ln B_p)' \tag{15}$$
$$+ \frac{1}{2(1 - a_s^2)} \left(\frac{E}{\mu}\right)^2 \left[M^4(M^2 - k_0)k_4' - (k_0 k_2 - 3k_2 M^2 - 2k_4 M^4)k_0' \right] ,$$

$$D = (M^2 - k_0)^2 \left[\left(\frac{a_s^2}{1 - a_s^2} - u_p^2 \right)(M^2 - k_0) + \left(\frac{E}{\mu}\right)^2 M^4 f^2 \right] , \tag{16}$$

and the prime $(\cdots)'$ denotes $\partial_r - (\partial_r\Psi/\partial_\theta\Psi)\partial_\theta$ along a stream line. The relativistic sound velocity a_s is given by

$$a_s^2 \equiv \left(\frac{\partial \ln \mu}{\partial \ln n}\right)_{ad} \tag{17}$$

$$= \frac{\Gamma P_{\rm inj}}{n_{\rm inj}\mu}\left(\frac{n}{n_{\rm inj}}\right)^{\Gamma-1} \tag{18}$$

$$= (\Gamma - 1)\frac{\mu - mc^2}{\mu} . \tag{19}$$

The denominator (16) can be reduced in the form of

$$D \propto \left(u_p^2 - u_{\rm AW}^2\right)^2 \left(u_p^2 - u_{\rm FM}^2\right) \left(u_p^2 - u_{\rm SM}^2\right) \ . \tag{20}$$

The relativistic Alfvén wave speed $u_{\rm AW}$, the fast magnetosonic wave speed $u_{\rm FM}$ and the slow manetosonic wave speed $u_{\rm SM}$ are defined by

$$u_{\rm AW}^2(r;\Psi) = \frac{B_p^2}{4\pi\mu n} k_0 \ , \tag{21}$$

$$u_{\rm FM}^2(r;\Psi) = \frac{1}{2}\left(A + \sqrt{A^2 - 4C_s^2 u_{\rm AW}}\right) \ , \tag{22}$$

$$u_{\rm SM}^2(r;\Psi) = \frac{1}{2}\left(A - \sqrt{A^2 - 4C_s^2 u_{\rm AW}}\right) \ , \tag{23}$$

where

$$A = u_{\rm AW}^2 + \frac{B_\phi^2}{4\pi\mu n \rho_w^2} + C_s^2 \ , \tag{24}$$

$$B_\phi = 4\pi\eta E \rho_w f \ , \tag{25}$$

$$C_s^2 = \frac{a_s^2}{1 - a_s^2} \ . \tag{26}$$

At the fast magnetosonic point ($r = r_{\rm F}, u_p = u_{\rm FM}$), the slow magnetosonic point ($r = r_{\rm S}, u_p = u_{\rm SM}$) and the Alfvén point ($r = r_{\rm A}, u_p = u_{\rm AW}$), the denomonator becomes zero. Therefore, at these critical points, we must require $N = 0$ to obtain physical wind and accretion solutions which pass through these critical points smoothly.

3. Critical Conditions at Magnetosonic Points

At the Alfvén point ($M^2 = k_0$), from the requirement $N = 0$, we get the following condition:

$$\frac{L\Omega_F}{E} = -\frac{g_{\phi\phi}^{\rm A}\Omega_F(\Omega_F - \omega_{\rm A})}{(g_{tt} + g_{t\phi}\Omega_F)_{\rm A}} \ . \tag{27}$$

It seem to be just the same critical condition as one of cold limit (see Takahashi 1994). However, from equations (8) and (13), to obtain the Alfvén

velocity $u_{\rm A} = u_p(r_{\rm A})$, we must solve a polinomial of degree N in $z = u_p^{1/N}$ for a politoropic index $\Gamma = 1 + 1/N$, while in cold limit it simply obtained as $u_{\rm A}^{\rm cold} = (k_0 B_p)_{\rm A}/(4\pi m c^2 \eta)$. We also find that the Alfvén velocity $u_{\rm A}^{\rm cold}$ of cold MHD model is always greater than that of hot MHD model.

At the fast magnetosonic point, from $N = 0$ and the poloidal equation (9), we obtain the following equation for the Mach-number $M_{\rm F} = M(r_F)$

$$AM_{\rm F}^6 + BM_{\rm F}^4 + CM_{\rm F}^2 + D = 0 \ , \tag{28}$$

where

$$A = K_4' \ , \tag{29}$$

$$B = 2(1 - 3a_s^2)(k_0 k_4 + k_2)(\ln B_p)' - k_0 K_4' + 2k_4 K_0' \ , \tag{30}$$

$$C = 3k_2 K_0' \ , \tag{31}$$

$$D = -k_0 k_2 K_0' \ , \tag{32}$$

with

$$k_2 \equiv (1 - L/E)^2 \ , \tag{33}$$

$$K_0' \equiv 2k_0 a_s^2 (\ln B_p)' + k_0' \ , \tag{34}$$

$$K_4' \equiv -2k_4 a_s^2 (\ln B_p)' + k_4' \ . \tag{35}$$

¿From the conditions $N = 0$ and $D = 0$ at the fast magnetosonic point, we obtain the energy flux ηE of the trans-fast accretion as functions of $x_{\rm F}$ and $M_{\rm F}^2$,

$$\eta E = \frac{1}{2\sqrt{2}\,\pi} \left[\frac{M^4 B_p^2 (M^2 - k_0)^3 (\ln B_p)'}{(k_0 k_2 - 3k_2 M^2 - 2k_4 M^4) k_0' - M^4 (M^2 - k_0) k_4'} \right]_{\rm F}^{1/2} \ , \tag{36}$$

where the Mach-number $M_{\rm F}$ is a solution of equation (28).

¿From the poloidal equation (9) and the definition of Mach-number (13), the poloidal velocity at the fast magnetosonic point is written by

$$u_{\rm F} = \left[\frac{k_0 k_4 - 2k_2 M^2 - k_4 M^4}{M^4 B_p^2 (k_0 - M^2)^2} (4\pi\eta E)^2 - 1 \right]_{\rm F}^{-1/2} \ , \tag{37}$$

and the total energy of the trans-fast MHD flow is written by

$$E_{\rm F} = \frac{4\pi u_{\rm F}\mu_{\rm F}}{B_p^{\rm F} M_{\rm F}^2}(\eta E) \ . \tag{38}$$

4. Concluding Remarks

To discuss the MHD flows passing through the slow magnetosonic point, we only replase the subscripts 'F' to 'S'. The quantities labeled by 'S' are to be evaluated at the slow magnetosonic point.

When the sound four-velocity C_s is greater than the Alfvén wave speed at the Alfvén radius, we find a limit of the hot trans-fast MHD accretion. In this case, it is possible that the condition $N = D = 0$ is not acheived between the Alfvén radius and the event horizon. This means that no physical trans-fast MHD accretion solution exists due to the over-pressure effects. We only obtain unphysical solutions that at the event horizon the plasma's pressure diverges and its radial velocity $u_{\rm H}^r$ becomes zero.

REFERENCES

Bondi,H. 1952, M.N.R.A.S., 112,195.

Camenzind,M. 1986a, Astron. Astrophys., 156, 137.

Camenzind,M. 1986b, Astron. Astrophys., 162, 32.

Camenzind,M. 1987, Astron. Astrophys., 184, 341.

Takahashi,M., Nitta,S., Tatematsu,Y., & Tomimatsu,A. 1990, Astrophys.J., 363, 206.

Takahashi,M. 1994, in Proceedings of the Third Workshop on General Relativity and Gravitation, p15, ed. K.Maeda.

Cold MHD Black Hole Magnetosphere Near Force-Free Limit

Toshio Uchida

Astronomical Institute, Faculty of Science, Tohoku University, Sendai 980, Japan

1. Introduction

When the thermal pressure force of the plasma is small and negligible compared with the inertial force and the electromagnetic force, the basic equations of the relativistic magnetohydrodynamics become

$$\mu n u^\nu \nabla_\nu u_\mu = F_{\mu\nu} J^\nu, \tag{1}$$

$$\nabla_\mu (n u^\mu) = 0, \tag{2}$$

$$F_{\mu\nu} u^\nu = 0, \tag{3}$$

$$\nabla_\lambda F_{\mu\nu} + \nabla_\mu F_{\nu\lambda} + \nabla_\nu F_{\lambda\mu} = 0, \tag{4}$$

$$\nabla_\nu F^{\mu\nu} = 4\pi J^\mu, \tag{5}$$

where $F_{\mu\nu}$ is the electromagnetic field, J^μ is the four current, u^μ is the macroscopic four velocity of the plasma, n is the particle number density and μ is the mass of the plasma particle. This limit is called the cold limit. Further when the inertial force is negligible compared with the electromagnetic force, the basic equations become

$$F_{\mu\nu} J^\nu = 0, \tag{6}$$

together with equations (4) and (5). This equation is most easily derived by setting $\mu \to 0$ in equation (1). This limit is called the force-free limit or the massless limit. Note that u^μ and n do not appear in this limit. That is, u^μ and n are not basic variables in the force-free limit and we need a complementary assumption different from the force-free condition in order to introduce these quantities in this limit.

In this work, first I will propose a new assumption to introduce u^μ and n to the force-free limit. The new assumption is general itself, but only

the stationary and axisymmetric configuration is treated in followings. The newly defined u^μ and n enable us to relate the force-free limit to the cold limit. Thus next, by regarding μ a small parameter, we will develop a perturbative expansion of physical quantities by μ in the cold limit near the force-free limit and derive expressions of the physical quantities which is correct up to first order in μ.

Although a black hole magnetosphere is constituted by both inflow and outflow, only inflow is considered. The background spacetime is Kerr spacetime, that is

$$ds^2 = -\alpha^2 dt^2 + \varpi^2 (d\phi - \omega dt)^2 + g_{rr} dr^2 + g_{\theta\theta} d\theta^2. \tag{7}$$

2. New definition of u^μ

Formally equations (2) and (3) do not disappear even if we set $\mu \to 0$. These equations, however, are not sufficient to determine u^μ and n uniquely. Thus one must introduce a complementary assumption to determine u^μ and n in addition to equations (2) and (3) . In many preceding works, it has been often assumed that the plasma is completely charge separated and the current is constituted by only the convective current. That is , u^μ is introduced by

$$qnu^\mu = J^\mu, \tag{8}$$

where q is the charge of the plasma particles. In the magnetohydrodynamics, however, the plasma is not completely charge separated in general. Thus the four velocity defined by equation (8) cannot smoothly be connected to the four velocity in the cold limit. Therefore, in order to relate the force-free limit to the cold limit, u^μ in the force-free limit is

chosen so as to be derived from u^μ in the cold limit by taking an appropriate limit. Thus we propose a new definition of u^μ and n. It is stated as follows:
u^μ and n in force-free limit must be coincide with the masless limit of u^μ and n in the cold limit. That is, they are obtained by taking $\mu \to 0$ limit in the expressions of u^μ and n in the cold limit.

3. Stationary and axisymmetric cold MHD configuration

In stationary and axisymmetric configurations, the basic equations of cold MHD yield integrals on the poloidal field line $\Omega_F(\Psi)$, $\eta(\Psi)$, $L(\Psi)$ and $E(\Psi)$. There are relations

$$u^r = \frac{\eta}{\sqrt{-g}n}\partial_\theta \Psi, \qquad u^\theta = -\frac{\eta}{\sqrt{-g}n}\partial_r \Psi, \tag{9}$$

$$u^\phi - \Omega_F u^t = \frac{\eta}{\alpha^2 \varpi^2 n} B_T, \tag{10}$$

$$\mu u_\phi - \frac{B_T}{4\pi\eta} = L(\Psi), \tag{11}$$

$$\mu u_t + \frac{B_T}{4\pi\eta}\Omega_F = -E(\Psi), \tag{12}$$

where $B_T = \alpha^2 \varpi^2 F_{r\theta}/\sqrt{-g}$. By equations (10), (11) and (12), we get

$$\frac{B_T}{4\pi\eta} = \frac{\varpi^2(\Omega_F - \omega)e - \Gamma L}{\Gamma - M^2}, \tag{13}$$

$$u^t = \frac{1}{\mu}\frac{1}{\alpha^2}\frac{(\alpha^2 - M^2)e - M^2(\Omega_F - \omega)L}{\Gamma - M^2}, \tag{14}$$

$$u^\phi = \frac{1}{\mu}\frac{1}{\alpha^2 \varpi^2}\frac{\varpi^2(\alpha^2\Omega_F - \omega M^2)e - [\Gamma + \varpi^2\Omega_F(\Omega_F - \omega)]M^2 L}{\Gamma - M^2}, \tag{15}$$

where Alfvem Mach number M is defined by

$$M^2 = \frac{4\pi\mu\eta^2}{n}, \tag{16}$$

e is defined by

$$e = E - \Omega_F L, \tag{17}$$

and Γ is given by

$$\Gamma = \alpha^2[1 - \frac{\varpi^2}{\alpha^2}(\Omega_F - \omega)^2]. \tag{18}$$

4. u^μ and n in force-free limit

Now let us take $\mu \to 0$ limit in equations (13), (14) and (15). In the force-free limit B_T becomes an integral on the poloidal field line $B_T(\Psi)$. By setting $\mu \to 0$, we have

$$L(\Psi) \to -\frac{B_T(\Psi)}{4\pi\eta}, \tag{19}$$

$$E(\Psi) \to -\frac{B_T(\Psi)}{4\pi\eta}\Omega_F(\Psi). \tag{20}$$

Thus we get

$$e = E - \Omega_F L \to 0. \tag{21}$$

This implies

$$\frac{e}{\mu} \to O(1). \tag{22}$$

Further we have

$$M^2 = \mu\frac{4\pi\eta^2}{n} \to 0, \tag{23}$$

as $\mu \to 0$. Thus from equation (14), we have

$$u^t \to \frac{1}{\Gamma}\{(\frac{e}{\mu}) + \frac{\eta}{n}\frac{B_T}{\alpha^2}(\Omega_F - \omega)\}, \tag{24}$$

and from equation (15)

$$u^\phi \to \frac{1}{\Gamma}\{(\frac{e}{\mu})\Omega_F + \frac{\eta}{n}\frac{B_T}{\alpha^2\varpi^2}[\Gamma + \varpi^2\Omega_F(\Omega_F - \omega)]\}. \tag{25}$$

Therefore the velocity field in the force-free limit derived from our new assumption becomes

$$u_0^r = \frac{\eta_0}{\sqrt{-g}n_0}\partial_\theta\Psi, \qquad u_0^\theta = -\frac{\eta_0}{\sqrt{-g}n_0}\partial_r\Psi, \tag{26}$$

$$u_0^t = \frac{1}{\Gamma}\{(\frac{e}{\mu})_0 + (\frac{\eta}{n})_0\frac{B_{T0}}{\alpha^2}(\Omega_F - \omega)\}, \tag{27}$$

$$u_0^\phi = \frac{1}{\Gamma}\{(\frac{e}{\mu})_0\Omega_F + (\frac{\eta}{n})_0\frac{B_{T0}}{\alpha^2\varpi^2}[\Gamma + \varpi^2\Omega_F(\Omega_F - \omega)]\}. \tag{28}$$

Here suffix $_0$ denotes the force-free limit. The particle number density n_0 is derived from $u_0^\mu u_{\mu 0} = -1$ and given by

$$n_0^2 = \frac{\eta_0^2}{\alpha^2\varpi^2}\frac{\Gamma|\nabla\Psi|^2 + B_{T0}^2}{(\frac{e}{\mu})_0 - \Gamma}. \tag{29}$$

It is evident that equations (2) and (3) are automatically satisfied.

In bellow, we restrict our consideration to the monopole field configuration on the equator and analysis along the poloidal field line. Then differentiating $u_0^\mu u_{\mu 0} = -1$, we have wind equation

$$\{\ln(\Delta^{1/2}u_p)\}' = \frac{N}{D}, \tag{30}$$

with

$$D = 2\Gamma[(\Gamma/r^2)\Phi^2 + B_{T0}^2], \tag{31}$$

$$N = \frac{\Delta'}{\Delta}\Gamma[(\Gamma/r^2)\Phi^2 + B_{T0}^2] + r^2(\Gamma/r^2)'B_{T0}^2 - \Delta(\frac{e}{\mu})_0^2(\frac{\eta}{n})_0^2\Gamma', \tag{32}$$

where $'$ denotes d/dr and Φ is the magnetic flux. D and N are both vanish at the event horizon (where $\Delta = 0$) and the light surface (where $\Gamma = 0$). This is respected result, because the event horizon is the fast magnetosonic point and the light surface is the Alfven point in the force-free limit. Further it should be noted that the critical conditions at two

critical points are automatically satisfied. This fact confirms the validity of our treatment.

5. Expansion by μ

Although the mass of the plasma particle μ is a constant which is fixed if the constituent of the plasma is given, formally we can regard μ as a continuous parameter in equation (1). Then it is natural to expect that solutions of equation (1) smoothly depend on μ. That is, the solution is written, for example, as

$$u^r = u^r(r;\mu). \tag{33}$$

Thus in the neighbourhood of $\mu = 0$, u^r is expanded as

$$u^r = u^r(r;0) + \mu\frac{\partial u^r}{\partial \mu} + \cdots, \tag{34}$$

and we can also expect that this will give a good approximation for sufficiently small value of μ. (Accuracy of the expansion depends on the configuration of force-free electromagnetic field, of course.)

The expression for n is derived from relation $u^\mu u_\mu = -1$ by setting $L = L_0 + L_1$, $(e/\mu) = (e/\mu)_0 + (e/\mu)_1$, and $\eta = \eta_0 + \eta_1$ while Φ is fixed. Here suffix $_1$ denotes the first order correction to the quantities by the effects of inertia of the plasma particles. Then straightforward calculation shows that the lowest order term yields equation (29) and the next order term yields

$$\begin{aligned}\frac{n_1}{n_0} &= \mu(4\pi\eta)_0^2\frac{\Gamma(\frac{L_1}{\mu}) + [(\frac{M_0^2}{\mu})L_0 - \varpi^2(\Omega_F - \omega)(\frac{e}{\mu})_0]}{\Gamma[\Gamma|\nabla\Psi|^2 + (4\pi\eta L)_0^2]} \\ &\quad + \frac{\eta_1}{\eta_0}\{1 + \frac{(4\pi\eta L)_0^2}{[\Gamma|\nabla\Psi|^2 + (4\pi\eta L)_0^2]}\} \\ &\quad - \frac{1}{(\frac{e}{\mu})_0 - \Gamma}(\frac{e}{\mu})_0(\frac{e}{\mu})_1.\end{aligned} \tag{35}$$

The expressions of other quantities are derived from equations (9), (13), (14) or (15) together with the above equation. For example, from equation (13) we have

$$\frac{B_T}{4\pi\eta} = -L_0 - \mu\frac{\mathcal{F}}{\Gamma - M_0^2}, \tag{36}$$

with

$$\begin{aligned}\mathcal{F} &= (\frac{M_0^2}{\mu})L_0 - \varpi^2(\Omega_F - \omega)(\frac{e}{\mu})_0 \\ &\quad +\Gamma(\frac{L_1}{\mu}) + (\frac{M_1^2}{\mu})L_0 - \varpi^2(\Omega_F - \omega)(\frac{e}{\mu})_1,\end{aligned} \tag{37}$$

where the first term in equation (36) is the term corresponds to the massless limit and the second term is the correction by inertia of the plasma.

6. Conclusion and discussion

In this work, we gave a new definition for u^μ and developed an expansion of the physical quantities by the mass of the plasma particle. However the result presented here is still preliminary and there are some problems not mentioned above.

First, as seen from equations (36) and (37), the first order corrections to the physical quantities also yield critical conditions. By these conditions, we have relations between η_1, $(e/\mu)_1$ and L_1 and also the first order changes in the position of the fast magnetosonic point and the Alfven point. Further, the treatment developed here must also be applied to the outflow and we must connect inflow and outflow to consider whole energetics of the black hole magnetosphere. We will treat these points elsewhere.

LARGE HYSTERETIC BEHAVIOR OF STELLAR BLACK HOLE CANDIDATE X-RAY BINARIES

Sigenori Miyamoto, Shunji Kitamoto,
Kiyoshi Hayashida & Wataru Egoshi
Department of Earth and Space Science,
Faculty of Science, Osaka University,
1-1, Machikaneyama, Toyonaka, Osaka 560, Japan

ABSTRACT

We show that stellar black hole X-ray binaries have two novel states; the power law hard state and the power law soft state, which depend not only X-ray luminosity but also on previous history of X-ray luminosity, i.e. the states show large hysteretic behavior which is dependent upon X-ray luminosity by a factor of about 100. This large hysteresis probably can not be explained by already existing accretion disk models.

The two states are represented by two (hard and soft) types of power law energy spectral components. In the rising phase of the outburst of an X-ray flare or an X-ray nova, the black hole X-ray binary is in the power law hard state and the power law component has its photon index ($-\gamma$) of about -1.7 (γ = 1.5-1.9) in the X-ray range of 3-40 keV. This state continues until near or just before the maximum X-ray flux (2-100 keV). The state then changes to the power law soft state, in which the photon index ($-\gamma$) of the power law component changes to about -2.7 (γ = 2.2-3.0) in the X-ray range of 3-40 keV. Following this change, a large multi-temperature (approximately represented by blackbody radiation of kT = 0.5-1 keV) disk blackbody component appears. This state continues until the X-ray flux has decreased to about 1/100 of its maximum. The disk blackbody component then decreases rapidly and the photon index ($-\gamma$) of the power law component changes to about -1.7. This is the beginning of the power law hard state. In the power law hard state, slight traces of or no disk blackbody component is observed. The short term variability of the power law components and the size of the X-ray emitting regions are different in these two power law states, implying completely different X-ray production processes in these two states. This result was derived from the combined observed results of GS1124-683, GX339-4 and Cyg X-1.

Subject heading: black hole physics -- radiation mechanism: non-thermal; thermal - binaries: close - individual (Cyg X-1, GS1124-683, GX339-4) - X-rays: stars

1. Introduction

Stellar black hole candidate X-ray binaries (BHC-XBs) have been considered to have two X-ray intensity states; the high state and the low state (e.g. Oda 1977; Liang & Nolan 1984; Tanaka 1989). However, Tanaka (1991) recently proposed the ultra-soft

state and the hard state, based on data from the recently observed black hole candidate GS2023+338, an X-ray nova, which showed a hard energy spectrum even in its X-ray high intensity state. Nowak (1994) also indicated that the distinction between the high and the low state could be confusing, since it was possible for the low state to actually be more luminous than the high state in the X-ray energy range of 1-70 keV for GX339-4. We propose here to use the power law soft state and the power law hard state which are dependent upon the value of the photon index of the X-ray power law energy spectral component in the energy range of 3-40 keV. Our proposal is similar to but different from Tanaka's proposal of the ultra-soft state and the hard state. While Tanaka's state is determined by whether the X-ray energy spectrum is ultra-soft or hard as a whole, in our case the power law soft or hard state is determined whether the power law component is soft (photon index $\gamma = 2.7$ (2.2-3.0)) or hard ($\gamma = 1.7$ (1.5-1.9)). (Hereafter, sometimes $\gamma =$ 2.7 and 1.7 is used to represent the γ values of the power law soft state (γ=2.2-3.0) and the hard state (γ=1.5-1.9)). This state depends largely on the previous history of the BHC-XB and shows large hysteresis as shown in the following.

2. The Power Law Hard and Soft States

2.1. GS1124-683

Nova Muscae 1991 or GS1124-683 is a BHC-XB. It was observed with the Ginga LAC from 1991 January 10 to September 3 intermittently. Its X-ray energy spectrum had two types. One is modeled with the soft power law component ($\gamma = 2.2$-3.0 in 3 - 40 keV X-rays) which is usually accompanied by a large multi-temperature disk blackbody component (approximately represented by blackbody radiation of kT = 0.5-1 keV), and the other is modeled with the hard power law component ($\gamma = 1.5$-1.9 in 3 - 40 keV X-rays) which is accompanied by either slight traces of or no multi-temperature disk blackbody component (Miyamoto et al. 1993; Ebisawa et al. 1994). The multi-temperature disk blackbody component presumably consists of X-rays from the optically thick accretion disk (Mitsuda et al. 1984). On MJD 48266 (1991 January 10), soon after the discovery of this Nova, the energy flux of the soft power law energy spectral component was larger than that of the disk blackbody component as shown in Fig.1-R. The disk blackbody component then increased rapidly, and at the X-ray maximum (1-37 keV) on 1991 January 15 this disk blackbody component became larger than the soft power law component. After the X-ray maximum, the soft power law component decreased with a time constant of about 12 days, while the disk blackbody component decreased gradually with a time constant of about 36 days. After about 60 days, the soft power law component became negligibly small and short term variability of X-rays also became small. After this, the soft power law component increased again by a factor of about 5. Finally the disk blackbody component decreased rapidly between MJD 48393 (May 17) and MJD 48420 (June 13), and the photon index (- γ) of the power law component changed to about -1.7. This was the beginning of the power law hard state (the so-called low state) as shown in

Fig. 1-R (Miyamoto et al. 1993). The X-ray energy flux (1-37 keV) at this moment was about 0.01 of the X-ray maximum. If the energy range is extended from 1-37 keV to 1-100 keV, the ratio becomes about 0.015. With this extension of the energy range, the energy flux of the hard power law component is increased by about 53 % and that of the soft power law component is increased only by about 4 %.

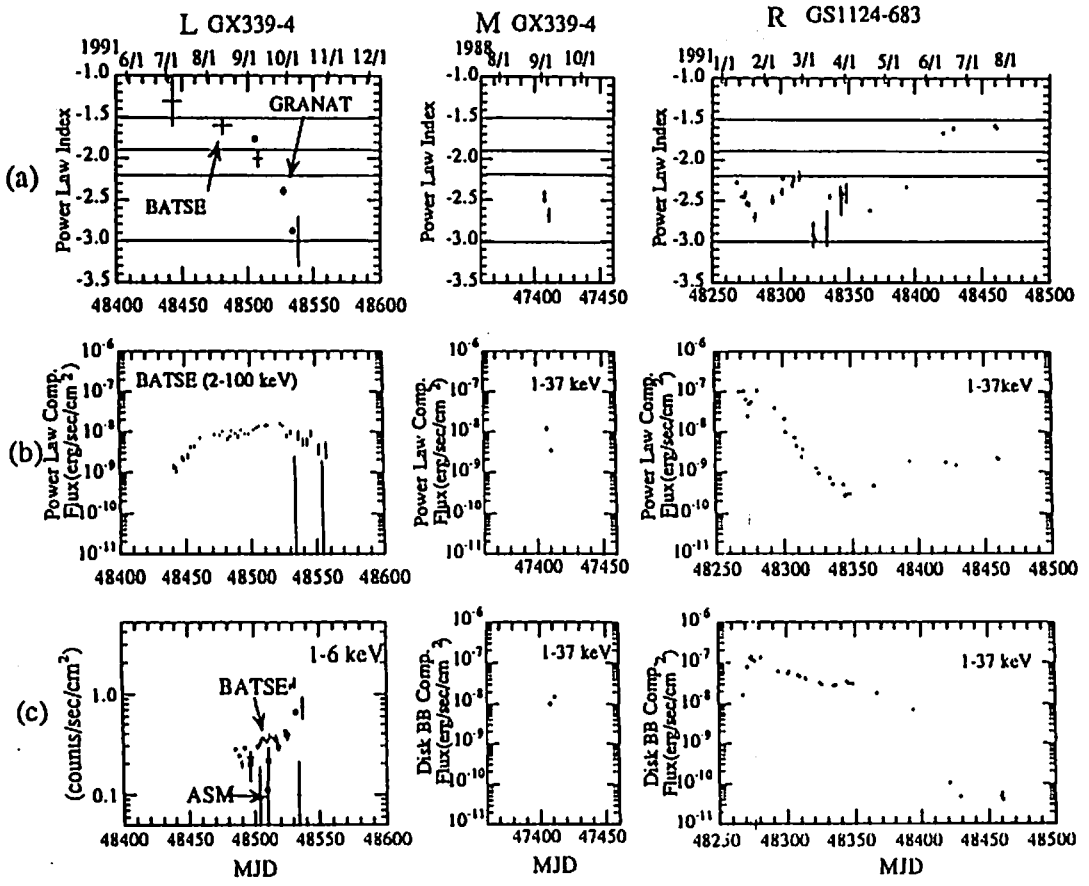

Fig. 1. Long term variation of black hole candidate X-ray binaries (GX339-4 & GS1124-683).

L: The outburst of GX339-4 in 1991 (Harmon et al. 1994, Grebenev et al. 1993, Kitamoto, 1992). (a) The photon index of the power law component; (b) X-ray energy flux (2-100 keV) of the power law component estimated from the 20-100 keV BATSE result; and (c) a comparison between X-ray counts (1- 6 keV) observed with the ASM and those of the power law component extrapolated from the 20-100 keV BATSE data.

M: The power law soft state observed in 1988 (Miyamoto et al. 1991).

(a) The photon index of the power law component; (b) X-ray energy flux (1-37 keV) of the power law component; and

(c) X-ray energy flux (1-38 keV) of the disk blackbody component.

R: The outburst of GS1124-683 (Miyamoto et al. 1993). (a) The photon index of the power law component; (b) X-ray energy flux (1-37 keV) of the power law component; and (c) X-ray energy flux (1-37 keV) of the disk blackbody component.

GS1124-683 was also observed with the GRANAT. Gilfanov et al (1991) reported that on 1991 January 9, the photon index ($-\gamma$) was - 2.6±0.1 in the X-ray energy range of 30-200 keV, and the flux in the energy range of 35-100 keV X-ray was 1450 mCrab. This corresponds to 2.7×10^{-7} erg/s/cm^2 (1-100 keV) of the soft power law component. The photon index of the power law energy spectrum in the energy range of 30-200 keV averaged over the period between January 16 and February 11 was - 2.45 ± 0.03. These are consistent with the Ginga results shown in Fig 1-R.

2.2. GX339-4

GX339-4 has been considered to be a black hole candidate, because its X-ray behavior is similar to that of a black hole candidate Cyg X-1. An outburst of this source was observed with the ASM and the LAC onboard the Ginga on 1988 September 3-7 (MJD 47407 -11). It was shown that just after the X-ray maximum (1-37 keV), the X-ray energy spectrum consisted of the soft power law component and the multi-temperature disk blackbody component (see Fig.1-M). The total X-ray flux (2-100 keV) at this time is estimated to be about 3×10^{-8} erg/s/cm^2 (assuming $\gamma = 2.7$) and the main component was the disk blackbody component (Miyamoto et al. 1991).

There is no direct observation of the transition of GX339-4 from the power law soft state to the power law hard state. However, in the low state of GX339-4 on 1985 April 25, the energy spectrum (2-10 keV) was well-fitted by a power law component of $\gamma = 1.85 \pm 0.15$ (Ilovaiskey et al. 1986) and we estimate the energy flux (2-100 keV) to be 1×10^{-10} erg/s/cm^2 assuming $\gamma = 1.7$, while on 1976 September 4-10, γ was 2.0 ±0.3 (16-251 keV) (Dolan et al. 1987) and the energy flux (2-100 keV) is estimated to be about 3×10^{-9} erg/s/cm^2.

Thus, GX339-4 is expected to evolve in a similar manner as that of GS1124-683. Near the maximum of its X-ray flux (1-37 keV), it was in the power law soft state with a large disk blackbody component. At about 1/100 of the maximum X-ray flux, it was in the power law hard state with slight traces of or no disk blackbody component. On 1976 September 4-10, however, the power law hard state was observed to exist even though the X-ray flux (2-100 keV) was at about 1/10 of the X-ray maximum.

How does the BHC-XB increase the X-ray flux in an X-ray outburst of a flare or an X-ray nova ? The answer can be given by combining data of GX339-4 observed with the Burst and Transient Source Experiment (BATSE) onboard the Compton Gamma Ray Observatory (CGRO) (Harmon et al. 1994), the GRANAT onboard the KVANT/ MIR (Grebenev et al. 1993) and the All Sky Monitor (ASM) onboard the GINGA (Kitamoto 1992).

Two X-ray outbursts (20-400 keV) of GX339-4 were observed in 1991 June - October and in 1992 September -1993 January with BATSE by Harmon et al. (1994). They found that these two outbursts were very similar in their flux and spectral evolution.

Harmon et al. (1994) fitted the energy spectra with the Sunyaev-Titarchuk Inverse-Compton Scattering Model (Sunyaev and Titarchuk 1980). This model can be represented by a power law in the energy range of less than kT_e (temperature of the Compton electron cloud). The values of the photon index of the power law component (- γ) of the outburst in 1991 (Harmon et al. 1994) are shown Fig.1-L-(a). Grebenev et al. (1993) also observed the same outburst of GX339-4 with the GRANAT and they also fitted the energy spectra with the same model. The values of the photon index (-γ) (Grebenev et al. 1993) are also shown in Fig.1-L-(a). From this figure, one can see that a transition from the power law hard state to the power law soft state took place between MJD 48506 and 48530 (1991 Sept. 5 - Oct.1).

To see long term variation of X-rays from GX339-4 in this transition in 1991 and to compare with the outburst in 1988 mentioned previously, the X-ray energy flux (2-100 keV) of the power law component from GX339-4 is estimated from the data by Harmon et al. (1994) assuming $\gamma = 1.7$ for MJD = 48441- 48528, $\gamma = 2.4$ for MJD = 48531, and $\gamma = 2.7$ for MJD = 48534- 48557. The result is shown in Fig. 1-L-(b). The contribution of X-rays above 100 keV, as compared to the total X-ray energy flux, is relatively small because this component decreases rapidly above 100 keV (Grebenev et al. 1993). The X-ray flux of the power law component reached its maximum around MJD = 48505-48525 (1991 Sept. 6 - 26), where the photon index also changed from $\gamma = 1.7$ to 2.7.

Ginga ASM also observed the same outburst of GX339-4 in 1991. In Fig. 1-L-(c), the photon counts (1- 6 keV) observed with the ASM (Kitamoto 1992) are shown. We compared the observed ASM counts (1-6 keV) with the photon counts of the power law component extrapolated from the spectrum at 20-100 keV observed by Harmon et al. (1994), assuming the photon index of the power law component as mentioned above and correcting for the efficiency of the ASM counter and the interstellar absorption. The results, shown in Fig.1-L-(c), demonstrate that photon counts observed with the ASM are almost equal to or smaller than the extrapolated values. Therefore the increase of 1-6 keV X-rays observed with the ASM can be explained by the change of the γ value. The multi-temperature disk blackbody component had not yet increased, which was expected from the result of GS1124-683 mentioned previously. Therefore little or no disk blackbody component exists in the power law hard state in either the rising phase of the X-ray outburst or just after the power law hard state has changed to the power law soft state. This explains why an initial increase of the X-ray novae in the power law hard state could not be found out with the ASM.

Maejima et al. (1984) observed with the Hakucho satellite a similar X-ray outburst (3-10 keV) of GX339-4 in 1981, which transited from the power law hard state ($\gamma = 1.74 \pm 0.04$) to the ultra-soft state ($\gamma = 4.3 \pm 0.2$, if approximated by a power law spectrum). This ultra-soft state suggested an appearance of the disk blackbody component. The X-ray intensity changed from about 0.1-0.2 Crab to 0.5 Crab (Maejima et al. 1984). This change corresponds to a transition from about 1.1 $\times 10^{-8}$ erg/s/cm^2 (2-100 keV, assuming

the photon index of -1.7) to 1.5 $\times 10^{-8}$ erg/s/cm^2 (2-20 keV). The latter value probably remains almost the same even if the energy range is extended to 2-100 keV because the ultra soft state shows a very soft energy spectrum. These values are similar to those of GX339-4 shown in Fig.1-L.

2.3. Cyg X-1

A similar transition was also observed in Cyg X-1 in 1980. Ling et al. (1983) observed with the JPL High Resolution Gamma-ray Spectrometer onboard the HEAO 3 an increase of gamma-rays (48-183 keV) from Cyg X-1 by a factor of about 2.7 on MJD 44150 - 44200 (1979 Oct. 4 - Nov. 19). This high gamma-ray intensity state continued until MJD 44378 (1980 April). The gamma-ray intensity then decreased about 20 days before Ogawara et al. (1982) observed a flare of X-rays (1-12 keV) on MJD 4400-30 (1980 June) with the Hakucho satellite. The energy spectra was approximated by a power law of indexes of - (1.7 - 2.0) during MJD 44143-44362 and -2.3 $\pm$ 0.2 during MJD 44383- 44389 for gamma rays of about 48 -93 keV (Ling et al. 1983), indicating that, at first, the state was the power law hard state and then it changed to the power law soft state. The maximum X-ray flux of the power law component is estimated to be about (6-8)$\times 10^{-8}$ erg/s/cm^2 (2-100 keV) by extrapolating the energy spectrum observed with the HEAO 3. The maximum X-ray flux of the flare observed with the Hakucho was about 4.5$\times 10^{-8}$ erg/s/cm^2 (1-12 keV) on MJD 44415 (Ogawara et al. 1982). Thus the black hole candidate, Cyg X-1, also shows the same transition from the power law hard state to the softer energy spectral state, which is probably the power law soft state with a large amount of the multi-temperature disk blackbody component.

2.4. Long Term Variation and The Power Law States

The transition from the power law hard state to the power law soft state was observed to take place near or just before the maximum X-ray luminosity in the outburst of flares of GX339-4 and Cyg X-1 as shown in the sections 2.1 and 2.3. In the decaying phase of the X-ray flare, the transition from the power law soft state to the power law hard state was observed to take place at about 1/100 of the maximum X-ray luminosity in GS1124-683 as shown in the section 2.1.

Combining these results, one can conclude that the BHC-XB starts its outburst in the power law hard state and changes to the power law soft state at around the X-ray maximum. In its decaying phase, at about 1/100 of the X-ray maximum flux the state changes again to the power law hard state. Thus there is hysteresis of about a factor of one hundred depending on X-ray luminosity between the power law hard state and the power law soft state. The soft power law component is usually accompanied by a large amount of the multi-temperature disk blackbody component, while the hard power law component is not.

3. Other Characteristics of The Power Law Two States

Moreover, as shown in the following, the soft ($\gamma = 2.7$) power law component and the hard ($\gamma = 1.7$) power law component are different not only in their photon index but also in their short term variability and the size of their X-ray emitting regions.

Short term variability (the normalized power spectrum density (NPSD) and the phase lag) is different for these two components. For instance, the NPSD is more than one order of magnitude larger in the hard power law component than that in the soft power law component at frequencies from 0.01 to 0.4 Hz (Miyamoto et al. 1994a; b). Moreover, in the power law soft state, just after the X-ray maximum, a peculiar large time (phase) lag of time variation between different energy X-rays up to about 0.1 sec was observed both in GX339-4 on 1988 September 5 (MJD 47409) (Miyamoto et al. 1991) and GS1124-683 on 1992 January 22 (MJD 48278) (Miyamoto et al. 1993).

To explain the peculiar large time lag and the energy spectrum of the soft power law component, Miyamoto & Kitamoto (1991) proposed a jet model in which large hot electron clouds of about 10^9 cm were formed above and below the central part of the accretion disk by rotating magnetic fields partly trapped in the accretion disk. In this model, low energy X-rays were inverse Compton scattered in the hot electron clouds and became the soft power law component. The size of the hot electron cloud, about 10^9 cm, was estimated from the time lag of about 0.1 sec (Miyamoto et al. 1991).

If we observe the evidence of the electron pair production in the high energy X-ray spectrum, the size of X-ray emitting region can be estimated using the compactness parameter $\ell = L\sigma_T/Rm_ec^3$, where L is the total luminosity produced within the source, R is the size of the emission region, σ_T is the Thomson scattering cross section, and m_e is the electron rest mass (e.g. Lightman & Zdziarski, 1987).

Liang & Dermer (1988) estimated the size of the X-ray production region of Cyg X-1 in the low state (the power law hard state) using the compactness parameter. The luminosity of Cyg X-1 was about 1.1×10^{37} erg/s (2.5 kpc) at the time interval γ_1 in the low state, when Ling et al. (1987) observed intense MeV emission lines. Assuming the compactness parameter (ℓ) was about 12 in this interval, Liang & Dermer estimated the linear size (R) of the X-ray emitting region in this low state to be about 2.5×10^7 cm. It is interesting to note that the time interval γ_1 (1979 Sept. 27- Oct.10, MJD 44133-56) is just before the increase of the hard power law component mentioned in section 2.3.

Similarly, one can estimate the size of the X-ray emitting region of GS1124-683 in the power law soft state. On 1991 January 20-21 (MJD 48276-77), soon after the nova GS1124-683 reached its X-ray maximum, the GRANAT team observed a broad Gaussian line of 474 keV (Sunyaev et al. 1992). In this case this source seemed to be just on the threshold of emitting the positron annihilation line, because the annihilation line was not observed on days before and after January 20-21. As the nova was near its maximum luminosity, the luminosity L is assumed to be near the Eddington limit, i.e. 10^{39} erg/s for a 10 solar mass black hole at this time. The linear size R is, therefore, estimated to be

about 2.7×10^9 cm for $l = 10$. This was one day before Miyamoto et al. (1993) observed the peculiar large phase lag mentioned above and is consistent with the size of the hot electron cloud estimated by Miyamoto et al. (1991).

Thus, the size of the X-ray emitting region and the X-ray short term variability as well as the energy spectrum in these two power law states are different. Thus X-ray production processes in these two different power law states should be different from each other.

4. One Exceptional Case: GS2023+338

However, one exceptional case has been observed. During an outburst of the X-ray nova, GS2023+338 (a BHC), in 1989, all of the X-ray spectra were observed to be hard. GS2023+338 was not observed to be in the power law soft state with the disk blackbody component (Tanaka 1989; 1991; Terada et al. 1994), i.e. it was always in the power law hard state and the transition from the power law hard state to the power law soft state was not observed. Thus, this nova does not agree with the evolution model mentioned in the section 2.4. In this case, although the X-ray flux (1-37 keV) reached a very large value, probably up to the Eddington limit, for a very short duration (about 13-16 minutes) on 1989 May 30, the mean X-ray flux was rather small and it decreased to 1/100 of the maximum X-ray flux within 3 hours (Tanaka 1989; Terada et al. 1994), suggesting that the mean matter density at the center of the accretion disk was rather low even at the time of this short maximum of X-ray flux. This suggests that the transition from the power law hard state to the power law soft state does not take place when the mean density at the center of the accretion disk is smaller than a certain value even if the source has flared up to about the Eddington limit for very short duration. However, the mean density at the center of the accretion disk seems to determine the transition from the power law hard state to the power law soft state in the hysteretic behavior of BHC-XBs as long as the mean density is larger than a certain value.

5. Conclusion

In conclusion, in BHC-XBs we found that there are two states, the power law hard and soft states. The states show large hysteretic behavior which is dependent upon the X-ray luminosity by a factor of about 100. The transition from the power law hard states to the power law soft state during this hysteretic behavior seems to be determined by the mean density at the center of the accretion disk. This large hysteretic behavior probably can not be explained by X-ray emitting models from the accretion disk. Hoshi & Inoue (1988) studied the hysteresis between the high and the low state theoretically and estimated that the hysteretic factor of X-ray luminosity could be about 3, which was too small to explain the hysteresis mentioned above. To explain this large hysteresis, some nonlinear phenomena seem to be necessary such as the magnetic accretion disk. Shibata et al. (1990) suggested that there could be two kinds of magnetic accretion disks; the high and

the low β (= p_{gas}/p_{magnet}) accretion disk. This may possibly explain the large hysteretic behavior observed in BHC-XBs.

The power law hard state and the power law soft state are different not only in their energy spectra, but also in their X-ray short term variability of the power law component, and the size of the X-ray emitting region. Moreover, either slight traces of or no X-ray disk blackbody component is observed in the power law hard state, although a large amount of the X-ray disk blackbody component is observed in the power law soft state.

The soft power spectral component appears near the X-ray maximum and continues to exist only during the decreasing phase of the X-ray outburst. Thus the power law soft state continues for a rather short duration compared to that of the power law hard state. This may be the reason why we observe the photon index ($-\gamma$) of the power law component to be about -1.7 in many AGNs, or large mass black holes in the center of the active galaxies (e.g. Turner & Pounds 1989).

It is also interesting to note that the intensive MeV emission lines were observed in Cyg X-1 just before a start of an X-ray increase in the power law hard state (Ling et al. 1987) and just after the X-ray maximum in GS1124-683 in the power law soft state (Sunyaev et al. 1992).

However, there are questions to be answered with observations. 1) Does the hysteresis really exist in an individual BHC-XB ? 2) Does a flare or nova exist in which a BHC-XB increases in the power law soft state and continues to be in the soft state ? 3) In the rising phase of the outburst in the power law hard state, is short term variability of X-rays (the normalized power spectrum density and the phase lag of time variations between different energy X-rays) the same as the canonical time variation observed in the so-called low state (Miyamoto et al. 1992) ? 4) Does similar evolution take place in neutron star X-ray binaries ? Variability similar to that of BHC-XBs was observed in X-rays from Cir X-1 and GX5-1 (Miyamoto 1994, Miyamoto et al. 1994a; 1994b).

We thank Amy R. Lesser for her help in editing this manuscript.

References

Dolan, J. F., Crannell, C. J., Dennis, B. R., & Orwig, L. E. 1987, ApJ. 322, 324

Grebenev, S. et al. 1993, A&AS 97, 281

Gilfanov, M. et al. 1991, Proceedings of the workshop on Nova Muscae 1991, ed. S. Brandt (Danish Space Research Institute, Lyngby) 51

Ebisawa, K. et al. 1994, PASJ, 46, 375

Harmon, B. A. et al. 1994, ApJ Lett. 425, L17

Hoshi, R, & Inoue, H. 1988, PASJ 40, 421

Ilovaisky, S. A. et al. 1986, A&A 164, 67

Kitamoto, S. 1992, Fourth International Toki Conference on Plasma Physics and Contorolled Nuclear Fusion, ed.T. D. Guyenne & J. J. Hunt, (Noordwijk, ESA Publications Division)

297
Liang, E. P. & Dermer, C. D. 1988, ApJ Lett. 325, L39
Liang, E. P. & Nolan, P. L. 1984, Space Sci. Rev. 38, 353
Lightman, A. P. & Zdziarski, A. A. 1987, ApJ. 319, 643
Ling, J. C., Mahoney, W. A., Wheaton, W. A., Jacobson, A.S., & Kaluzienski, L. 1983, ApJ. 275, 307.
Ling, J. C., Mahoney, W. A., Wheaton, W. A., & Jacobson A. S. 1987, ApJ. Letter, 321, L117
Maejima, Y., Makishima, K., Matsuoka, M., Ogawara, Y., & Oda, M. 1984, ApJ 285, 712
Mitsuda, K. et al. 1984, PASJ, 36, 741
Miyamoto, S. 1994, Proceedings of the IIAS workshop on mathematical approach to fluctuations II, ed. Hida T. (International Institute for Advanced Study,Kyoto), ISAS Research Note No. 548
Miyamoto, S., Kimura, K., Kitamoto, S., Dotani, T., & Ebisawa, K. 1991, ApJ, 383, 784
Miyamoto, S., & Kitamoto, S. 1991, ApJ, 374, 741
Miyamoto, S., Kitamoto, S., Iga, S., Negoro, H., & Terada, K. 1992, ApJ 391, L21
Miyamoto, S., Iga, S., Kitamoto, S., & Kamado, Y. 1993, APJ, 403, L39.
Miyamoto, S., Kitamoto, S., Iga, S., Hayashida, K., & Terada, K., 1994a, ApJ (Nov.1 issue) (in press)
Miyamoto,S., Kitamoto, S., Kamado, Y., Hashimotodani, K., Hayashida, K., Terada, K., & Negoro, H., 1994b, New Horizon of X-ray Astronomy, ed. Makino, F & Ohashi, T. (Tokyo, Universal Academy Press, Inc) 47
Nowak, M. A. 1994, ApJ. 422, 688
Oda, M. 1977, Space Sci. Rev. 20, 757
Ogawara, Y., Mitsuda, K., Masai, K., Vallerga, J. V., Cominsky, L. R., Grunsfeld, J. M., Kruper, J. S., & Ricker, G. R. 1982, Nature, 295, 675
Shibata, K., Tajima, T., & Matsumoto, R. 1990, ApJ. 350, 295
Sunyaev, R. A., & Titarchuk, L. G. 1980, A&A, 86, 121
Sunyaev, R. A. et al. 1992, ApJ Lett. 389, L75
Tanaka Y. 1989, in Proc. 23rd ESLAB Symp. on Two Topics in X-ray Astronomy, ed. J. Hunt, B. Battrick (Paris: ESA Publication Division), 1, 3
Tanaka, Y. 1991, Lecture Note in Physics (Springer-Verlag), 385, 98
Terada, K., Miyamoto, S., Kitamoto, S., & Egoshi, W. 1994, PASJ (in press)
Turner, T. J. & Pounds, K. A. 1989, MNRAS, 240, 833

Gamma Ray Bursts; Relativistic Astrophysical Objects?

Hitoshi HANAMI
Faculty of Humanities and Social Sciences, Iwate University, 020 JAPAN

1 Intorduction

Though it was about 20 years ago to discover gamma ray bursts, the orgin is still open question for astrophysists. The gamma ray bursts are contained from two categlies; classical gamma ray bursts which emit mainly in gamma ray episodically, and soft gamma ray repeaters whcih become active repeatedlly in hard X and soft gamma ray. Recently, ASCA and other observations find the evidence that the origin of the soft gamma ray repeaters is a neutron star, which is well explained by our presented model recently [1]. On the other hand, CGRO observations presented more serious problems to solve the orgin of the classical gamma ray bursts (CGRB) [2]. We have now a variety of the models from the orgin in the solar system to cosmological origin for CGRB. However, some relativistic effects can play important rules in the physical process of CGRB like relativistic fire-ball models. In this paper, then, we will consider the advatages and the problems the relativisitic effects, and check the privios presented fire ball models. We will also present magnetic cannon ball model.

2 Relativistic Fireball Models and Their Problems

When the gravitational collapse with coalesence of a neutron star and a neutron star or a black hole, or failed supernovae, the gravitational energy of baryon with $10^{53} erg$ is released. This is very similar to the situation in type II supernovae. In the supernovae, the neutrio emission from a new formed neutron star makes large contributions for the energy depostions. Since the baryon density is very high, the devided energy per one baryon is so low that the ejecta can emits only in X ray. It show us that the energy released in the high baryon density should be transfered to the low baryon density region for emitting in gamma ray through the graviational collapse [9]. To solve the problem, it was proposed that the precess of $\nu + \bar{\nu} \rightarrow 2\gamma$ forms the fireball of gamma ray.

The neutrios and the anti-neutrions are emitted from two hot neutron stars heated up by the tidal interaction in the coalecence [5]. The energy coversion rate becomes 1/100, which is esitated in optimistic situation. The maxmum gamma ray emission energy becomes $10^{51} erg$, which is enough for the cosmological origin. Some succeded process have been considered for

the situation after the energy deposition of $10^{51}erg$ occurs in the low baryon density region with the compact scale of $R_0 \simeq 100km$.

In the first phase, since the temperature of the fireball is $T = 35.7(E_0/10^{50}erg)^{1/4}(R_0/10km)^{-3/4}MeV$, generation of $e^+ - e^-$ occurs and the photon interacts with $e^+ - e^-$, which means the optical depth becomes very large. Then, the photon $\geq 0.5MeV$ cannot escape from the fireball due to the electron scattering. The fireball, however, can expand relativistically, while the internal energy can be converted to the kinetic energy of the plasma and the temperature and the density are decreasing. When the optical depth becomes lower than unity, the photon can escape from the the fireball. Without the baryon compornents, the most of the energy can be released as the radiation emission [6],[7].

In the neutron star binary coalencence, however, the fireball should contain large fraction of baryon compornents. For the large baryon contamination, the released energy is mainly converted to the kinetic energy of the baryon compornet expansion due to its large interia. The energy cannot be leaved for the gamma ray emission. Even if the fireball with the baryon contamination, the gamma ray emission can be produced by the secondary interactions.

When the baryon with the large momentum interacts with the interstellar medium and froms the shock fronts, the reproduction due to the synclotron emission fron the acclerated in the shocks was also considered [8]. As long as the baryon fraction is smaller than $10^{-6}M_\odot$, the relativistic expansion can be induced and the emission of $10 - 100keV$ from the fireball can be blueshifted to gamma ray. This relativistic motion effect is advatageous for the photon confinement problem induced by the production of $e^+ - e^-$ plasma due to the high energy depostion in the compact scale.

According to the fireball models, the photon is emitted from the region expanded larger than the magnetosphere region of a neutron star. Then, observed cyclotron absorption line cannot be explained by the fireball. Forthermore, the nesessary condition for the fireball is that the baryon fraction should be smaller than $10^{-6}M_\odot$ with the energy of $10^{50}erg$ [5],[8],[9]. We can consider the magnetic field can work like the neutrino which transports the energy into the low baryon density region.

3 Magnetic Cannon Ball with the Collapse of Magnetosphere

The typical observed strength of the magnetic field around neutron stars is $10^{12-13}G$. In the typical cases, the magnetic energy of $10^{42-44}erg$ is strong enough for the energy sources of galactic halo origin of CGRB. There are pulsars as the known objects which emit gamma ray from the magnetosphere of a neutron star. The magnetic fields of the pulsars, however, work as the energy channels through the electromagnetic and plasma processes, so that the rotation energy of the neutron star can be converted to the emissions.

On the other hand, when the neutron star with the magnetosphere collapses into a black hole, which may occur in the coalescence of a double neutron star binary, the current generating the magnetic fields also falls into the horizon of the black hole, so that the magnetosphere should disappear, and induces the emission of the electromagnetic waves. Let consider the

magnetosphere dynamics collapsing to a black hole whose background space-time structure is Schwarzshild geometry.

The dynamics of the electromagnetic field can be discribed by the Maxwell's equations [10],[11].

$$\frac{\partial \mathbf{E}}{\partial t} = \nabla \times (\alpha \mathbf{B}) - 4\pi\alpha \mathbf{j}\,, \qquad \nabla \cdot \mathbf{E} = 4\pi\rho\,,$$
$$\frac{\partial \mathbf{B}}{\partial t} = -\nabla \times (\alpha \mathbf{E})\,, \qquad \nabla \cdot \mathbf{B} = 0\,, \tag{1}$$

where the effects of curved space was included in the lapse function $\alpha = (1 - 2M/r)^{1/2}$. In this paper, we will assume the magnetosphere is vacuum because the matters fall onto the surface of the collapsing star. Introducing a gauge, we can present the fields by the potential as $\mathbf{B} = \nabla \times \mathbf{A}$, $\mathbf{E} = -\alpha^{-1}\partial \mathbf{A}/\partial t$. Using the potential presentation, we obtain the wave equations of the vector potential

$$-\frac{1}{\alpha^2}\frac{\partial^2 \mathbf{A}}{\partial t^2} = \frac{1}{\alpha}\nabla \times (\alpha \nabla \times \mathbf{A})\,. \tag{2}$$

We should solve the initial value problem under the equations for studying the evolution of the fields. As the initial condition, we assumed that there were dipole magnetic field of B_0 at the stellar surface R_0. Since the vector field $\mathbf{A}$ can be expaned by the vector spherical hermonics $\mathbf{X}_{lm}$ in general, the initial field is represented by only one vector spherical harimonics compornent of $l = 1, m = 0$ as $\mathbf{X}_{1,0} = \sqrt{3/8\pi} sin\theta \mathbf{e}_\phi$. Since neither the diffrential equation nor the boundary conditions mix different multipoles, the field will remain propotional to this harimics as it evolves. Separating variables by defining a new field variable $u(r,t)$ as $\mathbf{A}(\mathbf{r},t) = 4\pi/3 B_0 (R_0)^2 (u(r,t)/r) sin\theta \mathbf{e}_\phi$, the wave equation takes the form

$$\left[\frac{\partial^2}{\partial r^{*2}} - \frac{\partial^2}{\partial t^2} - V(r)\right] u(r,t) = 0\,, \tag{3}$$
$$V(r) = \left(1 - \frac{2M}{r}\right)\left[\frac{2}{r^2}\right]\,, r^* = r + 2M ln\left[\frac{r}{2M} - 1\right]\,.$$

This equation describes a one-dimensional wave subject to a potential $V(r)$ which has a grobal maximum at $r^* \simeq 4M$. The potential property induces the field decay near $r^* \simeq 4M$, and the wave propagetes inward and outward.

The figure 1 shows the result when the magnetic field does not change during the collapse and the stellar surface freely falls. We presented the magnetic field configurations after $t = 20$ in unit of light passing time through the Schwarzshild radius. We can see that the decay of the dipole magnetic field induces the electrmagnetic wave emission to outward. There are the outward Poynting vector $\mathbf{S} = \mathbf{E} \times \mathbf{B}$ at the bubble of the magnetic field which carries the momentum outward. This emission becomes $|\mathbf{S}| \propto 1/r^2$ as $r \to \infty$.

We will consider why the decay of the magnetosphere induces the outward emission of the electromagnetic wave. In the our result presented in figure 1, we give the boundary condition of the magnetic field at the stellar surface, which should be generated from the current in the stellar interior. The current falls into the event horizon at $r = 2M$ with the collapsing

stellar materials. The information of the magnetic field generation by the current disappears at the outside of the horizon as the collapse proceeds. It means that the observers at the outside observes the current loss. Then, even if the current is not dissipated in the stellar interior, we can see efectivelly the current dissipation as the current falls into the event horizon. Forthermore, all waves should propagates inward at the horizon. Then, the dissipated current energy means the wave energy of electromagnetic wave propageting into the horizon. It can be interpreated as there are inpedance determined from the wave boundary condition at the horizon where the wave can propagete only inside [12]. The backreaction of the falling waves induces outward propagating wave, which is observed as the expanding magnetic bubble in the calculated result. Since the time scale of the gravitational collapse is shorter than that of the changing the current in the stellar interior, the presented results can be valid in general case under the less dependence of the boundary condition at the stellar surface.

In this process, about half of the magnetosphere energy is lost into the horizon, left of it emits as the electromagnetic wave energy. When the neutron star collapses, the emitting wave frequency is $\simeq c^3/2GM \simeq 10^5 s^{-1}$. Since the wave of the lower frequency than plasma frequency $(4\pi ne^2/m)^{1/2} \simeq 9000 n^{1/2} s^{-1}$ is absorved or reflected, if there are plasma $n > 10^2 cm^{-3}$, most of the wave momentum can be transported to that of the plasma. After the momentum transfer, the simillar process occurs like the previous fireball models.

According above scenario of the collapsing magnetosphere, strong magnetic field of $10^{16}G$ is needed for the energy source of the cosmological origin. We have not yet observed such a strong field. It was pointed out, however, that such a strong field can be generated by the dynamo process of the turbulence induced from the convection in the gravitational collapse of supernovae[14]. Recent numerical simulations of collapse supernovae show that the strong convections are induced by the neutrio emission from the proto neutron star [15]. The turbulent motion reachs the velocity of $V_{com} \simeq 10^8 cms^{-1}$, whose saturated magnetic field becomes $B_{sat} \simeq (4\pi\rho V_{con}^2)^{1/2} \simeq 10^{15}G$;. If the coalecence of neutron star binary is the origin of CGRB, the similar turbulent and convective motions to the supernovae occurs in the pre-collapsing neutron stars, and they amplifies the magnetic field.

For the cosmological origin, the collapsing stellar magnetosphere should obtain the fraction of 1% in the released gravitational energy. The process of collapsing magnetosphere has some advantages for baryon contamination that baryon should fall into the stellar surface and the magnetic energy can be released in the magnetosphere contained no or little baryon. This our presented model can be called as magnetic cannon ball [16].

References

[1] H. Hanami, T. Nakamura, T. Murakami *Astrophys. J. L.*, in preparation, (1994)

[2] AIP Conf. Proceeding, *Compton Gamma Ray Observatory* (AIP Press, New York 1992).

[3] A.K. Harding, *Physics Rep.* , **206**, 327 (1991).

[4] T. Murakami, et al. *Nature*, **335**, 234 (1988).

[5] D. Eichler et al., *Nature*, **340**, 126 (1989).

[6] J.Goodman, *Astrophys. J.*, **308**, L47 (1986).

[7] B..Paczynshi, *Astrophys. J.*, **308**, L43 (1986).

[8] P.Meszaros & M. Rees, *Astrophys. J.*, **397**, 570 (1992).

[9] M. Rees & P.Meszaros *Astrophys. J.*, **405**, 278 (1993).

[10] Macdonald, D. A., and Thorne, K. S. 1982, Mon. Not. Roy. Astron. Soc. **198**, 345.

[11] Thorne, K. S., and Macdonald, D. A. 1982, Mon. Not. Roy. Astron. Soc. **198**, 339.

[12] K.S. Thorne, R.H. Price and D.A. Macdonald, *Black Holes: The Membrane Paradigm* (Yale University Press, New Heaven and London, 1986)

[13] P.Meszaros, *High-Energy Radiation from Magnetized Neutron Stars* (The University of Chicago Press, London 1992).

[14] C. Thompson & R.C. Duncan, *Astrophys. J.*, **408**, 194 (1993).

[15] A. Burrows & B.A. Fryxell, *Astrophys. J.*, **418**, L33 (1993).

[16] H. Hanami, in preparation (1994).

Figure Captions

Figure 1:The initial dipole magnetic field is represented as dushed lines. The magnetic field after $t = 20(2GM/c^3)$ is represented by the solid lines.

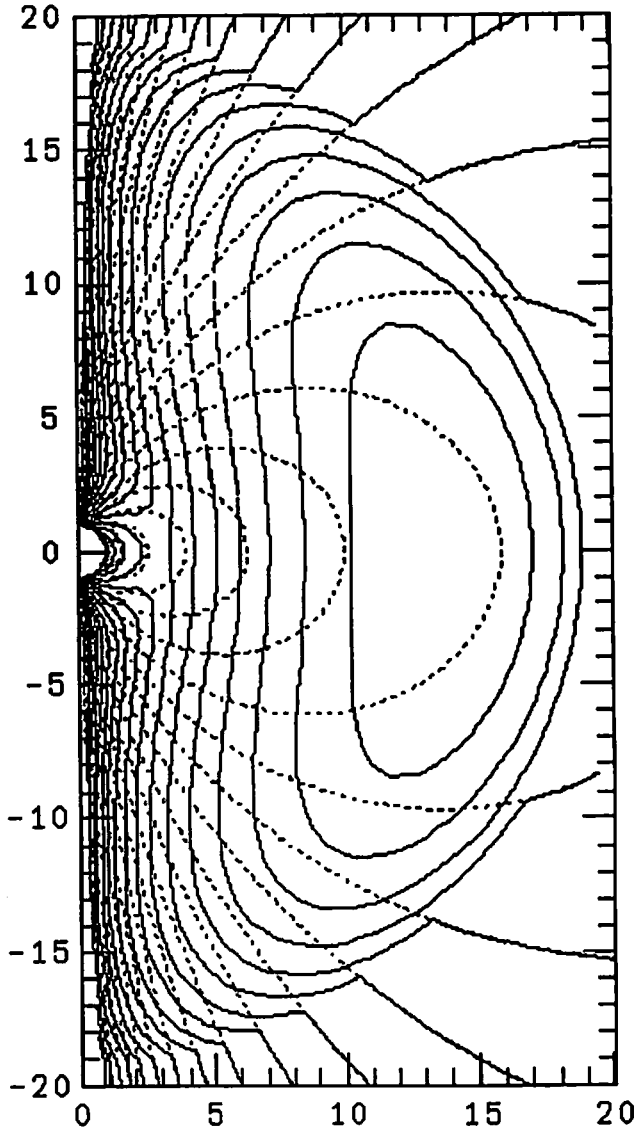

What Cavities?*

Yasunari Okuta†

Department of Astronomical Science,
The Graduate University for Advanced Studies,
Mizusawa, Iwate 023, Japan

and

Joseph Katz‡

Racah Institute of Physics,
Hebrew University, 91904 Jerusalem, Israel

Abstract

Most spherical thin shells, enclosing black body radiation satisfy the dominant energy condition if they have at least $\simeq 30\%$ of the total mass-energy. Containers with less mass energy, may be able to sustain high radiation pressures, contain mostly unstable radiation. Containers with negligible mass energy are either unable to sustain the radiation pressures or the radiation is unstable to gravitational collapse or both at the same time. Containers with black holes and radiation in thermal equilibrium, considered in the literature, are thus often unrealistic.

1. Introduction

Thermal equilibrium of black holes and radiation may exist in closed cavities (for recent reviews on the subject see papers by Landsberg [2] and Page [3]). The walls must be perfectly reflecting and able to resist pressures or tensions upon demand. Or so it seems for the resistance of the box is rarely questioned. The mass of the wall is ignored or explicitly neglected like in

*See Katz and Okuta [1] for complete discussions.

†e-mail: okuta@gprx.miz.nao.ac.jp

‡e-mail: jkatz@hujivms.bitnet

Sorkin, Wald and Zhang [4] though far reaching conclusions are sometimes drawn.

From an engineering view point, cavities with properties as asked for in black hole thermodynamics are incredible. Forces in the cavity must equilibrate the pressure due to radiation, attenuated by self-gravity attraction. But radiation pressure is of the order of its mass energy density. Therefore, how can a cavity have negligible mass energy (compared to that of radiation) and at the same time resist pressure forces comparable to those of radiation (divided by the radius of the box R)? Surely some 'energy condition' is strongly violated.

To shed some light on this question we have calculated the mass M_s of cavities with thin walls (thin spherical shells) and surfaces equal to $4\pi R^2$. The force F on half a sphere satisfies the dominant energy condition [5] if

$$-M_s c^2/2R \leq F \leq M_s c^2/2R. \tag{1}$$

The dominant energy condition is the only one to restrain pressures as well as tensions. One should not allow for unlimited pressure, this is not physical.

2. Elements of the Problem

We consider spherical cavities with perfectly reflecting walls enclosing black-body radiation (photons). The spacetime outside is thus Schwarzschild and the metric can be written in terms of the total mass energy M (in units of $G = c = 1$) as

$$ds^2 = \left(1 - \frac{2M}{r}\right) dt^2 - \left(1 - \frac{2M}{r}\right)^{-1} dr^2 - r^2 d\Omega^2, \qquad r \geq R \tag{2}$$
$$d\Omega^2 \equiv d\theta^2 + \sin^2\theta\, d\phi^2.$$

R is the 'radius' of the cavity. The radiation inside has pressure P, mass energy density ρ and local temperature T which all vary with r and, in Planck units, are related as follows:

$$P = \frac{1}{3}\rho, \quad \rho = \frac{\pi^2}{15} T^4. \tag{3}$$

The solution of Einstein's equations is well known, having been studied by Klein [8], Chandrasekhar [6], Sorkin, et al. [4], Landsberg [2] and Page [3]. Solutions are scale free and all quantities can be expressed in units of R.

Fig.1

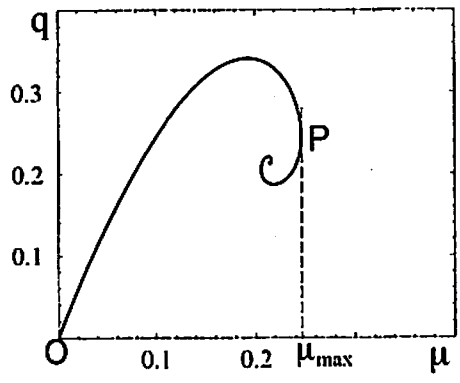

Fig.1
This represents the solution $q(\mu)$ of the TOV equation (8) and $\mu_{max} \simeq 0.246$

The metric inside can be written as

$$ds^2 = e^{2\nu(r)}dt^2 - \frac{dr^2}{1-2\mu(r)} - r^2 d\Omega^2, \qquad r \leq R. \tag{4}$$

where

$$\rho(R) = \frac{\pi^2}{15} T^4(R), \qquad \sqrt{1-\frac{2M}{R}}\, T(R) = T_\infty = \frac{1}{\beta}\,, \tag{5}$$

$$\mu(r) = \frac{\bar{m}(r)}{r}, \qquad \bar{m}(r) = \int_0^r 4\pi r'^2 \rho dr'. \tag{6}$$

Setting like in Sorkin et al. [4]

$$q(r) = \frac{d\bar{m}}{dr} = 4\pi r^2 \rho \quad \text{and} \quad z = \ln r\,, \tag{7}$$

one has Tolman-Oppenheimer-Volkoff equation for $q(\mu)$:

$$\frac{dq}{d\mu} = \frac{2q\left(1 - \frac{2}{3}q - 4\mu\right)}{(1-2\mu)(q-\mu)} \quad \text{with} \quad q = \mu = 0\,. \tag{8}$$

This equation is easily integrated (Fig.1).

$\nu(r)$ is thus completely defined and depends on β and on

$$\alpha = \frac{M}{R}\,. \tag{9}$$

$\nu(r)$ is independent of the shell, but $\mu(R) = \bar{m}(R)/R$ depends on the mass energy of the cavity.

3. The Cavities

Let σ be the mass energy density of the thin sphere enclosing the radiation and Π the pressure ($\Pi > 0$) or tension ($\Pi < 0$) in the shell. The relation between σ, Π and the metrics on both sides are readily found from second fundamental forms and from Gauss-Codazzi identities [9]. Following, for instance, Goldwirth and Katz [10], one finds that

$$4\pi R\,\sigma = \sqrt{1-2\mu} - \sqrt{1-2\alpha}, \qquad \mu = \mu(R) \tag{10}$$

and

$$4\pi R\,\Pi = \frac{1}{2}\left[\frac{1-\alpha}{\sqrt{1-2\alpha}} - \frac{1-\mu+\frac{1}{3}q(\mu)}{\sqrt{1-2\mu}}\right]. \tag{11}$$

In terms of the mass $M_s = 4\pi R^2\sigma$ of the shell (10) becomes

$$\alpha_s = \frac{M_s}{R} = \sqrt{1-2\mu} - \sqrt{1-2\alpha}\,. \tag{12}$$

α_s does not represent the mass energy of the shell E_s which is given by

$$E_s = \int \sqrt{-g}\, T^0_{0\,shell}\, d^3x = \sqrt{1-2\alpha}\, M_s\,. \tag{13}$$

Thus, in units of R,

$$\frac{E_s}{R} = \alpha_s\sqrt{1-2\alpha}\,. \tag{14}$$

It follows from (12) that

$$\frac{E_s}{R} = \sqrt{1-2\alpha}\left(\sqrt{1-2\mu} - \sqrt{1-2\alpha}\right) \le \sqrt{1-2\alpha}\left(1-\sqrt{1-2\alpha}\right) \le \alpha \tag{15}$$

and therefore $E_s \le M$. The fraction of mass energy in the shell is defined by

$$\eta \equiv \frac{E_s}{M} \le 1\,. \tag{16}$$

For a given η, equation (14) relates μ to both α and η. There is some advantage in introducing new variables instead of μ and α:

$$y \equiv \sqrt{1-2\mu}\,, \quad z \equiv \sqrt{1-2\alpha}\,, \quad 0 \le z \le y \le 1. \tag{17}$$

Fig.2

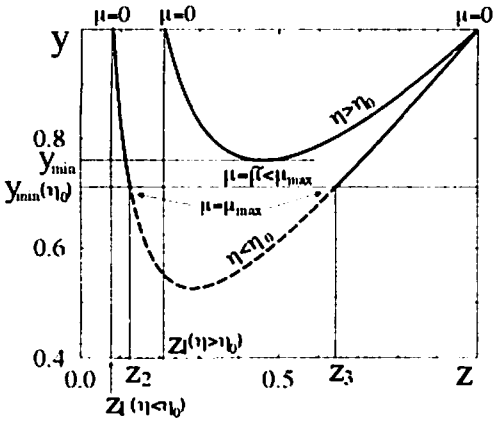

Fig.2
Two $y(z)$ lines, parameterized in μ: one for $\eta = 0.35 > \eta_0 \simeq 0.293$ whose minimum y_{min} is at $z = \sqrt{z_1(\eta)}$ for $\mu = \tilde{\mu} < \mu_{max}$ and another for $\eta = 0.15 < \eta_0$ whose minimum at $z = \sqrt{z_1(\eta)}$ is below $y_{min}(\eta_0)$ and not singled out on the figure.

Thus eq.(14) for $\mu(\alpha, \eta)$ is now replaced by an equation for $y(z, \eta)$:

$$y = \frac{\eta/2}{z} + \left(1 - \frac{\eta}{2}\right) z \,. \tag{18}$$

We know from Fig.1 that equilibrium configurations exist only for

$$\mu \leq \mu_{max} \simeq 0.246 \simeq \frac{1}{4} \quad \text{or} \quad y \geq y(\mu_{max}) \simeq \frac{1}{\sqrt{2}} \,. \tag{19}$$

This limit $1/\sqrt{2}$ divides the equilibrium configurations into two classes depending on whether the parabolic curve $y(z)$ in eq.(18) has a minimum below or above $1/\sqrt{2}$. The minimum of y is $y_{min} = \sqrt{\eta\,(2-\eta)}$. The dividing line at $\eta = \eta_0$ corresponds thus to $\sqrt{\eta_0\,(2-\eta_0)} = \frac{1}{\sqrt{2}}$ or $\eta_0 \simeq 0.293 \simeq 0.3$. If $\eta < \eta_0$, then $y_{min} < y_{min}(\eta_0)$. Equilibrium configurations exist for all values of μ: $0 \leq \mu \leq \mu_{max}$ but in two separate ranges of z: $z_1 < z < z_2$ and $z_3 < z < 1$ (Fig.2).

4. Viable Cavities

Among all equilibrium configurations of given η, what are those that do not violate the dominant energy conditions? Or equivalently, in what region of the (z, y) plane or the $(\alpha, \mu(R))$ plane or the $(M, \bar{m}(R))$ plane does the dominant energy conditions hold for $0 \leq \eta \leq 1$? The dominant energy

Fig.3

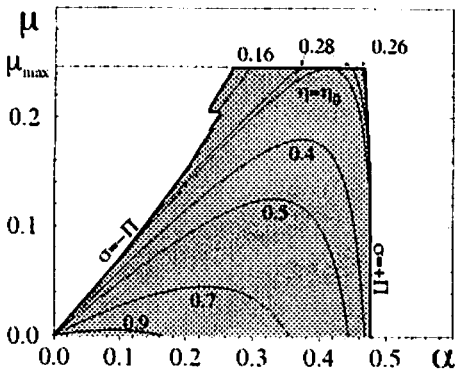

Fig.3
The dark region of the (α, μ) plane are points associated with equilibrium radiation in cavities satisfying the dominant energy conditions. All curves with $\eta > \eta_0 \simeq 0.3$ are inside that region. There are no curves for $\eta \lesssim 0.25$ that satisfies the condition $\Pi < \sigma$ (on the right) and no curve with $\eta \lesssim 0.097$ that satisfies $\Pi > -\sigma$ (on the left).

condition can be rewritten as

$$\left(\frac{1}{z} - 5y\right)(y - z) \leq \frac{2q}{3} \leq \left(\frac{1}{z} + 3y\right)(y - z). \tag{20}$$

The left hand side is a limit on pressures ($\Pi < \sigma$), the right hand side on tensions ($\Pi > -\sigma$). The limits on tensions or pressures in the wall correspond approximately to the dividing line between the two types of solutions ($\eta < \eta_0$ or $\eta > \eta_0$).

Fig.3 shows the region in the (α, μ) plane in which $|\Pi| < \sigma$; notice the relatively small domains of existence of the two classes of equilibrium for $\eta < \eta_0$ between the line $\eta = \eta_0$ and the border of the dark region.

All cavities with about 30% or more mass energy in the shell can resist any pressure or tension. On the other hand cavities with $\eta \lesssim 0.3$ are limited in two directions. For a given total mass energy M they cannot be too big ($\alpha = \frac{M}{R} \to 0$) for they are then unable to resist radiation pressure. There are no viable cavities for $\eta \lesssim 0.097$ when $\alpha \to 0$. They cannot also be too small ($\alpha \to 1$) either for they can then not resist gravitational collapse. There are no viable cavities for $\eta \lesssim 0.25$ when $\alpha \to \frac{1}{2}$.

5. Linear Series for Radiative Equilibrium

The three classes of solutions correspond to quite different $\beta(\mu)$ lines of equilibrium configurations. These lines can be deduces from eq.(5) and (7) which

Fig.4

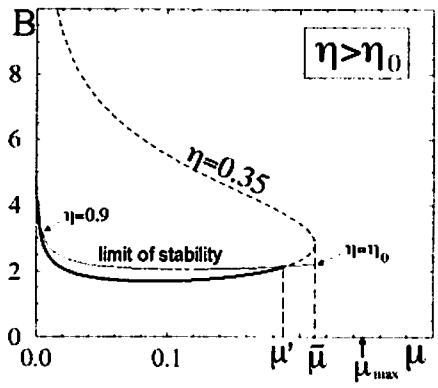

Fig.5a

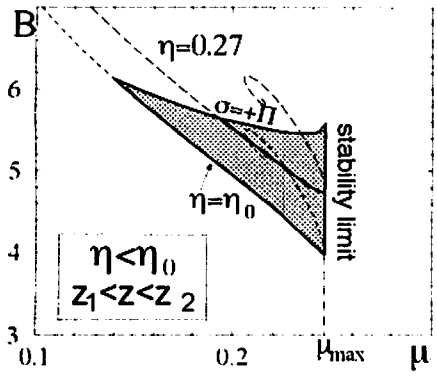

Fig.5b

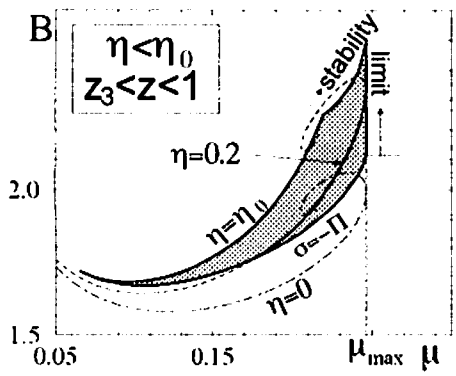

Fig.4
The linear series $B(\mu)$ for $\eta = 0.35$ is characteristic of all lines for $\eta > \eta_0$. The dashed part of the line represents unstable configurations and the thick lines are for stable ones. All configurations are unstable above the thin continuous line representing the limit of stability for $\eta_0 < \eta < 1$.

Fig.5a
The upper boundary of the dark region in this $B(\mu)$ plane corresponds to $\Pi = \sigma$ when $z_1 < z < z_2$. In the dark region, $0.25 \lesssim \eta \leq \eta_0$. There are no viable cavities for $\eta \lesssim 0.25$. The two linear series in this figure are in solid lines where configurations are stable and dashed for unstable ones.

Fig.5b
The lower boundary of the dark region in the plane correspond to $\Pi = -\sigma$ when $z_3 \leq z \leq 1$ and contains only curves with $0.097 \lesssim \eta < \eta_0$. The two linear series in the figure are in solid lines where stable and dashed where unstable. There are no *stable* lines in the dark region for $\eta \lesssim 0.11$.

give

$$B \equiv \left(\frac{15}{4\pi^3}\right)\frac{\beta}{R^{1/2}} = \frac{1}{zq^{1/4}} \tag{21}$$

with $q(\mu)$ and $z(y,\eta)$ defined by eq.(18) and with $y = \sqrt{1-2\mu}$, (21) gives $\beta(\mu,\eta)$ at fixed R.

When $\eta > \eta_0$, equilibrium configurations exist only for $0 \leq \mu \leq \tilde{\mu}(\eta) \leq \mu_{max}$. However, when μ varies from 0 to $\tilde{\mu}$, z varies from z_1 to $\sqrt{z_1}$ where $y = y_{min}$ and with increasing value of z, μ decreases again from $\tilde{\mu}(\eta)$ to zero.

The corresponding linear series $B(\mu)$ is an unwound spiral of the type shown in Fig.4. Here $B(\mu)$ tends to infinity twice, for $z = z_1$ and $z = 1$, since in both limits $y \to 1$, $\mu \to 0$ and $q \to \frac{1}{3}\mu$ so that $q \to 0$ and $B \to \infty$.

When $\eta < \eta_0$, consider first the class of equilibrium configurations for which z varies in the interval (z_1, z_2). Here μ grows from 0 at $z = z_1$ to μ_{max} at $z = z_2$ and q varies accordingly, as can be seen on Fig.1, from point O to P. But Fig.1 and Fig.2 show also that equilibrium configurations exists for decreasing z's, decreasing μ's and *further decreasing* $q(\mu)$. Thus for $\eta < \eta_0$ and $z_1 \leq z \leq z_2$, z and y may oscillate near z_2 a number of times for which $B(\mu)$ varies just as shown in Fig.5a, a result of $q(\mu)$'s behavior. The class of equilibria for $z_3 \leq z \leq 1$ shown in figure 5b are similar to those of Fig.5a but in a different range of temperature.

Thermodynamic stability limits for spherical perturbations are reached when the radiation energy E_r has a turning point in a linear series of equilibrium configurations $\beta(E_r)$. If the mass energy and field energy outside of the cavity are negligible, $E_r/R \simeq \mu(R) \simeq \alpha$, configurations are stable for $0 < \mu < \mu_{max} = 0.246$ (see Fig.5b) [12]. μ_{max} is also a limit where dynamical instability for radial perturbations sets in [4]. All the other configurations of a counterclockwise spiralling $\beta(E_r)$ curve are unstable [11]. Here we are interested to know how stability limits change when one takes account of the mass in the cavity ($\eta \neq 0$) and the field energy outside.

E_r is surely not $M - E_s$ because $M - E_s > 0$ even when there is no radiation. The difference must be in the field energy outside the cavity E_f ($r \geq R$). To calculate E_f, we use Lynden-Bell and Katz's method [13]. We replace the cavity with the radiation by a new empty cavity of the same radius R and enough mass energy $E'_s(\neq E_s)$ to produce the same gravitational field at $r \geq R$. Since the total mass energy is M and the mass energy of this shell is E'_s, the field energy $E_f = M - E'_s$ because the flat interior of the new

cavity has *no energy*. E_f/R depends on M/R or α only

$$\frac{E_f}{R} = \frac{1}{2}\left[1 - \sqrt{1 - \frac{2M}{R}}\right]^2 = \frac{1}{2}(1-z)^2. \tag{22}$$

Thus, radiation energy or

$$\varepsilon_r \equiv \frac{E_r}{R} = \alpha - \frac{E_s}{R} - \frac{E_f}{R} \tag{23}$$

with E_s/R given in (15) and y, z defined in (17), one can write

$$\varepsilon_r = z(1-y) = \frac{1}{2}(2-\eta)(1-z)(z-z_1). \tag{24}$$

ε_r is zero at $z = z_1$ and $z = 1$ and has one maximum ε_{rmax} at

$$z' = \frac{1+z_1}{2} \quad \text{where} \quad \varepsilon_{rmax} = \frac{(1-\eta)^2}{2(2-\eta)}. \tag{25}$$

The $\beta(\varepsilon_r)$ curves are similar to $\beta(\mu)$ which are inward spirals for $\eta < \eta_0$ (Fig.5) or U-type like curves for $\eta > \eta_0$ (Fig.4). Assuming radiation is thermodynamically stable at low temperature ($\beta \to \infty$) all configurations for which $0 < \varepsilon_r < \varepsilon_{rmax}$ and β has its lowest value are stable [11]. The spiral of $\beta(\varepsilon_r)$ at higher values of β represent unstable configurations. The limits of stability in the $\beta(\mu)$ plane depend on the value of η.

6. Concluding Remarks

Most cavities with more than $\simeq 30\%$ of the total mass energy containing thermal radiation can sustain high tensions or pressures without breaking the dominant energy condition. Cavities close to their Schwarzschild radius ($z_1 < z < z_2$) are unviable ($\Pi > \sigma$) for $\eta \lesssim 0.25$. Cavities with bigger radius ($z_3 < z < 1$) are also unviable ($\Pi > -\sigma$) for $\eta \lesssim 0.097$ and the radiation becomes anyway unstable for $\eta \lesssim 0.11$. Unstable radiation collapses to form a black hole [7].

Cavities with negligible mass energy ($\eta = 0$) are thus unviable and can, anyway, contain only unstable radiation as can be seen in Fig.5b. The points raised by Sorkin et al. [4] about total entropy becoming infinite in cavities with increasing radius or even reaching the Bekenstein [14] limit $S = 2\pi RM$ concerns thus unstable radiation in 'unviable' cavities.

References

[1] Katz J and Okuta Y 1994 gr-qc/940921

[2] Landsberg P T 1992 *Black Hole Physics* ed Sabbata V D and Zhang Z (Dordrecht: Kluwer Academic Publishers) p99

[3] Page D N *ibid.* p185

[4] Sorkin R D, Wald R M and Zhang Z 1981 *Gen. Rel. Grav.* **13** 1127

[5] Hawking S W and Ellis G F R 1973 *The Large Scale Structure of Space-time* (Cambridge: Cambridge University Press)

[6] Chandrasekhar S 1972 *General Relativity* p185 ed Raifeartaigh (Oxford: Clarendon Press)

[7] Gibbons G W and Perry M J 1978 *Proc. R. Soc.* A **358** 467

[8] Klein O 1947 *Arkiv för Matematik, Astronomi och Fysik* **19** 1

[9] Israel W 1966 Nuovo Cimento **44** 1; 1967 *Nuovo Cimento* **48** 463 (erratum)

[10] Goldwirth D and Katz J 1994 "*A Comment on Junction and Energy Conditions in Thin Shells*", gr-qc/9408034 (to appear in *Class. Quant. Grav.*)

[11] Katz J 1978 *Mon. Not. R. Astron. Soc.* **183** 765

[12] Parentani R, Katz J and Okamoto I 1994 "*Thermodynamics of a black hole in a cavity*", gr-qc/9410015

[13] Lynden-Bell D and Katz J 1985 *Mon. Not. R. Astron. Soc.* **213** 21p

[14] Bekenstein J D 1981 *Phys. Rev.* D **23** 287

[15] Hawking S W 1976 *Phys. Rev.* D **13** 191

Analysis of the Wheeler-DeWitt Equation beyond Planck Scale and Dimensional Reduction [1]

Kobe Univ. Kayoko Maeda

Introduction

One of our main purpose is to study four dimensional quantum gravity at short distance or hight energy. However, there are so many essential difficulties which disturb clear understanding with strict discussion.

We solve the Wheeler-DeWitt equation for four dimensional Einstein gravity as an expansion in powers of the Planck mass by means of a heat kernel regularization. This work to find out a solution is rather clear. The difficulty occurs to give a physical interpretation for our solution. Our results suggest that in the universe with a very small radius or with a very large curvature beyond a Planck scale expectation values of operators are reduced to calculations in a path integral representation of three dimensional Einstein gravity.

A treatment of the Wheeler-DeWitt equation

The (unregulated) Wheeler-DeWitt equation[1] without matter is

$$\left[-\frac{16\pi}{m_p^2}\,G_{ijkl}(x)\frac{\delta}{\delta h_{kl}(x)}\frac{\delta}{\delta h_{ij}(x)}+\frac{m_p^2}{16\pi}\sqrt{h(x)}\Big({}^3R(x)+2\Lambda\Big)\right]\Psi[h]=0\ , \tag{1}$$

where m_p is the Planck mass and G_{ijkl} is the metric on superspace

$$G_{ijkl}=\frac{1}{2\sqrt{h}}(h_{ik}h_{jl}+h_{il}h_{jk}-h_{ij}h_{kl})\ . \tag{2}$$

The ${}^3R(x)$ denotes the scalar curvature constructed from the three-metric h_{ij}. The Wheeler-DeWitt equation stands in need of regularization because it contains a product of two functional derivatives at the same spatial point,

$$\Delta(x)\equiv G_{ijkl}(x)\frac{\delta}{\delta h_{kl}(x)}\frac{\delta}{\delta h_{ij}(x)}\ . \tag{3}$$

[1]This result based on work with M. Sakamoto and T. Horiguchi, Phys.Lett.B (hep-th/9409152).

For example, $\Delta(x)$ acting on ${}^3R(y)$ is proportional to $(\delta(x,y))^2$, which is meaningless. To make eq.(1) well defined, we want to replace $\Delta(x)$ by a renormalized operator $\Delta_R(x)$, which is a finite operator preserving the three-dimensional general coordinate invariance. Recently Mansfield proposed a renormalization scheme to solve the Schrödinger equation for Yang-Mills theory in the strong coupling expansion [2]. We shall generalize the renormalization procedure developed by Mansfield to the Wheeler-DeWitt equation and solve it for the wave function of the universe as an expansion in powers of the Planck mass.

We have the finite version of the Wheeler-DeWitt equation,

$$\left[-\frac{16\pi}{m_p^2}\,\Delta_R(x)+\frac{m_p^2}{16\pi}\sqrt{h(x)}\Big({}^3R(x)+2\Lambda\Big)\right]\Psi[h]=0\ . \tag{4}$$

We have chosen the renormalization procedure to preserve three-dimensional general coordinate invariance but this is not enough to preserve the whole symmetry of the theory at the quantum level. We have to check that our renormalization procedure would be consistent with the constraints which are the generators of the symmetry.

A solution

Now we want to solve the (renormalized) Wheeler-DeWitt equation (4). To solve it, we attempt an expansion of the wave function in powers of the Planck mass. We assume that the wave function $\Psi[h]$ has the form

$$\Psi[h]\equiv\exp\Big\{-S[h]\Big\}=\exp\Big\{-\sum_{n=1}^{\infty}\Big(\frac{m_p^2}{16\pi}\Big)^{2n}S_n[h]\Big\}\ . \tag{5}$$

Then, the Wheeler-DeWitt equation becomes

$$\Delta_R(x)\,S-G_{ijkl}(x)\frac{\delta S}{\delta h_{kl}(x)}\frac{\delta S}{\delta h_{ij}(x)}+\Big(\frac{m_p^2}{16\pi}\Big)^2\sqrt{h(x)}\Big({}^3R(x)+2\Lambda\Big)=0\ , \tag{6}$$

so that to leading order

$$\Delta_R(x)\,S_1=-\sqrt{h(x)}\Big({}^3R(x)+2\Lambda\Big)\ . \tag{7}$$

We adopt an *ansatz* of locality[2] to solve the Wheeler-DeWitt equation in the expansion (5). We will assume that $S[h]$ is a sum of integrals of local functions of h_{ij}. Then we find a solution to leading order as

$$S_1 = \int d^3x\sqrt{h(x)}\Big\{c_1 + c_2\ {}^3R(x)\Big\}\ , \tag{8}$$

where

$$\begin{aligned} c_1 &= -\frac{3!}{\alpha_1\phi^{(3)}(0)}\Big(2\Lambda - \frac{3!\beta_1\phi^{(5)}(0)}{5!\beta_2\phi^{(3)}(0)}\Big)\ , \\ c_2 &= -\frac{3!}{\beta_2\phi^{(3)}(0)}\ . \end{aligned} \tag{9}$$

The semiclassical expansion corresponds to the expansion in powers of $\hbar$, while the expansion (5) corresponds to the expansion in powers of $\hbar^{-2}$ because $\hbar$ appears in the combination of $\hbar m_p^{-2}$ in quantum gravity. Thus the wave function to leading order in the expansion (5) is expected to describe quite different physics from the semiclassical one.

The accuracy of our solution to leading order may be gauged by comparing the magnitudes of the successive terms $(m_p^2/16\pi)^2 S_1$ and $(m_p^2/16\pi)^4 S_2$ in series for S. We can drop the next leading term when $\mu \gg m_p$ and ${}^3R \sim \mu^2$, $\nabla_i\nabla^i\,{}^3R \sim \mu^4$, etc.

If we apply the expansion (5) to a minisuperspace model, we can see that the expansion is essentially identical to a small radius expansion of the universe.

Discussion

Let us now discuss the physical interpretations of our result (8). We may compute expectation values of operators Ω for Ψ as

$$< \Omega > = \frac{\int \mathcal{D}h\, \Psi^*[h]\, \Omega\, \Psi[h]}{\int \mathcal{D}h\, \Psi^*[h]\, \Psi[h]}\ . \tag{10}$$

Since a precise definition of expectation values (or inner products) is not known in quantum gravity, the right hand side of eq.(11) is to be regarded as a formal definition of expectation values. If we put the wave function $\Psi[h]$ to leading order into eq.(11) and note that $\Psi[h]$ is real, we find that the expression is a path integral representation for the vacuum expectation values in three-dimensional Einstein gravity.

$$< \Omega > = \frac{\int \mathcal{D}h\, \Omega\, e^{(3-\mathrm{dimEinsteinGrav.})}}{\int \mathcal{D}h\, e^{(3-\mathrm{dimEinsteinGrav.})}}\ . \tag{11}$$

Therefore, we may conclude that in the universe with the very small radius or with the very large curvature beyond the Planck scale expectation values of operators can be

calculated as the vacuum expectation values of *three*-dimensional quantum Einstein gravity. Three-dimensional Einstein gravity has no local excitation, i.e., no graviton but a finite number of degrees of freedom, and is in fact a topological field theory [3, 4]. An interesting speculation from the above observations is that beyond the Planck scale dimensional reduction of four-dimensional quantum gravity occurs and topological phase appears [5].

References

[1] J. A. Wheeler, in *Battelle Rencontres*, edited by C. DeWitt and J. A. Wheeler (Benjamin, New York, 1968);

B. S. DeWitt, *Phys. Rev.* **160**(1967)1113.

[2] P. Mansfield, *Nucl. Phys.* **B418**(1994)113.

[3] E. Witten, *Nucl. Phys.* **B311**(1988/89)46.

[4] Y. Fujiwara, S. Higuchi, A. Hosoya, T. Mishima and M. Siino, *Phys. Rev.* **D44**(1991)1756; *Phys. Rev.* **D44**(1991)1763.

[5] E. Witten, *Phys. Lett.* **B206**(1988)601; *Commun. Math. Phys.* **117**(1988)353; **118**(1988)411.

ENTROPIES OF SCALAR FIELDS ON THREE DIMENSIONAL BLACK HOLES

IKUO ICHINOSE AND YUJI SATOH
Institute of Physics, University of Tokyo, Komaba, Tokyo 153 Japan

ABSTRACT

We briefly describe our recent work on thermodynamics of quantum scalar fields in three dimensional black hole backgrounds. We consider two approaches : One is mode expansions and direct computation of partition sum, and the other is the Euclidean path integral approach. A number of exact expressions are obtained, for example, mode functions, Hartle-Hawking Green functions on the black holes and entropies. They constitute reliable bases for the thermodynamics of quantum scalar fields. It is shown that thermodynamic quantities largely depend upon the approach, boundary conditions and regularization method. We find that, in general, the entropies are not proportional to the area of the horizon and that their divergent parts are not necessarily due to the existence of the horizon.

1 INTRODUCTION

Thermodynamics of black holes has been an interesting problem in theoretical physics. It stands just at the junction of general relativity, quantum mechanics and statistical mechanics. We have thought that its understanding leads to physics beyond that we have at present, in particular, quantum gravity.

However, we have not yet understood the true meaning of thermodynamic laws of black holes, and neither important related problems such as Hawking radiation and quantum coherence.

In respect of these issues, some proposals have been made recently [1, 2]. For example, (i) the Bekenstein-Hawking entropy and the entropy of a quantum field in a black hole background are the same object, i.e., the response of the Euclidean path integral to the introduction of a conical singularity to the underlying geometry [3, 2]. (ii) The entropy of the quantum field is obtained by tracing over local degrees of freedom inside the horizon (" geometric entropy ") [4, 2], by explicit counting of states [1] or by the Euclidean path integral. (iii) It is proportional to the area of the horizon and gives

the first quantum correction to the Bekenstein-Hawking entropy [1, 2]. (iv) Divergences appear due to the blow up of density of states associated to the horizon [5, 1, 2] and they can be removed by the renormalization of the gravitational coupling constant [1]. (v) Consequently, the problem of information loss and that of renormalizability of quantum gravity are intimately related.

Nevertheless, the system of a four dimensional black hole and a scalar field is quite complicated. Thus we have to resort to some approximations and somewhat formal arguments. Moreover, we do not know whether the various approaches for calculating the thermodynamic quantities are equivalent. There is no reason that the equivalence must hold a priori. These prevent us from clear understanding of the arguments.

In this article, we shall work with the three dimensional black holes of Einstein gravity discovered by Bañados, Teitelboim and Zanelli [6]. The three dimensional black holes share many of the features of those in four dimensions, and moreover they provide us with considerably simple systems. Thus we can expect to avoid technical difficulties in four dimensions and to be able to perform explicit analysis of their thermodynamics including matter.

Therefore, we shall mainly pursue two purposes in this article. One is to construct reliable bases for the thermodynamics of quantum scalar fields in the three dimensional black hole backgrounds. The other is to clarify the validity of the recent arguments explained above by explicit calculations. We believe that our results serve for deep understanding of thermodynamics of black holes. For details, see [7].

2 Three Dimensional Black Holes

Bañados et al. discovered three dimensional black holes of Einstein gravity with a negative cosmological term, $-2\,l^2$ [6], which are described by the metric

$$ds^2 = -\left[\frac{r^2}{l^2} - M\right] dt^2 - J dt d\phi + \left[\frac{r^2}{l^2} - M + \frac{J^2}{4r^2}\right]^{-1} dr^2 + r^2 d\phi^2 , \qquad (2.1)$$

with $-\infty < t < +\infty$, $0 \leq r < \infty$ and $0 \leq \phi < 2\pi$. Here M and J are identified with the mass and the angular momentum of the black hole, respectively. The black hole has inner and outer horizons represented by $r = r_\pm$ where $r_\pm$ is given by

$$M\,l^2 = r_+^2 + r_-^2 \quad , \quad J\,l = 2 r_+ r_- . \qquad (2.2)$$

Note that if the range of ϕ is extended as $-\infty < \phi < \infty$, the metric (2.1) describes the universal covering space of three dimensional anti-de Sitter space (AdS_3). Therefore the geometry of the 3 D black hole is locally that of AdS_3.

3 Entropies of Scalar Fields I : Partition Sum

In this section, we calculate entropies of scalar fields by mode expansion and direct computation of the partition sum. In this approach, the relation between the entropy and state counting is clear.

Now let us consider the scalar field satisfying the field equation,

$$(\Box - \mu l^{-2})\psi(x) \;=\; 0\,. \tag{3.1}$$

By making the separation of variables,

$$\psi_{n\omega} \;=\; e^{-i\omega t}\, e^{in\phi} f_{n\omega}(r)\,, \tag{3.2}$$

where n is an integer, we obtain the solution which does not diverge for arbitrary mass μ :

$$f_{n\omega}(v) \;=\; (v - v_+)^{\alpha_+}(v - v_-)^{\alpha_-} u^{-a_+} F(a_+, a_+ - c + 1; a_+ - a_- + 1; 1/u)\,. \tag{3.3}$$

Here F is the hypergeometric function, and the variables and parameters in the above expression are given by

$$v \;=\; \frac{r^2}{l^2}\,, \qquad v_\pm \;=\; \frac{r_\pm^2}{l^2}\,, \tag{3.4}$$

$$u \;=\; \frac{1}{v_+ - v_-}(v - v_-) \;=\; (r^2 - r_+^2)/d_H^2\,, \qquad d_H^2 \;=\; r_+^2 - r_-^2\,, \tag{3.5}$$

$$\alpha_\pm^2 \;=\; -\frac{1}{4(v_+ - v_-)^2}\left(r_\pm\omega - \frac{r_\mp}{l}n\right)^2\,, \tag{3.6}$$

$$a_\pm \;=\; (\alpha_+ + \alpha_-) + \frac{1}{2}(1 \pm \sqrt{1+\mu})\,, \quad c \;=\; 2\beta + 1\,. \tag{3.7}$$

At the horizon, it is expected that the scalar field becomes singular due to the infinite blue shift. Indeed this is the case. Therefore we impose the Dirichlet boundary condition just outside the horizon [5], namely, the condition that $f_{n\omega}$ vanishes at $u = 1 + \epsilon_H^2/l^2$ where ϵ_H is an infinitesimal number. Then we find that in the leading order of ϵ_H the energy spectrum is represented by two integers, k and n, as

$$\omega \;\sim\; \Omega_H\, n + C(k + \theta_0)\,, \quad C = \frac{2(v_+ - v_-)\pi}{r_+ \ln(l^2/\epsilon_H^2)}\,, \tag{3.8}$$

where θ_0 is a certain function of k and n and Ω_H is the angular velocity at the outer horizon, i.e., $\Omega_H = r_-/lr_+$.

Taking into account the fact that a rotating black hole has a chemical potential Ω_H, we find that the partition function with the inverse temperature β is given by

$$Z(\beta) \;=\; \prod_{k,n} \sum_{m=0}^{\infty} e^{-m\beta(\omega - \Omega_H n)}\,. \tag{3.9}$$

Then we get the entropy :

$$S(\beta) \sim \frac{r_+ l^2 \ln(l^2/\epsilon_H^2)}{2\pi d_H^2}\left[\frac{\pi^2}{3\beta}(2N_2+1) - \Omega_H \sum_{n=1}^{N_2} n \ln\left(1 - e^{-N_1\beta\Omega_H n}\right)\right.$$
$$\left. + \frac{2}{N_1\beta}\sum_{n=1}^{N_2}\int_0^{N_1\beta\Omega_H n} dt \ \ln\left(1 - e^{-t}\right)\right] + N_1 \sum_{n=0}^{N_2} \delta_{\theta_0(0,n),0} \,. \qquad (3.10)$$

Here N_1 is the cutoff for the occupation number of the particle for superradiant scattering modes, which are given by $\omega - \Omega_H n \leq 0$. N_2 is another cutoff for the quantum number n.

From (3.10), we see that the entropy is not proportional to the area of the outer horizon ($2\pi r_+$). We find also that divergences of the entropy come from the existence of the horizon, i.e., from ϵ_H. However we can show that this depends upon boundary conditions and that under different boundary conditions divergences are not due to the horizon (see [7]).

4 Entropies of Scalar Fields II : Hartle-Hawking Green Functions

In the preceding section, we obtained the entropy by the straightforward mode sum. In the following, we shall calculate the entropy in the Euclidean path integral approach in order to examine the equivalence between the various approaches.

First we find that the Green function of the scalar field is given by

$$\begin{aligned} -iG_{BH}(x,x') &= -i\sum_{n=-\infty}^{\infty} G_F(x,x'_n) \\ &\equiv \frac{1}{4\pi l}\sum_{n=-\infty}^{\infty}(z_n^2-1)^{-1/2}\left[z_n + (z_n^2-1)^{1/2}\right]^{1-\lambda} , \end{aligned} \qquad (4.1)$$

where $\lambda = 1 \pm \sqrt{1+\mu}$. $z_n(x,x')$ is defined by the distance between x and x' in the embedding space $\sigma(x,x')$ (recall that the 3 D black hole is locally AdS_3) through $z_n(x,x') = 1 + l^{-2}\sigma(x,x'_n)$, $x_n \equiv x \Big|_{\phi'-\phi'-2n\pi}$. For the massless scalar field with the conformal coupling, this Green function coincides with that obtained in [9, 10, 11]. Since the derivation of this result is lengthy, we omit it. For details, see [7].

Now let us study the properties of the Green function. First, it turns out that G_{BH} has the period

$$t \rightarrow t + i\beta_H \,, \qquad \phi \rightarrow \phi + i\frac{\Omega_H}{l}\beta_H \,, \qquad (4.2)$$

$$\beta_H = 2\pi r_+ l^2/d_H^2 \,. \qquad (4.3)$$

Thus G_{BH} can be regarded as a thermal Green function with the inverse temperature β_H and the chemical potential Ω_H. Note that β_H is nothing but the period around the outer

horizon in the Euclidean black hole geometry. Second we can demonstrate that G_{BH} satisfies the boundary conditions of the Hartle-Hawking type [8]. Therefore our result confirms and gives an explicit example to the literature of thermodynamics of black holes.

In order to compute the entropy, we need the Green function with a period slightly different from β_H. In the Euclidean geometry defined by the replacement in the metric (2.1), $it \to \tau$ and $-i\phi \to \varphi$, this corresponds to the problem to find a Green function on a cone geometry.

Such a Green function is obtained by the Sommerfeld integral representation [12, 13],

$$G_{BH}(x,x';\beta) = \sum_n G_F(x,x'_n;\beta), \tag{4.4}$$

$$G_F(x,x'_n;\beta) = \frac{\beta_H}{4\pi\beta i}\int_\Gamma d\zeta\, \tilde{G}_F(\zeta - w'_n;2\pi)\cot\left\{\frac{\beta_H}{2\beta}(\zeta - w)\right\}, \tag{4.5}$$

where we have explicitly denoted the period β. The contour Γ is given in Fig.1, and w and $\tilde{G}_F$ are defined by $iw \equiv 2\pi t/\beta_H$ and $\tilde{G}_F(w-w';2\pi) \equiv G_F(x,x')\,|_{r^{(\prime)},\phi^{(\prime)}-\Omega_H t^{(\prime)}:\text{fixed}}$ respectively.

Then we define the Euclidean Green function by

$$G^E_{BH}(\tau,\tau',\varphi,\varphi',r,r';\beta) \equiv iG_{BH}(t,t',\phi,\phi',r,r';\beta)\Big|_{\tau^{(\prime)}=it^{(\prime)},\varphi^{(\prime)}=-i\phi^{(\prime)}}. \tag{4.6}$$

Using G^E_{BH}, we obtain the free energy

$$\beta F(\beta) = -\frac{1}{2}\mathrm{tr}\log G^E_{BH}(x,x';\beta). \tag{4.7}$$

Consequently, we get the entropy :

$$S(\beta_H) = \beta_H F(\beta_H) + \frac{\Omega_H}{8\pi l^3}\beta_H^2 \sum_{n=-\infty}^{\infty}\int_{r_+^2}^{\infty} d(r^2)\lim_{r\to r'}\left[B\int_{A_n+B}^{\infty} dz \right. \tag{4.8}$$
$$\left. \times \frac{X^{1-\lambda}\{1+(\lambda-1)\log X\}}{\log^2 X\sqrt{z^2-1}}\frac{1}{\sqrt{(z-A_n)^2-B^2}}\frac{c_n^-(z-A_n)+B}{(z-A_n+c_n^-B)^2}\right] + c,$$

where

$$A_n = \frac{\sqrt{r^2-r_-^2}\sqrt{r'^2-r_-^2}}{d_H^2}c_n^+, \qquad B = \frac{\sqrt{r^2-r_+^2}\sqrt{r'^2-r_+^2}}{d_H^2}, \tag{4.9}$$

$$c_n^\pm = \cosh(2\pi n r_\pm/l), \quad X = z+\sqrt{z^2-1}. \tag{4.10}$$

c is a constant independent of μ and is ignored in the flat case. For $\lambda \le 1$, $\beta_H F(\beta_H)$ is divergent, but for $\lambda > 1$ we get

$$\beta_H\, F(\beta_H) = -\frac{l^{-2}\Omega_H}{8\pi^2 r_+}\beta_H^2 d_H^2 \sum_{n\ge 1}^{\infty}\frac{1}{n(\,c_n^+ - c_n^-\,)}\, e^{-2\pi(\lambda-1)nr_+/l} + c \qquad (\text{for } \lambda > 1). \tag{4.11}$$

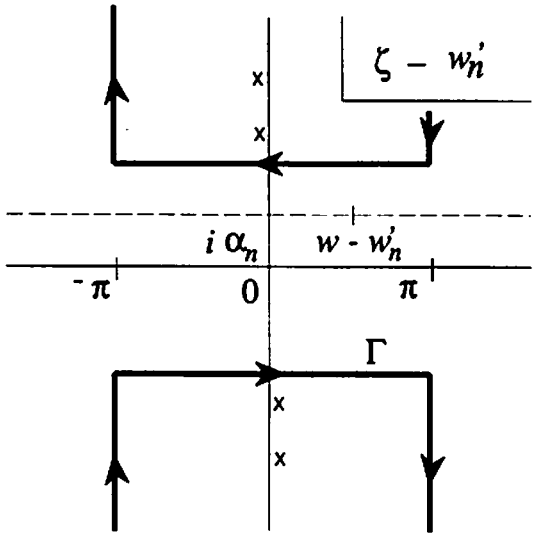

Fig. 1 : Contour Γ (solid line) in $\zeta - w'_n$ plane. The crosses ($\times$) indicate the singularities of $\bar{G}^E_F(\zeta - w'_n)$ in the region $-\pi < \mathrm{Re}\ (\zeta - w'_n) \leq \pi$ for $r,\ r' \geq r_+$. $\alpha_n = r_-(\Delta t - \Omega_H \Delta\phi + 2n\pi)/l$, $\Delta t = t - t'$, $\Delta\phi = \phi - \phi'$. In this figure, we show the contour Γ in the case of small $|\alpha_n|$. For large and positive α_n, for example, the line $\zeta - w'_n = i\alpha_n$ is above the crosses, and we can not take a contour as Γ in this figure. In this case we have only to deform Γ in a simple manner.

As we have exact expressions of the entropies, we can study the structure of their divergences without any ambiguity. At present, it is believed that the divergence of the entropy of quantum fields on black holes is closely related to important physical problems [1, 2].

In order to regularize the expression of (4.8), we introduce two cutoffs. We denote one by s, which concerns the trace and is given by $(r')^2 = r^2 + s^2$. The other is ϵ_H, which regularizes the lower end of the integral in (4.8) as $\int_{r_+^2} d(r^2) \to \int_{r_+^2+\epsilon_H^2} d(r^2)$. After some calculations, it turn out that the structure of the divergences depends upon the regularization method. For the case of $\epsilon_H \simeq s$ or $\epsilon_H >> s$, the divergences take the form

$$\Omega_H \beta_H^2 l^{-3} \left(d_H^3 \frac{1}{\epsilon_H} + \ b\ d_H^2 \log \epsilon_H^2 \right) , \tag{4.12}$$

where b is a constant. On the other hand, for $\epsilon_H << s$, they are of the form

$$\Omega_H \beta_H^2 l^{-3} \left(d_H^3 \frac{1}{s} + \ b\ d_H^2 \log s^2 \right) . \tag{4.13}$$

Therefore the divergences are given in terms of the larger cutoff, i.e., $\max\{\epsilon_H, s\}$.

From the above expressions, we find that they can contain various divergences coming from short distances such as $\epsilon_H^{-1}, \log \epsilon_H^2$, and s^{-1}. However not all of them are due to the existence of the outer horizon. We also find that the divergent terms are proportional to d_H. Hence they are not proportional to the area of the outer horizon ($2\pi r_+$).

5 CONCLUSION

We have investigated the thermodynamics of scalar fields on the three dimensional black holes in two approaches. One (approach I) is based on explicit mode expansion of the scalar fields and direct computation of the partition sum, and the other (approach II) is based on Hartle-Hawking Green functions. In both approaches, explicit expressions of the entropies are obtained. We believe that we have provided reliable bases for the study of thermodynamics of scalar fields on the three dimensional black holes and that our results give useful insight for understanding of thermodynamics of black holes in four dimensions.

Our results also allow us to answer the interesting questions listed in the introduction at least for the three dimensional case. First in approach I, we found that divergent terms of the entropy are not necessarily due to the existence of the outer horizon. They also depend upon the boundary conditions. In addition, the entropy is not proportional to the area of the outer horizon, namely, the Bekenstein-Hawking formula is invalid.

Second, we constructed exact Hartle-Hawking Green functions on the three dimensional black holes. By making use of them, we obtained the entropy. The divergent terms of the entropy, which come from short distances, are proportional to $d_H = \sqrt{r_+^2 - r_-^2}$. Thus the Bekenstein- Hawking formula is not satisfied again. Furthermore, the divergences are not always due to the existence of the outer horizon and depend upon the regularization method. In addition, the results obtained in approach I and II are quite *different.*

Therefore we conclude that the Bekenstein-Hawking formula including the quantum scalar fields is not valid in general. Thus the relationship between the divergence of the entropies and the renormalization of the gravitational coupling constant is not clear. It is also obscure whether the divergences are due to the existence of the horizon.

The expressions of the entropies largely depend upon the method of calculation, boundary conditions and regularization, namely, upon its definition. Hence it is quite important to consider which definition we should adopt. Without fixing the definition, we cannot discuss whether the entropies of scalar fields have a meaning as the number of states or whether they can be regarded as " geometric entropy ". Therefore we cannot understand the problem of the relationship between information loss and entropy of quantum fields until the problem of the definition is settled.

Fortunately, we have got explicit expressions of the thermodynamic quantities of scalar fields on the three dimensional black holes. Thus we think that it is possible to apply our results to various problems, for example, the problems discussed in this article and Hawking radiation [14]. Since the divergences appearing in our calculation can be absorbed into the renormalization of the *cosmological constant* , it may worth investigating the relationship between the divergence of the entropies and renormalization.

REFERENCES

[1] L. Susskind and J. Uglum, Phys. Rev. **D50** (1994) 2700.

[2] C. Callan and F. Wilczeck, Phys. Lett. **B333** (1994) 55.

[3] G.W. Gibbons and S.W.Hawking, Phys. Rev. **D15** (1977) 2752.

[4] M. Srednicki, Phys. Rev. Lett. **71** (1993) 666.

[5] G. 't Hooft, Nucl. Phys. **B256** (1985) 727.

[6] M. Bañados, C. Teitelboim and J. Zanelli, Phys. Rev. Lett. **69** (1992) 1849; M. Bañados, M. Henneaux, C. Teitelboim and J. Zanelli, Phys. Rev. **D48** (1993) 1506.

[7] I. Ichinose and Y. Satoh, University of Tokyo, Komaba, Report No. UT-Komaba 94-23, hepth/9412144.

[8] J.B. Hartle and S.W. Hawking, Phys. Rev. **D8** (1976) 2188.

[9] K. Shiraishi and T. Maki, Class. Quantum. Grav. **11** (1994) 695; Phys. Rev. **D49** (1994) 5286.

[10] G. Lifschytz and M. Ortiz, Phys. Rev. **D49** (1994) 1929.

[11] A.R. Steif, Phys. Rev. **D49** (1994) R585.

[12] A. Sommerfeld, Proc. Lond. Math. Soc. **xxviii** (1897) 417.

[13] H.S. Carslaw, Proc. Lond. Math. Soc. **xxx** (1898) 121; 8 (1910) 365; **18** (1919) 291.

[14] S.W. Hawking, Commun. Math. Phys. **43** (1975) 199; Phys. Rev. **D14** (1976) 2460.

Supersymmetry and general Killing-Yano tensors *

MASAYUKI TANIMOTO †

Department of Physics, Tokyo Institute of Technology, Oh-Okayama Meguro-ku, Tokyo 152, Japan

ABSTRACT

A Killing-Yano tensor of valence r is a r-form satisfying a first order differential equation. The role of Killing-Yano tensors is discussed in the context of the supersymmetric extension of charged point particle's motion. We find that the Killing-Yano tensors imply the existence of constants of motion commuting with the supercharge, in other word, superinvariants.

I. INTRODUCTION

Recently, Gibbons, Rietdijk and van Holten [2] investigated symmetries of spacetimes systematically in terms of the motion of pseudo-classical spinning point particles described by the supersymmetric extension of the usual relativistic point particle [3–7]. Such a supersymmetric theory possesses a supercharge Q generating the supersymmetry transformation between particle's position x^μ and particle's "spin" ξ^a, which must be introduced to forbid the negative norm state of spin due to the indefinite Lorentz metric η_{ab}. One outstanding feature of such a theory is to have an algebra like $\{Q, Q\} \propto H$, where H is the Hamiltonian. Due to this relation and the Jacobi identity, superinvariants J such as $\{Q, J\} = 0$ are simultaneously constants of motion $\{H, J\} = 0$, so that superinvariants are of particular importance in supersymmetric theories. It was a big success of Gibbons *et al.* to have been able to show that the Killing-Yano tensor, which had long been known for relativists as rather mysterious structure, can be understood as an object generating a 'nongeneric' supersymmetry, i.e. supersymmetry appearing only in specific spacetimes. The corresponding supercharge Q_f generated by the Killing-Yano tensor is a superinvariant rather than merely a constant of motion. The Killing-Yano tensor here is a 2-form, $f_{\mu\nu} = f_{[\mu\nu]}$, which satisfies the Penrose-Floyd equation [8]

---

*This article is based on Ref. [1]

†E-mail address: prince@th.phys.titech.ac.jp

$$D_{(\mu}f_{\nu)\lambda} = 0. \tag{1}$$

It is also worth noting that the square of a Killing-Yano tensor makes the associated Killing tensor $K_{\mu\nu}$ as

$$K_{\mu\nu} = f_{\mu\lambda}f_{\nu}{}^{\lambda}. \tag{2}$$

It is of some interest that so-called the Carter's constant $K_{\mu\nu}u^{\mu}u^{\nu}$ is the bosonic sector of square of Q_f, $\{Q_f, Q_f\}$. (u^{μ} is the particle's tangent.) We may call 2-forms satisfying Eq.(1) Killing-Yano tensors of usual type, whereas we call r-forms satisfying similar equation

$$D_{(\mu_1}f_{\mu_2)\mu_3\cdots\mu_{r+1}} = 0 \tag{3}$$

Killing-Yano tensors of valence r [9,10].

In this paper we discuss the role of these generalized Killing-Yano tensors, with the framework extended to include electromagnetic interactions.

We discuss the role of Killing-Yano tensors of valence r, $f_{\mu_1\cdots\mu_r}$. We know that, in the usual relativistic point particle theory, Killing tensors imply constants of motion, i.e., if the spacetime admits a Killing tensor $K_{\mu_1\cdots\mu_r}$ of valence r, then the phase space function $K_{\mu_1\cdots\mu_r}u^{\mu_1}\cdots u^{\mu_r}$ is constant along the geodesic [13]. What we point out in this paper is a counterpart to this in the supersymmetric theory. We will find the one-to-one correspondence between Killing-Yano tensors and superinvariants, of which forms are rather nontrivial. We also examine the brackets of such superinvariants with generic constants of motion, and thereby discuss the associated constants of motion with such superinvariants.

Although it has no obstacles in passing to quantum mechanics, we shall concentrate on classical analysis. Nevertheless, we know that Killing-Yano tensors can play a key role in the Dirac's theory on a curved spacetime [12]. Our results may strengthen the connection of Killing-Yano tensors with the supersymmetric classical and quantum mechanics on curved manifolds.

II. THE PSEUDO-CLASSICAL DESCRIPTION OF A CHARGED DIRAC PARTICLE

In this section, we establish the pseudo-classical description of our charged Dirac particle. Note first that, while usual point particle is described by its point x^{μ} on a Lorenzian manifold $(M, g_{\mu\nu})$, our pseudo-classical (charged) Dirac particle has also a freedom of spin which is represented by a Grassmann-valued pseudo-Lorentz vector ξ^a. Such descriptions was considered in Refs. [3–7], and in particular we shall employ the linearized Lagrangian treated in Ref. [7]. We thus start with the Lagrangian,

$$L = \frac{m}{2} g_{\mu\nu}\dot{x}^\mu \dot{x}^\nu + eA_\mu \dot{x}^\mu + \frac{i}{2}\left(\xi_a \frac{D\xi^a}{d\tau} - \frac{e}{m} F_{ab}\xi^a \xi^b\right), \tag{4}$$

where m and e are, respectively, the mass and the charge of a particle, and $A_\mu(x)$ and $F_{\mu\nu}(x)$, respectively, the vector potential and the field strength of the electromagnetic field, both of which are considered as external fields, and so is the spacetime metric $g_{\mu\nu}(x)$. Greek and Latin indices refer to world and Lorentz indices, respectively, and are converted into each other by the vielbein $e_a{}^\mu$. The dot over x^μ represents the derivative with respect to a parameter τ, while $D\xi^a/d\tau$ represents the covariant derivative with respect to τ;

$$\frac{D\xi^a}{d\tau} = \dot{\xi}^a + \omega^a{}_{b\mu}\xi^b \dot{x}^\mu, \tag{5}$$

where $\omega_{ab\mu}$ is the connection 1-form.

Since our Lagrangian is a gauge-fixed one, we have to add appropriate constraints. One is given by

$$H \equiv \frac{m}{2} g_{\mu\nu}\dot{x}^\mu \dot{x}^\nu + \frac{ie}{2m} F_{ab}\xi^a \xi^b \approx -\frac{m}{2}, \tag{6}$$

which ensures the time-reparametrization invariance. Also, this tells that the parameter τ is a generalization of the proper time. The other constraint is

$$Q \equiv e_{a\mu}\dot{x}^\mu \xi^a \approx 0, \tag{7}$$

which generates the supersymmetry transformation [‡]. The equations of motion derived from the above Lagrangian will be invariant under the transformation generated through appropriate Poisson-Dirac bracket with the above constraints. Variable ξ^a is the superpartner of x^μ for the supersymmetry transformation generated by Q. Our Lagrangian gives, in conjunction with the constraints H and Q, the pseudo-classical description of charged Dirac (spinning) particles.

Since the conjugate momenta are

$$p_\mu = \frac{\partial L}{\partial \dot{x}^\mu} = m g_{\mu\nu}\dot{x}^\nu + \omega_\mu + eA_\mu, \quad \pi_a = \frac{\partial L}{\partial \dot{\xi}^a} = -\frac{i}{2}\xi_a \tag{8}$$

[‡]The full Lagrangian contains, apart from the Lagrange multipliers, a Grassmann-valued pseudo-Lorents scaler ξ_5 as a variable, which must be introduced to 'carry' the mass. The supercharge (7) should have been $Q \equiv e_{a\mu}\dot{x}^\mu \xi^a + \xi_5 \approx 0$ to recover the massive Dirac equation when quantized. However, in the present gauge, ξ_5 is found to be a constant, so that the subsequent classical analysis will not be affected with ξ_5 suppressed. The constancy of ξ_5 will appear as the existence of the chiral charge (See Eq.(22)).

with $\omega_\mu \equiv (i/2)\omega_{ab\mu}\xi^a\xi^b$, the second class constraint for π_a yields the following Poisson-Dirac bracket;

$$\{F,G\} = \frac{\partial F}{\partial x^\mu}\frac{\partial G}{\partial p_\mu} - \frac{\partial F}{\partial p_\mu}\frac{\partial G}{\partial x^\mu} + i(\partial F/\partial \xi^a)\frac{\partial G}{\partial \xi_a}, \tag{9}$$

where $(\partial F/\partial \xi^a)$ is a right differentiation which will take the opposite sign to $\frac{\partial F}{\partial \xi^a}$ when F is Grassmann-odd. With this bracket, we can check the canonical relations, $\{x^\mu, p_\nu\} = \delta^\mu_\nu$ and $\left\{\xi^a, \xi^b\right\} = -i\eta^{ab}$. For convenience, we introduce the gauge-covariant variable Π_μ defined by

$$\Pi_\mu = p_\mu - \omega_\mu - eA_\mu (= mg_{\mu\nu}\dot{x}^\nu). \tag{10}$$

With this variable, the bracket becomes

$$\{F,G\} = (\mathcal{D}_\mu F)\frac{\partial G}{\partial \Pi_\mu} - \frac{\partial F}{\partial \Pi_\mu}(\mathcal{D}_\mu G) + (R_{\mu\nu} + eF_{\mu\nu})\frac{\partial F}{\partial \Pi_\mu}\frac{\partial G}{\partial \Pi_\nu} + i(\partial F/\partial \xi^a)\frac{\partial G}{\partial \xi_a}, \tag{11}$$

where we have defined the spin-valued Riemann tensor $R_{\mu\nu} \equiv (i/2)R_{ab\mu\nu}\xi^a\xi^b$, and the phase space covariant derivative operator

$$\mathcal{D}_\mu F \equiv \frac{\partial F}{\partial x^\mu} + \Pi_\lambda \Gamma^\lambda_{\mu\nu}\frac{\partial F}{\partial \Pi_\nu} - \omega^a{}_{b\mu}\xi^b\frac{\partial F}{\partial \xi^a}. \tag{12}$$

Now, with this bracket it is easy to see for the constraints

$$H = \frac{1}{2m}g^{\mu\nu}\Pi_\mu\Pi_\nu + \frac{ie}{2m}F_{ab}\xi^a\xi^b \approx -\frac{m}{2} \tag{13}$$

and

$$Q = \frac{1}{m}e_a{}^\mu\Pi_\mu\xi^a \approx 0 \tag{14}$$

that the usual supersymmetry algebra

$$\{Q,H\} = 0, \quad \{Q,Q\} = -\frac{2i}{m}H. \tag{15}$$

holds.

The equation for superinvariants is derived from the equation $\{Q,J\} = 0$. Such a superinvariant J is automatically a constant of motion, i.e., $\{H,J\} = 0$, as confirmed by the Jacobi identity with Eq.(15). With the bracket (11), we have

$$\xi^\mu\left(\mathcal{D}_\mu J - eF_{\mu\nu}\frac{\partial J}{\partial \Pi_\nu}\right) + i\Pi^a\frac{\partial J}{\partial \xi^a} = 0. \tag{16}$$

Following [2], let us expand $J(x,p,\Pi)$ in powers of Π_μ and ξ^a, and let the coefficients be $f^{(m,n)\mu_1\cdots\mu_n}_{a_1\cdots a_m}(x)$, i.e.,

$$J = \sum_{m,n=0}^{\infty}\frac{i^{[\frac{m}{2}]}}{m!n!}\xi^{a_1}\cdots\xi^{a_m}f^{(m,n)\mu_1\cdots\mu_n}_{a_1\cdots a_m}(x)\Pi_{\mu_1}\cdots\Pi_{\mu_n}. \tag{17}$$

We then obtain from Eq.(16) the component equation;

$$me_{[a}{}^\mu D_\mu f^{(m-1,n)\mu_1\cdots\mu_n}_{a_1\cdots a_{m-1}]} - meF_{\mu\nu}e_{[a}{}^\mu f^{(m-1,n+1)\mu_1\cdots\mu_n\nu}_{a_1\cdots a_{m-1}]} - nf^{(m+1,n-1)(\mu_1\cdots\mu_{n-1}}_{baa_1\cdots a_{m-1}}e^{b\mu_n)} = 0. \tag{18}$$

We may call this equation the generalized Penrose-Floyd equation.

III. THE ROLE OF KILLING-YANO TENSORS

Killing-Yano tensors give a special class of solutions of Eq.(18). This class is of the following form;

$$J = \frac{i^{[\frac{r-1}{2}]}}{(r-1)!} f^{(r-1,1)}_{a_1\cdots a_{r-1}}{}^{\mu}\Pi_\mu \xi^{a_1}\cdots\xi^{a_{r-1}} + \frac{i^{[\frac{r+1}{2}]}}{(r+1)!} f^{(r+1,1)}_{a_1\cdots a_{r+1}} \xi^{a_1}\cdots\xi^{a_{r+1}}. \tag{19}$$

It is easy to examine Eq.(18) for Eq.(19). We get the following theorem;

Theorem: *If the spacetime admits a Killing-Yano tensor of valence r, $f_{\mu_1\cdots\mu_r}$, and the electromagnetic field $F_{\mu\nu}$ satisfies the condition*

$$F_{\nu[\mu_r} f_{\mu_1\cdots\mu_{r-1}]}{}^{\nu} = 0, \tag{20}$$

then the function

$$Y_r = \xi^{\mu_2}\cdots\xi^{\mu_r} f_{\mu_1\cdots\mu_r}\Pi^{\mu_1} - \frac{i}{r+1}\xi^{\mu_1}\cdots\xi^{\mu_{r+1}} D_{[\mu_1} f_{\mu_2\cdots\mu_{r+1}]} \tag{21}$$

is a superinvariant, $\{Q, Y_r\} = 0$, for the bracket defined by Eq.(11). The converse also holds.

Here, $f_{\mu_1\cdots\mu_r}$ corresponds to $f^{(r-1,1)}_{a_1\cdots a_{r-1}}{}^{\nu} g_{\nu\mu_1} e^{a_1}{}_{\mu_2}\cdots e^{a_{r-1}}{}_{\mu_r}$.

What we want to note here is the Killing-Yano tensor of valence $d = \dim(M)$, which is generic and coincides with the volume form $\epsilon_{\mu_1\cdots\mu_d}$ up to a constant factor. This object appears in two generic constants of motion, the chiral charge [17]

$$\Gamma_* \equiv -\frac{i^{[\frac{d}{2}]}}{d!}\epsilon_{a_1\cdots a_d}\xi^{a_1}\cdots\xi^{a_d}, \tag{22}$$

and the dual supercharge

$$Q^* = i\{Q, \Gamma_*\} = \frac{-i^{[\frac{d}{2}]}}{(d-1)!}\epsilon_{a_1\cdots a_d} e^{a_1\mu}\Pi_\mu \xi^{a_2}\cdots\xi^{a_d}. \tag{23}$$

(The form of these generic charges is regardless of the existence of electromagnetic interactions.) We now know that

$$Q^* = \frac{-i^{[\frac{d}{2}]}}{(d-1)!} Y_d, \tag{24}$$

provided that $f_{\mu_1\cdots\mu_d} = \epsilon_{\mu_1\cdots\mu_d}$.

Eq.(3) implies that a Killing-Yano tensor of valence 1 is a usual Killing vector. Let ζ^μ be a Killing vector, then it is a direct consequence of the theorem that

$$Y_1 = \zeta^\mu\Pi_\mu - \frac{i}{2}\xi^\mu\xi^\nu D_\mu\zeta_\nu \tag{25}$$

is superinvariant, if

$$F_{\mu\nu}\zeta^{\nu} = 0 \tag{26}$$

holds. However, if we consider an alternative function

$$J_{\zeta} = \zeta^{\mu}(\Pi_{\mu} + eA_{\mu}) - \frac{i}{2}\xi^{\mu}\xi^{\nu}D_{\mu}\zeta_{\nu}, \tag{27}$$

this is superinvariant, regardless of Eq.(26), provided that the Lie derivative of the vector potential with respect to ζ^{μ} vanishes, $\mathcal{L}_{\zeta}A_{\mu} = 0$. We would have got Eq.(27) as a result of trying to obtain a constant of motion (not superinvariant) associated with a Killing vector (cf. Ref. [11]), however Eq.(27) happens to be superinvariant. This is a special feature for $r = 1$.

The case $r = 2$ is most well-known. Function

$$Q_f \equiv Y_2 = \xi^{\nu} f^{\mu}{}_{\nu}\Pi_{\mu} - \frac{i}{3}\xi^{\mu}\xi^{\nu}\xi^{\lambda}D_{[\mu}f_{\nu\lambda]}. \tag{28}$$

is superinvariant, provided that $f_{\mu\nu}$ is a Killing-Yano tensor and the electromagnetic tensor $F_{\mu\nu}$ satisfies the condition

$$f^{\lambda}{}_{[\mu}F_{\nu]\lambda} = 0. \tag{29}$$

The last condition is that the principal null directions (the PND) of the electromagnetic field must be aligned with those of the Killing spinor [11]. This type of superinvariants exists in the Kerr-Newman spacetime [2,12]. Although there are not so many physically interpretable spacetimes which admit a Killing-Yano tensor [9,14], another such interesting example would be the Taub-NUT spacetime [15,16], which admits four independent Killing-Yano tensors [16].

IV. THE CONSTANTS OF MOTION ASSOCIATED WITH Y_r

As already established, if a spacetime admits a Killing-Yano tensor of valence r and if the electromagnetic tensor satisfies Eq.(20), then Y_r is a constant of motion of a spinning particle in the spacetime. Possibly, there exist other constants of motion associated with Y_r, i.e., there may exist nonvanishing brackets of Y_r with other known constants of motion. We here discuss generic feature of such constants of motion, i.e., we suppose there are no nongeneric constants of motion other than Y_r for specific value of r.

It is obvious that we can construct such constants of motion first by taking brackets of Y_r with the four generic constants of motion, H, Q, Γ_*, and Q^*. Since Y_r is a (super)invariant, we cannot use H and Q for the present purpose. Moreover, since Q^* has connection with Γ_* through $Q^* = i\{Q, \Gamma_*\}$, we do not have to discuss Q^* and Γ_* separately. In fact, if $\dim(M) = d$, we have

$$
\begin{aligned}
\{Y_r, Q^*\} &= i\{Y_r, \{Q, \Gamma_*\}\} \\
&= -i(-1)^d \{\Gamma_*, \{Y_r, Q\}\} - i(-1)^{d(r-1)} \{Q, \{\Gamma_*, Y_r\}\} \\
&= i\{Q, \{Y_r, \Gamma_*\}\} \\
&(= \{Q, Y_r^*\}),
\end{aligned} \tag{30}
$$

where the second line is the consequence of the Jacobi identity and we have defined the dual of Y_r as $Y_r^* \equiv i\{Y_r, \Gamma_*\}$. Hence the bracket of Y_r with the dual supercharge Q^* is also the bracket of the supercharge Q and the dual of Y_r, so that we only need to start with seeing if there exist nonvanishing duals of Y_r.

Since $\mathcal{D}_\mu \Gamma_* = 0$ and $(\partial\Gamma_*/\partial\Pi_\mu) = 0$, we have

$$
Y_r^* = (-1)^r \frac{\partial Y_r}{\partial \xi^a} \frac{\partial \Gamma_*}{\partial \xi_a}. \tag{31}
$$

The numbers of the Grassmann vectors in Y_r and Γ_* are, respectively, $r-1$ (the least number) and d, so that that of Eq.(31) is $r-1+d-2 = r+d-3$, which must be not greater than d in order that Y_r^* do not vanish. We can therefore have nonvanishing Y_r^* only for $r \leq 3$. However, for $r = 1, 3$, we find by direct calculations that Y_r^* vanishes after all. Thus, we can generate new constants of motion only for $Y_2 = Q_f$.

We can immediately calculate $Y_2^* = Q_f^*$, which gives

$$
Q_f^* = \frac{-i^{[\frac{d}{2}]}}{(d-1)!} \epsilon_{a_1 \cdots a_d} e^{a_1 \mu} f^\nu{}_\mu \Pi_\nu \xi^{a_2} \cdots \xi^{a_d}. \tag{32}
$$

Then we can calculate the bracket of Q_f^* with the supercharge, for which we define $\mathcal{A}_f$;

$$
\begin{aligned}
\mathcal{A}_f &\equiv m\left\{Q, Q_f^*\right\} = m\{Q_f, Q^*\} \\
&= eF_{\mu\nu} f^{\nu\mu} \Gamma_* - \frac{i^{[\frac{d}{2}]+1}}{(d-2)!} \epsilon_{a_1 \cdots a_d} e^{a_1 \mu} \Pi_\mu e^{a_2 \nu} f^\lambda{}_\nu \Pi_\lambda \xi^{a_3} \cdots \xi^{a_d}.
\end{aligned} \tag{33}
$$

This is the end of our construction — Γ_*, Q, Q^*, Q_f, Q_f^* and $\mathcal{A}_f$ with $K \equiv \frac{i}{2}\{Q_f, Q_f\}$ and H constitute a closed algebra $\mathcal{G}_2$, where H is the Hamiltonian (13). The function K is given by

$$
\begin{aligned}
K &= \frac{1}{2} f^\mu{}_\lambda f^{\nu\lambda} \Pi_\mu \Pi_\nu \\
&+ \frac{i}{2} \xi^\mu \xi^\nu \left\{2(D_\lambda f^\sigma{}_\mu) f^\lambda{}_\nu \Pi_\sigma + c_{\mu\nu\lambda} f^{\sigma\lambda} \Pi_\sigma + eF_{\lambda\sigma} f^\lambda{}_\mu f^\sigma{}_\nu\right\} \\
&+ \frac{1}{4} \xi^\mu \xi^\nu \xi^\lambda \xi^\sigma \left\{R_{\mu\nu\kappa\omega} f^\kappa{}_\lambda f^\omega{}_\sigma - \frac{1}{2} c_{\mu\nu\kappa} c_{\lambda\sigma}{}^\kappa\right\},
\end{aligned} \tag{34}
$$

where

$$
c_{\mu\nu\lambda} = -2D_\mu f_{\nu\lambda} \; (= -2D_{[\mu} f_{\nu\lambda]}). \tag{35}
$$

FIG.1 summerizes the relation in $\mathcal{G}_2$.

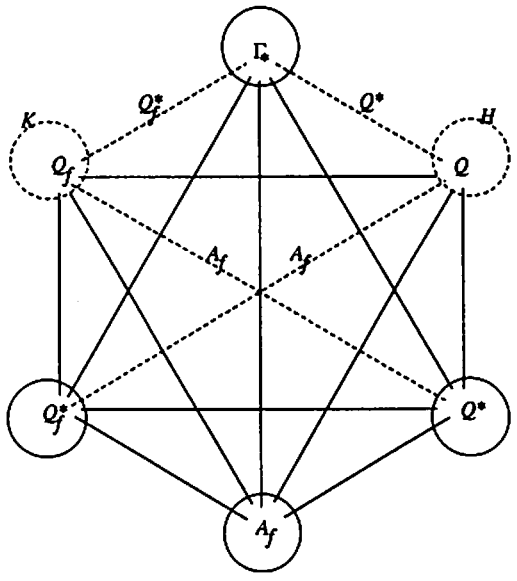

FIG. 1. The algebra $\mathcal{G}_2$. Real lines stand for vanishing of the Poisson-Dirac brackets, whereas dashed lines for non-zeros. Characters above dashed lines are reminders of the non-vanishing brackets, e.g., the bracket of Γ_* and Q is proportional to Q^*. Real circles stand for vanishing of the Poisson-Dirac brackets with oneself, whereas dashed circles for non-zeros. The meaning of characters above the dashed circles is the same as for the lines. H and K commute with any functions listed in the figure. Note that functions Γ_*, Q^*, Q_f^*, and $\mathcal{A}_f$ are mutually connected with real lines, so constitutes the (maximal) abelian subalgebra of $\mathcal{G}_2$. (See the last paragraph of this section.)

Of particular interest is the maximal abelian subalgebra, $\mathcal{H}$, of $\mathcal{G}_2$. We can easily find that Γ_*, Q^*, Q_f^* and $\mathcal{A}_f$ with K and H constitute such an algebra $\mathcal{H}$ and the dimension of it is six. In the Kerr-Newman spacetime, we have another two commuting constants of motion, J_ζ and J_ψ coming from the two commuting Killing vectors ζ and ψ, where, say, ζ is timelike and ψ is the spacelike Killing vector generating closed orbits. Functions J_ζ and J_ψ also commute with all elements of $\mathcal{H}$, and with $\mathcal{H}$ form the largest abelian algebra. This is a classical justification of the separability of the Dirac equation in the Kerr-Newman spacetime [18,19]. We can easily find that the Taub-NUT spacetime is also in the same situation.

V. CONCLUSIONS

We have shown that, if a spacetime admits a Killing-Yano tensor of valence r, the spinning particles moving on it possess the superinvariant Y_r defined by (21). To hold the symmetry associated with the Killing-Yano tensor, the electromagnetic tensor must satisfy Eq.(20). The function Y_2, which is made from the Killing-Yano tensor of usual type, is in a particular position, since only this can have nonvanishing bracket with the chiral charge, Γ_*, for which we can find the associated other constants of motion, (32) and (33).

It should be noted that these facts do not depend on the dimension of spacetime. This enables us to apply our results to other supersymmetric systems, e.g. supersymmetric cosmologies [20], where point particles in spacetimes are replaced by points in the minisuperspaces. Since the Lagrangians used there are not the same as the one used here, the form of Eq.(21) will vary. However, it is plausible that the Killing-Yano tensor can be a useful tool in investigating such systems.

Passing to quantum mechanics can formally be done by the substitutions

$$p_\mu \to -i\hbar\frac{\partial}{\partial x^\mu}, \quad x^\mu \to x^\mu, \quad \xi^\mu \to \sqrt{\frac{\hbar}{2}}\gamma_5\gamma^\mu, \tag{36}$$

where $(\gamma_5)^2 = 1$, $\gamma^a\gamma^b + \gamma^b\gamma^a = -2\eta^{ab}$, $\gamma_5\gamma^a = -\gamma^a\gamma_5$, and $\gamma^\mu \equiv \gamma^a e_a{}^\mu$. In particular,

$$\Pi_\mu \to -i\hbar\left(\frac{\partial}{\partial x^\mu} - \frac{1}{4}\omega_{ab\mu}\gamma^a\gamma^b - \frac{ie}{\hbar}A_\mu\right) \tag{37}$$

is the gauge-covariant derivative operator acting on the Dirac spinors. By these substitutions, Q_f defined by Eq.(28) becomes the operator commuting with the Dirac operator, first pointed out in [12]. It seems natural to expect that all Y_r become operators commuting with the Dirac operator. In particular, we can expect that the constants of motion constituting the largest abelian subalgebra mentioned in the last section become the operator commuting each other, and defines tha maximal number of quantum numbers in the Kerr or Taub-NUT spacetime.

The author thanks Professor A. Hosoya for continuous encouragements.

---

[1] M. Tanimoto, preprint (1995) TIT/HEP-277/COSMO-50.

[2] G.W. Gibbons, R.H. Rietdijk and J.W. van Holten, Nucl. Phys. B404 (1993) 42.

[3] F.A. Berezin and M.S. Marinov, Ann. Phys. (N.Y.) 104 (1977), 336

[4] R. Casalbuoni, Phys. Lett. B62 (1976), 49

[5] A. Barducci, R. Casalbuoni and L. Lusanna, Nuov. Cim. 35A (1976), 377; Nucl. Phys. B124 (1977), 93; id. 521

[6] L. Brink, S. Deser, B. Zumino, P. Di Vecchia and P. Howe, Phys. Lett. B64 (1976), 43

[7] L. Brink, P. Di Vecchia and P. Howe, Nucl. Phys. B118 (1977), 76

[8] R. Penrose, Ann. NY Acad. Sci. 224 (1973) 125; R. Floyd, PhD. Thesis, London (1973).

[9] W. Dietz and R. Rüdiger, Proc. R. Soc. Lond. A375 (1981) 361; Proc. R. Soc. Lond. A381 (1982) 315.

[10] K. Yano, Ann. Math. 55 (1952), 328.

[11] L.P. Hughston, R. Penrose, P. Sommers and M. Walker, Commun. Math. Phys. 27 (1972) 303.

[12] B. Carter and R.G. McLenaghan, Phys. Rev. D19 (1979) 1979.

[13] M. Walker and R. Penrose, Commun. Math. Phys. 18 (1970) 265.

[14] M. Tanimoto, Phys. Rev. D50 (1994) 2595.

[15] M. Visinescu, Phys. Lett. B339 (1994) 28.

[16] J.W. van Holten, preprint (1994) NIKHEF-H/94-29

[17] R.H. Rietdijk and J.W. van Holten, Class. Quantum Grav. 7 (1990) 247.

[18] S. Chandrasekhar, Proc. R. Soc. Lond. A349 (1976) 571

[19] D.N. Page, Phys. Rev. D14 (1976) 1509; N. Toop, (1976), unpublished.

[20] See, e.g., R. Graham, Phys. Rev. Lett. 67 (1991) 1381; P.D. D'Eath, S.W. Hawking and O. Obregón, Phys. Lett. B300 (1993) 44; M. Asano, M. Tanimoto and N. Yoshino, Phys. Lett. B314 (1993) 303; O. Obregón, J. Pullin and M.P. Ryan, Phys. Rev. D48 (1993) 5642; J. Bene and R. Graham, Phys. Rev. D49 (1994) 799; R. Graham and H. Luckock, Phys. Rev. D49 (1994) 2786; A.D.Y. Cheng, P.D. D'Eath and P.R.L.V. Moniz, Phys. Rev. D49 (1994) 5246.

Brans-Dicke Theory in Non-Commutative Geometry

Gaku KONISI, Takesi SAITO* and Ke WU**

Department of Physics, Kwansei Gakuin University, Nishinomiya 662, Japan
*Dept. of Phys., Kyoto Pref. Univ. of Medicine, Taishogun, Kyoto 603, Japan
**Inst. of Theor. Phys., Academia Sinica, P.O.Box 2735, Beijing 100080, China

Abstract

We derive exactly the Brans-Dicke theory on the manifold $M_4 \times Z_2$, where M_4 is the four-dimensional space-time and Z_2 is a discrete internal space with two points. We use the extended affine connection formalism, which is simpler than the vielbein formalism of the previous work and one can see more directly the effect of the Z_2 symmetry. A new formulation is given for the non-commutative differential calculus, which is proper in our discussion.

§ 1. Introduction

After the seminar work of Connes[1),2)] about an application to particle physics model building of the non-commutative geometry (NCG), the non-commutative differential calculus and geometry on $M_4 \times Z_2$ have been widely studied.[3)-14)] A very nice picture of these studies is that the Higgs field is introduced as an extended gauge field related to the Z_2 symmetry. Moreover, the extended Yang-Mills action constructed on $M_4 \times Z_2$ contains a Higgs potential which automatically generates the spontaneous-symmetry breaking. In our recent analysis,[15)] however, we have obtained different results and found a new mechanism which makes gauge fields and fermions massive without the Higgs potential and hence without any spontaneous-symmetry breaking.

Besides particle physics model building there are some works on gravity in terms of NCG on $M_4 \times Z_2$,[10)-14)] where a scalar field is coupled to gravity. However, the scalar fields in those papers are different with each other.[10),13),14)] The reason of this is partly owing to different torsion-free conditions used in their papers. So-called "partial" torsion-free condition used in Ref.14) exactly leads to the Brans-Dicke (BD) theory.[16)] However, the use of "total" torsion-free condition makes NCG into the usual CG and leads to the other kinds of scalar-gravity theory (including electromagnetism).[10),13)]

Another reason is mostly owing to lack of a proper formalism of gravity in terms of NCG. In this paper we propose a new formulation of the non-commutative differential calculus which is proper in gravity theory. The manifold $M_4 \times Z_2$ may be regarded as a pair of M_4's, each at the point $g = e$ or $g = r$ on Z_2. The physics requires that these two M_4-pieces should be equivalent with each other. We assume that the equivalence is attained by a limiting process with some parameter ε which tends to zero. As a technical tool to express the limiting process we introduce a coordinate $x^{\bullet}(g)$ on Z_2 such that their difference

$$\Delta x^{\bullet}(g) = x^{\bullet}(g) - x^{\bullet}(g') \sim \varepsilon \qquad (g \neq g') \tag{1.1}$$

is proportional to the limiting process parameter ε. Let a basis of the tangent space to $M_4 \times Z_2$ at a point $p = (x, x^{\bullet}(g))$ be $\mathcal{E}_N(x,g)$, where $N = (1,2,3,4,\bullet)$. An affine connection $\Gamma^L_{\bullet N}$ is then introduced by the mapping

$$\mathcal{E}_N(x,g') \sim \mathcal{E}_N(x,g) - \mathcal{E}_L(x,g)\Gamma^L_{\bullet N}\Delta x^{\bullet}(g). \tag{1.2}$$

Now, by the equivalence we mean that the basis $\mathcal{E}_N(x,g)$ is mapped to $\mathcal{E}_N(x,g')$ as ε tends to zero, i.e.,

$$\mathcal{E}_N(x,g') \sim \mathcal{E}_N(x,g) \quad as \quad \varepsilon \to 0. \tag{1.3}$$

In the next section, by using this equivalence assumption we propose a new formulation of the non-commutative differential calculus. We then derive the BD theory by using only an extended affine connection on $M_4 \times Z_2$. The result is exactly the same as what we got in the previous work[14] by the extended viel-bein formalism. Since the affine connection formalism is simpler than the latter one, one can see more directly the effect of the Z_2 symmetry. The final section is devoted to concluding remarks.

§ 2. Brans-Dicke theory on $M_4 \times Z_2$

The non-commutative differential calculus and geometry on $M_4 \times Z_2$ can be found in many papers. However, we propose here a modified one which is based on the equivalence assumption stated in § 1 and is proper in the following discussion.

1. Derivative on Z_2

Let $x^N = (x^n, x^\cdot)$, $n = 1,2,3,4$, be coordinates on $M_4 \times Z_2$, where $x^\cdot = x^\cdot(g)$, $g = (e, r) \in Z_2$, is a coordinate on Z_2. We then define a derivative on Z_2 for any function f by

$$\partial_{Z_2} f(x^\cdot(g)) = \lim \frac{\Delta f(x^\cdot(g))}{\Delta x^\cdot(g)} = \lim \frac{f(x^\cdot(g)) - f(x^\cdot(g'))}{x^\cdot(g) - x^\cdot(g')} = \lim \frac{f - f'}{x^\cdot - x^{\cdot\prime}}, \qquad (2.1)$$

where

$$\Delta x^\cdot(g) = x^\cdot(g) - x^\cdot(g') = x^\cdot - x^{\cdot\prime} \quad (g \neq g' \in Z_2) \qquad (2.2)$$

is proporsional to the limiting process parameter ε in (1.1) and we take the limit $\varepsilon \to 0$. From this definition we see that the second drivative always vanishes

$$\partial_{Z_2}\partial_{Z_2} f = \lim \partial_{Z_2} \frac{f - f'}{x^\cdot - x^{\cdot\prime}} = \lim \frac{1}{\Delta x^\cdot}\left(\frac{f - f'}{x^\cdot - x^{\cdot\prime}} - \frac{f' - f}{x^{\cdot\prime} - x^\cdot}\right) = 0. \qquad (2.3)$$

It should be noted that different from the usual NCG the Leibnitz rule is valid for this definition of derivative. This can be seen as follows:

$$\partial_{Z_2}(f_1 f_2) = \lim \frac{1}{\Delta x^\cdot}(f_1 f_2 - f_1' f_2')$$
$$= \lim \frac{1}{\Delta x^\cdot}(f_1 f_2 - f_1 f_2' + f_1 f_2' - f_1' f_2')$$
$$= f_1\, \partial_{Z_2} f_2 + \partial_{Z_2} f_1\, f_2', \tag{2.4}$$

where $f_2' = f_2$ in the limit, so that the Leibnitz rule is valid.

2. Exterior derivative

Let d_{Z_2} be the exterior derivative on Z_2. By introducing a one-form χ dual to ∂_{Z_2}, $\langle \chi, \partial_{Z_2} \rangle = 1$, the exterior derivative on f is defined by

$$d_{Z_2} f = (\partial_{Z_2} f)\chi. \tag{2.5}$$

The Leibnitz rule is also valid for this exterior derivative. We do not need the usual non-commutative relation $\chi f(g) = f(g')\chi$, because by the limiting process $\Delta x^\cdot \to 0$ we have $f(g) = f(g')$. Note, however, that effects of the difference between the two M_4 pieces are partially retained, in the first and second orders of ε, in the affine connection, torsion and curvature tensors.

The nilpotency $d_{Z_2}^2 = 0$ will be realized if

$$d_{Z_2}\chi = 0. \tag{2.6}$$

This can be seen as follows:

$$d_{Z_2}^2 f = d_{Z_2}(\partial_{Z_2} f\, \chi) = \partial_{Z_2}\partial_{Z_2} f\, \chi\wedge\chi + \partial_{Z_2} f\, d_{Z_2}\chi = 0. \tag{2.7}$$

Since the second-derivative vanishes by (2.3), then we have $d_{Z_2}\chi = 0$. This equation is different from the usual condition $d_{Z_2}\chi = -2\chi\wedge\chi$ in NCG. In (2.7) the product $\chi\wedge\chi$ needn't always vanish. In the following we assume

$$\chi\wedge\chi \neq 0. \tag{2.8}$$

This equation is characteristic in our formulation.

3. Exterior derivative on $M_4 \times Z_2$

Let d_4 be the exterior derivative on M_4. Then the exterior derivative on f is given by

$$df = d_4 f + d_{Z_2} f$$
$$= \partial_m f\, dx^m + \partial_{Z_2} f\, \chi. \qquad (m = 1,2,3,4) \tag{2.9}$$

In the following sometimes we use the notation as

$$df = \partial_N f\, dx^N. \qquad N = (m, \bullet), \; dx^\bullet = \chi. \tag{2.10}$$

From the requirement of nilpotency of $d^2 = 0$, $d_4^2 = 0$, $d_{Z_2}^2 = 0$ and hence $d_4 d_{Z_2} + d_{Z_2} d_4 = 0$, we get

$$dx^m \wedge dx^n = - dx^n \wedge dx^m, \tag{2.11}$$

$$dx^m \wedge \chi = - \chi \wedge dx^m. \tag{2.12}$$

However, the one-form χ on Z_2 with itself is not anticommetative by (2.8).

We now start with an extended affine connection on $M_4 \times Z_2$, which has the same formula as in the ordinary Riemann geometry

$$\Gamma^L{}_{MN} = \Gamma^L{}_{NM} = \frac{1}{2} G^{LK} (\partial_M G_{KN} + \partial_N G_{KM} - \partial_K G_{MN}), \tag{2.13}$$

where G_{MN} is a metric of this space. This formula can be derived in the usual way if we use the equivalence assumption. The detail will be given in Appendix.

In the following the metric G_{MN} and its inverse G^{MN} are chosen as

$$G_{MN} = \begin{pmatrix} g_{mn}(x) & 0 \\ 0 & \lambda^2(x) \end{pmatrix}, \tag{2.14}$$

$$G^{MN} = \begin{pmatrix} g^{mn}(x) & 0 \\ 0 & \lambda^{-2}(x) \end{pmatrix}. \tag{2.15}$$

We will consider a simple case that every field here is independent of $x^\bullet(g)$ on Z_2. Hence, in the following calculations one can set ∂_{Z_2} to be zero. Then we get all components of $\Gamma^L{}_{MN}$

$$\Gamma^m{}_{np} = \frac{1}{2} g^{ml} (\partial_n g_{lp} + \partial_p g_{ln} - \partial_l g_{np}), \tag{2.16 a}$$

$$\Gamma^m{}_{\bullet p} = \Gamma^\bullet{}_{mp} = 0, \tag{2.16 b}$$

$$\Gamma^\bullet{}_{\bullet p} = \frac{1}{\lambda} \partial_p \lambda, \tag{2.16 c}$$

$$\Gamma^m{}_{\bullet\bullet} = - \lambda \partial^m \lambda, \tag{2.16 d}$$

$$\Gamma^\bullet{}_{\bullet\bullet} = 0. \tag{2.16 e}$$

The extended Riemann curvature two-form is given by $\mathbb{\Gamma}^L{}_M \equiv \Gamma^L{}_{MN} dx^N$ as

$$
\begin{aligned}
\mathbb{R}^M{}_N &= d\mathbb{\Gamma}^M{}_N + \mathbb{\Gamma}^M{}_L \times \mathbb{\Gamma}^L{}_N \\
&= \partial_P \Gamma^M{}_{NQ}\, dx^P \wedge dx^Q + \Gamma^M{}_{LP} \Gamma^L{}_{NQ}\, dx^P \wedge dx^Q \\
&= (\partial_p \Gamma^M{}_{Nq} + \Gamma^M{}_{Lp} \Gamma^L{}_{Nq})\, dx^p \wedge dx^q \\
&\quad + (\partial_p \Gamma^M{}_{N\bullet} + \Gamma^M{}_{Lp} \Gamma^L{}_{N\bullet} - \Gamma^M{}_{L\bullet} \Gamma^L{}_{Np})\, dx^p \wedge \chi \\
&\quad + (\Gamma^M{}_{L\bullet} \Gamma^L{}_{N\bullet})\, \chi \wedge \chi .
\end{aligned}
\tag{2.17}
$$

The existence of the last $\chi \wedge \chi$ term is characteristic in NCG. Defining its components by

$$
\mathbb{R}^M{}_N = \frac{1}{2} R^M{}_{Npq}\, dx^p \wedge dx^q + R^M{}_{Np\bullet}\, dx^p \wedge \chi + R^M{}_{N\bullet\bullet}\, \chi \wedge \chi , \tag{2.18}
$$

we have

$$
R^M{}_{Npq} = \partial_p \Gamma^M{}_{Nq} - \partial_q \Gamma^M{}_{Np} + \Gamma^M{}_{Lp} \Gamma^L{}_{Nq} - \Gamma^M{}_{Lq} \Gamma^L{}_{Np} , \tag{2.19a}
$$

$$
R^M{}_{Np\bullet} = \partial_p \Gamma^M{}_{N\bullet} + \Gamma^M{}_{Lp} \Gamma^L{}_{N\bullet} - \Gamma^M{}_{L\bullet} \Gamma^L{}_{Np} , \tag{2.19b}
$$

$$
R^M{}_{N\bullet\bullet} = \Gamma^M{}_{L\bullet} \Gamma^L{}_{N\bullet} . \tag{2.19c}
$$

$$
R^M{}_{N\bullet q} = - R^M{}_{Nq\bullet} . \tag{2.19d}
$$

Substituting (2.16) into (2.19) one gets

$$
R^m{}_{npq} = \mathring{R}^m{}_{npq} \equiv \partial_p \Gamma^m{}_{nq} - \partial_q \Gamma^m{}_{np} + \Gamma^m{}_{\ell p} \Gamma^\ell{}_{nq} - \Gamma^m{}_{\ell q} \Gamma^\ell{}_{np} , \tag{2.20a}
$$

$$
R^\bullet{}_{m\bullet q} = -\mathring{\nabla}_q \left(\frac{1}{\lambda} \partial_m \lambda\right) - \frac{1}{\lambda^2} \partial_q \lambda \partial_m \lambda = -\frac{1}{\lambda} \mathring{\nabla}_q \partial_m \lambda , \tag{2.20b}
$$

$$
R^n{}_{\bullet\bullet q} = \mathring{\nabla}_q (\lambda \partial^n \lambda) - \partial^n \lambda \partial_q \lambda = \lambda \mathring{\nabla}_q \partial^n \lambda , \tag{2.20c}
$$

$$
R^\bullet{}_{mp\bullet} = \frac{1}{\lambda} \mathring{\nabla}_p \partial_m \lambda , \qquad (\mathring{\nabla}_p V_m \equiv \partial_p V_m - \Gamma^\ell{}_{mp} V_\ell) \tag{2.20d}
$$

$$
R^n{}_{\bullet p\bullet} = -\lambda \mathring{\nabla}_p \partial^n \lambda , \qquad (\mathring{\nabla}_p V^n \equiv \partial_p V^n + \Gamma^n{}_{\ell p} V^\ell) \tag{2.20e}
$$

$$
R^m{}_{n\bullet\bullet} = -\partial^m \lambda \partial_n \lambda , \tag{2.20f}
$$

$$
R^\bullet{}_{\bullet\bullet\bullet} = -\partial_\ell \lambda \partial^\ell \lambda , \tag{2.20g}
$$

and all other components are zero, where $\mathring{R}^m{}_{npq}$ and $\mathring{\nabla}_p$ are the usual four-dimensional Riemann curvature tensor and the covariant derivative on M_4.

Next, the extended Ricci curvature is given by

$$R_{MN} = \sum_{P} R^{P}{}_{MPN}$$
$$= R^{p}{}_{MpN} + R^{\bullet}{}_{M\bullet N}, \tag{2.21}$$

hence

$$R_{mn} = \mathring{R}_{mn} + R^{\bullet}{}_{m\bullet n}$$
$$= \mathring{R}_{mn} - \frac{1}{\lambda}\mathring{\nabla}_{n}\partial_{m}\lambda, \tag{2.22a}$$
$$R_{\bullet m} = R_{m\bullet} = 0, \tag{2.22b}$$
$$R_{\bullet\bullet} = R^{m}{}_{\bullet m\bullet} + R^{\bullet}{}_{\bullet\bullet\bullet}$$
$$= -\lambda\mathring{\nabla}_{m}\partial^{m}\lambda - \partial_{\ell}\lambda\partial^{\ell}\lambda, \tag{2.22c}$$

where

$$\mathring{R}_{mn} = \mathring{R}^{p}{}_{mpn}. \tag{2.23}$$

Finally we get the scalar curvature on $M_4 \times Z_2$

$$R = G^{MN}R_{MN} = \mathring{R} - 2\frac{1}{\lambda}\mathring{\nabla}_{m}\partial^{m}\lambda - \frac{1}{\lambda^2}\partial_{\ell}\lambda\partial^{\ell}\lambda. \tag{2.24}$$

By using $\det(G_{MN}) = \det(g_{mn})\lambda^2 \equiv g\lambda^2$, we obtain the gravity action

$$I = \int_{M_4}\int_{Z_2}\sqrt{-\det(G_{MN})}\,R$$
$$= \int_{M_4}\sqrt{-g}\,\lambda\left[\mathring{R} - 2\frac{1}{\lambda}\mathring{\nabla}_{m}\partial^{m}\lambda - \frac{1}{\lambda^2}\partial_{\ell}\lambda\partial^{\ell}\lambda\right]$$
$$= \int_{M_4}\sqrt{-g}\left(\lambda\mathring{R} - \frac{1}{\lambda}\partial_{\ell}\lambda\partial^{\ell}\lambda\right), \tag{2.25}$$

which is just the BD theory obtained in Ref. 14).

§ 3. Concluding remarks

Based on the equivalence assumption stated in the introduction we have derived the BD theory on the manifold $M_4 \times Z_2$. We have used only the extended affine connection formalism, which is simpler than the vielbein formalism previously proposed and one can see more directly the effect of the Z_2 symmetry. The BD kinetic term comes from the $\chi\wedge\chi$ term in the curvature two-form given by (2.17). The result shows that the BD scalar field is closely related to the

Z_2 discrete symmetry and is interpreted to discribing the distance between the two points in the internal space. The torsion of our space is given by

$$\begin{aligned} T^L &= \Gamma^L{}_{MN}\, dx^M \wedge dx^N \\ &= \Gamma^L{}_{mm}\, dx^m \wedge dx^m + (\Gamma^L{}_{m\bullet} - \Gamma^L{}_{\bullet m})\, dx^m \wedge \chi + \Gamma^L{}_{\bullet\bullet}\, \chi \wedge \chi \\ &= \Gamma^L{}_{\bullet\bullet}\, \chi \wedge \chi. \end{aligned} \tag{3.1}$$

From this formula we see that the total torsion is not zero. If we require $T^L = 0$, then we have $\chi \wedge \chi = 0$. This means that the most characteristic feature of the discrete symmetry disappears and we are led to another scalar-gravity theory.

It is a very interesting problem to introduce on $M_4 \times Z_2$ the electromagnetic field A_n together with the BD scalar field λ. At first sight this seems to be easily accomplished if we take the line element

$$\Delta s^2 = \lambda^2 (\Delta x^\bullet + A_m \Delta x^m)^2 + g_{mm} \Delta x^m \Delta x^m. \tag{3.2}$$

This is like that of the Kaluza-Klein theory where the fifth continuous dimension is replaced by two discrete points. However, the problem is not so simple, but we expect a different result from the KK theory, because there is a contribution to the curvature from the $\chi \wedge \chi$ term. The detail will be left for a future publication.

Appendix Derivation of Eq.(2.13)

We would like to derive Eq.(2.13). This equation is equivalent to

$$\partial_L G_{MN} = \Gamma_{MLN} + \Gamma_{NLM}, \tag{A.1}$$

where

$$\Gamma_{MLN} = G_{MK}\, \Gamma^K{}_{LN}. \tag{A.2}$$

Let a basis of the tangent space at $p = (x, g) \in M_4 \otimes Z_2$ be $e_N(x, g)$, $N = (n, \bullet)$, $n = 1,2,3,4$. Then, the affine connections are introduced by the mapping

$$e_N(x+\Delta x, g) \sim e_N(x,g) + e_L(x,g)\, \Gamma^L{}_{mN}\, \Delta x^m, \tag{A.3}$$

$$e_N(x, g') \sim e_N(x,g) - e_L(x,g)\, \Gamma^L{}_{\bullet N}\, \Delta x^\bullet, \tag{A.4}$$

where
$$\Delta x^{\bullet}(g) = x^{\bullet}(g) - x^{\bullet}(g') \tag{A.5}$$

is proporsional to the limiting process parameter ε in (1.1). The metric G_{MN} is defined by the inner product

$$G_{MN} = \langle \mathcal{E}_M , \mathcal{E}_N \rangle . \tag{A.6}$$

Let us first calculate for the general metric G_{MN}

$$\partial_{Z_2} G_{MN} = \lim_{\varepsilon \to 0} (G_{MN} - G'_{MN}) \frac{1}{\Delta x^{\bullet}} ,$$

where
$$\begin{aligned} G'_{MN} &= \mathcal{E}'_M \bullet \mathcal{E}'_N \\ &= (\mathcal{E}_M - \mathcal{E}_L \Gamma^L{}_{\bullet M} \Delta x^{\bullet}) \cdot (\mathcal{E}_N - \mathcal{E}_L \Gamma^L{}_{\bullet N} \Delta x^{\bullet}) \\ &= \mathcal{E}_M \bullet \mathcal{E}_N - (\mathcal{E}_M \bullet \mathcal{E}_L \Gamma^L{}_{\bullet N} + \mathcal{E}_N \bullet \mathcal{E}_L \Gamma^L{}_{\bullet M}) \Delta x^{\bullet} + O(\Delta x^{\bullet})^2 \\ &= G_{MN} - (\Gamma_{M \bullet N} + \Gamma_{N \bullet M}) \Delta x^{\bullet} + O(\Delta x^{\bullet})^2 . \end{aligned}$$

Taking the limit $\varepsilon \to 0$ we have

$$\partial_{Z_2} G_{MN} = \Gamma_{M \bullet N} + \Gamma_{N \bullet M} . \tag{A.7a}$$

In the same way we have for $\ell = 1,2,3,4$

$$\partial_{\ell} G_{MN} = \Gamma_{M \ell N} + \Gamma_{N \ell M} . \tag{A.7b}$$

Both equations (A.7a,b) are equivalent to (A.1). If $\Gamma^L{}_{MN} = \Gamma^L{}_{NM}$, then we obtain the result (2.13) in the usual way.

References

1) A. Connes, The Interface of Math. & Particle Phys., edited by D. Quillen, G. B. Segal & S. T. Tsou, Clarendon Press, Oxford (1990).

2) A. Connes and J. Lott, Nucl. Phys.(Proc. Suppl.) B18(1990), 29.

3) D.Kastler, *Introduction to non-commutative geometry and Yang-Mills model-building*, XIXth International Conference on Differential Geometric Methods in Theoretical Physics. Rapallo (Italy) June 1990. Springer Lect. Notes in Phys. 375(1990), 25.

4) R.Coquereaux, G.Esposito-Farese and G.Vaillant, Nucl. Phys. B353 (1991), 689.

5) A.Sitarz, *Non-commutative Geometry and Gauge Theory on Discrete Groups*, preprint TPJU-7/1992.

6) A. H. Chamseddine, G. Feldler and J. Frohlich, Phys. Lett. 296B(1992), 109; Nucl. Phys. B395(1993), 672.

7) H.G.Ding, H.Y.Guo, J.M.Li and K.Wu, *Higgs as Gauge Fields on Discrete Groups and Standard Models for Electroweak and Electroweak-Strong Interactions*, to appear in Z.Phys.

8) K.Morita, Prog. Theor. Phys. 90(1993), 219.
K.Morita and Y.Okumura, *Weinberg-Salam theory in Non-commutative Geometry*, Nagoya Univ. preprint, DPNU-93-25.
K.Morita and Y.Okumura, *Reconstruction of standard model in non-commutative geometry on $M_4 \otimes Z_2$*, Nagoya Univ. preprint, DPNU-93-38.
Y.Okumura, *Gauge theory and Higgs mechanism based on differential geometry on discrete space $M_4 \otimes Z_N$*, Chubu Univ. preprint, Jan. 8, 1994.
Y.Okumura, *Standard Model in Differential Geometry on Discrete Space $M_4 \otimes Z_3$*, Chubu Univ. preprint, Jan. 31, 1994.

9) S.Naka and E.Umezawa,
Prog. Theor. Phys. 92 (1994), 189.

10) A.H.Chamseddine,G.Felder,J.Frohlich, *Gravity in Non-Commutative Geometry*, Commun. Math. Phys. 155 (1993), 205.

11) W.Kalau and M.Waltze, *Gravity, Non-Commutative Geometry and the Wodzicki Residue*, preprint MZ-TH/93-38.

12) D. Kastler, The Dirac operator and gravitation, CPT-93/P2970.

13) G. Landi, N. A. Viet and K. C. Wali, Phys. Lett. B326(1994), 45.

14) B. Chen, T. Saito and K. Wu,
Prog. Theor. Phys. 92(1994), 881.

15) G. Konisi and T. Saito, "Higgs Scalar Fields and Discrete Symmetry," Kyoto Pref. Univ. of Medicine Preprint, Nov. 18, 1994.

16) C. H. Brans and R. H. Dicke, Phys. Rev. 124(1961), 925.

Quantum Smearing of Spacetime Singularity

Akio HOSOYA
Department of Physics
Tokyo Institute of Technology
Oh-Okayama, Meguro-ku,Tokyo 152
Japan

24, December 1994

Abstract

We propose a quantum mechanical generalization of affine length of a curve which gives a criterion whether a classical singularity is smeared out by quantum fluctuation of spacetime geometry. An explicit example is demonstrated in the (2+1)-dimensional black hole model.

1 Introduction

There seems to be a general belief that quantum gravity effects will somehow tame spacetime singularities, existence of which have been proven in classical theory of gravity.

Specifically, quantum cosmology is partly motivated by the intuition that the initial singularity can be avoided by considering quantum effects of spacetime. Less discussed is black hole singularity from quantum mechanical point of view, probably because of cosmic censorship conjecture. [1] In the case of naked singularities, which appear in some models of gravitational collapse in classical theory, many people are skeptical about its true existence in the real world, because violent quantum fluctuation of metrics will eventually wipe out that kind of singularity. Or at least, one cannot say for sure that naked singularity exists, if quantum effects of spacetime at Planck scale are taken into account.

However, the spacetime singularity is a completely different thing from the singularities which appear in classical electromagnetism or field theory in general. Those are normally expressible by distributions. In general relativity it is not the case, because of the nonlinearity of gravitational force. The spacetime singularity is characterized by the incompleteness of geodesics. More precisely

[1] There are literatures which study the vacuum expectation value of the metric tensor and then look at the global structure of spacetime. This approach seems to be limited in the semi-classical regime

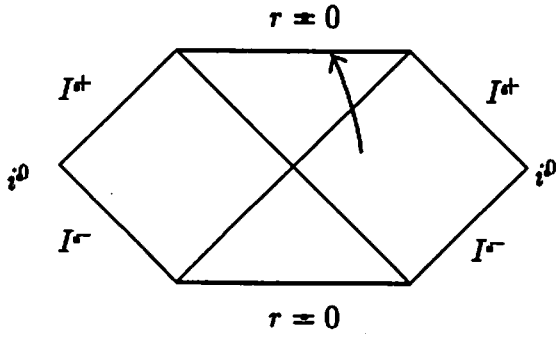

Figure 1: The Penrose diagram for the Schwarzschild black hole and a causal curve to the singularity

speaking, if a causal geodesic curve is incomplete with a finite affine parameter in a spacetime which has no further extension, we say that the spacetime is singular. The famous singularity theorem by Hawking and Penrose [1]states that such a singularity always exists if (a) energy condition (b)generic condition hold and if(c) a trapped surface exists.

The problem addressed in this paper is to propose a criterion for a singularity to be quantum mechanically smeared away. We shall demonstrate some explicit examples.

2 b-incompleteness

As briefly explained in the introduction, spacetime singularities are normally characterized by a geodesic of a finite affine length which ends up with nowhere in spacetime. Roughly, a free-falling observer will find an end of history after a finite proper time. On the other hand, if the affine length is infinite the would-be singularity is infinitely far away so that it is not a singularity at all. In two senses, this definition of singularity is unsatisfactory. For one thing, the geodesic incompleteness seems too restrictive to characterize the spacetime singularity. For example, a noninertial observer traveling by a rocket of a finite amount of fuel is a perfectly physical observer so that we need to tell him how singularity looks like. Second the concept of geodesic is a classical one so that it is rather difficult to generalize the definition of singularities on the basis of geodesics in quantum mechanics of spacetime . Very fortunately, a favorable generalization of spacetime singularity is available in classical general relativity which was first invented by Schmidt[2]. The time-like or null geodesic curve is replaced by a general C^1 causal curve so that we can make some instructions to a space traveler of a finite amount of fuel. He also ingeniously defined the so-called generalized affine parameter, which roughly measures how long it takes to get the singularity. If it is finite, the space traveler should worry his fate. Let M be the spacetime which is assumed to be non-extendible. We also assume

the spacetime is equipped with tetrads and connections. The generalized affine parameter associated with a causal curve :$\alpha : t \in [0,1) \to M$ is given by

$$|\alpha| = \int_0^1 dt \sqrt{\sum_{a=1}^{4} V^a(t) V^a(t)}. \tag{1}$$

Here V^a is a component of the tangent vector to the causal curve at the parameter t with respect to the parallelly transported tetrad from an arbitrarily chosen tetrad at the initial point :$\alpha(0)$. We can say that if the generalized affine parameter is finite for a causal curve which goes to the would-be singularity, the causal curve is *b-incomplete* (b for bundle). One of the virtues in the definition of the generalized affine parameter is the positive definiteness of quantity inside the square root. The generalized affine parameter coincides with the ordinary affine parameter when the curve is a geodesic curve. Therefore the b-completeness implies the geodesic completeness.

The generalized affine length $|\alpha|$ depends on the initial tetrad as well as the initial point. However, for new components of the tangent vector to the curve V' with respect to the parallelly transported tetrads from a different choice of the initial tetrad , which is obtained by a finite Lorentz transformation., it has been shown that there is some constant $C > 0$ such that

$$C \sum_{a=1}^{4} V^a V^a \leq \sum_{a=1}^{4} V'^a V'^a \leq C^{-1} \sum_{a=1}^{4} V^a V^a. \tag{2}$$

Namely, the finiteness or the infiniteness does not depend on the choice of the initial point and the chosen frame there. To express the generalized affine parameter to suit quantum gravity we use an expression for $V^a(t)$ in terms of the connection:

$$V^a(t) = V^\mu e_\mu^{\ b} [P \exp \int_0^t \omega]_b^a, \tag{3}$$

where V^μ and $e_\mu^{\ a}$ are the tangent vector and the frame tetrad at the point $\alpha(t)$, respectively. ω is the spin connection and P denotes the path ordered product.

In this paper we propose a quantum mechanical generalization of the b-length:

$$|\alpha|_q = \int_0^1 dt \sqrt{\sum_{a=1}^{4} < (V^\mu e_\mu^{\ b} [P \exp \int_0^t \omega]_b^a)^2 >}, \tag{4}$$

where <>means the expectation value with respect to a quantum state| > of the geometry. Here we stress that the curve is fixed in the coordinate space without referring the metric, which is now a quantum variable. In a sense, we study

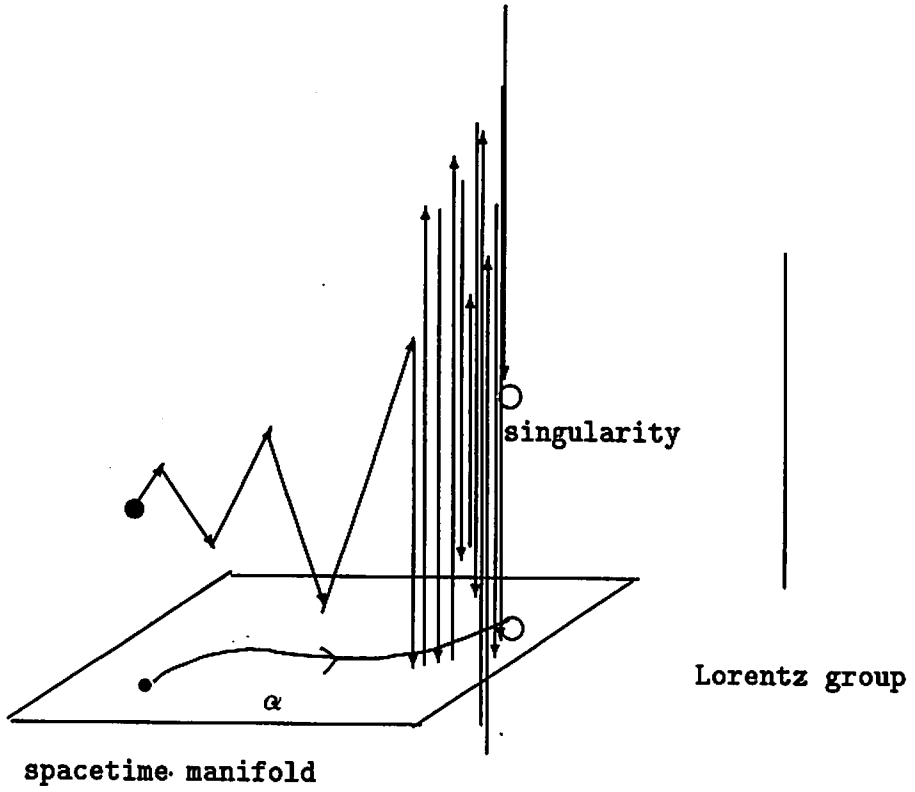

Figure 2: A conceptual picture of an infinite generalized affine parameter by large quantum fluctuation near the singularity

a classical test particle in quantum geometry. We will return to this point in the final section. The idea behind this definition of quantum b-(in)completeness is the following. Suppose we approach $t \to 1$ and the point $\alpha(1)$ is classically a singularity. So $|\alpha|$is finite classically . However, quantum mechanical fluctuation of the connection may be very large near the classical spacetime singularity so that the length of the curve α in the bundle space becomes infinite. This implies the observer will never reach the singularity in a finite lifetime due to the violent fluctuation of the geometry.

In the following sections, we will demonstrate how our definition of the smearing of singularity works in a simple (2+1)-dimensional black hole model [3]. Of course, the (2+1)-dimensional model is for the illustration only. One can in principle compute $|\alpha|_q$ in any model of quantum gravity.

3 The BTZ Black Hole

In this section we briefly review the (2+1)-dimensional black hole found by Bañodos et al. in the simplest circular symmetric case. The model is given by

the action which contains the Einstein-Hilbert action and the cosmological term in (2+1)-dimensions,

$$S = -\frac{1}{16\pi G}\int d^3x\sqrt{-g}[R - 2\Lambda], \tag{5}$$

where Λ is a negative cosmological constant and R is the scalar curvature. As is well known, in (2+1)-dimensions the Riemann tensor can be expressed by the Einstein tensor $R_{\mu\nu} - \frac{1}{2}g_{\mu\nu}R$. Hence the Einstein equation gives us the Riemann tensor as

$$R_{\mu\nu\rho\sigma} = \Lambda(g_{\mu\rho}g_{\nu\sigma} - g_{\mu\sigma}g_{\nu\rho}). \tag{6}$$

This implies the spacetime is a constant curvature spacetime with a sectional curvature being $\Lambda = -1/l^2$. The simplicity of the (2+1)-dimensional Einstein gravity is that it contains no gravitational wave modes and no Newtonian force. So one might wonder what is meant by quantization of black hole in (2+1)-dimensions. There are no gravitons to quantize and much worse there is no gravitational force to cause the gravitational collapse which eventually leads to the formation of a black hole in the physical (3+1)- dimensions! The point is, however, the existence of the global modes which describe the mass and angular momentum of a black hole, which appear as a consequence of the identification of spacetime by a discrete element of the isometry group of spacetime geometry. In the present case the covering spacetime is the anti-de Sitter spacetime and the isometry group is $SO(2,2)$. The best way to see this will be embedding the anti-de Sitter space in the 4 dimensional flat space with $++-$ signature. Let the coordinates of the 4-dimensional flat space be $X^A, A = 0,1,2,3$. The anti-de Sitter space is defined by the condition:

$$(X^0)^2 + (X^1)^2 - (X^2)^2 - (X^3)^2 = -1/l^2. \tag{7}$$

We introduce the parameterization which is convenient to describe the inside of the black hole as

$$\begin{aligned} X^0 &= \sqrt{1-\hat{r}^2/l^2}\sinh\hat{t}/l, \quad X^2 = \sqrt{1-\hat{r}^2/l^2}\cosh\hat{t}/l, \\ X^1 &= \hat{r}/l\cosh\hat{\theta}, \qquad\qquad X^3 = \hat{r}/l\sinh\hat{\theta}. \end{aligned} \tag{8}$$

Recall that we are actually interested in the inside of the black hole, because we are going to study the behavior of the generalized affine parameter near $r = 0$. The induced metric becomes

$$\begin{aligned} ds^2 &= (dX^0)^2 + (dX^1)^2 - (dX^2)^2 - (dX^3), \\ &= (1-\hat{r}^2/l^2)d\hat{t}^2 - (1-\hat{r}^2/l^2)^{-1}d\hat{r}^2 + \hat{r}^2 d\hat{\theta}^2 \end{aligned} \tag{9}$$

From the construction it is easy to see that the full isometry group is $SO(2,2)$. It may be more illuminating to rewrite the metric by rescaling $\hat{\theta} = \sqrt{M}\theta, \hat{t} = \sqrt{M}t, \hat{r} = r/\sqrt{M}$. We obtain

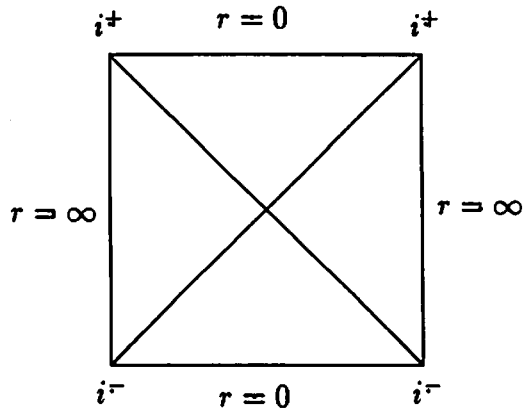

Figure 3: The Penrose diagram for the circular symmetric BTZ black hole

$$ds^2 = (M - r^2/l^2)dt^2 - (M - r^2/l^2)^{-1}dr^2 + r^2 d\theta^2 \tag{10}$$

The global structure of the spacetime of this metric is shown to be a circular symmetric black hole *if we identify* $\theta = 0$ *with* $\theta = 2\pi$, namely, $\hat{\theta} = 0$ with $\hat{\theta} = 2\pi\sqrt{M}$. Therefore the circular symmetric BTZ black hole spacetime can be represented as a quotient space of the anti-de Sitter spacetime by a certain amount of Lorentz boost, which is a discrete subgroup of the full isometry group $SO(2,2)$. The mass of the black hole M is introduced as a parameter of the identification, a Teichmüller parameter. The origin $r = 0$ turns out to be a space-like causal singularity as shown in the Penrose diagram (Fig.3), though the curvature is finite. So it is a rather mild singularity. In the next section we shall discuss a canonical quantization of the BTZ black hole system, in which the mass M will be treated as a dynamical variable.

4 A quantization of the circular symmetric BTZ black hole

It is by now well known that there are many ways to quantize the (2+1)-dimensional gravity and probably this ambiguity will also go over to the physical (3+1)-dimensional quantum gravity. For our present purpose, it is sufficient to show an example calculation in a specific scheme of quantization method, because it is not the issue addressed in this paper to decide which scheme is the correct one. We start with the first order formalism in which the triad and the spin connection are treated as independent variables. Only on-shell they are related by the metricity condition. We adopt the solution space approach to quantization[4] by making the ansatz for the triad and the spin connection one

forms,

$$\begin{cases} e^0 &= d\hat{r}/\sqrt{(1-\hat{r}^2/l^2)} \\ e^1 &= \alpha\sqrt{(1-\hat{r}^2/l^2)}dt \\ e^2 &= \beta\hat{r}d\phi \end{cases} \tag{11}$$

$$\begin{cases} \omega_1^0 &= -\alpha\hat{r}/l^2 dt \\ \omega_2^0 &= \sqrt{(1-\hat{r}^2/l^2)}\beta d\theta \\ \omega_2^1 &= 0 \end{cases} \tag{12}$$

The spacetime metric is given by

$$\begin{aligned} ds^2 &= -(e^0)^2 + (e^1)^2 + (e^2)^2 \\ &= \alpha^2(1-\hat{r}^2/l^2)d\hat{t}^2 - (1-\hat{r}^2/l^2)^{-1}d\hat{r}^2 + \beta^2\hat{r}^2 d\hat{\theta}^2, \end{aligned} \tag{13}$$

where the parameters α and β are related to the scales of the boost angles $\hat{t}$, $\hat{\phi}$. If they are constant, the triad and the spin connection satisfy the Einstein equation.

We now regard the parameters as functions of $\hat{r}$ and carry out the so-called the radial quantization, because inside the horizon the radial coordinate r plays a role of time. The curvature 2-form is calculated to be

$$\begin{aligned} R_1^0 &= -R^2 = -\tfrac{1}{l^2}e^0e^1 - \tfrac{\dot{\alpha}\hat{r}}{\alpha l^2}e^0e^1 \\ R_2^0 &= R^1 = -\tfrac{1}{l^2}e^0e^2 + \tfrac{\dot{\beta}(1-\hat{r}^2/l^2)}{\beta\hat{r}}e^0e^2 \\ R_2^1 &= R^0 = -\tfrac{1}{l^2}e^1e^2, \end{aligned} \tag{14}$$

where the dot indicates the differentiation with respect to r. In terms of the forms, the action can be written as

$$S = -\frac{2}{16\pi G}\int[-e_aR^a + \frac{1}{l^2}e^0e^1e^2], \tag{15}$$

so that the direct substitution and partial integration give

$$S = -\frac{1}{4G}\int \alpha\dot{\beta}drdt. \tag{16}$$

Here we have performed the integration over the angle ϕ. It is now clear that $p_\beta = -\frac{1}{4G}\alpha$ is the canonical momentum conjugate to β and that the Hamiltonian vanishes. Note that there are no contributions from the surface terms. This can be confirmed from the fact that the equations of motion derived from (16): $\dot{\alpha} = 0$ and $\dot{\beta} = 0$ reproduce the Einstein equation with the previous ansatz for the triad and the spin connection. The canonical quantization is straightforward;

$$[\alpha(t), \beta(t')] = 4Gi\hbar\delta(t-t'). \tag{17}$$

At this stage one might be puzzled that the parameters $\alpha(t)$and $\beta(t)$ which appear in the "spatial" metric do not commute with each other. This is because by making the anzatz for the triad and spin connection we have chosen a certain gauge, which makes a commutative Poisson bracket a non-commutative Dirac bracket. This phenomenon has already been observed by Carlip in his analysis of the torus universe[4]. The parameter β gives a scale of the boost angle between two spacetime points which we identify. As we saw in the previous section, this scale β is directly related to the mass of the BTZ black hole. Actually, $\beta^2 = M$. The physical meaning of the parameter α is less clear. If we are allowed to continue our metric defined inside the horizon to the outside and then Wick rotate the coordinate t, α would give a scale of the period of the Killing time t in the imaginary direction. So α is roughly related to the Hawking temperature or the "opening angle" in the Euclidean approach of Carlip and Teitelboim [5].

5 Quantum length

In this section we shall study the generalized affine parameter defined in §3 in quantum theory of the (2+1)-dimensional BTZ black hole analyzed in the previous section. This model has a technical advantage that the metric approaches the Minkowskii metric and connection becomes flat near the classical singularity. For comparison we start with a classical computation of the generalized affine parameters for a causal curve which approaches the black hole singularity.

5.1 classical case

For a simple illustration, consider a curve along which

$$e^1 = 0, \quad e^2 = ke^0 \tag{18}$$

with k being a constant. For the time-like curve, $|k| < 1$, while $|k| = 1$ for the null curve. We are interested in the case that the end point of the causal curve approaches the would-be singularity $r = 0$. It is therefore sufficient to consider a curve near $r = 0$. so that we can ignore ω_1^0 and use an approximation, $\omega_2^0 \approx \beta d\phi$. Therefore the path ordered product $P\exp\int\omega$ is simply a Lorentz boost in the direction 2 near $r = 0$. Namely,

$$V^\mu e_\mu^b [P\exp\int_0^t \omega]_b^a = V^\mu e_\mu^0 (1, 0, k) \begin{pmatrix} \cosh\theta & 0 & \sinh\theta \\ 0 & 1 & 0 \\ \sinh\theta & 0 & \cosh\theta \end{pmatrix} \tag{19}$$

For the path (18), the absolute value of the coordinate θ gets large like $\theta \approx -|k|\log r/\beta$ as r goes to zero as far as k is non-zero. Correspondingly the generalized affine parameter (4) tends to

$$
\begin{aligned}
|\alpha| &= \int dt \sqrt{\sum_{a=1}^{4} < (V^\mu e_\mu^b [P \exp \int \omega]_b^a)^2 >}, \\
&\approx \int^0 dr (1+|k|) \exp[|\phi|]/\sqrt{2} \\
&\approx \int^0 dr (1+|k|) r^{-|k|}/\sqrt{2}.
\end{aligned} \tag{20}
$$

It is now clear that for a time-like curve,$|k| < 1$ the above integration converges so that the path can reach the singularity $r = 0$ in a finite affine length. On the other hand, for some null or space-like paths $|k| \geq 1$, the generalized affine parameter diverges; the singularity is infinitely far away. However, according to the classical definition of singularity, $r = 0$ is a singularity, because we have at least one causal curve which is b-incomplete.

5.2 a gaussian wave packet

The previous classical analysis is suggestive in the sense that the null and space-like curves contribute more to the generalized affine parameter than the time-like one. Intuitively, in quantum gravity, the metric fluctuates so that the curve fluctuates between time-like and space-like. This fluctuation will effectively make the generalized affine parameter longer. Let us consider a gaussian wave packet spreading around a mass $M_0 = \beta_0^2$ with a width Δ:

$$
\Psi(\beta) = \exp[-\frac{(\beta - \beta_0)^2}{2\Delta}]. \tag{21}
$$

The expectation value $\sum_{a=0}^{2} < (V^\mu e_\mu^b [P \exp[\int_0^t \omega]_b^a)^2 >$, is readily evaluated to be proportional to

$$
\begin{aligned}
&\int d\beta \exp[2\beta\theta] |\Psi(\beta)|^2 \\
&= const. \times \exp[2\beta_0\theta + \Delta\theta^2].
\end{aligned} \tag{22}
$$

We obtain

$$
|\alpha|_q \approx \int^0 dr \exp[-|k| \log r + \frac{\Delta}{2\beta_0^2}(|k| \log r)^2], \tag{23}
$$

for the path in the previous subsection with β replaced by β_0, viz. $\theta \approx -|k| \log r/\beta_0$. (The choice β_0 is arbitrary, because it can be absorbed by $|k|$. We chose this for the comparison to the previous classical case.) Of course it is meaningless to define time-like or null curve in the theory of quantum metric, which is fluctuating. It is clear that the generalized affine parameter $|\alpha|_q$ is divergent however small the mass fluctuation Δ is. Roughly speaking, the mass fluctuation brings about an infinitely long random walk in the boost direction in the original universal covering anti-de Sitter space. We also note that the result does not depend whether the path is time-like ($|k| < 1$), null ($|k| = 1$) or space-like ($|k| > 1$), unless $k \neq 0$.

5.3 metric eigenstate

Since the Hamiltonian is zero in our system described in §4, the time evolution of the wave function is trivial. Among many possibilities consider the eigenstate of the metric operator:

$$\widehat{ds^2} = \alpha^2(1-\hat{r}^2/l^2)d\hat{t}^2 - (1-\hat{r}^2/l^2)^{-1}d\hat{r}^2 + \beta^2\hat{r}^2 d\hat{\theta}^2, \tag{24}$$

where θ and $\hat{t}$ are arbitrary functions of $\hat{r}$. Here α and β are considered as quantum operators, which satisfy the canonical commutation relation (17). In order to make the commutation relation make sense at equal $\hat{t}$'s, we replace $\delta(0)$ by $1/T$, where T is the range of the variable t. The "equal $\hat{t}$" commutation relation now reads

$$[\alpha, \beta] = 4Gi\hbar/T. \tag{25}$$

The eigenvalue problem

$$\widehat{ds^2}\psi(\beta) = ds^2\psi(\beta) \tag{26}$$

is mathematically the same as the harmonic oscillator problem in elementary quantum mechanics. The ground state wave function is given by

$$\psi_0(\beta) = \exp[-\frac{T}{8G\hbar\sqrt{1-r^2/l^2}}r|\frac{d\theta}{dt}|\beta^2] \tag{27}$$

and the generalized affine parameter is computed as

$$|\alpha|_q \approx const. \int^0 dr \exp[\frac{4G\hbar}{T}\frac{\sqrt{1-r^2/l^2}}{r}|\frac{dt}{d\theta}|\theta^2]. \tag{28}$$

We can immediately recognize that the generalized affine parameter is divergent, for a generic case $\frac{dt}{d\theta} \neq 0$ and $\theta \neq 0$ at $r = 0$. Otherwise, the curve is arbitrary. θ and t are arbitrary functions of r, which satisfy the genericness at $r = 0$. This should be so because the mass $M = \beta^2$ is fluctuating in the metric eigenstate, conforming with the previous analysis for the gaussian wave packet. We can argue that any quantum state prepared for a local observer should be an eigenstate of the observer's proper time. If so he cannot say what is the exact value of the black hole mass when he plunges into black hole, because the black hole mass and the proper time are not simultaneously diagolanizable.

6 Summary and Discussions

We have proposed a criterion for quantum fluctuation to smear out spacetime singularities which appear in classical gravity. That is, the spacetime is said to be smeared out if the quantum mechanically defined generalized affine length is infinite for a generic curve approaching the classical singularity. An explicit example is demonstrated in the (2+1)-dimensional circular symmetric black

hole. In this model, the computation of the Wilson-line becomes trivial near the black hole origin, where the spin connection becomes flat.

At this stage, we do not claim that the singularities are always wiped away. Probably it depends on quantum states and also types of singularity in classical solutions as well as Lagrangian models. We can even imagine the cases that the spacetime can be extendible in quantum gravity though it cannot classically in analogy to tunneling phenomena. This is beyond the scope of the present work. Without doubt, the physically interesting case is the curvature singularity which appears in the classical solutions of black hole and of cosmology. However, in this case the path ordered product is non-trivial. In general evaluation of the expectation value of the Wilson-line object may require some non-perturbative machinery in quantum gravity, possibly numerical method.

In the classical relativity, the spacetime is singular if at least one causal curve is b-incomplete. It seems to the present author that in quantum gravity "at least one causal curve" should be replaced by "a generic curve", because a single curve has a measure zero contribution to the path integral, when we quantize the position of a particle, though in the present work we fixed the particle trajectory in the coordinate space in analogy to the Wilson loop criterion of the phase of gauge theories. This belief is already included in the concluding statement of this section. The weakness of the definition proposed in this paper is that we have to refer to the classical theory to study the behavior of the generalized affine parameter near the singularity. Without the global spacetime structure obtained by the classical analysis, we cannot say where is the singularity let alone its quantum smearing. At the moment the present author has no idea how to proceed without classical solution.

References

[1] S. W. Hawking and G.F.R. Ellis, *Large Scale Structure of Spacetime* , Cambridge University Press, (1973)

[2] B.G. Schmidt, *J. Gen.Rel.and Grav.* **1** (1971) 269

[3] M. Bañados, C. Teitelboim and J. Zanneli, *Phys. Rev. Lett.* **69** (1992) 1849.

[4] S. Carlip and J.E. Nelson,
Comparative Quantizations of (2+1)-dimensional Gravity, UCD preprint , gr-qc/9411031.

[5] S. Carlip and C. Teitelboim, *Aspects of Black Hole Quantum Mechanics and Thermodynamics in 2+1 Dimensions*, UCD-94-13, gr-qc/9405070.

Wave Function of Black Hole Decay

Akira Tomimatsu

Department of Physics, Nagoya University, Chikusa-ku, Nagoya 464-01, Japan

Abstract

Based on the Hamiltonian formulation for self-similar gravitational collapse of a massless scalar field, we construct a minisuperspace model of quantum black holes. We study a tunneling solution of the wave function satisfying the Schrödinger equation. The quantum decay of black hole states into scattering states of outgoing scalar waves is found in terms of the time evolution of the wave function.

I. INTRODUCTION

The quantum instability of black holes due to the Hawking radiation remains as one of the most important problems in field theories. The two-dimensional models have been developed by neglecting the quantum fluctuations of the metric and calculating only the back reaction of the radiation. In this paper we consider spherically symmmetric gravitational collapse of a massless scalar field in four-dimensional spacetime and treat quantum-mechanically the metric as well as the matter field. In the framework of the canonical quantization procedure, the spherically symmetric system is described by a wave function, which is defined on the superspace of metrics and scalar field configurations. The direct application of the usual Hamiltonian formulation should lead to the Wheeler-DeWitt equation for the wave function. Even if the fields are assumed to be spherically symmetric, it would of course be very difficult to solve the functional differetial equation in full generality. To avoid this mathematical difficulty and pick up interesting informations from the wave function, we must develop a tractable minisuperspace model for the spherical collapse. Our key idea is to restrict the metric components and the scalar field to a self-similar functional form.

In classical general relativity there exist one-parameter families of solutions of the Einstein-scalar equations with initial data of ingoing wave packets. The important property is that while weak fields bounce and disperse to infinity, strong fields form a black

hole [1]. A critical parameter value separates the supercritical (black hole) solutions from the subcritical (dispersed wave) solutions. The self-similar family originally derived by Roberts [2] is a simple and analytical example to observe such dynamical effects [3]. In quantum version of the self-similar model we regard such supercritical and subcritical solutions as classical trajectories on the minisuperspace. Quantum fluctuations of the trajectories will enhance the dispersive effect of initially ingoing scalar waves, and one may find a tunneling wave function which allows initial supercritical states to evolve finally into outgoing wave states without leaving black hole states.

The main purpose of this paper is to give a brief summary on quantum mechanics of the spherical collapse in the context of our self-similar minisuperspace model. The full version will be published elsewhere. In Sec. II we construct the canonical formulation for the dynamical variables. By virtue of the restricted choice of coordinates for self-similarity, the system is reduced to its true dynamical degrees of freedom without introducing a Hamiltonian constraint. In this ADM quantization we obtain the Schrödinger equation instead of the Wheeler-DeWitt equation to describe the evolution of the wave function. The Hamiltonian operator is used to define quantum states corresponding to the supercritical and subcritical solutions. In Sec. III we solve the Schrödinger equation by giving the initial data of black hole states. It is concluded that our model succeeds in proposing the wave function which reveals a quantum process of black hole decay.

II. QUANTUM SELF-SIMILAR MODEL

We consider the Einstein-scalar action for the metric g_{ab} plus the massless scalar field ϕ (in units $G = c = 1$), which is given by

$$I = -\frac{1}{16\pi}\int d^4x\sqrt{-g}(R + 2\partial^a\phi\partial_a\phi) \ . \tag{1}$$

In spherical symmetry, the line-element may be written in double-null form as

$$ds^2 = -2hdudv + r^2 d\Omega^2 \ , \tag{2}$$

where $d\Omega^2$ refers to the unit sphere and h and r depend on the retarded and advanced null coordinates u and v. A time coordinate defined by $\xi = -v/u$ which runs in the range $0 < \xi < \infty$ is used to assume the self-similarity of the form

$$h = h(\xi) \ , \ r = -uf(\xi) \ , \ \phi = \phi(\xi) \ , \tag{3}$$

where the positive variable f is introduced as a self-similar field instead of the radius r. The action (1) generates the Hamiltonian which contains only the kinetic terms as follows,

$$H = \frac{1}{2l^2}(f^{-2}\Pi_\phi^2 - f^{-1}\Pi_f f \Pi_f) , \tag{4}$$

where l is an arbitrary parameter with dimension of length. Note that the gravity part of the kinetic terms becomes negative. Our choice of coordinates leaves just the two degrees of freedom, because h turns out to be a constant of motion for the Hamiltonian.

In canonical quantization we replace the momenta conjugate to f and ϕ by the operators

$$\Pi_f = \frac{l_p^2}{i}\frac{\partial}{\partial f} , \ \Pi_\phi = \frac{l_p^2}{i}\frac{\partial}{\partial \phi} , \tag{5}$$

where l_p is the Planck length. Though the Hamiltonian operator contains the ambiguity in the ordering of factors f and $\partial/\partial f$, for mathematical simplicity we assume the form written by (4). Then, because the momentum operator Π_ϕ is commutable with H, we represent the Hamiltonian eigenfunction as follows,

$$\Psi_E = A_E(f)\exp(ik\phi) , \tag{6}$$

which satisfy the equations

$$H\Psi_E = l_p^2 E\Psi_E , \ \Pi_\phi\Psi_E = l_p^2 k\Psi_E \tag{7}$$

with the dimensionless eigenvalues k and E. To eliminate the constants l and l_p from the mathematical expressions, we rewrite lf/l_p simply by f in the following. For $E > 0$ we obtain a black hole state corresponding to the classical supercritical solution. Because the region $f \to \infty$ in the minisuperspace is classically forbidden, the eigenfunction A_E is given by the modified Bessel function

$$A_E = A_0(E,k)K_{ik}(f\sqrt{2E}) , \tag{8}$$

which decreases exponentially at large f. For $E < 0$ the eigenfunction A_E has two linearly independent oscillatory solutions written by the Hankel functions $H_{ik}^{(1)}(f\sqrt{-2E})$ and $H_{ik}^{(2)}(f\sqrt{-2E})$. The latter solution corresponds to the subcritical state of the spherical collapse. Note that the function $H_{ik}^{(2)}(f\sqrt{-2E})$ reduces to the WKB approximate form e^{iS} in the limit $f \to \infty$, which describes the classical dynamics of f according to the equation $\Pi_f = \partial S/\partial f = -\sqrt{-2E}$. The negative value of $\Pi_f = -df/d\xi$ means the evolution due to outgoing scalar waves at large ξ. Then the former solution describes a

time reversal of the subcritical process, in which at large ξ scalar waves propagate inwards rather than outwards. These Hamiltonian eigenfunctions which behave like a bound state and a scattering state constitute a basic set to study the properties of the wave function satisfying the Schrödinger equation.

III. BLACK HOLE DECAY

The new aspect of the quantum system obtained here is that the Hamiltonian operator has the form of a Klein-Gordon equation in two dimensions. Then we can obtain the black hole state (8) as a bound state without any effect of a potential term. However such a state will not remain stable under a time evolution of the wave function. In fact we find the breakdown of orthogonality of the Hamiltonian eigenstates corresponding to different eigenvalues E and E' as follows,

$$K_{ik}(f\sqrt{2E}) \;=\; \frac{1}{2}\int_{-\infty}^{0}(\frac{-E'}{E})^{ik/2}(E-E')^{-1}J_{ik}(f\sqrt{-2E'})dE' \;, \tag{9}$$

where J_{ik} is the Bessel function. This motivates us to explain the black hole state with $E > 0$ as a wave packet defined by a superposition of the scattering states with $E' < 0$. By virtue of the expansion (9) we can consider two different types of time evolution of the wave packet according to the Schrödinger equation

$$i\frac{\partial\Psi}{\partial\xi} \;=\; H\Psi \;, \tag{10}$$

where $\Psi = K_{ik}(f\sqrt{2E})$ at $\xi = 0$. If all the scattering states corresponding to various eigenvalues E' evolve coherently, we obtain

$$\Psi \;=\; \exp(-i\xi E)K_{ik}(f\sqrt{2E})e^{ik\phi} \;, \tag{11}$$

which means that the initial black hole state never decays. For a distant observer who cannot receive any information inside the black hole, such a coherence may break down. Another possible way of the evolution is

$$\Psi \;=\; \frac{1}{2}\int_{-\infty}^{0}\exp(-i\xi E')(\frac{-E'}{E})^{ik/2}(E-E')^{-1}J_{ik}(f\sqrt{-2E'})dE'e^{ik\phi} \;. \tag{12}$$

Now each scattering state evolves incoherently, and the packet will begin to spread. We can evaluate the integral with respect to E' in (12), by using the Wick rotation $\tau = -i\xi$ of the time coordinate. This tunneling solution

$$\Psi \;=\; \frac{1}{2}e^{ik\phi}(f^2/2E)^{ik/2}e^{E\tau}\int_{\tau}^{\infty}d\tau\tau^{-(1+ik)}e^{-(2E\tau^2+f^2)/2\tau)} \;, \tag{13}$$

reduces to

$$\Psi \sim \exp(-if^2/2\xi) \times \exp(ik\phi) \tag{14}$$

at large ξ. Recall that outgoing scalar waves dominate in the subcritical evolution at large ξ. The subcritical Hamiltonian eigenstate behaves asymptotically as follows,

$$\exp(-i\xi E) H^{(2)}_{ik}(f\sqrt{-2E}) \sim \exp(-if^2/2\xi) \ , \tag{15}$$

where E is eliminated by the equation $f = \xi\sqrt{-2E}$ which is valid on the classical trajectory at large ξ. Though the wave function Ψ is not a Hamiltonian eigenfunction, the asymptotic form (14) (which should be compared with (15)) clearly shows that the initial black hole state completely disappears to generate outgoing scalar waves.

In summary, for the quantum self-similar collapse of a scalar field we derived the wave function (13) of black hole decay. The decay mechanism is essentially due to the principle of superposition in quantum mechanics, which allows us to treat the initial black hole state as a wave packet of various scattering states. In this simple self-similar model no force can work to keep the wave packet stable, and if the incoherent evolution (12) goes on, the black hole decay accompanied with the generation of outgoing scalar waves is an inevitable quantum process.

ACKNOWLEDGMENTS

I would like to thank Yoshimi Oshiro and Kouji Nakamura for valuable discussions.

REFERENCES

[1] D. S. Goldwirth and T. Piran, Phys. Rev. D **36**, 3575 (1987).

[2] M. D. Roberts, Gen. Rel. Grav. **21**, 907 (1989).

[3] Y. Oshiro, K. Nakamura and A. Tomimatsu, Prog. Theor. Phys. **91**, 1265, (1994).

Four Dimensional Quantum Topology Changes

Masaru Siino*
Department of Physics, Tokyo Institute of Technology
Meguroku, Tokyo 152, Japan
Department of Physics, Kyoto University
Sakyouku, Kyoto 606-01, Japan

We investigate topology-changing processes in 4-dimensional quantum gravity with a negative cosmological constant. By playing the "gluing-polytope game" for hyperbolic geometry, we explicitly construct instanton-like solutions without singularity. Because of cusps, these solutions are non-compact but have a finite volume. Then we evaluate topology change amplitudes in the WKB approximation in terms of the volume of these solution.

I. INTRODUCTION

The works of the many authors [1] about the change of the topology of the universe tell that it is an unusual phenomenon. In the situation where we need quantum gravity, however, topology changing process is essential, for example Coleman's mechanism, the birth of the universe, the evaporation of a black hole and so on. Further, the possibilities of the topology change even in the classical gravity provides important physics (Lorentz cobordism theory and time-machine).

Some recent works demonstrated that the topology changes are possible in the physical spacetime. In 3-dimensional spacetime with a negative cosmological constant, two cases with the topology changes were investigated. One of the present author (M. S.) [2] showed that the compactified three dimensional black hole (the higher genus universe with negative cosmological constant) provides the topology change by its analytical continuation around the coordinate singularity of the spacetime. On the other hand, in the quantum gravity, Fujiwara, Higuchi, Hosoya, Mishima and one of the present author (M. S.) [3] constructed the topology changing solutions by quantum tunneling. To discuss real topology changes these works should be applied to the four dimensional spacetime. The former will be adapted to the (3+1)-dimensional compact hyperbolic cosmology [4]. Then, the purpose of this paper is the investigation of the quantum topology change through the tunneling process in the four dimensions.

According to Gibbons and Hartle [5], the quantum tunneling spacetime is semi-classically approximated by a Riemannian manifold with totally geodesic boundaries. In Ref. [3] such 3-manifolds were constructed from regular truncated polyhedra embedded into a hyperbolic 3-space. In this paper we construct topology changing solutions of the Einstein equation using 4-dimensional regular truncated polytope embedded into a hyperbolic 4-space [6].

In the next section we briefly review about the quantum tunneling of a spacetime. The section 3 gives topology changing solutions. We investigate their amplitudes in the section 4. The final section is devoted to a summary and discussions.

II. QUANTUM TUNNELING OF SPACETIME

A topology changing process is characterized by two spatial hypersurfaces, an initial hypersurface Σ_i and a final hypersurface Σ_f (they may be composed of some disconnected components.). Gibbons and Hartle [5] stated that the tunneling process is approximated by a Riemannian manifold which has the boundaries Σ_i and Σ_f. In the ADM-formalism with a real lapse function N and a real shift vector N^i, the spatial hypersurface has a set of valuables, a spatial metric h_{ij} and an extrinsic curvature K_{ij}. In a semi-classical picture, an ordinary spacetime manifold and a quantum tunneling manifold are connected on the hypersurface Σ, (see Fig.1).

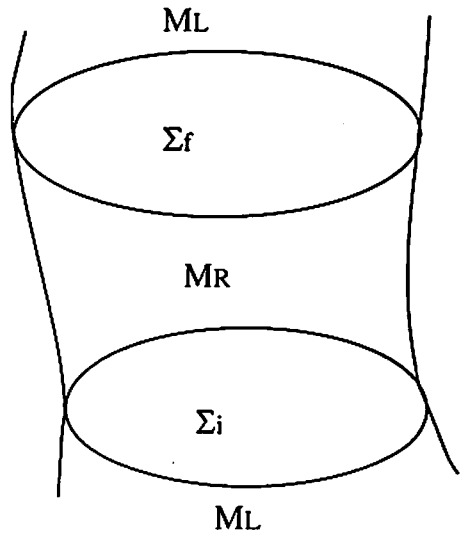

FIG. 1. A manifold with a Euclidean signature M_R intermediates the two manifolds with a Lorentz signature M_L through $\Sigma_{i,f}$

Since there are a time τ in the quantum tunneling manifold M_E with a Euclidean signature and a time t in the ordinary spacetime manifold M_L with a Lorentz signature, there are two definitions of the extrinsic curvature of Σ for M_E and M_L,

$$K_{ij} = -\frac{1}{2N}\left(\frac{\partial h_{ij}}{\partial t} - D_{(i}N_{j)}\right) \quad for M_L \tag{1}$$

$$= -\frac{1}{2N}\left(\frac{\partial h_{ij}}{\partial \tau} - D_{(i}N_{j)}\right) \quad for M_E, \tag{2}$$

where D_i is a covariant derivative in terms of h_{ij}. Since the time τ in M_E is analytically continued to the time t in M_L as $\tau = it$ at Σ, the analytical continuation of geometrical valuables, h_{ij} and K_{ij}, requires vanishing K_{ij} and N_i at Σ. We call these boundary hypersurfaces with vanishing extrinsic curvature as totally geodesic boundaries.

For simplicity, in this paper, we consider spacetimes with constant curvature where the Weyl tensor vanishes everywhere. The Riemannian manifold (tunneling manifold) becomes locally isometric to any one case of S^4 (4-sphere), R^4 (4-plane) or H^4 (4-hyperboloid). In Ref. [5], however, it is also stated that if we require that the Σ_i and Σ_f are disconnected, the spacetime should at some points violate an energy condition, which demands

$$R_{\mu\nu}V^\mu V^\nu > 0 \tag{3}$$

for all vector V^μ. Therefore we can exclude S^4 from our considerations of topology changing manifolds because the curvature is positive.

From the Gauss-Codazzi equation, the vanishing extrinsic curvature makes Σ_i and Σ_f also have a constant curvature (locally isometric to S^3, R^3 or H^3). To consider the change of topology we need the variety of the topology. If we choose R^4, the topology of Σ is so restricted. On the contrary, since the variety of hyperbolic 3-manifolds (Riemannian manifolds locally isometric to H^3) is very rich, we shall consider the vacuum spacetime with negative cosmological constant (locally isometric to H^4). Then the following question arises;

> Can we construct a hyperbolic 4-manifold with totally geodesic boundaries Σ_i and Σ_f which have different topologies?

Any 4-manifold with the hyperbolic structure is the quotient manifold of a 4-hyperboloid H^4 with a discrete subgroup of its isometry group $SO(4,1)$. The fundamental region of this quotient 4-manifolds is a 4-polytope embedded into H^4. The boundaries of the fundamental region are identified with each other and the fundamental region forms manifold. If the 4-manifold has boundaries, some of the boundaries of the foundamental region are not identified and form the boundary of the 4-manifold. Following the procedure of 3-dimensional case [3], we determine the fundamental region and the identifications of its boundaries in the hyperbolic geometry [6].

A. Hyperbolic Geometry and Klein Model

In our construction, we use n-dimensional Klein model as the model of hyperbolic geometry. To give a hyperbolic structure to 4-dimensional polytopes we embed them into the 4-Klein model. The n-Klein model is a model on an open n-disk

$$D^n = \{x^i \in R^n | x^i x_i < 1\}, \tag{4}$$

in which a metric is

$$ds^2 = \frac{1}{1-r^2}\left(\frac{dr^2}{1-r^2} + r^2 d\Omega^2_{n-1}\right). \tag{5}$$

When r goes to 1, one approaches to a sphere at infinity ∂D^n. This metric gives a constant sectional curvature -1 and has hyperbolic structures. Then this Klein-mode is isometric to the well-known n-dimensional open-universe ($k = -1$).

Here we briefly review the virtues of this model. First, it is easily confirmed that all totally geodesic (extrinsic curvature vanishing) $m(< n)$-hypersurface becomes m-plane in this model. Then we can construct totally geodesic boundaries by correcting such m-planes. Of course we know that each m-planes can exactly be identified by the isometry of this model $SO(n,1)$. Further, the most important property arises when we consider points on the outside of the sphere at infinity ∂D^n. As depicted in Fig.2, most of parallel $(n-1)$-plane, not crossing on the Klein model D^n, cross on the outside of the sphere at infinity ∂D^n.

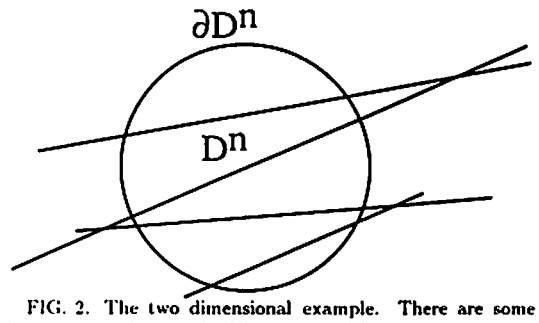

FIG. 2. The two dimensional example. There are some lines not crossing on the Klein model D^n. They are palarell lines and cross on the outside of the sphere at infinity ∂D^n.

Suppose some $(n-1)$-planes share only one outside point a. There ought to be $(n-1)$-dimensional cone with thevertex a, which is tangent to the sphere at infinity Then there also exists $(n-1)$-plane through the touching points of the cone and the sphere at infinity (examplifyed in Fig.3). The virtue of the Klein model guarantees that this $(n-1)$-plane is orthogonal to all original planes.

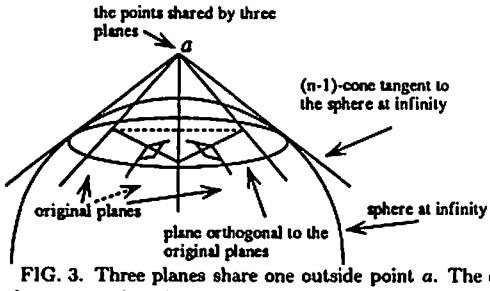

FIG. 3. Three planes share one outside point a. The cone whose vertex is a, is tangent to the sphere at infinity. Then the plane through the touching points is perpendicular to the three planes.

These facts make our procedure possible. For example, we show a simple example in a 2-Klein model of H^2. In Fig.4, two regular triangles are drawn in the 2-Klein model so that each vertex protrudes from D^2. As mentioned above, we can draw dotted lines which are orthogonal to the edges of the triangle and truncate off the vertices along these dotted lines. We call such a truncation as a regular truncation. Gluing the triangles for the labeled edges to match, we get a hyperbolic space with three S^1 boundaries. Since the line composing the boundary is geodesic and orthogonal to the edges of the regular triangle, the boundary becomes totally geodesic S^1 [7].

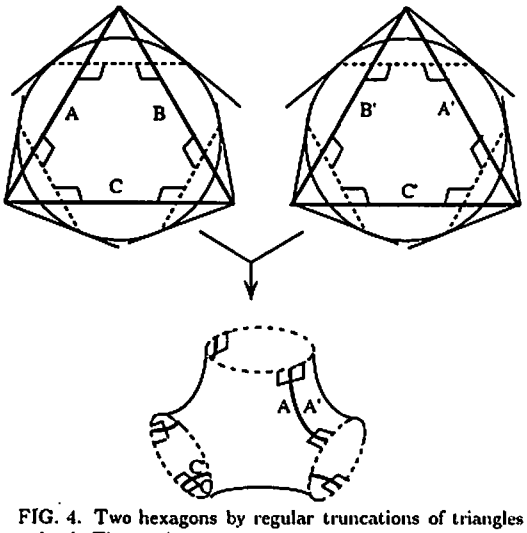

FIG. 4. Two hexagons by regular truncations of triangles are glued. The resultant space is one of the simplest topology changing manifolds.

Finally we should remark upon the relation between the size of an object surrounded by planes and the angles between these planes. In the hyperbolic geometry, if we enlarge an object, the angles decreases. When the size approaches zero, the angle becomes the value in Euclidean geometry. The angle on the sphere at infinity ∂D^n vanishes and we have no angle in the outside of ∂D^n.

B. Four Dimensional Polytopes

First we prepare regular truncated 4-polytopes in the 4-Klein model of 4-hyperbolic space. Regular 4-polytopes are 5-cell, 8-cell, 16-cell, 24-cell, 120-cell and 600-cell. The size of these polytopes in the 4-Klein model are restricted as follows. For regular truncation of the vertices of the polytopes we must impose following two conditions to the size of the polytopes.

1) There are all vertices on the outside of the sphere at infinity.

2) The edges of polytopes does not belong completely to the outside of the sphere at infinity.

From above conditions, a single vertex shared by 3-planes that are cells bounding the polytope can be regularly truncated off. The vertex determines a unique 3-plane which is perpendicular to the polyhedra bounding polytope as mentioned in the previous subsection. Also as mentioned in the previous subsection, the dicellular angle (the angle between two adjacent polyhedra in a 4-dimensional space) decreases as the size of the polytope increases in the hyperbolic geometry. To produce regular and smooth structure after gluing of polytopes the dicellular angle must be $2\pi/n$ (n is an integer). Then the size of the polytopes are restricted further. From a geometrical calculation we find the allowed dicellular angles of the polytopes. The allowed polytopes are shown in the following table.

polytope	dicellular angle	polyhedra made by truncation	solid angle around the vertices
5-cell	$\pi/3$	five tetrahedra	0
8-cell	$\pi/3$	sixteen tetrahedra	0
16-cell	$\pi/2$	eight octahedra	0
24-cell	$2\pi/5$	twenty-four octahedra	$4\pi/20$
	$\pi/3$	twenty-four octahedra	0
120-cell	$\pi/3$	600 tetrahedra	0
600-cell	$2\pi/3$	120 icosahedra	$4\pi/12$

The first column is the name of polytope. Allowed dicellular angles are on the second column. Here it should be noted that the edges of the polytope are tangent to the sphere at infinity except for the cases of the 24-cell with the dicellular angle being $2\pi/5$ and the 600-cell with the dicellular angle being $2\pi/3$. Therefore after regular truncation, the polytopes have several points at infinity and are non-compact (examplified for the case of 8-cell in the next subsection). In this paper, we only consider these non-compact case. By admitting the points at infinity, the construction becomes much easier. On those points at infinity, the restriction that the spacetime should be a manifold around the vertex of the truncated polytope does not work.

In the next subsection we demonstrate the construction of the topology changing Euclidean solution from twelve 8-cell's [8] which are 4-polytopes bounded by eight congruent hexahedra. The development of the 8-cell on 3-space is shown in Fig.5. Gluing faces in four dimensions according to arrows in Fig.5 we get a 4-dimensional polytope surrounded by these eight hexahedra, which has sixteen vertices.

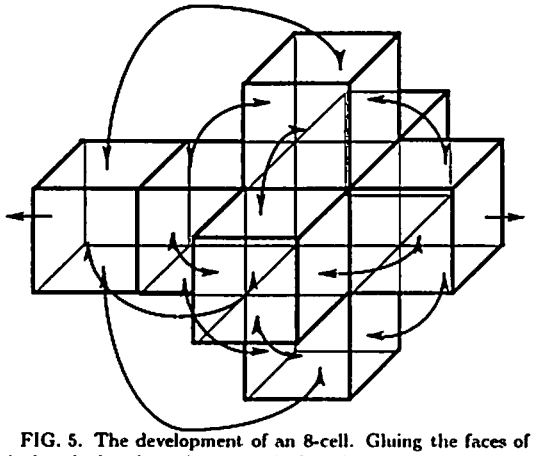

FIG. 5. The development of an 8-cell. Gluing the faces of the hexahedra along the arrows in four dimensions, we get the 8-cell of a 4-dimensional polytope.

C. Construction from 8-cell

The size of the embedded 8-cell is determined so that its dicellular angles (the angle between two neighboring hexahedra in 4-dimensions) becomes $\pi/3$. Since in this size every vertices are out of a sphere at infinity ∂D^4 and edges of the 8-cell are tangent to the sphere at infinity. Each hexahedron of the 8-cell is embedded into a 3-Klein model (sub-model of the 4-projective model) as shown Fig.6. Also in this three dimensional figure, every vertices are out of the sphere at infinity ∂D^3 and all edges are tangent to the sphere.

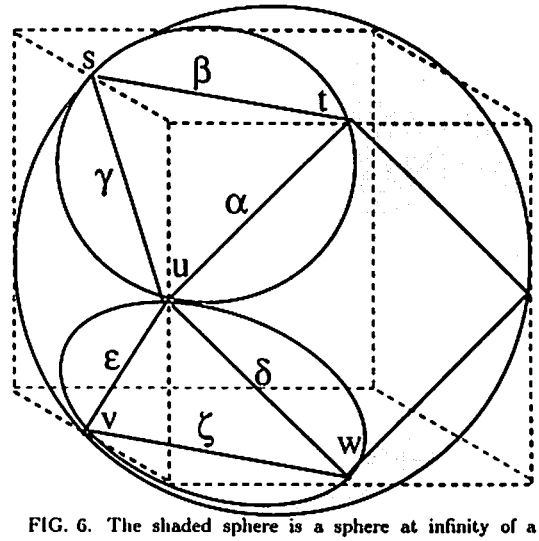

FIG. 6. The shaded sphere is a sphere at infinity of a 3-projective model. Each edge of the hexahedra is tangent to the sphere at s, t, u.... The sphere is cut by planes through s, t, u.... Along these planes we truncate the vertices of the hexahedron.

To get a totally geodesic boundary hypersurface, we truncate each vertex of the 8-cell in the same way to the 2-dimensional example. Let us pay attention to the four hexahedra having a vertex in common in Fig.5. A property of the Klein model guarantees the existence of a unique 3-hyperplane which is perpendicular to all of the four hexahedra as mentioned above. We cut the sixteen vertices of the 8-cell along these 3-hyperplanes to get a regular truncated 8-cell embedded completely in the 4-projective model. These truncations of 8-cell induce truncations on each hexahedron bounding the 8-cell. The resultant hexahedron is shown in Fig.6. On the section by the truncation of the vertex of the 8-cell a triangle appears and its three vertices (s, t, u) are on the sphere at infinity ∂D^3. It is noted that the triangles share vertices with adjacent triangles (the vertex (u) is shared in Fig.6) and all original edges of the hexahedron are truncated off. Because four hexahedra share one vertex in an 8-cell (see Fig.7), each 3-boundary of the 8-cell made by the truncation is bounded by four triangles. From Fig.7 we see that the 3-boundary is a tetrahedron whose vertices are on the sphere at infinity. Since each tetrahedron is orthogonal to the hexahedra in the 4-hyperbolic space, the dihedral angle of the tetrahedron is equal to the dicellular angle of the 8-cell $\pi/3$. The volume integration tells that such tetrahedra have a finite volume [6] though they are non-compact. A single 8-cell includes sixteen vertices and has sixteen tetrahedra on the boundary after regular truncation.

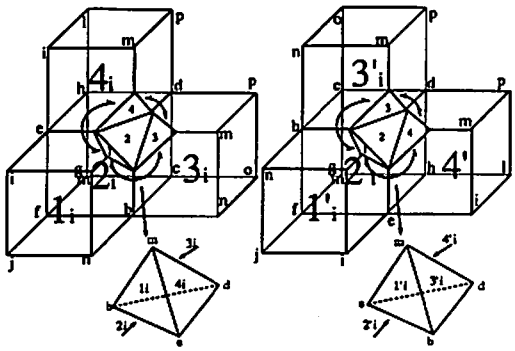

FIG. 7. Four hexahedra meet at a vertex. When we truncate the vertex, a tetrahedron appears. We label the faces and the vertices of the tetrahedra at the vertices (a) by the number of the cell which the face belongs to and the vertices of the 8-cell's on the opposite side of (a), respectively.

Hence the construction requires us to find certain gluing between the hexahedra of appropriate numbers of regular truncated hyperbolic 8-cell's, so that the resultant space becomes smooth manifold. First we try a natural extension of the above mentioned simple 2-dimensional example to this 4-dimensional case. We prepare two regular truncated 8-cell's and they are reflection symmetric as depicted in Fig.8.

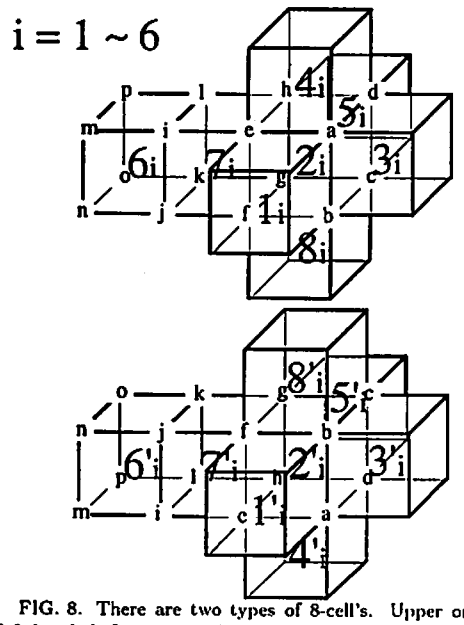

FIG. 8. There are two types of 8-cell's. Upper ones are left-handed. Lower ones (with prime) are right-handed. The corresponding cells (for example, 1_1 and $1'_1$, 4_1 and $4'_3$ ...) are identified.

Gluing the hexahedra $X(1 \sim 8)$ and X' so that all vertices $(a) \sim (p)$ match, we get 4-topological space with sixteen boundaries. To see the smoothness of this 4-topological space, it is sufficient to check the smoothness on the boundaries. The inside of a truncated hyperbolic 8-cell is smooth and regular. Further we can exactly glue the two hexahedra because the glued two hexahedra are totally geodesic. Therefore singular structures can appear only on the faces, edges and vertices of each hexahedra. From Fig.6 we see that if they are singular, the singularity must appear on the boundary tetrahedra. The gluing of the hexahedra induces the gluing on the boundary tetrahedra. Fig.7, for example, shows the gluing of two tetrahedra corresponding to vertex (a) both in the unprimed 8-cell and the primed 8-cell is determined by the identifications of the truncated hexahedra. Since each umprimed hexahedra is identified with its primed partner, each face of unprimed tetrahedra are glued with its primed partner so that all vertices match. In this configuration, the topology of this space composed of the two tetrahedra is S^3. Nevertheless we have only $2\pi/3$-rotation after gluing around each edges of the tetrahedra, since only two edges of the tetrahedra with a dihedral angle being $\pi/3$ are identified into one edge. There is a singularity by the dificit angle.

To avoid this singularity on the edges, we consider a branched covering space of this singular space. The appropriate branched covering space can be given by sixth-cover (twelve tetrahedra) of the original singular space. The faces and vertices of the twelve tetrahedra are labeled as Fig.9. We call these primed tetrahedra as right-handed and the others as left-handed. The following pairs of the face of right-handed tetrahedra and the face of the left-handed tetrahedra are glued so that each labeled vertices match.

$$\begin{array}{llll} A_1 - A'_1 & B_1 - B'_3 & C_1 - C'_2 & D_1 - D'_4 \\ A_2 - A'_2 & B_2 - B'_1 & C_2 - C'_4 & D_2 - D'_3 \\ A_3 - A'_3 & B_3 - B'_2 & C_3 - C'_5 & D_3 - D'_6 \\ A_4 - A'_4 & B_4 - B'_6 & C_4 - C'_1 & D_4 - D'_5 \\ A_5 - A'_5 & B_5 - B'_4 & C_5 - C'_6 & D_5 - D'_1 \\ A_6 - A'_6 & B_6 - B'_5 & C_6 - C'_3 & D_6 - D'_2 \end{array} \tag{6}$$

For instance, A_1 is matched with A'_1. All the vertices p_1, p_2, p_3 of A_1 are identified to the vertices p_1, p_2, p_3 of A'_1, respectively.

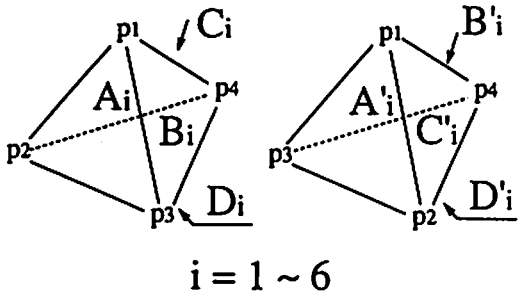

FIG. 9. We consider six left-handed tetrahedra and six right-handed tetrahedra. Twelve tetrahedra form M_{B8}.

Fig.10 shows that the consistency of the gluing around all edges. There remain twelve edges after gluing (6). Each six dihedral angles meet at one edge. There is no dificit angle since a single dihedral angle is $\pi/3$.

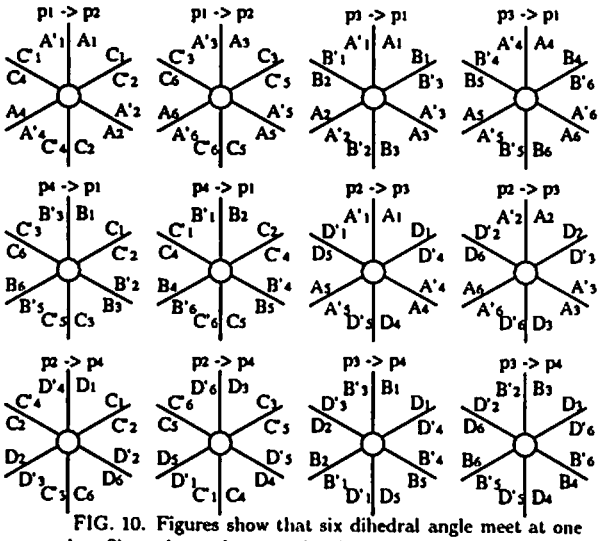

FIG. 10. Figures show that six dihedral angle meet at one edge. Since the angles are $\pi/3$, there is no dificit angle.

On the other hand, the vertices of the tetrahedra are on the sphere at infinity ∂D^3. By the gluing these vertices are identified into four points at infinity, p_1, p_2, p_3, p_4. Such a point at infinity is called as a cusp of the hyperbolic manifold and is no singularity, topologically looking like a torus cross a half-open interval (see Fig.11). There is no singular structure and the space composed of twelve tetrahedra is non-compact smooth manifold M_{B8}.

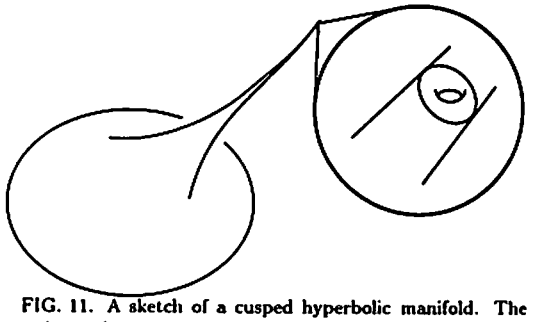

FIG. 11. A sketch of a cusped hyperbolic manifold. The cusp is topologically looks like a torus cross a half-open interval.

The cusp will not cause any physical problem because one cannot observe the infinity of the universe. Further the existence of such points at infinity makes the manifold pretty flexible. If the vertices were at finite distance, also another restriction that space should be smooth around the vertices, would be imposed. This restriction makes manifolds so rigid. In fact, we know much more cusped 3-manifolds than compact 3-manifolds [9]. Hence, admitting the cusp to our manifold we get the following most simple example of topology changing solutions.

Now we expect that the branched covering proceeded above can be straightforwardly extended to the whole of 8-cell's. Since the previous identification of two 8-cell's provides the singular boundaries whose sixth-covers are smooth manifold, the sixth-cover of the previous identification of 8-cell's will provide smooth boundary manifold M_{B8}'s. We prepare six pairs of a unprimed 8-cell and a primed 8-cell as Fig.8 (the pairs are labeled by $i = 1 \sim 6$.). The each vertices and the cells (hexahedra) of the 8-cell's are labeled as Fig.8. All following gluing will be done matching these labeled vertices. For vertex (a), the gluing of related hexahedra (cell1 $\sim$ 4) is determined so that it induces a gluing which is equivalent to (6) forming M_{B8}, on tetrahedra made by the truncation of the vertex (a)'s. Fig.7 shows these tetrahedra from the vertices (a)'s. In this figure, the face of the tetrahedra are labeled by the cell which the face belongs to and the vertices of tetrahedra have the same label as the adjacent vertices of the 8-cell. From Fig.7 and 9 we find a correspondence, $1_i \equiv A_i$, $4_i \equiv B_i$, $3_i \equiv C_i$, $2_i \equiv D_i$. Then their gluings are determined as

$$\begin{array}{llll} 1_1 - 1'_1 & 4_1 - 4'_3 & 3_1 - 3'_2 & 2_1 - 2'_4 \\ 1_2 - 1'_2 & 4_2 - 4'_1 & 3_2 - 3'_4 & 2_2 - 2'_3 \\ 1_3 - 1'_3 & 4_3 - 4'_2 & 3_3 - 3'_5 & 2_3 - 2'_6 \\ 1_4 - 1'_4 & 4_4 - 4'_6 & 3_4 - 3'_1 & 2_4 - 2'_5 \\ 1_5 - 1'_5 & 4_5 - 4'_4 & 3_5 - 3'_6 & 2_5 - 2'_1 \\ 1_6 - 1'_6 & 4_6 - 4'_5 & 3_6 - 3'_3 & 2_6 - 2'_2 \ . \end{array} \tag{7}$$

It is non-trivial problem whether it is possible for the tetrahedra of the other vertices $(b) \sim (p)$ to form M_{B8} by the appropriate choice of the gluing of the other cells (cell5 $\sim$ 8). Determining the other gluings as follows,

we see the adjacent two tetrahedra, for example (a) and (b) (see Fig.12), are reflection symmetric because of the symmetry of the 8-cell.

$$\begin{array}{llll} 5_1-5'_1 & 8_1-8'_3 & 7_1-7'_2 & 6_1-6'_4 \\ 5_2-5'_2 & 8_2-8'_1 & 7_2-7'_4 & 6_2-6'_3 \\ 5_3-5'_3 & 8_3-8'_2 & 7_3-7'_5 & 6_3-6'_6 \\ 5_4-5'_4 & 8_4-8'_6 & 7_4-7'_1 & 6_4-6'_5 \\ 5_5-5'_5 & 8_5-8'_4 & 7_5-7'_6 & 6_5-6'_1 \\ 5_6-5'_6 & 8_6-8'_5 & 7_6-7'_3 & 6_6-6'_2 \end{array} \tag{8}$$

Since the reflection of M_{B8} is M_{B8}, each twelve tetrahedra, forms M_{B8} of (b) $\sim$ (p). Therefore the glued twelve 8-cell's have sixteen M_{B8}'s on their boundary. Here it should be noted that the fact that the tetrahedra are orthogonal to the cells (hexahedra) of the 8-cell gurantees that the M_{B8} is smooth at their joint. Then M_{B8} is totally geodesic smooth manifold in the H^4.

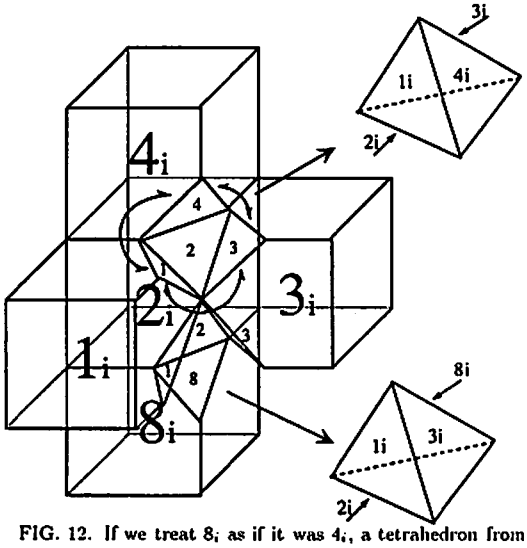

FIG. 12. If we treat 8_i as if it was 4_i, a tetrahedron from vertex (a) and a tetrahedon from vertex (b) would be reflection symmetric.

Of course these identifications are orientation preserving isometry transformation because of the reflection symmetry between the unprimed 8-cell's and the primed 8-cell's. The resultant space is orientable.

To check that this 4-space is complete smooth 4-manifold, we consider the neighborhood of faces, edges and vertices. In 4-dimensions, when we turn around each face completely the total angle has to be 2π by consistency. On the boundary 3-hypersurface, however, this amounts to checking the 2π turn around the edges (α, β, γ... in Fig6) of the boundary. This consistency is guaranteed because the boundary is an already checked manifold M_{B8}. The remaining vertex after the regular truncation (s, t, u... in Fig6) causes no problem since they form 4-cusps at infinity. The edges are located only on the boundaries which form 3-manifold after the gluing (α, β, γ... in Fig6). As mentioned above, this does not bring any trouble. Hence this space is a hyperbolic complete smooth 4-manifold with totally geodesic 3-boundaries. The boundaries are sixteen M_{B8}'s.

D. Other Solutions

As shown previously in the table, there are seven kinds of 4-polytopes admitting a regular truncation. Two of them, 24-cell with a dicellular angle being $2\pi/5$ and 600-cell with a dicellular angle $2\pi/3$, are compact and the others are non-compact. We can try our method of twelve non-compact 8-cell's in these non-compact cases. Only, from 16-cell's (sixteen tetrahedra) with a dicellular angle being $\pi/2$ or 24-cell's (twenty-four octahedra) with a dicellular angle being $\pi/3$ we successfully get hyperbolic complete smooth 4-manifolds with totally geodesic 3-boundaries in the similar way to the 8-cell. Four such 16-cell's form a manifold whose 3-boundaries are eight M_{B16}'s with six cusps which is composed of four octahedra. Six 24-cell's also construct a manifold whose 3-boundaries are twenty-four M_{B24}'s with eight cusps which is composed of six hexahedra.

Here we point out a peculiarity of the hyperbolic manifold by reffering to a mathematically known fact. For three or four dimensional hyperbolic manifold $M_{3,4}$, $\pi_1(M_{3,4})$ determines $M_{3,4}$ uniquely up to an isometry and a choice of normalizing constants [11]. This is known as the Mostow rigidity. Then it is valid to determine the H_1 of the hyperbolic manifold in order to distinguish the manifolds, where H_1 is a Abelian group such that $H_1 = \pi_1/[\pi_1, \pi_1]$. To characterize these boundaries topologically we calculate the homology group H_1,

$$H_1(M_{B8}) = Z + Z + Z + Z \tag{9}$$

$$H_1(M_{B16}) = Z + Z + Z + Z + Z + Z \tag{10}$$

$$H_1(M_{B24}) = Z + Z + Z + Z + Z + Z + Z + Z. \tag{11}$$

Clearly they are topologically inequivalent. Since the rank of the free finitely generated abelian group part of H_1 counts the number of two dimensional holes, the latter has more complicated topology than the former [12]. The fact that there is no torsion part is plesant for our universe. It also implies that our construction is so simple. If we had a method which can produce a solution whose boundaries have torsion part, much more solutions would be found.

Incidentally, it is impossible to construct the solution from 5-cell's or 120-cell's in our way. The remaining polytopes are compact. It may be possible to construct a compact topology changing solution from these polytopes though it is more complicated. This is our future problem [10].

III. SUMMARY AND DISCUSSIONS

In this paper, we have found the topology changing solutions by quantum tunneling. Here we summary the results in a following table.

building block	boundary $\Sigma_{i,j}$	$H_1(\Sigma)$
8-cell×12	$16 \times M_{B8}$	Z+Z+Z+Z
16-cell×4	$8 \times M_{B16}$	Z+Z+Z+Z+Z+Z
24-cell×6	$24 \times M_{B24}$	Z+Z+Z+Z+Z+Z+Z+Z

People might be amused for the existence of the cusps. However, it physically causes no problem since the cusps are at infinity and we cannot see. We see only the pattern of spatial periodicity [14]. If we observe the pattern of spatial periodicity as the super large scale strucutre of the universe, we may be able to determine what is the topology of our universe and whether the universe has the cusps or not.

Some people may think that our construction is so restricted. First, the identification is determined so as to preserve the symmetry of the polytope. Further the polytopes are symmetric each other even after the identification. From these restriction, for example, it is not allowed to identify the polyhedra belonging to a single polytope. We have believed that our restriction makes the construction simple. It is likely that there are much more solutions ruled out by the restrictions. To complete the discussion about the topology change by the quantum tunneling, we should include such solutions. The structure of the tunneling manifold will become complicated. The construction by a computer will be needed in such complicated case [10].

When we evaluate the topology changing ampritude, the context of Hartle and Hawking will be used. Originaly, however, the boundary condition of Hartle and Hawking, no-boundary boundary condition, does not accept the existence of the boundary at infinity. In our solutions, the tunneling manifold has cusped boundary at infinity. Since the cusped boundary is infinitly small and the manifold has finite volume, we have accepted the cusped manifold. If we rigorously impose the no-boundary boundary condition, we need compact tunneling manifold. As mentioned above, the compact manifold is difficult to find. We will need wide search of the solution using a computer [10].

Acknowledgments

We would like to thank Professor A. Hosoya and Professor S. Kojima for helpful discussions. One of the authors (M. S.) thanks the Japan Society for the Promotion of Science for financial support. This work was supported in part by the Japanese Grant-in-Aid for Scientific Research Fund of the Ministry of Education, Science and Culture.

[1] R. P. .Geroch, *J. Math. Phys.* **8** (1967) 782, P. Yodzis, *Gen. Rel. Grav.* **4** (1973) 299, D. Gannon, *J. Math. Phys.* **16** (1975) 2364, F. J. Tipler, *Ann. Phys.* **108** (1977) 1, R. D. Sorkin, *Phys. Rev.* **D33** (1986) 978.
[2] M. Siino, *Class. Quantum Grav.* **11** (1994) 1995.
[3] Y. Fujiwara, S. Higuchi, A. Hosoya, T. Mishima and M. Siino, *Phys. Rev.* **D44** (1991) 1756, *Phys. Rev.* **D44** (1991) 1763, *Class. Quantum Grav.* **7** (1992) 163.
[4] A. Ishibashi, T. Koike, M. Siino, in preparation.
[5] G. W. Gibbons and J. B. Hartle, *Phys. Rev.* **D42** (1990) 2458.
[6] W. P. Thurston, *The Geometry and Topology of 3-manifold*, to be published by Princeton University Press, 1978/79.
[7] D. Brill *Euclidean Maxwell-Einstein Theory*, to appear in Luis Witten Festschrift (World Scientific).
[8] H. S. M. Coxeter, *Regular Polytopes*, New York, Dover Publications, 1973.
[9] ftp.geo.ed/pub/game/Snappea
[10] T. Chiba and M. Siino, in preparation.
[11] G. D. Mostow, *Strong Rigidity of Locally Symmetric Spaces, Annals of Mathematics Studies*, Princeton, Princeton University Press, 1973.
[12] C. Nash and S. Sen, *Topology and geometry for physics*, London, Academic Press, 1983.
[13] T. Koike, A. Hosoya and M. Tanimoto
[14] L. Z. Fang and H. Sato, *Gen. Rel. Grav.*17 (1985) 1117

Hirosaki University

January 17, 1995

Equation of Motion in the Slow-Motion Approximation in General Relativity

T. FUTAMASE

Department of Physics, Hirosaki University, Hirosaki, 036, Japan

ABSTRACT

We shall give a review of the present stage of the research on the slow-motion approximation and the equation of motion in general relativity.

1. Introduction

Although the research on the equation of motion of a self-gravitating system in general relativity has a long history, we have not yet obtained a fully satisfactory theoretical picture. The research has been activated by the discovery of binary pulsar system PSR1913+16 at 1975.[1] Various relativistic effects have been observed by analyzing the motion of the system. The most surprising among them was the observation of the orbital period change due to the emission of the graviational radiation. The observed change of the period $\dot{P}_{obs}$ coincides with the theoretical prediction by general relativity $\dot{P}_{G.R}$ with a very good accuracy.

$$\frac{\dot{P}_{G.R}}{\dot{P}_{obs}} = 1.0023 \pm 0.0041$$

The predicted value above is calculated by the so-called quadrupole formula. The formula is based on the slow motion approximation and thus neglects higher order radiation such as the graviatational radiation emitted by the change of the octopole moment of the system. The text book version of the formula predicts how much energy is carried out by graviational radiation from the system to infinity. Sometimes such a version of the formula is called as the far-zone version.[2] In order to obtain the piriod change of the system, one needs to have the equation of motion with radiation damping and to solve it. This can be done as follows.[3] One assumes that the damping is supposed to be described by the reaction force F^i_{react} in the equation of motion and assumes the global conservation of the energy of the following form:

$$< \frac{dE}{dt} >= - < \int F^i_{react} v_i d^3x >= -\frac{1}{5} < Q^{(3)}_{ij} Q^{(3)}_{ij} >$$

where $Q_{ij} = I_{ij} - \frac{1}{3}\delta_{ij} I^k_{.k}$ and I_{ij} is the quadrupole moment. Then one is able to derive the reaction force.

$$F^i_{react} = -\frac{2}{5}\rho x^k Q^{(5)}_{ik}$$

The above reaction force is ϵ^5 smaller than the Newtonian force in the equation of motion where $\epsilon = v/c$ (v is the magnitude of the typical velocity of the system

and c is the velocity of light). Since the magnitudes of the graviatational potential is of the order ϵ^2, the first relativistic correction is ϵ^2 smaller than the Newtonian order and is called as the first post Newtonian correction. Thus it has been said that the reaction force appears at 2.5 post-Newtonian order.

The above derivation is obviously not satisfactory because the reaction force is not actually derived. One should be able to derive the equation of motion with radiation reaction from the informations in the so-called near zone only.[2] In fact such a derivation of the reaction force has been carried out by various people by various methods under the assumption that the typical velocity of the system is much smaller than the velocity of light. Every calculations confirm essencially the above result. Thus there exist no difficulty in deriving the equation of motion of slowly moving and weekly self-gravitating object in general relativity.

Although higher order radiation and their effects on the motion of the system are interesting in a theoretical point of view, it was thought that they play no important role in our understanding of the nature of, say, coalescing binary systems. However the approval of RIGO project[4] by US congress changes the situation. One of the most realsitic target for RIGO are coalescing compact binary systems. It turns out that we need much higher order (at least 4 post-Newtonian) calculation to make the theoretical template to extract the detailed informations of the system from the observed properties of gravitational radiation.[5] [6] Although partial results which are very interesting are obtained, no fully consistent calculation up to such a higher order has been done yet. Thus it is now urgent to have some sort of the theoretical scheme within general relativity which allows us to do explicit calculations up to arbitrary higher post-Newtonian order. It might happen that the very concept of the radiation reaction force may not be appropriate and the equation of motion may take a quite different form such as an integro-differential equation in higher post-Newtonian orders.

In this report we shall review the present status of the slow-motion approximation in general relativity.

2. Difficulties in General Relativity

The equation of motion is rather simple in Newtonian theory. However the situation become unclear as we go to general relativity becouse of the nonlinearity of Einstein equation.[7] The concept of the definition and energy of gravitational radiation near the source are not well defined. This makes difficult to have the global energy consevation. In fact the relation between the near-zone field and the far-zone field is not yet well understood in general situation which causes a difficulty to subtract the gravitational radiation in numerical relativity. Since the gravitational field contributs to the source of Einstein equation as well as the material contribution, the definition of the body becomes unclear.

Here we shall concentrate only the previous treatments for the description of the body. It should be mentioned in this context that an exact treatrment of extended body has been developed by Dixon.[8] In his treatment the four partial differential equations

$$T^{\mu\nu}{}_{;\nu} = 0$$

may be replaced by ten ordinary differential equations for the multipole moment of the body.

$$\dot{P}^{\mu} + \frac{1}{2} R^{\mu}{}_{\nu\rho\sigma} \dot{z}^{\nu} S^{\rho\sigma} = F^{\mu}(z, I^{\cdots}; g)$$

$$\dot{S}^{\mu\nu} + 2\dot{z}^{[\mu} P^{\nu]} = L^{\mu\nu}(z, I^{\cdots}; g)$$

where $z^{\mu}(\lambda)$ is the center of mass worldline, P^{μ} the 4-momentum, $S^{\mu\nu}$ the angular momentum and $I^{\cdots}$ is appropriatelly defined relativistic multiple moment. If the metric tensor is somehow expressed in terms of the body's multipole moments by the use of Einstein equation, then the above equations become "the equation of motion". However this final step has not been taken yet. In this sense his treament has no use for the study of the radiation reaction problem. Perhaps some sort of approximation would be necessary to couple his approach with Einstein equation. This direction of reaserch might be very important.

Avoiding the complicity of treating internal motion of the source, the following form of the point particle is sometimes used.

$$T^{\mu\nu}(x) = m \int dt\, \delta^{(4)}(x - z(\lambda))\, \dot{x}^{\mu}\dot{x}^{\nu}\, (-g g_{\rho\sigma}\dot{z}^{\rho}\dot{z}^{\sigma})^{-1/2}$$

However as is well-known, such singular source is not compatible with Einstein equation. Physically there is no naive point particle limit in general relativity. Furthermore the covariant conservation of the stress-energy tensor for the above form implies the geodesic equation and thus it is unable to take into account the backreaction. However it is possible to define a strong field point particle limit in the slow-motion case in general relativity by constructing an appropriate one-parameter family perfect fluid solution of Einstein equation.[9]

There is another way to describe the body, namely one construct a timelike cylindrical hypersurface around the body and describe the body in terms of the gravitational field on the surface. THis approach has been used to obtain the equation of motion of a slowly moving source by Einstein, Infelt and Hoffman[10] A. Einstein, L. Infeld and B. Hoffmann, Ann. Math., **39**, 65, (1938) and successifly applied the fast-moving charged source in electromagnetic case by Dirac. It has also been applied to describe the motion of a compact star and black hole.[11] However this approach has been appled for slowly moving sources so far in general relativity.

3. Slow-Motion Approximation

Let us first state a general theory of approximation in general relativity which is asymptotically valid as some parameter tends to zero. This can be formulated in terms of an one-parameter family of the solution[12]

$$\{g_{\mu\nu}(x;\epsilon), T^{\mu\nu}(x;\epsilon)\}$$

which satisfy Einstein equation for each ϵ.

$$G_{\mu\nu}(g_{\alpha\beta}(x;\epsilon)) = 8\pi T_{\mu\nu}(x; g_{\alpha\beta};\epsilon)$$

Then the approximation is obtained as

$$g_{\mu\nu}(x;\epsilon) = g_{\mu\nu}(x,0) + \epsilon\partial_\epsilon g_{\mu\nu}(x;0) + ...$$

$$T^{\mu\nu}(x;\epsilon) = T^{\mu\nu}(x;0) + \epsilon\partial_\epsilon T^{\mu\nu}(x;0) + ...$$

This can be seen geometrically as follows:[13] One can regard the family of solution as a fiber bundle where the base manifold is R(the parameter space) and the fiber is the spacetime manifold for each ϵ. Then the derivative with respect to *epsilon* may be taken along a congruence of curves in the fiber bundle, thus it is Lie derivative with respect to the tangent vector to this congruence. Each congruence defines a map between each fiber and the nature of the approximation. It should be also noted that the limit $\epsilon = 0$ may be singular, namely $\epsilon = 0$ fiber is not the solution of Einstein equation.

The slow-motion approximation is defined by taking the small parameter ϵ as the ratio between the typical velocity of the source and the velocity of light, and the congruence to define the limit is defined as ϵt fixed. The latter condition comes from the fact that the typical time interval such as the orbital period in the case of a binary system scales like ϵ^{-1} in the Newtonian situation.

There are choices of the slow-motion approximation depending on how to define the family of solution. Namely one can define the solution by specifying the initial data at a spatial hypersurface[13] or at past null infinity. In both cases one have to make sure that the system is physically isolated, namely there will be no incoming radiation at the initial stage because one is interested in the effect of self-field. The no incoming radiation condition is not simple at all within the approximation scheme because of the ambiguity of the definition of gravitational radiation.

The post-Minkowski approximation is also defined by taking the small parameter as the gravitational coupling constant G. Damour and others have developed a systematic formulation of the post-Minkowski approximation coupled with the matching technique as well as the multipolar expansion technique.[14] They have used the approximation in the slow motion case and obtained very interesting phenomena at higher orders. So far they are the most advanced group in this subject.

4. The present status

In the conventional slow-motion approximation[15] [16] it has been suggested that the logarithimic divergence appears at some higher post-Newtonian (pN) order. This can be easily understood by realizing that the retarded expansion is nothing but Taylor expansion at the instantenious time t of the integrand of the retarded integral.

$$\frac{T(t-\frac{r}{c},y)}{r} = \frac{T(t,y)}{r} - \frac{1}{c}\dot{T}(t,y) + \frac{1}{2}\frac{r}{c^2}\ddot{T}(t,y) + ...$$

Thus if the T has no compact support in y, the intergal over y will diverge at some higher order.

The divergences are regularized by constructing a family of the solutions by appropriate initial data with Newtonian scaling at an intial spacelike hypersurface and taking appropriate limiting process on the so-constructed fiber bundle. Namely one defines the Newtonian time as $\tau = \epsilon t$ and the congruence by fixing τ. This means we take the limit $\epsilon \to 0$ by following the same physical events along the family of solution (For example, the orbital period of a Newtonian binary system scales like ϵ^{-1} as the orbital velocity $v \sim \epsilon$) and it gurantees the limit is actually the Newtonian limit. Then the integral region also depends on ϵ such a way that the region gets large as $\epsilon \to 0$. The following simple example shows how the reguralization happens in this approach.

$$\epsilon^n \int^{\tau/\epsilon} \frac{dr}{r} \sim \epsilon^n \log \epsilon$$

If one would take the conventiona approach, namely the integral reion is infinite from the first, one would have had the logarithmic divergence at the order ϵ^n. Above example shows that the divergence-free slow-motion approximation is not analytic in ϵ. In the harmonic coordinate it occurs at 3 pN order.[17] Its explicit form depends strongly on the choice of the coordinate system. In fact it has been suggested by recent calculation by Asada that such behaviour wont appear up to 4th pN order in the maximal slicing and the conformal gauge.

At the moment there is no comlete calculation in the slow-motion approximation higher than 3rd pN order. However the slow-motion approximation is recently formulated in 3+1 formalism and some explicit calculation has been done in the conformal time slice and the transverse gauge to obtain the near and far zone quadrupole formula in a covenient form.[18] Details of this calculation will be presented in this volume by Asada. It is expected that the calculations at higher order in this gauge makes the situation rather simple and higher order calculation is now in progress. It should be also noted that the conformal time slice turned out to be a very convenient to use in numerical relativity[19] . Developing the slow-motion approximation in this gauge thus gives us the brigde between analytical approach and numerical approach.

As far as the far zone calculation is concerned, Branchet and Damour have developed a new post-Newtonian a gravitational wave generation formalism based on the post-Minkowski approximation with multipole expansion technique and obtained the first-post Newtonian corrections to the standard quadrupole formula.[20] [21] They have obtained the following form of a past-dependent reaction force

$$F^i_{react} = \rho \frac{\partial}{\partial x^i} (\phi_{react} + \delta\phi)$$

where $\phi_{react} = \frac{1}{5} x^i x^j Q^{ij}$ is the reaction force at 2.5 pN order and $\delta\phi$ is the past-dependent force associated with the tails generated by the backscatter of the gravitational raiation off the background curvature.

$$\delta\phi = \frac{4}{5} x^i x^j I(t) \int_0^\infty dy \log\left(\frac{y}{2b}\right) I^{(7)}_{ij}(t-y)$$

Branchet and Wiseman has recently obtained the expressions of asymptotic gravitational waveform and the associated energy generated by the source at the 2 pN approximation.[22]

5. Conclusion

We have reviewed the present status of the slow-motion approximation in general relativity. It may be able to formulate it manifestly divergence-free. However sufficently higher order near zone calculations in this approximation have not yet been done because of the complexity of the calculation. It is hoped that one may find a convenient gauge to simplify the calculation at such higher orders.

REFERENCES

1. R. A. Hulse and J. H. Taylor, Astrophys. J., 205, 580, (1975)
2. See for example, T. Damour, in 300 Years of Gravitation, edited by S. Hawking and W. Isreal, Cambridge University Press, (1987)
3. For example, L. D. Landau and E. M. Lifshitz, Classical Theory of Fields, Pergamon, Oxford, (1975)
4. A. Abramovici et al. Science, **256**, 325, (1992)
5. A. G. Wiseman and C. M. Will, Phys. Rev D44, 2945, (1991)
6. B. F. Schutz, in Journees Relativistes 1992
7. See, for example, J. Ehlers, Ann. N. Y. Acad. Sci., 336, 279, (1980)
8. W. G. Dixon, in Isolated Gravitating System in General Relativity, edited by J. Ehlers, (North-Holland, Amsterdam 1979)
9. T. Futamase, Phys. Rev. D36, 321, (1987)
10.
11. see for example, K. S. Throne, in Gravitational Radiation, edited by N. Dreuelle and T. Piran, (North Holland: Amsterdam , 1983)
12. R. E. Kates, Ann. Phys. N. Y., **132**, 1, (1981)
13. T. Futamase and B. F. Schutz, Phys. Rev. D28, 2363, (1983)
14. T. Damour, in Gravitational Radiation, edited by N. Deruelle and T. Piran (North-Holland, Amsterdam, 1983)

15. S. Chandrasekher, Astrophys. J. **158**, 45, (1969)

16. J. L. Anderson and T. C. DeCanio, Gen. Rel. Grav. **6**, 197, (1975)

17. T. Futamase, Phys. Rev, D28, 2373, (1983)

18. H. Asada, M. Shibata and T. Futamase, in preparation

19. M. Shibata and T. Nakamura, Prog. Theor. Phys. **88**, 317, (1992)

20. L. Branchet and T. Damour, C. R. Acad. Sc. Paris, series II, 298, 431, (1984)

21. L. Branchet and T. Damour, Phys. Rev. D46, 4304, (1990)

22. L. Branchet, preprint

Post-Newtonian Approximation in the (3+1) Formalism and the Quadrupole Radiation-Reaction

HIDEKI ASADA[1], MASARU SHIBATA[1] AND TOSHIFUMI FUTAMASE[2]

[1] *Department of Earth and Space Science, Faculty of Science, Osaka University, Toyonaka, Osaka 560, Japan*

[2] *Department of Physics, Faculty of Science, Hirosaki University, Hirosaki 036, Japan*

ABSTRACT

The Post-Newtonian (PN) approxiamtion is useful for the prediction of the gravitational radiation and the evolution due to the radiation reaction of the slow-motion system such as a compact binary. In order to clarify the gauge freedom, the PN approximation is formulated in the (3+1) formalism here. The quadrupole radiation and the radiation reaction are investigated using the conformal time slice and the transverse gauge. It is found that the meaning of PN metric is much clearer in our gauge condition than in the use of other condition including the Harmonic gauge.

1. Introduction

One of the most promising sources of gravitational waves for the planned laser-interferometric gravitational wave detectors such as LIGO[1]or VIRGO[2]is the inspiralling compact binary. The typical velocity of this system is so small compared with the light velocity even in the late stage that the Post-Newtonian (PN) approximation can be used to predict the waveform and the orbital evolution due to the gravitational radiation. Nevertheless, there is some complexity such as the log-term[3][4]at higher orders in the PN approximation, which originates from the non-linearlity of the Einstein equation. Some gauge condition might decrease the complexity of non-linearlity. Also it is difficult to compare the result of the standard PN approximation with other calculations such as the perturbation method around the black hole[5]and the numerical relativity[6], since the PN approximation is performed under the Harmonic condition in most cases.

The (3+1) formalism is convenient to see the gauge issue. Therefore we consider the PN approximation in the (3+1) formalism in this article. This has been already treated by many people[7]. They essentially make use of the ADM gauge[8]. In this article we adopt the conformal time slice[9]and the transverse gauge, which clarify the physical meaning of each PN metric. It is shown that our choice of gauge simplify the calculation of the quadrupole radiation and the radiation reaction.

We use the units of $c = G = 1$. Greek and Latin indices take $0, 1, 2, 3$ and $1, 2, 3$, respectively.

2. (3+1) Formalism for Post-Newtonian Approximation

2.1 (3+1) Formalism

We consider the (3+1) formalism to perform the PN approximation. In the (3+1) formalism, the metric is split as

$$g_{\mu\nu} = \gamma_{\mu\nu} - n_\mu n_\nu, \tag{2.1}$$

and

$$\begin{aligned} n_\mu &= (-\alpha,\ 0), \\ n^\mu &= \left(\frac{1}{\alpha},\ -\frac{\beta^i}{\alpha}\right), \end{aligned} \tag{2.2}$$

where α, β^i and γ_{ij} are the lapse function, shift vector and metric on 3D hypersurface,

respectively. Then the line element is written as

$$ds^2 = -(\alpha^2 - \beta_i\beta^i)dt^2 + 2\beta_i dt dx^i + \gamma_{ij}dx^i dx^j. \tag{2.3}$$

Using the (3+1) formalism, the Einstein equation is split into the constraint equations and the evolution equations.

To distinguish the wave part from the non-wave part(for example, Newtonian potential) in the metric, we use the conformal factor $\psi = \det(\gamma_{ij})^{1/12}$ and $\tilde{\gamma}_{ij} = \psi^{-4}\gamma_{ij}$ so that $\det(\tilde{\gamma}_{ij}) = 1$ is satisfied. We also define $\tilde{A}_{ij}$ as

$$\tilde{A}_{ij} \equiv \psi^{-4}A_{ij} \equiv \psi^{-4}\Big(K_{ij} - \frac{1}{3}\gamma_{ij}K\Big). \tag{2.4}$$

Using these variables, the evolution equations can be rewritten as follows;

$$\frac{d}{dt}\tilde{\gamma}_{ij} = -2\alpha\tilde{A}_{ij} + \tilde{\gamma}_{il}\frac{\partial\beta^l}{\partial x^j} + \tilde{\gamma}_{jl}\frac{\partial\beta^l}{\partial x^i} - \frac{2}{3}\tilde{\gamma}_{ij}\frac{\partial\beta^l}{\partial x^l}, \tag{2.5}$$

$$\begin{aligned}\frac{d}{dt}\tilde{A}_{ij} = {} & \frac{1}{\psi^4}\Big[\alpha\Big(R_{ij} - \frac{1}{3}\gamma_{ij}R\Big) - \Big(D_iD_j\alpha - \frac{1}{3}\gamma_{ij}D^kD_k\alpha\Big)\Big] \\ & + \alpha(K\tilde{A}_{ij} - 2\tilde{A}_{il}\tilde{A}^l{}_j) + \frac{\partial\beta^m}{\partial x^i}\tilde{A}_{mj} + \frac{\partial\beta^m}{\partial x^j}\tilde{A}_{mi} - \frac{2}{3}\frac{\partial\beta^m}{\partial x^m}\tilde{A}_{ij} \\ & - 8\pi\frac{\alpha}{\psi^4}\Big(S_{ij} - \frac{1}{3}\gamma_{ij}S^l{}_l\Big),\end{aligned} \tag{2.6}$$

$$\frac{d}{dt}\psi = \frac{\psi}{6}\Big(-\alpha K + \frac{\partial\beta^i}{\partial x^i}\Big), \tag{2.7}$$

$$\frac{d}{dt}K = \alpha\Big(\tilde{A}_{ij}\tilde{A}^{ij} + \frac{1}{3}K^2\Big) - D^iD_i\alpha + 4\pi\alpha(S^i{}_i + E), \tag{2.8}$$

where

$$\frac{d}{dt} = \frac{\partial}{\partial t} - \beta^i\frac{\partial}{\partial x^i}. \tag{2.9}$$

E and S_{ij} are defined as

$$\begin{aligned} E &= T_{\mu\nu}n^\mu n^\nu, \\ S_{ij} &= T_{kl}\gamma^k{}_i\gamma^l{}_j. \end{aligned} \tag{2.10}$$

The constarint equations are also written as

$$\tilde{\Delta}\psi = \frac{1}{8}\tilde{R}\psi - 2\pi E\psi^5 - \frac{\psi^5}{8}\Big(\tilde{A}_{ij}\tilde{A}^{ij} - \frac{2}{3}K^2\Big), \tag{2.11}$$

and

$$\tilde{D}_j(\psi^6\tilde{A}^j{}_i) - \frac{2}{3}\psi^6\tilde{D}_iK = 8\pi\psi^6 J_i, \tag{2.12}$$

where $\tilde{R}$ is the scalar curvature with respect to $\tilde{\gamma}_{ij}$ and J_i is defined as

$$J_j = -T_{\mu\nu}n^\mu\gamma^\nu_j. \tag{2.13}$$

Now let us consider R_{ij} in Eq.(2.6), which is one of the main source terms of the evolution equation for $\tilde{A}_{ij}$. First we split R_{ij} into two parts as

$$R_{ij} = \tilde{R}_{ij} + R^\psi_{ij}, \tag{2.14}$$

where $\tilde{R}_{ij}$ is the Ricci tensor with respect to $\tilde{\gamma}_{ij}$,

$$R^\psi_{ij} = -\frac{2}{\psi}\tilde{D}_i\tilde{D}_j\psi - \frac{2}{\psi}\tilde{\gamma}_{ij}\tilde{D}^k\tilde{D}_k\psi + \frac{6}{\psi^2}(\tilde{D}_i\psi)(\tilde{D}_j\psi) - \frac{2}{\psi^2}\tilde{\gamma}_{ij}(\tilde{D}_k\psi)(\tilde{D}^k\psi). \tag{2.15}$$

and $\tilde{D}_i$ is the covariant derivative with respect to $\tilde{\gamma}_{ij}$. We split $\tilde{\gamma}_{ij}$ as $\eta_{ij} + h_{ij}$, where η_{ij} is the flat 3D metric.

In this article, we consider only the linear order in h_{ij} assuming $|h_{ij}| \ll 1$. This implies that we neglect the non-linear couplig between gravitational waves, but does not imply that we neglect the non-linear couplig between the Newtonian potentials and between gravitational waves and the Newtonian poterntials. In other words, although we can not see the non-linear memory of gravitational waves[10], we can see the tail term of gravitational waves and can derive the exact quadrupole formula(see below). Here, to guarantee the wave property of $\tilde{\gamma}_{ij}$, we impose the *TT gauge*(transverse-traceless gauge, where the traceless property is already guaranteed) to the 3D metric as

$$h_{ij,j} = 0. \tag{2.16}$$

This condition leads to

$$\tilde{R}_{ij} = -\frac{1}{2}\Delta_{flat}h_{ij}, \tag{2.17}$$

where Δ_{flat} is the Laplacian with respect to η_{ij}.

It is possible to consider several slice conditions providing the Newtonian picture; the maximal slice[11], harmonic slice[12], and conformal time slice[9]. Among them, we find that the conformal time slice is most tractable and useful to distinguish the wave part and the non-wave parts. The conformal time slice is defined[9] as

$$\alpha = \exp\Big(-2\epsilon - \frac{2}{3}\epsilon^3 - \frac{2}{5}\epsilon^5\Big), \tag{2.18}$$

where $\epsilon = \psi - 1$. Then the equations (2.6) is rewritten as

$$\begin{aligned}\frac{d}{dt}\tilde{A}_{ij} = &-\frac{1}{2}\frac{\alpha}{\psi^4}\Delta_{flat}h_{ij} + \frac{2\alpha}{\psi^4}\Big[\Big(\tilde{D}_i\tilde{D}_j\psi - \frac{\tilde{\gamma}_{ij}}{3}\tilde{D}_k\tilde{D}^k\psi\Big)\frac{\epsilon}{\psi}(1+\epsilon+\epsilon^2+\epsilon^3+\epsilon^4) \\ &- \frac{1}{\psi^2}\Big(\tilde{D}_i\psi\tilde{D}_j\psi - \frac{1}{3}\tilde{\gamma}_{ij}\tilde{D}^k\psi\tilde{D}_k\psi\Big) \\ &\qquad (3+6\epsilon+6\epsilon^2+6\epsilon^3+6\epsilon^4+12\epsilon^5+10\epsilon^6+8\epsilon^7+6\epsilon^8+4\epsilon^9+2\epsilon^{10})\Big] \\ &+ \alpha(K\tilde{A}_{ij} - 2\tilde{A}_{il}\tilde{A}^l{}_j) + \beta^m{}_{,i}\tilde{A}_{mj} + \beta^m{}_{,j}\tilde{A}_{mi} - \frac{2}{3}\beta^m{}_{,m}\tilde{A}_{ij} - 8\pi\frac{\alpha}{\psi^4}\Big(S_{ij} - \frac{1}{3}\gamma_{ij}S^l{}_l\Big),\end{aligned} \tag{2.19}$$

where we use the TT gauge condition as well as the linear approximation for h_{ij} in the above equation. From Eqs.(2.5) and (2.19) the wave equation for h_{ij} is written as

$$\begin{aligned}\Box\, h_{ij} = &-\Big(\frac{\alpha^2}{\psi^4} - 1\Big)\Delta_{flat}h_{ij} + \Big(\frac{d^2}{dt^2} - \frac{\partial^2}{\partial t^2}\Big)h_{ij} \\ &+ \frac{4\alpha^2}{\psi^4}\Big[\Big(\tilde{D}_i\tilde{D}_j\psi - \frac{\tilde{\gamma}_{ij}}{3}\tilde{D}_k\tilde{D}^k\psi\Big)\frac{\epsilon}{\psi}(1+\epsilon+\epsilon^2+\epsilon^3+\epsilon^4) \\ &- \frac{1}{\psi^2}\Big(\tilde{D}_i\psi\tilde{D}_j\psi - \frac{1}{3}\tilde{\gamma}_{ij}\tilde{D}^k\psi\tilde{D}_k\psi\Big) \\ &\qquad (3+6\epsilon+6\epsilon^2+6\epsilon^3+6\epsilon^4+12\epsilon^5+10\epsilon^6+8\epsilon^7+6\epsilon^8+4\epsilon^9+2\epsilon^{10})\Big] \\ &+ 2\alpha^2(K\tilde{A}_{ij} - 2\tilde{A}_{il}\tilde{A}^l{}_j) + 2\alpha\Big(\beta^m{}_{,i}\tilde{A}_{mj} + \beta^m{}_{,j}\tilde{A}_{mi} - \frac{2}{3}\beta^m{}_{,m}\tilde{A}_{ij}\Big) \\ &- 16\pi\frac{\alpha^2}{\psi^4}\Big(S_{ij} - \frac{1}{3}\gamma_{ij}S^l{}_l\Big) - \frac{d}{dt}\Big(\beta^m{}_{,i}\tilde{\gamma}_{mj} + \beta^m{}_{,j}\tilde{\gamma}_{mi} - \frac{2}{3}\beta^m{}_{,m}\tilde{\gamma}_{ij}\Big) + 2\frac{d\alpha}{dt}\tilde{A}_{ij} \\ &\equiv \tau_{ij},\end{aligned} \tag{2.20}$$

where

$$\Box = -\frac{\partial^2}{\partial t^2} + \Delta_{flat}. \tag{2.21}$$

In the above, we use $\epsilon = \psi - 1$, where ψ satisfies

$$\tilde{\Delta}\psi = -2\pi E\psi^5 - \frac{\psi^5}{8}\Big(\tilde{A}_{ij}\tilde{A}^{ij} - \frac{2}{3}K^2\Big). \tag{2.22}$$

In the original conformal slice[9], ϵ is constructed from ψ which satisfies Eq.(2.11)($\tilde{R} \neq 0$). However, in the present article, we assume $\tilde{R} = 0$, and this treatment is justified in the case where $\tilde{R}$ is small, *i.e.*, the gravitational wave is not extremely strong($h_{ij} < 1$) and the gauge part in $\tilde{R}$ is removed ingeniously.

Finally, we assume the perfect fluid as the matter. It is expected that we can avoid the extra divergent terms in the case of point sources.

2.2 Post Newtonian approximation

We consider the PN approximation of the above equations. First of all, ψ (and α in the conformal time slice) is determined by the Hamiltonian constraint. In the lowest order, it becomes

$$\Delta_{flat(2)}\psi = -2\pi\rho, \tag{2.23}$$

where ρ is the mass density and the subscript (n) denotes the quantity of $O(c^{-n})$. Thus, ${}_{(2)}\alpha = -2{}_{(2)}\psi = -U$ is satisfied in this gauge, where U is the Newtonian potential.

Let us consider the wave equation for h_{ij}. In the lowest order PN approximation, Eq.(2.20) is written as

$$\begin{aligned} \Box\, h_{ij} = &\left(UU_{,ij} - \frac{1}{3}\eta_{ij}U\Delta_{flat}U - 3U_{,i}U_{,j} + \eta_{ij}U_{,k}U_{,k}\right) \\ &- 16\pi\left(\rho v_i v_j - \frac{1}{3}\eta_{ij}\rho v^2\right) - \left({}_{(3)}\dot{\beta}_{i,j} + {}_{(3)}\dot{\beta}_{j,i} - \frac{2}{3}\eta_{ij}{}_{(3)}\dot{\beta}_{k,k}\right) = {}_{(4)}\tau_{ij}, \end{aligned} \tag{2.24}$$

where we use $\epsilon = 2U$ which holds in the lowest order approximation. We should note that ${}_{(4)}\tau_{ij}$ has the TT property, *i.e.*, ${}_{(4)}\tau_{ij,j} = 0$ and ${}_{(4)}\tau_{ii} = 0$ as a natural consequence of the TT gauge, $h_{ij,j} = h_{ii} = 0$. In addition, it should be noted that h_{ij} begins with the second PN order thanks to the conformal transformation.

Therefore, ${}_{(4)}h_{ij}$ is determined from

$$\Delta_{flat(4)}h_{ij} = {}_{(4)}\tau_{ij}. \tag{2.25}$$

A part of the quadrupole back reaction potential in the near zone, ${}_{(5)}h_{ij}$, is derived from

$${}_{(5)}h_{ij}(t) = \frac{1}{4\pi}\frac{\partial}{\partial t}\int {}_{(4)}\tau_{ij}(t, \mathbf{x}')d^3x'. \tag{2.26}$$

Also, the quadrupole mode of gravitational waves in the wave zone is written as

$$h_{ij}^{rad} = -\frac{1}{4\pi} \lim_{|\mathbf{x}|\to\infty} \int \frac{{}_{(4)}\tau_{ij}(t - |\mathbf{x} - \mathbf{x}'|, \mathbf{x}')}{|\mathbf{x} - \mathbf{x}'|} d^3x'. \tag{2.27}$$

In the next section, we derive the quadrupole radiation-reaction force, the quadrupole formula in the near zone and the gravitational waves using Eqs.(2.26) and (2.27).

We note that for the PN equation of motion up to the 2.5PN order, we need ${}_{(2)}\alpha$, ${}_{(4)}\alpha$, ${}_{(6)}\alpha$, ${}_{(7)}\alpha$, ${}_{(2)}\psi$, ${}_{(4)}\psi$, ${}_{(3)}\beta$, ${}_{(5)}\beta$, ${}_{(4)}h_{ij}$ and ${}_{(5)}h_{ij}$. Therefore, if we solve the above set of the equations, we can obtain the 2.5 PN equation of motion.

3. Quadrupole Radiation and the Radiation Reaction

3.1 Near Zone

Inserting ${}_{(4)}\tau_{ij}$ of Eq.(2.24) into (2.26), we obtain ${}_{(5)}h_{ij}$ in the near zone,

$${}_{(5)}h_{ij} = -\frac{4}{5} I_{ij}^{(3)}. \tag{3.1}$$

Then the Hamiltonian constariant at the 2.5PN order turns out to be

$$\Delta_{flat}{}_{(7)}\psi = -\frac{2}{5} I_{ij}^{(3)} U_{,ij}\ , \tag{3.2}$$

From this, we find ${}_{(7)}\psi$ and ${}_{(7)}\alpha$ take the following form,

$${}_{(7)}\alpha = -2\ {}_{(7)}\psi = -\frac{2}{5} I_{ij}^{(3)} \int \rho(t, \mathbf{x}') \frac{(x^i - x'^i)(x^j - x'^j)}{|\mathbf{x} - \mathbf{x}'|^3} d^3x'. \tag{3.3}$$

We consider the PN equation of motion,

$$\dot{v}_i + v^j v_{i,j} = -P_{,i} + U_{,i} + F_i^{1PN} + F_i^{2PN} + F_i^{2.5PN} + O(c^{-8}), \tag{3.4}$$

where F_i^{1PN} and F_i^{2PN} are 1PN and 2PN force respectively and conserve the energy of

the system. The radiation reaction force per unit mass, $F_i^{2.5PN} \equiv F_i^r$, is

$$\begin{aligned} F_i^r &= -\Big(({}_{(5)}h_{ij}v^j)^{\cdot} + v^k v^j_{,k}{}_{(5)}h_{ij} + {}_{(7)}\alpha_{,i}\Big) \\ &= \Big[\frac{4}{5}(I^{(3)}_{ij}v^j)^{\cdot} + \frac{4}{5}I^{(3)}_{ij}v^k v^j_{,k} + \frac{2}{5}I^{(3)}_{kl}\frac{\partial}{\partial x^i}\int \rho(t,\mathbf{x}')\frac{(x^k - x'^k)(x^l - x'^l)}{|\mathbf{x}-\mathbf{x}'|^3}d^3x'\Big]. \end{aligned} \tag{3.5}$$

The work done by the force (3.5) is given by

$$\begin{aligned} W &\equiv \int \rho F_i^r v^i d^3x \\ &= \frac{4}{5}\frac{\partial}{\partial t}\Big(I^{(3)}_{ij}\int \rho v^i v^j d^3x\Big) - \frac{1}{5}I^{(3)}_{ij}I^{(3)ij} \end{aligned} \tag{3.6}$$

We obtain the so-called quadrupole formula of the energy loss by the quadrupole radiation reaction force by averaging the Eq.(3.6) in time, which is reasonable to the periodic system such as the binary pulsar,

$$\left\langle \frac{dE_N}{dt} \right\rangle = -\frac{1}{5}\left\langle I^{(3)}_{ij}I^{(3)ij}\right\rangle + O(c^{-6}). \tag{3.7}$$

3.2 Far Zone

Since h_{ij} is tansverse and traceless, Eq.(2.24) turns out to be

$$\begin{aligned} \Box\, h_{ij} =& \tau^{TT}_{ij} \\ =& \Big(-16\pi\big(\rho v_i v_j - \frac{1}{3}\delta_{ij}\rho v^2\big) \\ &+ \big(UU_{,ij} - \frac{1}{3}\delta_{ij}U\Delta_{flat}U - 3U_{,i}U_{,j} + \delta_{ij}U_{,k}U_{,k}\big)\Big)^{TT}, \end{aligned} \tag{3.8}$$

where TT means the transverse and traceless part. Note that the spatial derivative of the shift vector consists of the longitudinal part of h_{ij}. From Eq.(3.8) we see the quadrupole wave,

$$h_{ij}(t,\mathbf{x}) = \frac{2I^{(2)TT}_{ij}(t-|\mathbf{x}|)}{|\mathbf{x}|}. \tag{3.9}$$

Then the luminosity of the quadrupole radiation is given by

$$\begin{aligned} L =& \frac{1}{32\pi}\int \dot{h}^{TT}_{ij}\dot{h}^{TT}_{ij}r^2 d\Omega \\ =& \frac{1}{5}I^{(3)}_{ij}I^{ij(3)} \end{aligned} \tag{3.10}$$

This is same as the energy loss due to the quadrupole radiation reaction force as expected.

4. Concluding Remarks

The prescription for the PN approximation in the (3+1) formalism is given in this article. The gauge issue should be clear in this formalism. As an example the conformal time slicing and the transverse gauge are adopted so that the wave part and the non-wave part are identified as h_{ij} and ψ respectively. In fact we derive the quadrupole radiation-reaction metric and the energy loss by the reaction force in the near zone. Also the quadrupole waveform and the luminosity are derived in the far zone. In addition, since the wave part and the non-wave part are distinguishable easily in this gauge condition, it would be easier than other gauges including the Harmonic gauge to perform higher order calculations.

For example, it is found from Eq.(2.20) that the first term in the right hand side is only the non-linear term of the monopole part and the quadrupole wave. Thus we obtain the equation for the tail effect

$$\Box\, h_{ij}^{tail} = 4U\ddot{h}_{ij}^{Q}, \tag{4.1}$$

where h_{ij}^{Q} means the linearlized quadrupole waves. This equation is just same as the Blanchet and Damour's[4]. Although the linealized quadrupole wave propagates on the flat light cone, the existence of the massive source deviates the light cone. The tail effect expresses the correction due to propagation on the curved light cone. Thus it is realized that the gauge condition in this areticle is useful in the PN approximation beyond the 2.5PN order too. The higher order treatment will be done in the future work.

Acknowledgements:

We would like to thank T. Nakamura for his encouragement and useful comments.

REFERENCES

1. R. E. Vogt, in proceedings of the sixth Marcel Grossmann meeting on general relativity, edited by H. Sato and T. Nakamura(World Scientific, 1991), 244;
   A. Abramovici et al. Science, **256**, 325, (1992);
   K. S. Thorne, in proceedings of the eighth Nishinomiya-Yukawa memorial symposium on Relativistic Astrophysics, Edited by M. Sasaki(Universal Academy Press, Tokyo, 1994), 67.
2. C. Bradaschia et al., Nucl. Instrum. Method Phys. Res. Sect. **A289**, 518, (1990).
3. T.Futamase and B.F.Schutz, Phys. Rev. **D28**, 2362 (1983);
   T.Futamase, Phys. Rev. **D28**, 2373(1983).
4. L.Blanchet and T.Damour, Phys.Rev.**D37**, 1410 (1988);
   L.Blanchet and T.Damour, Phys Rev **D46**, 4304 (1992).
5. T. Regge and J. A. Wheeler, Phys. Rev. **108**, 1063 (1957);
   S. A. Teukolsky, Astrophys. J. **185**, 635 (1973).
6. T. Nakamura, K. Oohara and Y. Kojima, Prog. Theor. Phys. Supp. **90**, 76, (1987);
   T. Nakamura, in the proceedings of the eighth Nishinomiya-Yukawa memorial symposium on Relativistic Astrophysics, Edited by M. Sasaki(University Academy Press, Tokyo, 1994), 155.
7. T. Ohta. H. Okamura, T. Kimura and K. Hiida, Prog. Thor. Phys. **51**, 1598, (1974);
   G. Schafer, Ann. Phys. **161**, 81, (1985);
   L. Blanchet, T. Damour and G. Schafer, Mon.Not.R.Astr.Soc. **242**, 289 (1990).
8. R. Arnowitt, S. Deser and C. W. Misner, The Dynamics of General Relativity in Gravitation: An Introduction to Current Research, ed. L. Witten (1962).
9. M. Shibata and T. Nakamura, Prog. Theor. Phys. **88**, 317 , (1992).
10. Christodoulou, Phys. Rev. Lett. **67**,1486, (1991) ;
    A. G. Wiseman and C. M. Will, Phys. Rev. **D44**,2945, (1991) ;
    Kip. S. Thorne, Phys. Rev. **D45**,520, (1992).
11. Futamase, Proceedings of Gravitational wave astronomy (in Japanese, 1991).
12. Bona and Masso, Phys. Rev. Lett. **68**, 1097, (1992).

Post-Newtonian expansion of gravitational waves from a particle orbiting around a rotating black hole

Hideyuki Tagoshi
Department of Physics, Kyoto University, Kyoto 606-01, Japan

Using the Teukolsky and Sasaki-Nakamura equations, we calculate the post-Newtonian expansion of the energy and angular momentum luminosities of gravitational waves from a test particle with slightly eccentric orbit around a rotating black hole up to $O(v^5)$ beyond the quadrupole formula. We find that circular orbit is stable up through the order $O(v^5)$ even if the spin of a black hole exists. Using the results, we argue the total phase of gravitational waves from coalescing compact binaries. We find that the eccentricity is important at $O(v^5)$ order if the initial eccentricity in the LIGO's band is greater than 0.4. There are possibilities that binaries which have a non-negligible eccentricity will be observed by laser interferometers and our results will be useful to analyze gravitational waves from such binaries.

1 Introduction

Among the possible sources of gravitational waves, coalescing compact binaries are the most promising candidates which can be detected by the near-future, ground based laser interferometric gravitational wave detectors such as LIGO [1] and VIRGO [2]. One reason is that we expect such events to occur 3/yr within 200Mpc [3]. The other reason is that we expect sufficiently large amplitude of gravitational waves to be detected by LIGO and VIRGO if such events occur.

We can extract physical information of binaries, such as masses and spins etc., from *inspiral wave forms* by the matched filtering technique [4]. In this method, binaries' parameters are determined by cross-correlating the noisy signal from detectors with theoretical templates. If the signal and the templates lose phase with each other by one cycle over the thousands as the waves sweep through the LIGO/VIRGO band, their cross correlation will be significantly reduced. This means that it is important to construct theoretical templates which are accurate to better than one cycle during entire sweep through the LIGO/VIRGO band [4]. If we have accurate templates, we can determine the chirp mass of the systems within 1% error [5]. Thus, much effort has been recently made to construct accurate theoretical templates [6–11].

To calculate inspiraling wave forms from coalescing binaries, the standard method is the post-Newtonian expansion of the Einstein equations, in which the equations are expanded in terms of a small parameter $v \sim (M/r)^{1/2}$, where M and r are the total mass and orbital length-scale of the system, respectively. However, calculations have been successful to only a few orders in v beyond the leading (Newtonian) order so far.

Recently the post-Newtonian expansion based on the perturbation formalism of a black hole is developed. In such analysis, we consider gravitational waves from a particle of mass μ orbiting around a black hole of mass M assuming $\mu \ll M$. Although this method is restricted to the case of $\mu \ll M$, we can calculate higher order post-Newtonian corrections of gravitational waves by means of relatively simple analysis compared to the standard post-Newtonian analysis. This direction of research was first done analytically by Poisson [12] to $O(v^3)$ order and numerically by Cutler et. al. [13] to $O(v^6)$ order. Then a highly accurate numerical calculation was done by Tagoshi and Nakamura [14] to $O(v^8)$ order and they found the appearance of $\log v$ terms in the energy flux at $O(v^6)$ and at $O(v^8)$. They also clarified that the accuracy of the energy flux to at least $O(v^6)$ is needed to construct template wave forms. An analytical calculation to the same order was done by Tagoshi and Sasaki [15] which was based on the formulation built up by Sasaki [16] and they confirmed the result of Tagoshi and Nakamura. These calculation were extended to a rotating black hole case by Shibata et.al. [17] to $O(v^5)$ order. They calculated gravitational waves from a particle in circular orbit with small inclination from the equatorial plane to see the effect of spin at higher post-Newtonian orders. They found that the effect of spin to the orbital phase is important at $O(v^5)$ order when one of the star is a rapidly rotating neutron star with its pulse period less than 2 ms or a rapidly rotating black hole with $q = J_{BH}/M^2 \geq 0.2$.

In this paper, we extend the analysis of Shibata et.al. to a case of eccentric orbit. The post-Newtonian expansion of gravitational waves including the effect of the eccentricity have already been done to $O(v^3)$

order for arbitrary eccentricity by Blanchet and Schäfer [10] and the spin effect at $O(v^3)$ order was calculated by Shibata [18].

The binary pulsars such as PSR 1913+16 have now non-negligible eccentricity, but when gravitational waves from such systems can be detected by LIGO/VIRGO, their eccentricity will have significantly decreased due to radiation reaction and it will become negligible. However there are some possibilities that close binary systems are produced in dense stellar systems [19] which may evolve to super massive black holes in the center of AGN's. Those binaries may have highly eccentric orbit when they emit the gravitational waves which can be detected by LIGO/VIRGO. Since LIGO's advanced detector systems have sensitivities for BH-BH inspirals at < 5 Gpc, such binaries seem to be possible sources for LIGO/VIRGO. Then to construct the template for such binaries, it seems important to investigate the effect of eccentricity at higher post-Newtonian order. Hence, in this paper, we study the effect of eccentricity to $O(v^5)$ order including spin effect.

On the other hand, a laser interferometric detector in space, LISA, was proposed[20]. LISA will observe the gravitational waves which have amplitude $h \sim 10^{-23}$ at frequency $f \sim 10^{-1} - 10^{-3}$ by one year integration. Then gravitational waves from compact stars orbiting around supermassive black holes in galactic centers will become a possible sources for such detectors and a few events per year can be expected [18]. Then it is important to investigate the gravitational waves from super massive black holes. Since $\mu/M \ll 1$ for such cases, our formulas give the correct value under the assumption $v \ll 1$.

The paper is organized as follows. In section 2, we show the Teukolsky equation and review the method of the post-Newtonian expansion of a homogeneous solution of the Teukolsky equation for a Kerr black hole using the Sasaki-Nakamura equation. In section 3, we solve the geodesic equation assuming that eccentricity e of a particle is small ($e \ll 1$), and integrate the source term of the Teukolsky equation. In section 4, we show the energy and angular momentum luminosity to $O(e^2)$ and $O(v^5)$. In section 5, we study the stability of circular orbit under radiation reaction. In section 6, we study the effect of the eccentricity to orbital phase of coalescing binaries. Section 7 is devoted to the summary. Throughout this paper we use the units of $c = G = 1$.

2 General formulation

2.1 The Teukolsky equation

We consider the case when a test particle of mass μ travels a slightly eccentric orbit around a Kerr black hole of mass $M \gg \mu$. We follow the notation used by Shibata et.al., but for definiteness, we recapitulate necessary formulae and definitions of symbols.

To calculate gravitational radiation from a particle orbiting around a Kerr black hole, we start with the Teukolsky equation. [21, 22] We focus on the radiation going out to infinity described by the fourth Newman-Penrose quantity, ψ_4 [23], which may be expressed as

$$\psi_4 = (r - ia\cos\theta)^{-4} \int d\omega e^{-i\omega t} \sum_{\ell,m} \frac{e^{im\varphi}}{\sqrt{2\pi}} {}_{-2}S^{a\omega}_{\ell m}(\theta) R_{\ell m\omega}(r), \tag{2.1}$$

where ${}_{-2}S^{a\omega}_{\ell m}$ is the spheroidal harmonic function of spin weight $s = -2$, which are normalized as

$$\int_0^\pi |{}_{-2}S^{a\omega}_{\ell m}|^2 \sin\theta d\theta = 1. \tag{2.2}$$

The radial function $R_{\ell m\omega}(r)$ obeys the Teukolsky equation with spin weight $s = -2$,

$$\Delta^2 \frac{d}{dr}\left(\frac{1}{\Delta}\frac{dR_{\ell m\omega}}{dr}\right) - V(r)R_{\ell m\omega} = T_{\ell m\omega}(r), \tag{2.3}$$

where $T_{\ell m\omega}(r)$ is the source term whose explicit form will be shown later, and $\Delta = r^2 - 2Mr + a^2$. The potential $V(r)$ is given by

$$V(r) = -\frac{K^2 + 4i(r-M)K}{\Delta} + 8i\omega r + \lambda, \tag{2.4}$$

where $K = (r^2 + a^2)\omega - ma$ and λ is the eigenvalue of ${}_{-2}S^{a\omega}_{\ell m}$.

The solution of the Teukolsky equation at infinity ($r \to \infty$) is expressed as

$$R_{\ell m\omega}(r) \to \frac{r^3 e^{i\omega r^*}}{2i\omega B^{in}_{\ell m\omega}} \int_{r_+}^{\infty} dr' \frac{T_{\ell m\omega}(r') R^{in}_{\ell m\omega}(r')}{\Delta^2(r')} \equiv \tilde{Z}_{\ell m\omega} r^3 e^{i\omega r^*}, \tag{2.5}$$

where $r_+ = M + \sqrt{M^2 - a^2}$ denotes the radius of the event horizon and $R^{in}_{\ell m\omega}$ is the homogeneous solution which satisfies the ingoing-wave boundary condition at horizon,

$$R^{in}_{\ell m\omega} \to \begin{cases} D_{\ell m\omega} \Delta^2 e^{-ikr^*} & \text{for } r^* \to -\infty \\ r^3 B^{out}_{\ell m\omega} e^{i\omega r^*} + r^{-1} B^{in}_{\ell m\omega} e^{-i\omega r^*} & \text{for } r^* \to +\infty, \end{cases} \tag{2.6}$$

where $k = \omega - ma/2Mr_+$ and r^* is the tortoise coordinate defined by

$$\frac{dr^*}{dr} = \frac{r^2 + a^2}{\Delta}. \tag{2.7}$$

For definiteness, we fix the integration constant such that r^* is given explicitly by

$$\begin{aligned} r^* &= \int \frac{dr^*}{dr} dr \\ &= r + \frac{2Mr_+}{r_+ - r_-} \ln \frac{r - r_+}{2M} - \frac{2Mr_-}{r_+ - r_-} \ln \frac{r - r_-}{2M}, \end{aligned} \tag{2.8}$$

where $r_\pm = M \pm \sqrt{M^2 - a^2}$.

2.2 Post-Newtonian expansion of the homogeneous solution

In the previous papers [16, 17], the post-Newtonian expansion of the homogeneous solution was performed to $O(\epsilon^2)$ where $\epsilon \equiv 2M\omega$. In this section, we review the method [16, 17].

In order to calculate gravitational waves emitted to infinity from a particle in slightly eccentric orbit, we need to know the explicit form of the source term $T_{\ell m\omega}(r)$, which has support around $r = r_0$ where r_0 is the radius which is the value of order of the orbital radius in the Boyer-Lindquist coordinate, the ingoing-wave Teukolsky function $R^{in}_{\ell m\omega}(r)$ around $r = r_0$, and its incident amplitude $B^{in}_{\ell m\omega}$ at infinity. We consider the expansion of these quantities in terms of a small parameter, $v^2 \equiv M/r_0$. In addition, we need to expand those quantity in terms of $\epsilon \equiv 2M\omega$ since $\omega = O(\Omega)$ where Ω is the orbital angular velocity of the particle and $M\omega = O(v^3)$. In case of Kerr black hole, the another combination of parameters $a\omega$ appears in the Teukolsky equation. We define $a \equiv qM$ and we have $a\omega = q\epsilon/2 = O(\epsilon^3)$.

First we perform the expansion of the spheroidal harmonics ${}_{-2}S^{a\omega}_{\ell m}$ and their eigenvalues λ in terms of $a\omega$. Since the spheroidal harmonics will appear only in the source term and since $a\omega = O(\epsilon)$, we have only to evaluate ${}_{-2}S^{a\omega}_{\ell m}$ up to $O(a\omega)$. On the other hand, the angular eigenvalues λ comes into play in the radial equation, we evaluate it up to $O(a^2\omega^2)$. The spheroidal harmonics ${}_{-2}S^{a\omega}_{\ell m}$ is given by

$${}_{-2}S^{a\omega}_{\ell m} = {}_{-2}P_{\ell m} + a\omega S^{(1)}_{\ell m} + O((a\omega)^2), \tag{2.9}$$

where ${}_{-2}P_{\ell m}$ are the spherical harmonics of spin weight $s = -2$ [24] and

$$S^{(1)}_{\ell m} = \sum_{\ell'} c^{\ell'}_{\ell m}\ {}_{-2}P_{\ell' m}, \tag{2.10}$$

where $c^{\ell'}_{\ell m}$ are non-zero only for $\ell' = \ell \pm 1$ and they are given by

$$\begin{aligned} c^{\ell+1}_{\ell m} &= \frac{2}{(\ell+1)^2} \left[\frac{(\ell+3)(\ell-1)(\ell+m+1)(\ell-m+1)}{(2\ell+1)(2\ell+3)} \right]^{1/2}, \\ c^{\ell-1}_{\ell m} &= -\frac{2}{\ell^2} \left[\frac{(\ell+2)(\ell-2)(\ell+m)(\ell-m)}{(2\ell+1)(2\ell-1)} \right]^{1/2}. \end{aligned}$$

The eigenvalue λ is given by

$$\lambda = \lambda_0 + a\omega\lambda_1 + a^2\omega^2\lambda_2 + O((a\omega)^3) \tag{2.11}$$

where $\lambda_0 = (\ell-1)(\ell+2)$, $\lambda_1 = -2m(\ell^2+\ell+4)/(\ell^2+\ell)$ and

$$\lambda_2 = -2(\ell+1)(c_{\ell m}^{\ell+1})^2 + 2\ell(c_{\ell m}^{\ell-1})^2 + \frac{2}{3} - \frac{2}{3}\frac{(\ell+4)(\ell-3)(\ell^2+\ell-3m^2)}{\ell(\ell+1)(2\ell+3)(2\ell-1)}. \tag{2.12}$$

Next we solve the homogeneous solution $R^{in}_{\ell m\omega}$. The Teukolsky equation is transformed into Sasaki-Nakamura equation [25], which is given by

$$\left[\frac{d^2}{dr^{*2}} - F(r)\frac{d}{dr^*} - U(r)\right]X_{\ell m\omega} = 0. \tag{2.13}$$

The explicit forms of $F(r)$ and $U(r)$ are given in the Appendix A. The relation between $R_{\ell m\omega}$ and $X_{\ell m\omega}$ is

$$R_{\ell m\omega} = \frac{1}{\eta}\left\{\left(\alpha + \frac{\beta_{,r}}{\Delta}\right)\chi_{\ell m\omega} - \frac{\beta}{\Delta}\chi_{\ell m\omega,r}\right\}, \tag{2.14}$$

where $\chi_{\ell m\omega} = X_{\ell m\omega}\Delta/(r^2+a^2)^{1/2}$, and the functions α, β and η are shown in Appendix A. Conversely, we can express $X_{\ell m\omega}$ in terms of $R_{\ell m\omega}$ as

$$X_{\ell m\omega} = (r^2+a^2)^{1/2}\, r^2\, J_-J_-\left[\frac{1}{r^2}R_{\ell m\omega}\right], \tag{2.15}$$

where $J_- = (d/dr) - i(K/\Delta)$. Then the asymptotic behavior of the ingoing-wave solution $X^{in}_{\ell m\omega}$ which corresponds to Eq.(2.6) is

$$X^{in}_{\ell m\omega} \to \begin{cases} A^{out}_{\ell m\omega}e^{i\omega r^*} + A^{in}_{\ell m\omega}e^{-i\omega r^*} & \text{for } r^* \to \infty \\ C_{\ell m\omega}e^{-ikr^*}, & \text{for } r^* \to -\infty, \end{cases} \tag{2.16}$$

where $A^{in}_{\ell m\omega}$, $A^{out}_{\ell m\omega}$ and $C_{\ell m\omega}$ are respectively related to $B^{in}_{\ell m\omega}$, $B^{out}_{\ell m\omega}$ and $D_{\ell m\omega}$ defined in Eq.(2.6) as

$$\begin{aligned} B^{in}_{\ell m\omega} &= -\frac{1}{4\omega^2}A^{in}_{\ell m\omega}, \\ B^{out}_{\ell m\omega} &= -\frac{4\omega^2}{c_0}A^{out}_{\ell m\omega}, \\ D_{\ell m\omega} &= \frac{1}{d_{\ell m\omega}}C_{\ell m\omega}, \end{aligned} \tag{2.17}$$

where c_0 is given in Eq.(A.3) of Appendix A and

$$\begin{aligned} d_{\ell m\omega} &= \sqrt{2Mr_+}[(8 - 24iM\omega - 16M^2\omega^2)r_+^2 \\ &\quad +(12iam - 16M + 16amM\omega + 24iM^2\omega)r_+ - 4a^2m^2 - 12iamM + 8M^2]. \end{aligned}$$

First we introduce the variable $z = \omega r$ and

$$\begin{aligned} z^* &= z + \epsilon\left[\frac{z_+}{z_+ - z_-}\ln(z - z_+) - \frac{z_-}{z_+ - z_-}\ln(z - z_-)\right] \\ &= \omega r^* + \epsilon\ln\epsilon, \end{aligned} \tag{2.18}$$

where $z_\pm = \omega r_\pm$. To solve $X^{in}_{\ell m\omega}$ by expanding it in terms of ϵ, we set

$$X^{in}_{\ell m\omega} = \sqrt{z^2 + a^2\omega^2}\,\xi_{\ell m}(z)\exp\left(-i\phi(z)\right), \tag{2.19}$$

where

$$\begin{aligned}\phi(z) &= \int dr\left(\frac{K}{\Delta}-\omega\right)\\ &= z^*-z-\frac{\epsilon}{2}mq\frac{1}{z_+-z_-}\ln\frac{z-z_+}{z-z_-},\end{aligned} \tag{2.20}$$

which generalizes the phase function $\omega(r^*-r)$ of the Schwarzschild case. This prescription makes it easy to implement the ingoing-wave boundary condition on $X^{in}_{\ell m\omega}$.

Inserting Eq.(2.19) into Eq.(2.13) and expanding it in terms of $\epsilon = 2M\omega$, we obtain

$$L^{(0)}[\xi_{\ell m}] = \epsilon L^{(1)}[\xi_{\ell m}] + \epsilon Q^{(1)}[\xi_{\ell m}] + \epsilon^2 Q^{(2)}[\xi_{\ell m}] + O(\epsilon^3), \tag{2.21}$$

where $L^{(0)}$, $L^{(1)}$, $Q^{(1)}$ and $Q^{(2)}$ are differential operators given by

$$L^{(0)} = \frac{d^2}{dz^2}+\frac{2}{z}\frac{d}{dz}+\left(1-\frac{\ell(\ell+1)}{z^2}\right), \tag{2.22}$$

$$L^{(1)} = \frac{1}{z}\frac{d^2}{dz^2}+\left(\frac{1}{z^2}+\frac{2i}{z}\right)\frac{d}{dz}-\left(\frac{4}{z^3}-\frac{i}{z^2}+\frac{1}{z}\right), \tag{2.23}$$

$$Q^{(1)} = \frac{iq\lambda_1}{2z^2}\frac{d}{dz}-\frac{4imq}{l(l+1)z^3}+\frac{4mq}{l(l+1)z^2}+\frac{\lambda_1 q+2mq}{2z^2}, \tag{2.24}$$

for arbitrary ℓ and

$$\begin{aligned}Q^{(2)} &= -\frac{q^2}{4z^2}\frac{d^2}{dz^2}-\left(\frac{9q^2-2m^2q^2-6imq}{36z^3}+\frac{i(2m^2q^2-9q^2)-18mq}{108z^2}\right)\frac{d}{dz}\\ &+\left(\frac{9q^2+5m^2q^2-3imq}{9z^4}+\frac{i(2m^2q^2-9q^2)}{54z^3}\right.\\ &\left.-\frac{-63imq+81q^2-2m^2q^2}{378z^2}\right),\end{aligned}$$

for $\ell = 2$. We do not need $Q^{(2)}$ for $\ell \geq 3$ for the post-Newtonian order we consider in this paper (i.e., up to $O(v^5)$ beyond Newtonian). Expanding $\xi_{\ell m}$ in terms of ϵ as

$$\xi_{\ell m} = \sum_{n=0}^{\infty}\epsilon^n\xi^{(n)}_{\ell m}(z), \tag{2.25}$$

we obtain from Eq.(2.21) the iterative equations,

$$L^{(0)}[\xi^{(0)}_{\ell m}] = 0, \tag{2.26}$$

$$L^{(0)}[\xi^{(1)}_{\ell m}] = L^{(1)}[\xi^{(0)}_{\ell m}] + Q^{(1)}[\xi^{(0)}_{\ell m}] \equiv W^{(1)}_{\ell m}, \tag{2.27}$$

$$L^{(0)}[\xi^{(2)}_{\ell m}] = L^{(1)}[\xi^{(1)}_{\ell m}] + Q^{(1)}[\xi^{(1)}_{\ell m}] + Q^{(2)}[\xi^{(1)}_{\ell m}] \equiv W^{(2)}_{\ell m}. \tag{2.28}$$

The general solution to Eq.(2.26) is immediately obtained as

$$\xi^{(0)}_{\ell m} = \alpha^{(0)}_{\ell} j_\ell + \beta^{(0)}_{\ell} n_\ell, \tag{2.29}$$

where j_ℓ and n_ℓ are usual spherical Bessel functions. The boundary condition for $n \leq 2$ is that $\xi^{(n)}_{\ell m}$ is regular at $z = 0$. Hence $\beta^{(0)}_{\ell} = 0$ and we set $\alpha^{(0)}_{\ell} = 1$ for convenience.

To calculate $\xi_{\ell m}^{(n)}$ for $n \geq 1$, we rewrite Eq.(2.27) and (2.28) in the indefinite integral form by using the spherical Bessel functions as

$$\xi_{\ell m}^{(n)} = n_\ell \int^z dz z^2 j_\ell W_{\ell m}^{(n)} - j_\ell \int^z dz z^2 n_\ell W_{\ell m}^{(n)} \quad (n = 1, 2). \tag{2.30}$$

For $n = 1$, we have

$$\begin{aligned}
\xi_{\ell m}^{(1)} &= \alpha_\ell^{(1)} j_\ell + \frac{(\ell-1)(\ell+3)}{2(\ell+1)(2\ell+1)} j_{\ell+1} - \frac{\ell^2-4}{2\ell(2\ell+1)} j_{\ell-1} \\
&+ z^2(n_\ell j_0 - j_\ell n_0) j_0 + \sum_{k=1}^{\ell-1} \left(\frac{1}{k} + \frac{1}{k+1}\right) z^2 (n_\ell j_k - j_\ell n_k) j_k \\
&+ n_\ell(\mathrm{Ci}(2z) - \gamma - \ln 2z) - j_\ell \mathrm{Si}(2z) + i j_\ell \ln z \\
&+ \frac{imq}{2}\left(\frac{\ell^2+4}{\ell^2(2\ell+1)}\right) j_{\ell-1} + \frac{imq}{2}\left(\frac{(\ell+1)^2+4}{(\ell+1)^2(2\ell+1)}\right) j_{\ell+1},
\end{aligned} \tag{2.31}$$

where $\mathrm{Ci}(x) = -\int_x^\infty dt \cos t/t$ and $\mathrm{Si}(x) = \int_0^x dt \sin t/t$ are cosine and sine integral functions, γ is the Euler constant, and $\alpha_\ell^{(1)}$ is an integration constant which represents the arbitrariness of the normalization of $X_{\ell m\omega}^{in}$. We set $\alpha_\ell^{(1)} = 0$ for simplicity.

As noted previously, the source term $T_{\ell m\omega}$ has support only around $r = r_0$ and $\omega r_0 = O(\Omega r_0) = O(v)$. Hence we only need $X_{\ell m\omega}^{in}$ at $z = O(v) \ll 1$ to evaluate the source integral, apart from the value of the incident amplitude $A_{\ell m\omega}^{in}$. Hence the post-Newtonian expansion of $X_{\ell m\omega}^{in}$ corresponds to the expansion not only in terms of $\epsilon = O(v^3)$ but also z by assuming $\epsilon \ll z \ll 1$. In order to evaluate the gravitational wave luminosity to $O(v^5)$ beyond the leading order, we must calculate the series expansion of $\xi_{\ell m}^{(n)}$ in powers of z for $n = 0$ to $\ell = 4$, for $n = 1$ to $\ell = 3$ and for $n = 2$ to $\ell = 2$.

When we evaluate $A_{\ell m\omega}^{in}$, we examine the asymptotic behavior of $\xi_{\ell m}^{(n)}$ at infinity. Since the accuracy of $A_{\ell m\omega}^{in}$ we need is $O(\epsilon)$, we don't have to calculate $\xi_{\ell m}^{(2)}$ in analytic form. We need only the series expansion formulas for $\xi_{\ell m}^{(2)}$ around $z = 0$, which is easily obtained by Eq.(2.30). Inserting $\xi_{\ell m}^{(n)}$ into Eq.(2.19) and expanding it by z and ϵ assuming $\epsilon \ll z \ll 1$, we obtain

$$\begin{aligned}
X_{2m\omega}^{in} &= \frac{z^3}{15} - \frac{z^5}{210} + \frac{z^7}{7560} + O(z^9) + \epsilon\left(\frac{imqz^2}{30} - \frac{13z^4}{630} - \frac{11imqz^4}{3780} + O(z^6)\right) \\
&+ \epsilon^2\left(\frac{q^2 + 2imq - m^2q^2}{120} z - \frac{mq}{30} z^2 + O(z^3)\right),
\end{aligned} \tag{2.32}$$

$$X_{3m\omega}^{in} = \frac{z^4}{105} - \frac{z^6}{1890} + O(z^8) + \epsilon\left(-\frac{z^3}{126} + \frac{2imq}{945} z^3 + O(z^5)\right), \tag{2.33}$$

$$X_{4m\omega}^{in} = \frac{z^5}{945} + O(z^7). \tag{2.34}$$

Using the transformation of Eq.(2.14), we obtain $R_{\ell m\omega}^{in}$ as

$$\begin{aligned}
\omega R_{2m\omega}^{in} &= \frac{z^4}{30} + \frac{i}{45} z^5 - \frac{11\, z^6}{1260} - \frac{i}{420} z^7 + \frac{23\, z^8}{45360} + \frac{i}{11340} z^9 \\
&+ \epsilon\left(\frac{-z^3}{15} - \frac{i}{60} m\, q\, z^3 - \frac{i}{60} z^4 + \frac{m\, q\, z^4}{45}\right. \\
&- \left.\frac{41\, z^5}{3780} + \frac{277\, i}{22680} m\, q\, z^5 - \frac{31\, i}{3780} z^6 - \frac{7\, m\, q\, z^6}{1620}\right) \\
&+ \epsilon^2\left(\frac{z^2}{30} + \frac{i}{40} m\, q\, z^2 + \frac{q^2\, z^2}{60} - \frac{m^2\, q^2\, z^2}{240}\right. \\
&- \left.\frac{i}{60} z^3 - \frac{m\, q\, z^3}{30} + \frac{i}{90} q^2\, z^3 - \frac{i}{120} m^2\, q^2\, z^3\right),
\end{aligned} \tag{2.35}$$

$$
\begin{aligned}
\omega R^{in}_{3m\omega} &= \frac{z^5}{630} + \frac{i}{1260} z^6 - \frac{z^7}{3780} - \frac{i}{16200} z^8 \\
&+ \epsilon\Big(\frac{-z^4}{252} - \frac{i}{1890} m q z^4 - \frac{i}{756} z^5 + \frac{11 m q z^5}{22680}\Big), \qquad (2.36)\\
\omega R^{in}_{4m\omega} &= \frac{z^6}{11340} + \frac{iz^7}{28350}. \qquad (2.37)
\end{aligned}
$$

We calculate $A^{in}_{\ell m\omega}$ by examining the asymptotic behavior of $\xi^{(n)}_{\ell m}$ and Eq.(2.19) at infinity. The results are expressed as

$$
A^{in}_{\ell m\omega} = \frac{1}{2} i^{\ell+1} e^{-i\epsilon \ln \epsilon} \left[1 + \epsilon\left(-\frac{\pi}{2}\mathrm{sgn}(\omega) + i q^{(1)}_{\ell m}\right) + \ldots\right], \qquad (2.38)
$$

where

$$
\begin{aligned}
q^{(1)}_{\ell m} &= \frac{1}{2}\left[\psi(\ell) + \psi(\ell+1) + \frac{(\ell-1)(\ell+3)}{\ell(\ell+1)}\right] - \ln 2 - \frac{2imq}{\ell^2(\ell+1)^2}, \qquad (2.39)\\
\psi(\ell) &= \sum_{k=1}^{\ell-1} \frac{1}{k} - \gamma. \qquad (2.40)
\end{aligned}
$$

The corresponding incident amplitudes $B^{in}_{\ell m\omega}$ for the Teukolsky function are obtained from Eq.(2.17).

3 Source terms

3.1 The geodesic equations

In this section, we solve the geodesic equation for a slightly eccentric motion. The same procedure was previously performed by Apostolatos et.al. [26] for Schwarzschild geometry.

The geodesic equations in Kerr geometry are given by

$$
\begin{aligned}
\Sigma\frac{d\theta}{d\tau} &= \pm\Big[C - \cos^2\theta\Big\{a^2(1-E^2) + \frac{l_z^2}{\sin^2\theta}\Big\}\Big]^{1/2} \equiv \Theta(\theta),\\
\Sigma\frac{d\varphi}{d\tau} &= -\Big(aE - \frac{l_z}{\sin^2\theta}\Big) + \frac{a}{\Delta}\Big(E(r^2+a^2) - al_z\Big) \equiv \Phi,\\
\Sigma\frac{dt}{d\tau} &= -\Big(aE - \frac{l_z}{\sin^2\theta}\Big)a\sin^2\theta + \frac{r^2+a^2}{\Delta}\Big(E(r^2+a^2) - al_z\Big) \equiv T,\\
\Sigma\frac{dr}{d\tau} &= \pm\sqrt{R}, \qquad (3.1)
\end{aligned}
$$

where E, l_z and C are the energy, the z-component of the angular momentum and the Carter constant of a test particle, respectively.[1] $\Sigma = r^2 + a^2\cos^2\theta$ and

$$
R = [E(r^2+a^2) - al_z]^2 - \Delta[(Ea - l_z)^2 + r^2 + C]. \qquad (3.2)
$$

We consider the motion of a particle in the equatorial plane $\theta = \pi/2$. In this case we can set $C = 0$. We define $r = r_0$ as the radius where the potential R/r^4 becomes the minimum $\partial(R/r^4)/\partial r\,|_{r=r_0} = 0$. We also define the eccentricity e so that $r = r_0(1+e)$ is a turning point of the radial motion, at which $R(r = r_0(1+e)) = 0$. In this paper we assume $e \ll 1$. Using above two equations and expanding E and l_z as

$$
\begin{aligned}
E &= E^{(0)} + eE^{(1)} + e^2E^{(2)} + e^3E^{(3)} + O(e^4),\\
l_z &= l_z^{(0)} + el_z^{(1)} + e^2l_z^{(2)} + e^3l_z^{(3)} + O(e^4),
\end{aligned}
$$

[1] In this section, these constants of motion are those measured in units of μ. That is, if expressed in the standard units, E, l_z and C in Eq.(3.1) are to be replaced with E/μ, l_z/μ and C/μ^2, respectively.

we obtain $E^{(n)}$ and $l_z^{(n)}$ for $n = 0, 1$ and 2 as

$$
\begin{aligned}
E^{(0)} &= \frac{1 - 2v^2 + qv^3}{(1 - 3v^2 + 2qv^3)^{(1/2)}}, \\
E^{(1)} &= 0, \\
E^{(2)} &= \frac{v^2(1 - 3v^2 + qv^3 + q^2v^4)(-1 + 6v^2 - 8qv^3 + 3q^2v^4)}{2(1 - 3v^2 + 2qv^3)^{3/2}(-1 + 2v^2 - q^2v^4)}, \\
l_z^{(0)} &= \frac{r_0 v(1 - 2qv^3 + q^2v^4)}{(1 - 3v^2 + 2qv^3)^{(1/2)}}, \\
l_z^{(1)} &= 0, \\
l_z^{(2)} &= \frac{q\, r_0\, v^5(q - 3v + qv^2 + q^2v^3)(-1 + 6v^2 - 8qv^3 + 3q^2v^4)}{2(1 - 3v^2 + 2qv^3)^{3/2}(-1 + 2v^2 - q^2v^4)},
\end{aligned}
$$

The post-Newtonian expansion forms of $E^{(n)}$ and $l_z^{(n)}$ up to the required orders are

$$
E = 1 - \frac{M}{2\,r_0} + \frac{3\,M^2}{8\,r_0{}^2} - \frac{q\,M^{\frac{3}{2}}}{r_0{}^{\frac{3}{2}}} + e^2\left(\frac{M}{2\,r_0} - \frac{5\,M^2}{4\,r_0{}^2} + \frac{3\,q\,M^{\frac{3}{2}}}{r_0{}^{\frac{3}{2}}}\right) + O(v^6), \tag{3.3}
$$

$$
\begin{aligned}
l_z &= (Mr_0)^{1/2}\left[1 + \frac{3M}{2r_0} - \frac{3qM^{3/2}}{r_0^{3/2}} + \left(\frac{27}{8} + q^2\right)\frac{M^2}{r_0^2} - \frac{15qM^{5/2}}{2r_0^{5/2}}\right. \\
&\quad \left. + e^2\left(\frac{q^2M^2}{2r_0^2} - \frac{3qM^{5/2}}{2r_0^{5/2}}\right) + O(v^6)\right].
\end{aligned} \tag{3.4}
$$

Next we solve the geodesic equations for slightly eccentric orbits. The radial equation is

$$
\left(\frac{dr}{dt}\right)^2 = \frac{R}{T^2}. \tag{3.5}
$$

We expand $r(t)$ as

$$
r(t) = r_0\left[1 + er^{(1)}(t) + e^2r^{(2)}(t) + O(e^3)\right], \tag{3.6}
$$

and R/T^2 in terms of e and v using Eq.(3.3) and (3.4). Collecting terms of equal order in e, we obtain

$$
\left(\frac{dr^{(1)}}{dt}\right)^2 = \Omega_r^2(1 - (r^{(1)})^2), \tag{3.7}
$$

and

$$
\frac{1}{\Omega_r^2}\frac{dr^{(1)}}{dt}\frac{dr^{(2)}}{dt} = -r^{(1)}r^{(2)} + q_0 + q_1r^{(1)} + q_2(r^{(1)})^2. \tag{3.8}
$$

In this paper, since we don't need the exact expression of Ω_r, q_0, q_1 and q_2, we only show its post-Newtonian forms:

$$
\Omega_r = \frac{M^{1/2}}{r_0^{3/2}}\left[1 - \frac{3M}{r_0} + \frac{3qM^{3/2}}{r_0^{3/2}} - \frac{(9 + 3q^2)M^2}{2r_0^2} + \frac{15qM^{5/2}}{r_0^{5/2}} + O(v^6)\right], \tag{3.9}
$$

$$
q_0 = -1 + \frac{M}{r_0} - \frac{2\,q\,M^{3/2}}{r_0{}^{3/2}} + \frac{(6 + q^2)\,M^2}{r_0{}^2} - \frac{20\,q\,M^{5/2}}{r_0{}^{5/2}} + O(v^6), \tag{3.10}
$$

$$
q_1 = \frac{2\,M}{r_0}\left[1 + \frac{2\,M}{r_0} - \frac{3\,q\,M^{\frac{3}{2}}}{r_0{}^{\frac{3}{2}}} + \frac{4\,M^2}{r_0{}^2} - \frac{6\,q\,M^{\frac{3}{2}}}{r_0{}^{\frac{3}{2}}} + O(v^6)\right], \tag{3.11}
$$

$$
q_2 = 1 - \frac{3\,M}{r_0} + \frac{2\,q\,M^{\frac{3}{2}}}{r_0{}^{\frac{3}{2}}} + \frac{(-10 - q^2)\,M^2}{r_0{}^2} + \frac{26\,q\,M^{\frac{3}{2}}}{r_0{}^{\frac{3}{2}}} + O(v^6). \tag{3.12}
$$

We obtain $r^{(1)}(t)$ from Eq.(3.7) as

$$r^{(1)}(t) = \cos\Omega_r t, \tag{3.13}$$

where we set $r(t=0) = r_0(1+e)$. Substitution of Eq. (3.13) into Eq. (3.8) yields after integration

$$r^{(2)}(t) = q_3(1-\cos\Omega_r t) + q_4(1-\cos 2\Omega_r t), \tag{3.14}$$

where $q_3 = -q_0$ and $q_4 = q_2/2$.

In the same way, we can calculate $\varphi(t)$. From Eq.(3.1), we have $d\varphi/dt = \Phi/T$, which can be expanded in terms of e using Eq.(3.3), (3.4), (3.6), (3.13) and (3.14). Integrating the resulting equation, we obtain

$$\varphi(t) = \Omega_\varphi t + ep_1 \sin\Omega_r t + e^2 p_2 \sin\Omega_r t + e^2 p_3 \sin 2\Omega_r t + O(e^3), \tag{3.15}$$

where

$$\begin{aligned}
p_1 &= -2 - \frac{4M}{r_0} + \frac{6qM^{\frac{3}{2}}}{r_0^{\frac{3}{2}}} + \frac{(-17-q^2)\,M^2}{r_0^2} + \frac{48qM^{\frac{3}{2}}}{r_0^{\frac{5}{2}}} + O(v^6),\\
p_2 &= 2 + \frac{2M}{r_0} - \frac{2qM^{\frac{3}{2}}}{r_0^{\frac{3}{2}}} + \frac{(1-q^2)\,M^2}{r_0^2} + \frac{6qM^{\frac{3}{2}}}{r_0^{\frac{5}{2}}} + O(v^6),\\
p_3 &= \frac{5}{4} + \frac{M}{4r_0} - \frac{2qM^{\frac{3}{2}}}{r_0^{\frac{3}{2}}} - \frac{(9+7q^2)\,M^2}{8r_0^2} + \frac{59\,(-1+q^2)\,M^3}{8r_0^3} + O(v^6),
\end{aligned} \tag{3.16}$$

and

$$\begin{aligned}
\Omega_\varphi &= \frac{\sqrt{M}}{r_0^{\frac{3}{2}}}\left[1 - \frac{qM^{3/2}}{r_0^{3/2}}\right.\\
&\quad \left. + e^2\left(-\frac{3}{2} + \frac{9M}{2r_0} - \frac{9qM^{3/2}}{2r_0^{3/2}} + \frac{3\,(6+q^2)\,M^2}{r_0^2} - \frac{60qM^{5/2}}{r_0^{5/2}}\right) + O(v^6)\right].
\end{aligned} \tag{3.17}$$

The fact that $\Omega_r \neq \Omega_\varphi$ implies that these eccentric orbits are not closed.

3.2 Integration of the source term

In this section, using the results of the previous section, we derive the source term of the Teukolsky equation and integrate it to give the amplitude of the Teukolsky function at infinity.

The energy momentum tensor of a test particle of mass μ is given by

$$T^{\mu\nu} = \frac{\mu}{\Sigma\sin\theta dt/d\tau}\frac{dz^\mu}{d\tau}\frac{dz^\nu}{d\tau}\delta(r-r(t))\delta(\theta-\pi/2)\delta(\varphi-\varphi(t)). \tag{3.18}$$

The source term of the Teukolsky equation is given by

$$T_{\ell m\omega} = 4\int d\Omega dt \rho^{-5}\bar{\rho}^{-1}(B_2' + B_2'^*)e^{-im\varphi+i\omega t}\frac{{}_{-2}S^{a\omega}_{\ell m}}{\sqrt{2\pi}}, \tag{3.19}$$

where

$$\begin{aligned}
B_2' &= -\frac{1}{2}\rho^8\bar{\rho}L_{-1}[\rho^{-4}L_0(\rho^{-2}\bar{\rho}^{-1}T_{nn})]\\
&\quad - \frac{1}{2\sqrt{2}}\rho^8\bar{\rho}\Delta^2 L_{-1}[\rho^{-4}\bar{\rho}^2 J_+(\rho^{-2}\bar{\rho}^{-2}\Delta^{-1}T_{\bar{m}n})],\\
B_2'^* &= -\frac{1}{4}\rho^8\bar{\rho}\Delta^2 J_+[\rho^{-4}J_+(\rho^{-2}\bar{\rho}T_{\bar{m}\bar{m}})]\\
&\quad - \frac{1}{2\sqrt{2}}\rho^8\bar{\rho}\Delta^2 J_+[\rho^{-4}\bar{\rho}^2\Delta^{-1}L_{-1}(\rho^{-2}\bar{\rho}^{-2}T_{\bar{m}n})],
\end{aligned} \tag{3.20}$$

with

$$
\begin{aligned}
\rho &= (r - ia\cos\theta)^{-1}, \\
L_s &= \partial_\theta + \frac{m}{\sin\theta} - a\omega\sin\theta + s\cot\theta, \\
J_+ &= \partial_r + iK/\Delta,
\end{aligned}
\tag{3.21}
$$

and $\overline{\rho}$ etc. denoting the complex conjugate of ρ.

In the present case, the tetrad components of the energy momentum tensor, T_{nn}, $T_{\overline{m}n}$ and $T_{\overline{m}\overline{m}}$, are in the forms,

$$
\begin{aligned}
T_{nn} &= \frac{C_{nn}}{\sin\theta}\delta(r - r(t))\delta(\theta - \pi/2)\delta(\varphi - \varphi(t)), \\
T_{\overline{m}n} &= \frac{C_{\overline{m}n}}{\sin\theta}\delta(r - r(t))\delta(\theta - \pi/2)\delta(\varphi - \varphi(t)), \\
T_{\overline{m}\overline{m}} &= \frac{C_{\overline{m}\overline{m}}}{\sin\theta}\delta(r - r(t))\delta(\theta - \pi/2)\delta(\varphi - \varphi(t)),
\end{aligned}
\tag{3.22}
$$

where

$$
\begin{aligned}
C_{nn} &= \frac{\mu}{4\Sigma^3 \dot{t}}\left[E(r^2 + a^2) - al_z + \Sigma\frac{dr}{d\tau}\right]^2, \\
C_{\overline{m}n} &= -\frac{\mu\rho}{2\sqrt{2}\Sigma^2 \dot{t}}\left[E(r^2 + a^2) - al_z + \Sigma\frac{dr}{d\tau}\right]\left[i\sin\theta\left(aE - \frac{l_z}{\sin^2\theta}\right)\right], \\
C_{\overline{m}\overline{m}} &= \frac{\mu\rho^2}{2\Sigma\dot{t}}\left[i\sin\theta\left(aE - \frac{l_z}{\sin^2\theta}\right)\right]^2,
\end{aligned}
\tag{3.23}
$$

and $\dot{t} = dt/d\tau$.

Substituting Eq.(3.20) into Eq.(3.19) and performing integration by part, we obtain

$$
\begin{aligned}
T_{\ell m\omega} &= \frac{4}{\sqrt{2\pi}}\int_{-\infty}^{\infty} dt \int d\theta e^{i\omega t - im\varphi(t)} \\
&\times \Big[-\frac{1}{2}L_1^\dagger\{\rho^{-4}L_2^\dagger(\rho^3 S)\}C_{nn}\rho^{-2}\overline{\rho}^{-1}\delta(r - r(t))\delta(\theta - \pi/2) \\
&+ \frac{\Delta^2\overline{\rho}^2}{\sqrt{2}\rho}(L_2^\dagger S + ia(\overline{\rho} - \rho)\sin\theta S)J_+\{C_{\overline{m}n}\rho^{-2}\overline{\rho}^{-2}\Delta^{-1}\delta(r - r(t))\delta(\theta - \pi/2)\} \\
&+ \frac{1}{2\sqrt{2}}L_2^\dagger\{\rho^3 S(\overline{\rho}^2\rho^{-4})_{,r}\}C_{\overline{m}n}\Delta\rho^{-2}\overline{\rho}^{-2}\delta(r - r(t))\delta(\theta - \pi/2) \\
&- \frac{1}{4}\rho^3\Delta^2 S J_+\{\rho^{-4}J_+(\overline{\rho}\rho^{-2}C_{\overline{m}\overline{m}}\delta(r - r(t))\delta(\theta - \pi/2))\}\Big],
\end{aligned}
\tag{3.24}
$$

where

$$
L_s^\dagger = \partial_\theta - \frac{m}{\sin\theta} + a\omega\sin\theta + s\cot\theta,
\tag{3.25}
$$

and S denotes ${}_{-2}S_{\ell m}^{a\omega}(\theta(t))$ for simplicity.

We further rewrite Eq.(3.24) as

$$
\begin{aligned}
T_{\ell m\omega} &= \int_{-\infty}^{\infty} dt e^{i\omega t - im\varphi(t)}\Delta^2\Big[(A_{nn0} + A_{\overline{m}n0} + A_{\overline{m}\overline{m}0})\delta(r - r(t)) \\
&+ \{(A_{\overline{m}n1} + A_{\overline{m}\overline{m}1})\delta(r - r(t))\}_{,r} + \{A_{\overline{m}\overline{m}2}\delta(r - r(t))\}_{,rr}\Big],
\end{aligned}
\tag{3.26}
$$

where $A_{n\,n\,0}$ etc. are given in Appendix B. Inserting Eq.(3.26) into Eq.(2.5), we obtain $\tilde{Z}_{\ell m\omega}$ as

$$\begin{aligned}
\tilde{Z}_{\ell m\omega} &= \frac{1}{2i\omega B^{in}_{\ell m\omega}}\int_{-\infty}^{\infty} dt e^{i\omega t - im\varphi(t)}\Big[R^{in}_{\ell m\omega}\{A_{n\,n\,0}+A_{\overline{m}\,n\,0}+A_{\overline{m}\,\overline{m}\,0}\} \\
&\quad -\frac{dR^{in}_{\ell m\omega}}{dr}\{A_{\overline{m}\,n\,1}+A_{\overline{m}\,\overline{m}\,1}\}+\frac{d^2R^{in}_{\ell m\omega}}{dr^2}A_{\overline{m}\,\overline{m}\,2}\Big]_{r=r(t)}, \\
&\equiv \frac{1}{2i\omega_n B^{in}_{\ell m\omega}}\int_{-\infty}^{\infty} dt e^{i\omega t - im\varphi(t)}W_{\ell m\omega}\,. \qquad (3.27)
\end{aligned}$$

Eq. (3.27) can be simplified by noting the result of the previous section that the orbits of our interest have the properties,

$$r(t+\Delta t)=r(t), \qquad d\varphi/dt\,|_{t=t+\Delta t}=d\varphi/dt\,|_{t=t}, \qquad (3.28)$$

where $\Delta t = 2\pi/\Omega_r$. Using this fact, we can rewrite the above integral as

$$\begin{aligned}
\tilde{Z}_{\ell m\omega} &= \frac{1}{2i\omega B^{in}_{\ell m\omega}}\int_{-\infty}^{\infty} dt e^{i\omega t - im\varphi(t)}W_{\ell m\omega} \\
&= \frac{1}{2i\omega B^{in}_{\ell m\omega}}\frac{2\pi}{\Delta t}\int_0^{\Delta t} dt e^{i\omega t - im\varphi(t)}W_{\ell m\omega}\sum_n \delta(\omega-\omega_n) \\
&\equiv \sum_n \delta(\omega-\omega_n)Z_{\ell m\omega}, \qquad (3.29)
\end{aligned}$$

where

$$\omega_n = n\Omega_r + m\Omega_\varphi, \quad (n=0,\pm1,\pm2,\ldots). \qquad (3.30)$$

Using the solution of the geodesic equation for $r(t)$, we expand $W_{\ell m\omega_n}$ in terms of e. We can see that the resulting equation has the structure up to the order $O(e^2)$,

$$\begin{aligned}
W_{\ell m\omega} &= f_0 + e\left(f_1 r^{(1)} + f_2\frac{dr^{(1)}}{dt}\right) + e^2\left(f_3 r^{(2)} + f_4\frac{dr^{(2)}}{dt} + f_5 (r^{(1)})^2\right. \\
&+ \left. f_6\left(\frac{dr^{(1)}}{dt}\right)^2 + f_7 r^{(1)}\frac{dr^{(1)}}{dt} + f_8\right) + O(e^3). \qquad (3.31)
\end{aligned}$$

We insert Eq.(3.13), (3.14), (3.15) and (3.31) into Eq.(3.32) and expand it in terms of e. Finally, using the relations $\cos(\Omega_r t) = (e^{i\Omega_r t}+e^{-i\Omega_r t})/2$ and $\sin(\Omega_r t) = (e^{i\Omega_r t}-e^{-i\Omega_r t})/2i$, we obtain

$$\begin{aligned}
I_{\ell m\omega_n} &\equiv \int_0^{\Delta t} dt e^{i\omega_n t - im\varphi(t)}W_{\ell m\omega_n} \\
&= \Delta t\,\Big[\Big\{f_0 + e^2\Big(\frac{f_5}{2}+f_8-\frac{m^2p_1^2}{4}f_0 \\
&\quad +(q_3+q_4)f_3+\frac{im\Omega_r p_1}{2}f_2+\frac{\Omega_r^2}{2}f_6\Big)\Big]\,\delta_{n,0} \\
&\quad +e\left(\frac{f_1}{2}+\frac{mp_1}{2}f_0-\frac{i\Omega_r}{2}f_2\right)\delta_{n,1} \\
&\quad +e\left(\frac{f_1}{2}-\frac{mp_1}{2}f_0+\frac{i\Omega_r}{2}f_2\right)\delta_{n,-1} \\
&\quad +e^2\Big(\frac{3f_5}{4}+f_8+\frac{f_1\,m\,p_1}{4}-\frac{f_0\,m^2\,{p_1}^2}{8}+\frac{f_0\,m\,p_3}{2}+f_3\,q_3 \\
&\quad +\frac{f_3\,q_4}{2}-\frac{i}{4}f_7\,w+\frac{i}{4}f_2\,m\,p_1\,w+i\,f_4\,q_4\,w+\frac{f_6\,w^2}{4}\Big)\,\delta_{n,2}
\end{aligned}$$

$$+e^2\left(\frac{3f_5}{4}+f_8-\frac{f_1\,m\,p_1}{4}-\frac{f_0\,m^2\,{p_1}^2}{8}-\frac{f_0\,m\,p_3}{2}+f_3\,q_3\right.$$
$$\left.+\frac{f_3\,q_4}{2}+\frac{i}{4}f_7\,w+\frac{i}{4}f_2\,m\,p_1\,w-i\,f_4\,q_4\,w+\frac{f_6\,w^2}{4}\right)\delta_{n,-2}\Bigg] \tag{3.32}$$

We can see from Eq.(3.32) that $n=\pm 2$ modes occur at $O(e^2)$. Then when we evaluate the luminosity, $n=\pm 2$ modes contribute from $O(e^4)$. Therefore we have only to calculate $n=0,\pm 1$ modes to evaluate the luminosity up to $O(e^2)$.

4 The energy and angular momentum fluxes

In this section, we calculate the energy and angular momentum fluxes to $O(v^5)$ beyond the quadrupole formula and to $O(e^2)$ in the eccentricity. From Eq.(2.1), ψ_4 at $r\to\infty$ takes the form,

$$\psi_4=\frac{1}{r}\sum_{n=-2}^{2}\sum_{\ell=2}^{4}\sum_{m=-\ell}^{\ell}Z_{\ell m\omega_n}\frac{{}_{-2}S^{a\omega_n}_{\ell m}}{\sqrt{2\pi}}e^{i\omega_n(r^*-t)+im\varphi}. \tag{4.1}$$

At infinity, ψ_4 is related to the two independent modes of gravitational waves h_+ and $h_\times$ as

$$\psi_4=\frac{1}{2}(\ddot{h}_+-i\ddot{h}_\times). \tag{4.2}$$

From Eqs.(4.1) and (4.2), the energy flux averaged over $t\gg\Delta t$ is given by

$$\left\langle\frac{dE}{dt}\right\rangle=\sum_{\ell,m,n}\frac{\left|Z_{\ell m\omega_n}\right|^2}{4\pi\omega_n^2}\equiv\sum_{\ell,m,n}\left(\frac{dE}{dt}\right)_{\ell mn}. \tag{4.3}$$

In the same way, the angular momentum flux is given by

$$\left\langle\frac{dJ_z}{dt}\right\rangle=\sum_{\ell,m,n}\frac{m\left|Z_{\ell m\omega_n}\right|^2}{4\pi\omega_n^3}\equiv\sum_{\ell,m,n}\left(\frac{dJ_z}{dt}\right)_{\ell mn}=\sum_{\ell,m,n}\frac{m}{\omega_n}\left(\frac{dE}{dt}\right)_{\ell mn}. \tag{4.4}$$

In order to express the post-Newtonian corrections to the luminosity, we define $\eta_{\ell mn}$ as

$$\left(\frac{dE}{dt}\right)_{\ell mn}\equiv\frac{1}{2}\left(\frac{dE}{dt}\right)_N\eta_{\ell,m,n}, \tag{4.5}$$

where $(dE/dt)_N$ is the Newtonian quadrupole luminosity:

$$\left(\frac{dE}{dt}\right)_N=\frac{32\mu^2M^3}{5r_0^5}=\frac{32}{5}\left(\frac{\mu}{M}\right)^2v^{10}.$$

For $\ell=2$, $\eta_{\ell,m,n}$ which contribute to the luminosity to $O(v^5)$ are given by the following formulae. We only show $\eta_{\ell mn}$ for $m\geq 0$ mode. $\eta_{\ell,m,n}$ for $m\leq 0$ is easily obtained from the symmetry $\eta_{\ell,m,n}=\eta_{\ell,-m,-n}$.

$$\begin{aligned}\eta_{2,2,0}\;=\;&1-\frac{107\,v^2}{21}+4\,\pi\,v^3-6\,q\,v^3+\frac{4784\,v^4}{1323}+2\,q^2\,v^4\\&-\frac{428\,\pi\,v^5}{21}+\frac{4216\,q\,v^5}{189}\\&+e^2\left(-10+\frac{932\,v^2}{21}-46\,\pi\,v^3+84\,q\,v^3-\frac{14417\,v^4}{147}-23\,q^2\,v^4\right.\\&\left.+\frac{4748\,\pi\,v^5}{21}+\frac{2675\,q\,v^5}{189}\right)\end{aligned}$$

$$
\begin{aligned}
\eta_{2,2,1} &= e^2\left(\frac{729}{64}-\frac{3645\,v^2}{64}+\frac{2187\,\pi\,v^3}{32}-\frac{3645\,q\,v^3}{32}\right.\\
&\quad\left.+\frac{24057\,v^4}{256}+\frac{2187\,q^2\,v^4}{64}-\frac{6561\,\pi\,v^5}{16}+\frac{9477\,q\,v^5}{112}\right)\\
\eta_{2,2,-1} &= e^2\left(\frac{9}{64}+\frac{1041\,v^2}{448}+\frac{9\,\pi\,v^3}{32}-\frac{153\,q\,v^3}{32}\right.\\
&\quad\left.+\frac{2224681\,v^4}{112896}+\frac{99\,q^2\,v^4}{64}+\frac{615\,\pi\,v^5}{112}-\frac{27857\,q\,v^5}{336}\right)\\
\eta_{2,1,0} &= \frac{v^2}{36}-\frac{q\,v^3}{12}-\frac{17\,v^4}{504}+\frac{q^2\,v^4}{16}+\frac{\pi\,v^5}{18}-\frac{793\,q\,v^5}{9072}\\
&\quad+e^2\left(\frac{-2\,v^2}{9}+\frac{2\,q\,v^3}{3}+\frac{93\,v^4}{112}-\frac{q^2\,v^4}{2}-\frac{19\,\pi\,v^5}{36}-\frac{27113\,q\,v^5}{18144}\right)\\
\eta_{2,1,1} &= e^2\left(\frac{4\,v^2}{9}-\frac{4\,q\,v^3}{3}-\frac{172\,v^4}{63}+q^2\,v^4+\frac{16\,\pi\,v^5}{9}+\frac{2794\,q\,v^5}{567}\right)\\
\eta_{2,0,\pm1} &= e^2\left(\frac{1}{96}-\frac{145\,v^2}{672}+\frac{\pi\,v^3}{48}+\frac{3\,q\,v^3}{16}+\frac{282521\,v^4}{169344}-\frac{3\,q^2\,v^4}{32}\right.\\
&\quad\left.-\frac{83\,\pi\,v^5}{168}-\frac{1255\,q\,v^5}{504}\right),
\end{aligned}
$$

and $\eta_{2,1,-1}$ becomes $O(v^6)$. Putting together the above results, we obtain $(dE/dt)_\ell \equiv \sum_{mn}(dE/dt)_{\ell mn}$ for $\ell = 2$ as

$$
\begin{aligned}
\left(\frac{dE}{dt}\right)_2 &= \left(\frac{dE}{dt}\right)_N\left\{1-\frac{1277\,v^2}{252}+4\,\pi\,v^3-\frac{73\,q\,v^3}{12}+\frac{37915\,v^4}{10584}\right.\\
&\quad+\frac{33\,q^2\,v^4}{16}-\frac{2561\,\pi\,v^5}{126}+\frac{201575\,q\,v^5}{9072}\\
&\quad+e^2\left(\frac{37}{24}-\frac{2581\,v^2}{252}+\frac{1087\,\pi\,v^3}{48}-\frac{211\,q\,v^3}{6}+\frac{325393\,v^4}{21168}+\frac{105\,q^2\,v^4}{8}\right.\\
&\quad\left.\left.-\frac{29857\,\pi\,v^5}{168}+\frac{11293\,q\,v^5}{672}\right)\right\}. \qquad (4.6)
\end{aligned}
$$

For $\ell = 3$, we obtain

$$
\begin{aligned}
\eta_{3,3,0} &= \frac{1215\,v^2}{896}-\frac{1215\,v^4}{112}+\frac{3645\,\pi\,v^5}{448}-\frac{1215\,q\,v^5}{112}\\
&\quad+e^2\left(\frac{-10935\,v^2}{448}+\frac{37665\,v^4}{256}-\frac{142155\,\pi\,v^5}{896}+\frac{134865\,q\,v^5}{448}\right)\\
\eta_{3,3,1} &= e^2\left(\frac{640\,v^2}{21}-\frac{46720\,v^4}{189}+\frac{5120\,\pi\,v^5}{21}-\frac{1280\,q\,v^5}{3}\right)\\
\eta_{3,3,-1} &= e^2\left(\frac{15\,v^2}{14}+\frac{1055\,v^4}{126}+\frac{30\,\pi\,v^5}{7}-\frac{435\,q\,v^5}{14}\right)\\
\eta_{3,2,0} &= \frac{5\,v^4}{63}-\frac{40\,q\,v^5}{189}+e^2\left(\frac{-65\,v^4}{63}+\frac{520\,q\,v^5}{189}\right)\\
\eta_{3,2,1} &= e^2\left(\frac{3645\,v^4}{1792}-\frac{1215\,q\,v^5}{224}\right)\\
\eta_{3,2,-1} &= e^2\left(\frac{5\,v^4}{1792}-\frac{5\,q\,v^5}{672}\right)\\
\eta_{3,1,0} &= \frac{v^2}{8064}-\frac{v^4}{1512}+\frac{\pi\,v^5}{4032}-\frac{17\,q\,v^5}{9072}
\end{aligned}
$$

$$+e^2\left(\frac{-v^2}{4032}+\frac{65\,v^4}{16128}-\frac{\pi\,v^5}{1152}+\frac{199\,q\,v^5}{36288}\right)$$

$$\eta_{3,1,1} = e^2\left(\frac{v^2}{126}-\frac{23\,v^4}{126}+\frac{2\,\pi\,v^5}{63}+\frac{122\,q\,v^5}{567}\right)$$

$$\eta_{3,0,\pm1} = e^2\left(\frac{v^4}{2688}-\frac{q\,v^5}{1008}\right)$$

and $\eta_{3,1,-1}$ becomes $O(v^6)$. Thus we obtain

$$\left(\frac{dE}{dt}\right)_3 = \left(\frac{dE}{dt}\right)_N\left\{\frac{1367\,v^2}{1008}-\frac{32567\,v^4}{3024}+\left(\frac{16403\,\pi}{2016}-\frac{896\,q}{81}\right)v^5 +e^2\left(\frac{1801\,v^2}{252}-\frac{78509\,v^4}{864}+\left(\frac{40083\,\pi}{448}-\frac{8913\,q}{56}\right)v^5\right)\right\} \tag{4.7}$$

For $\ell = 4$, we have

$$\eta_{4,4,0} = \frac{1280\,v^4}{567}-\frac{37120\,e^2\,v^4}{567},$$

$$\eta_{4,4,1} = \frac{48828125\,e^2\,v^4}{580608},$$

$$\eta_{4,4,-1} = \frac{32805\,e^2\,v^4}{7168},$$

$$\eta_{4,2,0} = \frac{5\,v^4}{3969}-\frac{25\,e^2\,v^4}{3969},$$

$$\eta_{4,2,-1} = \frac{5\,e^2\,v^4}{254016},$$

$$\eta_{4,0,\pm1} = \frac{e^2\,v^4}{225792},$$

and $\eta_{4,2,1}$ becomes $O(v^6)$. Hence we have

$$\left(\frac{dE}{dt}\right)_4 = \left(\frac{dE}{dt}\right)_N\left\{\frac{8965\,v^4}{3969}+\frac{2946739\,e^2\,v^4}{127008}\right\}. \tag{4.8}$$

Finally, gathering all the above results, we have the energy luminosity up to $O(v^5)$ as

$$\left\langle\frac{dE}{dt}\right\rangle = \left(\frac{dE}{dt}\right)_N\left\{1-\frac{1247\,v^2}{336}+4\,\pi\,v^3-\frac{73\,q\,v^3}{12}-\frac{44711\,v^4}{9072}+\frac{33\,q^2\,v^4}{16} -\frac{8191\,\pi\,v^5}{672}+\frac{3749\,q\,v^5}{336}+e^2\left(\frac{37}{24}-\frac{65\,v^2}{21}+\frac{1087\,\pi\,v^3}{48}-\frac{211\,q\,v^3}{6} -\frac{474409\,v^4}{9072}+\frac{105\,q^2\,v^4}{8}-\frac{118607\,\pi\,v^5}{1344}-\frac{95663\,q\,v^5}{672}\right)\right\} \tag{4.9}$$

This result agrees with those derived in Shibata et.al. [17] if we set $e = 0$. To compare our results to those derived in the previous papers, it is convenient to change the parameter from v to $v' \equiv (M\Omega_\varphi)^{1/3}$. The relation between v and v' is given by

$$v = v'\left[1+\frac{q}{3}v'^3+e^2\left\{\frac{1}{2}-\frac{3}{2}v'^2+\frac{8}{3}qv'^3 -6v'^4-q^2v'^4+\frac{31}{2}qv'^5\right\}\right]. \tag{4.10}$$

Then we can see that the terms which are proportional to e^2 agree with the formulae derived by Peters and Mathews [27] at reading order, Galt'sov et.al. [28] and Blanchet and Schäfer at v^2 order [29], Blanchet and Schäfer at v^3 order without q term [10] and Shibata at v^3 order with q term [18] when we expand their formulae by e assuming $e \ll 1$ and set $\mu/M \ll 1$.

From Eq.(4.4), the averaged angular momentum fluxes for $\ell = 2$, 3 and 4 are calculated to give

$$\begin{aligned}
\left(\frac{dJ_z}{dt}\right)_2 &= \left(\frac{dJ_z}{dt}\right)_N \left\{1 - \frac{1277\,v^2}{252} + 4\,\pi\,v^3 - \frac{61\,q\,v^3}{12} + \frac{37915\,v^4}{10584} + \frac{33\,q^2\,v^4}{16}\right. \\
&\quad - \frac{2561\,\pi\,v^5}{126} + \frac{22229\,q\,v^5}{1296} + e^2\left(-\frac{5}{8} + \frac{137\,v^2}{24} + \frac{49\,\pi\,v^3}{8} - \frac{57\,q\,v^3}{4}\right. \\
&\quad \left.\left. - \frac{249787\,v^4}{14112} + \frac{203\,q^2\,v^4}{32} - \frac{20437\,\pi\,v^5}{504} - \frac{164449\,q\,v^5}{4536}\right)\right\} \\
\left(\frac{dJ_z}{dt}\right)_3 &= \left(\frac{dJ_z}{dt}\right)_N \left\{\frac{1367\,v^2}{1008} - \frac{32567\,v^4}{3024} + \left(\frac{16403\,\pi}{2016} - \frac{88049\,q}{9072}\right) v^5\right. \\
&\quad \left. + e^2\left(\frac{67\,v^2}{32} - \frac{66497\,v^4}{2016} + \left(\frac{43193\,\pi}{1008} - \frac{1675571\,q}{18144}\right), v^5\right)\right. \\
\left(\frac{dJ_z}{dt}\right)_4 &= \left(\frac{dJ_z}{dt}\right)_N \left\{\frac{8965\,v^4}{3969} + \frac{478195\,e^2\,v^4}{42336}\right\}
\end{aligned}$$

where $(dJ_z/dt)_N$ is defined to be

$$\left(\frac{dJ_z}{dt}\right)_N = \frac{32\mu^2 M^{5/2}}{5 r_0^{7/2}} = \frac{32}{5}\left(\frac{\mu}{M}\right)^2 M v^7. \tag{4.11}$$

Total angular momentum luminosity is then given by

$$\begin{aligned}
\left\langle\frac{dJ_z}{dt}\right\rangle &= \left(\frac{dJ_z}{dt}\right)_N \left\{1 - \frac{1247\,v^2}{336} + \left(4\,\pi - \frac{61\,q}{12}\right) v^3 + \left(-\frac{44711}{9072} + \frac{33\,q^2}{16}\right) v^4\right. \\
&\quad + \left(\frac{-8191\,\pi}{672} + \frac{417\,q}{56}\right) v^5 + e^2\left(-\frac{5}{8} + \frac{749\,v^2}{96} + \left(\frac{49\,\pi}{8} - \frac{57\,q}{4}\right) v^3\right. \\
&\quad \left.\left. + \left(-\frac{238229}{6048} + \frac{203\,q^2}{32}\right) v^4 + \left(\frac{773\,\pi}{336} - \frac{28807\,q}{224}\right) v^5\right)\right\}
\end{aligned} \tag{4.12}$$

From above results, we find that q^2 terms appear at v^4 order and linear terms in q appear at v^3 and v^5 orders in all of the above formulae. Those feature are the same as in Shibata et.at.

5 Stability of circular orbit under radiation reaction

Apostolatos et.al. [26] investigated the stability of circular orbit of a test particle around a Schwarzschild black hole under the influence of radiation reaction, and they show that a circular orbit is stable only if the orbital radius is greater than a critical radius $r_c \simeq 6.6792M$. In this section, we extend their analysis to a Kerr black hole case and investigate the stability of circular orbit under radiation reaction using the post-Newtonian approximation.

We are interested in the evolution of the radius r_0 and eccentricity e. Since E and l_z of a particle which we are considering is determined by e and r_0, the knowledge of the rates of loss of energy and angular momentum due to gravitational radiation is sufficient to determine the evolution of e and r_0. The evolution equations for e and r_0 are determined by

$$\begin{aligned}
\dot{E} &= \frac{\partial E(r_0, e)}{\partial r_0}\frac{dr_0}{dt} + \frac{\partial E(r_0, e)}{\partial e}\frac{de}{dt}, \\
\dot{l}_z &= \frac{\partial l_z(r_0, e)}{\partial r_0}\frac{dr_0}{dt} + \frac{\partial l_z(r_0, e)}{\partial e}\frac{de}{dt},
\end{aligned} \tag{5.1}$$

where $\dot{E}$ and $\dot{l}_z$ represent the time derivatives. We concentrate our attention to the secular evolution of e and r_0. We therefore set $\dot{E} = -\langle dE/dt \rangle$ and $\dot{l}_z = -\langle dJ_z/dt \rangle$. Solving Eq.(5.1) in terms of de/dt and dr_0/dt, we have

$$\begin{aligned}
\frac{dr_0}{dt} &= \left[-\frac{\partial L_z}{\partial e}\left\langle\frac{dE}{dt}\right\rangle + \frac{\partial E}{\partial e}\left\langle\frac{dJ_z}{dt}\right\rangle\right] \Big/ \left[\frac{\partial L_z}{\partial e}\frac{\partial E}{\partial r_0} - \frac{\partial E}{\partial e}\frac{\partial L_z}{\partial r_0}\right], \\
\frac{de}{dt} &= \left[\frac{\partial L_z}{\partial r_0}\left\langle\frac{dE}{dt}\right\rangle - \frac{\partial E}{\partial r_0}\left\langle\frac{dJ_z}{dt}\right\rangle\right] \Big/ \left[\frac{\partial L_z}{\partial e}\frac{\partial E}{\partial r_0} - \frac{\partial E}{\partial e}\frac{\partial L_z}{\partial r_0}\right],
\end{aligned} \tag{5.2}$$

We expand E and l_z in terms of e as

$$\begin{aligned}
E &= E^{(0)} + eE^{(1)} + e^2E^{(2)} + e^3E^{(3)} + O(e^4), \\
l_z &= l_z^{(0)} + el_z^{(1)} + e^2l_z^{(2)} + e^3l_z^{(3)} + O(e^4).
\end{aligned} \tag{5.3}$$

Note that $E^{(1)}$ and $l_z^{(1)}$ are zero. We also rewrite $\langle dE/dt \rangle$ and $\langle dJ_z/dt \rangle$ of the previous section as

$$\left\langle\frac{dE}{dt}\right\rangle = \dot{E}^{(0)} + e\dot{E}^{(1)} + e^2\dot{E}^{(2)} + O(e^3), \tag{5.4}$$

$$\left\langle\frac{dJ_z}{dt}\right\rangle = \dot{j}_z^{(0)} + e\dot{j}_z^{(1)} + e^2\dot{j}_z^{(2)} + O(e^3). \tag{5.5}$$

Then using the fact that

$$\dot{E}^{(0)} = \Omega_\varphi \dot{j}_z^{(0)}, \quad \dot{E}^{(1)} = \dot{j}_z^{(1)} = 0, \tag{5.6}$$

we have $\dot{e}$ and $\dot{r}_0$ to the reading order of e as

$$\dot{e} = e\frac{\left(\dot{E}^{(2)}L_z^{(0)\prime} + \dot{E}^{(0)}L_z^{(2)\prime} + \dot{j}_z^{(2)}E^{(0)\prime} + \dot{j}_z^{(0)}E^{(2)\prime}\right)}{-2L_z^{(0)\prime}E^{(2)} + 2E^{(0)\prime}L_z^{(2)}}, \tag{5.7}$$

$$\dot{r}_0 = \frac{2\dot{j}_z^{(0)}E^{(2)} - 2\dot{E}^{(0)}L_z^{(2)}}{-2L_z^{(0)\prime}E^{(2)} + 2E^{(0)\prime}L_z^{(2)}}. \tag{5.8}$$

where $' = \partial/\partial r_0$. Note that $\dot{e}$ is proportional to e. This means that circular orbit remains circular under radiation reaction since $\dot{e}(e=0) = 0$. This fact hold if Eq.(5.6) is correct. In this paper, we only give the proof of Eq.(5.6) using the post-Newtonian approximation, but the formulation of the previous section, especially Eq.(3.31) and (3.32), suggests that Eq.(5.6) will also hold in the relativistic cases.

If we expand Eq.(5.7) in terms of v, we have

$$\begin{aligned}
\frac{de}{dt} &= -\frac{304}{15}\frac{\mu}{M^2}ev^8\left[1 - \frac{6849\,v^2}{2128} + \frac{985\,\pi\,v^3}{152} - \frac{879\,q\,v^3}{76} - \frac{286397\,v^4}{38304} + \frac{1345\,q^2\,v^4}{304}\right. \\
&\quad \left. - \frac{87947\,\pi\,v^5}{4256} - \frac{23201\,q\,v^5}{2128}\right]
\end{aligned} \tag{5.9}$$

$$\begin{aligned}
\frac{dr_0}{dt} &= -\frac{64}{5}\frac{\mu}{M}v^6\left[1 - \frac{743\,v^2}{336} + 4\,\pi\,v^3 - \frac{133\,q\,v^3}{12} + \frac{34103\,v^4}{18144} + \frac{81\,q^2\,v^4}{16}\right. \\
&\quad \left. - \frac{4159\,\pi\,v^5}{672} - \frac{1451\,q\,v^5}{56}\right].
\end{aligned} \tag{5.10}$$

From Eq.(5.9) and (5.10), we obtain

$$\begin{aligned}
\frac{de}{dr_0} &= \frac{19}{12}\frac{e}{r_0}\left[1 - \frac{3215\,v^2}{3192} + \frac{377\,\pi\,v^3}{152} - \frac{55\,q\,v^3}{114} - \frac{111813545\,v^4}{9652608} - \frac{97\,q^2\,v^4}{152}\right. \\
&\quad \left. - \frac{253409\,\pi\,v^5}{51072} + \frac{53203\,q\,v^5}{19152}\right]
\end{aligned} \tag{5.11}$$

We see from Eq.(5.9) that in the slow motion limit $v \ll 1$, $\dot{e}$ is always negative and this means that circular orbit is stable under the influence of radiation reaction. We also find that if $q > 0\,(q < 0)$, the rate of change of the eccentricity and radius decrease (increase) at order $O(v^3)$ and $O(v^5)$ and always increase at order $O(v^4)$. Note however that since the Teukolsky equation is constructed to the first order of μ/M, the radiation reaction to the particle is not taken into account. Then we must keep in mind that above results are valid only in the restricted situations when the adiabatic approximation is valid and the mass ratio is large (i.e. $\mu/M \ll 1$).

Using Eq.(5.9), we examine the critical radius where $\dot{e}$ changes sign. We see that $\dot{e}$ become zero at $r_0 \simeq 3.7M$ when $q = 0$. This value contradicts with the fact that there are the last circular stable orbit at $r = 6M$ in the Schwarzschild space time. This value also disagrees with the critical radius $r \simeq 6.6792M$ obtained by Apostolatos et.al. This is because that the post-Newtonian approximation does not give the good approximation around $r = 6M$ [30] even if we calculate the post-Newtonian expansion to order $O(v^5)$.

6 Implications to coalescing compact binaries

In this section, we discuss the effects of post-Newtonian terms in the luminosity to the orbital evolution of inspiraling compact binaries. Although our results are valid only in the test particle limit, we ignore this fact in the following.

The total cycle N of the phase of gravitational waves from an inspiraling binaries from $r = r_i$ $(t = t_i)$ to $r = r_f$ $(t = t_f)$ is given by

$$N \equiv \int_{t_i}^{t_f} f dt = \frac{1}{\pi}\int_{r_f}^{r_i} dr\, \Omega_\varphi \frac{dE/dr}{|dE/dt|}, \tag{6.1}$$

where f is the frequency of the wave.

From Eq.(5.11), we see that the eccentricity e of the orbit decreases according to $e \propto r^{19/12}$ where r is the orbital radius. We estimate the effects of the eccentricity to the total cycle of the gravitational wave in the LIGO's band.

Expanding Ω_φ, dE/dt, and dE/dr with respect to $v = (M/r)^{1/2}$, N is expressed as

$$N = \frac{5}{64\pi}\frac{M}{\mu}\int_{r_f}^{r_i} \frac{dr r^{3/2}}{M^{5/2}} \frac{\sum_{k=0}^{\infty} b_k(e)(M/r)^{k/2} \sum_{k=0}^{\infty} c_k(e)(M/r)^{k/2}}{\sum_{k=0}^{\infty} d_k(e)(M/r)^{k/2}}, \tag{6.2}$$

where the series forms in the denominator and numerator represent the post-Newtonian corrections to the Ω_φ, dE/dt, and dE/dr, that is

$$\begin{aligned}
\sum_{k=0}^{\infty} b_k(e)(M/r)^{k/2} &= \frac{\Omega_\varphi}{(\Omega_\varphi)_N}, \\
\sum_{k=0}^{\infty} c_k(e)(M/r)^{k/2} &= \frac{(dE/dr)}{(dE/dr)_N}, \\
\sum_{k=0}^{\infty} d_k(e)(M/r)^{k/2} &= \frac{(dE/dt)}{(dE/dt)_N},
\end{aligned}$$

and the argument e is given to the coefficients b_k, c_k and d_k to emphasize the e-dependence of the post-Newtonian corrections.

Since the effect of post-Newtonian corrections in the case $e = 0$ has been studied, we examine only the effect due to non-vanishing value of e. For this purpose, we define

$$\begin{aligned}
N^{(n)} = \frac{5}{64\pi}\frac{M}{\mu}\Bigg[\int_{r_f}^{r_i} \frac{dr r^{3/2}}{M^{5/2}} \Bigg\{ & \frac{\sum_{k=0}^{n} b_k(e)(M/r)^{k/2} + b_{n+1}(0)(M/r)^{(n+1)/2}}{\sum_{k=0}^{n} d_k(e)(M/r)^{k/2} + d_{n+1}(0)(M/r)^{(n+1)/2}} \\
& \times \Big(\sum_{k=0}^{n} c_k(e)(M/r)^{k/2} + c_{n+1}(0)(M/r)^{(n+1)/2}\Big)\Bigg\}\Bigg],
\end{aligned} \tag{6.3}$$

and $\Delta N^{(n)} \equiv | N^{(n)} - N^{(n-1)} |$ which describe the effect of e at the $O(v^n)$ order. Then we insert $e = e_i(r/r_i)^{19/12}$ into Eq.(6.3), where e_i is eccentricity at $r = r_i$, and integrate it numerically. The results are listed in Table 2. In this calculation, we define r_i as the radius at which $f(r_i) = 10$Hz. Then

$e_i(q=0)$	$\Delta N^{(4)}$	$\Delta N^{(5)}$	$e_i(q=1)$	$\Delta N^{(4)}$	$\Delta N^{(5)}$
0.1	0.36	0.09	0.1	0.37	0.07
0.2	1.37	0.32	0.2	1.38	0.26
0.3	2.77	0.63	0.3	2.81	0.48
0.4	4.28	0.95	0.4	4.37	0.68
0.5	5.63	1.22	0.5	5.83	0.80

Table 2 (a)

$e_i(q=0)$	$\Delta N^{(4)}$	$\Delta N^{(5)}$	$e_i(q=1)$	$\Delta N^{(4)}$	$\Delta N^{(5)}$
0.1	0.54	0.20	0.1	0.55	0.18
0.2	2.01	0.76	0.2	2.07	0.65
0.3	4.06	1.50	0.3	4.22	1.25
0.4	6.25	2.24	0.4	6.57	1.76
0.5	8.22	2.85	0.5	8.76	2.08

Table 2 (b)

$e_i(q=0)$	$\Delta N^{(4)}$	$\Delta N^{(5)}$	$e_i(q=1)$	$\Delta N^{(4)}$	$\Delta N^{(5)}$
0.1	0.19	0.09	0.1	0.21	0.08
0.2	0.72	0.33	0.2	0.76	0.30
0.3	1.46	0.64	0.3	1.56	0.57
0.4	2.23	0.97	0.4	2.42	0.81
0.5	2.94	1.21	0.5	3.22	0.96

Table 2 (c)

Table 1: The effect of the eccentricity to the total cycle of the coalescing binaries in the case $q = 0$ (left) and $q = 1$ (right) and (a) $(m_1, m_2) = (1.4M_\odot, 1.4M_\odot)$, (b) $(m_1, m_2) = (1.4M_\odot, 10M_\odot)$, (c) $(m_1, m_2) = (10M_\odot, 10M_\odot)$.

we set $r_i = 175M$ for $(m_1, m_2) = (1.4M_\odot, 1.4M_\odot)$, $r_i = 68M$ for $(1.4M_\odot, 10M_\odot)$ and $r_i = 47M$ for $(10M_\odot, 10M_\odot)$ respectively. We set $r_f = 8M$ for all cases since the post-Newtonian expansion of the luminosity does not give a good approximation around $r \sim 6M$ (for instance, dE/dt changes the sign around $r \sim 6M$ for certain value of q and e).

The required accuracy as a template of the gravitational waves from coalescing binaries is $\Delta N < 0.5$. We see from Table 2 that the effects of the eccentricity is important at the order $O(v^4)$ if initial eccentricity is larger than 0.2 or 0.3. On the other hand, the effect of the eccentricity at $O(v^5)$ is important if initial eccentricity is greater than 0.4 or 0.5. These properties hold for all the values of q. Above facts suggest that if the initial eccentricity is $e_i \sim 1$, terms of order $O(v^6)$ may become important and we must calculate those terms to construct the template of binaries with a highly eccentric orbit.

Shapiro and Teukolsky [31] considered a formation scenario of super massive black hole which may exist in the center of galaxies via the collapse of a dense cluster of compact stars. Quinlan and Shapiro [19] investigated the role of binary formation in the evolution of dense stellar systems. In their scenario, formation of binaries through the dissipative two-body encounter dominates formation through three body encounters in the initial stage of cluster evolution. The maximum periastron separation of binaries formed by dissipation of gravitational radiation can be estimated as

$$\begin{aligned} r_{p,max} &= \left(\frac{85\pi}{6}\right)^{2/7} \frac{Gm}{c^{10/7} v^{4/7}} \\ &\sim 115\mathrm{km} \left(\frac{m}{M_\odot}\right) \left(\frac{v}{10^3\,\mathrm{km}}\right)^{-4/7}, \end{aligned}$$

where v is initial relative velocity of the encounter. Those binaries are in the bandwidth of LIGO when they are formed. Binaries formed by two body encounters have typically large eccentricity $e \sim 1$. The advanced detector system of LIGO will have sensitivity to detect the merger of NS-NS binaries within 1 Gpc and BH-BH binaries within 5 Gpc [4]. Then binaries in dense stellar systems may become possible sources of gravitational waves for LIGO/VIRGO. In such case, eccentricity will play an important role to obtain physical informations of the binary systems.

7 Summary

We performed the post-Newtonian expansion of gravitational waves from a test particle in slightly eccentric orbit around a Kerr black hole. The effect of the deviation from circular orbit was expressed by the eccentricity e and we treated e as a perturbation. We calculated the gravitational wave luminosity of both the energy and the angular momentum to order $O(v^5)$ and $O(e^2)$. Our formulas agree with the formulas of the luminosity to the order $O(v^3)$ which were calculated so far by several authors.

We examine the stability of circular orbit in the slow motion situation. We find that if eccentricity e is zero, de/dt is also zero and this means that circular orbit remains circular under the influence of radiation reaction. We also find that circular orbit is stable against radiation reaction even if the central black hole is spinning. Above these results are consistent with the previous works. We also find that if $q > 0$ ($q < 0$), the rate of decrease of eccentricity become small (large) compared to the case of $q = 0$ at $O(v^3)$ and $O(v^5)$ and become always large at $O(v^4)$.

We have also estimated the accuracy of the post-Newtonian expansion to predict the total cycle of coalescing binaries. We found that if the initial eccentricity, at which binaries can be observed with laser interferometers, is greater than 0.2 and 0.4, the effect of the eccentricity become important at order $O(v^4)$ and $O(v^5)$ respectively. There are possibilities that compact binaries with high eccentricity was formed in the dense stellar systems and they may be detected with laser interferometers. Although our results are restricted to case of the large mass ratio and small eccentricity, they will be useful to analyze gravitational waves from such binaries.

On the other hand, gravitational waves from compact stars orbiting around a supermassive black hole in a galactic center will become a possible sources for a proposed laser interferometric detector in space, LISA. Since our formulas give the correct value for such waves, they will give a useful guideline to investigate those cases.

The author thanks T. Nakamura, M. Sasaki and M. Shibata for useful discussions and collaborations. The details of this paper will be published elsewhere [32].

A The formulae of F and U

In this Appendix we show the potential functions F and U of the SN equation (2.13). Details of the derivation are given in Ref. [25].

The function $F(r)$ is given by

$$F(r) = \frac{\eta_{,r}}{\eta}\frac{\Delta}{r^2 + a^2}, \tag{A.1}$$

where

$$\eta = c_0 + c_1/r + c_2/r^2 + c_3/r^3 + c_4/r^4, \tag{A.2}$$

with

$$\begin{aligned} c_0 &= -12i\omega M + \lambda(\lambda + 2) - 12a\omega(a\omega - m), \\ c_1 &= 8ia[3a\omega - \lambda(a\omega - m)], \\ c_2 &= -24iaM(a\omega - m) + 12a^2[1 - 2(a\omega - m)^2], \\ c_3 &= 24ia^3(a\omega - m) - 24Ma^2, \\ c_4 &= 12a^4. \end{aligned} \tag{A.3}$$

The function $U(r)$ is given by

$$U(r) = \frac{\Delta U_1}{(r^2+a^2)^2} + G^2 + \frac{\Delta G_{,r}}{r^2+a^2} - FG, \tag{A.4}$$

where

$$\begin{aligned}
G &= -\frac{2(r-M)}{r^2+a^2} + \frac{r\Delta}{(r^2+a^2)^2}, \\
U_1 &= V + \frac{\Delta^2}{\beta}\left[\left(2\alpha + \frac{\beta_{,r}}{\Delta}\right)_{,r} - \frac{\eta_{,r}}{\eta}\left(\alpha + \frac{\beta_{,r}}{\Delta}\right)\right], \\
\alpha &= -i\frac{K\beta}{\Delta^2} + 3iK_{,r} + \lambda + \frac{6\Delta}{r^2}, \\
\beta &= 2\Delta\left(-iK + r - M - \frac{2\Delta}{r}\right).
\end{aligned} \tag{A.5}$$

B Functions of the source term

In this Appendix we show the A's in Eq.(3.19).

$$\begin{aligned}
A_{nn0} &= \frac{-2}{\sqrt{2\pi}\Delta^2} C_{nn}\rho^{-2}\overline{\rho}^{-1} L_1^+\{\rho^{-4}L_2^+(\rho^3 S)\}, \\
A_{\overline{m}n0} &= \frac{2}{\sqrt{\pi}\Delta} C_{\overline{m}n}\rho^{-3}\Big[(L_2^+ S)\left(\frac{iK}{\Delta} + \rho + \overline{\rho}\right) \\
&\qquad -a\sin\theta S\frac{K}{\Delta}(\overline{\rho}-\rho)\Big], \\
A_{\overline{m}\overline{m}0} &= -\frac{1}{\sqrt{2\pi}}\rho^{-3}\overline{\rho}C_{\overline{m}\overline{m}}S\left[-i\left(\frac{K}{\Delta}\right)_{,r} - \frac{K^2}{\Delta^2} + 2i\rho\frac{K}{\Delta}\right], \\
A_{\overline{m}n1} &= \frac{2}{\sqrt{\pi}\Delta}\rho^{-3}C_{\overline{m}n}[L_2^+ S + ia\sin\theta(\overline{\rho}-\rho)S], \\
A_{\overline{m}\overline{m}1} &= -\frac{2}{\sqrt{2\pi}}\rho^{-3}\overline{\rho}C_{\overline{m}\overline{m}}S\left(i\frac{K}{\Delta} + \rho\right), \\
A_{\overline{m}\overline{m}2} &= -\frac{1}{\sqrt{2\pi}}\rho^{-3}\overline{\rho}C_{\overline{m}\overline{m}}S,
\end{aligned}$$

where S denotes ${}_{-2}S^{a\omega}_{\ell m}$.

References

[1] A. Abramovici et al., Science, **256**, (1992), 325.

[2] C. Bradaschia et al., Nucl. Instrum. & Methods, **A289** (1990), 518 .

[3] E.S. Phinney, Astrophys. J. **380**, L17 (1991).

[4] C. Cutler et al. Phys. Rev. Lett. **70** (1993), 2984.

[5] C.Cutler and E.E.Flanagan, Phys. Rev. **D49** (1994), 2658.

[6] C.W. Lincoln and C.M. Will, Phys. Rev. **D42**, (1990), 1123.

[7] A.G. Wiseman, Phys. Rev. **D46** (1992), 1517.

[8] L. E. Kidder, C. M. Will and A. G. Wiseman, Phys. Rev. D47, R4183 (1993).

[9] A.G. Wiseman, Phys. Rev. **D48** (1993) 4757.

[10] L. Blanchet and G Schäfer, Class. Quantum Grav. **10** (1993), 2699.

[11] C. M. Will, in *Proceedings of the 8th Nishinomiya-Yukawa Memorial Symposium: Relativistic Cosmology*, ed. M. Sasaki (Universal Academy Press, Tokyo, 1994), p83, and references therein.

[12] E. Poisson, Phys. Rev. **D47** (1993) 1497.

[13] C. Cutler, L.S. Finn, E. Poisson and G.J. Sussman, Phys. Rev. **D47** (1993), 1511.

[14] H.Tagoshi and T. Nakamura, Phys. Rev. D49 (1994), 4016.

[15] H.Tagoshi and M.Sasaki, Prog. Theor. Phys. **92** (1994), 745.

[16] M. Sasaki, Prog. Theor. Phys. **92** (1994), 17.

[17] M.Shibata, M.Sasaki, H.Tagoshi and T.Tanaka, preprint KUNS-1268, OU-TAP-9, (1994).

[18] M.Shibata, preprint OU-TAP-10(1994).

[19] G.D.Quinlan and S.L.Shapiro, Ap. J. **321** (1987), 199.

[20] K.Danzmann et.al. *'LISA : Proposal for a Laser-Interferometric Gravitational Wave detector in Space'*, MPQ-177 (1993) unpublished.

[21] S. A. Teukolsky, Astrophys. J. **185** (1973), 635.

[22] R. A. Breuer, *Gravitational Perturbation Theory and Synchrotron Radiation*, Lecture Notes in Physics **44**, (1975), (Springer Verlag).

[23] E.T.Newman and R.Penrose, J. Math. Phys. **7** (1966) 863.

[24] J. N. Goldberg, A.J. MacFarlane, E. T. Newman, F. Rohrlich, and E. C. G. Sudarshan, J. Math. Phys. **8**, (1967), 2155.

[25] M. Sasaki and T. Nakamura, Prog. Theor. Phys. **67** (1982), 1788; M. Sasaki and T. Nakamura, Phys. Lett. **89A** (1982), 68.

[26] T. Apostolatos, D. Kennefick, A. Ori and E. Poisson, Phys. Rev. **D47** (1993), 5376.

[27] P.C.Peters and J.Mathews, Phys. Rev.**131** (1963), 435.

[28] D.V. Gal'sov, A.A. Matiukhin and V.I. Petukhov, Phys. Lett. **77A** (1980), 387.

[29] L. Blanchet and G. Schäfer, Mon. Not. R. astr. Soc. **239** (1989), 845.

[30] L.E. Kidder, C.M. Will and A.G. Wiseman, Class. Quantum. Grav. **9** (1992), L125.

[31] S.L. Shapiro and S.A. Teukolsky, Ap. J. **292** (1985), L41.

[32] H. Tagoshi, Prog. Theor. Phys. **93** (1995) in press

GRG meeting at Kyoto, 1994

Radiation Reaction in Kerr Geometry

Yasushi Mino

Department of Physics, Kyoto University, Kyoto 606-01

abstract

We consider the radiation reaction to a particle motion rotating around a rotating black hole. We assume the mass of the particle μ is much smaller than the mass of black hole M and treat the gravitational degree of freedom as a perturbation of Kerr black hole.

We calculate the Green function of the metric perturbation. It is quite complicated to use the retarded Green function in order to obtain the radiation reaction force. Hence we consider the possibility to use the antisymmetric Green function to calculate the radiation reaction force.

Applying the technique developed by H. Tagoshi and M. Sasaki, the post-Newtonian expansion of the radiation reaction is now under calculation.

I. INTRODUCTION

In this paper, we consider the new method to investigate the radiation reaction to a particle motion around a black hole. We assume that the black hole is far more massive than the particle and the gravitational field induced by the particle can be treated as a perturbation of the black hole.

The method previously developed by H. Tagoshi and M. Sasaki [1,2] is used to consider such situations until now [3–7]. In that method, one calculates the gravitational waves at the null infinity and obtains the flux of the energy and the angular momentum propagated by the waves. If the orbit in the background spacetime can be specified by the energy and the angular momentum, and if the background geometry is at least stationary and axial symmetric, the radiation reaction to the orbit can be calculated by using the conservation laws which come from the symmetry of the background geometry.

This method is powerful in computing the radiation reaction in the higher order post-Newtonian expansion. However the condition that the orbit is determined by only the energy and the angular momentum, restricts its application. When the background geometry is a Schwarzchild black hole, the orbit can fully determined by the energy and the angular momentum and one can, therefore, compute

*E-mail: mino@murasaki.scphys.kyoto-u.ac.jp

the radiation reaction to the orbit [4,5]. But in the case that the background geometry is a Kerr black hole, one needs three parameters to specify the orbit, i.e. the energy, the angular momentum, and the Carter constant. One can compute the radiation reaction to the energy and the angular momentum, but one cannot get the radiation reaction to the Carter constant in this method. In order to get the radiation reaction to the orbit, one must put one constraint on the orbit by hand, such that the orbit remains circular [6], or that the orbit is restricted to the equatorial plane [7]. These constraints are arbitrary and restricts the situation to be considered. Thus, we need to find another method to compute the radiation reaction to the orbit.

In [8], it is argued that the radiation reaction force can be calculated by using the antisymmetric Green function of the metric perturbation in Kerr geometry. The antisymmetric Green function is constructed by extracting the time-antisymmetric part from the retarded Green function which was derived in [9]. If it is correct, we can calculate the complete radiation reaction to the orbit by integrating the equation of motion. However the use of the antisymmetric Green function instead of the retarded Green function was not clearly justified in [8] and seems just for convenience of obtaining the finite radiation reaction force. If we try to calculate the reaction force with the retarded Green function, it becomes divergent since the particle has the infinite density.

In this paper, applying the regularization technique of classical electro-magnetic radiation reaction force in the curved spacetime [10] to the case of gravitational radiation, we obtain a divergence-free equation of motion considering a extended particle, and find that the use of the antisymmetric Green function is justified if and only if the orbit is bound.

The geodesic close to the equatorial circular orbit in a Kerr geometry can be solved by the perturbation. Post-Newtonian expansion of the radiation reaction can be obtained in the similar way that is used in [3–7], and is now under computation.

II. RADIATION REACTION FORCE

We adopt the technique developed in [10]. The computation depends on the Hadamard expansion of the Green function, and on the conservation law of the energy-momentum tensor [†].

We first explain the Hadamard expansion of the tensor Green function $G_{mnab}(x,z)$ [‡].

The Hadamard expansion is the technique to expand the Green function from the lightcorn of the source, using the square of the geodetic interval σ [§]. For example, the Feynman propagator G_{mnab} for the tensor potential is expanded as,

---

[†]Since the contents of this section need too much mathematics around the Riemannian geometry, the calculations in detail are put in my master thesis and the forth coming paper [12].

[‡]The tensors which depend on the two different spacetime points, say x and z, are called bi-tensors. A simplest example of bi-tensors is the product of two vectors, $A^m(x), B_a(z)$,

$$C^m{}_a(x,z) = A^m(x)B_a(z). \tag{2.1}$$

In the following, indices taken from a to l are always associated with the point z, while the rest of the alphabets are with the point x.

[§]σ is the square of the geodetic interval between x and z. It is determined by,

$$g^{ab}\sigma_{;a}\sigma_{;b} = g^{mn}\sigma_{;m}\sigma_{;n} = \pm\frac{1}{2}\sigma, \qquad \lim_{x\to z}\sigma = 0. \tag{2.2}$$

$$G_{mnab}(x,z) = \frac{1}{(2\pi)^2}\left(\frac{u_{mnab}}{\sigma + i0} + v_{mnab}\log|\sigma + i0| + w_{mnab}\right), \tag{2.3}$$

$$v_{mnab} = \sum_{N=0}^{\infty} v^N_{mnab}\sigma^N, \qquad w_{mnab} = \sum_{N=0}^{\infty} w^N_{mnab}\sigma^N, \tag{2.4}$$

In the following, we assume that the background is the vacuum spacetime in order to avoid the complexity of the computation. The metric perturbation h_{mn} must satisfy,

$$\frac{1}{2}\left(-g^{op}\bar{h}_{mn;op} - 2R_m{}^o{}_n{}^p\bar{h}_{op}\right) = 8\pi\frac{G}{c^5}T_{mn}, \tag{2.5}$$

$$\bar{h}_{mn} = h_{mn} - \frac{1}{2}g_{mn}h, \tag{2.6}$$

$$T^{mn} = \mu c\int\left[\frac{1}{\sqrt{g}}\bar{g}^m{}_a\bar{g}^n{}_b\dot{z}^a\dot{z}^b\right]_{z=z(\tau)}\delta^{(4)}(x - z(\tau))d\tau. \tag{2.7}$$

This can be solved by the Green function method with the Hadamard expansion **.

The radiation reaction force to the particle can directly be calculated by the metric perturbation induced by it. As was noticed, the radiation reaction to the point particle becomes diverge. We have to consider the extended particle with finite density so that we can get the finite equation of motion.

Instead of considering the extended density distribution of the particle, we use the covariant conservation law to calculate the radiation reaction force. The advantage to use the conservation law is to change the volume integral into the surface integral. If we take the surface outside the particle, we can implement the surface integration without the extended density distribution of the particle.

We explain how to construct the covariant conservation law of the matter and the gravitational waves, which was derived in [11]. Suppose that $g_{mn} + \bar{h}_{mn}$ is a solution of the full Einstein equation. Expanding the Einstein equation in terms of $\bar{h}_{mn}$ ††, we get,

$$G^{(1)\,mn}[\bar{h}] + G^{(2)\,mn}[\bar{h}] = 8\pi\frac{G}{c^5}\left(T^{(1)\,mn} + T^{(2)\,mn}[\bar{h}]\right) + O(\bar{h}^3). \tag{2.9}$$

Here we expand the Einstein tensor and the energy-momentum tensor of the upper indices to the second order of $\bar{h}_{mn}$. The numbers on the right of the tensors show the order of the metric perturbation ‡‡. For the energy-momentum tensor of the point particle,

---

Possibly σ becomes multi-valued when the geodetic interval becomes larger than the scale of the background curvature. However we don't mind such situations because a region close to the particle is only of our interest.

**$\bar{g}_{ma}$ is the bi-vector of geodetic parallel displacement and is defined by,

$$\bar{g}_{ma;n}g^{no}\sigma_{;o} = \bar{g}_{ma;b}g^{bc}\sigma_{;c} = 0, \qquad \lim_{x\to z}\bar{g}_m{}^a = \delta_m{}^a. \tag{2.8}$$

Its geometrical significance may be at once inferred.

††In expanding the energy-momentum tensor, we pay attention just to the metric in it, and we leave the orbit as it is. This is because we want to derive the equation motion which is valid even when the deviation of the orbit by the radiative effect becomes large [11].

‡‡Since the background spacetime is vacuum, $G^{(0)\,mn}$ vanish, $T^{(1)\,mn}$ is $O(h)$ though independent of $\bar{h}_{mn}$ and $T^{(2)\,mn}$ is $O(h^2)$ though linear in $\bar{h}_{mn}$. As was noted, the orbit in the energy-momentum tensor is not expanded. This is why (2.9) does not stand in each order of $\bar{h}_{mn}$.

$$T^{(2)\,mn}[\tilde{h}] = \frac{c^3}{16\pi G}\tilde{h}_{op}\left(\bar{g}^{o}{}_{a}\bar{g}^{p}{}_{b}\dot{z}^{a}\dot{z}^{b} - c^2 g^{op}\right) G^{(1)\,mn}[\tilde{h}] + O(\tilde{h}^2). \tag{2.10}$$

Noting $\tilde{h}_{mn} - h_{mn} = O(h^2)$, $T^{(1)\,mn} = \frac{c^5}{8\pi G}G^{(1)\,mn}[h] + O(h^2)$, we get,

$$T^{(1)\,mn} = \frac{c^5}{8\pi G}\left\{G^{mn\,(1)}[\tilde{h}] + G^{mn\,(2)}[h] - \frac{1}{2c^2}h_{op}\left(\bar{g}^{o}{}_{a}\bar{g}^{p}{}_{b}\dot{z}^{a}\dot{z}^{b} - c^2 g^{op}\right) G^{(1)\,mn}[h]\right\} + O(h^3). \tag{2.11}$$

Taking the covariant divergence with respect to the background metric, we finally get the covariant conservation law for h_{mn},

$$\left(T^{(1)\,mn} + T^{mn}_{GW}[h]\right)_{;n} = O(h^3), \tag{2.12}$$

$$T^{(1)\,mn} = \mu c \int \left[\frac{1}{\sqrt{\bar{g}}}\bar{g}^{m}{}_{a}\bar{g}^{n}{}_{b}\dot{z}^{a}\dot{z}^{b}\right]_{x=z(\tau)} \delta^{(4)}(x - z(\tau))d\tau, \tag{2.13}$$

$$T^{mn}_{GW}[h] = \frac{c^5}{8\pi G}\left\{\frac{1}{2c^2}h_{op}\left(\bar{g}^{o}{}_{a}\bar{g}^{p}{}_{b}\dot{z}^{a}\dot{z}^{b} - c^2 g^{op}\right) G^{(1)\,mn}[h] - G^{(2)\,mn}[h]\right\}. \tag{2.14}$$

We integrate (2.12). The region of integration is shown in Fig. 1.

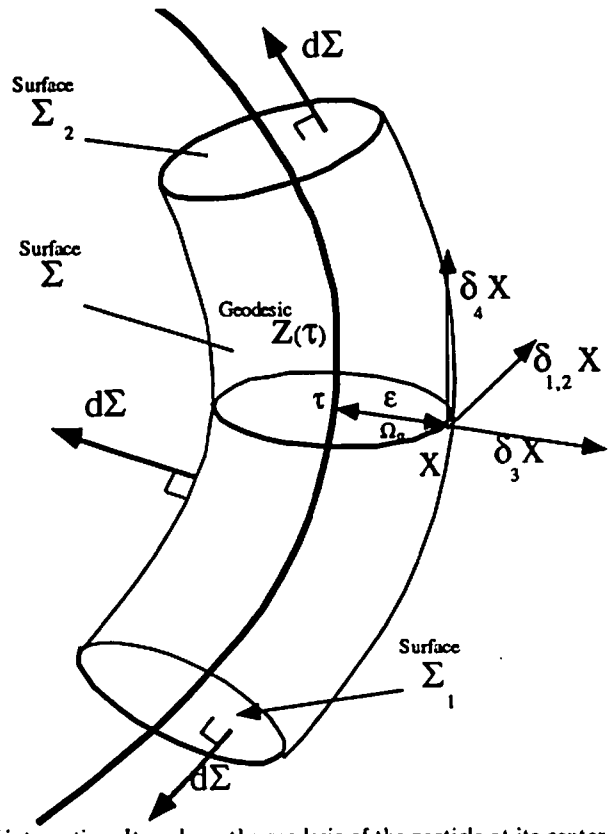

FIG. 1. The region of integration; It encloses the geodesic of the particle at its center and has the spatial radius ϵ_{tube} larger than the radius of the particle. The time-like length is delimited between τ_2 and τ_1.

$$0 = \int_V dx^4 \sqrt{-g}\bar{g}_m{}^a \left(T^{(1)\ mn} + T^{mn}_{GW}\right)_{;n}$$
$$= \int_{\Sigma_1,\Sigma_2} d\Sigma_n \bar{g}_m{}^a T^{(1)\ mn} + \int_{\Sigma,\Sigma_1,\Sigma_2} d\Sigma_n \bar{g}_m{}^a T^{mn}_{GW} - \int_V dx^4 \sqrt{-g}\bar{g}_m{}^a{}_{;n} \left(T^{(1)\ mn} + T^{mn}_{GW}\right). \tag{2.15}$$

It is found that taking the point particle limit $\epsilon_{tube} \to 0$, the last term of (2.15) vanishes.

The first term can be calculated in the point particle limit,

$$\int_{\Sigma_1,\Sigma_2} d\Sigma_n \bar{g}_m{}^a T^{(1)\ mn} = \mu \left[\bar{g}_{b'}{}^a(z(\tau'), z(\tau))\dot{z}^{b'}(\tau')\right]_{\tau'=\tau_1}^{\tau'=\tau_2}$$
$$= \mu \ddot{z}^a \delta\tau + O(\delta\tau^2). \tag{2.16}$$

Here we define $\delta\tau = \tau_2 - \tau_1$ and assume it sufficiently small.

The second term becomes divergent when we take the point particle limit. Its contribution to the surface Σ can be obtained, using the metric perturbation induced by the point particle. Since the surface Σ is outside the particle, the integral is finite as long as the radius of tube ϵ_{tube} is finite.

$$\int_\Sigma d\Sigma_n \sqrt{-g}\bar{g}_m{}^a T^{mn}_{GW} = -\frac{7}{2}\left(\frac{1}{\epsilon_{tube}}\right)\frac{G\mu^2}{c^2}\ddot{z}^a \delta\tau$$
$$+\frac{G\mu^2}{2c^5}\delta\tau\left(2\dot{z}^a \bar{g}^m{}_b \bar{g}^n{}_c \bar{g}^o{}_d \dot{z}^b \dot{z}^c \dot{z}^d + 2c^2 \bar{g}^{ma}\bar{g}^n{}_b \bar{g}^o{}_c \dot{z}^b \dot{z}^c - c^2 \dot{z}^a g^{mn} \bar{g}^o{}_b \dot{z}^b - c^4 \bar{g}^{oa} g^{mn}\right)$$
$$\times \int_{-\infty}^{\tau} d\tau' v_{mna'b';o} \dot{z}^{a'} \dot{z}^{b'}$$
$$+O(\ddot{z}, \dddot{z}). \tag{2.17}$$

The last term, $O(\ddot{z}, \dddot{z})$, is finite in the point particle limit. However it will be shown that $\ddot{z}, \dddot{z}$ are of order ϵ_{tube}, and thus, it has a negligible contribution to the equation of motion.

In order to calculate the contribution to the surface Σ_1, Σ_2, we need to consider the extended density distribution of the particle. But the order of divergence can be seen by the metric perturbation induced by the point particle. We found that there appears only a $\frac{1}{\epsilon_{tube}}$-divergent term and that no finite terms contribute to the integral in the point particle limit. This corresponds to the divergence of the gravitational self-interaction energy of the point particle because the integrand is the energy density of the gravitational waves observed by the particle and because Σ_1, Σ_2 are space-like surfaces normal to the orbit of the particle. We put the contribution on the surface Σ_1, Σ_2 as,

$$\int_{\Sigma_1} d\Sigma_n \sqrt{-g}\bar{g}_m{}^a T^{mn}_{GW} = -\frac{1}{2}\left(\frac{\alpha}{\epsilon_{tube}}\right)\frac{G\mu^2}{c^2}\ddot{z}^a(\tau_1), \tag{2.18}$$
$$\int_{\Sigma_2} d\Sigma_n \sqrt{-g}\bar{g}_m{}^a T^{mn}_{GW} = \frac{1}{2}\left(\frac{\alpha}{\epsilon_{tube}}\right)\frac{G\mu^2}{c^2}\ddot{z}^a(\tau_2), \tag{2.19}$$

where α is a non-dimensional parameter which represents the structure of the extended density distribution of the particle. We expect that the particle is so compact that its structure does not change in time. α is independent of time and we get,

$$\int_{\Sigma_1,\Sigma_2} d\Sigma_n \sqrt{-g}\bar{g}_m{}^a T^{mn}_{GW} = \frac{1}{2}\left(\frac{\alpha}{\epsilon_{tube}}\right)\frac{G\mu^2}{c^2}\ddot{z}^a \delta\tau. \tag{2.20}$$

In summary, we obtain a regular equation of motion which includes the radiation reaction,

$$\left(1+\frac{\alpha-7}{2\epsilon_{tube}}\frac{G\mu}{2c^2}\right)\mu\ddot{z}^a+\frac{G\mu^2}{2c^5}F^a[\tau,-\infty]=0, \tag{2.21}$$

$$F^a[\tau_2,\tau_1]=\left(2\dot{z}^a\bar{g}^m{}_b\bar{g}^n{}_c\bar{g}^o{}_d\dot{z}^b\dot{z}^c\dot{z}^d+2c^2\bar{g}^{ma}\bar{g}^n{}_b\bar{g}^o{}_c\dot{z}^b\dot{z}^c-c^2\dot{z}^a g^{mn}\bar{g}^o{}_b\dot{z}^b-c^4\bar{g}^{oa}g^{mn}\right)$$
$$\times\int_{\tau_1}^{\tau_2}d\tau' v_{mna'b';o}\dot{z}^{a'}\dot{z}^{b'}. \tag{2.22}$$

Now it becomes clear why the equation of motion becomes divergent in the point particle limit.

Exactly speaking, the linear approximation of the Einstein equation is valid only when the radius of the particle ($\leq \epsilon_{tube}$) is much larger than its Schwarzchild radius $\frac{G\mu^2}{2c^5}$. In this situation, the equation of motion becomes,

$$\mu\ddot{z}^a+\frac{G\mu^2}{2c^5}F^a[\tau,-\infty]=0. \tag{2.23}$$

The ignorance of the last term $O(\ddot{z},\dddot{z})$ in (2.17) is now justified because as is shown in (2.23), $\ddot{z},\dddot{z}$ are $O(\epsilon_{tube})$.

This equation of motion has an interesting characters. The force comes only from the 'tail' terms involving the integration over the past history of the particle. The appearance of the 'tail' is characteristic in the curved background. In fact, the 'tail' terms appear in the electro-magnetic radiation reaction to a charged particle [10]. This term is thought to represent the reaction by the gravitational waves which were emitted in the past, and scattered by the curvature in the background spacetime.

For the comparison, we calculate the equation of motion, following the proposal of Gal'tsov [8].

$$\mu\ddot{z}^a+\frac{G\mu^2}{4c^5}F^a[\infty,-\infty]=0 \tag{2.24}$$

(We call this the Gal'tsov equation of motion.) Comparing (2.24) and (2.23), the difference is just the domains of integration of the 'tail' terms. If the particle is bound, these can be though to give the same value. The proposal of Gal'tsov [8] is correct when we consider the radiation reaction to the bound orbit.

III. METRIC PERTURBATION

In this section, we briefly explain how to construct the metric perturbation of a Kerr spacetime. The calculation in detail is in [9,8,12]. The construction of the metric perturbation depends on the Teukolsky equations [13] and the Wald's theorem [14].

The Teukolsky equations are the equations of perturbed Weyl scalars Ψ_0,Ψ_4. The most remarkable character is that the variables are separable in these equations. In the following, we express one of the Teukolsky equations as,

$$E\cdot\psi=\tau_{ab}\cdot T^{ab}, \tag{3.1}$$

where E is a linear differential operator and is separable. $\tau_{ab}T^{ab}$ is the source term of the Teukolsky equation. τ_{ab} is a linear differential operator and T^{ab} is a energy-momentum tensor which induces the perturbation. (In this stage, we need just one Teukolsky equation.) The perturbed Einstein equation is written as

$$E^{ab}{}_{cd}\cdot h^{cd}=T^{ab}, \tag{3.2}$$

where $E^{ab}{}_{cd}$ is a tensor differential operator and h^{cd} is a metric perturbation induced by the energy-momentum T^{ab}.The Weyl scalar ψ is related to the metric perturbation h^{cd}.

$$\psi = \Psi_{cd} \cdot h^{cd} \tag{3.3}$$

Eliminating ψ and T^{ab} from (3.1), (3.2), (3.3), we obtain an identity.

$$E \cdot \Psi_{cd} = \tau_{ab} \cdot E^{ab}{}_{cd} \tag{3.4}$$

The central idea of the Wald's theorem is the notion of the 'adjoint' of the differential operator. A (m,n)-tensor differential operator $\mathcal{O}^{i_1,i_2,\cdots,i_m}{}_{j_1,j_2,\cdots,j_n}$ is the operator which acts on a n-tensor $\phi^{j_1,j_2,\cdots,j_n}$ and makes m-tensor.

$$(\mathcal{O}\phi)^{i_1,i_2,\cdots,i_m} = \mathcal{O}^{i_1,i_2,\cdots,i_m}{}_{j_1,j_2,\cdots,j_n}\phi^{j_1,j_2,\cdots,j_n} \tag{3.5}$$

The adjoint of a (m,n)-tensor operator $\mathcal{O}^{i_1,i_2,\cdots,i_m}{}_{j_1,j_2,\cdots,j_n}$ is a (n,m)-tensor operator $\mathcal{O}^{*\,j_1,j_2,\cdots,j_n}{}_{i_1,i_2,\cdots,i_m}$ which is defined for some vector s^i as,

$$\psi_{i_1,i_2,\cdots,i_m}(\mathcal{O}\phi)^{i_1,i_2,\cdots,i_m} - (\mathcal{O}^*\psi)_{j_1,j_2,\cdots,j_n}\phi^{j_1,j_2,\cdots,j_n} = s^i{}_{;i} \tag{3.6}$$

Especially, when $\mathcal{O}$ is a (n,n)-tensor differential operator and $\mathcal{O} = \mathcal{O}^*$, $\mathcal{O}$ is said self-adjoint. (Here and in what follows, we omit the indices of the operators.) Most readers may understand that this is the same procedure to integrate by parts and that the adjoint of a operator always exists. The example of a self-adjoint operator, which is of importance in the later use is the (2,2)-tensor differential operator of the perturbed Einstein equation $E^{ab}{}_{cd}$.

$$E^{ab}{}_{cd} = \frac{1}{2}\left(-g^a{}_c g^b{}_d \nabla_e \nabla^e - g^{ab}\nabla_c\nabla_d + g^a{}_c\nabla^b\nabla_d + g^b{}_d\nabla^a\nabla_c + g^{ab}g_{cd}\nabla_e\nabla^e - g_{cd}\nabla^a\nabla^b\right) \tag{3.7}$$

There stands a sum rule in taking the adjoint. When the $\mathcal{O}$ and $\mathcal{P}$ are the same class of differential operators,

$$(\mathcal{O} + \mathcal{P})^* = \mathcal{O}^* + \mathcal{P}^* \tag{3.8}$$

This guarantees that the adjoint operator of a separable operator is also separable. The composition rule stands as,

$$(\mathcal{O} \cdot \mathcal{P})^* = \mathcal{P}^* \cdot \mathcal{O}^* \tag{3.9}$$

Theorem - Suppose the identity $\mathcal{S} \cdot \mathcal{E} = \mathcal{O} \cdot \mathcal{T}$ holds for the tensor differential operator $\mathcal{S}, \mathcal{E}, \mathcal{O}, \mathcal{T}$. Suppose a tensor ϕ satisfies $\mathcal{O}^* \cdot \phi = 0$. Then $\mathcal{S}^* \cdot \phi$ satisfies $\mathcal{E}^* \cdot (\mathcal{S}^* \cdot \phi) = 0$. In particular, if $\mathcal{E}$ is self-adjoint, $\mathcal{S}^* \cdot \phi = 0$ is a solution of the differential equation $\mathcal{E}(f)$.

Proof - Taking the adjoint of $\mathcal{S} \cdot \mathcal{E} = \mathcal{O} \cdot \mathcal{T}$, we have

$$\mathcal{E}^* \cdot \mathcal{S}^* = \mathcal{T}^* \cdot \mathcal{O}^* \tag{3.10}$$

Applying these operators to ϕ, we get,

$$\mathcal{E}^* \cdot \mathcal{S}^* \cdot \phi = 0 \tag{3.11}$$

which is the desired result.

Applying this theorem to the identity (3.4), and noting that $E^{ab}{}_{cd}$ is self-adjoint, what we have to do to construct the metric perturbation is to find the solution of a scalar linear differential equation;

$$E^{*} \cdot \psi^{*} = 0 \tag{3.12}$$

Since E is separable, E^{*} is also separable and we can find the explicit solutions. Then the metric perturbation h^{cd} becomes,

$$h^{cd} = \tau^{*\ cd} \cdot \psi^{*} \tag{3.13}$$

We briefly comment where the gauge freedom appears in (3.13). This comes from the fact that the operator τ_{ab} is not uniquely defined in (3.1). Since the energy-momentum tensor satisfies the covariant conservation law $T^{ab}{}_{;b}$, one is free in adding $\xi_a \nabla_b + \xi_b \nabla_a$ to τ^{ab}. This uncertainty in defining τ_{ab} reflects the gauge freedom in (3.13).

The metric perturbation (3.13) is a homogeneous solution of the perturbed Einstein equation. Using the Green function method, we can construct the inhomogeneous solution of the perturbed Einstein equation induced by the energy-momentum tensor T^{ab} for the point particle (2.7).

The metric perturbation obtained by the retarded Green function is not well-behaved around the particle as was note in Sec.II. Thus we follow the proposal of Gal'tsov [8] and use the antisymmetric Green function to calculate the radiation reaction force, which is justified for the bound orbit.

IV. POST NEWTONIAN EXPANSION

In this section, we will explain how to proceed the post-Newtonian expansion of the radiation reaction to the orbit.

The radiation reaction force can be obtained from the metric perturbation, which is constructed from the tensor radiative Green function and the geodesic in a Kerr spacetime.

In order to get the post-Newtonian expansion of the radiative Green function, we must solve (3.12). The technique of the post-Newtonian expansion to solve (3.12) is in [2]. We use the result in [6] [§§].

The geodesic around a Kerr black hole are not known in general. We solve the geodesic equation $\ddot{z}^a$ by the perturbation of the equatorial and circular orbits of the Kerr black hole.

The post-Newtonian expansion of the radiation reaction to the energy, the angular momentum and the Carter constant of a orbit is now under calculation.

V. SUMMARY

In this paper, we show the way to obtain the local description of the gravitational radiation force to the extended particle. It is found that the gravitational radiation reaction is from the 'tail' effect.

[§§] In [6], the post-Newtonian expansion of the Teukolsky radial function R_{-2} and of the spin-weighted spheroidal harmonics are derived. These constitute ψ^{*}. See [12] for the detail.

The use of the antisymmetric Green function, as was proposed in [8], is justified as long as the particle is bound around the black hole.

The post-Newtonian expansion of the radiation reaction to the orbit in a Kerr geometry is now under calculation.

Acknowledgement

I thank to Prof. H. Sato for his continuous encouragement. I thank Prof. T. Nakamura, Prof. M. Sasaki, M. Shibata, T. Tanaka, and H. Tagoshi for many helpful discussions. I am also grateful to K. Nakao for carefully reading my manuscript.

---

[1] H. Tagoshi and T. Nakamura, *Phys. Rev.* D49(1994), 4016
[2] M. Sasaki, Prog. Theor. Phys. 92(1994), 17
[3] H. Tagoshi and M. Sasaki, 92(1994), 754
[4] T. Apostolatos, D. Kennefick, A. Ori, and E. Poisson, *Phys. Rev.* D47(1993), 5376
[5] C. Cutler, D. Kennefick and E. Poisson, *Phys. Rev.* D50(1994), 3816
[6] M.Shibata, M. Sasaki, H. Tagoshi and T. Tanaka, gr-qc 9409054
[7] H. Tagoshi, to be appeared in *Prog. Theor. Phys.*
[8] D. V. Gal'tsov, *J. Phys.* A15(1982), 3737
[9] Chrzanowski, *Phys. Rev.* D11(1975), 2042
[10] B. S. DeWitt, and R. W. Brehme, *Ann. Phys.*(N.Y.) 9(1960), 220
[11] M. Sasaki, *Prog. Theor. Phys.*, 65, 489(1981)
[12] Y. Mino, *Master thesis* (in Japanese); Y. Mino *in preparation*
[13] For example, see S. Chandrasekha, *Mathematical Theory of Black Holes* (Oxford University Press, New York, 1983)
[14] R. M. Wald, *Phys. Rev. Lett.* 41(1978), 203

Review and Comment on Critical Behavior in Gravitational Collapse

Yoshi Fujiwara

Uji Research Center, Yukawa Institute for Theoretical Physics, Kyoto University, Uji 611, Japan

Abstract The so-called "critical behavior" in gravitational collapse, found first by Choptuik in numerical simulation, is little understood at present. In this contribution, some important aspects of this non-linear behavior of gravity are briefly reviewed. Some comments are also made, especially on the dependence of this phenomenon on the collapsing matter.

1 Introduction

Gravity is a non-linear phenomenon of nature. Classical theory of gravity is described by Einstein's general relativity which obeys the non-linear partial differential equations. At present we have little knowledge of the non-linear nature of general relativity.

Numerical relativity has been and is increasing its importance in role of understanding non-linear aspects of gravitational phenomena. One of the most important practical applications would be the study of gravitational radiation from compact astronomical objects, whose observation is believed to be done in near future.

On the other hand, the non-linear problems of general relativity theory such as cosmic censorship, no hair conjecture and so on would be uncovered with the help of numerical simulations. Generally speaking, non-linearity in physics has a variety of features as is familiar in fluid dynamics and other areas. Moreover, another aspect of general relativity, namely general covariance, renders another difficulty. (See the talk by M. Shibata.) So each of the non-linear phenomena should be understood step by step in each situation.

Choptuik found an interesting non-linear phenomenon in studying gravitational collapse of scalar field in spherical symmetry. It is widely called "critical behavior" in gravitational collapse. Following this, other people made numerical simulations of gravitational collapse for completely different physical systems and found that a similar phenomenon could be observed. (See [1] for the reference.)

In this talk, some important aspects of this phenomenon are briefly reviewed with some comments being made. In particular, it is questioned how "universal" of this phenomenon by showing a simple exactly solvable model of gravitational

collapse. It is discussed the relevance of this non-linear phenomenon in general relativity to other problems in non-linear physics.

2 Critical Behavior in Gravitational Collapse

Let me summarize what is called the "critical behavior". The reader is referred to the literature [1] for the details and to [2]~[12] for recent analytic study about this phenomenon.

Numerical simulations were done so far for the gravitational collapse of (A) massless scalar field in spherical symmetry (with minimal coupling), (B) gravitational wave in axisymmetry, and (C) perfect fluid of radiation in spherical symmetry. Note that the physical system is obviously different from each other and that the matter has "null" character in propagation.

Consider a smooth initial data of a matter field. Suppose that the initial data have a parameter p which represents the typical strength of gravity of the system, typically (gravitational mass)/(characteristic length). Let us denote the one-parameter family of initial data by $D[p]$, and consider different families $D_k[p_k]$. Solve the Cauchy problem by following the time evolution of each initial data to obtain the space-time solution $S_k[p_k]$.

One would expect two different final-states: either the initial concentration of energy create a large enough mass, compared to its size, to form a black hole, or the initial field is finally dispersed to infinity to leave a flat space-time behind. As the parameter p changes in a family, there would be a certain critical value p^* that divides these two final-states. Since classical general relativity has no intrinsic scale, one may naively expect that almost zero mass of black hole is formed for $S[p^*]$. This is called "critical point".

Now the following phenomena were found in the numerical simulations above:
(I) Universal evolution near critical point

Sufficiently close to critical point $p \simeq p^*$, a family-dependent strong-field region $\mathcal{R}_k$ exists, after enough time of evolution to forget the details of initial data, such that the solution $S_k[p_k]$ in R_k is independent of the family k. In particular, except for the case (C), there was found a discrete scaling relation for a scale-invariant quantity ϕ:

$$\phi(\rho - \Delta, \tau - \Delta) \simeq \phi(\rho, \tau). \tag{1}$$

Here ρ and τ are logarithms of proper areal radius[1] r and central proper time t, that is,

$$\rho = \ln r + \kappa_k\,; \quad \tau = \ln(t_0 - t) + \kappa_k, \tag{2}$$

where κ_k is a family-dependent quantity for shifting and t_0 is the finite accumulation time of these "echoes". (Precisely critical solution $p = p^*$ is conjectured to exhibit an infinite train of echoes.) Δ in (1) is universal, *i.e.* independent of family

[1] In axisymmetric case, one restricts to the symmetry plane.

k. The value of Δ was found to be $\simeq 3.4$ for (A) and $\simeq$ for (B). It seems that this "echoing" phenomenon is non-linear oscillation of wave which is shrinking in size with the strong-field region $\mathcal{R}_k$.

(II) Power-law of black hole mass for near and super-critical point

For $p > p^*$, as $p \to p^*$, the mass of formed black hole which is actually defined by the proper size of apparent horizon formed) is found to obey a power-law:

$$M_{BH} = c_k \, |p - p^*|^\gamma, \tag{3}$$

where c_k is a family-dependent constant. γ is independent of the family k. What is most surprising is the numerical result that γ takes almost the same value for any case (A)(B)(C), $\gamma \simeq 0.36 - 0.37$ within numerical accuracy. This implies that (3) does not depend even on the physical system, being in contrast with the other phenomenon (I).

3 Discussion

Many analytic studies have been done from several viewpoints. Most of the works concentrates on the argument of the critical exponent in the power-law black hole mass (3).

Some comments are made in order. It is clear that in order to understand the non-linear wave behavior in the phenomenon (I), we should analyze the Einstein equations and the equation of motion for the matter field in the strong-field region. Many people believe that "self-similarity" plays an important role in the nature of this behavior.

The concept of self-similarity appears in many problems in physics such as self-gravitating system, fluid mechanics, diffusion problems etc [13]. Dimensional analysis usually allows one to have an ansatz of solution for the long-time and intermediate behavior of a system. In classical general relativity, the unit of length is the only scalable quantity with dimension, when one adopts the geometrized unit $c = 1 = G$. Since any specific coordinate system has no intrinsic meaning, one has to implement the self-similarity analysis in a geometrically invariant way. This can be achieved by considering a transformation of space-time such that the space-time metric changes its overall scale under it, which is called homothetic motion. Then, due to the Einstein equation, matter field is subject to a certain transformation. Requirement of self-similarity reduces the equations of motion to ordinary differential equations. (See [14] and the talk by K. Nakamura.) In this way, the space-time structure and the behavior of matter field were analyzed in [3] through [6]. Except for [6], the critical exponent was argued and found to be 1/2. How the self-similar solution is an attractor of the full theory is yet to be investigated as well as the finite size effect of such a self-similar region. Furthermore, the relation of this continuous self-similarity to the discrete scaling in the phenomenon (I) is not known.

One can consider some toy models — two-dimensional dilaton gravity [7], spherical shell inside Minkowski and outside Vaidya [8], three-dimensional gravity [9], also discussing the critical exponent.

The problem of the relevant mode in the echoing phenomenon was addressed in [10] [11]. Pullin presented that if one assumes the power-law of black hole mass (3) and that the relevant mode is the quasi-normal mode on a fixed background of Schwarzschild space-time, the critical exponent is necessarily 1/2 independently of the matter field involved.

As for the matter field, what is the features that are necessary for such critical behavior? The critical behavior does not exist for a certain matter field. In [12], a simple exactly solvable model was considered in order to show this point. The model was spherical collapse of dust in cosmic expansion, namely the so-called Tolman-Bondi model with cosmological constant. Dust field does not possess the null character in propagation. The cosmological constant introduced an intrinsic scale in the system, but is irrelevant in the strong-field region of collapse. Then it was shown that the critical exponent is essentially dependent on the parameter p in the initial data, although the solution is self-similar locally in the strong-field region.

The dependence of critical behavior on the theory of gravity, the Einstein theory and on the space-time dimension is now under investigation [15].

The dependence of the critical exponent on dimension, in particular, is expected to be essential from the following viewpoint. The critical exponent appears as a power in a singular behavior of a certain quantity in the set of non-linear partial differential equations. An analogous exponent to it, for example, appears in a self-gravitating system [16]. When the system is spatially on-dimensional, the set of partial differential equations which governs the time evolution of this system can be reduced so that a singular behavior is expressed as a map from Lagrange to Eulerian coordinate. The singular behavior of the map is predicted by the catastrophe theory. Essentially it depends on the dimension of the system.

Recently, the so-called renormalization group approach is tested in various non-linear partial differential equations appearing in wide areas of mathematical physics, condensed matter physics, fluid mechanics and so on. (For example, see [17] and the references therein for the relation of this approach to the above self-similarity method.) The basic nature of critical behavior in gravitational collapse would be clarified also from such a viewpoint, possibly opening a completely new way to understand the non-linearity of gravity.

References

[1] Numerical simulations of gravitational collapse:
• Massless scalar field with minimal coupling in spherical symmetry
M. W. Choptuik, *Phys. Rev. Lett.* **70** (1993) 9.
• Gravitational wave in axisymmetry
A. M. Abrahams and C. R. Evans, *Phys. Rev. Lett.* **70** (1993) 2980; *Gen. Rel. Grav.* **26** (1994) 379.
• Radiation fluid in spherical symmetry
C. R. Evans and J. S. Coleman, *Phys. Rev. Lett.* **72** (1994) 1782.
• Choptuik's model was checked by different way in
C. Gundlach, R. H. Price and J. Pullin, *Phys. Rev.* **D49** (1994) 890.
D. Garfinkle, *Choptuik scaling in null coordinates*, gr-qc/9412008.

[2] D. Christodoulou, *Comm. Math. Phys.* **105** (1986) 337; **106** (1986) 587; **109** (1987) 591; **109** (1987) 613.

[3] Y. Oshiro, K. Nakamura and A. Tomimatsu, *Critical Behavior of Black Hole Formation in a Scalar Wave Collapse*, *Prog. Theor. Phys.* **91** (1994) 1265.

[4] V. Husain, E. A. Martinez and D. Núñez, *Exact solution for scalar field collapse*, *Phys. Rev.* **D50** (1994) 3783.

[5] P. R. Brady, *Analytic example of critical behaviour in scalar field collapse*, *Class. Quantum Grav.* **11** (1994) 1255; *Self-similar scalar field collapse: naked singularities and critical behaviour*, gr-qc/9409035.

[6] E. W. Hirschmann and D. M. Eardley, *Universal Scaling and Echoing in Gravitational Collapse of a Complex Scalar Field*, gr-qc/9409045.

[7] A. Strominger and L. Thorlacius, *Universality and Scaling at the Onset of Quantum Black Hole Formation*, *Phys. Rev. Lett.* **72** (1994) 1584.

[8] T. Koike and T. Mishima, *An analytic model with critical behavior in black hole formation*, gr-qc/9409045.

[9] Y. Peleg and A. R. Steif, *Phase Transition for Gravitationally Collapsing Dust Shells in 2+1 Dimensions*, gr-qc/9412023.

[10] J. Pullin, *Is there a connection between no-hair behavior and universality in gravitational collapse?*, gr-qc/9409044.

[11] J. Traschen, *Discrete Self-Similarity and Critical Point Behavior in Fluctuations about Extremal Black Holes*, gr-qc/9403016.

[12] Y. Fujiwara and J. Yokoyama, *Black hole mass in Tolman-Bondi model with cosmological constant*, in preparation.

[13] G. I. Barenblatt, "Similarity, Self-Similarity and Intermediate Asymptotics", (Consultants Bureau, New York, 1979).

[14] D. M. Eardley, *Comm. Math. Phys.* **37** (1974) 287.

[15] Y. Fujiwara, in preparation.

[16] N. Gouda and T. Nakamura, *Prog. Theor. Phys.* **79** (1988) 765;
N. Gouda, *Prog. Theor. Phys.* **81** (1989) 648.

[17] N. Goldenfeld, "Lectures on Phase Transitions and the Renormalization Group", (Addison-Wesley, 1992).

Critical behavior in scalar wave collapse

Yoshimi OSHIRO, Kouji NAKAMURA
and Akira TOMIMATSU

Department of Physics, Nagoya University
Chikusa-ku, Nagoya 464-01, Japan

We study the critical behavior of black hole formation in spherical symmetric massless scalar field collapse. We analyze the evolution of the local mass near the singularity and find that the origin of power-law behavior is the transition from the scalar charge σ to the Schwarzschild mass m.

1 Introduction

Recently critical behaviors has been shown to occur near the zero mass black hole formation in three types of gravitational collapse. These behaviors were observed in the scalar wave collapse [1], in the axisymmetric gravitational collapse [2] and in the radiation fluid collapse [3]. These critical phenomena are characterized by a power-law behavior, a scaling relation and a universality. Near the critical point, black hole mass m_B serves as an order parameter and has a power-law dependence on a parameter p which present the field strength : $m_B \simeq c_f \mid p - p^* \mid^\beta$ where p^* is a critical value, c_f is a family-dependent constant. The critical exponent β is universal in the sense of being independent of the details of the initial data in both scalar and gravitational collapse [1] [2]. Surprisingly, the values of the critical exponent β are given by $\beta \simeq 0.37$ in these three systems. This power-law behavior comes from the nonlinearity of the fields. Nonlinear effects also induce the scaling relation of the field near the critical point. For example, the scalar field ϕ asymptotically approaches a scaling relation of the form $\phi(\rho - \Delta, \tau - \Delta) \simeq \phi(\rho, \tau)$, where ρ and τ are logarithms of proper radius r and central proper time T: $\rho = \ln r + \kappa$ and $\tau = \ln(T^* - T) + \kappa$. The time T^* is the finite accumulation time of the echoes and κ is a family-specific constant and Δ is a universal constant in the sense of being independent of the initial data.

An analytic explanation of these phenomena would be important. Several authors discussed these critical phenomena [5] [6], however a consequence of these papers is $\beta = 1/2$ which is slightly different form the numerical result $\beta \simeq 0.37$. An essential point of these papers is that the gravitational mass is estimated on the apparent horizon in some dynamical stage. However, after the dynamical stage, the scalar field exists which contributes to the final black hole mass. Since they missed the effect of this scalar field, the analytic method presents a mass which smaller than the numerical one.

In this paper, our main purpose is make it clear the mechanism of the power-law behavior in the scalar wave collapse. For this purpose we analyze the evolution of the

local mass after the dynamical region. Because in the supercritical case ($p > p^*$), one expects that near the future time-like infinity space-time settles down to a Schwarzschild black hole (no-hair theorem of black hole). At that stage the local mass which estimate at the origin corresponds to the Schwarzschild mass. Hence the analysis of the evolution of local mass at the origin is relevant for the estimation of a final black hole mass.

A scenario of our analysis is as follows. In section 2 we discuss the boundary condition. In section 3, fundamental equations are present and in section 4, we obtain the power-law in the zero mass limit. In section 5, results are discussed. In this paper we use $G = c = 1$ unit.

2 Boundary condition

We start with the setting of boundary condition. The Roberts solution [7] used in refs [5] [6] is an appropriate solution for the initial imploding wave, because it has a parameter to control the black hole formation. In this paper we also use this solution to represent the initial imploding wave. The Roberts solution is given by

$$ds^2 = -2hdUdV + \chi d\Omega^2, \tag{2.1}$$

$$\chi = \frac{1}{4}\{(1-p)V - U\}\{(1+p)V - U\}, \tag{2.2}$$

$$h = \frac{1}{2}, \tag{2.3}$$

$$\psi = \pm\frac{1}{2}\log\frac{(1+p)V - U}{(1-p)V - U}, \tag{2.4}$$

with the energy-momentum tensor

$$T_{\mu\nu} = \frac{1}{4\pi}(\partial_\mu\psi\partial_\nu\psi - \frac{1}{2}g_{\mu\nu}\partial^\alpha\psi\partial_\alpha\psi).$$

This space-time is asymptotically flat at the past null infinity $U \to -\infty$. The scalar waves implode from the past null infinity with $\phi \simeq \mp pV/\sqrt{\chi}$. The parameter p turns out to give the amplitude of imploding scalar wave and $p \geq 1$ correspond to the supercritical case and $p < 1$ correspond to the subcritical case (See refs [5] [6]). Since our main purpose is to make it clear that the mechanism of the power-law behavior, we consider only supercritical case. As mentioned in references [5] [6], this solution can not be use to represent the whole space-time of asymptotically flat gravitational collapse. For realistic evolution we replace the region $V \leq 0$ by flat space-time which is smoothly matched to the region $V \geq 0$. Furthermore, for the gravitational collapse of wave packets, the Roberts solution is approximately valid in a strong-field region of $V \leq V_0$. We use this solution only $0 \leq V \leq V_0$ for the realistic gravitational collapse of wave packets.

In the refs [5] and [6], the author estimate the local mass M_h on the apparent horizon and obtain $M_h \simeq (p-1)^{1/2}V_0$ in the limit $p \to 1$. This is slightly different from the numerical result $\beta \simeq 0.37$. This difference of critical exponents gives

$$M_{numerical} \simeq (p-1)^{0.37} > (p-1)^{1/2} \simeq M_h, \tag{2.5}$$

since $p-1<1$. This means that the after dynamical stage ($V>V_0$), the scalar wave exists which contributes to the final black hole mass. Thus the analysis after dynamical region ($V>V_0$) is important to determine the final black hole mass.

From no-hair theorem of black hole, we expect that the space-time settles down to a Schwarzschild black hole at the time-like infinity. At that stage the local mass estimated at the origin correspond to the Schwarzschild mass. Hence the evolution of the local mass at the origin is relevant for a final black hole mass. To analyze the evolution of the local mass at the origin, we estimate the local mass due to imploding scalar wave $\phi \simeq \mp pv/\sqrt{\chi}$. Near the point P (see figure, $U=(1-p)V_0$) the local mass behaves

$$M \simeq \frac{p^2(p-1)V_0^2}{8\sqrt{\chi}}. \tag{2.6}$$

This local mass diverge at the origin. Thus the nature of this singularity is different from the Schwarzschild one. In fact the Ricci scalar R diverge at the origin like $R \simeq \chi^{-2}$ in the Roberts space-time. However, we expect that this local mass goes to constant and the Ricci scalar goes to zero at the time-like infinity. This dynamical evolution of the singularity will be relevant for the critical behavior of gravitational collapse.

To analyze the evolution of the local mass at the origin we use the Wymann-like solution

$$ds^2 = Fdv^2 + 2dvdr + \chi d\Omega^2, \tag{2.7}$$

$$\chi = r^2\left(\frac{2\eta}{r}-1\right)^{1-m/\eta}, \tag{2.8}$$

$$F = \left(\frac{2\eta}{r}-1\right)^{m/\eta}, \tag{2.9}$$

$$\psi = \pm\frac{\sigma}{2\eta}\log\left(\frac{2\eta}{r}-1\right), \tag{2.10}$$

$$\eta = \sqrt{\sigma^2+m^2}, \tag{2.11}$$

where σ and m is constant and v is advanced time. σ is called scalar charge and for $\sigma=0$ we obtain the Schwarzschild solution. If one replace $F\to -F$ and $(2\eta/r-1)$ to $(1-2\eta/r)$, we obtain the Wymann solution [8]. This Wymann-like solution has a pathological space-time structure, because the circumference radius χ is restricted by some maximum radius $\chi_{max} = (\eta-m)^{1-m/\eta}(\eta+m)^{1+m/\eta}$. However, this Wymann-like solution is useful to understand the evolution of the singularity, if we use it near the origin $\chi \simeq 0$ ($r\simeq 0$). We expect that some regular solution exists in the $\chi >> 1$ region which can be smoothly matched to this Wymann-like solution near $\chi \simeq 0$.

To analyze the evolution of the local mass, we need to match the Wymann-like solution to the Roberts solution at point P(see figure). One simple way to obtain the matching condition is to look at the behavior of the local mass. The local mass in the Wymann-like space-time is given by

$$M = m\left\{\frac{(\eta+m)^2}{2mr}-1\right\}\left(\frac{2\eta}{r}-1\right)^{-(\eta+m)/2\eta}. \tag{2.12}$$

Near the origin this local mass behaves as

$$M \simeq \frac{1}{8}\left(1+\frac{m}{\eta}\right)^2 (2\eta)^{2\eta/(\eta+m)}\,\chi^{-(\eta-m)/2(\eta+m)} \tag{2.13}$$

To match to the initial condition (2.6), the local mass (2.13) must behave like $\chi^{-1/2}$. Then, we find that m must be equal to zero at point P and obtain a relation between σ and p as follows

$$\sigma^2 = \frac{1}{4}p^2(p-1)V_0^2. \tag{2.14}$$

This relation means that the imploding scalar wave has the effective scalar charge $\sigma \propto p(p-1)^{1/2}$. It can be shown that metric is also continue at point P.

On the other hand, from no-hair theorem we expect that the scalar charge σ goes to zero at time-like infinity i^+ ($v \to \infty$). When the scalar charge σ equal to zero and equation (2.13) gives

$$M = m. \tag{2.15}$$

Thus, at the time-like infinity, the remaining m gives the Schwarzschild black hole mass.

Before closing this section, we summarize the condition for the scalar charge σ and for m. To match to the Roberts solution, m must equal to zero at point P and scalar charge σ must vanish at time-like infinity. Then, as one goes from P to i^+, σ and m must vary with v (we set $v = 0$ at P) as follows

$$v : 0 \to \infty, \tag{2.16}$$

$$\sigma : \sigma_i \to 0, \tag{2.17}$$

$$m : 0 \to m_B. \tag{2.18}$$

From these conditions, we can obtain the power-law behavior. Of course, Wymann-like solution is a static solution. We must extend Wymann-like solution to a dynamical one. In the next section we try to extend this solution to a dynamical one.

3 Basic equations

Near the origin $r \simeq 0$, we assume v, r dependence of η and m as follows

$$\eta(v,r) \simeq \eta_0(v) + \eta_1(v)(\frac{r}{2\eta_0})^{n(v)}, \tag{3.1}$$

$$\frac{m(v,r)}{\eta(v,r)} \simeq f(v) + g(v)(\frac{r}{2\eta_0})^{n(v)}, \tag{3.2}$$

where η_0, η_1, n, f, are functions of v. From (2.8) and (2.9) we obtain

$$\begin{aligned}\chi &= (2\eta_0)^2(\frac{r}{2\eta_0})^{1+f}\{1-(1-f)(\frac{r}{2\eta_0}) - \frac{f}{2}(1-f)(\frac{r}{2\eta_0})^2 \\ &\quad +a_1(\frac{r}{2\eta_0})^n \log kr + a_2 \log 2k\eta_0 (\frac{r}{2\eta_0})^n \}, \end{aligned} \tag{3.3}$$

$$\begin{aligned}F &= (2\eta_0)^f(\frac{r}{2\eta_0})^{1-n}\{1-f(\frac{r}{2\eta_0}) \\ &\quad +b_1(\frac{r}{2\eta_0})^n \log kr + b_2 \log 2k\eta_0 (\frac{r}{2\eta_0})^n \}, \end{aligned} \tag{3.4}$$

where k is constant which has $[r^{-1}]$ dimension. a_1, a_2, b_1 and b_2 are functions of v and their order are $O((\eta_0)^0)$.

Note that there are two limits $r \to 0$ and $\eta_0 \to 0$. First, we take $r \to 0$ limit, to find basic equations for η_0 and f. Next, we take $\eta_0 \to 0$ limit, to analyze the critical behavior.

From order estimation of Einstein equation $G_{\mu\nu} = 8\pi T_{\mu\nu}$, we obtain following equations,

$$n = f + 1 \tag{3.5}$$

$$(2\eta_0)\dot{f} = n(n+1)a_1, \tag{3.6}$$

$$2\dot{\eta_0} = \frac{1}{2}n(n+1)(a_1 + a_2)\log 2k\eta_0 - \frac{n}{2}(2n+1)a_1, \tag{3.7}$$

and scalar filed ψ is given by

$$\psi = \pm\frac{1}{2}\sqrt{1-f^2}\ \log 2kr + O(1). \tag{3.8}$$

Here dot denoted the v derivative. These equations are not so simple, however in the $\eta_0 \to 0$ limit these equations become simple and give the power-law behavior. In the next section, we take the $\eta_0 \to 0$ limit.

4 Zero mass limit and power-law behavior

In this section we show that the power-law behavior automatically appears in the zero mass limit. Since a_1 has the order $O(1)$, then from equations (3.6) and (3.7) we obtain

$$2\dot{\eta_0} = (1-\gamma)\eta_0\dot{f}\log 2k\eta_0, \tag{4.1}$$

in the $\eta_0 \to 0$ limit. Where γ is given by

$$\gamma = -\frac{a_2}{a_1}. \tag{4.2}$$

For integration of (4.1), we use the condition (2.16) $\sim$ (2.18). Under this condition we find the relation between final black hole mass m_B and initial scalar charge σ_i as follows

$$(2km_B) = (2k\sigma_i)^{\bar{\beta}},$$

where $\bar{\beta}$ is given by

$$\bar{\beta} = \exp(1-\bar{\gamma}), \tag{4.3}$$

and

$$\bar{\gamma} = \int_0^1 \gamma df. \tag{4.4}$$

Note that the function f is given by $f = m/\eta$, then f vary 0 to 1. From (2.14) and (4.3) we obtain power law

$$m_B \simeq c_f(p-1)^{\beta}, \tag{4.5}$$

here the critical exponent β is given by

$$\beta = \frac{1}{2}\bar{\beta}. \tag{4.6}$$

We obtain the power-law (4.5) and the critical exponent (4.6). Above analysis make it clear that the mechanism of the power-law behavior. The power-law behavior crucially related to evolution of scalar charge σ and m. Note that the critical exponent β is independent for the cut off parameter V_0. The V_0 affects only family-dependent constant c_f.

5 discussion

Our analysis is limit to the origin, then we can not determine the value of β exactly. However, this analyses show the possibility of the value of $\beta \neq 1/2$ even if previous paper give $\beta = 1/2$. For example, if $\bar{\gamma} = 3/2$ we obtain $\beta = (\exp(-1/4))/2 \simeq 0.39$.

Our analyses show that the behavior of scalar field during point P to time-like infinity is crucially related to the critical exponent β. The dependence of behavior of the scalar field for the critical exponent β is suggest that some attractor will appear in the zero mass limit for the universality. Such attractor will be related to the scaling relation.

Let we summarize our results. In this paper we make it clear that the mechanism of the power-law behavior. The mechanism of the power-law is expressed by the evolution of the local mass(as same as the evolution of singularity). The critical exponent β is related to the behavior of the scalar field during point P to time-like infinity. These results suggest that the dynamics of singularity is important for the critical behavior.

Universality and scaling relation is difficult to explain by this analysis. However, our analyze suggest that the universality and the critical exponent β are crucially related each other. The critical behavior were also observed in the axisymmetric gravitational collapse [2] and in the radiation fluid collapse [3]. The singularity evolution in these space-time are future problem.

References

[1] M.W.Choptuik, Phys. Rev. Lett. **70**, 9, (1993).

[2] A.M.Abrahams and C.R.Evans, Phys. Rev. Lett. **70**, 2980, (1993). A.M.Abrahams and C.R.Evans, Phys. Rev. **D 49**, 3998, (1994).

[3] C.R.Evans and J.S.Coleman, Phys. Rev. Lett. **72**, 1782, (1994).

[4] D.M. Eardley, in *Texas/PASCOS 92: Relativistic Astrophysics and Particle Cosmology,* eds. C.W.Akerlof and M.A.Srednicki (N.Y.Acad. Sci.,New York),1993.

[5] Y.Oshiro,K.Nakamura and A.Tomimatsu, Prog. Theor. Phys. **91**, 1265, (1994).

[6] P.R.Brady, Class. Quantum Grav. **11**, 1255, (1994).

[7] M.D.Roberts, Gen. Rel. Grav. **21**, 907, (1989).

[8] M.Wymann, Phys. Rev. **D 24**, 839, (1981).

Figure caption

Figure Penrose diagram for black hole formation due to wave-packet collapse. The region I is the flat space-time and in the region II, initial imploding wave is dominant. Wymann-like solution present the shadowed region. Roberts solution and Wymann-like solution is connected at the the point P.

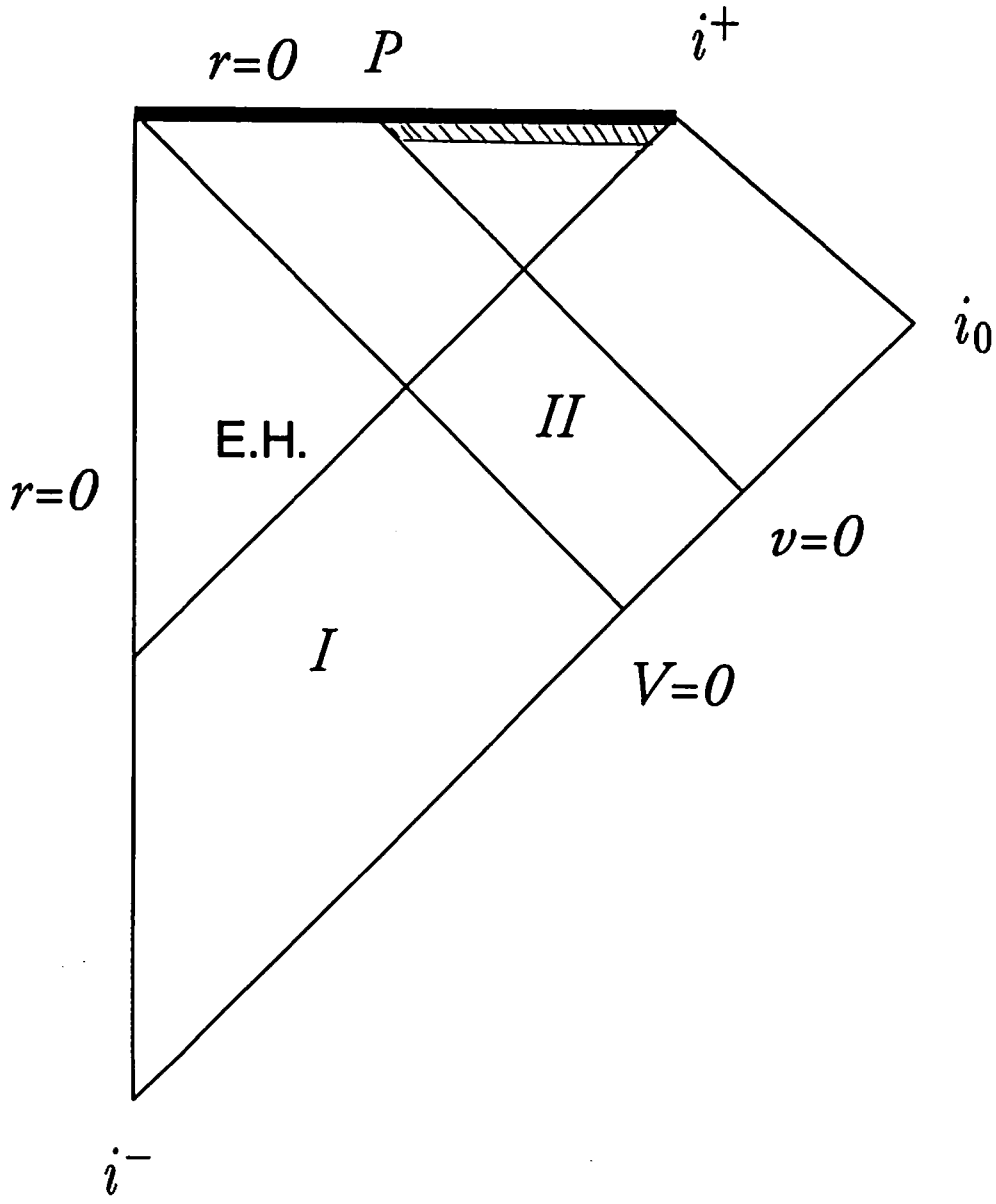
r=0
P
i+
i0
E.H.
II
r=0
v=0
I
V=0
i−

Critical phenomena in gravitational collapse

Tatsuhiko Koike*

Department of Physics, Tokyo Institute of Technology, Oh-Okayama, Meguro, Tokyo 152, Japan

and

Takashi Mishima†

Laboratories of Physics, College of Science and Technology, Nihon University, Narashinodai, Funabashi, Chiba 274, Japan

A simple analytic model is presented which exhibits a critical behavior in black hole formation. It is collapse of a thin shell coupled with outgoing null fluid. We see that the critical behavior is caused by the gravitational nonlinearity near the event horizon. We calculate the value of the critical exponent analytically and find that it is very dependent on the coupling constants of the system.

Gravitational collapse with formation of black holes is one of the main problems of general relativity. Recently, Choptuik [1] numerically discovered a critical behavior of the gravitational collapse of massless scalar field. His result can be summarized as follows. Let $\{S_i(p)\}$ be one-parameter families of solutions of Einstein's equations for spherically symmetric massless scalar field minimally coupled to gravitational field, where p is a parameter which smoothly specifies the initial value of the scalar and gravitational fields and i is an index which specifies one of the several one-parameter families. For each family $S_i(p)$ there is a critical value p^* of the parameter p such that solutions $S_i(p > p^*)$ contain a black hole while $S_i(p < p^*)$ do not, which are referred to as supercritical and subcritical, respectively. He found that near-critical solutions satisfy the following: (1) the strong field region is universal in the sense that it approaches the identical spacetime for all families (*i.e.* for all i), (2) the strong field region has a discrete self similarity, and (3) for supercritical solutions

---

*JSPS fellow, e-mail: bartok@phys.titech.ac.jp

†e-mail: tmishima@phys.titech.ac.jp

the black hole mass is proportional to a certain power of the deviation of the parameter p from the critical value p^* as

$$M_B \propto (p - p^*)^\beta, \tag{1}$$

and the critical exponent β is universal, *i.e.* independent of i. The numerical value of the β was given as $\beta \simeq 0.37$. Abrahams and Evans [2] found the similar phenomena in axisymmetric collapse of gravitational wave. Evans and Coleman [3] also found the similar phenomena in spherically symmetric collapse of radiation fluid, in which case the self similarity is not discrete but local one. In the both cases the obtained values of the exponent were very close. It suggest that the universality in (3) can be extended to independence of the critical exponent from details of systems, though in the first suggestion it meant its independence of initial data. There have been some attempts to understand the phenomena [4–6], but we are yet to obtain a totally satisfactory explanation.

If the critical behavior has very universal feature we may expect the similar behavior in seemingly very different models, which may enable us to investigate it in a simple model. On the other hand, the model should have some essential properties which the above models have in common. First, the spacetime should be asymptotically flat. Second, there must be energy transportation to the null infinity. This is because otherwise the spacetime necessarily ends up with a black hole with the mass of the initially prepared matter whenever a black hole forms (apart from the possibility that a star forms outside a black hole of small mass) so that there would be no criticality, which is the case of the Lemaitre–Tolman–Bondi spacetimes. Third, the matter content was "massless" in all of the above numerical studies. It is preferable that our model should also have the similar property.

A simple model possessing these properties is the collapse of a thin shell coupled with outgoing null flux. We will find such a model which exhibits the critical behavior in black hole formation. We treat it analytically, which may help find the mechanism of the critical behavior. We shall find the critical exponent and its dependence on the details of the systems.

Let us assume that the outer side of the shell is coupled with outgoing null flux which may transport the energy of the shell to infinity and the inner side of the shell does not have any interaction. The exterior spacetime is the Vaidya spacetime. The interior spacetime is assumed to be flat, *i.e.* , is the Minkowski spacetime. We can write the line element as

$$ds^2 = -(1-2\Phi)du^2 - 2dudr + r^2 d\Omega^2, \tag{2}$$

where u is the retarded time, r the area radius, and $d\Omega^2$ the line element on a unit sphere, and

$$\Phi = \begin{cases} \Phi_+ = M(u)/r & \text{(exterior)} \\ \Phi_- = 0 & \text{(interior).} \end{cases} \tag{3}$$

A similar situation is considered in [7] in the context of the creation of man-made universes. Note that $M(u)$ gives the Bondi–Sachs mass of the null infinity at u. Let τ denote the proper time of the shell. Let $r = R(\tau)$ represent the trajectory of the shell. Note that R is the shell's radius. We assume that the shell consist of perfect fluid with surface density ρ and tension $\zeta = -\eta\sigma$, where η a constant. For simplicity, we assume that the coupling of the shell and the spacetime is given by

$$(\sigma R^{1-\omega})^{\cdot} = 0, \tag{4}$$

where ω and C are constants. In the $\omega = -1$ case of the above equation the mass M of the shell conserves, while $\omega = 1$ is said to hold in the case of false vacuum bubbles [8]. Our assumption is a slight generalization of them in the parameter space. Using the metric junction formalism first considered by Israel [9], we have the following equation of motion of the shell,

$$\dot{R}^2 + 1 = f^2, \tag{5}$$

$$\dot{\sigma} + \frac{2\dot{R}}{R}(\sigma - \zeta) = \frac{\dot{M}}{4\pi R^2}\frac{1}{\sqrt{\dot{R}^2 + 1 - 2\Phi} + \dot{R}}, \tag{6}$$

where

$$f = \frac{1}{2}\left(\frac{\mathcal{M}}{R}\right) + \Phi\left(\frac{\mathcal{M}}{R}\right)^{-1}, \quad p = 2\eta + \omega + 1, \quad \tilde{M} = CM, \quad \tilde{R} = CR. \tag{7}$$

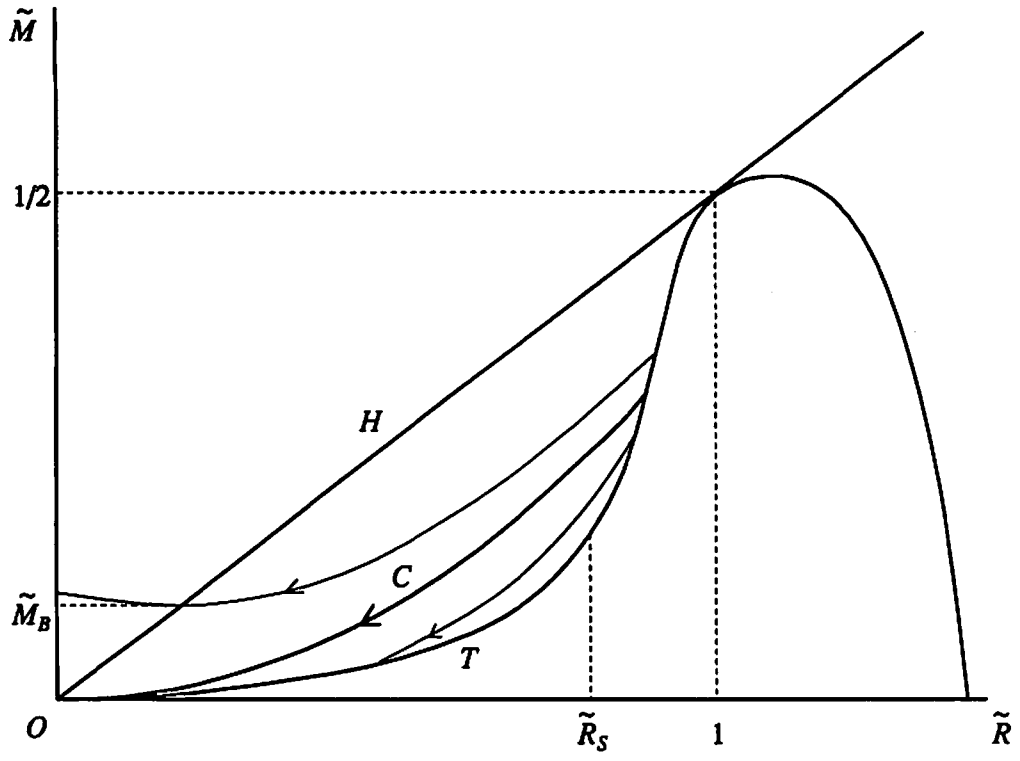

FIG. 1. The evolutions of the Bondi—Sachs mass and the radius of the shell are illustrated. The line H corresponds to the apparent horizon and the line T is the set of states with $\dot{R} = 0$. Region I is between H and T, where we can set initial data. The thick line C with an arrow denotes the critical solution which hits the origin. The thin line with an arrow above C is a supercritical solution which cross H. The value M_B of the mass function is the mass of the formed black hole. The thin line with an arrow below C is a subcritical solution.

Let us look at the qualitative behavior of the shell and search models which exhibits a critical behavior in the black hole formation. First we assume that there is some mechanism to prevent negative flux to emit from the shell and the shell will be static after then. It follows from eqs. (4), (5), (6), (7) and $d\tilde{M}/d\tilde{R} = \dot{\tilde{M}}/\dot{\tilde{R}}$ that the orbit of the collapsing shell outside the event horizon is given by a first order ordinary differential equation

$$\frac{d\tilde{M}}{d\tilde{R}} = p\tilde{R}^{\omega}(f - \tilde{R}^{\omega} + \frac{\dot{\tilde{R}}}{|\dot{\tilde{R}}|}\sqrt{f^2 - 1}). \tag{8}$$

One immediately finds that the motion of the shell is scale invariant, which is another feature

which our model has in common with the case of spherically symmetric scalar field collapse. The set T of turning points (boundary of the forbidden region) in the $\tilde{M}$-$\tilde{R}$ space is given by the points where $\dot{\tilde{R}} = 0$ hence $f = 1$. The line H of $\tilde{M} = \tilde{R}/2$ corresponds to the apparent horizon where the expansion of the outgoing null ray vanishes. Further, it coincides with the event horizon for the outgoing Vaidya spacetime. We assume that ω is positive, for otherwise the mass is not bounded from below and can be negative. Then the shape of the potential is as shown in fig. 1.

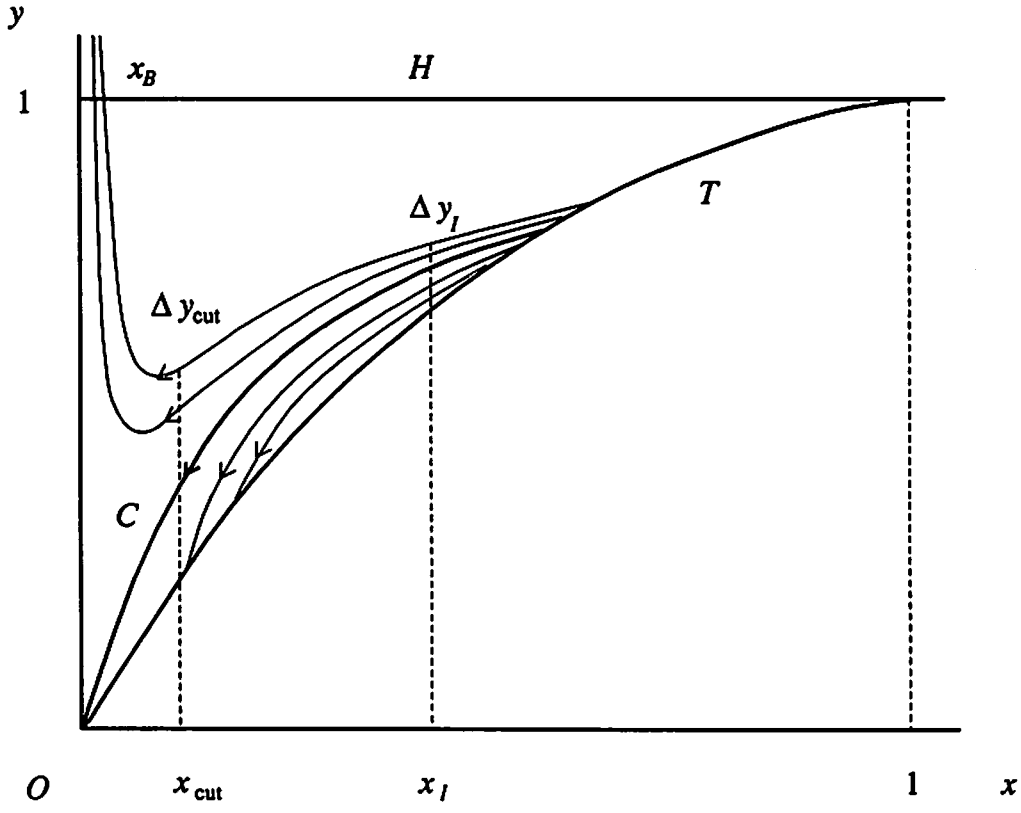

FIG. 2. The evolution in variables x and y. The line H corresponds to the apparent horizon and the line T is the set of states with $\dot{R} = 0$. Region I is between H and T, where we can set initial data. The thick line C with an arrow denotes the critical solution which hits the origin. The thin line with an arrow above C is a supercritical solution which crosses H. The coordinate x_B of the point intersecting H gives the mass of the formed black hole. The thin line with an arrow below C is a subcritical solution.

The initial condition $(\tilde{R}_I, \tilde{M}_I)$ can be given in the region between H and T with $0 \leq \tilde{R} < 1$, which we will call Region I, if the shell is not contained in a black hole from the beginning. We require that the mass decreases when the shell is collapsing. This is given by the condition $p = 2\eta + \omega + 1 > 0$. Then it can be shown [10] that the critical point exists if and only if the both of η and ω are positive. The phase diagram is shown in fig. 1.

We change variables of the equation (8) by

$$x = \tilde{R}^{\omega}, \quad y = 2\tilde{M}\tilde{R}^{-1}. \tag{9}$$

Eq. (8) for $\dot{\tilde{R}} < 0$ is given by

$$\frac{dy}{dx} = \frac{1}{\omega}\left((p-1)\frac{y}{x} - px - p\left(\left(\frac{y}{x} + x\right)^2 - 4\right)^{\frac{1}{2}}\right). \tag{10}$$

The behavior of the solutions is illustrated in fig. 2.

The critical solution $y = y_C$ in y-x diagram hits the origin. The supercritical solutions diverge at $\tilde{R} = 0$. The event horizon H is given by the straight line $y = 1$. The mass of the black hole $\tilde{M}_B$ is related to the value x_B of x at the point intersecting H as $M_B \propto x_B^{1/\omega}$. A convenient choice for initial conditions of $(\tilde{R}, \tilde{M}) = (\tilde{R}_I, \tilde{M}_I)$ is those with fixed $\tilde{R}$, which correspond to initial conditions of $(x, y) = (x_I, y_I)$ with fixed x_I. A power-law relation $x_B \propto \Delta y_I^{\beta'}$ implies $\tilde{M}_B \propto \Delta \tilde{M}_I^{\beta}$, where $\beta = \beta'/\omega$. Let us devide Region I into two, $x \geq x_{\rm cut}$ and $x \leq x_{\rm cut}$, with $x_{\rm cut}$ being a small positive constant. We will call the former the *linear (deviation) region* and the latter the *scaling region*. In the linear region, the expansion of the deviation vector of the solution curves, or the rate of change of the gradient along nearby curves, is bounded because the denominator vanishes only on T. This implies that the deviation vector field which is finite on x_I is always finite along the curve up to $x_{\rm cut}$. Therefore we have

$$\Delta y_{\rm cut} \propto \Delta y_I \tag{11}$$

in the linear region. It should noted that the cutoff $x_{\rm cut}$ can be chosen to be an arbitrarily small constant. The nonlinearity in $\Delta\tilde{M}$ occures only in a infinitesimal region in $\tilde{R}$. In the scaling region, if we ignore x compared to unity, eq. (10) reads

$$\frac{dy}{dx} = \frac{1}{\omega}\left((p-1)\frac{y}{x} - p\left(\left(\frac{y}{x}\right)^2 - 4\right)^{\frac{1}{2}}\right). \tag{12}$$

Note that y/x is not necessarily large compared to unity for near-critical solutions. One finds a scaling law in the sense that the transformation $(x, y) \mapsto (ax, ay)$ does not change the differential equation (12), which says that if $y = y_1(x)$ is a solution, $y = a^{-1}y_1(ax)$ gives general solutions. In fact, one integrates eq. (12) to find

$$k = x(\sqrt{f^2-1} + f)^{\frac{\omega p}{p^2-q^2}} \left|p\sqrt{f^2-1} - qf\right|^{\frac{\omega q}{p^2-q^2}}, \tag{13}$$

where $q = 2\eta$, k is the constant of integration, and $2f = y/x$ in the present approximation. The critical solution is the one passing the origin hence the one having finite limit of $f = y/2x$ as $x \to 0$. It is the $k = 0$ solution, namely,

$$y_C = \frac{2px}{\sqrt{p^2-q^2}}, \tag{14}$$

Positive k corresponds to all of the other solutions. For small k, by setting $y = 1$ one finds

$$k \sim x_B^{1-\frac{\omega}{p-q}}. \tag{15}$$

Setting $x = x_{\rm cut}$ one has

$$k \sim (\Delta y_{\rm cut})^{\frac{\omega q}{p^2-q^2}}. \tag{16}$$

Combining these equations, one has the critical exponent

$$\beta = \frac{q}{p+q} = \frac{2\eta}{4\eta+\omega+1}. \tag{17}$$

It can be shown that the above value is exact [10].

Let us summarize our result. We constructed an analytic model which exibits a critical behavior of black hole formation, namely, collapse of a thin shell coupled with outgoing null fluid. In that model the dynamics of the shell is described by an ordinary differential equation. We investigated the dynamics of the shell and the evolution of the Bondi–Sachs mass. It was seen that the near-critical solutions have the linear region and the scaling region.

The deviation of the Bondi–Sachs mass from that of the critical solution gets nonlinear only in the scaling region, which is near the $\tilde{M} = 0$ and near the event horizon.

It is remarkable that in our model the critical exponent β is dependent on the constants η and ω specifying the system. The exponent β can take the values in the range $0 < \beta < 1/2$ for $\eta > 0$ and $\omega > 0$. We can easily adjust β to be ~ 0.38, but there seems to be no strong physical reason to prefer such values for η and ω. This suggests that the critical exponent is not so universal in the extended sense. There may be many different *universality classes*, and the critical exponent β may serve as an index specifying them.

There will be a question why the numerically calculated cases seem to fall into the same universality class with $\beta \sim 0.38$, even if we admit the existence of many universal classes. One may think that the massless property of the matter is crucial. In our case, even if we require that the shell consists of radiation fluid having a trace free equation of state, $\eta = 1/2$, then β is equal to $1/(3+\omega)$ and cannot exceed $1/3$. This may suggest that the massless property is not so important. Another possibility is that self-similarity is crucial. A support for this possibility is that the critical solution in our model does not have spacetime self-similarity. If the near-critical solutions necessarily fall into a self-similar spacetime in the systems with *smoothly* distributed matter, then types of self-similar spacetimes may determine the universality classes.

The universality in the initial value is not verified in our model because the solutions are parametrized by a single parameter M_I (or R_I), apart from an irrelevant parameter C. However, if the situations are similar to our model in the numerically investigated collapses the universality in initial data can be naturally understood. Namely, Choptuik originally showed in his model that almost all modes or fluctuations in initial data damp away in the final stage so that the spacetime fall into a unique one. On the other hand, it is shown in our model that the value of β is completely determined in the scaling region, which is an infinitely small portion of the spacetime corresponding the very last stage of the collapse. This may suggest that the solutions have the linear and scaling regions, and the fluctuations are washed out within the linear region. This explains the universality of the

critical exponent β in initial data. The above point of view may also explain the universality in the extended sense if the spacetimes fall into the same one in the last stage of the collapse in several different systems.

This work is supported in part by the Grant-in-Aid for Scientific Reserch Fund of the Ministry of Education of Japan (T. K.).

---

[1] M. W. Choptuik, *Phys. Rev. Lett.* **70** (1993) 9.

[2] A. M. Abrahams and C. R. Evans, *Phys. Rev. Lett.* **70** (1993) 2980.

[3] C. R. Evans and J. S. Coleman, *Phys. Rev. Lett.* **72** (1994) 1782.

[4] Y. Oshiro, K. Nakamura, and A. Tomimatsu, *Prog. Theor. Phys.* **91** (1994) 1265.

[5] P. R. Brady, Does scalar field collapse produce 'zero mass' black holes?, 1994, gr-qc/9402023.

[6] V. Husain, E. A. Martinez, and D. Nunez, Exact solution for scalar field collapse, 1994, gr-qc/9402021.

[7] T. Mishima, H. Suzuki, and N. Yoshino, Creation of a child universe in Vaidya spacetimes with out-going negative energy radiation, in *Proceeding of the Third Workshop on General Relativity and Gravitaion*, edited by K. Maeda *et. al.*, pages 375–381, Tokyo, 1994.

[8] S. K. Blau, E. Guendelman, and A. H. Guth, *Phys. Rev.* **D35** (1987) 1747.

[9] W. Israel, *Nuovo Cim.* **44B** (1966) 1.

[10] T. Koike and T. Mishima, An analytic model with critical behavior in black hole formation, 1994, Tokyo Inst. Tech. preprint TIT/HEP-266/COSMO-46, gr-qc/9409045.

Einstein-scalar spacetime with local symmetry

Kouji Nakamura*

Department of Physics, Nagoya University, Chikusa-ku, Nagoya 464-01, Japan

Abstract

A simple model is suggested to investigate the universality of critical exponent of black hole mass which is independent of initial conditions in Choptuik's numerical calculation. This model is a self-similar model of spherically symmetric spacetime with minimally coupled scalar field and one-parameter extension of Roberts solution which shows the critical exponent is 1/2. In this toy model, the phase space of $\kappa^2 > 1$ and one of $\kappa^2 < 1$, where κ is an extended parameter, shows different features.

I. INTRODUCTION

Recently, Choptuik [1] discovered the phenomenon by numerical calculation. This phenomenon seems to suggest that the gravitational collapse is a sort of phase transition. His model was a simple model of self-gravitating system, *i.e.*, gravitational collapse of minimally coupled massless scalar filed in spherically symmetric spacetime. In this system, the collapse of strong scalar field leads to the black hole formation and the collapse of weak scalar field do not lead to the black hole formation but the scalar wave bounce at origin and escape infinity.

Choptuik discovered the one-parameter families of solutions of this system. This parameter p represents the strength of initial scalar field. Suppose that in the case $p > p^*$ black

*e-mail address: kouchan@allegro.phys.nagoya-u.ac.jp

hole formation occurs and in the case $p < p^*$ black hole does not form. He also investigated the behavior of this system in the limit $p \to p^*$ in detail. He discovered the two fact in this limit. One is about the mass of black hole which is formed by the collapse of scalar wave. This mass M_{BH} depends on p and have the behavior,

$$M_{BH} \propto |p - p^*|^\gamma, \qquad \gamma = 0.37, \tag{1.1}$$

where γ is a "universal" constant. Another fact is the discrete self-similarity of scalar field near the apparent horizon,

$$Z(\rho - \Delta, \tau - \Delta) = Z(\rho, \tau), \qquad \Delta = 3.4, \tag{1.2}$$

where Z corresponds to the derivative of scalar field. Δ is also a "universal" constant.

The words "universal" above in this case means that γ and Δ do not depend on the initial conditions. After his discovery, it was shown by numerical calculation that the behavior similar to Eq.(1.1) appears and the near value of γ was obtained [2] when one considers other massless field collapse. This may means that γ is a "universal constant". In this case "universal" means that γ does not depend on not only initial conditions but also the collapsing massless matter. On the other hand, the analytic examples which have this critical behavior shows $\gamma = 1/2$ [3,4] or γ depends on the collapsing matter [5]. These examples show that the γ is not "universal" only by imposing that the spacetime is a solution of Einstein equation.

So, it is natural to consider that there are some universal classes. These classes consist of one-parameter families of solutions which have a common value of Δ and γ. In this sense, Roberts solution which shows $\gamma = 1/2$ [3] may not belong to a universal class, for Roberts solution is only one parameter family of solutions which characterized by only one parameter and, in general, the analytic examples are idealized one as a model of black hole formation. Then, it is possible to consider that Roberts solution may be isolated family of solutions and $\gamma = 1/2$ may be a special case. So it is meaningful to consider the behavior of solutions which have similar characters to Roberts solutions. In this talk, I suggest the simplified

model to consider the universality of γ which contains more one parameter and the system is self-similar. To find self similar variables, one must consider the symmetries of differential equations.

II. SYMMETRIES OF DIFFERENTIAL EQUATIONS

In this section, I show the method to find self-similar variables [6]. Let us consider a system of partial differential equation,

$$\Delta^\alpha \left(x^i, u^a, \frac{\partial u^b}{\partial x^j}, \frac{\partial^2 u^c}{\partial x^l x^k}, \ldots\ldots \right) = 0. \tag{2.1}$$

where α is the number of equations of this system. x^i and u^a are independent and dependent variables respectively ($i = 1, ..., n$, $a = 1, ..., m$). When $\Delta^\alpha = 0$ are Einstein equations, x^i are coordinates and u^a are metric components and matter fields. A solution of Eq.(2.1) $u^a = u^a(x^i)$ is said to be a self-similar solution when there exist a group of transformation $g : \{x^i, u^a\} \to \{\tilde{x}^i, \tilde{u}^a\}$ such that $g(u^a - u^a(x^i)) = \tilde{u}^a - \tilde{u}^a(\tilde{x}^i) = 0$. The existence of g is closely related to the symmetries of the system of the differential equation (2.1), i.e. g must be a group of transformation which remains Eq.(2.1) invariant. Let us call a group G whose every element remains Eq.(2.1) invariant g to be symmetry group of differential equation. The symmetry group G is determined by Eq.(2.1). For a $g \in G$, one can obtain $m + n - 1$ functions $\tilde{u}^p(x^i, u^a)$ which are invariant under the transformation g, i.e., $g(\tilde{u}^p) = 0$. We call these variables to be self-similar variables. When one adopts these variables as independent and dependent variables of Eq.(2.1), Eq.(2.1) can be reduced to a set of total differential equations. The solutions of these total differential equations are self-similar solutions which are invariant under the transformation g.

Hence, to find self-similar variables is to find a symmetry group of Eq.(2.1). If one restricts his consideration to the case when the symmetry group G is a Lie group, all elements of G can be find systematically [6].

Although I do not show the detail of this method to find all elements of G systematically, the idea of this method as follows. Suppose that $g \in G$ where G a Lie group of transforma-

tion, $G : \{x^i, u^a\} \to \{\tilde{x}^i, \tilde{u}^a\}$ and its generator can be written in the form $\mathbf{v}^a = \xi^i(x^j, u^b)\partial_{x^i} + \phi^a(x^j, u^b)\partial_{u^a}$[1]. If G is the symmetry group of Eq.(2.1), Eq.(2.1) may be invariant under the transformation which generated by $\mathbf{v}^a$. On the contrary, If one imposes that Eq.(2.1) is invariant under the transformation which generated by general $\mathbf{v}^a$, this imposition leads to the restrictions to $\mathbf{v}^a$ which can be expressed by differential equations of $\xi^i(x^j, u^b)$ and $\phi^a(x^j, u^b)$. Solving these equations, one can obtain the generators $\mathbf{v}^p$ which are generator of symmetry group of Eq.(2.1). And then, obtaining the integrals of $\mathbf{v}^a$, one can obtain self-similar variables.[2]

We adapt this method to the Einstein equations for spherically symmetric spacetime with minimally coupled massless scalar field ψ,

$$h = -(r^2)_{,uv}, \qquad (r^2\psi_{,v})_{,u} + (r^2\psi_{,u})_{,v} = 0,$$
$$\left(\frac{r_{,v}}{h}\right)_{,v} = -\frac{r}{h}\psi_{,v}^2, \qquad \left(\frac{r_{,u}}{h}\right)_{,u} = -\frac{r}{h}\psi_{,u}^2,$$

where spacetime metric is $ds^2 = -2h(u,v)dudv + r^2(u,v)d\Omega_2^2$, $d\Omega_2^2$ is the metric of unit sphere. One can obtain the 4 generators,

$$\mathbf{v}^1 = \xi(u)\partial_u - h\xi(u)_{,u}\partial_h, \qquad \mathbf{v}^2 = \eta(v)\partial_v - h\eta(v)_{,v}\partial_h,$$
$$\mathbf{v}^3 = r\partial_r + 2h\partial_h, \qquad \mathbf{v}^4 = \partial_\psi,$$

where $\xi(u)$ and $\eta(v)$ are arbitrary function of u and v respectively. Here, we must note that $\mathbf{v}^1, ..., \mathbf{v}^4$ is a generator of transformation which defined on the space spanned by $\{u, v, r, h, \psi\}$. $\mathbf{v}_1$ and $\mathbf{v}_2$ correspond to the coordinate transformations of null coordinates u and v respectively. $\mathbf{v}^4$ corresponds to the translation of ψ. The general form of generator can be written by

---

[1]This form of transformation represents a point to point transformation on the space which is spanned by $\{x^i, u^a\}$, *i.e.*, local transformation. So, the symmetry group whose generator is written by this form called local symmetry group.

[2]Detail of this calculation and proofs of theorems can be seen in Ref. [6].

$$\mathbf{v} = \xi(u)\partial_u + \eta(v)\partial_v + 2\lambda r\partial_r + h(2\lambda - \xi(u)_{,u} - \eta(v)_{,v})\partial_h + \kappa\partial_\psi, \tag{2.2}$$

where λ and κ are arbitrary constant. Denoting $\mathbf{v}_0 = \xi(u)\partial_u + \eta(v)\partial_v$, Eq.(2.2) can be written as follows,

$$\pounds_{\mathbf{v}_0} g_{\mu\nu} = -2\lambda g_{\mu\nu}, \qquad \pounds_{\mathbf{v}_0}\psi = \kappa. \tag{2.3}$$

These equations are obtained by Cahill and Taub as the conditions of self-similarity in general relativity [7].

III. SPACETIMES WITH LOCAL SYMMETRY

Using the condition (2.3), one can obtain Einstein equations as total differential equations. Whether λ or κ vanishes or not, these total differential equations have different solutions. If $\lambda = 0$, $\mathbf{v}_0$ becomes to be a Killing vector. Then, one can obtain the homogeneous spacetime when $\mathbf{v}_0$ is spacelike and static spacetime when $\mathbf{v}_0$ is timelike. If $\lambda \neq 0$, general solution of the condition (2.3) can be obtained by

$$ds^2 = -2h\left(\frac{u}{v}\right)dudv + v^2 f^2\left(\frac{u}{v}\right)d\Omega_2^2, \tag{3.1}$$

$$\psi = g\left(\frac{u}{v}\right) - \kappa \ln v. \tag{3.2}$$

In this case, $\mathbf{v}_0$ becomes to be a conformal Killing vector $\mathbf{v}_0 = u\partial_u + v\partial_v$. This vector $\mathbf{v}_0$ is a generator of a transformation of $u + v$. So, in the nonvanishing λ case, the condition (2.3) means that the metric of spacetime is invariant under the scale transformation of $u+v$, therefore, the spacetime which is obtained by using ansatz (3.1) is a scale invariant solution of Einstein equations. This can be easily seen by considering vacuum solution.

The vacuum solution can be obtained by imposing $g = 0$ and $\kappa = 0$. Then the possible vacuum solution is only flat Minkowski spacetime. The spherically symmetric vacuum solution is only Schwarzschild solution. Imposing the scale invariance (2.3), Schwarzschild mass parameter must vanish, *i.e.*, the scale invariance leads to vanishing mass scale.

The Einstein equations whose solution is Roberts solution can be obtained by $\kappa = 0$. So, if λ does not vanish and $\kappa = 0$, the solution which becomes Minkowski spacetime in the vacuum limit is only Roberts solution. On the other hand, when $\kappa \neq 0$, Einstein equations can be written,

$$2\xi(f^2 g')' + \kappa(f^2)' = 0, \qquad h = -(f^2)' + \xi(f^2)'' \tag{3.3}$$

$$\left(\frac{f'}{h}\right)' = -\frac{fg'^2}{h}, \qquad \left(\frac{f - \xi f'}{h}\right)' = \frac{f}{\xi h}(\xi g' + \kappa)^2 \tag{3.4}$$

where $\xi = u/v$ and $' = d/d\xi$. From two equations (3.4), one can easily obtain, $h = \xi^{-\kappa^2} e^{-2\kappa g}$. The factor $\xi^{-\kappa^2}$ of this h can be eliminated using coordinate transformation,

$$u = ((1-\kappa^2)U)^{1/(1-\kappa^2)}, \qquad v = ((1+\kappa^2)V)^{1/(1+\kappa^2)}, \qquad (\kappa^2 \neq 1) \tag{3.5}$$

$$u = e^U, \qquad v = \sqrt{2|V|}, \qquad (\kappa^2 = 1) \tag{3.6}$$

Furthermore, first equation of (3.3) can be formally integrate, then the Einstein equations (3.3) and (3.4) can be written as follows,

$$f'' + 2\kappa g' f' = -fg'^2, \qquad 2\xi g' f' + \xi f g'' + \kappa f' = 0 \tag{3.7}$$

$$h = e^{-2\kappa g}, \qquad f^2 = \int_{\xi_i}^{\xi} dx x \int_{\xi_i}^{x} dy y^{-2} e^{-2\kappa g(y)} \tag{3.8}$$

These equations cannot be solved by hand. So, we only show the local structure of the phase space of these equations. We transforming the variables as follows,

$$x = g^{\mu\nu}\partial_\mu r \partial_\nu r, \qquad y = \frac{ff'}{h}, \qquad z = \frac{fg'}{f'}, \tag{3.9}$$

where x corresponds to the expansions of radial null ray, *i.e.*, $x > 0$ means untrapped region and $x < 0$ means trapped region and z corresponds to the scalar fields. Einstein equations (3.3) and (3.4) can be written,

$$\dot{x} = 1 - (z^2+1)x, \qquad \dot{y} = \frac{y(2x-1)}{x} \tag{3.10}$$

$$\dot{z} = \frac{2\kappa xy - z(1-2xy)}{y(1+2x)}, \qquad (z+\kappa)^2(1-2y)x = (1+\kappa^2)x - 1$$

where $\cdot = f/f'd/d\xi$. Last equation of (3.10) is a constraint equation. Then, the phase space is essentially two dimensional. In the phase space, there are fixed points $(x, y, z) = (1/2, 1/(1 \pm \kappa), \pm 1)$. These fixed points shows the spacetime whose metric is

$$ds^2 = -(1 - \kappa^2)dudv + uvd\Omega_2^2. \tag{3.11}$$

By the linear analysis near the fixed points, these fixed points are both local attractors when $\kappa > 1$ and both saddle points when $\kappa < 1$. Hence, one can expect that the behavior of solutions when $\kappa > 1$ are quite different with it when $\kappa < 1$[3].

IV. DISCUSSIONS

In summary, we consider the self-similarity of Einstein equation of spherically symmetric spacetime with massless scalar filed which is different with self-similarity of Roberts solution. These self-similarity solutions have a parameter which vanishes in the Roberts solution. So, the solutions which have this self-similarity is a one-parameter extension. So, this model is useful to consider the universality γ of critical behavior.

The problems are as follows. I. The global structure of these solutions and whether black hole solutions exist or not. II. If exist, the initial condition dependence of the black hole mass and its critical exponent. If $\gamma = 1/2$, there may be a universal class of $\gamma = 1/2$ around Roberts solution. Unless, the problem of the κ-dependence of critical exponent arises, in this case, Roberts solution may be an isolated family of solution in the sense that there are may solutions which have a critical exponent $\gamma = 1/2$. So, this model is useful to investigate the universality of γ.

---

[3]Unfortunately, these results were already known by Brady [8]. He investigated the structure of this phase space by numerical calculation.

REFERENCES

[1] M. Choptuik, Phys. Rev. Lett. **70**, 9, (1993).

[2] A.M. Abrahams and C.R. Evans, Phys. Rev. Lett. **70**, 2, (1993). Evans and J.S. Coleman, Phys. Rev. Lett. **72**, 1782, (1994).

[3] Y. Oshiro, K. Nakamura and A. Tomimatsu, Prog. Theor. Phys. Lett. **91**, 6, 1265 (1994). P.R. Brady, Class. Quantum Grav. **11**, 1255, (1994).

[4] A. Strominger and L. Thorlacius, Phys. Rev. Lett. **72**, 1584, (1994).

[5] T. Koike and T. Mishima, *"An analytic model with critical behavior in black hole formation"*, preprint TIT-HEP-266 and gr-qc/9409045.

[6] P.J. Olver, *"Applications of Lie Groups to Differential Equations.* GTM, No,107, Springer-Verlang, New York.

[7] M.E. Cahill and A.H. Taub, Commun. Math. Phys. **21**, 1, (1971).

[8] P.R. Brady, "Self-similar scalar field collapse: naked singularities and critical behavior" preprint NCL94-TP12 and gr-qc/9409035.

Cosmic Colored Black Holes

TAKASHI TORII [a], KEI-ICHI MAEDA[b] and TAKASHI TACHIZAWA[c],

Department of Physics, Waseda University, Shinjuku-ku, Tokyo 169, Japan

Abstract

We present spherically symmetric static solutions (a particle-like solution and a black hole solutions) in the Einstein-Yang-Mills system with a cosmological constant. Although their gravitational structures are locally similar to the Bartnik-McKinnon particles or the colored black holes, the asymptotic behavior becomes quite different because of the existence of a cosmological horizon. We also discuss their stability by means of a catastrophe theory as well as a linear perturbation analysis and find the number of unstable modes.

(a) electronic mail: 64L514@cfi.waseda.ac.jp, (b) electronic mail: maeda@cfi.waseda.ac.jp
(c) electronic mail: 63L507@cfi.waseda.ac.jp

The self-gravitating structures with non-Abelian fields have been intensively studied from various points of view since Bartnik and McKinnon (BM) particle[1] and colored black hole solutions[2] were found by numerical method. Since such new type of solution with non-Abelian hair show a variety of features and have many interesting properties, those may reveal a new important aspect in general relativity through the study of them such as the no hair conjecture or a stability analysis via a catastrophe theory[3, 4]. Those objects may be very small even if they exist and they would be important only in the early history of the universe[5, 6]. In the early universe, however, we usually expect a vacuum energy, which is equivalent to a cosmological constant. From observational cosmological point of view, some astrophysicists have pointed out that a small cosmological constant may explain the observation of number count of galaxies[7]. We then wonder why a self-gravitating non-Abelian structure with the cosmological constant has not been studied yet. Such non-Aberian structures might be formed in the early universe and play an important role in cosmology. Hence, it may be worth studying such objects.

In this short note we present both a particle-like and a black-hole non-Abelian solutions with a cosmological constant, and discuss those structures and thermodynamical properties.

We also study their stability by means of a catastrophe theoretical method as well as a linear perturbation analysis.

We start with the following Lagrangian,

$$S = \int d^4x\sqrt{-g}\left[\frac{1}{16\pi G}(R-\Lambda) - \frac{1}{16\pi g^2}\mathrm{Tr}F^2\right], \tag{1}$$

where SU(2) Yang-Mills(YM) field strength F is expressed by its potential A as $F = dA + A\wedge A$. g is a coupling constant of the YM field.

Since we are interested in the case that a YM field is localized and a spacetime approaches asymptotically de Sitter solution because of a cosmological constant Λ, the metric in the spherically symmetric static spacetime is written as

$$ds^2 = -\left(1 - \frac{2Gm(r)}{r} - \frac{\Lambda}{3}r^2\right)e^{-2\delta(r)}dt^2 + \left(1 - \frac{2Gm(r)}{r} - \frac{\Lambda}{3}r^2\right)^{-1}dr^2 + r^2(d\theta^2 + \sin^2\theta d\phi^2). \tag{2}$$

As for a SU(2) YM potential, we adopt the following form,

$$A = w(r)\tau_1 d\theta + \{w(r)\tau_2 + \cot\theta\tau_3\}\sin\theta d\phi. \tag{3}$$

which is the same as that of the colored black hole and is obtained from the most generic spherically symmetric one with the ansatz of being static and no "electric" charge.

The field equations derived from(1) are

$$\tilde{m}' = \left(1 - \frac{2\tilde{m}}{\tilde{r}} - \frac{1}{3}\tilde{r}^2\right)\frac{w'^2}{\alpha^2} + \frac{(1-w^2)^2}{2\alpha^2\tilde{r}^2}, \tag{4}$$

$$\delta' = -\frac{2w'^2}{\alpha^2\tilde{r}}, \tag{5}$$

$$\left[\left(1 - \frac{2\tilde{m}}{\tilde{r}} - \frac{1}{3}\tilde{r}^2\right)e^{-\delta}w'\right]' - \frac{w(1-w^2)}{\tilde{r}^2} = 0, \tag{6}$$

where we have used normalized variables as $\tilde{r} \equiv \sqrt{\Lambda}r$, $\tilde{m} \equiv \sqrt{\Lambda}Gm$, and a prime denotes a derivative with respect to $\tilde{r}$. $\alpha \equiv g/\sqrt{G\Lambda}$ is a normalized coupling constant, which is only one parameter appeared in those basic equations.

We consider two class of solutions: One is a particle-like solution (first class) such as the BM solution and the other is black hole solutions (second class) such as the colored black hole. Before showing our results, we have to discuss boundary conditions of the field functions. Because of the asymptotic structure of our spacetime, we expect a cosmological horizon. Hence we need two boundary conditions both at the origin ($r = 0$) or at the black hole horizon (r_h) and at the cosmological horizon (r_c). As for the metric functions, $m(r)$ and $\delta(r)$, those must be

finite in whole region. We set $\delta = 0$ at the cosmological horizon. For the YM field, a regularity at the origin requires $w = \pm 1$ and $w' = 0$. We can choose $w = 1$ without loss of generality. At the black hole horizon, we use the same boundary condition as that of the colored black hole, i.e., $w'(r_h)$ is described by $w(r_h)$ from the condition for a regular horizon and $w(r_h)$ becomes a shooting parameter. At the cosmological horizon, although a value of w seems to be free in the present coordinate system, it must be analyzed more carefully. Since the de Sitter spacetime is closed in spatial section, the present coordinate system does not cover whole 3-space but its half bounded by the cosmological horizon. Hence we transform the radial coordinate as $r = R \sin\chi$ ($\chi \in [0, \pi]$), where R is a radius of the cosmological horizon located at $\chi = \pi/2$. This new coordinates cover the whole 3-space beyond the cosmological horizon. It is natural to assume that energy density of the YM field ρ_{YM} varies smoothly throughout whole spacetime. Further we demand $d\rho_{YM}/d\chi = 0$ at the cosmological horizon, which means that the spacetime has a reflection symmetry at the cosmological horizon, and it guarantees a regular particle-like and black hole solutions. We shall discuss a particle-like solution and a black hole separately.

1. Particle-like solution

Under the above boundary conditions, we have two types of trivial analytic solutions as a particle-like solution. One is $w \equiv 1$, $m \equiv 0$, $\delta \equiv 0$, which is the de Sitter solution. The other solution, which is found by Ding and Hosoya(DH)[8], is $w = \cos\chi = \sqrt{1 - r^2/R^2}$. It seems to be a non-trivial solution if we see only a distribution of the YM potential. However, the energy density of YM field ρ_{YM} keeps constant throughout the spacetime; i.e., $\rho_{YM} = \Lambda/8\pi G$, and it gives a trivial homogeneous spacetime (a static 3-sphere with a constant radius). Note that the DH solution requires a certain relation for parameters, i.e., $\Lambda = 3g^2/4G$, then a fine-tuning is needed.

Non-trivial particle-like solutions we have found are some kind of extension of the BM solution. In the region where the YM field is located, new solution is very similar to the BM solution. We find a family of discrete solutions each of which is characterized by the node number i of the YM potential. The asymptotic behaviors, however, become quite different from the BM solution because of the existence of Λ. The YM field of the BM solution damps faster than $\sim r^{-2}$ and it has no global charge relating to the gauge field. This is the reason why we classified the BM solution into a globally neutral type in the previous paper[3]. In case of the new solutions, however, the YM field does not vanish and continues to exist over the cosmological horizon. This produces an effective charge at $r = r_c$ defined by $Q_{eff} = \int_{r_c} \sqrt{\mathrm{tr}F^2} r^2 \sin\theta d\theta d\phi$.

Hence we expected that the spacetime approaches to the Reissner-Nordström-de Sitter (RNdS) spacetime asymptotically. We have confirmed it numerically. We also find that the effective charge gets large when the normalized coupling constant α becomes small, i.e., when g decreases or Λ increases.

A new family of solutions has a critical coupling constant $\alpha_{cr} \sim 1.75$, below which no solution exists except for trivial ones. That is to say a non-trivial solution disappears when Λ gets large and/or g gets small. We can easily understood this as follows. For a general relativistic fluid with nonzero vacuum energy density ρ_{vac} (or a cosmological constant Λ), if $\rho_f/\rho_{vac} \leq 2$, the perfect fluid cannot be localized as an isolated star-like object, where ρ_f is a fluid density[9]. For our new solution, we shall introduce the mean energy density of the YM field, $\bar{\rho}_{YM} \equiv M/(\frac{4}{3}\pi r_0^3)$. r_0 is the effective radius at which ρ_{YM} of the YM field drops by half. Comparing $\bar{\rho}_{YM}$ with $\rho_{vac} = \Lambda/8\pi G$, we find that a new solution does not exist for the case of $\bar{\rho}_{YM}/\rho_{vac} \lesssim 5$. This result is consistent with the perfect fluid case and we expect that this property may be universal for any matter with a cosmological constant. The physical reason why there is the critical value α_{cr} may be explained as follows. The size of the self-gravitating non-trivial structure is $r_0 \sim \sqrt{G}/g$. while the radius of cosmological horizon is $r_c \sim (3\Lambda)^{1/2}$. Then, if $r_0 > r_c$, i.e., $\alpha \lesssim O(1)$, no particle-like solution cannot exist in the de Sitter background spacetime.

2. Black hole solution

Now we turn to the black hole solutions. It is easy to check that the Schwarzschild-de Sitter solution ($w \equiv \pm 1$) and the RNdS solution ($w \equiv 0$) are trivial solutions.

As for a non-trivial black hole solution, (we call it the cosmic colored black hole), we plot the mass-horizon radius relation in Fig. 1. Note that the mass of a black hole M is defined by

$$M = m(r_c) + \frac{Q_{eff}^2}{2r_c}. \tag{7}$$

The reason is as follows. A new solution has an effective charge at the cosmological r_c horizon and it approaches the RNdS spacetime asymptotically. Then the mass function m includes a contribution of a gauge field. It is plausible to subtract it in the definition of the mass of a black hole just as in the RNdS solution. Furthermore, this definition of M provides the conserved AD mass for the RNdS black hole, although it is not sure whether it is true for the present cosmic colored black holes.

For the RNdS solution, there are in general three horizons, an inner horizon, a black hole

horizon and a cosmological horizon (the dotted lines in Fig. 1). In Fig. 1, the solid lines denote the black hole and the cosmological horizons ($r_h < r_c$) of the cosmic colored black holes. In the limit of $r_h \to 0$, these branches end up with particle-like solutions. The behaviors of solutions depend on the coupling constant α. For a large coupling constant $\alpha > 2.3$, the black-hole branch reaches that of RNdS solutions, and makes a bifurcation point. This behavior is similar to a family of monopole black holes in the Einstein-Yang-Mills-Higgs system [4], where a family of monopole black holes merges to the Reissner-Nordström black hole branch. The monopole black hole has interesting properties depending on their self-coupling constant λ such that there are two types of non-trivial solutions for small λ, one of which is more stable than the other. One may expect that the cosmic colored black hole has the similar properties, but it turns to be forbidden from the catastrophe theory. Because a family of monopole black holes constructs a swallow tail catastrophe, which needs at least three independent parameters, but the present system has only two parameters, i.e., α and a radius of the black hole horizon.

For a small coupling constant $\alpha < 2.3$, the cosmic colored black hole solution is not bound up with the RNdS branch but disappears on the way. We can understood the reason by looking at the branch of the cosmological horizon. The end point of the branches merges to the extreme line of the RNdS black holes, where the black hole horizon and cosmological horizon coincide each other. When the mass of a cosmic colored black hole gets large, the radius of its cosmological horizon would become smaller than that of extreme RNdS black holes. However, although a cosmic colored black hole is different from the RNdS black hole, the asymptotic behavior should be same. Hence it is likely for cosmic colored black holes to disappear at the extreme point of the RNdS black hole. When the coupling constant gets further smaller ($\alpha < \alpha_{cr} \sim 1.75$), the cosmic colored black hole dose not exist as the particle-like solution.

To discuss the thermodynamical properties of the cosmic colored black hole, we plot temperatures at both black hole and cosmological horizons of the cosmic colored black holes in Fig. 2. The temperature at the cosmological horizon has the similar mass-dependence to that of RNdS black hole qualitatively, while there is a big difference for that at the black hole horizon. In the RNdS black hole case, when the mass of a black hole gets small, a sign of the heat capacity at the black hole horizon changes from negative to positive, and the temperatures at both horizons coincide at a point E in Fig. 2. In the limit of the extreme black hole, the temperature vanishes. On the other hand, for the cosmic colored black hole when the mass of the black hole gets small, its temperature diverges though there is some range where the sign of its heat capacity becomes positive. This behavior is similar to the colored black hole. This

may be understood by the same mechanism explained in Ref. [10].

Those thermodynamical properties may allow us to discuss the evolution of the cosmic colored black holes. If there is initially a RNdS black hole which mass is large enough, its mass gradually decreases via the Hawking radiation because the temperature at its black hole horizon is higher than that at the cosmological horizon. At the point E in Fig. 2 where two temperatures eventually becomes equal, however, the energy fluxes from both horizons balance and the black hole does not evaporate further. On the other hand, this scenario cannot be applied to the SU(2) YM system, because of the existence of the cosmic colored black holes. The cosmic colored black hole has larger entropy than the RNdS black hole with the same mass. Hence, the RNdS black hole shifts to the cosmic colored black hole at the bifurcation point. After this, since there is no intersection of two temperature curves unlike the RNdS case, the evaporation does not stop, but rather it will be accelerated, and finally a particle-like solution will remain.

Are the cosmic colored black holes stable or not? Here we use two methods in order to answer this question. One is the catastrophe theoretical method[11], which is useful to discuss a relative stability among several families of solutions and widely applied in various research fields including astrophysics. The other is the usual linear perturbation method, with which we can find unstable modes explicitly and show the number of such modes.

First we show the former method. We choose the mass M and the entropy S of the black hole as a control parameter and a potential function in the catastrophe theory, respectively. The entropy S is related to a radius of the black hole horizon as $S = \pi r_h^2$, hence r_h is qualitatively equivalent to the entropy S. We show the $M - r_h$ relation for $\alpha = 0.1$ in Fig. 3. B_i $(i = 1,2)$ describe the bifurcation points consist of branches of cosmic colored black holes with i modes and of the RNdS black hole, and M_i $(i = 1,2)$ are masses of black holes at these bifurcation points B_i. The structure at each bifurcation point in a plane spanned by the control parameter and the potential function is classified into a cusp catastrophe. Since the cosmic colored black hole has larger entropy than that of the RNdS black hole, the cosmic colored black hole is more stable than RNdS black hole with the same mass by means of catastrophe theory. Provided that RNdS black hole with $M > M_1$ has n unstable modes, it will find another unstable mode at the bifurcation point B_1 and then has $(n+1)$ unstable modes in the range of $M_2 < M < M_1$. On the other hand the cosmic colored black hole with one node has n unstable modes. Similarly at the point B_2 the RNdS black hole will get another unstable mode while the cosmic colored black hole with two nodes has $(n+1)$ unstable modes, and so forth. The particle-like solution

has the same number of unstable modes of their branch. Note that if $n = 0$, i.e., the RNdS black hole with $M > M_1$ is stable, then the cosmic colored black hole with one node is also stable. Hence we only have to investigate the stability of RNdS black hole. However it is impossible to study it by the catastrophe theory, and then we apply the linear perturbation method. Before showing our results it should be stressed that the RNdS black hole with a U(1) gauge field is stable!

Here we consider only radial perturbations. Writing down the perturbation equations and drawing its potential form, we can see that a cosmological constant has a tendency to stabilize the umperturbed solution. Analyzing the stability in detail numerically, however we find that, the RNdS solution with $M > M_1$ has one unstable mode. We have also confirmed that the number of unstable modes of the RNdS black holes increases one by one at the bifurcation points (B_i). Hence we conclude that the cosmic colored black hole with i nodes has i unstable modes. This result does not depend on the coupling constant α.

In this paper we have investigated a particle-like solution with a cosmological constant and the cosmic colored black hole, which are the first self-gravitating non-Abelian structures with a cosmological constant. The gravitational structure is definitely changed by the cosmological constant, in particular an effective charge appears at the cosmological horizon. Although new solution is not stable, we may expect some important effects in the astrophysical process caused by the BM solutions and/or the colored black holes[6].

This work was supported partially by the Grant-in-Aid for Scientific Research Fund of the Ministry of Education, Science and Culture (No. 06302021 and No. 06640412), by the Grant-in-Aid for JSPS Fellow (No. 053769), and by the Waseda University Grant for Special Research Projects.

References

[1] R. Bartnik and J. McKinnon, Phys. Rev. Lett. **61**, 141

[2] M.S. Volkov and D.V. Galt'sov, Pis'ma Zh. Eksp. Teor. Fiz. **50** 312 (1989); Sov. J. Nucl. Phys. **51**, 747 (1990);
P. Bizon, Phys. Rev. Lett. **64** 2844, (1990) ;
H.P. Künzle and A.K. Masoud-ul-Alam, J. Math. Phys. **31**, 928 (1990).

[3] K. Maeda, T. Tachizawa, T. Torii and T. Maki, Phys. Rev. Lett. **72** 450, (1994). See also T. Torii, K. Maeda and T. Tachizawa, preprint WU-AP/39/94 (gr-qc9406013) (1994, to be published in Phys. Rev. **D**), and references therein.

[4] T. Tachizawa, K. Maeda, and T. Torii, WU-AP/40/94 (gr-qc9410016) (1994, to be published in Phys. Rev. **D**).

[5] I. G. Moss and A. Wray, Phys. Rev. **D46** R1215, (1992)

[6] W. G. Gibbons and A. R. Steif, Phys. Lett. B **314** 13 (1993); Phys. Lett. B **320** 245 (1993)

[7] M. Fukugita, F. Takahara, K. Yamashita and Y. Yoshii, Astrophys. J. **361** (1990) Part2 L1.

[8] S Ding and A Hosoya, TIT/HEP-242/COSMO-39 (1993).

[9] W. A. Hiscock, J. Math. Phys. **29**, 443 (1988)

[10] T. Torii and K. Maeda, Phys. Rev. **D48**, 1643 (1993).

[11] R. Thom, *Structural Stability and Morphogenesis*, Benjamin (1975).

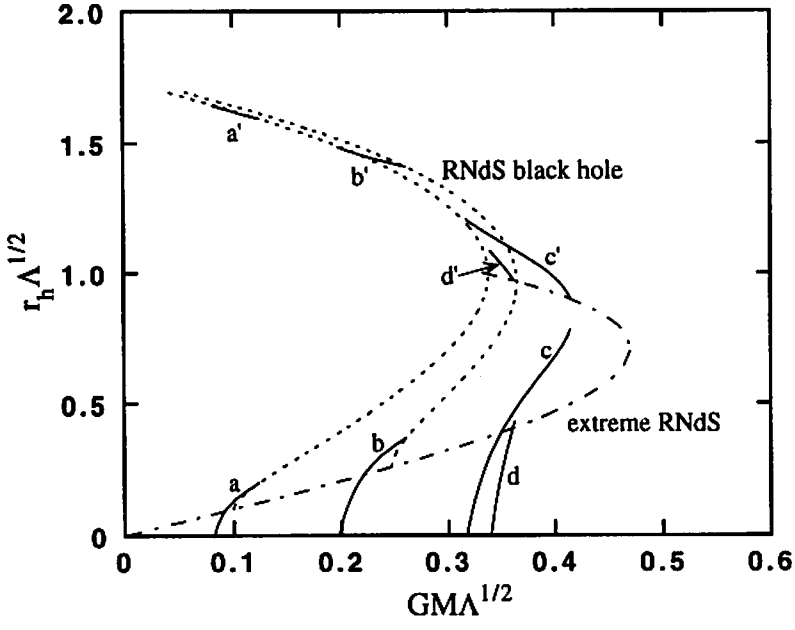

FIG 1: The mass-horizon radius diagrams of the cosmic colored black holes for $\alpha \equiv g/\sqrt{G\Lambda} = 10.0$($a$(the black hole horizon(BH)), a'(the cosmological horizon(CH))), =4.0(b(BH), b'(CH)), =2.2(c(BH), c'(CH)),and =1.9(d(BH), d'(CH)). We also plot those of the RNdS black holes for their charges $\sqrt{G\Lambda}Q = 0.1$ and 0.25 (the dotted lines) and the extreme points of all RNdS black holes (the dot-dashed line). We find that the cosmic colored black holes for a, a' and b, b' coincide with the RNdS black holes with the same charge at the cosmological horizons, while the cosmological horizons for c' and d' finish on the extreme line.

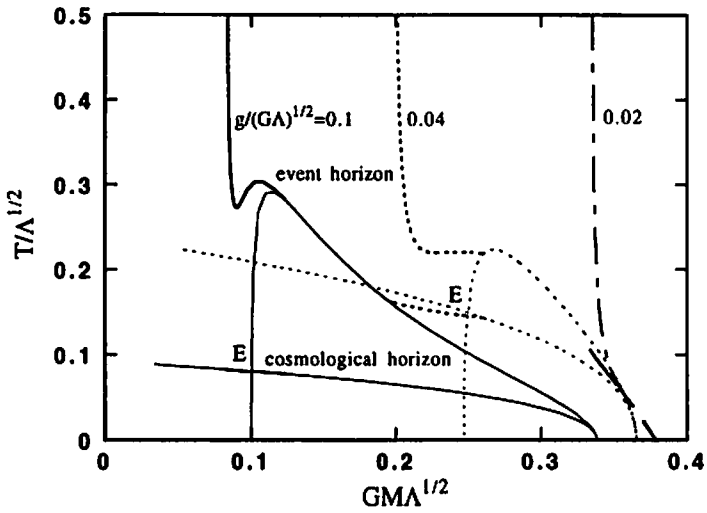

FIG 2: The mass-temperature diagram of the cosmic colored black holes for $\alpha = 10.0$ (solid lines), =4.0 (dotted lines), and =2.0 (dot-dashed lines). We also plot those for the RNdS black holes with the same charges. For the large coupling constant α (e.g. 10.0), the specific heat will changes its sign two times, but no changes for small α (e.g. 2.0). The temperatures of both black hole and cosmological horizons of RNdS black holes intersect at the point E, but the cosmic colored black holes do not have such a point. This will changes the fates of two types of black holes.

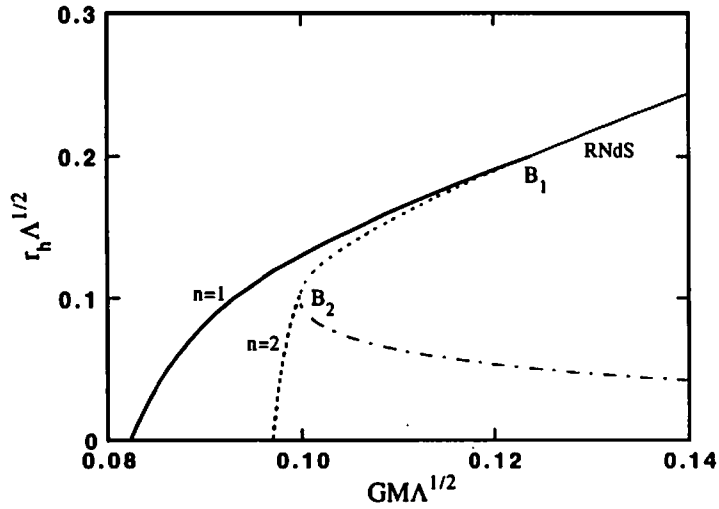

FIG 3: The mass-horizon radius diagram of the cosmic colored black holes with node number $i = 1, 2$ and the RNdS black holes for $\alpha = 10.0$. There are two bifurcation points B_i ($i = 1, 2$), which correspond to the cusp catastrophes. The solid, the dotted and the dot-dashed lines have one, two and three unstable modes, respectively.

Evolution of Dilatonic Black Holes by Hawking Radiation

JUN-ICHIROU KOGA and KEI-ICHI MAEDA[(a)]

Department of Physics, Waseda University, Shinjuku-ku, Tokyo 169, Japan

(a) electronic mail : maeda@cfi.waseda.ac.jp

Abstract

We calculate Hawking radiation from the electrically charged dilatonic black holes, and study its dependence of the dilaton coupling constant α. As for non-rotating holes, our calculation shows the emission rate of Hawking radiation increases in the extreme limit for $\alpha > 1$, while it decreases in the $\alpha < 1$ case. So we find the critical value of $\alpha = 1$ which is predicted from superstring theory. We also consider rotating holes. By analyzing Kerr-Newman ($\alpha = 0$), Kaluza-Klein ($\alpha = \sqrt{3}$) and Sen ($\alpha = 1$ with axion) solutions, with our previous calculation on superradiance, we find the value $\alpha \sim 1$ is again critical in this case. The evolutions of these three types of holes show that Kaluza-Klein hole inevitably goes to the naked singularity in the semiclassical approximation.

1 Introduction

In the effective theories of the higher-dimensional unified theories of fundamental interactions, the dilaton field appears and couples to other known matter fields. It may play some important role in the history of the early universe or in astrophysics. We may get some implications of higher-dimensional unification by investigating the physics in these theories. The coupling constant of dilaton field depends on the dimension of an internal space and a unification theory, so it is important to see a dependence of the coupling constant.

In this paper, we consider the black hole solutions mainly in Einstein-Maxwell-dilaton theory in which the action is written as

$$S = \frac{1}{16\pi} \int d^4x \sqrt{-g} \left[R - 2(\nabla\phi)^2 - e^{-2\alpha\phi} F^2 \right], \tag{1}$$

where dilaton field ϕ couples to Maxwell field F through the coupling constant α. (We adopt the units of $c = \hbar = G = k_B = 1$). If we set $\alpha = 0$, it is just usual Einstein-Maxwell theory, and the axisymmetric stationary black hole is Kerr-Newman solution. In the $\alpha = 1$ case, it is a low energy effective action of a superstring theory, and $\alpha = \sqrt{3}$ corresponds to 5-dimensional Kaluza-Klein theory with the dimension reduced to four.

Although the spherically symmetric black hole solution for the action (1) is known for the arbitrary coupling constant[1], the exact rotating black hole solutions we know are only two: Kerr-Newman ($\alpha = 0$) and "Kaluza-Klein" [2] ($\alpha = \sqrt{3}$). In addition to these, there is another exact solution derived by Sen[3] for $\alpha = 1$ with an additional axion field (three-rank tensor $H_{\mu\nu\rho}$), which we call "Sen" solution. We analyze Hawking radiation from these black holes and study the coupling constant dependence.

All these solutions approach to Kerr when the charge of the hole becomes zero, so the differences by the coupling constant is small when the charge is small. Hence, if we consider the discharge process in Hawking radiation, the coupling constant dependence will be quickly lost, since the time scale of discharge is much smaller than that of the loss of the mass or the angular momentum for sufficiently massive black holes.

Because of this, we pay our attentions to the cases where the charge of the black hole is conserved (it is true for a central charge), and consider a massless neutral scalar particle which does not couple to dilaton.

2 Hawking Radiation from Non-Rotating Black Holes

First, we consider the non-rotating dilatonic black hole, since we know the exact solution for any α in this case. This solution[1] is expressed as

$$\begin{aligned} ds^2 &= -\frac{\Delta(\rho)}{R^2(\rho)}dt^2 + \frac{R^2(\rho)}{\Delta(\rho)}d\rho^2 + R^2(\rho)(d\theta^2 + \sin^2\theta d\varphi^2)\,, \\ A_t &= \frac{Q}{\rho}, \quad \phi = \frac{\alpha}{1+\alpha^2}\ln\left(1 - \frac{\rho_-}{\rho}\right). \end{aligned} \tag{2}$$

where

$$\Delta(\rho) = (\rho - \rho_+)(\rho - \rho_-)\,, \quad R(\rho) = \rho\left(1 - \frac{\rho_-}{\rho}\right)^{\alpha^2/(1+\alpha^2)}. \tag{3}$$

The outer and 'inner' horizon ρ_+, ρ_- are given by the mass M, the electric charge Q of the black hole and α as follows

$$\rho_\pm = \frac{(1+\alpha^2)(M \pm \sqrt{M^2 - (1-\alpha^2)Q^2})}{(1 \pm \alpha^2)}. \tag{4}$$

When ρ_+ and ρ_- coincide ($Q = Q_{\max} \equiv \sqrt{1+\alpha^2}M$ then), we call it the extreme state, beyond which no black hole exists. It has to be emphasized that, in this case, the naked singularity appears at $\rho = \rho_+$ and the area of the hole is zero for $\alpha > 0$, so it is not a black hole solution. ($\rho = \rho_-$ is the curvature singularity for $\alpha > 0$).

The temperature is expressed as

$$T = \frac{1}{4\pi\rho_+}\left(1 - \frac{\rho_-}{\rho_+}\right)^{(1-\alpha^2)/(1+\alpha^2)}, \tag{5}$$

and this quantity shows an interesting property[1]. When we consider $\alpha < 1$, T goes to zero in the extreme limit, whereas it diverges in the $\alpha > 1$ case, and it becomes non-zero finite value for $\alpha = 1$ in that limit. This property indicates that the Hawking radiation may be drastically affected by the coupling constant, and especially, the emission rate diverges in the extreme limit for $\alpha > 1$, because the spectrum of Hawking radiation is thermal. However Holzhey and Wilczek[4] pointed out that the effective potentials (through which barrier particles tunnel to be created) around these holes with $\alpha > 1$ grow infinitely high in the extreme limit and the transmission probability for particles to escape into infinity may become very small. These two properties have the opposite effects on

Hawking radiation. Here we clarify which effect overcomes the other.

The energy emission rate of Hawking radiation[5] is given by

$$\frac{dM}{dt} = \frac{-1}{2\pi}\sum_{l,m}\int_0^\infty \frac{\omega\left(1-|A|^2\right)}{\exp\left[\omega/T\right]-1}\,d\omega, \tag{6}$$

where l, m are the angular momentum and ω is the energy of the particle. The quantity $|A|^2$ is the reflection coefficient of the scalar wave, which is calculated by solving Klein-Gordon equation

$$\Phi_{,\mu}^{\ ;\mu} = 0\,. \tag{7}$$

This becomes separable, by setting

$$\Phi = \frac{\chi(\rho)}{R(\rho)}S(\theta)e^{im\varphi}e^{-i\omega t}. \tag{8}$$

Eq.(7) is reduced to the Legendre equation and the radial equation,

$$\left[\frac{d^2}{d\rho^{*2}} + \omega^2 - V^2(\rho)\right]\chi(\rho^*) = 0, \tag{9}$$

where

$$\begin{aligned} V^2(\rho) &\equiv \frac{\Delta(\rho)}{R^2(\rho)}\left[\frac{l(l+1)}{R^2(\rho)} + \frac{1}{R(\rho)}\frac{d}{d\rho}\left(\frac{\Delta(\rho)}{R^2(\rho)}\frac{dR(\rho)}{d\rho}\right)\right], \\ d\rho^* &= \frac{R^2(\rho)}{\Delta(\rho)}\,d\rho. \end{aligned} \tag{10}$$

We calculate the emission rate Eq.(6) by solving Eq.(9) numerically, integrating by ω, and summing on l and m (here and hereafter we neglect $l \geq 2$ modes because $1-|A|^2$ for these modes are sufficiently small for the centrifugal barriers). We plot the results in Fig.1. Here we have assumed the charge is positive without losing generality. In this figure, we see that the emission rate for $\alpha > 1$ increases rapidly as the charge approaches to the extreme value. On the other hand, in the $\alpha < 1$ case, the emission rate goes to zero in the extreme limit (since $T \to 0$), so we find that there exists the critical value at $\alpha = 1$, which is predicted by superstring theory.

3 Hawking Radiation from Rotating Black Holes

Next, we consider rotating black holes. As we pointed out before, we know the black hole solution in a few cases. The most familiar one is Kerr-Newman solution which we do not show explicitly here. Another is Kaluza-Klein black hole which is given by

$$\begin{aligned} ds^2 &= -\frac{\Delta - a^2\sin^2\theta}{B\Sigma}dt^2 - 2a\sin^2\theta\frac{1}{\sqrt{1-v^2}}\frac{Z}{B}dtd\varphi \\ &\quad + \left[B\left(r^2+a^2\right) + a^2\sin^2\theta\,\frac{Z}{B}\right]\sin^2\theta\,d\varphi^2 + \frac{B\Sigma}{\Delta}dr^2 + B\Sigma\,d\theta^2\,, \\ A_t &= \frac{v}{2(1-v^2)}\frac{Z}{B^2},\quad A_\varphi = -a\sin^2\theta\frac{v}{2\sqrt{1-v^2}}\frac{Z}{B^2},\quad \phi = -\frac{\sqrt{3}}{2}\ln B \end{aligned} \tag{11}$$

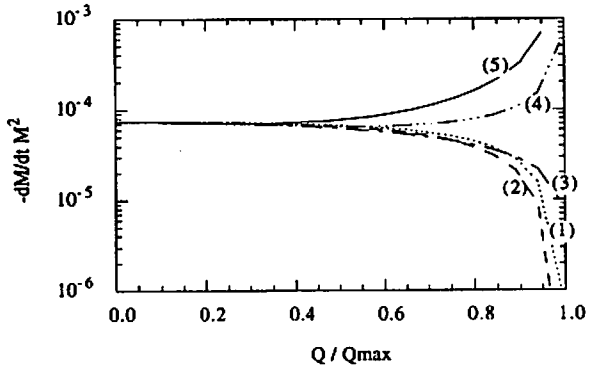

Fig. 1: The emission rate of non-rotating dilatonic black hole by Hawking radiation The charge is normalized by $Q_{\max} = \sqrt{1+\alpha^2}M$ and the vertical axis is logarithm of the emission rate $-dM/dt$ normalized by the mass. Each line denotes (1):$\alpha = 0$, (2):$\alpha = 0.5$, (3):$\alpha = 1$, (4):$\alpha = 1.5$, (5):$\alpha = 2$. The $\alpha = 0.5$ line is below the $\alpha = 0$ line. This is because the effective potential suppresses the emission rate. But, for $\alpha > 1$, the emission rate increases rapidly near the extreme limit.

where, Δ, Σ, Z and B are functions of r and θ, and given by,

$$\Delta = r^2 - 2\mu r + a^2, \quad \Sigma = r^2 + a^2\cos^2\theta, \quad Z = \frac{2\mu r}{\Sigma}, \quad B = \left(1 + \frac{v^2 Z}{1-v^2}\right)^{\frac{1}{2}}. \tag{12}$$

The coordinate r here, and ρ in the previous section are related by $r = \rho - \rho_-$. The mass M, the electric charge Q and the angular momentum J of the black hole are described by the parameters v ($|v| < 1$) , μ and a as,

$$M = \mu\left[1 + \frac{v^2}{2(1-v^2)}\right], \quad Q = \frac{\mu v}{1-v^2}, \quad J = \frac{\mu a}{\sqrt{1-v^2}}. \tag{13}$$

The horizon radius r_H is given by,

$$r_H = \mu + \sqrt{\mu^2 - a^2}, \quad (\mu^2 \geq a^2). \tag{14}$$

The condition of $\mu^2 \geq a^2$ for the horizon to exist is rewritten as

$$\left(\frac{J}{M^2}\right)^2 \leq \frac{1}{4}\left[2 - 10\left(\frac{Q}{M}\right)^2 - \left(\frac{Q}{M}\right)^4 + 2\left(1 + 2\left(\frac{Q}{M}\right)^2\right)^{3/2}\right]. \tag{15}$$

(see Fig.2). The temperature T and the angular velocity Ω_H of this black hole are expressed as

$$T = \frac{\sqrt{1-v^2}}{2\pi}\frac{\sqrt{\mu^2 - a^2}}{r_H^2 + a^2}, \quad \Omega_H = \frac{a\sqrt{1-v^2}}{r_H^2 + a^2}. \tag{16}$$

Here, we can see interesting behaviours of these quantities. When the black hole is non-rotating, T diverges in the extreme limit as we mentioned before (since Kaluza-Klein solution corresponds to

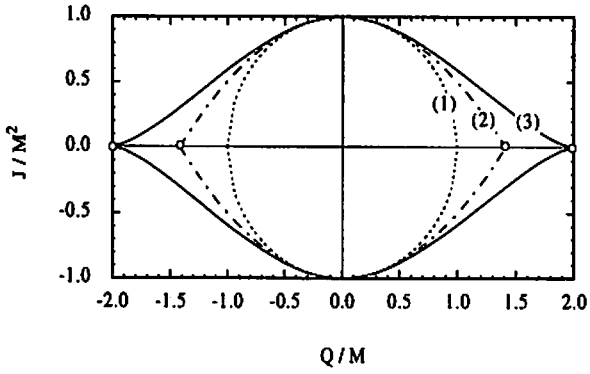

Fig. 2: The parameter space of three types of black hole solutions
The extreme lines are shown in Q/M–J/M^2 plane for (1):Kerr-Newman, (2):Sen, and (3):Kaluza-Klein black hole solutions. The region inside each line gives the black hole solution, except the points denoted by the small circles where the naked singularity appears.

$\alpha = \sqrt{3} > 1$). But if we consider the extreme limit in the rotating solution ($\mu = a$), T goes to zero. Hence, in the limit of $Q \to Q_{\max} = 2M$, we find it is discontinuous at this point. (Remind here that it is not a black hole solution there). The similar thing occurs for Ω_H. The angular velocity of the non-rotating hole is always zero, even in the extreme limit, whereas if we consider the limit, $J \to 0$ of the extremely charged black hole with $J \neq 0$, Ω_H diverges in the limit of $Q \to Q_{\max}$.

Thirdly, we consider Sen black hole solution which is as follows :

$$\begin{aligned} ds^2 &= -\frac{\Delta - a^2\sin^2\theta}{\Sigma}dt^2 + \frac{\Sigma}{\Delta}dr^2 + \Sigma d\theta^2 - \frac{4\mu r a\cosh^2\beta\sin^2\theta}{\Sigma}dtd\theta + \frac{\Lambda}{\Sigma}\sin^2\theta\, d\varphi^2\,, \\ A_t &= \frac{1}{\sqrt{2}}\frac{\mu r\sinh 2\beta}{\Sigma}\,, \quad A_\varphi = -\frac{a}{\sqrt{2}}\sin^2\theta\,\frac{\mu r\sinh 2\beta}{\Sigma}\,, \\ \phi &= -\frac{1}{2}\ln\frac{\Sigma}{r^2 + a^2\cos^2\theta}\,, \quad B_{t\varphi} = 2a\sin^2\theta\,\frac{\mu r\sinh^2\beta}{\Sigma} \end{aligned} \tag{17}$$

where Δ, Σ and Λ are given by

$$\begin{aligned} \Delta &= r^2 - 2\mu r + a^2, \quad \Sigma = r^2 + a^2\cos^2\theta + 2\mu r\sinh^2\beta\,, \\ \Lambda &= \left(r^2 + a^2\right)\left(r^2 + a^2\cos^2\theta\right) + 2\mu r a^2\sin^2\theta + 4\mu r\left(r^2 + a^2\right)\sinh^2\beta + 4\mu^2 r^2\sinh^4\beta. \end{aligned} \tag{18}$$

The physical mass M, the electric charge Q, and the angular momentum J are described by the parameters μ, β and a as

$$M = \frac{\mu}{2}(1 + \cosh 2\beta)\,, \quad Q = \frac{\mu}{\sqrt{2}}\sinh 2\beta, \quad J = \frac{a\mu}{2}(1 + \cosh 2\beta)\,. \tag{19}$$

$B_{\mu\nu}$ generates antisymmetric three-rank tensor $H_{\mu\nu\rho}$ (axion). The present model includes H^2 term interaction which is absent in Kerr-Newman and Kaluza-Klein case. But, if we set $J = 0$, this

is reduced to the non-rotating solution Eq.(2) with $\alpha = 1$, and when $Q = 0$, it is Kerr, as the above two solutions. So we use this solution complementarily.

The horizon radius of this hole is given by the same equation as Eq.(14), and it exists only when

$$|J| \leq M^2 - \frac{Q^2}{2}. \tag{20}$$

(see Fig.2 again). The temperature and the angular velocity of this solution are calculated as

$$T = \frac{\sqrt{(2M^2 - Q^2)^2 - 4J^2}}{4\pi\left[2M^2 - Q^2 + \sqrt{(2M^2 - Q^2)^2 - 4J^2}\right]}, \quad \Omega_H = \frac{J}{M\left[2M^2 - Q^2 + \sqrt{(2M^2 - Q^2)^2 - 4J^2}\right]}. \tag{21}$$

As in Kaluza-Klein solution, T and Ω_H of this black hole are also discontinuous at $Q = Q_{\max} = \sqrt{2}M$, but never diverge and become non-zero finite value instead.

Here we discuss Hawking radiation from these two black holes in addition to Kerr-Newman hole, setting Q and J positive (which does not lose generality). In this case, since the black holes rotate, they emit their angular momentum in addition to the energy. They can be calculated by

$$\frac{dM}{dt} = \frac{-1}{2\pi}\sum_{l,m}\int_0^\infty \frac{\omega\,(1 - |A|^2)}{\exp\left[(\omega - m\Omega_H)/T\right] - 1}\,d\omega\,, \quad \frac{dJ}{dt} = \frac{-1}{2\pi}\sum_{l,m}\int_0^\infty \frac{m\,(1 - |A|^2)}{\exp\left[(\omega - m\Omega_H)/T\right] - 1}\,d\omega\,. \tag{22}$$

Klein-Gordon equation can be separated also in the rotating hole cases, and its radial part, for each case, is written as

$$\left[\frac{d^2}{dr^{*2}} + (\omega - m\Omega(r))^2 - V^2(r)\right]\chi(r^*) = 0. \tag{23}$$

where the tortoise coordinate r^* is defined by

$$dr^* = \frac{R^2(r)}{\Delta(r)}\,dr. \tag{24}$$

The functions in these equations for Kerr-Newman are defined by

$$\begin{aligned} \Omega(r) &\equiv (2Mr - Q^2)\frac{a}{R^4(r)}\,, \quad R^2(r) \equiv r^2 + a^2\,, \\ V^2(r) &\equiv \frac{\Delta(r)}{R^2(r)}\left\{\frac{\lambda}{R^2(r)} + \frac{1}{R(r)}\frac{d}{dr}\left[\frac{\Delta(r)}{R^2(r)}\frac{dR(r)}{dr}\right] - \frac{m^2a^2}{R^6(r)}(r^2 + a^2 - Q^2 + 2Mr)\right\}\,, \end{aligned} \tag{25}$$

where

$$\Delta \equiv r^2 + a^2 + Q^2 - 2Mr\,. \tag{26}$$

For Kaluza-Klein, they are given by

$$\begin{aligned} \Omega(r) &\equiv \frac{2\mu r}{\sqrt{1 - v^2}}\frac{a}{R^4(r)}\,, \quad R^2(r) \equiv B\Sigma|_{\theta=0} = (r^2 + a^2)\left(1 + \frac{v^2}{1 - v^2}\frac{2\mu r}{r^2 + a^2}\right)^{\frac{1}{2}}\,, \\ V^2(r) &\equiv \frac{\Delta(r)}{R^2(r)}\left\{\frac{\lambda}{R^2(r)} + \frac{1}{R(r)}\frac{d}{dr}\left[\frac{\Delta(r)}{R^2(r)}\frac{dR(r)}{dr}\right] - \frac{m^2a^2}{R^6(r)}\left[r^2 + a^2 + \frac{2\mu r}{1 - v^2}\right]\right\}. \end{aligned} \tag{27}$$

and, in Sen case,

$$\Omega(r) \equiv 2\mu r\cosh^2\beta\frac{a}{R^4(r)}, \quad R^2(r) \equiv \Sigma|_{\theta=0} = r^2 + a^2 + 2\mu r\sinh^2\beta\,,$$

$$V^2(r) \equiv \frac{\Delta(r)}{R^2(r)}\left\{\frac{\lambda}{R^2(r)} + \frac{1}{R(r)}\frac{d}{dr}\left[\frac{\Delta(r)}{R^2(r)}\frac{dR(r)}{dr}\right] - \frac{m^2a^2}{R^6(r)}\left(r^2 + a^2 + 2\mu r\cosh 2\beta\right)\right\}. \quad (28)$$

The spheroidal equations are the same with Kerr case for all these three types, and the separation constant λ can be calculated perturbatively[6] as

$$\lambda = l(l+1) + \frac{1}{2}\left[\frac{(2m-1)(2m+1)}{(2l-1)(2l+3)} + 1\right]a^2\omega^2 + \frac{1}{2}\left[\frac{(l-m-1)(l-m)(l+m-1)(l+m)}{(2l-3)(2l-1)^3(2l+1)}\right.$$
$$\left. - \frac{(l-m+1)(l-m+2)(l+m+1)(l+m+2)}{(2l+1)(2l+3)^3(2l+5)}\right]a^4\omega^4 + \mathcal{O}(a^6\omega^6). \quad (29)$$

This approximation is valid since we introduce a high energy cut-off in the integration by ω of Eq.(22), which is justified for the suppression of energy spectrum of Planckian distribution at higher energy, and $a\omega < 1$ for all considered cases with cut-off, although $\omega M > 1$ in some cases.

We focus on the highly charged holes, since the coupling constant dependence of the emission rate becomes small in the opposite limit. We choose $J = 0.01M^2$ and calculate the emission rates. In Fig.3, we plot them against the charge normalized by $Q_{\rm ex}$ which is the maximal value of the charge for $J = 0.01M^2$ and is a little less than $Q_{\rm max}$. (See Fig.2). In Fig.3 (a), it can be seen that the behaviour of the emission rate is very similar to that of the non-rotating case (Fig.1), except the vicinity of the extreme limit. Near the extreme limit, the emission rate of Kaluza-Klein hole drops sharply, because the temperature goes to zero in this case, in contrast to the non-rotating case. Since the temperatures of all these three types with non-zero angular momentum go to zero in the extreme limit, the emission rates becomes superradiant[7] in this limit as is well known (only the $0 \le \omega \le m\Omega_H$ mode survives in the limit of $T \to 0$ in Eq.(22)). In Ref.[8], we calculated the emission rates by superradiance for these holes, and found the emission rates increase very rapidly near the extreme limit for $\alpha > 1$ and the behaviours of them are changed at $\alpha \sim 1$. (We cannot conclude that the critical value is exactly unity, because we analyzed the approximate black hole solution in Ref.[8] which is valid only for the slowly rotating and not so highly charged cases). Remembering there exists the critical value at $\alpha = 1$ in the non-rotating case, all these facts tell us that the coupling constant $\alpha \sim 1$ is critical in the rotating case as well. As for the angular momentum emission in Fig.3 (b), we can see the similar feature. This is due to the behaviour of Ω_H which is zero in the limit $Q \to Q_{\rm max}$ for the small coupling constant (Kerr-newman), but becomes infinity when the coupling constant is large enough (Kaluza-Klein). Ω_H of Sen black hole goes to non-zero finite value in this limit so it seems that $\alpha = 1$ is critical in the behaviour of Ω_H, but this solution has non-zero axion field and is not in the same model (1) as Kerr-Newman and Kaluza-Klein. Despite this fact, our calculation shows that the behaviours of the emission rates are drastically changed at $\alpha \sim 1$.

Next, we consider the evolution of these rotating holes by Hawking radiation. Calculating $d(\frac{Q}{M})/dt$

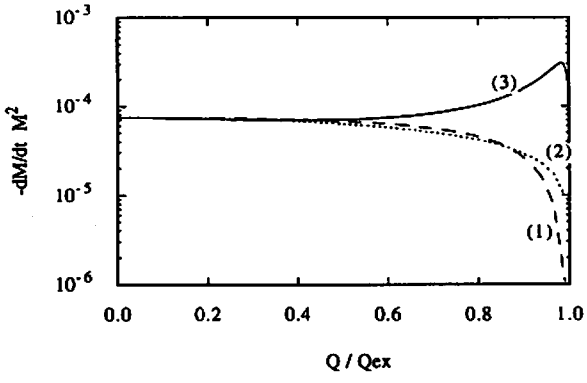

(a)

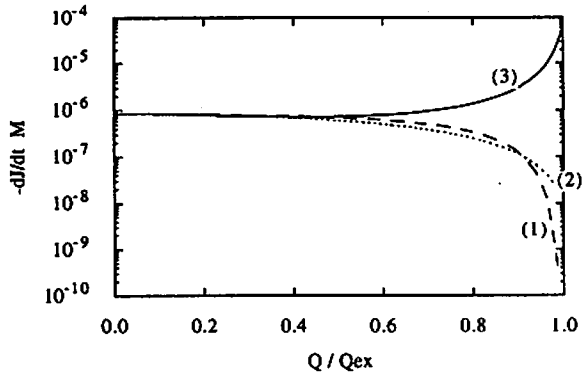

(b)

Fig. 3: The emission rate from three types of rotating black holes
(a): the energy emission rate $-dM/dt$, (b): the angular momentum emission rate $-dJ/dt$ with each quantity normalized by the mass of the black hole. The horizontal axis is normalized by $Q_{\rm ex}$ now. In the figures the lines denote (1):Kerr-Newman, (2):Sen, and (3):Kaluza-Klein. The value of $Q_{\rm ex}$ for each case is, $0.999\,Q_{\rm max}$ for Kerr-Newman, $0.995\,Q_{\rm max}$ for Sen and $0.972\,Q_{\rm max}$ for Kaluza-Klein hole. Since we set $J = 0.01M^2$, the temperature becomes zero and the emission rates are described only by superradiant modes in the extreme limit for each hole.

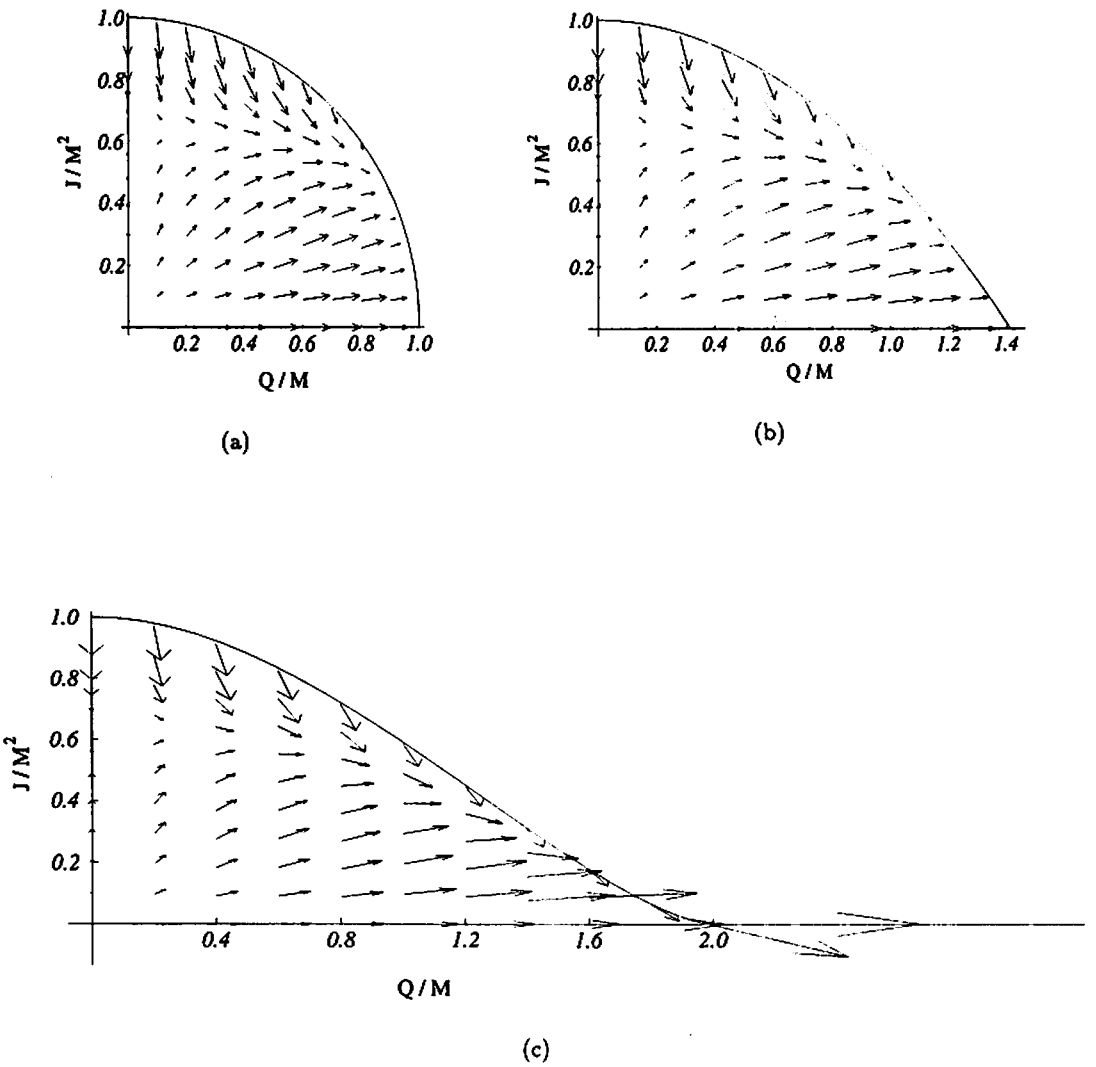

Fig. 4: The vector field representation of the evolution of three types of black holes Each figure represents (a):Kerr-Newman, (b):Sen, and (c):Kaluza-Klein black hole. The vectors near the extreme lines direct inside the lines in all cases. The shown amplitudes of the vectors are enlarged by 2500 times. They are very small for Kerr-Newman and Sen holes near $Q = Q_{\max}$, although in Kaluza-Klein case they are considerably large around the $Q = Q_{\max}$.

and $d(\frac{J}{M^2})/dt$ using Eq.(22), we show this pair as a vector field on the plane of Fig.2, which represents a direction in which the black hole evolves (Fig.4). Because we assume the charge is conserved and the black holes lose their mass, Q/M increases. From Fig.4, we see that although the evolution of Kerr-Newman hole stops as it approach $Q = Q_{\max}$, Kaluza-Klein hole inevitably goes to $Q = Q_{\max}$ where the naked singularity appears. This is because the emission rates of Kaluza-Klein are very large around this point. So we cannot avoid the naked singularity in this case, and this situation is very similar to the evaporation of Schwarzschild black hole where the area of the hole goes to zero and the emission rate increases infinitely large in the last stage.

4 Conclusion

In summary, we considered Hawking radiation by the neutral scalar field from dilatonic black holes with the assumption that the black hole charge is conserved, and calculated the emission rate to see the dependence on the coupling constant of dilaton. In the non-rotating case, our calculation shows the emission rate increases near the extreme limit for the coupling constant greater than unity, whereas they drops down to zero for smaller coupling constant. So we can see the coupling constant $\alpha = 1$ is the critical value in the behaviour of Hawking radiation. Furthermore, also in the rotating case, we found $\alpha \sim 1$ is the critical value, and this value is predicted by superstring theory. As a result, the evolutions of the holes become completely different depending on the coupling constant. In particular, Kaluza-Klein hole inevitably goes to the naked singularity.

The back reaction onto spacetime is not considered here, although the emission rates near $Q = Q_{\max}$ grows very large and the area of the hole approaches Planck scale in the limit of $Q \to Q_{\max}$ for Kaluza-Klein hole. The semiclassical approximation may not be valid any more and we need further study to confirm our results.

References

[1] G. W. Gibbons and K. Maeda, Nucl. Phys. B 298 (1988) 741;
D. Garfinkle, G. T. Horowitz and A. Strominger, Phys. Rev. D 43 (1991) 3140

[2] V. Frolov, A. Zelnikov and U. Bleyer, Ann. Phys. (Leipzig) 44 (1987) 371

[3] A. Sen, Phys. Rev. Lett. 69 (1992) 1006

[4] C. F. E. Holzhey and F. Wilczek, Nucl. Phys. B 380 (1992) 447

[5] S. W. Hawking, Commun. math. Phys. 43 (1975) 199

[6] C. J. Bouwkamp, Phillips. Res. Rep. 5 (1950) 87

[7] W. G. Unruh, Phys. Rev. D 10 (1974) 3194

[8] J. Koga and K. Maeda, Phys. Lett. B 340 (1994) 29

On the Phase Transitions of Kerr-Newman Black Holes

Osamu Kaburaki

Astronomical Institute, Faculty of Science, Tohoku University,

Aoba, Sendai 980-77, Japan

The previously suggested existence of second-order phase transitions in a series of Kerr-Newman states is examined in the framework of equilibrium black-hole thermodynamics. Some unusual physical situations in one of such transitions which is shown very likely to occur at the extremal state are discussed together with a usual critical exponent. The possibility of a first-order transition is also pointed out.

1. Introduction

It has often been claimed that there are second-order phase transitions in black-hole equilibrium states. For example, Davies [1] regards the appearance, under a certain condition, of the infinite discontinuity in the heat capacity at constant angular momentum and electric charge as a sign of its existence. Another kind of second-order transition at the extremal states has been proposed by Pavón and Rubí [2] for Kerr holes and by Pavón [3] for Reissner-Nordström holes, both based on the divergences of some non-equilibrium thermodynamic fluctuations. Generally speaking, however, it is premature to conclude the existence of a second-order phase transition only from the divergence in the fluctuations or susceptibilities such as the heat capacity. Indeed, as shown by the present author [4], such divergences do appear also at a state where the stability changes. Therefore, one must carefully distinguish such phenomena from actual phase transitions.

There is a very powerful and systematic method called the "turning-point method"

[5] to find the points on a equilibrium sequence where the changes of stability occur. According to it, a change of stability occurs only at a point with vertical tangent in a continuous part of a curve which we shall call the conjugacy diagram. The curve plots, against some intrinsic variable, its conjugate variable [4, 5]. It has also been shown that, at such a point of stability change, the Massieu function plotted against the relevant intrinsic variable always has a cusp [4]. In the present paper, the former result is used to exclude irrelevant divergences of thermodynamic fluctuations from those possibly associated with some second-order phase transition.

In considering the thermodynamic fluctuations, one must specify first in which thermodynamic environment he is interested. This is because, although various statistical ensembles are equivalent in the sense that they give the same results for the equilibrium quantities they predict different fluctuations around such equilibrium values. As a thermodynamic environment of a Kerr-Newman black hole, we are now interested in the three cases: the microcanonical, canonical and grand canonical conditions. In the first situation the black hole is placed in a perfectly reflecting wall so that it can exchange nothing with the exterior, in the second it is placed in a heat bath with which it can exchange only heat reversibly, while in the last it keeps contact with three types of reservoirs so that it can exchange not only heat but also angular momentum and electric charge with them.

2. Search for Second-Order Phase Transitions

As shown in ref. [4], one can calculate the second moments of fluctuating quantities from the formula

$$< \delta X_i \, \delta X_j >= \frac{k_B}{\lambda_i} \, \delta_{ij} = k_B \left(\frac{\partial^2 \Psi}{\partial x_i^2} \right)_{\pm_i} \delta_{ij}. \tag{1}$$

It is evident from Eq. (1) that a divergence of fluctuations appears at a point of vanishing

λ_i (e.g. at a point of vertical tangent on the i-th conjugacy diagram). If such a point occurs in a *continuous* part of the curve, it indicates that there is a change of stability [4]. Thus we have divergent fluctuations at a point, on the equilibrium sequence, where a change of stability occurs. However, the cases in which such a divergence occurs *asymptotically* needs further considerations. Needless to say, the formula like (1) is useless where the eigenvalues become negative.

It is a straightforward task to calculate various correlations of fluctuations in the three ensembles of our present interest [6].

(1) microcanonical ensemble

In this ensemble, the intrinsic variables, their conjugate counterparts and eigenvalues are $\{x_i\} = \{M,\ J,\ Q\}$, $\{X_i\} = \{\beta,\ -\omega,\ -\phi\}$ and $\{\lambda_i\} = \{-C_{JQ}/\beta^2,\ -I_{MQ}/\beta,\ -K_{MJ}/\beta\}$, where M, J and Q are the mass, angular momentum and electric charge of a hole, respectively, and $\beta \equiv T^{-1}$, $\omega \equiv \Omega/T$ and $\phi \equiv \Phi/T$, with T, Ω and Φ being the temperature, angular velocity and electrostatic potential of its horizon. The eigenvalues in every ensemble are closely related to the hole's susceptibilities: heat capacity $C_\mu \equiv -\beta^2(\partial M/\partial\beta)_\mu$, moment of inertia $I_\nu \equiv \beta(\partial J/\partial\omega)_\nu$ and electrostatic capacity $K_\rho \equiv \beta(\partial Q/\partial\phi)_\rho$ as defined in ref. [4] (α_J and α_Q are used there, instead of ω and ϕ here). For each of these susceptibilities, there are altogether four variations (denoted by μ, ν and ρ, respectively) according to the difference of the sets of quantities which are fixed in calculating them. In the present case, the relevant suffixes are $\nu = \{J,\ Q\}$, $\mu = \{M,\ Q\}$ and $\rho = \{M,\ J\}$.

Typical second moments of the fluctuations in this ensemble are

$$
\begin{aligned}
&< (\delta\beta)^2 > = -k_B\frac{\beta^2}{C_{JQ}}, \quad < (\delta\omega)^2 > = -k_B\frac{\beta}{I_{MQ}}, \quad < (\delta\phi)^2 > = -k_B\frac{\beta}{K_{MJ}}, \\
&< (\delta\Omega)^2 > = -k_B\left[\frac{\Omega^2}{C_{JQ}} + \frac{T}{I_{MQ}}\right], \quad < (\delta\Phi)^2 > = -k_B\left[\frac{\Phi^2}{C_{JQ}} + \frac{T}{K_{MJ}}\right], \\
&< \delta T\ \delta\Omega > = -k_B\frac{T\Omega}{C_{JQ}}, \quad < \delta T\ \delta\Phi > = -k_B\frac{T\Phi}{C_{JQ}}, \quad < \delta\Omega\ \delta\Phi > = -k_B\frac{\Omega\Phi}{C_{JQ}}.
\end{aligned}
\tag{2}
$$

For the discussion of divergent fluctuations, however, it is more convenient to return to the eigenvalues themselves. Their concrete expressions are

$$\lambda_1 = \frac{1-h^4}{1+j^2}\frac{B_1}{A_1}, \quad \lambda_2 = -\frac{4(1-h^2)}{1+h^2}\frac{B_1}{B_2}M^2, \quad \lambda_3 = -2(1-h^2)\frac{B_1}{B_3}. \tag{3}$$

The non-dimensional parameters appeared here are defined as $j = \mid J \mid / M r_H$, $q = \mid Q \mid / r_H$ and $h = \sqrt{j^2+q^2}$, where r_H denotes radii of the outer and inner horizons of a hole. The parameters j and q measure the degrees of rotation and charging up of the hole, respectively, and h serves as a parameter which specifies the position of a black hole state on the equilibrium sequence. The range $0 \leq h < 1$ corresponds to the states of the outer horizons while that $1 < h$ does to the inner horizons. The extremal states in which the outer and inner horizons merge together are specified as the states of $h = 1$ (see ref. [7] where, however, h_J and h_Q are used instead of j and q). Other quantities such as A_i and B_i ($i = 1, \ldots, 4$) are also defined in ref. [7], and we cite here only the relevant ones:

$$A_1 = (1+j^2)[1-2(h^2+2j^2)-3h^4], \quad B_1 = (1+j^2)(1-h^2)^2,$$
$$B_2 = (1+j^2)[(1-h^2)^2+4j^4], \quad B_3 = (1+j^2)[1+3h^4-2(1+h^2)j^2]. \tag{4}$$

The zeros of the eigenvalues occur only at $h = 1$. As seen from the conjugacy diagrams given in ref. [7] (Figs. 3(a) and 3(d)), each divergence of the tangent does not occur in a continuous part of these diagrams but does asymptotically as h approaches to 1 both from below and from above. It can also be confirmed that the entropy (the proper Massieu function in the present case) as a function of M does not have a cusp at the point of $h = 1$ but is folded smoothly there (Fig. 1). Therefore, this divergences are not related to any change of stability at a turning point and is strongly suggested to be reflecting the existence of a second-order phase transition there. This point will further be discussed in section 3.

(2) canonical ensemble

In this ensemble, $\{x_i\} = \{\beta,\ J,\ Q\}$, $\{X_i\} = \{-M,\ -\omega,\ \phi\}$ and $\{\lambda_i\} = \{\beta^2/C_{JQ},\ -I_{\beta Q}/\beta,\ -K_{\beta J}/\beta\}$, and typical non-vanishing second moments are

$$
\begin{aligned}
&< (\delta M)^2 > = k_B T^2 C_{JQ}, \quad < (\delta\omega)^2 > = -k_B \frac{\beta}{I_{\beta Q}}, \quad < (\delta\phi)^2 > = -k_B \frac{\beta}{K_{\beta J}}, \\
&< (\delta S)^2 > = k_B C_{JQ}, \quad < \delta S\ \delta M > = k_B T\ C_{JQ}, \\
&< (\delta\Omega)^2 > = -k_B \frac{T}{I_{\beta Q}}, \quad < (\delta\Phi)^2 > = -k_B \frac{T}{K_{\beta J}},
\end{aligned}
\tag{5}
$$

where S is the entropy. The explicit expressions of the eigenvalues are

$$
\lambda_1 = -\frac{1+j^2}{1-h^4}\,\frac{A_1}{B_1}, \quad \lambda_2 = -\frac{4(1-h^2)}{1+h^2}\,\frac{A_1}{A_2}\,M^2, \quad \lambda_3 = -2(1-h^2)\,\frac{A_1}{A_3}, \tag{6}
$$

where the newly appeared quantities are given by

$$
\begin{aligned}
A_2 &= (1+h^2)[1-3h^2+(5+h^2)j^2], \\
A_3 &= 1-h^4-(5+10h^2+9h^4)j^2+2(1+3h^2)j^4.
\end{aligned}
\tag{7}
$$

The eigenvalues become zero at $h = 1$ and the zero of A_1. However, the former possibility can be almost excluded. This is because the hole's temperatures in this ensemble are fixed at those of the heat reservoirs and hence the states of $h = 1$ are not attainable unless the reservoir has zero temperature. In the latter case (i.e. $A_1 = 0$), the divergence of fluctuations occurs at the turning points associated with the simultaneous changes of stability in the three modes on the outer horizons (see Figs. 4(a), 5(a) and 6(a) of ref. [7]). Since C_{JQ} diverges at this point, this case corresponds to the one which Davies has pointed out. As confirmed here, however, these divergences are irrelevant to any phase transition of the holes.

(3) grand canonical ensemble

In this ensemble, $\{x_i\} = \{\beta,\ \omega,\ \phi\}$, $\{X_i\} = \{-M,\ J,\ Q\}$ and $\{\lambda\} = \{\beta^2/C_{\omega\phi},\ \beta/I_{\beta\phi},\ \beta/K_{\beta\omega}\}$, and typical non-vanishing second moments are

$$< (\delta M)^2 > = k_B T^2 C_{\omega\phi}, \quad < (\delta J)^2 > = k_B T I_{\beta\phi}, \quad < (\delta Q)^2 > = k_B T K_{\beta\omega},$$
$$< (\delta S)^2 > = k_B \left[C_{\omega\phi} + \beta\Omega^2 I_{\beta\phi} + \beta\Phi^2 K_{\beta\omega} \right], \tag{8}$$
$$< \delta M \ \delta S > = k_B T C_{\omega\phi}, \quad < \delta J \ \delta S > = -k_B \Omega I_{\beta\phi}, \quad < \delta Q \ \delta S > = -k_B \Phi K_{\beta\omega}.$$

The explicit expressions of the eigenvalues are

$$\lambda_1 = -\frac{1+j^2}{1-h^4}\frac{A_4}{B_4}, \quad \lambda_2 = \frac{1+h^2}{4(1-h^2)}\frac{A_4}{A_3}M^{-2}, \quad \lambda_3 = \frac{1}{2(1-h^2)}\frac{A_4}{A_2}, \tag{9}$$

where the newly appeared quantities are given by

$$A_4 = (1+h^2)[1-h^2+3(1+h^2)j^2-2j^4], \tag{10}$$
$$B_4 = (1+j^2)[1+3h^4+2(1-h^2)j^2].$$

The second moments cited above correspond to those obtained by Pavón and Rubí [8] for Kerr holes (i.e. $Q = 0$) when the limit of infinitely large volume is taken for their box containing the Hawking radiation. The divergence of fluctuations appears in this ensemble only at the zero of A_4, where the simultaneous changes of stability occur in the three modes on the inner horizons. Therefore, there is no divergence of fluctuations in this ensemble which is relevant to some second-order phase transition.

3. Critical Behavior of Extremal Holes

From the above discussions for the three different ensembles, we have found that a second-order phase transition is very likely to exist on the equilibrium sequence of isolated Kerr-Newman black holes at their extremal limits as some authors have predicted (e.g. ref. [2,3]). In fact, a physical interpretation of such a transition has also been proposed more than a decade ago by Curir [9] for Kerr holes based on an analogy of the black hole states with laser systems. In this theory, a non-extremal Kerr hole, which amplifies waves in the

spectral range $2\pi\nu < n\Omega$ (where ν is the frequency and n is the natural number) through superradiance, is regarded as a coexistence system of the outer and inner horizons. At the extremal state where $T = 0$, however, both horizons merge together and emit only at the critical frequency $2\pi\nu = n\Omega$. The extremal state is thus regarded as the critical point of a second-order phase transition whose critical temperature is zero. The ordered phase is proposed to be that of naked singularities while the disordered phase consists of non-extremal Kerr states ($T > T_c = 0$).

We follow here the idea of coexistence system but propose a somewhat different physical interpretation from Curir's. The main point to be noted for this system of coexisting two horizons of a Kerr-Newman hole is that the thermodynamic variables which are common in this system are not the intensive variables as in usual systems but the extensive variables, M, J and Q. On the contrary, the differences in the intensive variables such as temperature, angular velocity and electrostatic potential are the characteristics of the existence of different two phases. Since these quantities are expressed in terms of the mass M and non-dimensional parameters, h and j (or equivalently q) [7], the quantity defined by $\epsilon \equiv (M - M_X)/M_X$ measures the closeness of a state to the critical point, where the critical mass $M_X \equiv (Q^2 + \sqrt{4J^2 + Q^4}\,)/2$ is the mass of the extremal hole for a given set of J and Q. Contrary to the Curir's case, the difference in temperature serves rather as an order parameter, $\zeta \equiv (T_+ - T_-)M_X$, where the suffixes $+$ and $-$ indicate the quantities associated with the outer and inner horizons, respectively. Thus, in our interpretation, the non-extremal states on a Kerr-Newman sequence are regarded as ordered states whereas the extremal state as disordered.

As an example of the critical exponents in this transition, we calculate the one for temperature. We can show from the definition of M_X and the parameter expressions for J and Q that $\epsilon = (1-h)^2/2h$. This equation yields $h_+ + h_- = 1 + \epsilon$ and $h_+ h_- = 1$, which

are used to evaluate ζ. In the limit of $\epsilon \to 0$, we have $\zeta \propto \epsilon^{1/2}$. Although the value 1/2 for a critical exponent is familiar as a result of classical thermodynamics, it may not be reliable since the critical point is the place where the classical thermodynamics lose its validity [10].

Another unusual point to be mentioned is the stability of the inner horizons. The turning point method concludes only that there is a change of stability, in the microcanonical ensemble, neither on the outer nor on the inner horizons [7], since the conjugacy diagrams for the outer and inner horizons are all disconnected. However, on some other grounds the inner horizons are suggested to be always unstable [11]. This fact contrasts with usual cases in which coexisting two phases are both, at least, in locally stable equilibria.

4. First-Order Phase Transition

Although no one seems to have insisted on the existence of a first-order phase transition in the Kerr-Newman black hole states, we propose here that there may be such a transition between a Schwarzschild state ($J = Q = 0$) and a non-Schwarzschild state ($J \neq 0$ and/or $Q \neq 0$) with a common mass, if there is a perturbation of sufficient strength. This statement is based on the fact that the plot of the black hole entropy against mass have two topologically different branches, one for the Schwarzschild sequence and the other for the non-Schwarzschild one (see Fig. 1). The transition seems to be easier to occur the lager the mass of the holes. However, whether such a transition in which a non-Schwarzschild hole abruptly abandon its angular momentum and charge can actually occur or not should be examined dynamically. In any case, it may be worth noting in this regard that the spacetime characters of the horizons of both types (regarded as phases) of black holes are quite different as can be confirmed by the conformal diagrams.

References

[1] P. C. W. Davies, Proc. R. Soc. London A 353 (1977) 499.

[2] D. Pavón and J. M. Rubí, Phys. Rev. D 37 (1988) 2052.

[3] D. Pavón, Phys. Rev. D 43 (1991) 2495.

[4] O. Kaburaki, Phys. Lett. A 185 (1994) 21.

[5] H. Poincaé, Acta Math. 7 (1885) 259;
J. Katz, Mon. Not. Roy. Astr. Soc. 183 (1978) 765; *ibid.* 189 (1979) 817.

[6] Some of the results on such moments have been presented before:
O. Kaburaki, Proc. of the Third Workshop on General Relativity and Gravitation, eds. K. Maeda et al. (Tokyo, 1994) p. 107.

[7] J. Katz, I. Okamoto and O. Kaburaki, Class. Quantum Grav. 10 (1993) 1323.

[8] D. Pavón and J. M. Rubí, Gen. Rel. Grav. 17 (1985) 387.

[9] A. Curir, Gen. Rel. Grav. 13 (1981) 417; *ibid.* 13 (1981) 1177.

[10] H. B. Callen, Thermodynamics and an Introduction to Thermostatistics (John Wiley, New York, 1985).

[11] O. Kaburaki, Proc. of the Seventh Marcel Grossmann Meeting on General Relativity and Gravitation, (1994) in press.

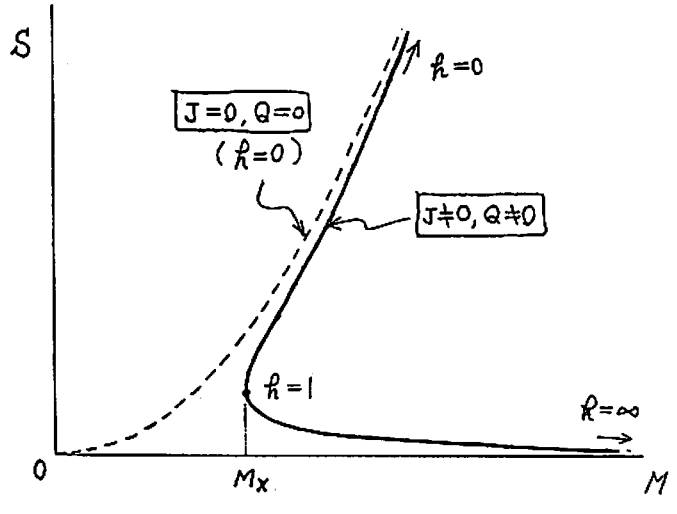

Fig. 1

Ergoregions and preferred time

Sean A. Hayward

Department of Physics, Kyoto University, Kyoto 606-01, Japan

hayward@murasaki.scphys.kyoto-u.ac.jp

Abstract. Ergoregions can be defined to consist of points where test particles may have positive or negative energy. The energy of a test particle can be defined (i) in stationary space-times, using the Killing vector; (ii) in spherically symmetric space-times, using the Misner-Sharp energy, as suggested by Hájíček. In case (ii), the energy is conserved and has the desired Newtonian limit, and the ergoregion coincides with the trapped region. In both cases there is a preferred time, (i) the Killing vector and (ii) the Kodama vector, which maps the test particle's momentum to its energy. In both cases, the ergoregion consists of the points where this vector is spatial. This vector provides a natural candidate for the preferred time of quantum theory. In case (ii), this raises the possibility of generalising Hawking radiation to non-stationary black holes and thereby obtaining a consistent quantum theory of black holes. Moreover, for a different choice of time, the expected energy of a wave packet will usually not reduce to the classical energy in the classical limit, thus violating the correspondence principle.

I. Introduction

Gravitational theory and quantum theory collide in the *Hawking effect*, whereby a black hole may lose energy by radiation of a quantum field. More precisely, Hawking and others showed [1] that on a stationary black-hole space-time, a quantum field produces particles with a thermal spectrum at a characteristic temperature as measured by stationary observers. This loss of energy presumably reduces the black hole's energy and therefore its area, leading to the possibility of a complete evaporation of the black hole. To describe this consistently requires generalising the Hawking effect to non-stationary black holes. Immediately one encounters the *problem of time* in quantum theory [2]: the canonical formalism involves a choice of time, with different choices leading to inequivalent predictions, even at the semi-classical level. In stationary space-times, it seems natural to use the Killing vector to define a preferred time, but for general space-times there is no preferred vector.

Thus there is a fundamental conceptual problem. One is forced to consider the physical basis of Hawking radiation in intuitive terms. Hawking's original explanation was that the uncertainty principle allows the production of pairs of particles, of which one could fall into the hole and the other escape, taking away energy. This points towards the concept of an *ergoregion*: a region of points where a test particle may have positive or negative energy. Classically, ergoregions allows *energy extraction* by the Penrose process [3]: a test particle may split into two fragments, one with negative energy and the other therefore having greater energy than the original. There is a continuous version of the Penrose process, for a test field, known as super-radiant scattering [4]. Taking into account the uncertainty principle, the location of the ergoregion is uncertain, so that one would expect energy extraction by a quantum field to be possible from a neighbourhood of the classical

ergoregion. This leads to the idea that *the Hawking effect is the quantum field version of energy extraction* by the Penrose process. This is supported by the fact that quantum field theory predicts particle production if and only if a classical test field has both positive and negative frequencies [4,5], where the frequencies are eigenvalues of the energy operator. The mixture of positive and negative energies (or frequencies) is the crucial feature of both processes.

Thus attention focusses on the concept of ergoregion. To define this properly requires a definition of the energy of a test particle. In stationary space-times, this is standard and determined by the Killing vector. In spherically symmetric space-times, there is a natural definition suggested by Hájíček [6], who also argued along lines similar to the above. In the following, the Hájíček energy is reviewed and shown to have various properties which support its physical interpretation. An equivalent definition is given which is formally identical to the standard stationary one, with the Killing vector replaced by a preferred vector introduced by Kodama [7]. The Kodama vector provides a *preferred time* and so offers a natural resolution to the problem of time in spherical symmetry. This provides a basis for the quantum theory of non-stationary black holes.

II. Stationary space-times

First recall the standard definition of energy of a test particle in a stationary space-time. Such space-times are defined by a Killing vector ξ which generates asymptotic time translations. For a test particle with rest mass m and velocity v, where $m > 0$ and $g(v,v) = -1$, the energy is defined [4] by

$$\mathcal{E} = -g(\xi, mv). \tag{1}$$

Here g denotes the metric and the sign convention is that spatial metrics are positive-definite. Because the test particle moves along a geodesic, it follows that $\mathcal{E}$ is conserved: $v(\mathcal{E}) = 0$. Thus $\mathcal{E}$ is a constant of the motion, and also agrees with the usual definition of energy in flat space-time, so is usually accepted as the standard energy of a test particle.

It follows immediately that the ergoregion—where $\mathcal{E}$ may be positive or negative, depending on v—consists of the points where ξ is spatial. Specifically: (i) if ξ is future-causal then $\mathcal{E} > 0$ for all v, assumed future-causal; (ii) if ξ is past-causal then $\mathcal{E} < 0$ for all v; (iii) if ξ is spatial then there exist v_1 and v_2 such that $\mathcal{E}_1 > 0$ and $\mathcal{E}_2 < 0$.

For the Schwarzshild black hole, the ergoregion coincides with the trapped region. Thus classical energy extraction from the black hole cannot occur for global reasons. This becomes possible for quantum fields due to the blurring caused by the uncertainty principle.

III. Spherically symmetric space-times

Spherically symmetric space-times may be defined by the line-element

$$\mathrm{d}s^2 = r^2 \mathrm{d}\Omega^2 - 2\mathrm{e}^{-f} \mathrm{d}\xi^+ \mathrm{d}\xi^- \tag{2}$$

where $\mathrm{d}\Omega^2$ refers to the unit 2-sphere and the areal radius r and function f depend on the null coordinates $\xi^\pm$. For such space-times there is a widely (though not universally) accepted definition of active gravitational energy due to Misner & Sharp [8]:

$$E = \tfrac{1}{2} r + \mathrm{e}^f r \partial_+ r \partial_- r \tag{3}$$

where $\partial_\pm = \partial/\partial\xi^\pm$. Various physically important properties of E were recently established or reviewed [9], of which the following are relevant.

(i). A sphere is trapped if $E > \frac{1}{2}r$ and untrapped if $E \leq \frac{1}{2}r$. Here a trapped surface is one for which $\partial_+ r \partial_- r > 0$, following Penrose's definition [10], and an untrapped surface is one for which $\partial_+ r \partial_- r \leq 0$.

(ii). E reduces to the standard asymptotic energies for an asymptotically flat space-time, namely the Bondi-Sachs energy at $\mathcal{I}^\pm$ and the Arnowitt-Deser-Misner energy at i^0.

(iii). E reduces to the Schwarzschild mass in vacuo.

(iv). In the Newtonian limit $c \to \infty$ of an ideal fluid,

$$E = Mc^2 + K + V + O(c^{-2}) \tag{4}$$

where the mass M, kinetic energy K and gravitational potential energy V are defined by

$$M = \int_\Sigma *\varepsilon \qquad K = \int_\Sigma *\tfrac{1}{2}\varepsilon\dot{r}^2 \qquad V = -\int_\Sigma *\frac{M\varepsilon}{r} \tag{5}$$

where ε is the density of the fluid, Σ is a spatial hypersurface orthogonal to the flow, with volume element $*$ and a regular centre.

It should also be noted that more general definitions of energy such as those of Hawking and Penrose [11] reduce to E in spherical symmetry.

One formula will be required below, namely that determining the evolution of E:

$$\partial_\pm E = 4\pi e^f r^2 (T_{+-}\partial_\pm r - T_{\pm\pm}\partial_\mp r) \tag{6}$$

where T is the stress-energy tensor, $T_{\pm\pm} = T(\partial_\pm, \partial_\pm)$ and $T_{+-} = T(\partial_+, \partial_-)$. This follows from the Einstein equation with units $G = 1$ [9].

Hájíček's idea was to define the energy of a spherical shell of test particles as the variation in E induced by the perturbation of the test particles [6]. Denote perturbations of $(T, E \ldots)$ by script letters $(\mathcal{T}, \mathcal{E} \ldots)$. For a spherical shell of test particles with rest mass m and velocity v, where $m > 0$ and $g(v, v) = -1$, the stress-energy tensor is

$$\mathcal{T} = g(v) \otimes g(v) m\delta \tag{7}$$

where δ is the Dirac distribution with support at the intersection S of the shell with a spatial hypersurface Σ:

$$\int_\Sigma *\delta X = X|_S \,. \tag{8}$$

Then the Hájíček energy $\mathcal{E}$ of the shell is defined by the perturbed analogue of (6):

$$\partial_\pm \mathcal{E} = 4\pi e^f r^2 (\mathcal{T}_{+-}\partial_\pm r - \mathcal{T}_{\pm\pm}\partial_\mp r). \tag{9}$$

Taking an orthonormal basis $\{v, z\}$, i.e. such that $g(z, v) = 0$ and $g(z, z) = 1$, and denoting $\dot{X} = v(X)$ and $X' = z(X)$, this formula may be rewritten as

$$\dot{\mathcal{E}} = 0 \qquad \mathcal{E}' = 4\pi r^2 r' m\delta. \tag{10}$$

The first equation expresses conservation of $\mathcal{E}$. The second equation integrates to

$$\mathcal{E} = \pm m \left(1 + \dot{r}^2 - \frac{2E}{r}\right)^{1/2}\Bigg|_S \tag{11}$$

where the sign is that of r'. It follows that $\mathcal{E}$ has the desired Newtonian limit:

$$\pm\mathcal{E} = mc^2 + \tfrac{1}{2}m\dot{r}^2 - \frac{mM}{r} + O(c^{-2}). \tag{12}$$

The terms represent the mass, kinetic energy and gravitational potential energy of the shell. These properties support the physical interpretation of $\mathcal{E}$ as the active energy of the shell of test particles.

It follows, as Hájíček showed, that the ergoregion coincides with the trapped region. Specifically: (i) if S is untrapped, with orientation fixed by $\partial_+ r > 0$, then $r' > 0$ for all v and so $\mathcal{E} > 0$; (ii) similarly, if untrapped S has the opposite orientation then $\mathcal{E} < 0$; (iii) if S is trapped, then there exist v_1 and v_2 such that $r_1' > 0$ and $r_2' < 0$, so that $\mathcal{E}_1 > 0$ and $\mathcal{E}_2 < 0$. As in the stationary case, the overall sign of $\mathcal{E}$ is conventional.

IV. Preferred time in spherical symmetry

Both the Misner-Sharp energy and the Hájíček energy can be defined equivalently in terms of a preferred vector identified by Hájíček and introduced earlier by Kodama [7]. In its relation to the energy, the Kodama vector plays the same role in spherically symmetric space-times that the Killing vector plays in stationary space-times. The Kodama vector may be defined, up to orientation, by

$$\xi = \operatorname{curl} r \tag{13}$$

where the curl refers to the two-dimensional space-time obtained by taking the quotient by the spheres of symmetry. An equivalent definition is

$$\xi(r) = 0 \qquad g(\xi,\xi) = \frac{2E}{r} - 1. \tag{14}$$

One finds explicitly that, up to sign,

$$\xi = e^f(\partial_+ r \partial_- - \partial_- r \partial_+). \tag{15}$$

One can show [9] that both ξ and $T(\xi)$ have zero divergence and that the Misner-Sharp energy satisfies

$$E = \int_\Sigma *T(\xi, v) \tag{16}$$

where Σ is a spatial hypersurface with regular centre, volume form $*$ and unit normal vector v. That is, E is the charge associated with the conserved current $T(\xi)$. Similarly, the Hájíček energy satisfies

$$\mathcal{E} = \int_\Sigma *T(\xi, v) = -\int_\Sigma *g(\xi, mv\delta) = -g(\xi, mv)|_S. \tag{17}$$

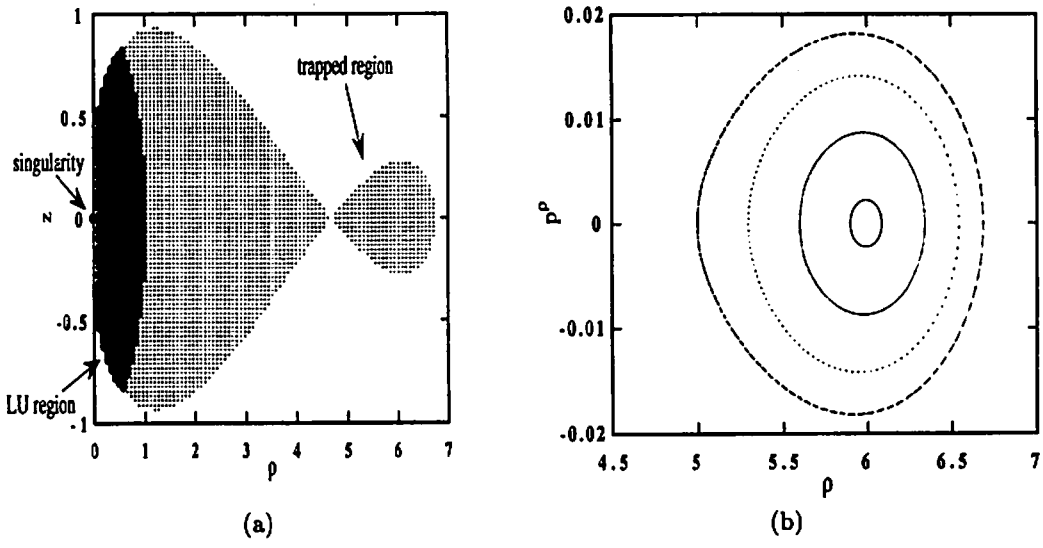

Fig. 1: (a) is the unstable region and the trapped region of 1-Curzon spacetime. In this picture, the LU region can be seen only around singularity, and trapped orbit can go through only the LS region. (b) is Poincaré map of the orbit which is completely included the LS region. All of the tori are not broken.

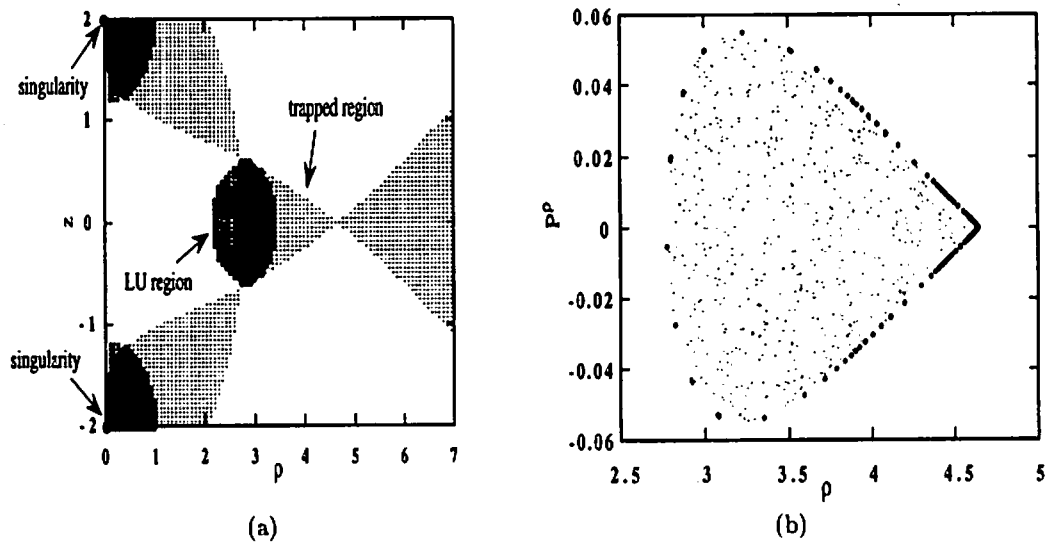

Fig. 2: Chaos in the 2-Curzon spacetime with two equal masses. (a) is the LU region and the trapped region. Some bounded orbit pass through the LU region. (b) is the Poincaré map of th orbit of (a). The tori are completely broken.

2 Homoclinic tangle

In our previous study, we showed that the LU region plays an important role in causing chaotic behavior of test particles. It seems that the passing of the orbit through the LU region is a necessary condition for strong chaos. However we found a counterexample of our criterion (Fig.3). Fig.3 shows that the particle cannot pass through the LU region

but the motion is chaotic. We can explain this from another point of view, that is, the existence of homoclinic orbit and homoclinic tangle.

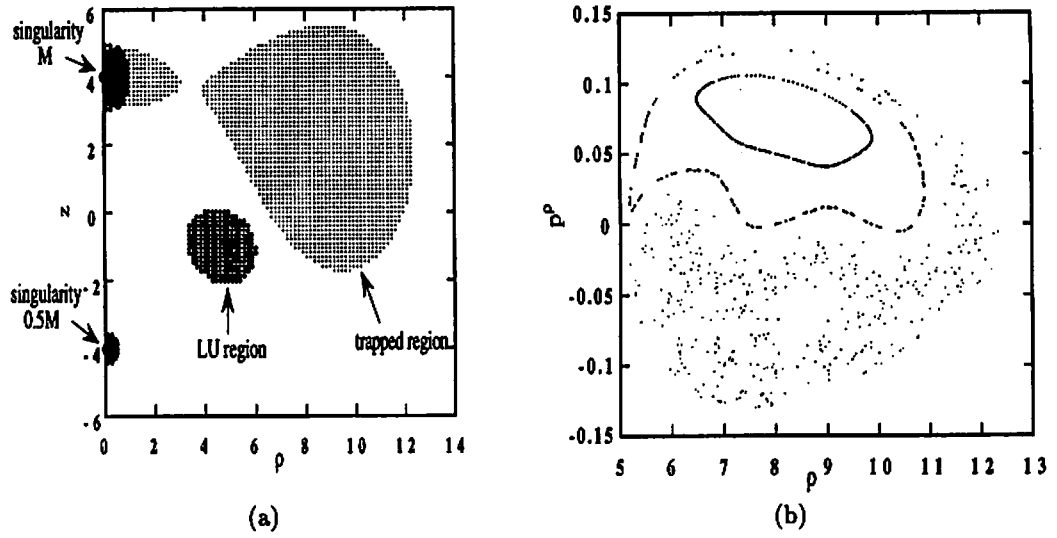

Fig. 3: Chaos in the 2-Curzon spacetime with two different masses. The mass ratio is 2:1. (a) shows the unstable region and the trapped region. (b) is the Poincaré map of the orbit of (a). Although the trapped region do not overlap with the LU region, the orbit of test particle is chaotic.

In GR, a single point-mass system has usually an unstable equilibrium point around it. And there exists an orbit which gradually departs at this point and asymptotically approach it after infinite time interval, if the angular momentum and energy of the particle is chosen appropriately (Fig.4). This orbit is called a homoclinic orbit and is known to play an important role in causing strong chaos.

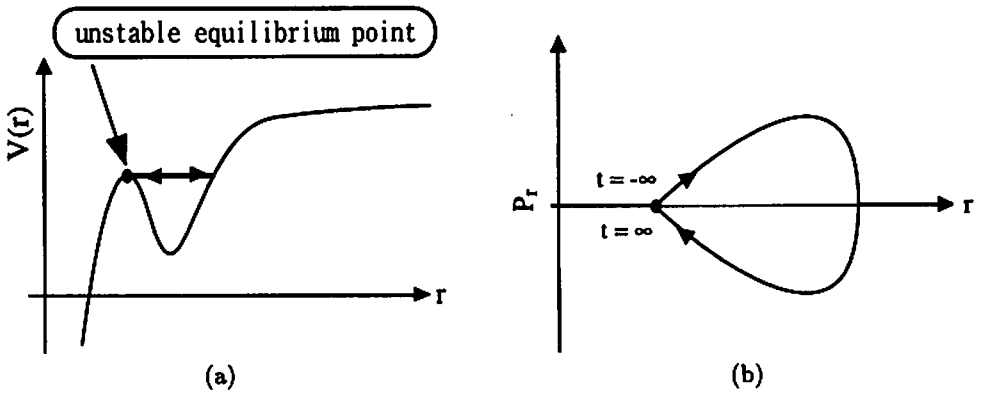

Fig. 4: (a) The effective potential of the test particle in Schwarzschild spacetime. There exists an unstable equilibrium point and a homoclinic orbit. (b) A homoclinic orbit in phase space

In our previous study, all spacetime we examined have a reflection symmetry about the equatorial plane, which makes it possible that homoclinic orbit always exists. However it is more natural that the spacetime around a gravitational source does not have such

symmetry because of another gravitational source around it as Fig.3. In this case the homoclinic orbit no longer exists in the spacetime, but it is split and tangled complicatedly. This is called a homoclinic tangle and is one of causes of strong chaos. From this point of view, for example, Bombelli et al [3] showed that strong chaos occurs in Schwarzschild spacetime perturbed by gravitational wave. They claimed that the time symmetry of the spacetime is broken by the perturbation then homoclinic orbit tangles and chaos occurs. Moeckel [4] also showed similar chaotic phenomena in the other type of perturbed Schwarzschild spacetime.

3 Conclusion

We have analyzed the motion of test particles in axisymmetric static spacetimes systematically to find the criterion for strong chaos to occur. We conclude that there are two causes of the strong chaos.

(1) the local instability caused by negative curvature of spacetime. (As the energy of the particle increases the orbit becomes chaotic as it approaches that of the unstable equilibrium point.)

(2) homoclinic tangle caused by the perturbation which breaks some symmetries of the spacetime.

We do not know whether or not these criteria are independent each other. We continue to analyze the particles motion in various spacetimes to verify our criterion.

As we mentioned in section 1, it seems that the distribution of the LU region has some kind of relationship with Petrov classification of the spacetime. So we may be able to classify the spacetimes by analyzing the motions of particles.

So far, the spacetimes we examined are around naked singularities and are not realistic. So we will apply our criterion to the investigation the motion of a particle in other more realistic system, for example, the motion of a spinning particle in Kerr spacetime.

References

[1] Y. Sota, S. Suzuki and K. Maeda, *Proceeding of the Third Workshop on General Relativity and Gravitation* (1994) 233.

[2] M. Szydlowski, Phys. Lett. **A176** (1993) 22

[3] L. Bombelli and E. Calzetta, Class. Quantum. Grav. **9** (1992) 2573.

[4] R. Moeckel, Commun. Math. Phys. **150** (1992) 415

Quantum "de" coherence and real time quantum tunneling

MASAHIRO MORIKAWA
Department of Physics, Ochanomizu University
1-1, Otsuka 2, Bunkyo-ku, Tokyo 112 JAPAN
e-mail: hiro@phys.ocha.ac.jp

Abstract

The subjects in this report are to develop the approximation formalism of quantum evolution by using the classical statistical mechanics and then, to apply this formalism to the quantum tunneling problem in the real-time scheme. We first clarify the fundamental effects of dissipation on the classical-quantum correspondence in quantum mechanics. We study the effect of friction and fluctuation induced from the environmental degrees of freedom, and emphasize that the friction always reduces the entropy while the diffusion enhances it. Using this property, we construct the Fokker-Planck equation which reasonably approximates quantum mechanics while asymptotically preserving entropy and energy. We demonstrate that this Fokker-Planck equation also reproduces the symmetric part of the quantum correlation function. Applying these facts, we formulate the real time quantum tunneling process not relying upon the ordinary instanton method.

I. INTRODUCTION

We often encounter the problem of quantum-classical correspondence in various issues in physics; such as a) quantum coherence in macroscopic systems [1], b) quantum chaos [2], c) the dissipative quantum tunneling [3], d) decoherence of the wave function of the Universe [4], e) classicalization of the density perturbations in the early Universe [5],... The quantum-classical correspondence is highly non-trivial and, for instance, a simple limit $\hbar \to 0$ does not always guarantee the correct classical behavior. In this report, let us consider this problem especially in the context of quantum tunneling problem.

The central problem in the quantum-classical correspondence will be the classicalization mechanism of the quantum system. In a wide class of physical systems, the classical behavior is gradually recovered via the process of quantum decoherence (*i.e.* the destruction of quantum coherence) which is naturally induced from the environment that couples with the system of interest [6]. For example in quantum cosmology, the Universe begun as a wave function, which should eventually describe the classical space-time and the ordinary gas dynamics at the later stage of the Universe. Moreover the density fluctuations produced

from the quantum fluctuations in the early Universe are supposed to reduce to the classical curvature perturbations in order to trigger the galaxy formation. In the measurement theory of quantum mechanics, the information of the quantum system is extracted by the measurement apparatus as classical signals.

The main criteria for the classicalization has been the quantum decoherence. Actually, we naively expect that the off-diagonal part of the density matrix represents the quantum transition and coherence. Therefore we have been focused on the diagonalization of the density matrix when we would like to confirm the classicalization of the system [7].

However the criteria and the measure of the classicality are not so straightforward. Many other criteria have been proposed so far for the classicalization. For example, Lyth, Guth, Pi and others [8] propose that the condition $\langle x^2\rangle\langle p^2\rangle \gg \hbar$ should be satisfied for the classicalized system. The condition for WKB approximation is another criterion. The Machida-Namiki [9] proposes the reduction of the quantum correlation due to the thermal fluctuation in the measurement apparatus. Fukuda [1] proposes the reduction of the fluctuations due to the macroscopic property of the collective mode. ... In this report, we first review the measure of classicality [10]. Especially, we emphasize that the above criteria for classicality are classified into two conditions: a) the destruction of quantum coherence (= decoherence, QD) and b) the establishment of the classical correlation (CC) in the phase space of the system.

There are various external perturbations which affect the classicalization of the system. They are a) frictional effect which violates the time reversal symmetry, b) diffusion effect which violates the quantum coherence and c) the external classical force which makes the system coherent or squeeze... We study how these external perturbations affect the classicalization with the above different criteria. For example for the first criterion decoherence, we show that the diffusion always reduces the quantum coherence while the friction always enhances it. Thus the classicality measured by decoherence is determined by the balance of friction and diffusion.

In order to demonstrate the formalism of classicalization, in the second part of this report, we study the quantum tunneling problem in real time. Especially based on the balance of the enhancement and the reduction of quantum coherence by friction and diffusion mentioned above, we construct the Fokker-Planck equation which represents quantum mechanical evolution in the semiclassical and asymptotic region. Then by applying the standard method of first order phase transition in statistical mechanics [11], we obtain the tunneling rate. We compare this formula with the tunneling amplitude derived from the standard instanton method in the imaginary time formalism [12]. We emphasize that our real time formalism is particularly suitable for studying the dissipative quantum tunneling.

II. EVOLUTION EQUATION FOR THE STATE AND THE MEASURE OF CLASSICALITY

We study, in this section, a general evolution equation for the density matrix $\rho(t)$ of the dissipative system with the local approximation, which is the Markovian limit of the dissipative corrections induced from the environment [13]. A general evolution equation would be non-local in space-time and is quite complicated. The approximated density matrix for a quantum mechanical system obeys the evolution equation

$$\begin{aligned}\dot{\rho}(x,x';t) = \Big[&\frac{i}{2m}(\partial_x^2 - \partial_{x'}^2) - i\frac{m}{2}\omega^2(x^2 - x'^2) - i(v(x) - v(x')) \\ &-\epsilon x_\Delta(\partial_x - \partial_{x'}) - \Lambda x_\Delta^2\Big]\rho(x,x';t),\end{aligned} \tag{2.1}$$

where $\rho(x,x';t) \equiv \langle x|\rho(t)|x'\rangle$, $2x_C = x + x'$, and $x_\Delta = x - x'$. The variables $v(x), m, \omega, \epsilon$ and, Λ are, respectively, potential, mass, frequency, friction coefficient, and the diffusion constant. This form is derived from the general argument of dissipative quantum systems [13]. Note that the probability is preserved ($d\mathrm{Tr}\rho/dt = 0$) even if the system is dissipative.

In the following, we will mainly consider Gaussian approximation of the above equation:

$$\rho(x,x',t) = \exp[\alpha^2 x_C^2 + i\beta x_C x_\Delta - \gamma^2 x_\Delta^2 + \lambda]. \tag{2.2}$$

Then the above evolution equation Eq.(2.1) becomes

$$\begin{aligned}
\frac{d\alpha^2}{dt} &= -\frac{2}{m}\beta\alpha^2 \\
\frac{d\beta}{dt} &= \frac{4}{m}\alpha^2\gamma^2 - \frac{1}{m}\beta^2 - 2\epsilon\beta - m\omega^2 \\
\frac{d\gamma^2}{dt} &= -4\epsilon\gamma^2 + \Lambda - \frac{2}{m}\beta\gamma^2,
\end{aligned} \tag{2.3}$$

and λ is a normalization constant. We Fourier transform Eq.(2.2) with respect to the variable x_C to a new variable q. Then the state is

$$\rho(x_\Delta, q; t) = \exp[-A(t)x_\Delta^2 - 2B(t)x_\Delta q - C(t)q^2 - D(t)], \tag{2.4}$$

and the Eq.(2.3) becomes

$$\begin{aligned}
\dot{A} &= -4\epsilon A - 2m\omega^2 B + \Lambda, \\
\dot{B} &= m^{-1}A - 2\epsilon B - m\omega^2 C, \\
\dot{C} &= 2m^{-1}B, \\
\dot{D} &= 0.
\end{aligned} \tag{2.5}$$

In the above, there are three fundamental effects from the environment: a) dissipation effect on the system which is represented by the friction coefficient ϵ, b) fluctuation effect on the system which is represented by the diffusion coefficient Λ, c) renormalization effects which forces the parameters in the original Hamiltonian shift.

Now we study the criteria for classicality of the system. All the criteria proposed so far mentioned above can be classified in the following two conditions: a) destruction of the quantum coherence (= decoherence, QD) and b) the establishment of the classical correlation (CC) in the phase space of the system.

A. Quantum Decoherence condition

The environmental degrees of freedom which couples to the system reduces the quantum coherence by the random perturbations on the system. This decoherence can be a measure for the classicality. Actual measure may be $\delta_{QD} := \mathrm{Tr}\rho^2$ for the system density matrix ρ or the statistical entropy $S := -\mathrm{Tr}\rho\ln\rho$. δ_{QD} becomes 1 for a pure state because in this case ρ is a projection operator ($\rho^2 = \rho$) and reduces to 0 if the quantum coherence is destroyed. Therefore smaller value of δ_{QD} means that the system is much classicalized. The entropy S becomes 1 for a pure state and increases to infinity if the quantum coherence is destroyed. These values are independent from the representation (choice of canonical variables). For a general state Eq.(2.1), we have

$$\langle x(t)x(t')\rangle_\xi = \frac{\Lambda}{4m^2\epsilon\omega^2}\cos(\omega(t-t')), \tag{3.4}$$

in the $\epsilon \to 0$ limit. This reduces to $\cos(\omega(t-t'))/(4m\omega)$ if we choose the above values for ϵ and Λ. This is precisely the symmetric correlation function in quantum mechanics: $\mathrm{Re}\langle x(t)x(t')\rangle$. We can also show that another classicality measure δ_{CC} is of order 1, which means that the system is well quantum also in the sense of classical correlation.

Thus we conclude that, provided that we choose the special values of Λ and ϵ, the statistical mechanical Fokker-Planck equation reproduces quantum mechanics: quantum correlations and coherence while preserving energy.

B. non-Gaussian case

In the general case, we compare the quantum mechanical generating functional and the statistical mechanical one. The statistical mechanical generating functional, whose variation with respect to the source yields n-point correlation function of the statistical variable $x(t)$, is given by averaging the Langevin equation with the statistical weight of the random force:

$$\begin{aligned} Z(J) &= \int[dx_C]\int[d\xi]\exp[-\int dt(\xi^2/2\Lambda)] \\ &\qquad \times\delta(\ddot{x}_C + m\omega^2 x_C + 2\epsilon m\dot{x}_C - \xi + V'(x_C)) \\ &= \int[dx_C]\int[dx_\Delta/2\pi]\exp[i\int x_\Delta V'(-i\delta_J)] \\ &\qquad \times\exp[i\int x_\Delta(m\partial_t^2 + m\omega^2 + 2\epsilon m\partial_t)x_C + iJx_C - \Lambda\int x_\Delta^2/2]. \end{aligned} \tag{3.5}$$

This becomes after the x_Δ, x_C integration,

$$Z(J) = \exp[-i\int x_\Delta V'(-i\delta_J)]\exp[-\frac{\Lambda}{2}\int(SJ)^2]|_{x_\Delta\to SJ}, \tag{3.6}$$

where $S = (m\partial_t^2 + m\omega^2 - 2\epsilon m\partial_t)^{-1}$. The perturbation expansion of the generating functional based on this expression is the same in quantum mechanics case except the following points. a) The propagator in statistical mechanics is the symmetric part of the two-point correlation in quantum mechanics $Re\langle x(t)x(t')\rangle$, and b) All the vertex in the statistical mechanics is accompanied with at least one external line. Relevant differences become manifest in the three and higher number loop-corrections. Therefore in the semiclassical region, we expect that the approximation of the quantum mechanics by statistical mechanics is still effective.

IV. APPLICATION TO QUANTUM TUNNELING

We now apply our method to approximate the quantum mechanics by statistical mechanics to the problem of quantum tunneling. By doing so, we can use real-time formalism, not relying upon the popular instanton method which is based on the imaginary time formalism. The advantage of the real time formalism will be a) that several dissipative effects (such as diffusion, friction, and energy shifts) induced from the environment on the tunneling amplitude will be studied independently, b) that the state change during the tunneling can be studied, and c) that the tunneling time variation, which is an observable by experiment, can be studied in principle.

In the previous sections, we derived the Fokker-Planck equation which approximates quantum mechanics, and the quantum fluctuation is represented by the diffusion term in the Fokker-Planck equation. Therefore the problem of quantum *tunneling* through a potential barrier is replaced by the problem of the transition *over* the potential barrier. This latter problem has been well studied in statistical mechanics, especially by Langer [11]. We follow the systematic method by Langer in the following.

We consider the statistical field $\varphi(\vec{x},t)$ and its distribution function $W[\varphi(\vec{x}),p_\varphi(\vec{x});t]$. The Hamiltonian for this field is

$$H=\int d\vec{x}[\frac{1}{2}(p_\varphi^2+\nabla\varphi^2)+\frac{1}{2}\mu^2\varphi^2+V(\varphi)]. \tag{4.1}$$

The potential V is supposed to have the absolute minimum which corresponds to the stable state and a local minimum which corresponds to the metastable state. If we use the vector notation defined by

$$\begin{pmatrix}\varphi(\vec{x})\\ p_\varphi(\vec{x})\end{pmatrix}\to\eta(\vec{x}),\ \begin{pmatrix}\delta/\delta\varphi(\vec{x})\\ \delta/\delta p_\varphi(\vec{x})\end{pmatrix}\to\delta/\delta\eta(\vec{x}), \tag{4.2}$$

the Fokker-Planck equation becomes

$$\frac{\partial W}{\partial t}=-\int d\vec{x}\frac{\delta J(vecx)}{\delta\eta(\vec{x})}, \tag{4.3}$$

where the current is defined by

$$J(\vec{x})=-\begin{pmatrix}0 & -1\\ 1 & 2\epsilon\end{pmatrix}\begin{pmatrix}(\delta_\varphi H)W & \frac{\lambda}{2\epsilon}(\delta_\varphi W)\\ (\delta_p H)W & \frac{\lambda}{2\epsilon}(\delta_p W).\end{pmatrix} \tag{4.4}$$

The standard strategy for obtaining the transition amplitude (=tunneling amplitude) is as follows: We look for the stationary solution of the Fokker-Planck equation with the boundary condition that there is a source at the metastable state and the sink at the stable state. The flow most probably cross the saddle point configuration $\bar{\eta}(\vec{x})$. Therefore the total flow over the saddle point yields the transition amplitude. We notice that the static solution of the Fokker-Planck equation is

$$W_0[\varphi,p]=\exp[-\frac{2\epsilon}{\Lambda}H]. \tag{4.5}$$

In order to obtain the stationary solution, we set the anzats that the desired solution has the form: $\sigma\times$ (the static solution). Then we obtain the equation of motion for σ, which is linearized near the saddle point configuration $\bar{\eta}(\vec{x})$. This linearized equation is solved by the method of eigenvalue problem. It turns out that there is only one negative eigenvalue ($\lambda_1<0$) which corresponds to the steepest descent path through the saddle point. Evaluating the probability flow in this direction, the final result for the transition probability is given by

$$I=\frac{|\kappa|}{2\pi}\left(\frac{2\pi}{|\lambda_1|}\frac{\Lambda}{2\epsilon}\right)^{1/2}Z_0^{-1}\exp[-\frac{2\epsilon}{\Lambda}\bar{H}]\prod_n''\left(\frac{2\pi}{\lambda_n}\frac{\Lambda}{2\epsilon}\right)^{1/2}, \tag{4.6}$$

where the double prime means that the summation is over all the positive eigenvalues, and the $\bar{H}$ means the Hamiltonian evaluated at the saddle point $\bar{\eta}$. The most sensitive and relevant part in the above expression will be the exponential factor. ¿From this form, it is evident that a) the diffusion effect Λ enhances the transition amplitude, b) the friction effect reduces the amplitude, and c) the renormalization of energy is also an important factor to determine the amplitude.

Now we apply the above result for the vacuum case and compare with the result obtained from the ordinary instanton method.

A. one-dimensional system

We consider the system with the Hamiltonian:

$$H = \frac{p^2}{2m} + V,$$
$$V = \frac{1}{2}m\omega^2 x^2 - \frac{\lambda}{3!}x^3. \tag{4.7}$$

Neglecting the $\lambda\partial_p^3$ term which is $O(\hbar^3)$, the Fokker-Planck equation becomes

$$\dot{W}[x,p;t] = \left[\frac{p}{m}\partial_x - V'(x)\partial_p + 2\epsilon\partial_p p + \Lambda\partial_p^2\right] W[x,p;t]. \tag{4.8}$$

The metastable state is on $x = 0$ and the stable state is $x \to +\infty$ in this model. The saddle point is located at $\bar{x} = 2m\omega^2/\lambda$. The saddle point is a solution of $\delta H = 0$. Though there are other solutions which oscillate around $\bar{x}$, they do not yield the desired stationary solution for W; therefore discarded. The parameters for this model becomes

$$\kappa = \epsilon - \sqrt{\epsilon^2 + \omega^2} < 0,$$
$$\lambda_1 = -m\omega^2,$$
$$\lambda_2 = 1/m,$$
$$\bar{H} = \frac{2(m\omega^2)^3}{3\lambda^2}. \tag{4.9}$$

By setting $2m\epsilon/\Lambda = 2/\omega$ so that the system represent the pure quantum state and for $\epsilon \ll \omega$, we have

$$I = Z_0^{-1}\frac{\omega}{2}\exp[-\frac{4}{3}\frac{m^3\omega^5}{\lambda^2}]. \tag{4.10}$$

¿From the instanton method, the exponent, which is the Euclidean action for the imaginary-time saddle point, becomes $-(24/5)(m^3\omega^5/\lambda^2)$. The inverse frequency ω^{-1} approximately gives the time scale of one instanton in imaginary time. Moreover the Hamiltonian in real time is the Euclidean Lagrangean density in the imaginary time. Therefore $2\bar{H}/\omega$ is of order of the Euclidean action. This is the reason that our real time method yields the correct factor in the exponent in the transition amplitude. On the other hand with respect to the numerical coefficient of the exponent, our value is smaller than that derived from the instanton method by the factor 5/18. This may be due to the still incomplete approximation in our method: we approximate the potential $V(x)$ near the saddle point by the harmonic potential. On the other hand in the instanton method, the whole history (in imaginary time) of the instanton is considered and therefore the whole shape of the potent

B. $\lambda\phi^4$ model with the thin-wall approximation

Next we consider the field theory model with double well potential slightly shifted.

$$H = \int d\vec{x}\left[\frac{1}{2}(\dot{\phi}^2 + (\nabla\phi)^2) + V(\phi)\right]$$
$$V(\phi) = \frac{\lambda}{8}(\phi^2 - \frac{\mu^2}{\lambda})^2 + \frac{\nu}{2a}(\phi - a), \tag{4.11}$$

where λ, μ, ν, and $a(=\sqrt{\mu^2/\lambda})$ are, respectively, the coupling strength, mass, a slight asymmetry in the double well, and the field strength at the bottom of the potential. In our real time scheme, the saddle point is the three-dimensional sphere inside of which is the true vacuum and the outside is the false vacuum. In the imaginary time scheme with the thin wall approximation ($\mu^4 \gg \lambda\nu$), the saddle point is the four-dimensional sphere. The real time scheme yields the exponential factor in the transition amplitude

$$\exp[-\frac{2^5\pi}{\sqrt{3}3^4}\left(\frac{\mu^{12}}{\lambda^4\nu^3}\right)]. \tag{4.12}$$

The imaginary time scheme yields

$$\exp[-\frac{\pi^2}{6}\left(\frac{\mu^{12}}{\lambda^4\nu^3}\right)]. \tag{4.13}$$

Thus our value of the numerical coefficient in the exponent is smaller than that derived from the instanton method by the factor ≈ 1.64. The discrepancy in the numerical values will be due to the same reason: incomplete approximation in our real time method.

V. SUMMARY

In order to clarify the quantum-to-classical correspondence, we first classified the classicality conditions into two criteria: quantum decoherence and the classical correlation. We also investigated how these classicality is affected by the effects of environment (diffusion, dissipation, and the renormalization of parameters) which linearly couples with the system. Especially, we found that the diffusion effect forces the energy and the entropy increase while the dissipation effect forces them reduce. The balance of them determines the equilibrium value. If we choose the special ratio of the diffusion and dissipation ($(\Lambda/\epsilon) = m\omega$), which is inferred from the zero-temperature limit of the Caldeira-Legget model, then the entropy asymptotically approaches to unity, and the energy asymptotically conserves. Moreover, the symmetric part of the quantum two-point function is recovered from the Fokker-Planck equation in the semi-classical limit. In this sense, the quantum system can be approximated by the statistical mechanics.

Applying this fact, we considered the quantum tunneling problem in the real time. Because the dynamics of this system is transformed into the statistical mechanics, we can apply the well developed method for the Fokker-Planck equation for the derivation of the transition amplitude. Actually we derived the correct form for the exponent except some discrepancy in the numerical factors. This discrepancy is considered to be due to the incomplete approximation in our real time method. Our scheme will be particularly relevant in the case of dissipative quantum tunneling. All the dissipative effects are clearly incorporated in the formula for the tunneling probability: a) The diffusion increases the tunneling amplitude. b) The friction reduces it. c) The shift of the parameters in the Hamiltonaian affects it.

We have to further study the quantum tunneling amplitude in the dissipative case. Because the various factors of dissipative effects are manifest in the formula of transition amplitude, we hope our real time method will have some advantage in this evaluation. With respect to the discrepancy in the numerical coefficients, we may be able to improve our method considering the anharminicity around the saddle point.

There may be several other applications of our scheme of approximation. For example, a) quantum chaos. The chaotic property of the dynamical system is manifest in the classical

mechanics. However in general, it disappears in the quantized system. In order to clarify the missing link between the classical chaos and the quantum chaos, our method may be relevant. b) stochastic quantization. The Euclidean quantum n-point functions can be reproduced from the correlation function of the statistical system in the asymptotic limit of the fictitious time. The situation is quite similar to our method. By examining this stochastic quantization method, we would like to clarify how extent the quantum mechanics is approximated from the statistical mechanics. These issues will be reported in our future publications.

Acknowledgments

The author would like to thank Kurata foundation for financial support.

REFERENCES

[1] Fukuda, Prog. Theor. Phys. **81** 34 (1989).
[2] W. D. Heiss, *Chaos and Quantum Chaos, Proceedings, Blydepoort, Eastern Transvaal South Africa* Springer-Verlag, Berlin (1992).
[3] A. J. Leggett, Rev. Mod. Phys. **59** 1 (1987).
[4] M. Morikawa, Phys. Rev. **D40** 4023 (1989).
[5] M. Morikawa, Prog. Theor. Phys. **77** 1163 (1987).
[6] E. Joos and H. D. Zeh, Z. Phys. **B 59** 223 (1985).
[7] W. H. Zurek, Phys. Rev. **D24** 1516 (1981); **D26** 1862 (1982); W. G. Unruh and W. H. Zurek, Phys. Rev. **D 40** 1071 (1989).
[8] D. H. Lyth, Phys. Rev. **D 31** 1792 (1985); A. H. Guth and S. Y. Pi, *ibid.* **D 32** 1899 (1985)
[9] S. Machida and M. Namiki, Prog. Theor. Phys. **63** 1457 (1980); **63** 1833 (1980).
[10] M. Morikawa, Phys. Rev. **D 42** , 2929 (1990).
[11] J. S. Langer, Ann. Phys. **41** , 108 (1967); **54** , 258 (1969).
[12] S. Coleman, Phys. Rev. **D 15** , 2929 (1977).
[13] A. O. Caldeira and A. J. Leggett, Physica **121A** 587 (1983).
[14] J. -P. Vigier et al. in *Quantum Implications* Ed. by B. J. Hiley, Routledge & Kegan Paul, London 169 (1987).
[15] A. Starobinsky, in *Fundamental Interactions*, Ed. by V. N. Ponomarev (MGPI, Moscow) 55 (1983); A. Linde, *Particle Physics and Inflationary Cosmology*, Harwood Academic Publisher GmbH, Switzerland (1990).
[16] R. F. Streater, J. Phys. A. Math. Gen. **15** 1477 (1982).

Gravitational waves from boson stars

Shijun Yoshida, Yoshiharu Eriguchi and Toshifumi Futamase*

Department of Earth Science and Astronomy,
University of Tokyo, Komaba, Meguro, Tokyo 153, Japan

* *Department of Physics, Hirosaki University, Hirosaki 036, Japan*

Abstract

We investigate non-radial oscillations of a boson star by taking into account of the emission of gravitational waves in the framework of general relativity. We solve the linearized perturbed equations for even parity modes and find that there exists a new type of quasi-normal mode for boson stars. Contrary to the behavior of quasi-normal modes of compact fluid stars, imaginary parts of frequencies of normal modes of boson stars are large, which implies short damping time scale of oscillations.

1. Introduction

Several authors[1,2] analyzed the behavior of massive scalar fields in general relativity. In particular, Ruffini and Bonazzola[1] solved the semi-classical Einstein equation and obtained a gravitationally bound state of a self-gravitating scalar field. This bound system has been called a boson star. The self-gravity is supported by the dispersive effect due to the wave character of the scalar field. They have shown that the pressure of the scalar field is anisotropic and that there exists a critical mass of the order of M_{pl}^2/m for boson stars, where M_{pl} and m are the Planck mass and the mass of the scalar field, respectively.

Recently the importance of scalar fields has been recognized in cosmology. Many models of the inflationary universe have been constructed by assuming the existence of a scalar field called inflaton whose energy density causes the inflationary expansion.[3] A possibility that a part of the dark matter could be made up of bosonic particles has also been discussed in relation to the studies of primordial nucleosynthesis. It is then natural to ask the question if there exist gravitationally bound systems made up from such bosonic particles.

Since the situation for the scalar field is as mentioned above, some authors[4,5] began to re-construct equilibrium states of boson stars which consists of a complex scalar field coupled with gravity. It is important to note that, although metric components and the energy-momentum tensor of the scalar field for equilibrium models should be static, the

scalar field ϕ itself must depend on the time because it obeys the wave type equation. The time dependency of the scalar field is included by assuming that the field takes a form of $\phi(r,t) = \phi_0(r)e^{-i\omega t}$, where r is the radial coordinate and ω is the frequency of the scalar field. Under this assumption equilibrium states of scalar fields can be considered as standing waves. Thus there can be many energy levels for boson stars. In this paper we study only the behavior of the ground state of equilibrium configurations. The energy of the ground state of a boson star is the lowest and there is no node in the distribution of the scalar field along the radial direction.

As for the gravitational radiation emission from boson stars, Ferrell and Gleiser[6] calculated the amount of gravitational energy which is expected to release during the transition from an excited state to the ground state. Although their work is important in understanding connections between boson stars and ordinary stellar collapse, we are interested in the detailed information about the gravitational radiation from equilibrium configurations of boson stars. Such an information is obtained only by studying non-radial oscillations of boson stars in the framework of general relativity.

Moreover, since the gravitational wave observatories are expected to operate in the near future, it is important to have detailed knowledge about features of gravitational waves which are deeply related to the nature of sources and to study differences and similarities of gravitational waves from different kinds of sources. So far many authors have studied gravitational radiations from black holes[7,8] and neutron stars.[9-14] Since boson stars, if they exist, are potential sources of gravitational waves, we will study here boson stars, in particular non-radial pulsations and associated gravitational waves.

As the first step to the full analysis of non-radial oscillations of boson stars, Kojima, Yoshida and Futamase presented a formulation of non-radial pulsations of a boson star in the framework of general relativity.[15] They found that perturbations with odd parity do not couple with gravitational waves and that the set of equations reduces to a sixth-order differential equation for even parity modes. Therefore in this paper we consider only even parity perturbations. Since it is not practical to use their original formulation because of its numerical subtlety, we reformulate the perturbed equations so as to perform numerical integrations for even parity without difficulty.

2. Basic equations for perturbations

We assume the unperturbed state of a boson star is static and spherically symmetric. The equilibrium solution is given by a solution of the Einstein-Klein-Gordon equations whose appropriate boundary conditions it must satisfy. Detailed expression for the equilibrium configuration of a boson star is given by Yoshida et al.[16] and thus we do not write it down here.

Since the unperturbed state is spherical and static, the perturbed quantities can be decomposed by tensor harmonics for the angular variables θ and φ and by the Fourier expansion for the time t. Thus the normal modes are characterized by indices l and m of the tensor harmonics, the parity and the frequency σ. The metric in the Regge-Wheeler gauge[7,12] are given by

$$\begin{aligned} ds^2 = & e^{\nu}\left(-1+\mu^l H_0 Y_{lm} e^{-i\sigma t}\right) dt^2 - 2i\sigma r \mu^l H_1 Y_{lm} e^{-i\sigma t} dt dr \\ & + e^{\lambda}\left(1+\mu^l H_0 Y_{lm} e^{-i\sigma t}\right) dr^2 + r^2\left(1+\mu^l K Y_{lm} e^{-i\sigma t}\right)\left(d\theta^2+\sin^2\theta d\varphi^2\right), \end{aligned} \tag{2.1}$$

where the quantity μ is defined by

$$\mu = \begin{cases} r/R_s & 0 \le r < R_s, \\ 1 & r \ge R_s. \end{cases} \tag{2.2}$$

Here R_s is a radius of a boson star. The coefficient functions H_0, H_1 and K for the metric perturbation are functions of only the radial coordinate r. Here $Y_{lm}(\theta,\varphi)$ is the spherical harmonics. Note that this expression is valid for $l \ge 2$ and that we consider only even parity perturbations since gravitational waves couple only to that mode as discussed in the introduction.

For the scalar field we take the following form:

$$\phi = e^{-i\omega t}\left[\phi_0(r) + \left\{\mu^l \Phi_1(t,r) + i\left(\mu^l \dot{\Phi}_2(t,r)\right)\right\} Y_{lm}\right]. \tag{2.3}$$

Perturbed quantities Φ_1 and Φ_2 for scalar fields are expressed as follows:

$$\Phi_j(t,r) = \phi_j(r) e^{-i\sigma t}, \tag{2.4}$$

where $j = 1, 2$ and ϕ_j are the functions of only r and the dot denotes differentiation with respect to t.

By using the above expression, it is straightforward to calculate each component of the perturbed Einstein equation and the perturbed scalar field equation. Although there is a freedom of choice for the basic equations, we choose the following form of equations as our basic equations for even parity modes:

$$\begin{aligned} &\frac{d}{dr}\mathbf{X}(r) = A(r,l,\sigma)\,\mathbf{X}(r)\,, \quad L(\mathbf{X}) = 0\,, \\ &\mathbf{X}(r) = (Y,\, K,\, H_1,\, F_+,\, F_-,\, F_+{}',\, F_-{}')\,, \end{aligned} \tag{2.5}$$

where $Y \equiv (K - H_0)/r^2$, $F_\pm \equiv \phi_1 \pm \sigma\,\phi_2$ and the prim denotes differentiation with respect to r. Explicit expressions for above equations are given by Yoshida et al.[16] .

The above equations consist of a system of seven first order differential equations and one algebraic equation for Y, K, H_1, F_+, F_-, $F_+{}'$ and $F_-{}'$. Thus we can reduce these equations to six first order differential equations. This is clear contrast to the case of perfect fluid where basic equations can be reduced to a fourth-order differential equation. This difference comes from the fact that both real and imaginary parts of the perturbed scalar field are dynamical quantities of the matter.

i) Behavior of the solution at the center of the star

Due to the regularity of physical quantities at the center, there remain only three free parameters, $H_1(r=0)$ and $F_\pm(r=0)$. They have to be determined from other boundary conditions discussed later.

ii) Behavior of the solution outside the star

Outside the star, the magnitude of background scalar fields tends to zero very quickly so that the background geometry becomes almost the Schwarzschild space-time. We find that the system of Eqs.(2.5) is reduced to the system of perturbation equations for a Schwarzschild black hole derived by Zerilli,[8] if we set $\phi_0 = 0$. Thus we obtain the following second-order differential equation for the perturbed metric:

$$\left[e^{-\lambda}\frac{d}{dr}e^{-\lambda}\frac{d}{dr} + \sigma^2 - e^{-\lambda}\frac{2n^2(n+1)r^3 + 6n^2Mr^2 + 18nM^2r + 18M^3}{r^3(nr+3M)^2}\right]Z = 0\,, \tag{2.6}$$

where $n \equiv \frac{1}{2}(l+2)(l-1)$ and M is the mass of the boson star. The relation between the perturbed metric and the Zerilli function Z is written as follows:

$$\begin{aligned} e^{-\lambda}\frac{dZ}{dr} &\equiv e^{-\lambda}\frac{n(n+1)r^2 + 3nMr + 6M^2}{(nr+3M)^2}H_1 - \frac{nr^2 - 3nMr - 3M^2}{(nr+3M)^2}K\,, \\ Z &\equiv -e^{-\lambda}\frac{r^2}{nr+3M}H_1 + \frac{r^2}{nr+3M}K\,. \end{aligned} \tag{2.7}$$

For a large radius, the function Z in Eq.(2.6) behaves as

$$Z = A_{in}\exp(-i\sigma r_*) + A_{out}\exp(i\sigma r_*) + O[1/r]\,, \tag{2.8}$$

where $r_* = r + 2M\log(r-2M)$. The second term in Eq.(2.8) represents an outgoing gravitational wave, while the first term represents an incoming wave because we choose the time dependency of the form $e^{-i\sigma t}$ for the perturbed quantities.

Concerning the perturbed scalar fields, we have two second-order differential equations for a massive free scalar field around a Schwarzschild black hole.[17] Equations for perturbed scalar fields in Eqs.(2.5) reduce to Schrödinger-type wave equations as follows:

$$\left[e^{-\lambda}\frac{d}{dr}e^{-\lambda}\frac{d}{dr} + (\sigma\pm\omega)^2 - e^{-\lambda}\left(1+\frac{l(l+1)}{r^2}+\frac{2M}{r^3}\right)\right]G_\pm = 0\,, \tag{2.9}$$

where $G_\pm \equiv r\mu^l F_\pm$. As the radius becomes large, the functions $G_\pm$ in Eq.(2.9) behave as

$$G_\pm \sim B_{\pm in}\exp\left[-i\sqrt{(\sigma\pm\omega)^2-1}\,r_*\right] + B_{\pm out}\exp\left[i\sqrt{(\sigma\pm\omega)^2-1}\,r_*\right]. \tag{2.10}$$

Here we choose the branch of the square root with $Re(\sqrt{(\sigma\pm\omega)^2-1}) \geq 0$ if σ is complex.

iii) Physical boundary conditions

As discussed above, basic equations of our problem are seven first order differential equations. At the center of the star we can specify only four boundary conditions so that three solutions of seven independent solutions remain unfixed near the origin. In order to determine a unique and physically acceptable solution, we need to use other boundary conditions. We are interested in quasi-normal modes associated with the emission of the gravitational radiation and the scalar radiation, that is, oscillations *without incoming radiations.* Thus we require three more boundary conditions at spatial infinity, which represent no-incoming radiation conditions as follows:

$$\frac{A_{in}}{A_{out}} = \frac{B_{+in}}{B_{+out}} = \frac{B_{-in}}{B_{-out}} = 0\,. \tag{2.11}$$

Thus our problem forms an eigenvalue problem for σ and frequencies of quasi-normal modes will be discrete. Moreover they will be complex so that those modes represent damping oscillations due to the emission of the gravitational radiation and the scalar radiation.

As shown in the next chapter, imaginary parts of eigen frequencies are not so small that we cannot use the "resonance" scheme but need to use the WKB approximation or other scheme[14] to solve the Zerilli equation and the massive scalar perturbation equations outside the star. In this paper we adopt the WKB scheme because of its simplicity for numerical computations. This scheme was proposed by Kokkotas and Schutz[13] for searching w-modes of stars whose imaginary parts of frequencies are large.

3. Numerical results

We define the surface of the unperturbed boson star by the following condition. If the absolute value of the scalar field becomes less than a certain small value, we define the distance to that point as the radius of the boson star *for the perturbation analysis.* In the actual computations the surface distance R_s is defined by $\phi_0(R_s) \sim 5 \times 10^{-5}$. The matter outside the surface thus defined contributes little to the mass of the boson star. Thus for the region outside R_s we set the amplitude of the background scalar field to vanish so that the metric in that region reduces to the Schwarzschild metric.

Models of unperturbed boson stars are characterized by the central value of the scalar field. Physical quantities for models investigated in this paper are shown in Table 1. Here the mass, the frequency, the radius and the value of the scalar field at the surface are tabulated for three models: stable configuration (Model 1), marginal stable one (Model 2) and unstable one (Model 3) against small radial perturbations. Here we use the scalar field without self-interaction. And we only investigate a quadrupole oscillation $l = 2$ in this paper.

Also, in order to perform numerical integration easily, we solve equations only for the range of the positive real part of $(\sigma \pm \omega)^2 - 1$, which is expressed as $(Re(\sigma) \pm \omega)^2 - 1 - Im(\sigma)^2 > 0$. Here we use $Im(\sigma) < 0$ because we consider only stable solutions.

Obtained frequencies are very similar to w-modes of relativistic stellar models found by Kokkotas and Schutz[13] . The imaginary part of the frequency is plotted against the real part of the frequency in Fig. 1. From this figure we can see two important features of quasi-normal modes of boson stars. First, imaginary parts of frequencies are large. This is different from situation for f- and p-modes of relativistic stars. It implies that damping time scales are very short compared to those of ordinary stars. Secondly, difference of real parts of frequencies between any two nearest modes is almost the same as seen from this figure.

The absence of the above "orderly nature" for lower eigenvalues is probably due to numerical inaccuracies or a breakdown of the WKB approximation. Actually when $Re(\sigma) \sim \omega + 1$, iterations of our numerical procedure converge very slowly or do not converge. Therefore in this region it is very difficult to obtain eigenvalues, even if they exist.

In Fig. 2 the metric perturbation function H_1 and scalar field perturbation function F_- for the lowest and the second lowest frequencies of our results are plotted for the model with $\phi_0 = 0.1916$ (Model 2 in Table 1). In this figure we set the value of the function $K = 1$ at the center of the star. From this figure it is found that the amplitude of the metric perturbation is comparable to that of the scalar field perturbation. This feature of the eigen function is different from that of w-modes of ordinary stars.[13,14] This implies that quasi-normal modes of boson stars are different from w-modes, though they have eigen-frequencies with large imaginary parts.

These "peculiar" behaviors may come from the wave character of the scalar field. For ordinary stars, the perturbed quantities for the matter such as the density, the pressure, the velocity and so on as well as unperturbed quantities are confined to a finite region. On the contrary, perturbations for scalar fields extend to infinity, though we cut the unperturbed boson field at a finite radius. These behaviors of quasi-normal modes of boson stars can be explained by using a simple model with two strings connected by a spring.[16]

4. Conclusion

In order to study non-radial pulsations of boson stars and its associated gravitational waves, we have reformulated linearized perturbation equations around an equilibrium state of a boson star. We have written down basic perturbation equations for even parity mode. After that we have solved the basic equations numerically by specifying appropriate boundary conditions for *quasi-normal modes*.

The obtained results are different from those of perfect fluid stars in the following points: 1) $Im(\sigma)/Re(\sigma)$ is larger than that of f- and p-modes of perfect fluid stars. 2) Although $Im(\sigma)/Re(\sigma)$ is large, amplitudes of perturbations of the metric are comparable to those of perturbations of scalar fields. These can be clearly explained by the fact that the scalar field extends to infinity. Thus the quasi-normal mode found in this paper is a new mode which has not been found for normal stars.

In the present investigation, we have calculated quasi-normal modes for boson stars whose surfaces are defined rather artificially. If we use a different definition of the surface, we will

obtain slightly different eigen-frequencies, because the eigen frequencies depend crucially on the position of the surface or the boundary. This is clearly seen from the results of ordinary stars for which the determination of the precise boundary is essential to obtain precise values of frequencies. However, since the exact surface of the boson star is at infinity, we need to define the finite surface by some means. Moreover the field strength of the unperturbed boson fields decays exponentially. Thus we may neglect those fields far distant from the main part of the boson star, though it is not exact from the mathematical point of view. However, from the physical point of view, it is important to know the nature of the quasi-normal modes. Thus as far as differences which arise from different definitions of surfaces are of the order of a few percent, we can use our results to understand the behavior of quasi-normal modes of boson stars.

REFERENCES

1. R. Ruffini and S. Bonazzola, Phys. Rev. **187**, 1767 (1969).
2. D. J. Kaup, Phys. Rev. **172**, 1331 (1968).
3. K. Sato, Mon. Not. R. Astron. Soc. **195**, 467 (1981); Phys. Lett. **99B**, 66 (1981); A. H. Guth, Phys. Rev. D **23**, 347 (1981).
4. M. Colpi, S. L. Shapiro and I. Wasserman, Phys. Rev. Lett. **57**, 2485 (1986).
5. R. Friedberg, T. D. Lee and Y. Pang, Phys. Rev. D **35**, 3640 (1987).
6. R. Ferrell and M. Gleiser, Phys. Rev. D **40**, 2524 (1989).
7. T. Regge and J. A. Wheeler, Phys. Rev. **108**, 1063 (1957).
8. F. J. Zerilli, Phys. Rev. Lett. **24**, 737 (1970); Phys. Rev. D **2**, 2141 (1970).
9. K. S. Thorne and A. Campolattaro, Astrophys. J. **149**, 591 (1967); K. S. Thorne, Astrophys. J. **158**, 1 (1969).
10. T. Nakamura, K. Oohara and Y. Kojima, Prog. Theor. Phys. Suppl. **90**, (1987).
11. Y. Kojima, Prog. Theor. Phys. **79**, 665 (1988).
12. L. Lindblom and S. Detweiler, Astrophys. J. Suppl. **53**, 73 (1983); S. Detweiler and L. Lindblom, Astrophys. J. **292**, 12 (1985).
13. K. D. Kokkotas and B. F. Schutz, Mon. Not. R. Astron. Soc. **255**, 119 (1992).
14. M. Leins, H. P. Nollert and M. H. Soffel, Phys. Rev. D **48**, 3467 (1993).

15. Y. Kojima, S. Yoshida and T. Futamase, Prog. Theor. Phys. **86**, 401 (1991).

16. S. Yoshida, Y. Eriguchi and T. Futamase, Phys. Rev. D **50**, 6235 (1994).

17. L. E. Simone and C. M. Will, Class. Quantum Grav. **9**, 963 (1992).

Table 1

Model	$\phi_0(0)$ $[M_{pl}/\sqrt{4\pi}]$	M $[M_{pl}^2/m]$	ω $[m]$	R_s $[m^{-1}]$	$\phi_0(R_s)$ $[M_{pl}/\sqrt{4\pi}]$
Model 1	0.1000	0.584	0.9137	22.405	4.98E-05
Model 2	0.1916	0.633	0.8531	16.755	4.87E-05
Model 3	0.2500	0.622	0.8229	14.855	4.91E-05

Table 1 : Physical quantities of boson stars used in this paper are listed. M_{pl} and m are the Planck mass and the mass of the scalar field, respectively. Note that our scaling of scalar fields differ from that used by Gleiser[6] by a factor of $1/\sqrt{2}$.

Figure Captions

Figure 1 : The negative value of the imaginary part of the frequency, $-Im(\sigma)$, is plotted against the real part of the frequency, $Re(\sigma)$, for quasi-normal modes of $l = 2$ of boson stars. All frequencies are measured in units of the mass of scalar field m. Different curves and marks correspond to different unperturbed boson stars. Dotted curve and diamond marks denote quasi-normal frequencies for the stable model (Model 1) against radial perturbations. Dash-dotted curve and plus marks for those of the marginally stable model (Model 2). Long dashed-dotted curve and box marks for those of the unstable model (Model 3).

Figure 2 : Amplitudes of perturbation functions H_1 and F_- for two quasi-normal modes of Model 2 in Fig. 1 are plotted against the distance from the center. All functions are normalized so as to keep the value of the function K at the center of the star to be unity, i.e. $K(0) = 1$. It should be noted that the metric perturbation and the scalar perturbation are of the same order everywhere.

Fig.1

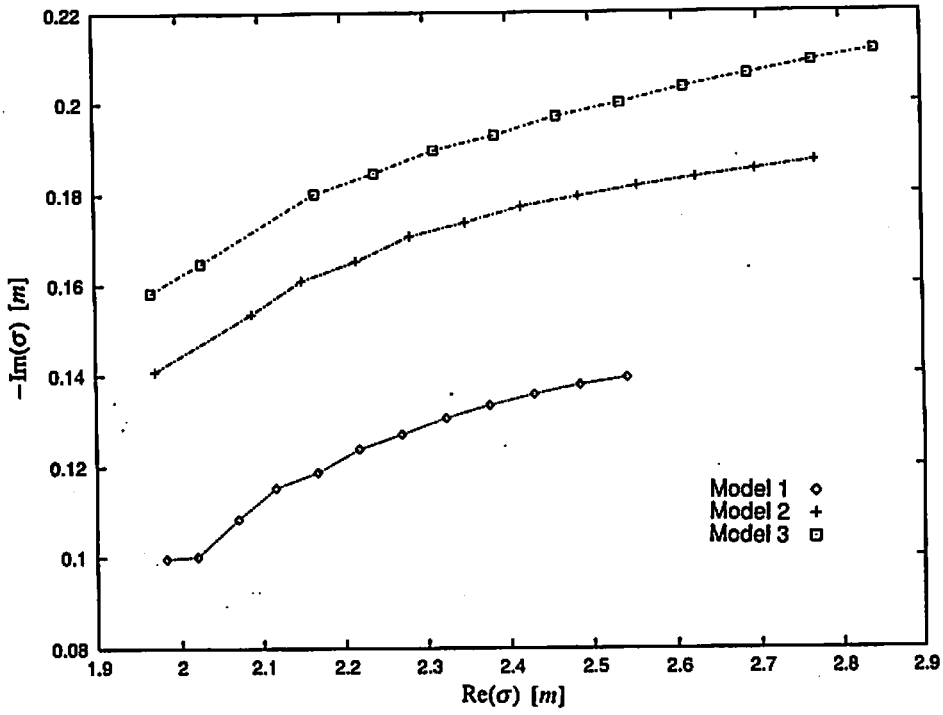
0.22
0.2
0.18
0.16
0.14
0.12
0.1
0.08
$-\mathrm{Im}(\sigma)$ [m]
1.9
2
2.1
2.2
2.3
2.4
2.5
2.6
2.7
2.8
2.9
$\mathrm{Re}(\sigma)$ [m]
Model 1
Model 2
Model 3

Fig.2

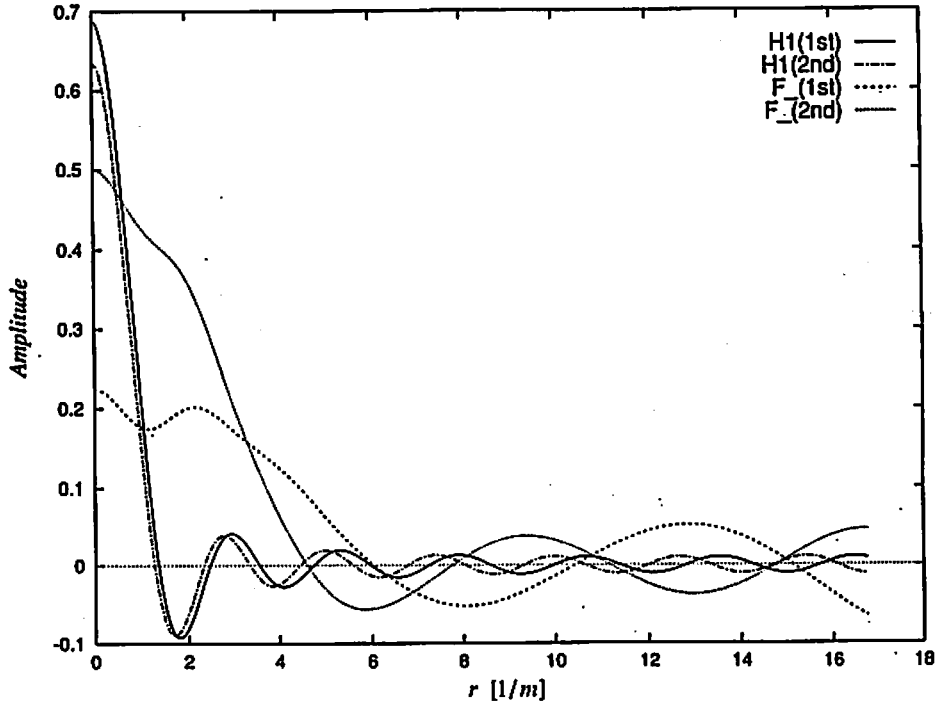
0.7
0.6
0.5
0.4
0.3
0.2
0.1
0
-0.1
Amplitude
0
2
4
6
8
10
12
14
16
18
r [$1/m$]
H1(1st)
H1(2nd)
F_(1st)
F_(2nd)

Non-radial oscillations of ultra compact stars [1]

Yasufumi Kojima

Department of Physics, Tokyo Metropolitan University,
Hachioji, Tokyo 192-03, Japan

ABSTRACT

Normal modes of polar perturbation in a highly compact star with uniform energy density are calculated. In the less compact stars, there is only one mode, the Kelvin f-mode, for each spherical harmonic index $l(\geq 2)$. Different resonance states become possible in sufficiently compact stars. The characteristic resonance frequencies agree with the counterparts regarding the axial mode. This oscillation is related to the gravitational waves, not to fluid motions, and hence there is no difference between axial and polar perturbations like in the perturbations of the Schwarzschild spacetime.

1. Introduction

In pulsations of a spherically symmetric star, the polar and axial modes are quite different. The former is coupled to the density and pressure perturbations, while the latter is never. The incident gravitational wave can induce the stellar pulsation and exhibits the resonance only in the polar mode in the Newtonian limit. Chandrasekhar and Ferrari (1991b) recently showed that this is not true in the relativistic case. If star is located inside the Regge-Wheeler potential peak, $\sim 3M$, gravitational waves can be trapped inside the barrier and the system exhibits resonances even in the axial mode. They calculated the quasi-normal frequencies for such resonance states in highly compact stars, $M/R > 0.41$, where M and R are the mass of radius of the star. Kokkotas (1994) calculated the higher overtone modes.

These modes are associated with the dynamical degree of freedom of gravitational waves. In the gravitational perturbation of the Schwarzschild black hole, the polar and axial perturbations are related each other by a certain transformation, and hence, the quasi-normal frequencies are exactly the same (e.g., Chandrasekhar 1983). Natural questions arise. What is the relation between the polar and axial perturbations in a compact star? Is there the polar mode corresponding to the axial mode found by Chandrasekhar & Ferrari (1991b) and Kokkotas (1994)? Do the characteristic frequencies coincide with the values of the axial modes, if exist?

In this paper, these problems are numerically examined in the stellar models with uniform energy density, for which compact stellar model is possible $M/R \leq 4/9$.

[1]This is based on Y. Kojima, N. Andersson and K. D. Kokkotas, *On the oscillation spectra of ultra compact stars,* submitted to Proc. Roy. Soc. London.

2. Equations of non-radial oscillations of the star with homogeneous energy density

The basic equations are summaried briefly in this section. The energy density ϱ is constant throughout the star in the equilibrium state. We also assume that the Eulerian change of the energy density is zero, $\delta\varrho = 0$. In the Newtonian pulsation theory, this approximation gives only one oscillation mode, the Kelvin f-modes. We use this approximation to avoid uninteresting fluid oscillations like p- and g- modes. The relativistic perturbation equations of the polar mode can be obtained by imposing $\delta\varrho = 0$, equivalently $C^{-2} = 0$, in eqs. (38)-(39) of Kojima (1992). The same notations will be used here. The basic equations inside the star are two second-order differential equations for certain components of the metric perturbations, $H_{0,l}$ and K_l. They are given by

$$
\begin{aligned}
&(K_l - H_{0,l})'' - \frac{e^\lambda}{r^2}[2r - 10M + \kappa(\varrho - 5p)r^3](K_l - H_{0,l})' \\
&+\frac{e^\lambda}{r^2}(\sigma^2 e^{-\nu} r^2 - 2n)(K_l - H_{0,l}) \\
&+\frac{4e^\lambda}{r^4}[3Mr - \kappa\varrho r^4 - e^\lambda(M + \kappa p r^3)^2]H_{0,l} = 0
\end{aligned} \tag{1}
$$

and

$$
\begin{aligned}
&K_l'' + \frac{e^\lambda}{r^2}[3r - 5M - \kappa\varrho r^3]K_l' - \frac{ne^\lambda}{r^2}K_l - \frac{1}{r}H_{0,l}' \\
&-\frac{e^\lambda}{r^3}[(n+2)r - 2\kappa\varrho r^3]H_{0,l} = 0,
\end{aligned} \tag{2}
$$

where the prime denotes derivative with respect to r. Near the center of the star, $r \sim 0$, the non-singular solutions for eqs. (1)-(2), have the form,

$$
K_l \sim r^l, \quad H_{0,l} - K_l \sim u r^{l+2}, \tag{3}
$$

where k and u are constants.

The Lagrangian change in pressure, Δp should vanish at the stellar surface. The Lagrangian change can be written as

$$
\begin{aligned}
2\sigma^2 e^{-\nu}\kappa\Delta p \;=\; & \frac{1}{e^\lambda r^4}[-\sigma^2 e^{-\nu} r^3 + e^\lambda(n+1)(M + \kappa p r^3)](K_l - H_{0,l})' \\
&+\frac{1}{r^6}[-\sigma^2 e^{-\nu} r^3(nr + 5M + 3\kappa p r^3) \\
&+2(n+1)e^\lambda(M + \kappa p r^3)^2](K_l - H_{0,l}) \\
&+\frac{1}{r^6}[\sigma^4 e^{-2\nu} r^6 + \sigma^2 e^{-\nu} r^2\{e^\lambda(M + \kappa p r^3)^2 + 4Mr + 2\kappa p r^4\} \\
&-2(n+1)e^\lambda(M + \kappa p r^3)^2]K_l.
\end{aligned} \tag{4}
$$

Outside the star in vacuum, the perturbation equations are reduced to a second-order differential equation. The solutions are a linear combination of out-going and in-coming waves at infinity;

$$\begin{aligned} K_l &\longrightarrow A_{out}\exp(i\sigma r^*) + A_{in}\exp(-i\sigma r^*), \\ H_{0,l} &\longrightarrow i\sigma(r+2M)\{A_{out}\exp(i\sigma r^*) - A_{in}\exp(-i\sigma r^*)\}, \end{aligned} \tag{5}$$

where r^* denotes tortoise coordinate, and A_{in}, A_{out}, are constants, which represent the amplitudes of the in-coming and out-going gravitational waves at infinity. We impose out-going wave condition at infinity, i.e., $A_{in} = 0$. This condition is satisfied only for a discrete set of complex frequencies in general. We use the usual resonance method to get the complex eigen-frequencies (e.g., Chandrasekhar & Ferrari 1991a). That is, assuming the small imaginary part of the eigen-value, we calculate $|A_{in}|$ for real numbers of σ. The curve of $|A_{in}|$ exhibits a deep minimum as $|A_{in}|^2 = \text{const}\ \{(\sigma - \sigma_R)^2 + \sigma_I^2\}$. From the minimum, we have σ_R and σ_I, which correspond to the real and imaginary parts of a complex eigen-frequency. This method is valid only for the solution with small imaginary part. Different technique is necessary to get other class of solutions, like w-modes (gravitational *w*ave modes, Kokkotas & Schutz 1992) in which the imaginary part is comparable to the real part. We therefore limit our calculation to eigen-frequencies with small imaginary part in this paper.

3. Numerical calculation of characteristic frequencies

Normal frequencies of $l = 2$ are calculated and the results are given in this section. In Fig.1, the amplitude of in-coming wave $|A_{in}|$ is shown as a function of real frequency σ. One resonance minimum is evident in the stellar model with $M/R = 0.2$. The oscillation frequency is $\sigma_R(R^3/M)^{1/2} = 0.887$. In the Newtonian limit, $M/R \to 0$, the value tends to the frequency of the Kelvin f-mode, $\sigma_R(R^3/M)^{1/2} = \sqrt{2l(l-1)/(2l+1)} = 0.894$ (e.g., Tassoul 1978). In this way, there is only one oscillation mode in less compact stars as expected from Newtonian pulsation theory.

There is a tiny dent at $\sigma(R^3/M)^{1/2} \sim 1.7$ in the model with $M/R = 0.40$. The minimum becomes evident in the model with $M/R = 0.42$, although the frequency is shifted to $\sigma(R^3/M)^{1/2} \sim 1.3$. The new resonance mode is possible for $M/R \geq 0.4$. This criterion is almost the same as obtained in the axial mode (Chandrasekhar & Ferrari 1991b). Notice that this critical value depends on the numerical technique of the normal frequency calculation. The resonance point near $\sigma(R^3/M)^{1/2} \sim 1.7$ in the model with $M/R = 0.40$ is so ambiguous that reliable conclusion is impossible only by our numerical method. If it is possible to determine the characteristic frequency by a different method, the critical compactness M/R may be reduced.

As the star becomes more compact, lots of resonance states are evident as shown in the model with $M/R = 0.44$. The number of the evident resonance states increases with the compactness. The number of the resonance states also depends on the numerical method.

Kokkotas (1994) calculated lots of higher overtone modes using the WKB method. The imaginary part of those modes is so large that the present method can not calculate the modes. Further study is necessary to know the whole spectrum of the resonance states.

In Fig.2, the normal frequencies of the polar perturbation are shown as a function of M/R. The frequencies obtained in the axial one are also denoted. Our numerical calculation is limited up to $\sigma_I/\sigma_R \sim 0.01$, since the minimum of the amplitude $|A_{in}|$ becomes less clear as the star becomes less compact. We have also limited to $M/R \sim 0.44$. This value is slightly smaller than the extreme case $M/R = 4/9 = 0.444\cdots$. As the star becomes more compact, the mode crossing between the f-mode and gravitational wave mode occurs near $M/R = 0.44$ as inferred from Fig.2. Two minimums of $|A_{in}|$ merge there, so that it is inaccurate to calculate the frequencies near the crossing point.

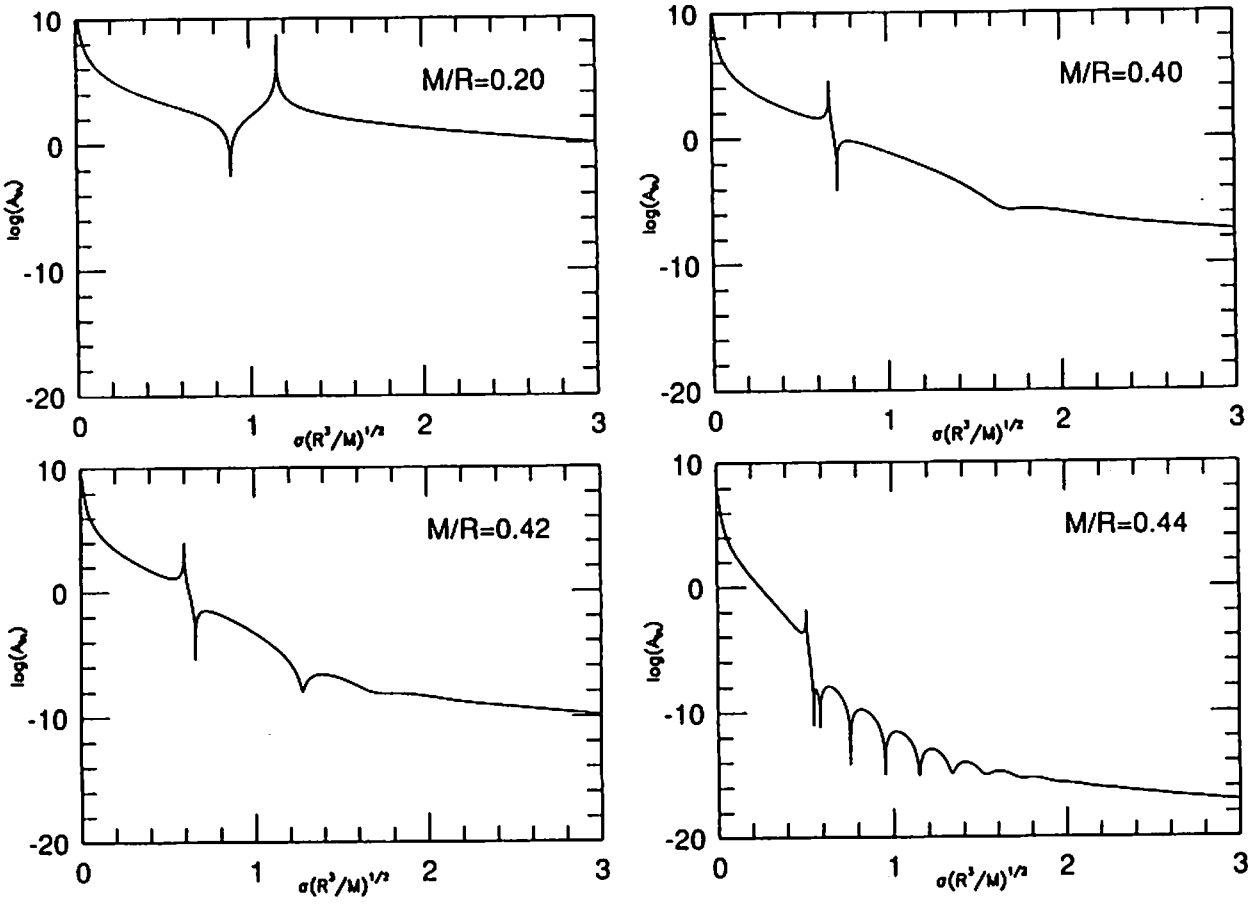

Fig.1. The amplitude of the incoming gravitational wave, $|A_{in}|$ as a function of frequency, $\sigma(R^3/M)^{1/2}$ for different stellar models. From the minimums, the quasi-normal frequencies can be calculated.

The agreement between the polar and axial modes is fairly good for all cases. The somewhat larger discrepancies in the imaginary part are due to the numerical accuracy. Outside the star, both polar and axial perturbations can be described by the Regge-Wheeler equation. When the stellar surface is smaller than the peak radius of the potential barrier, gravitational wave is temporarily trapped inside the barrier and gradually decayed. The complex eigen-frequency represents such situation. As the star becomes more compact, the decay rate, i.e., the imaginary part, decreases because of the deeper potential well. This mechanism is inherent in the gravitational wave irrespective of the fluid motions, and hence works in a similar way in the polar and axial perturbations.

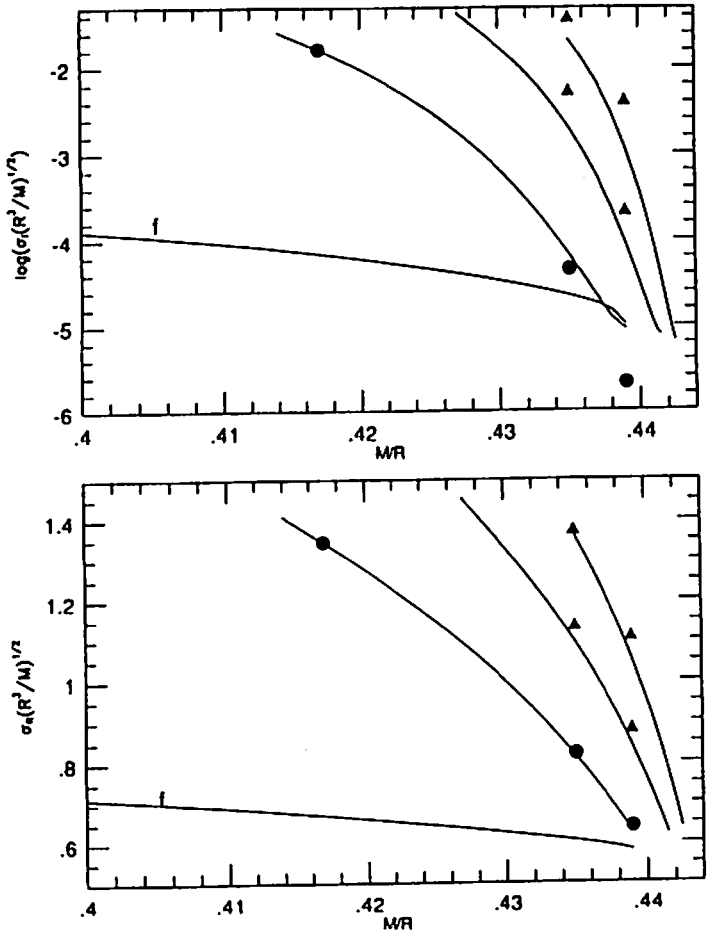

Fig.2. The quasi-normal frequency of the polar perturbation as a function of the compactness M/R. The upper panel shows the imaginary part and the lower one the real part. The dots represent the values of the lowest mode of the axial perturbation obtained by Chandrasekhar & Ferrari (1991b) and the triangles those of the higher modes by Kokkotas (1994). The line indicated by f is the quasi-normal frequency of the Kelvin f-mode.

4. Concluding remarks

We have confirmed the similar quasi-normal modes in the polar perturbation corresponding to those in the axial perturbation in the previous section. The characteristic frequencies are the same as those of the axial mode within the numerical accuracy. These modes are mainly related to dynamical freedom of gravitational waves, and hence there is no essential difference between the polar and axial modes like in the perturbations of Schwarzschild black hole. The characteristic frequencies are however quite different from the quasi-normal frequencies of the black hole.

These modes resemble the w-modes found in the polar perturbation (Kojima 1988, Kokkotas & Schutz 1992) in a sense that gravitational waves play an essential role. The decay rate is comparable to the oscillation frequency in the w-modes of a typical star $M/R \sim 0.2$. As inferred from Fig.2, the imaginary part of the new modes exponentially increases with decrease of M/R. The modes may be connected to the w-modes in the less compact star. If this is true, what happens in the axial perturbation? There are no w-modes in the axial perturbation because the coupling with matter is necessary as suggested in a simple toy model (Kokkotas & Schutz 1986). It is necessary to calculate eigen-frequency with large decay rate, but the problem is beyond this work.

Finally, although the ultra compact stars considered here are astrophysically unrealistic, the normal frequencies of them may be useful as a clue of understanding whole spectrum of the oscillation modes in relativistic stars.

Acknowledgment

This work stemmed from inspiring concern of Prof. S. Chandrasekhar at the MG7 meeting. I am grateful to Nils Andersson for useful comments. This work was supported in part by the Japanese Grant-in-Aid for Scientific Research on Priority Area (03250212, 04234104, 04234209, 05218208).

REFERENCES

Chandrasekhar, S. 1983 *The mathematical theory of black holes* Oxford: Clarendon Press.
Chandrasekhar, S. & Ferrari, V. 1991a Proc. R. Soc. Lond. A **432**, 247-249.
Chandrasekhar, S. & Ferrari, V. 1991b Proc. R. Soc. Lond. A **434**, 449-457.
Kokkotas, K.D., 1994 Mon. Not. Roy. Astr. Soc, **268**, 1015-1018.
Kokkotas , K.D., & Schutz B.F., 1986 Gen. Rel. and Grav., **18**, 913-921.
Kokkotas , K.D., & Schutz B.F., 1992 Mon. Not. Roy. Astr. Soc, **255**, 119-128.
Kojima, Y., 1988 Prog. Theor. Phys. **79**, 665-675.
Kojima, Y., 1992 Phys. Rev. D. **46**, 4289-4303.
Tassoul, J., 1978 *The theory of rotating stars* Princeton: Princeton Univ. Press.

Evolution of Pure Gravitational Waves in 3D Numerical Relativity

MASARU SHIBATA

Department of Earth and Space Science, Faculty of Science, Osaka University, Toyonaka, Osaka 560, Japan

and

TAKASHI NAKAMURA

Yukawa Institute for Theoretical Physics Kyoto University, Kyoto 606-01, Japan

ABSTRACT

Using the technique of the three dimensional(3D) numerical relativity, we have simulated the dynamical evolution of pure gravitational waves. We use the conformal flat and $K = 0$ initial condition for the evolution of the spacetime. To test the slice conditions, we adopt several slices. We find that the geodesic slice($\alpha = 1$) is not appropriate for the evolution of the above initial condition. On the other hand, the harmonic slice works well even for initial conditions with high(and not too high) amplitude gravitational waves. As in the axisymmetric case, also in the 3D case, gravitational waves with a sufficiently high amplitude collapse by their self-gravity and the collapsed gravitational waves seem to form a black hole. In this case, the singularity avoidance property of the harmonic slice seems weak, so that it may be inappropriate for the formation problems of the black hole. By means of the gauge invariant wave extraction technique, we see the wave form of gravitational waves at the outer region. We find that the non-linearity of the Einstein gravity induces the higher multipole modes even if the only quadrupole mode exists initially.

1. Introduction

Gravitational waves from the last a few minutes of coalescing binary systems[1](neutron star-neutron star, black hole-neutron star and black hole-black hole binaries) are main targets of the kilometer-size Laser Interferometric Gravitational Wave Observatory(LIGO)[2]and VIRGO[3]. These binaries first emit periodic gravitational waves because their orbits will be circular. During this stage, the emission time scale of gravitational waves is much longer than that of the orbital period, so that we may assume the adiabatic evolution of the binary. Hence, "mild" gravitational waves are emitted in this stage. However, once the two stars in the binary approach up to $\sim 6-8M$, where M is the total mass of the binary, they can not maintain the circular orbit because the centrifugal force can not be balanced with the strong relativistic gravity[4]. At this stage, the circular orbit of binary changes to the plunge one, and finally they merge and will become a rotating black hole in a few milli-second. In such a process, much gravitational waves will be emitted violently[5]and they are just general relativistic in contrast to periodic gravitational waves emitted during the inspiral stage. This means that the gravitational waves trace the strong gravitational field and the fast motion of the matter there. Hence, if we can detect such gravitational waves by LIGO and VIRGO, we will be able to see a strong gravitational field, that is impossible by many other observations.

Such gravitational waves, however, have the frequency of ~kHz, so that the sensitivity of the laser interferometric detectors will be not so high(the signal-to-noise ratio is at most 10) even for the advanced LIGO[2]. To confirm the detection of such signal of gravitational waves, we have to prepare the theoretical template of gravitational waves which can be compared with the detected signal of gravitational waves. Here, any approximations for general relativity break down to calculate gravitational waves at the binary merging. We must solve the fully general relativistic equation without any approximations. Therefore, we need to perform the fully general relativistic three dimensional(3D) numerical simulation of coalescing binaries to obtain the wave form of gravitational waves with a sufficient accuracy. This paper is an effort toward the success of such a simulation.

In 3D numerical relativity, there are several points to be developed. One of them is the choice of the appropriate coordinate conditions, such as a spatial gauge and a slice, and another is the establishment of the method to extract gravitational waves from the 3D metric. As for the spatial gauge, we require that it escapes the appearance of coordinate singularity as well as it deletes the spurious gauge modes. The minimal distortion(MD)

gauge was proposed by Smarr and York[6]sixteen years ago as a spatial gauge which has the required property. However to adopt it, we must solve the complicated vector Laplacian equation and no one has tried to use it except for the spherically symmetric calculations. Recently, Nakamura used a similar type gauge to the MD gauge for the test simulations of merging binary neutron stars, rotating core collapse and so on, and made sure that this type of the gauge is a good gauge[7]. Therefore we should make a thorough investigation of the MD-type gauge although we do not pursue this problem any more in this paper.

As for the slice, there are several slices proposed. The maximal slice ($K = 0$) is a well-known slice which has the singularity avoidance property. However to adopt this slice, we need to solve a 3D elliptical equation, that is somewhat troublesome. In addition, it is not appropriate to see gravitational waves in the wave zone because the spurious gauge wave in the wave zone behaves like $\propto r^{-1}$[8]. Shibata and Nakamura proposed the conformal slice which seems to be appropriate to see gravitational waves in the wave zone as well as which has the singularity avoidance property for the formation problem of the black hole[8]. Nakamura used the conformal slice for simulations of merging binary neutron stars and rotating core collapse, and found that the conformal slice has an excellent property to see gravitational waves in the wave zone[7]. However as shown in section 4.2 and appendix A, this slice is not almighty and can be used only in a restricted case. Furthermore, even in the restricted cases, we need to solve a 3D elliptical equation for the conformal factor to use the conformal slice. If possible, we like to avoid to solve 3D elliptical equations. Recently, the harmonic slice($\Box\, t = 0$) has been proposed[9]. The harmonic slice seems to have the singularity avoidance property[9], and is very tractable because we have only to solve the evolution equation for the lapse function which is the same type equation as that for the 3D metric. However, this slice has not been investigated so much compared with other slices and the detailed properties have not been known. We should clarify how situations we can use this slice. In this way, we should research several slices in more detail and compare them.

As for the wave extraction, recently, the gauge invariant wave extraction technique has been developed by NCSA group[10]. In their method, they assume that the numerically calculated spacetime metric in the wave zone can be split into the Schwarzschild metric and the metric of the linear part. Then, they calculate the gauge invariant quantity from the linear part. Using this technique, they calculated the quasi-normal modes clearly in their axisymmetric calculation of black hole spacetimes. We need to extend this technique to the

3D calculation to see the wave form clearly.

For those purposes, we simulate the evolution of the 3D vacuum spacetime composed of gravitational waves in this paper. To check the slice and to investigate that the wave extraction technique works well for various situations, we consider high amplitude gravitational waves as well as low amplitude one. The paper is organized as follows. We describe the basic equations as well as the boundary conditions and the numerical methods in section 2. In section 3, we show the conformal flat and $K = 0$ initial conditions of gravitational waves. In section 4, we investigate the property of several slices. In this paper we adopt the geodesic slice($\alpha = 1$), harmonic slice, and the maximal slice. We show the advantages and disadvantages of them, briefly. In section 5, we show the methods for the analysis and numerical results. Section 6 is devoted to summary.

Throughout this paper, we use the units of $c = 1$, and Greek and Latin indices take $0, 1, 2, 3$ and $i = 1, 2, 3$, respectively.

2. Formulation

In this paper, the basic equation is the vacuum Einstein equation as

$$G_{\mu\nu} = 0. \tag{2.1}$$

We solve this equation imposing no symmetries except for equatorial plane symmetry. To solve the Eq.(2.1), we use the (3+1) formalism and write the line element as

$$ds^2 = -(\alpha^2 - \beta_i\beta^i)dt^2 + 2\beta_i dt dx^i + \gamma_{ij} dx^i dx^j, \tag{2.2}$$

where α, β^i and γ_{ij} are the lapse function, shift vector and metric on 3D hypersurface, respectively. Using the (3+1) formalism, the Einstein equation is split into the constraint equations and the evolution equations. The formers are the so-called Hamiltonian and momentum constraints which respectively become

$$R - K_{ij}K^{ij} + K^2 = 0, \tag{2.3}$$

$$D_i K^i{}_j - D_j K = 0, \tag{2.4}$$

where K_{ij}, K, R and D_i are the extrinsic curvature, the trace part of K_{ij}, the scalar curvature of a 3D hypersurface and the covariant derivative with respect of γ_{ij}. Evolution

equations for the metric and extrinsic curvature are respectively

$$\frac{\partial}{\partial t}\gamma_{ij} = -2\alpha K_{ij} + D_i\beta_j + D_j\beta_i, \tag{2.5}$$

$$\begin{aligned}\frac{\partial}{\partial t}K_{ij} &= \alpha(R_{ij} + KK_{ij} - 2K_{il}K^l{}_j) - D_iD_j\alpha \\ &\quad + (D_j\beta^m)K_{mi} + (D_i\beta^m)K_{mj} + \beta^m D_m K_{ij},\end{aligned} \tag{2.6}$$

$$\frac{\partial}{\partial t}\ln(\gamma) = -2\alpha K + 2D_i\beta^i, \tag{2.7}$$

$$\frac{\partial}{\partial t}K = \alpha(R + K^2) - D^iD_i\alpha + \beta^j D_j K, \tag{2.8}$$

where R_{ij} and γ are the Ricci tensor with respect to γ_{ij} and determinant of γ_{ij}, respectively. Hereafter we use $\phi = \ln(\gamma)/12$ instead of γ.

Although it is possible to treat these evolution equations for numerical integration, in our numerical code we solve $\tilde{\gamma}_{ij} = \exp(-4\phi)\gamma_{ij}$ instead of γ_{ij} for convenience. Here we define $\det(\tilde{\gamma}_{ij}) = 1$. We also define $\tilde{A}_{ij}$ as

$$\tilde{A}_{ij} \equiv \exp(-4\phi)A_{ij} \equiv \exp(-4\phi)\Big(K_{ij} - \frac{1}{3}\gamma_{ij}K\Big). \tag{2.9}$$

We should note that in our notation, indices of $\tilde{A}_{ij}$ are raised and lowered by $\tilde{\gamma}_{ij}$, so that the relations, $\tilde{A}^i{}_j = A^i{}_j$ and $\tilde{A}^{ij} = \exp(4\phi)A^{ij}$, hold. Using these variables, the evolution equations (2.5)-(2.8) can be rewritten as follows;

$$\frac{d}{dt}\tilde{\gamma}_{ij} = -2\alpha\tilde{A}_{ij} + \tilde{\gamma}_{il}\frac{\partial\beta^l}{\partial x^j} + \tilde{\gamma}_{jl}\frac{\partial\beta^l}{\partial x^i} - \frac{2}{3}\tilde{\gamma}_{ij}\frac{\partial\beta^l}{\partial x^l}, \tag{2.10}$$

$$\begin{aligned}\frac{d}{dt}\tilde{A}_{ij} &= \exp(-4\phi)\Big[\alpha\Big(R_{ij} - \frac{1}{3}\gamma_{ij}R\Big) - \Big(D_iD_j\alpha - \frac{1}{3}\gamma_{ij}D^kD_k\alpha\Big)\Big] \\ &\quad + \alpha(K\tilde{A}_{ij} - 2\tilde{A}_{il}\tilde{A}^l{}_j) + \frac{\partial\beta^m}{\partial x^i}\tilde{A}_{mj} + \frac{\partial\beta^m}{\partial x^j}\tilde{A}_{mi} - \frac{2}{3}\frac{\partial\beta^m}{\partial x^m}\tilde{A}_{ij},\end{aligned} \tag{2.11}$$

$$\frac{d}{dt}\phi = \frac{1}{6}\Big(-\alpha K + \frac{\partial\beta^i}{\partial x^i}\Big), \tag{2.12}$$

$$\frac{d}{dt}K = \alpha\Big(\tilde{A}_{ij}\tilde{A}^{ij} + \frac{1}{3}K^2\Big) - D^iD_i\alpha, \tag{2.13}$$

where

$$\frac{d}{dt} = \frac{\partial}{\partial t} - \beta^i\frac{\partial}{\partial x^i}. \tag{2.14}$$

Now let us consider R_{ij} which is the main source term of the evolution equation for $\tilde{A}_{ij}$.

First we split R_{ij} into two parts as

$$R_{ij} = \tilde{R}_{ij} + R^{\phi}_{ij}, \tag{2.15}$$

where $\tilde{R}_{ij}$ is the Ricci tensor with respect to $\tilde{\gamma}_{ij}$,

$$R^{\phi}_{ij} = -2\tilde{D}_i\tilde{D}_j\phi - 2\tilde{\gamma}_{ij}\tilde{D}^k\tilde{D}_k\phi + 4(\tilde{D}_i\phi)(\tilde{D}_j\phi) - 4\tilde{\gamma}_{ij}(\tilde{D}_k\phi)(\tilde{D}^k\phi). \tag{2.16}$$

and $\tilde{D}_i$ is the covariant derivative with respect to $\tilde{\gamma}_{ij}$. Using the property of $\det(\tilde{\gamma}_{ij}) = 1$, $\tilde{R}_{ij}$ is written as

$$\tilde{R}_{ij} = \frac{1}{2}\Big[\tilde{\gamma}^{kl}(\tilde{\gamma}_{lj,ik} + \tilde{\gamma}_{li,jk} - \tilde{\gamma}_{ij,lk}) + \tilde{\gamma}^{kl}{}_{,k}(\tilde{\gamma}_{lj,i} + \tilde{\gamma}_{li,j} - \tilde{\gamma}_{ij,l})\Big] - \tilde{\Gamma}^l_{kj}\tilde{\Gamma}^k_{li}\ , \tag{2.17}$$

where $_{,i}$ denotes $\partial/\partial x^i$ and $\tilde{\Gamma}^k_{ij}$ is the Christoffel symbol with respect to $\tilde{\gamma}_{ij}$. Following Nakamura[11], we split $\tilde{\gamma}_{ij}$ and $\tilde{\gamma}^{ij}$ as $\eta_{ij} + h_{ij}$ and $\eta^{ij} + f^{ij}$, where η_{ij} denotes the Minkowski geometry, and rewrite $\tilde{R}_{ij}$ as

$$\begin{aligned}\tilde{R}_{ij} = \frac{1}{2}\Big[&-h_{ij,kk} + h_{jl,li} + h_{il,lj} + f^{kl}{}_{,k}(h_{lj,i} + h_{li,j} - h_{ij,l}) \\ &+ f^{kl}(h_{lj,ik} + h_{li,jk} - h_{ij,lk})\Big] - \tilde{\Gamma}^l_{kj}\tilde{\Gamma}^k_{li}\ .\end{aligned} \tag{2.18}$$

As shown by Nakamura[11], the first term is the main part of the wave equation, that is, in the linear approximation of the vacuum Einstein equation, it only appears irrespective of the gauge condition. The other terms are non-linear terms or gauge terms in the linear approximation, i.e., the second and third terms are the gauge terms or have essentially the non-linear nature. This is because the source terms of the evolution equation for $h_{ij,j}$ are either the non-linear terms or the gauge terms, and if we take the linear approximation, we can set them zero. To guarantee the non-linearity of them as well as to avoid the appearance of the spurious wave terms, we introduce a new variable as

$$F_i \equiv h_{ij,j}, \tag{2.19}$$

and rewrite the second and third terms of $\tilde{R}_{ij}$ as $F_{i,j} + F_{j,i}$. Using the momentum constraint equation, the evolution equation of F_i can be written as

$$\begin{aligned}\frac{d}{dt}F_i = 2\alpha\Big(&f^{kj}\tilde{A}_{ik,j} + f^{kj}{}_{,j}\tilde{A}_{ik} - \frac{1}{2}\tilde{A}^{jl}h_{lj,i} + 6\phi_{,k}\tilde{A}^k{}_i - \frac{2}{3}K_{,i}\Big) \\ &- 2\alpha_{,j}\tilde{A}_{ij} + \beta^k{}_{,j}h_{ij,k} + (\tilde{\gamma}_{il}\beta^l{}_{,j} + \tilde{\gamma}_{jl}\beta^l{}_{,i} - \frac{2}{3}\tilde{\gamma}_{ij}\beta^l{}_{,l})_{,j}\ .\end{aligned} \tag{2.20}$$

Eqs.(2.10)-(2.13) and (2.20) are the evolution equations to be solved.

To solve them, we must give some slice and spatial gauge conditions for α and β^i, respectively. In our numerical code, any choices of the slice and spatial gauge conditions are possible. However in the present paper, we choose $\beta^i = 0$ as the spatial gauge condition because any troubles such as an appearance of the coordinate singularity are not expected in the dynamical evolution of gravitational waves even if we choose such a simple condition. If we perform, for example, the simulation of coalescing binary neutron stars, we should consider an appropriate spatial gauge conditions such as minimal distortion gauge[7]. On the other hand, we adopt several slice conditions to test them; geodesic slice, harmonic slice, algebraic slice similar to the harmonic slice($\alpha \propto \exp(n\phi)$, n is an integer) and maximal slice. We discuss their properties in the subsequent section(see below).

In the numerical simulation, we use the Cartesian grid, so the components of the metric and extrinsic curvature which appear in the numerical code are $\tilde{\gamma}_{xx}, \tilde{\gamma}_{xy}, \ldots$ and $\tilde{A}_{xx}, \tilde{A}_{xy}, \ldots$. Since we assume equatorial plane symmetry, the following relations of symmetry hold;

$$\begin{aligned}
&\phi(z) = \phi(-z), && \alpha(z) = \alpha(-z), \\
&\tilde{\gamma}_{ab}(z) = \tilde{\gamma}_{ab}(-z), && \tilde{\gamma}_{zz}(z) = \tilde{\gamma}_{zz}(-z), \\
&\tilde{A}_{ab}(z) = \tilde{A}_{ab}(-z), && \tilde{A}_{zz}(z) = \tilde{A}_{zz}(-z), \\
&\tilde{\gamma}_{az}(z) = -\tilde{\gamma}_{az}(-z), && \tilde{A}_{az}(z) = -\tilde{A}_{az}(-z), \\
&F_a(z) = F_a(-z), && F_z(z) = -F_z(-z),
\end{aligned} \tag{2.21}$$

where a and b denote x or y.

As for the outer boundary condition, we use the following one for $\tilde{\gamma}_{ij}$, F_i, ϕ and $\tilde{A}_{ij}$;

$$rQ(u) = \text{constant}, \tag{2.22}$$

where Q denotes geometric quantities, and we define u as

$$u = \alpha t - \exp(2\phi) r. \tag{2.23}$$

More explicitly,

$$Q(t, r) = \left(1 - \frac{\Delta r}{r}\right) Q(t - \Delta t, r - \Delta r), \tag{2.24}$$

where Δt is the time step in the simulation, and $\Delta r = \alpha \exp(-2\phi)\Delta t$. In practice, $Q(t - \Delta t, r - \Delta r)$ is obtained by the interpolation from the nearby mesh points. We note that this

condition can be interpreted not only as the outgoing boundary condition for the wave, but also as the boundary condition for $1/r$ potential. This is because in the case of $Q(t-\Delta t, r) = Q(t, r)$ =constant, Eq.(2.22) becomes $Q(r)r$ =constant.

In numerical code, we use the second order finite difference for $\partial/\partial x^i$ such as

$$\begin{aligned} \frac{\partial}{\partial x} &\rightarrow \frac{1}{x_{i+1}-x_{i-1}}\Big(\frac{Q_{i+1}-Q_i}{x_{i+1}-x_i}(x_i-x_{i-1})+\frac{Q_i-Q_{i-1}}{x_i-x_{i-1}}(x_{i+1}-x_i)\Big), \\ \frac{\partial^2}{\partial x^2} &\rightarrow \frac{2}{x_{i+1}-x_{i-1}}\Big(\frac{Q_{i+1}-Q_i}{x_{i+1}-x_i}-\frac{Q_i-Q_{i-1}}{x_i-x_{i-1}}\Big). \end{aligned} \tag{2.25}$$

The grid points are determined by the rule as

$$\begin{aligned} x_i &= x_{i-1}+w(x_{i-1}-x_{i-2}), \\ y_j &= y_{j-1}+w(y_{j-1}-y_{j-2}), \\ z_k &= z_{k-1}+w(z_{k-1}-z_{k-2}), \end{aligned} \tag{2.26}$$

where w is a constant with $w \geq 1$. Usually, we use $w = 1$, but we find that for $w \neq 1$, the numerical accuracy is as good as that for $w = 1$. The grid covers $-x_{max} \leq x \leq x_{max}$, $-y_{max} \leq x \leq y_{max}$ and $0 \leq z \leq z_{max}$. We fix x_{max}, y_{max} and z_{max} as $4 \sim 5r_0$, where r_0 is a width of the wave packet(see section 3). As for the grid numbers, we take $(N_x, N_y, N_z) = (59, 59, 30)$ mesh points typically. In this case, we use a YHP 715-50 work station. We also perform simulations on the FACOM VP-2600(in data processing center of Kyoto University) taking $(121, 121, 61)$ mesh points in order to see the dependence on the grid number and resolution, but the results does not change so much. In the typical case, the memory required is about 30 Mbytes and the computational time on a YHP 715-50 work station is about 10 hours for 2000 time steps.

For the numerical time evolution, we use the leapflog method[12]; we put $\tilde{\gamma}_{ij}$, F_i, ϕ and α on t, $t+\Delta t$, $t+2\Delta t, \ldots$ and put $\tilde{A}_{ij}$ and K on $t+0.5\Delta t$, $t+1.5\Delta t, \ldots$.

3. Initial Condition for Gravitational Waves

In this section, we consider the initial condition for pure gravitational waves. To give the initial condition, we must solve the constraint equations, Eqs.(2.3) and (2.4). Using the

conformal factor $\psi = \exp(\phi)$, Eq.(2.3) is written as

$$\tilde{\Delta}\psi = \frac{1}{8}\Big[\tilde{R}_j^{\ j}\psi - (\tilde{A}_{ij}\tilde{A}^{ij} - \frac{2}{3}K^2)\psi^5\Big], \tag{3.1}$$

where $\tilde{\Delta} = \tilde{D}_k\tilde{D}^k$ is the Laplacian with respect to $\tilde{\gamma}_{ij}$. Using $\tilde{D}_i$ instead of D_i, Eq.(2.4) is also rewritten as

$$\tilde{D}_i(\hat{A}^i{}_j) - \frac{2}{3}\psi^6\tilde{D}_jK = 0, \tag{3.2}$$

where $\hat{A}^i{}_j \equiv \psi^6\tilde{A}^i{}_j$. Note that indices of $\hat{A}^i{}_j$ are raised and lowered by $\tilde{\gamma}^{ij}$ and $\tilde{\gamma}_{ij}$, respectively.

One of the most simple choices to set the initial condition for the vacuum Einstein equation is to consider the conformal flat, $\tilde{\gamma}_{ij} = \eta_{ij}$ and $K = 0$ slice, initially. In this case, we have only to consider the initial form of the tracefree extrinsic curvature(i.e., $\tilde{A}_{ij}$) and the conformal factor. Nakamura derived such initial conditions as well as the general solution of the the linearized vacuum Einstein equation[11]to compare the numerical solution with the analytical one. (Hereafter we call the solution of this type the TT wave.) The solutions of the linearized TT wave for $\hat{A}_{ij}$ are composed of two independent modes, even and odd parity modes, but in this paper, we consider only the even parity mode of the TT waves, which is written as

$$\hat{A}_{ij} = \sum_{lm}\begin{pmatrix} a_{lm}Y_{lm} & b_{lm}Y_{lm,\theta} & b_{lm}Y_{lm,\varphi} \\ * & g_{lm}Y_{lm} + f_{lm}W_{lm} & f_{lm}X_{lm} \\ * & * & (g_{lm}Y_{lm} - f_{lm}W_{lm})\sin^2\theta \end{pmatrix}, \tag{3.3}$$

where $*$ denotes the relations of symmetry. $a_{lm}, b_{lm}, g_{lm}, f_{lm}$ are functions of r and t, and described as

$$\begin{aligned} a_{lm} &= r^{l-2}\Big(\frac{1}{r}\frac{\partial}{\partial r}\Big)^l\frac{P_{lm}(t-r) + Q_{lm}(t+r)}{r}, \\ g_{lm} &= -\frac{r^2}{2}a_{lm}, \\ b_{lm} &= \frac{1}{l(l+1)r}\frac{\partial}{\partial r}(r^3a_{lm}), \\ f_{lm} &= \frac{1}{(l-2)(l+1)}\Big[g_{lm} + \frac{\partial}{\partial r}\Big(\frac{r}{l(l+1)}\frac{\partial}{\partial r}(r^3a_{lm})\Big)\Big]. \end{aligned} \tag{3.4}$$

Y_{lm} is the spherical harmonic function and

$$\begin{aligned} X_{lm} &= 2\frac{\partial}{\partial\varphi}\Big(\frac{\partial}{\partial\theta} - \cot\theta\Big)Y_{lm}, \\ W_{lm} &= \Big(\frac{\partial^2}{\partial\theta^2} - \cot\theta\frac{\partial}{\partial\theta} - \frac{1}{\sin^2\theta}\frac{\partial^2}{\partial^2\varphi}\Big)Y_{lm}. \end{aligned} \tag{3.5}$$

We use $\hat{A}_{ij}$ at $t = 0$ as the initial condition.

In this paper, we only consider the quadrupole mode($l = |m| = 2$) for initial conditions. Even in this case, the various choices for P_{22}, P_{2-2} and Q_{22}, Q_{2-2} are possible. As one choice, we select

$$
\begin{aligned}
P_{22} = P_{2-2} &= \frac{C}{4}\sqrt{\frac{32\pi}{15}}\frac{\partial}{\partial t}\exp\Big(-\frac{(r-t)^2}{2r_0^2}\Big), \\
Q_{22} = Q_{2-2} &= -\frac{C}{4}\sqrt{\frac{32\pi}{15}}\frac{\partial}{\partial t}\exp\Big(-\frac{(r+t)^2}{2r_0^2}\Big),
\end{aligned}
\tag{3.6}
$$

where C and r_0 denote an arbitrary amplitude of the TT wave and an width of the wave packet. For simplicity, hereafter, we set $r_0 = 1$, i.e., we fix the unit of the length scale to the width of the wave packet. In this case, components of $\bar{A}_{ij}$ at $t = 0$ are written as

$$
\begin{aligned}
\hat{A}_{xx} &= C_{12}\exp(-r^2/2)\Big[12 - 8y^2 - 16z^2 + 2z^4 + z^2(x^2 + 3y^2) + y^4 - x^2y^2\Big], \\
\hat{A}_{yy} &= C_{12}\exp(-r^2/2)\Big[-12 + 8x^2 + 16z^2 - 2z^4 - z^2(3x^2 + y^2) - x^4 + x^2y^2\Big], \\
\hat{A}_{zz} &= C_{12}\exp(-r^2/2)(x^2 - y^2)(-8 + 2z^2 + x^2 + y^2), \\
\hat{A}_{xy} &= C_{12}\exp(-r^2/2)xy(x^2 - y^2), \\
\hat{A}_{xz} &= C_{12}\exp(-r^2/2)xz(12 - 2r^2 + x^2 - y^2), \\
\hat{A}_{yz} &= C_{12}\exp(-r^2/2)yz(-12 + 2r^2 + x^2 - y^2),
\end{aligned}
\tag{3.7}
$$

where $C_{12} = C/12$. Another one is

$$
\begin{aligned}
P_{22} = P_{2-2} &= \frac{C'}{2}\sqrt{\frac{32\pi}{15}}\frac{\partial}{\partial t}\Big[\Big\{\Big(\frac{r-t}{r_0}\Big)^2 + 1\Big\}\exp\Big(-\frac{(r-t)^2}{2r_0^2}\Big)\Big], \\
Q_{22} = Q_{2-2} &= -\frac{C'}{2}\sqrt{\frac{32\pi}{15}}\frac{\partial}{\partial t}\Big[\Big\{\Big(\frac{r+t}{r_0}\Big)^2 + 1\Big\}\exp\Big(-\frac{(r+t)^2}{2r_0^2}\Big)\Big],
\end{aligned}
\tag{3.8}
$$

where C' and r_0 also denote an amplitude and an width of the wave packet. We also set

$r_0 = 1$. Then components of $\tilde{A}_{ij}$ at $t = 0$ are written as

$$
\begin{aligned}
\hat{A}_{xx} &= C'_{12}\exp(-r^2/2)\{-60 + 124z^2 + 12x^2 + 68y^2 - 4z^4 - 17y^4 + x^2y^2 \\
&\qquad + z^2(5x^2 - 21y^2) - 30r^2z^2 + 2r^4z^2 - r^2(x^2 - y^2)(y^2 + z^2)\}, \\
\hat{A}_{yy} &= C'_{12}\exp(-r^2/2)\{60 - 124z^2 - 68x^2 - 12y^2 + 4z^4 + 17x^4 - x^2y^2 \\
&\qquad + z^2(21x^2 - 5y^2) + 30r^2z^2 - 2r^4z^2 - r^2(x^2 - y^2)(x^2 + z^2)\}, \\
\hat{A}_{zz} &= C'_{12}\exp(-r^2/2)(x^2 - y^2)(56 - 17r^2 - 9z^2 + r^4 + r^2z^2), \\
\hat{A}_{xy} &= C'_{12}\exp(-r^2/2)xy(x^2 - y^2)(r^2 - 9), \\
\hat{A}_{xz} &= C'_{12}\exp(-r^2/2)xz\{-84 + 30r^2 - 2r^4 + (r^2 - 9)(x^2 - y^2)\}, \\
\hat{A}_{yz} &= C'_{12}\exp(-r^2/2)yz\{84 - 30r^2 + 2r^4 + (r^2 - 9)(x^2 - y^2)\},
\end{aligned}
\tag{3.9}
$$

where $C'_{12} = C'/12$. Hereafter we call the former(Eq.(3.7)) and the later(Eq.(3.9)) initial conditions models(A) and (B), respectively. In both cases, exchange $x \leftrightarrow y$ corresponds to exchange $C(C') \leftrightarrow -C(C')$, so that even if we choose negative $C(C')$, we does not obtain any new results. Hence, we only consider the cases of $C,\ C' > 0$.

Once $\hat{A}_{ij}$ is obtained, we can solve the Hamiltonian constraint as follows:

$$\Delta_{flat}\psi = -\frac{1}{8}\psi^{-7}\hat{A}_{ij}\hat{A}^{ij}, \tag{3.10}$$

where Δ_{flat} is the Laplacian with respect to η_{ij}. This equation is solved with the boundary condition

$$\psi = 1 + \frac{M}{2} + O(r^{-3}), \tag{3.11}$$

where M is the gravitational mass of the system. Numerically, we use the following standard method:(1) We put the trial value of ψ in the right-hand side(RHS) of Eq.(3.10). (2) We solve the Poisson equation for a given source term by ICCG method[13]. (3) We put new ψ in the RHS of Eq.(3.10). We continue these procedure the sufficient convergence is achieved. After ψ is obtained, $\tilde{A}_{ij}$ is given by

$$\tilde{A}_{ij} = \psi^{-6}\hat{A}_{ij}. \tag{3.12}$$

4. Slice Conditions

We have tried to calculate the dynamical evolution of the TT wave using several slice conditions. We summarize their properties in this section.

4.1 Geodesic slice: $\alpha = 1$

The geodesic slice has been well-known as an inappropriate slice because it does not have the singularity avoidance property for the black hole formation problems[14]. We here show that it is also inappropriate to compute the dynamical evolution of the TT wave for a long time integration even if the amplitude of the TT wave is low. Let us explain this using the variable K as an example. In the case of the geodesic slice, $\alpha = 1$, Eq.(2.13) becomes

$$\frac{\partial K}{\partial t} = \tilde{A}_{ij}\tilde{A}^{ij} + \frac{1}{3}K^2. \tag{4.1}$$

For the low amplitude wave, $\tilde{A}_{ij}$ is regarded as gravitational waves, so even if they initially exist in the central region, in a little while, they must disperse to infinity. Although $K = 0$ initially(at $t = 0$), K becomes positive for $t > 0$ due to the term $\tilde{A}_{ij}\tilde{A}^{ij} > 0$. After gravitational waves($\tilde{A}_{ij}$) disperse, K obeys the equation as

$$\frac{\partial K}{\partial t} = \frac{1}{3}K^2. \tag{4.2}$$

The solution of it is immediately obtained as

$$K = \frac{3K_1}{3 - K_1(t - t_1)}, \tag{4.3}$$

where K_1 denotes K at $t = t_1 > 0$. From the above argument, K_1 will be positive, so that K will diverge at $t \sim t_1 + 3/K_1$. Clearly, this means the appearance of the coordinate singularity. Therefore, we can conclude that the geodesic slice is not appropriate even for the evolution of the low amplitude TT waves(see also fig.3).*

* Note that if we choose an appropriate K initially, this coordinate singularity may be escaped. This point is not clear.

4.2 Harmonic slice and similar algebraic slices

Next, we consider the slices such as

$$\alpha = \alpha_0(\mathbf{r})\exp(n\phi), \tag{4.4}$$

where n is a constant and $\alpha_0(\mathbf{r})$ is an arbitrary function of $\mathbf{r}$ which is set initially. In the case of $n = 6$, the slice becomes the harmonic slice with $\beta^i = 0$[9]. Substituting Eq.(4.4) into Eq.(2.12), we obtain

$$\frac{\partial}{\partial t}\alpha^{-1} = \frac{n}{6}K. \tag{4.5}$$

From Eqs.(2.13) and (4.5), we obtain

$$\frac{\partial^2\alpha}{\partial t^2} = \left(\frac{\partial\alpha}{\partial t}\right)^2\alpha^{-1} + \frac{n}{6}\alpha^2\left[-\alpha(\tilde{A}_{ij}\tilde{A}^{ij} + \frac{1}{3}K^2) + D^iD_i\alpha\right]. \tag{4.6}$$

Let us consider the case of the linear TT waves, in which geometric variables are expanded as

$$\begin{aligned}
\tilde{\gamma}_{ij} &= \eta_{ij} + \epsilon h^{(1)}_{ij}, \\
\tilde{A}_{ij} &= \epsilon A^{(1)}_{ij}, \\
K &= \epsilon^2 K^{(2)}, \\
\alpha &= 1 + \epsilon^2\alpha^{(2)},
\end{aligned} \tag{4.7}$$

where ϵ is small parameter. Then, for the lowest order in $\epsilon(O(\epsilon^2))$, Eq.(4.6) becomes

$$\frac{\partial^2\alpha^{(2)}}{\partial t^2} = \frac{n}{6}\left(\Delta_{flat}\alpha^{(2)} - \tilde{A}^{(1)}_{ij}\tilde{A}^{(1)}_{ij}\right). \tag{4.8}$$

For $n < 0$, Eq.(4.8) becomes a 4D elliptical equation. In this case, we can expect that the system is unstable for numerical time evolution. This is because the dispersion relations for homogeneous equation of Eq.(4.8) become

$$\omega = \pm i\sqrt{\frac{|n|\mathbf{k}\cdot\mathbf{k}}{6}}, \tag{4.9}$$

where the expansion of $\alpha^{(2)}$ by $\exp(i\omega t - i\mathbf{k}\cdot\mathbf{r})$ is assumed. Since unstable modes($\mathrm{Im}(\omega) < 0$) always exist, any slice conditions with $n < 0$ will not be appropriate to evolve the spacetime numerically.

This fact can be also applied to the conformal slice[6],

$$\alpha = \exp\Big(-2\overline{\psi} - \frac{2}{3}\overline{\psi}^3 - \frac{2}{5}\overline{\psi}^5\Big), \tag{4.10}$$

where $\overline{\psi} = \exp(\phi) - 1$. In this case, the evolution equation in $O(\epsilon^2)$ is written as

$$\frac{\partial^2 \alpha^{(2)}}{\partial t^2} = -\frac{1}{3}\Big(\Delta_{flat}\alpha^{(2)} - \tilde{A}^{(1)}_{ij}\tilde{A}^{(1)}_{ij}\Big), \tag{4.11}$$

or

$$\frac{\partial^2 \psi^{(2)}}{\partial t^2} = -\frac{1}{3}\Big(\Delta_{flat}\psi^{(2)} + \frac{1}{2}\tilde{A}^{(1)}_{ij}\tilde{A}^{(1)}_{ij}\Big). \tag{4.12}$$

Since Eq.(4.12) is the same as Eq.(4.8) with $n = 2$ and the RHS of Eq.(4.12) does not vanish even if we use the Hamiltonian constraint, it is unstable for the numerical time evolution. Therefore, the conformal slice is not appropriate for the time evolution of the TT wave. However, that is not always the case, and the stable numerical time evolution is possible if the spacetime is different from those composed only of gravitational waves. This point is explained in appendix A.

For $n > 0$, Eq.(4.8) is a hyperbolic equation with the source term, $-\tilde{A}^{(1)}_{ij}\tilde{A}^{(1)}_{ij}$. In particular, in the case of $n = 6$, i.e., for the harmonic slice, it becomes the wave equation. In contrast with $n < 0$ cases, the slices with $n > 0$ seem to be allowed the stable time evolution in numerical simulations adopting Eqs.(2.11)-(2.14). Indeed, we try to calculate the time evolution of the TT wave for a variety of initial conditions and for various $n(= 2, 6, 12)$, and see the stable time evolution of the TT wave. From the various calculations using different $n(> 0)$, we do not find noticeable differences of results(but, the slice with larger n has somewhat stronger singularity avoidance). Therefore in this paper, we mainly use the harmonic slice as an example.

Even if we fix $n = 6$, another freedom remains; choice of $\alpha_0(\mathbf{r})$. For the low amplitude TT wave, its choice is not important, but in the case of the higher amplitude TT wave, in particular, for the cases where the shrink of the TT wave by its self-gravity leads to the high density peaks in the central region or the collapse of the TT wave results in a black hole formation, its choice seems to be important. In section 5, we mention the importance of the choice of $\alpha_0(\mathbf{r})$ in more detail.

4.3 MAXIMAL SLICE

The maximal slice, $K = 0$, is well-known because for the singularity avoidance property both for the black hole formation problem[14] and for the dynamical evolution of gravitational waves and the subsequent black hole formation[15]. In the case of the maximal slice, the equation for α becomes

$$\tilde{\Delta}\alpha + 2\tilde{D}_i\phi\tilde{D}^i\alpha = \alpha\exp(4\phi)\tilde{A}_{ij}\tilde{A}^{ij}. \tag{4.13}$$

We solve this equation by the relaxation method as follows: (1) We rewrite the equation as

$$\Delta_{flat}\alpha = -(f^{ij}\alpha_{,i})_{,j} - 2\tilde{\gamma}^{ij}\phi_{,i}\alpha_{,j} + \alpha\exp(4\phi)\tilde{A}_{ij}\tilde{A}^{ij}. \tag{4.14}$$

(2) We first substitute the trial value of α in the RHS of Eq.(4.13), and by ICCG method we solve the Poisson equation with the boundary condition as

$$\alpha = 1 - \frac{M_a}{r} + O(r^{-3}), \tag{4.15}$$

where

$$M_a = M_a(t) = \lim_{r\to\infty}\frac{1}{4\pi}\oint \nabla_i\alpha dS^i.$$

(3) We continue the above procedure until α sufficiently converges.

We try to test the convergence for several numerical simulations of the evolution of the TT wave. For the low amplitude TT wave, the convergence of the relaxation is good. (Note, however, that even in this case, the computational time is about ten times as long as that by means of of the harmonic slice for our typical simulations on a work station.) For the higher amplitude TT wave, the convergence of the relaxation becomes even worse. This seems due to the first and second terms in the RHS of Eq.(4.14). To overcome this troublesome property, we need to find a more suitable method to solve Eq.(4.13). For these reasons, in the following calculations, we mainly use the harmonic slice to save the computational time. Investigation for the maximal slice is left as one of future problems.

5. Numerical Results

5.1 Method for analysis

Since the metric involves the gauge modes except for the physical quantities such as gravitational waves, we must think some ideas to extract some meaningful quantities. To see the some "density" of gravitational waves, we make use of the curvature invariant as follows:

$$I = 8E_{ij}E^{ij} + 4P_{ijk}P^{ijk}, \tag{5.1}$$

where

$$\begin{aligned} E_{ij} &= R_{ij} + KK_{ij} - K_{ik}K^{k}_{j}, \\ P_{ijk} &= D_j K_{ik} - D_i K_{jk}. \end{aligned} \tag{5.2}$$

I is the so-called the Bel-Robinson's energy density. Since I is a gauge invariant quantity as well as positive definite, it will be able to extract some physical "energy density" of gravitational waves.

To see the wave form of gravitational waves, we use the gauge invariant wave extraction technique, which has recently developed by NCSA group[10]. Following their method, we assume that the numerically calculated spacetime metric near the outer boundary can be split as

$$g_{\mu\nu} = \eta_{\mu\nu} + \xi_{\mu\nu}, \tag{5.3}$$

where $\xi_{\mu\nu} = \sum_{lm} \xi^{lm}_{\mu\nu}$ and

$$\xi^{lm}_{\mu\nu} = \begin{pmatrix} H_{0lm}Y_{lm} & H_{1lm}Y_{lm} & h_{0lm}Y_{lm,\theta} & h_{0lm}Y_{lm,\varphi} \\ * & H_{2lm}Y_{lm} & h_{1lm}Y_{lm,\theta} & h_{1lm}Y_{lm,\varphi} \\ * & * & r^2(K_{lm}Y_{lm} + G_{lm}W_{lm}) & r^2 G_{lm}X_{lm} \\ * & * & * & r^2(K_{lm}Y_{lm} - G_{lm}W_{lm})\sin^2\theta \end{pmatrix}, \tag{5.4}$$

and $H_{0lm}, H_{1lm}, H_{2lm}, h_{0lm}, h_{1lm}, K_{lm}$ and G_{lm} are all functions of r and t. These variables

are calculated from the numerically derived metric as

$$
\begin{aligned}
H_{0lm} &= \int d\Omega Y^*_{lm} \alpha^2, \\
H_{2lm} &= \int d\Omega Y^*_{lm} \exp(4\phi) \tilde{\gamma}_{rr}, \\
h_{1lm} &= \frac{1}{l(l+1)} \int d\Omega \exp(4\phi) \Big(Y^*_{lm,\theta} \tilde{\gamma}_{r\theta} + \frac{Y^*_{lm,\varphi}}{\sin^2\theta} \tilde{\gamma}_{r\theta} \Big), \\
G_{lm} &= \frac{1}{2(l-1)l(l+1)(l+2)} \int d\Omega \exp(4\phi) r^{-2} \Big(W^*_{lm} \tilde{\gamma}_- + 2X^*_{lm} \frac{\tilde{\gamma}_{\theta\varphi}}{\sin^2\theta} \Big), \\
K_{lm} &= \frac{1}{2} \int d\Omega Y^*_{lm} \exp(4\phi) \tilde{\gamma}_+ r^{-2},
\end{aligned}
\tag{5.5}
$$

where $d\Omega = \sin\theta d\theta d\varphi$, Y^* denotes the complex conjugate of Y, and

$$
\tilde{\gamma}_\pm = \tilde{\gamma}_{\theta\theta} \pm \frac{\tilde{\gamma}_{\varphi\varphi}}{\sin^2\theta}. \tag{5.6}
$$

Note that $H_{1lm} = h_{0lm} = 0$ in the present gauge condition. In practice, $\tilde{\gamma}_{rr}, \tilde{\gamma}_{r\theta}, \ldots$ are transformed from $\tilde{\gamma}_{xx}, \tilde{\gamma}_{xy}, \ldots$.

Using these variables, the gauge invariant quantity for gravitational waves can be written;

$$
R_{lm}(t,r) = \sqrt{\frac{2}{(l-1)l(l+1)(l+2)}} \Big(4k_{2lm} + l(l+1)k_{1lm} \Big), \tag{5.7}
$$

where

$$
\begin{aligned}
k_{1lm} &= K_{lm} + l(l+1)G_{lm} + 2rG_{lm,r} - 2\frac{h_{1lm}}{r}, \\
k_{2lm} &= \frac{H_{2lm}}{2} - \frac{1}{2}\frac{\partial}{\partial r}\Big(r\{K_{lm} + l(l+1)G_{lm}\} \Big).
\end{aligned}
\tag{5.8}
$$

We note that $R_{lm}(t,r)$ obeys the flat-space wave equation as

$$
\Big(\frac{\partial^2}{\partial t^2} - \frac{1}{r^2}\frac{\partial}{\partial r} r^2 \frac{\partial}{\partial r} + \frac{l(l+1)}{r^2} \Big) R_{lm}(t,r) = 0. \tag{5.9}
$$

5.2 Results

We consider the various initial conditions with $0.01 \leq C \leq 7$ for model(A) and $0.01 \leq C' \leq 1$ for model(B). In fig.1, the relations between the gravitational mass, M, and C(C') are shown for models(A) and (B). In the case of model(A), the relation $M = M_0 C^2$ holds for $C \lesssim 0.3$, where M_0 is a constant $\simeq 0.145$. For $C \sim 2$, the mass is about 50% different from the extrapolated value $4M_0$, so that we can expect that for $C \gtrsim 2$, the non-linearity of the TT wave plays an important role in the dynamical evolution. In the case of model(B), the relation $M = M_0' C'^2$ also holds for $C' \lesssim 0.1$, and $M_0' \simeq 2.6$. In this case, the ratio of the mass to the extrapolated mass formula becomes less than 50% for $C' \gtrsim 0.5$.

In fig.2, we show the time evolution of $h_{yy} = \tilde{\gamma}_{yy} - 1$ and $h_{zz} = \tilde{\gamma}_{zz} - 1$ for $C = 0.01$ of model(A) at $(x_{max}, 0, 0)$. This calculation is performed using the harmonic slice with $\alpha_0(\mathbf{r}) = 1$. In order to see the numerical accuracy, we show both numerical and analytical results in the figures. The solid and dotted lines denote the results by the numerical and the analytical calculations, respectively. Here, the analytical result corresponds to a solution of the linearized Einstein equation. We can see that both results agree well. We also find that after wave disperses, h_{ij} remains zero except for the small numerical errors for a long time. Thus the harmonic slice works well for the evolution of the low amplitude TT wave. Next, in figs.3(a) and(b), we show the results of the same quantities as in fig.2, but by means of the geodesic slice and the maximal slice. For the case of the geodesic slice, h_{ij} gradually deviates from zero after the wave disperses, and the deviation becomes larger and larger. This bad behavior seems due to the property of the geodesic slice explained in section 3.1, and this clearly shows that the geodesic slice is not appropriate to follow even the low amplitude TT wave for a long time. On the other hand, the maximal slice works well for this problem.

In figs.4(a-d), we show the time evolution of the Bel-Robinson's energy density(I) for $C = 0.1$, 2, 4 and 7 of model(A). We also show I for $C' = 0.3$, 0.5 and 1 of model(B) in figs.4(e-g) to see whether the difference of the initial condition affects the time evolution of I. The figures denote the density contours of I in the $z = 0$ plane. First we pay attention to model(A). For $C = 0.1$, we see that the wave only disperses to infinity. In this case, the non-linearity of the TT wave is not important, so that we may regard the time evolution of I for $C = 0.1$ as the typical behavior of I for the low amplitude TT wave. For $C = 2$, the behavior of I is different from that for the low amplitude TT wave due to the non-linearity. At early times in the evolution, the wave packet shrinks by its self-gravity and high density peaks appear near the origin. Then it disperses to infinity like in the case of $C = 0.1$. For

$C = 4$, concentration of the wave is more remarkable: After the wave packet shrinks to the central region, it does not disperse soon and oscillates around the origin for a few times. In this case, the amplitude of the oscillation is also very high, but the wave disperses after the oscillation. Finally we show I for $C = 7$. In this case, the initial behavior is essentially the same as for $C = 4$. But after the wave packet shrinks to the central region, the behavior is different; without oscillating, the wave merely collapses and the amplitude becomes higher and higher. Although we do not try to find the apparent horizon in the present simulations, we may expect that a black hole will be formed in the central region like in the case of axisymmetric calculations[15].

We note that the above calculations are performed using the harmonic slice with $\alpha_0(\mathbf{r}) = 1$ for $C = 0.1$ and 2, but for $C = 4$ and 7, we adopt

$$\alpha_0(\mathbf{r}) = \exp\left(-2\overline{\psi}_0 - \frac{2}{3}\overline{\psi}_0{}^3 - \frac{2}{5}\overline{\psi}_0{}^5\right), \tag{5.10}$$

where $\overline{\psi}_0$ denotes $\exp(\phi) - 1$ at $t = 0$. In this initial slice, outer region of the spacetime is guaranteed to be the Schwarzschild one as well as the lapse function in the inner region becomes sufficiently small for the high amplitude TT waves[6]. In the case of $C = 0.1$ and 2, we also perform the calculations with $\alpha_0(\mathbf{r}) \neq 1$, but the results are essentially the same. (This is the same for $C \lesssim 3$.) However, for $C \gtrsim 4$, if we use $\alpha_0(\mathbf{r}) = 1$ as an initial condition for the harmonic slice, we obtain the results in which values of geometric variables at the origin become very large and computation breaks down. The behavior is not due to the true singularity at the origin, but seems due to the appearance of the coordinate singularity. So that, this fact does not show a drawback of the harmonic slice because it can be escaped easily by choosing an appropriate initial α_0. However, it also shows that we should carefully choose $\alpha_0(\mathbf{r})$ for the highly distorted spacetime such as the high amplitude TT wave.

We should also notice that in the case of $C = 7$, i.e., in the case that the TT wave collapses by its self-gravity, the harmonic slice even with Eq.(5.10) does not have the singularity avoidance property: The 3D hypersurface seems to hit the singularity(or approach very near it) soon after the collapse of the TT wave. We also perform simulations with other $\alpha_0(\mathbf{r})$, but the results are essentially the same. Bona and Masso[9]proofed that the harmonic slice avoids the singularity in the case of the well-known and idealized spacetimes. However, in the present case, the spacetimes do not have any symmetries and it is not clear that their proof can be applied. Also, in the numerically generated spacetimes, the truncation errors are certainly generated. In their proof, they assumed that the behavior of α near

the singularity is $\alpha(\tau) \sim (\tau_s - \tau)^p$, where τ and τ_s, respectively, denote the proper time and proper time at which the spacetime hits the singularity. They assumed $p \geq 1$, and in this case, the harmonic slice has the singularity avoidance property because the singularities can not be reached in a finite coordinate time. If $p < 1$, it does not have such a property. Let us consider the singularity with $p \gtrsim 1$. If a small truncation error is generated in the numerical simulation and p happens to become < 1, then the time slice hits the singularity soon. Further worse, in the harmonic slice, the time slice approaches infinitely close to the singularity; near the singularity, the spacetime is highly distorted and values of geometric variables become very large(for example, $|K| \to \infty$.) So that, we can expect that the large truncation error is largely accumulated. In such a case, it is very questionable that the harmonic slice can avoid the singularity as discussed above. Thus, the singularity avoidance property of the harmonic slice seems to be week in the numerically generated spacetime. This point should be clarified by means of several other calculations in future works.

Now, we see I for $C' = 0.3$, 0.5 and 1 of model(B) in figs.4(e-g). We soon find that features of the time evolution of I for each model is very similar to that for $C = 2$, 4 and 7 of model(A): In the case of $C' = 0.3$, the wave packet first shrinks to the central region by its self-gravity and then disperses to infinity. In the case of $C' = 0.5$, after the wave packet shrinks to the central region, the high amplitude oscillations of the wave continue for a few times, and finally the wave disperses to infinity. In the case of $C' = 1$, after the wave packet shrinks, it collapses without oscillating so much. The difference between models(A) and (B) is the steepness of the initial configuration of I in the central region: The initial configuration of I for model(B) are steeper than that for model(A) in the central region even if the gravitational masses of the system are the same. This difference seems to affect the threshold value of $M/r_0 \equiv \sigma_{crit}$, beyond which the wave packet must collapse. In the case of model(A), $\sigma_{crit} \sim 0.5$ for $C \sim 7$, but in the case of model(B), it is slightly different from that for model(A) and becomes about 0.3 for $C' \sim 1$. However, the difference we find is only this point. Initial configuration of the TT wave does not seem to change the final fate of the TT wave extremely.

Next, let us see the wave form of the TT wave at the outer region. In figs.5(a-f), we show $R_{lm}(t, r)$ at $r = 3.9r_0$ for $C = 0.1, 2$, 4 of model(A) and for $C' = 0.03$, 0.3 and 0.5. In these figures, the solid, dotted, dashed, long dashed, and dotted-dashed lines denote $(l, m) = (2, 2+)$, $(2, 0)$, $(4, 4+)$, $(4, 2+)$ and $(4, 0)$ modes. 2+ and 4+ denote the combination of mode like $(Y_{l2} + Y^*_{l-2})/\sqrt{2}$ and $(Y_{l4} + Y^*_{l-4})/\sqrt{2}$. Note that in the initial slice, only the

$(2,2+)$ mode exists. For $C = 0.1$ of model(A) and $C' = 0.03$ of model(B), $(2,2+)$ mode dominates over other modes throughout the whole time. (Small values of the other modes will be the numerical error.) This is quite natural because the nature of the TT wave is linear and the non-linear couplings with the other modes are negligible. To check whether the wave extraction works well or not, we also write the gauge invariant wave form of gravitational waves at $3.9r_0$ by the analytical calculation in fig.6. It is written as

$$\begin{aligned} R_{22+} = \sqrt{\frac{16\pi}{15}}\frac{1}{r^3}\Big[& \exp\Big(-\frac{(r+t)^2}{2}\Big)\Big(-3 - 3r^2 - 3r^4 + r^6 - 3rt - 3r^3t + 4r^5t \\ & + 3t^2 + 3r^2t^2 + 6r^4t^2 + 3rt^3 + 4r^3t^3 + r^2t^4\Big) \\ & + \exp\Big(-\frac{(r-t)^2}{2}\Big)\Big(3 + 3r^2 + 3r^4 - r^6 - 3rt - 3r^3t + 4r^5t \\ & - 3t^2 - 3r^2t^2 - 6r^4t^2 + 3rt^3 + 4r^3t^3 - r^2t^4\Big)\Big] . \end{aligned} \tag{5.11}$$

We find that fig.5(a) and fig.6 agree well. Therefore, we can consider that the wave extraction technique works well. (We note that the wave form is different from that at infinity. To see that with an accuracy less than $\sim 1\%$, we have to take the grid up to $r \sim$ a few $\times\, 10r_0$, but this point is not important in this paper.)

For $C \gtrsim 2$ of model(A) and $C' \gtrsim 0.3$ of model(B), the non-linearity becomes important; $(2,0)$ mode comes to have a high amplitude. The ratio of peak amplitudes for $(2,0)$ mode to $(2,2+)$ mode is about 40% for $C = 2$ of model(A) and $C' = 0.3$ of model(B). For $C = 4$ of model(A) and $C' = 0.5$ of model(B), the ratio becomes about 60%, and the ratio of peak amplitudes for $l = 4$ modes to $(2,2+)$ mode also becomes large($\sim 10\%$). Thus the excitation of the higher multipole modes is expected as the amplitude of the TT wave becomes large.

Let us apply the above analysis to the wave form of merging compact binaries such as binary neutron stars and binary black holes. At the merging of such binaries, the amplitude of gravitational waves at the Schwarzschild radius of the binaries will be of order unity. In reality, Newtonian 3D numerical simulations[5]showed that its value is about 0.3 for quadrupole gravitational waves. In the present calculation, this value corresponds to that for the cases of $C \sim 1$ or $C' \sim 0.3$, so that we are allowed to expect that a sufficient excitation of the higher multipole modes by the quadrupole mode. This implies that the perturbation analysis[16]may be inappropriate for emission problems of gravitational waves from the merging binary unless the merged object is swallowed inside the event horizon rapidly enough.

6. Summary

In this paper, we have simulated the dynamical evolution of the vacuum spacetimes composed of gravitational waves. As the initial condition of gravitational waves, we use the conformal flat and $K = 0$ initial condition. (We call it the TT wave in this paper.) We consider both the low and high amplitude TT waves to see the property of several slices in the various spacetimes and to investigate that the gauge invariant wave extraction technique works well. As for the slices, we reach following conclusions.

(1) Geodesic slice: This slice is not appropriate to follow the evolution of the TT wave for a long time even if its amplitude is low.

(2)Harmonic slice: This slice is appropriate to follow the evolution of the TT wave for a long time unless the amplitude of the TT wave is too high. However, in the case in which the amplitude of the TT wave is so high that it collapses to a black hole, this slice seems inappropriate: Our simulations seems to indicate the following behavior. The time slice approaches very near the singularity and values of geometric variables become very large(e.g., $|K| \to \infty$) because of the strong distortion of the spacetime. As a result, the truncation error is accumulated and the slice hits the singularity. Thus, the singularity avoidance property of the harmonic slice seems weak. We had better consider a slice in which time slices do not approach the singularity too closely. We should find out a slice at least satisfying the condition $|K| \leq K_c$, where K_c a finite value.

(3)Maximal slice: This slice will have a suitable property to follow the evolution of the TT wave even in the case in which the black hole is formed from the high amplitude TT wave. (This was shown by axisymmetric calculations[15].) However, to use this slice, we must solve a 3D elliptical equation which is troublesome. If we can develop a good method to solve it, this slice will become useful slice.

We also investigate whether the gauge invariant wave extraction technique works well or not, and make sure that it is good. Using this technique, we also see the non-linearity of the Einstein equation: Even if only the quadrupole mode of gravitational waves exists initially, the non-linearity of the Einstein equation induces the other multipole modes. This means that in the case of the merging of compact binary, non-linear excitation of the higher multipole modes from the quadrupole mode is allowed to be expected. Hence, to detect the signal of the last phase of coalescing binary may lead to see the non-linearity of the Einstein

gravity.**

In this paper, we have described the numerical results of the dynamical evolution of gravitational waves with even parity and with one wave packet. As the subsequent works, we plan to investigate the dynamical evolution of odd parity gravitation waves or collision between two wave packets of high amplitude gravitational waves. These subjects can be studied by the present numerical code, so we will report these results in the near future. Like in the case of $C = 7$ of model(A), the high amplitude TT wave collapses and probably a black hole is formed. To make sure of it, 1)we must construct the numerical code to find the apparent horizon , and 2)we must find an appropriate slice which has the singularity avoidance property. As for 2), the maximal slice may be the required slices. If so, we need to construct an appropriate method to solve a 3D elliptical equation. In this way, many interesting subjects remain and many problems should be solved even for the evolution of pure gravitational waves in 3D numerical relativity. Thus, much more works should be done in this area.

Acknowledgments

We thank K. Nakao for frequent conversations and useful discussions. This work was in part supported by the Japanese Grant-in-Aid Scientific Research of the Ministry of Education, Science and Culture, Nos. 04234104 and 06740343.

APPENDIX A

In this appendix, we show the property of the conformal slice in the spacetime with the perfect fluid and show that the stable time evolution seems to be allowed contrary to in the vacuum spacetime composed only of gravitational waves. In the case of the conformal slice with $\beta^i = 0$, the evolution equation of ψ and K become

$$\frac{\partial}{\partial t}\psi = -\frac{\psi}{6}\alpha K, \tag{A.1}$$

$$\begin{aligned}\frac{\partial K}{\partial t} &= 2\frac{\alpha}{\psi^4}\left[\tilde{\Delta}\psi(1+\overline{\psi}^2+\overline{\psi}^4) - \frac{2}{\psi}\tilde{D}_k\psi\tilde{D}^k\psi(3\overline{\psi}^5+2\overline{\psi}^6+2\overline{\psi}^7+\overline{\psi}^8+\overline{\psi}^9)\right] \\ &\quad + \alpha\left(\tilde{A}_{ij}\tilde{A}^{ij}+\frac{1}{3}K^2\right) + 4\pi\alpha(S^l{}_l + E),\end{aligned} \tag{A.2}$$

** Note that if we can detect the *non-linear memory* of coalescing binaries, we may also see the non-linearity of the Einstein gravity[17].

where $\overline{\psi} = \psi - 1$, $S_{ij} = T_{kl}\gamma^k{}_i\gamma^l{}_j$, $E = T_{\mu\nu}n^\mu n^\nu$, and $T_{\mu\nu}$ is

$$T_{\mu\nu} = (\rho + \rho\varepsilon + P)u_\mu u_\nu + P g_{\mu\nu}. \tag{A.3}$$

Here, n^μ, u_μ, ρ, ε and P are the timelike unit normal, four velocity, baryon density, internal energy and pressure, respectively. From the Hamiltonian, the equation for ψ becomes

$$\tilde{\Delta}\psi = \frac{1}{8}\tilde{R}\psi - 2\pi E\psi^5 - \frac{\psi^5}{8}\Big(\tilde{A}_{ij}\tilde{A}^{ij} - \frac{2}{3}K^2\Big). \tag{A.4}$$

As far as not so strong field is concerned, the post-Newtonian approximation will be a good one. In this case, the following expansions are possible[16];

$$\begin{aligned}
\psi &= 1 + \psi^{(2)} + \psi^{(4)} + \dots \\
K &= K^{(3)} + K^{(5)} + \dots \\
\tilde{A}_{ij} &= \tilde{A}^{(3)}_{ij} + \dots \\
h_{ij} &= h^{(2)}_{ij} + \dots \\
f^{ij} &= f^{ij(2)} + \dots \\
E &= \rho + (\rho v^2 + \rho\varepsilon) + \dots \\
S_i{}^i &= \rho v^2 + 3P + \dots,
\end{aligned} \tag{A.5}$$

where $v_i = u^i/u^0$, $v^2 = v_i v_i$ and each variable is expanded by v^2. Making use of the Hamiltonian constraint, the evolution equations are written as

$$\begin{aligned}
\frac{\partial\psi^{(2)}}{\partial t} &= -\frac{1}{6}K^{(3)} \\
\frac{\partial\psi^{(4)}}{\partial t} &= -\frac{1}{6}\Big(K^{(5)} - \psi^{(2)}K^{(3)}\Big) \\
\frac{\partial K^{(3)}}{\partial t} &= 2\tilde{\Delta}\psi^{(4)} + 4\pi(4\rho\psi^{(2)} + 2\rho v^2 + 3P + \rho\varepsilon) + 2(f^{ij(2)}\psi^{(2)}_{,i})_{,j}.
\end{aligned} \tag{A.6}$$

Thus, the simple relation such as Eq.(4.11), which is derived assuming the linear approximation in h_{ij}, never holds for $\psi^{(2)}$ and $\psi^{(4)}$. Furthermore, we exchange $\psi^{(2)}$ into $U/2$, we obtain the equation of the Newtonian potential from the Hamiltonian constraint as

$$\Delta_{flat}U = -4\pi\rho. \tag{A.7}$$

Also, the equations for $\psi^{(4)}$ and $\psi^{(6)}$ become the 3D elliptical equations[16]. Therefore using the conformal slice, the stable numerical time evolution may be allowed. In practice, using

the conformal slice, Shibata and Nakamura[8] performed the simulation of the spherical symmetric dust collapse and subsequent black hole formation, and Nakamura[7] performed the simulation of the coalescence of binary neutron stars. In both cases, the stable numerical time evolutions were allowed when they used the Hamiltonian constraint to obtain ψ. This will be because the spurious unstable modes are generated in the case in which we use the evolution equation to obtain ψ. In any case, if we use the Hamiltonian constraint, the stable time evolution is possible. In conclusion, the conformal slice is not adequate for the simulation of the spacetime in which the Newtonian description of the system is not possible, but will be able to be used for the simulation of the black hole formation and the coalescence binary neutron stars, i.e., the spacetimes where the Newtonian description is possible. This is very natural conclusion because the conformal slice was originally designed to agree with the Newtonian description.

REFERENCES

1. C. Cutler et al., Phys. Rev. Lett **70**(1993), 2984.
2. R. E. Vogt, in proceedings of the sixth Marcel Grossmann meeting on general relativity, edited by H. Sato and T. Nakamura(World Scientific, 1991), 244;
   A. Abramovici et al. Science, **256**(1992), 325;
   K. S. Thorne, in proceedings of the eighth Nishinomiya-Yukawa memorial symposium on Relativistic Astrophysics, Edited by M. Sasaki(Universal Academy Press, Tokyo, 1994), 67.
3. C. Bradaschia et al., Nucl. Instrum. Method Phys. Res. Sect. **A289**(1990), 518.
4. C. W. Lincoln and C. M. Will, Phys. Rev. **D42**(1990), 1123.
5. For example, M. Shibata, T. Nakamura and K. Oohara, Prog. Theor. Phys. **88**(1992), 1079 and references therein.
6. L. Smarr and J. W. York, Phys. Rev. **D17**(1978), 1945 and 2529.
7. T. Nakamura, in the proceedings of the eighth Nishinomiya-Yukawa memorial symposium on Relativistic Astrophysics, Edited by M. Sasaki(University Academy Press, Tokyo, 1994), 155.
8. M. Shibata and T. Nakamura, Prog. Theor. Phys. **88**(1992), 317.

9. Bona and Masso, Phys. Rev. **D38**(1988), 2419; Phys. Rev. Lett. **68**(1992), 1097.

10. A. Abrahams, D. Bernstein, D. Hobill, E. Seidel and L. Smarr, Phys. Rev. **D45**(1992), 3544; P. Anninos et al., Phys. Rev. **D50**(1994), 3801; D. Berstein et al., Phys. Rev. **D50**(1994), 5000.

11. T. Nakamura, K. Oohara and Y. Kojima, Prog. Theor. Phys. supp. **90**(1987), 76.

12. W. H. Press et al., Numerical Recipes, (Cambridge University Press, 1989).

13. K. Oohara and T. Nakamura, Prog. Theor. Phys. **81**(1989), 360.

14. D. M. Eardley and L. Smarr, Phys. Rev. **D19**(1979), 2239.

15. M. Shibata, K. Nakao, T. Nakamura and K. Maeda, Phys. Rev. **D50**(1994), 708.

16. R. H. Price and J. Pullin, Phys. Rev. Lett. **72**(1994), 3297.

17. K. S. Thorne, Phys. Rev. **D45**(1992), 520 ; A. G. Wiseman and C. M. Will, Phys. Rev. **D44**(1991), R2945 ; D. Kennefick, Phys. Rev. **D50**(1994), 3587.

18. H. Asada, M. Shibata and T. Futamase, in preparation.

Figure Captions

Fig.1 : The relation between the amplitude of the TT wave(C) and the gravitational mass(M) at $t = 0$ for models(A) and (B). The solid and dashed lines denote the gravitational mass and $M = M_0C^2$, respectively. The open squares are the data points by numerical calculations.

Fig.2 : The time evolution of h_{yy} and h_{zz} for $C = 0.01$ of model(A) at $(x_{max}, 0, 0)$. In this calculation, we use the harmonic slice with $\alpha_0(\mathbf{r}) = 1$. Solid and dotted lines show the numerical and analytical results, respectively. Here, the analytical results correspond to the solution of the linearized Einstein equation.

Fig.3 : The same as in fig.2 except for the slice; (a) for the geodesic slice and (b)for the maximal slice.

Fig.4 : The contours of the Bel-Robinson's energy density I in the $z = 0$ plane.
(a) For $C = 0.1$ of model(A) and for $t = 0.015,\ 2.265,\ 4.515,\ 6.765$.
(b) For $C = 2$ of model(A) and for $t = 0.015,\ 2.265,\ 4.515,\ 6.765,\ 9.015$.
(c) For $C = 4$ of model(A) and for $t = 0.015,\ 2.265,\ 4.515,\ 6.765,\ 9.015,\ 11.265,\ 13.515,\ 15.765$.

(d) For $C = 7$ of model(A) and for $t = 0.015,\ 2.265,\ 4.515,\ 6.765,\ 9.015$. In this calculation, the 3D hypersurface seems to hit the singularity at $t \lesssim 12$.

(e) For $C' = 0.3$ of model(B) and for $t = 0.015,\ 2.265,\ 4.515,\ 6.765$.

(f) For $C' = 0.5$ of model(B) and for $t = 0.015,\ 2.265,\ 4.515,\ 6.765,\ 9.015,\ 11.265,\ 13.515$.

(g) For $C' = 1$ of model(B) and for $t = 0.015,\ 2.265,\ 4.515,\ 6.765$. In this calculation, the 3D hypersurface seems to hit the singularity at $t \sim 10$.

Fig.5 : Several modes of gravitational waves at $r = 3.9r_0$ are shown for various initial conditions of models(A) and (B). Gravitational waves are extracted from the gauge invariant technique. The solid, dotted, dashed, long dashed, and dotted-dashed lines denote $(l, m) = (2, 2+)$, $(2, 0)$, $(4, 4+)$, $(4, 2+)$ and $(4, 0)$ modes. 2+ and 4+ denote the combination of mode like $(Y_{l2} + Y^*_{l-2})/\sqrt{2}$ and $(Y_{l4} + Y^*_{l-4})/\sqrt{2}$. Each figure shows for (a)$C = 0.1$, (b)$C = 2$, (c)$C = 4$ of model(A) and (d)$C' = 0.03$, (e)$C' = 0.3$, (f)$C' = 0.5$ of model(B).

Fig.6 : R_{22+} at $r = 3.9r_0$ for $C = 0.1$ of model(A) by means of the analytical calculation(Eq.(5.11)). The figure agrees with R_{22+} in fig.5(a) well.

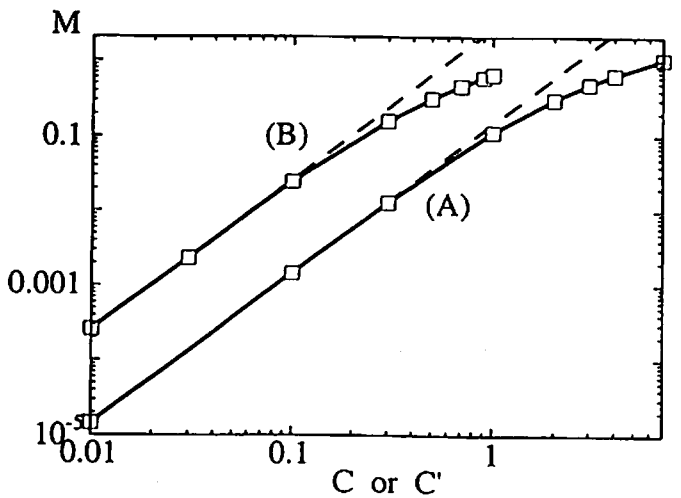
M
0.1
0.001
10^{-5}
0.01
0.1
1
C or C'
(B)
(A)

Fig.1

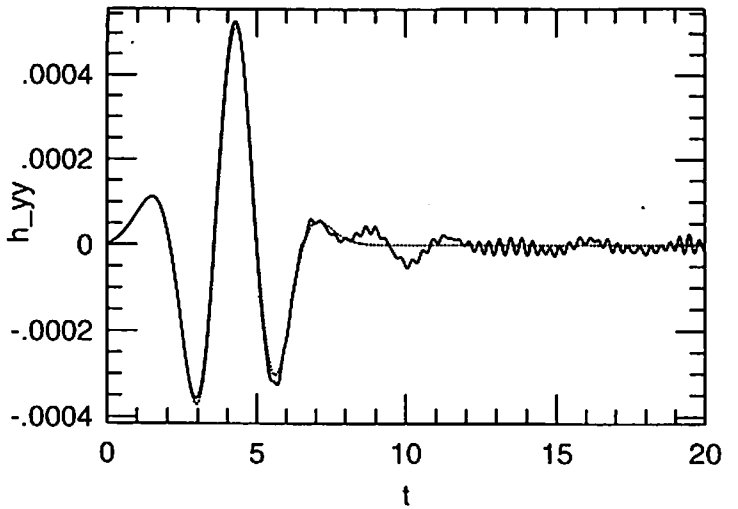
.0004
.0002
0
-.0002
-.0004
h_yy
0
5
10
15
20
t

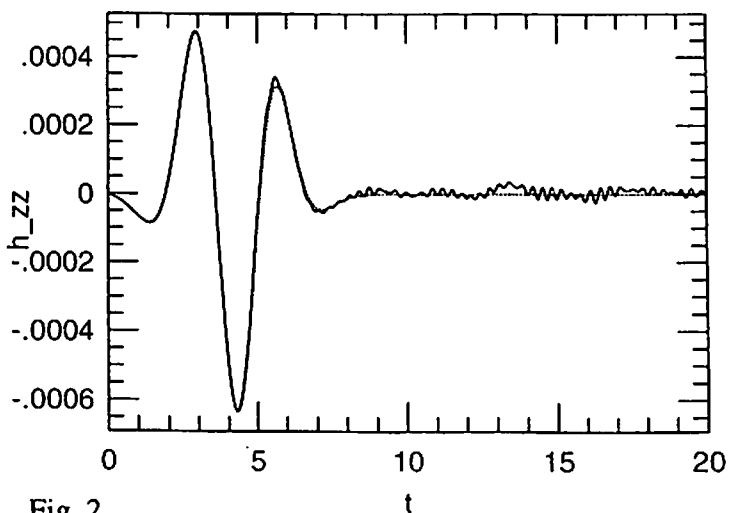
.0004
.0002
0
-.0002
-.0004
-.0006
h_zz
0
5
10
15
20
t

Fig. 2

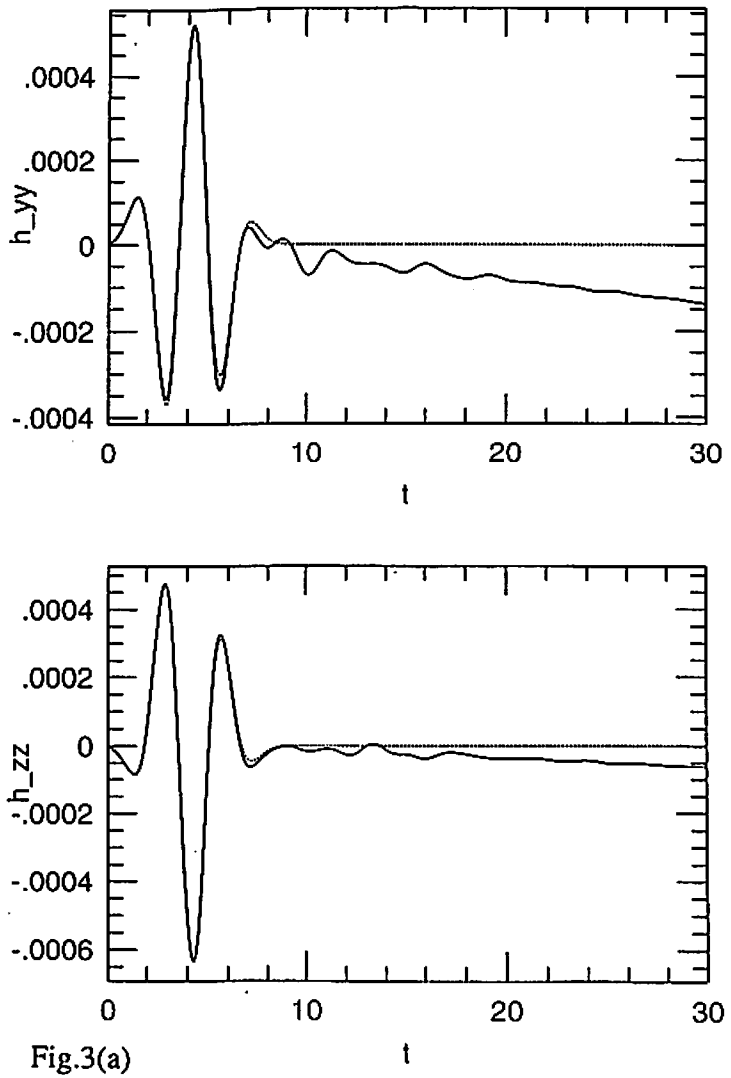
.0004
.0002
0
-.0002
-.0004
h_yy
0
10
20
30
t
.0004
.0002
0
-.0002
-.0004
-.0006
h_zz
0
10
20
30
t

Fig.3(a)

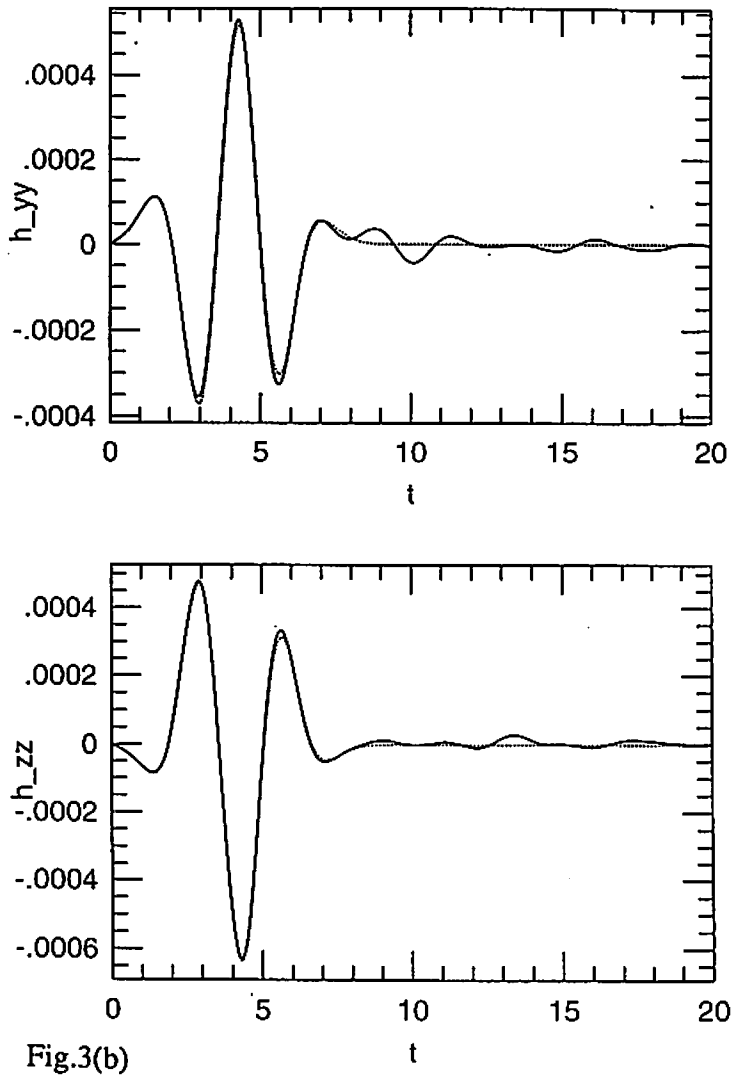
.0004
.0002
0
-.0002
-.0004
h_yy
0
5
10
15
20
t
.0004
.0002
0
-.0002
-.0004
-.0006
h_zz
0
5
10
15
20
t

Fig.3(b)

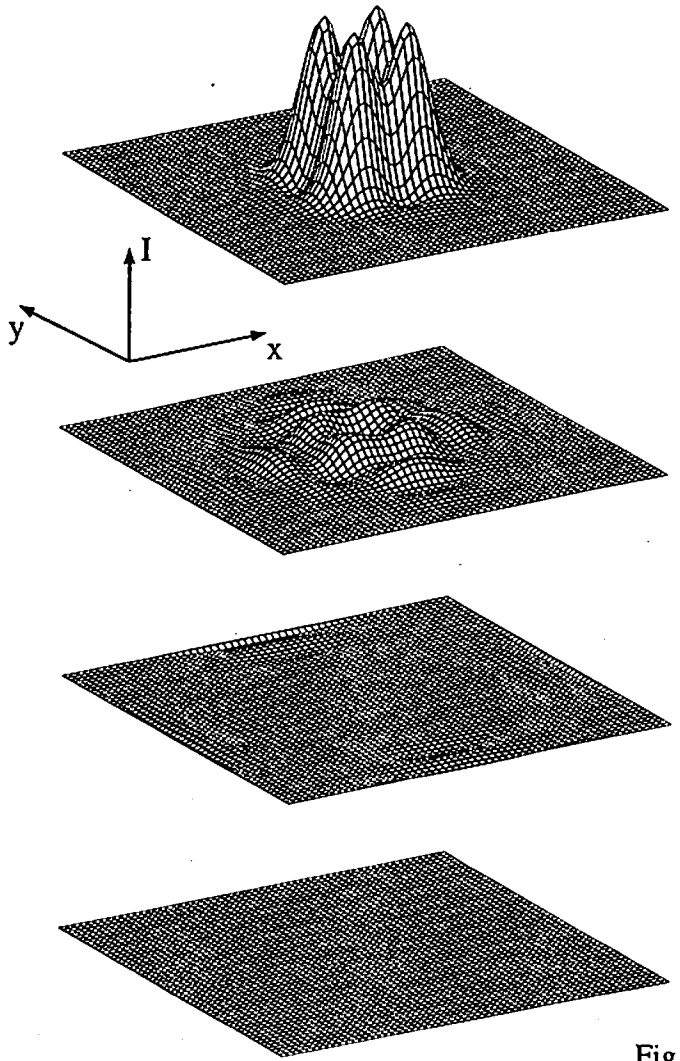

Fig.4(a)

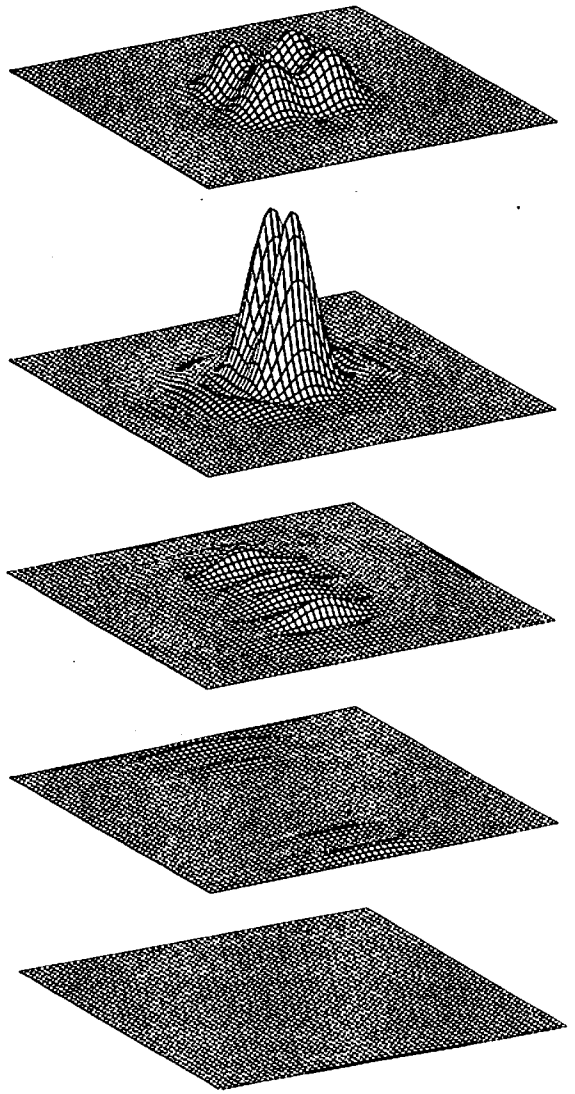

Fig4.(b)

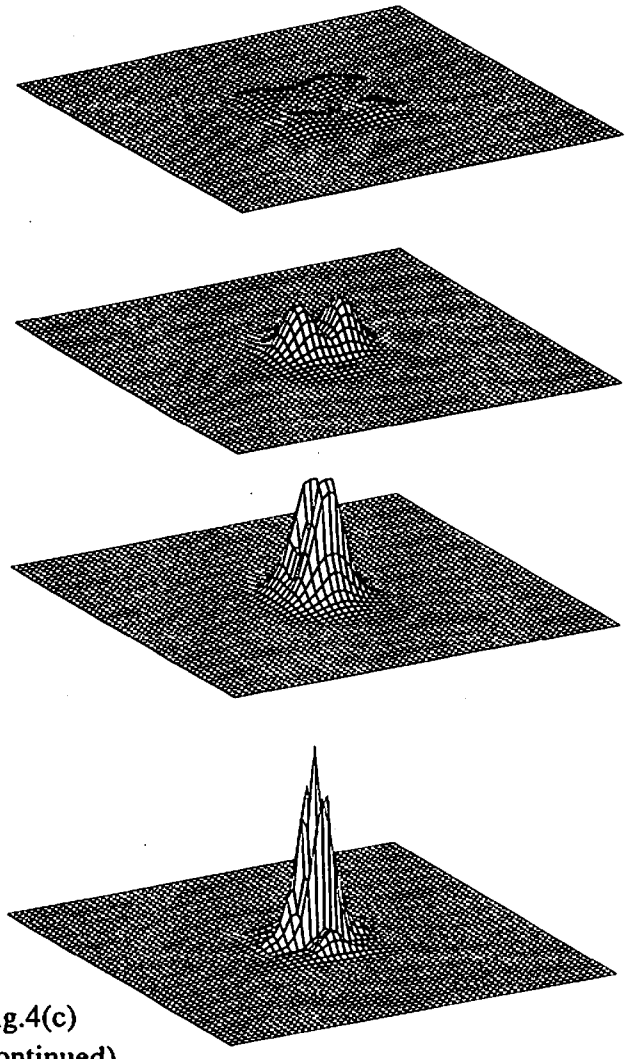

Fig.4(c)
(Continued)

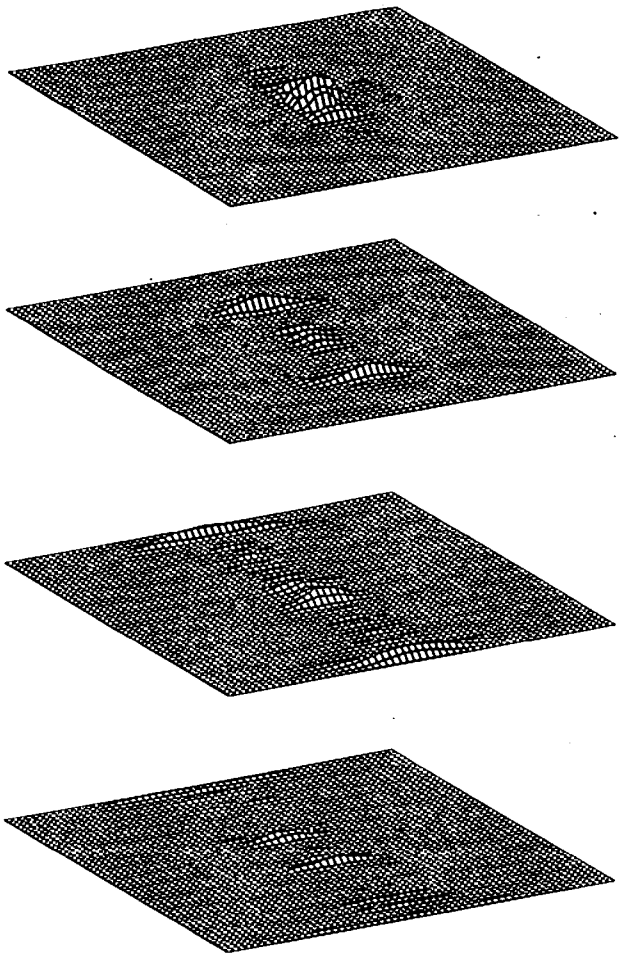

Fig.4(c)

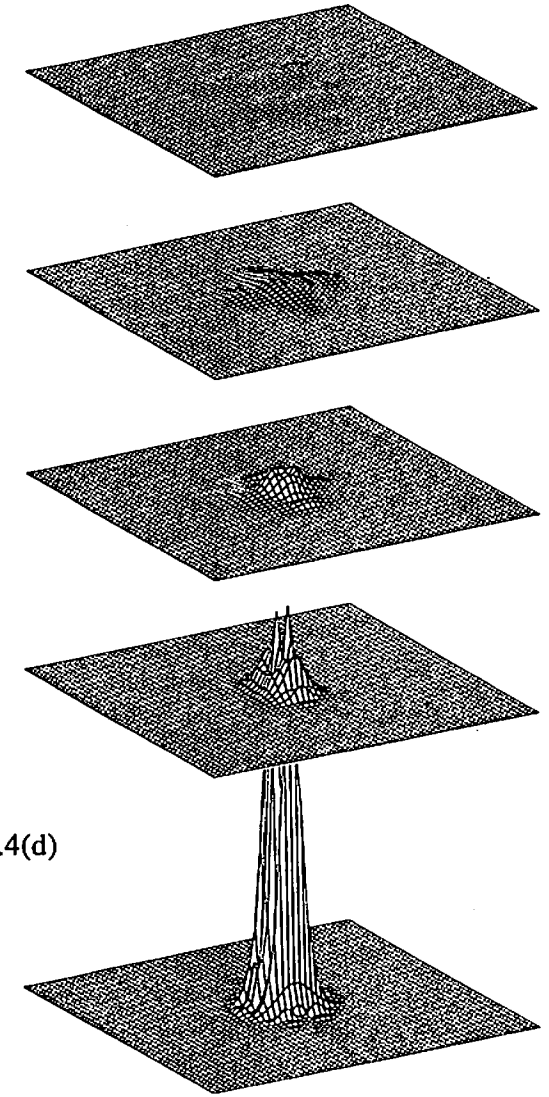

Fig.4(d)

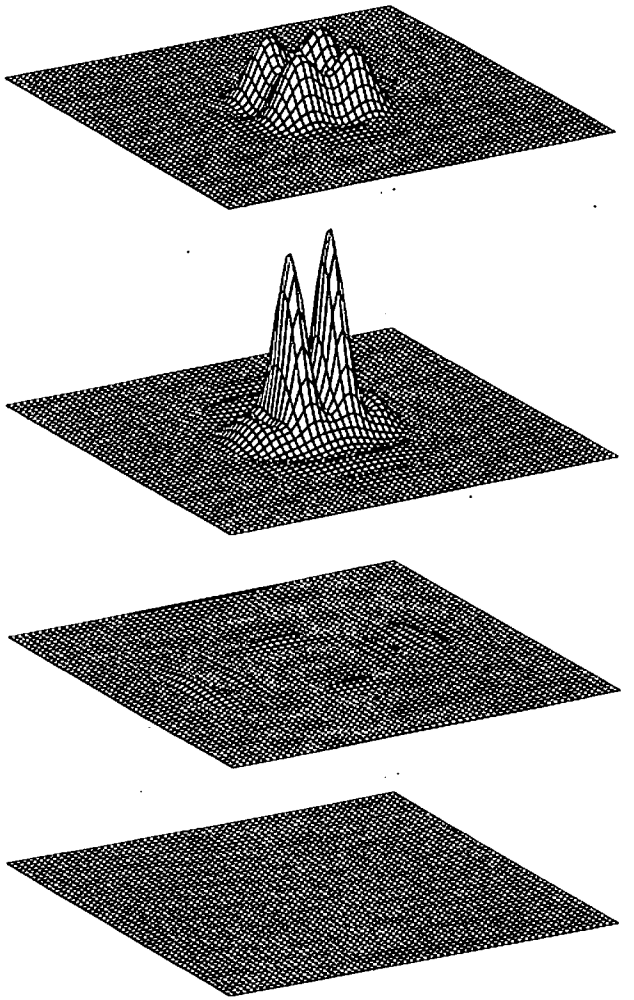

Fig.4(e)

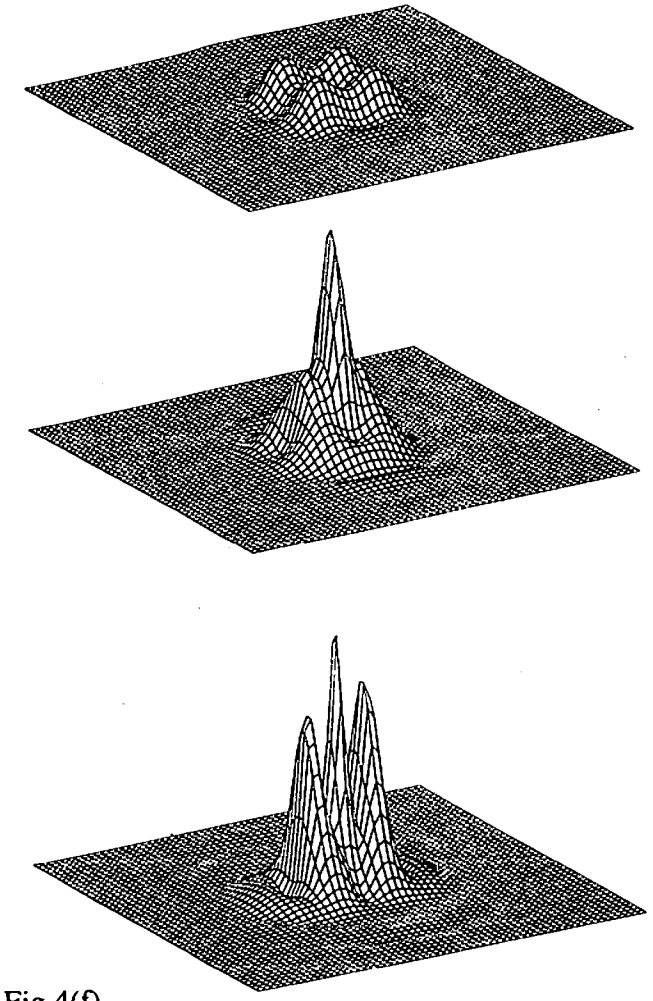

Fig.4(f)
(Continued)

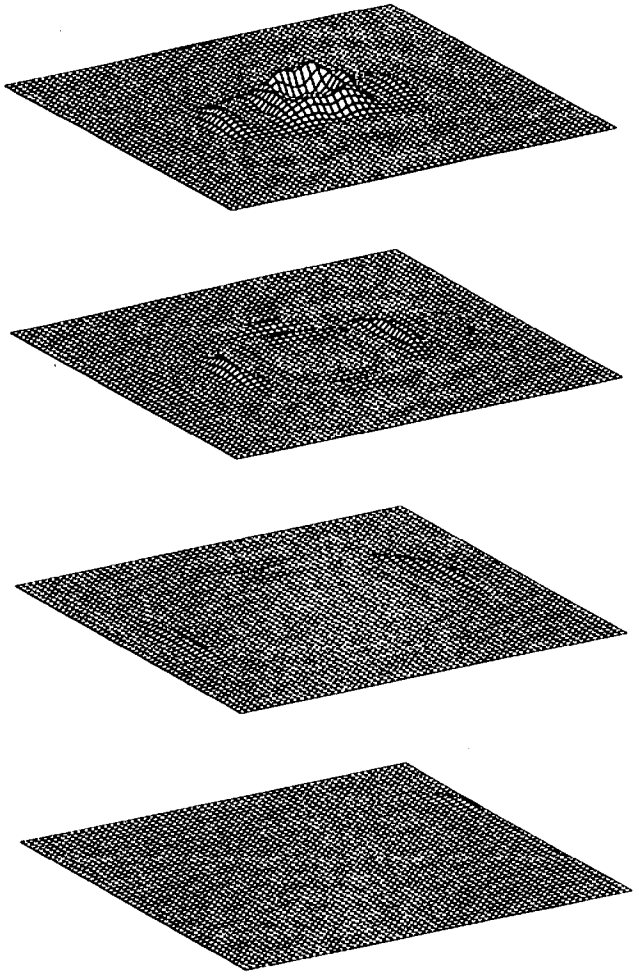

Fig.4(f)

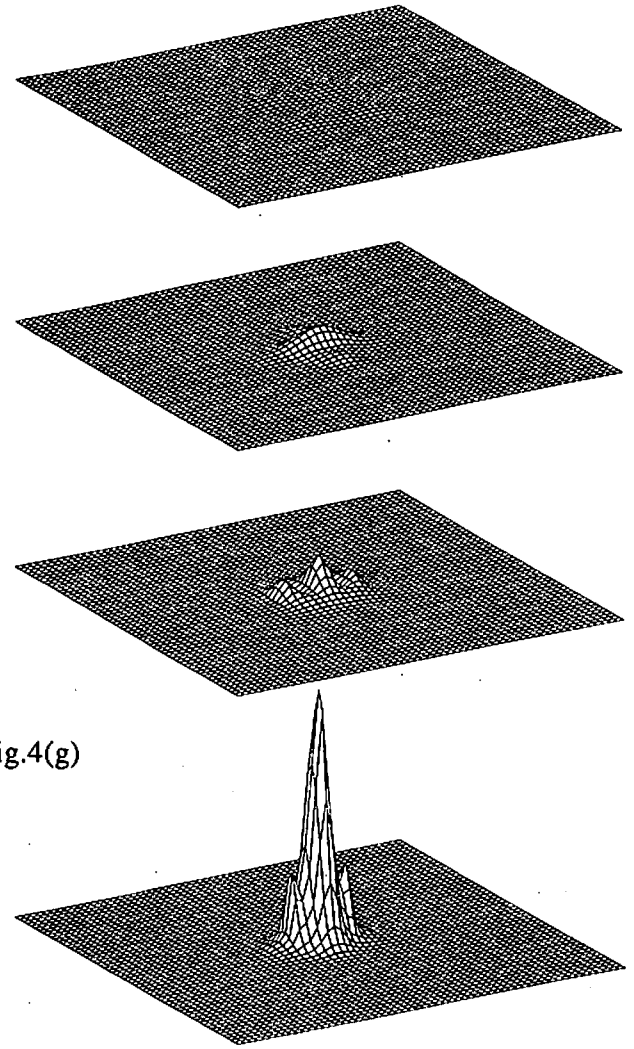

Fig.4(g)

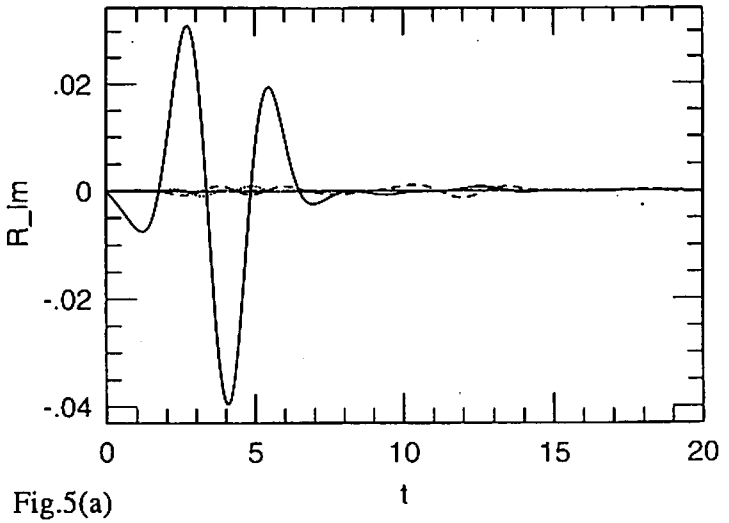

Fig.5(a)

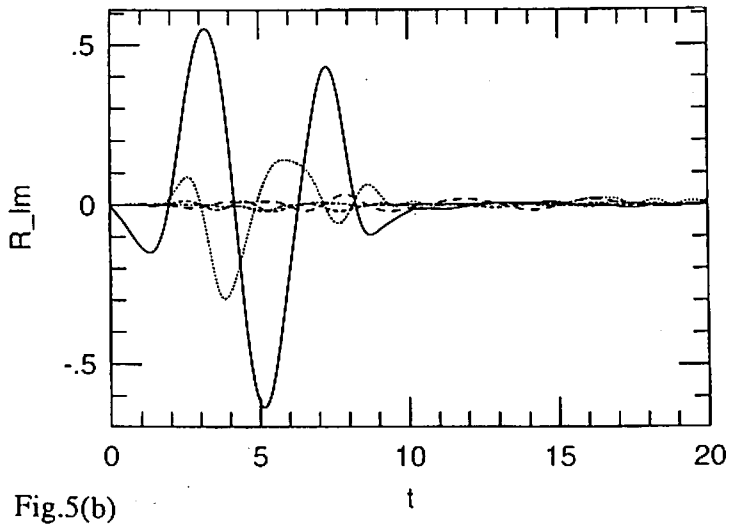

Fig.5(b)

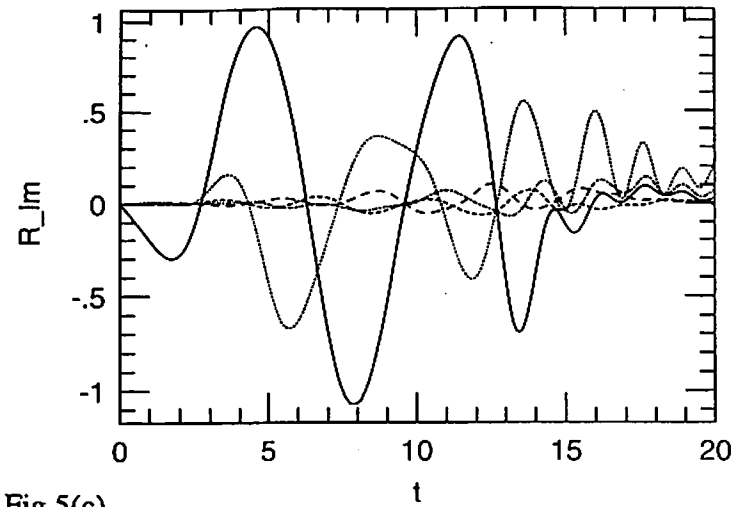

Fig.5(c)

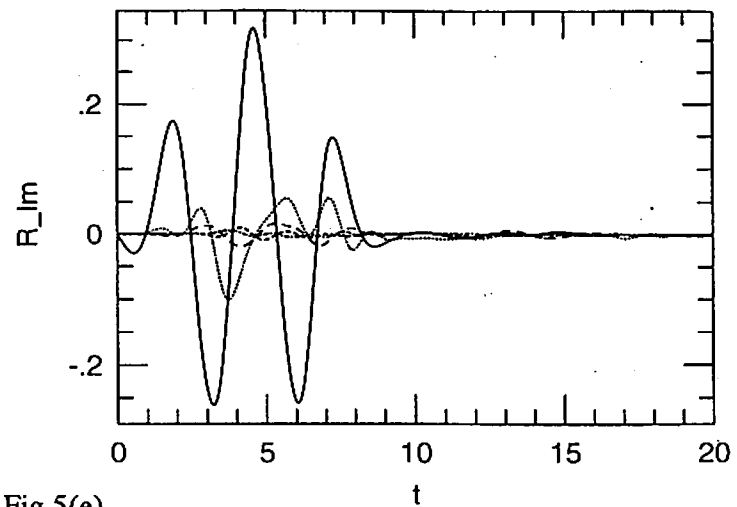

Fig.5(e)

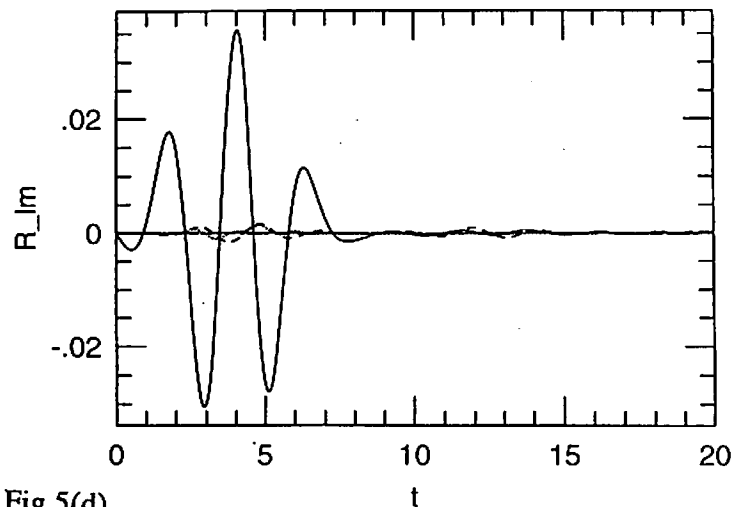

Fig.5(d)

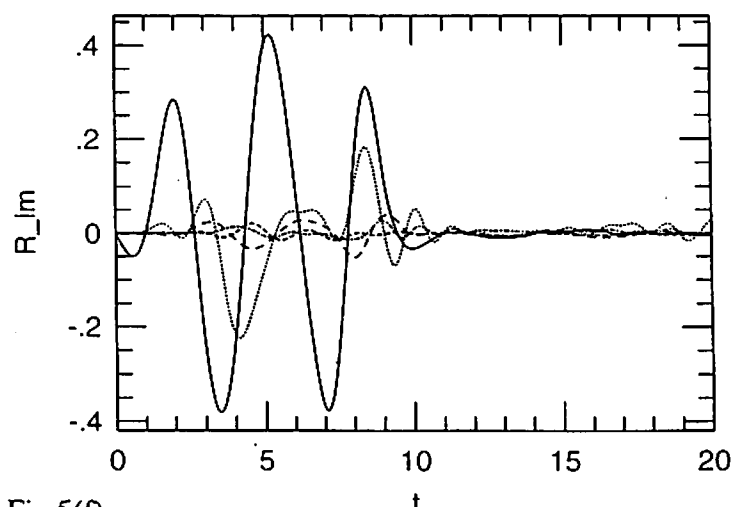

Fig.5(f)

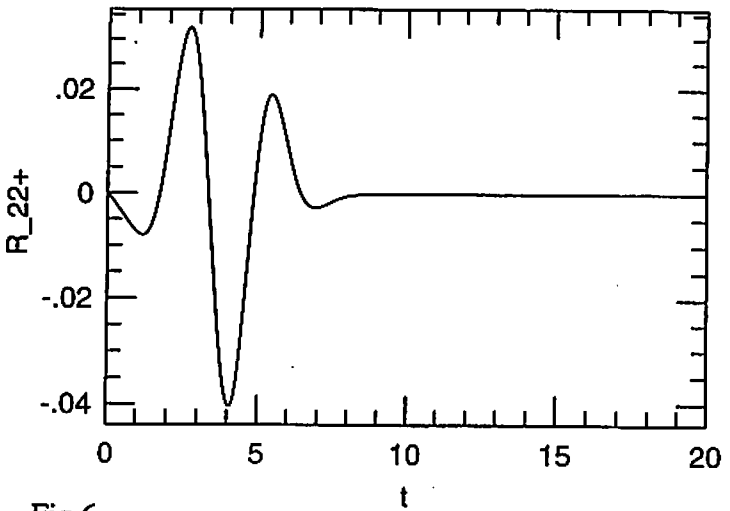

Fig.6

Fully Relativistic 3D Numerical Simulations of Coalescing Binary Neutron Stars

TAKASHI NAKAMURA

Yukawa Institute for Theoretical Physics
Kyoto University, Kyoto 606, Japan

ABSTRACT

Basic equations and numerical methods of a 3D numerical relativity code developed recently are shown. For a time slice and 3-space coordinate condition, conformal time slicing and pseudo-minimal shear condition are adopted. Preliminary numerical simulations for coalescing binary neutron stars using $(80)^3$ Cartesian grids are shown. The results of spherically symmetric collapse to black hole, formation of rotating black hole and collision of two dust spheres are also shown. Qualitatively the code works well without serious difficulties. Full scale simulations with $\sim (400)^3$ grids are urgently required for quantitative arguments on the results.

1. Introduction

Coalescing binary neutron stars (or black holes) is one of the most important sources of gravitational waves for LIGO/VIRGO projects .[1] Comparing observed wave patterns in *The Last Three Minutes* of coalescing binary neutron stars (or black holes) with theoretical templates, mass and spin of neutron stars may be determined.[2] Sasaki[3] argued various aspects of post Newtonian calculations to obtain accurate templates in this conference.

In the last three minutes, v_{rot}/c is a good parameter for expansion since $v_{rot}/c \sim 0.1$. However in the final phase of the coalescence, there is no such small parameters. So one must abandon post Newtonian expansion. Numerical relativity is one of the methods to study such nonlinear phase of coalescing binary neutron stars which I like to call it as *The Last Three Milli Seconds.* For this problem, there are many numerical simulations using Newtonian hydrodynamics code either with or without radiation reaction forces by gravitational waves and Post-Newtonian corrections.[4] From these numerical results there are many perspectives on wave patterns of gravitational waves and dynamics of coalescing events. However since Newtonian hydrodynamics is not so good approximation in this case, I think that these simulations should be considered as preludes of full general relativistic ones.

Here I like to discuss recent development of my fully general relativistic code to simulate *The Last Three Milli Seconds.* In the workshop on numerical relativity, Wilson[5] as well as Seidel[6] presented development of their 3D code which can be found in this volume. As for cosmological problem Kurki-Suonio, Laguna and Matzner[7] have already published numerical results of their fully general relativistic 3D code. But here I restrict the problem only for asymptotically flat space-times for which I have already developed full 3D code for the propagation of localized gravitational waves.[8] Combining this with a 3D hydrodynamics code used for coalescing binary neutron stars[4] previously, I have tried to make a full 3D general relativistic code for the final phase of coalescing binary neutron stars.

2. Basic Equations

A)Initial Value Equations

In the (3+1)- formalism of the Einstein equations the line element is expressed as

$$ds^2 = -\alpha^2 dt^2 + \gamma_{ij}(dx^i + \beta^i dt)(dx^j + \beta^j dt), \tag{1}$$

where α, β^i and γ_{ij} are the lapse function, the shift vector and the intrinsic metric of 3-space, respectively. The initial data should satisfy the constraint equations;

$$^{(3)}R + K^2 - K_{ij}K^{ij} = 16\pi\rho_H, \tag{2}$$

$$K^j_{i;j} - K_{;j} = 8\pi J_i \tag{3}$$

where ${}^{(3)}R$, K_{ij}, K, ρ_H and J_i are scalar curvature, extrinsic curvature and its trace, energy density and momentum density of matter, respectively. In Eq.(3), ; means the covariant derivative with respect to metric γ_{ij}. Now we assume that γ_{ij} is conformally flat as

$$\gamma_{ij} = \phi^4 \tilde{\gamma}_{ij}, \tag{4}$$

where $\tilde{\gamma}_{ij}$ is the flat metric. We define the conformal transformation as

$$\begin{aligned} \tilde{K}_{ij} \equiv \phi^2 K_{ij}, \tilde{K}^j_i \equiv \phi^6 K^j_i, \tilde{K}^{ij} \equiv \phi^{10} K^{ij} \\ \rho_B \equiv \rho_H \phi^6 \text{ and } \tilde{J}_i \equiv J_i \phi^6. \end{aligned} \tag{5}$$

Now if we assume K = 0, Eq.(3) becomes

$$\tilde{K}^j_{i|j} = 8\pi \tilde{J}_i, \tag{6}$$

where | means the covariant derivative with respect to the flat metric $\tilde{\gamma}_{ij}$. We decompose $\tilde{K}_{ij}$ as

$$\tilde{K}_{ij} = \tilde{K}^{TT}_{ij} + (\tilde{W}_{i|j} + \tilde{W}_{j|i} - \frac{2}{3}\tilde{\gamma}_{ij}\tilde{W}^l_{|l}), \tag{7}$$

where $\tilde{K}^{TT}_{ij}$ is the transverse traceless part of $\tilde{K}_{ij}$ and $\tilde{W}_i$ is the longitudinal part of $\tilde{K}_{ij}$. Assuming $\tilde{K}^{TT}_{ij} = 0$ for simplicity, we rewrite Eq.(6) as

$$\Delta_f \tilde{W}_i + \frac{1}{3}(\tilde{W}^l_{|l})_{|i} = 8\pi \tilde{J}_i, \tag{8}$$

where Δ_f is the flat Laplacian. In the real coalescing binary neutron stars, $\tilde{K}^{TT}_{ij}$ at t=0 is needed from the results of post-Newtonian calculations or other methods.

Let us define the divergence of W^i as

$$DIV \equiv W^i_{|i}. \tag{9}$$

Taking the divergence of Eq.(8), we have

$$\Delta_f \ (DIV) = 6\pi \tilde{J}^i_{|i}. \tag{10}$$

We first solve Eq.(10) for given $\tilde{J}_i$. Using DIV, we can rewrite Eq.(8) as

$$\Delta_f \tilde{W}_i = -\frac{1}{3}(DIV)_{|i} + 8\pi \tilde{J}_i. \tag{11}$$

Although Eq.(8) was the coupled elliptic type equation of $\tilde{W}_i$ originally, the above procedure enables us to decouple Eq.(8). The boundary conditions for Eq.(10) and

Eq.(11) are

$$\tilde{W}_i = \frac{1}{r^3}\epsilon_{ijk}x^j M^k + O(\frac{1}{r^3}) \tag{12}$$

and

$$DIV = O(\frac{1}{r^4}), \tag{13}$$

where M^k is the constant related to angular momentum of the system. Now Eq.(2) is rewritten as

$$\Delta_f(\phi) = -\frac{2\pi\rho_B}{\phi} - \frac{1}{8}\phi^{-7}\tilde{K}_{ij}\tilde{K}^{ij}, \tag{14}$$

We solve Eq.(14) for given ρ_B under the boundary condition

$$\phi = 1 + \frac{M_G}{2r} + O(\frac{1}{r^3}), \tag{15}$$

where M_G is the gravitational mass of the system.

B) Relativistic Hydrodynamics

We assume the perfect fluid. Then the energy momentum tensor $T_{\mu\nu}$ becomes

$$T_{\mu\nu} = (\rho + \rho\epsilon + P)u_\mu u_\nu + P g_{\mu\nu}, \tag{16}$$

where ρ, ϵ, P and u_μ are the proper mass density, specific internal energy, pressure and the four velocity of the fluid, respectively. We define the projection tensor $h_{\mu\nu}$ as

$$h_{\mu\nu} = g_{\mu\nu} + n_\mu n_\nu, \tag{17}$$

where n_μ is the normal vector to the hypersurface. ρ_H, J_i and S_{ij} are defined as

$$\rho_H \equiv T_{\mu\nu}n^\mu n^\nu, J_i \equiv -T_{\mu\nu}n^\mu h_i^\nu$$

and

$$S_{ij} \equiv T_{\mu\nu}h_i^\mu h_j^\nu. \tag{18}$$

Then the relativistic hydrodynamics equation ($T^\mu_{\nu;\mu} = 0$ where ; is the covariant derivative with respect to $g_{\mu\nu}$) is written as

$$\begin{aligned}\frac{\partial}{\partial t}(\sqrt{\gamma}\, J_i) + \frac{\partial}{\partial x^l}(\sqrt{\gamma}J_i V^l) = -\alpha\sqrt{\gamma}\frac{\partial P}{\partial x^i} - \sqrt{\gamma}(P+\rho_H)\frac{\partial \alpha}{\partial x^i} \\ +\frac{1}{2}\alpha\sqrt{\gamma}\frac{\partial \gamma_{kl}}{\partial x^i}\frac{J^k J^l}{(P+\rho_H)} + \sqrt{\gamma}J_l\frac{\partial \beta^l}{\partial x^i},\end{aligned} \tag{19}$$

$$\frac{\partial}{\partial t}(\sqrt{\gamma}\alpha u^0\rho\epsilon) + \frac{\partial}{\partial x^l}(\sqrt{\gamma}\alpha u^0\rho\epsilon V^l) = -P\frac{1}{\alpha\sqrt{\gamma}}\frac{\partial}{\partial x^\nu}(\alpha\sqrt{\gamma}u^\nu), \tag{20}$$

$$\frac{\partial}{\partial t}(\sqrt{\gamma}\alpha u^0\rho) + \frac{\partial}{\partial x^l}(\sqrt{\gamma}\alpha u^0\rho V^l) = 0, \tag{21}$$

$$\gamma = det(\gamma_{ij}), \tag{22}$$

and

$$V^l = \alpha J^l/(P + \rho_H) - \beta^l = u^l/u^0. \tag{23}$$

Left hand sides of Eq.(19),(20) and (21) are similar to the corresponding equations in Newtonian hydrodynamics if we define the following quantities corresponding to variables in Newtonian hydrodynamics as

$$\rho_N \equiv \sqrt{\gamma}\alpha u^0\rho$$

and

$$u_i^N \equiv J_i/(\alpha u^0\rho). \tag{24}$$

Then left hand sides become as

$$\frac{\partial}{\partial t}(\rho_N u_i^N) + \frac{\partial}{\partial x^l}(\rho_N u_i^N V^l) = \text{.....}, \tag{19$'$}$$

$$\frac{\partial}{\partial t}(\rho_N\epsilon) + \frac{\partial}{\partial x^l}(\rho_N\epsilon V^l) = \text{.....}, \tag{20$'$}$$

and

$$\frac{\partial}{\partial t}\rho_N + \frac{\partial}{\partial x^l}(\rho_N V^l) = 0. \tag{21$'$}$$

Using the variables ρ_N, u_i^N and ϵ, we can apply Newtonian hydrodynamics code developed by Nakamura and Oohara[4)] almost as it is. To complete relativistic hydrodynamics equations, we need the equation of state,

$$P = P(\epsilon, \rho)$$

C) Time evolution of the extrinsic curvatures

The evolution equations of the extrinsic curvatures are

$$\frac{\partial}{\partial t}K_{ij} - \frac{\partial}{\partial x^l}(K_{ij}\beta^l) = (SK)_{ij}^{main} + (SK)_{ij}^{non} + (SK)_{ij}^{\beta}, \tag{25}$$

where

$$(SK)_{ij}^{main} = \alpha\{{}^{(3)}R_{ij} - 8\pi(S_{ij} + \frac{1}{2}\gamma_{ij}(\rho_H - S_l^l))\} - \alpha_{|ij}, \tag{26}$$

$$(SK)_{ij}^{non} = \alpha(KK_{ij} - 2K_{il}K_j^l), \tag{27}$$

and

$$(SK)_{ij}^{\beta} = K_{mj}\frac{\partial\beta^m}{\partial x^i} + K_{mi}\frac{\partial\beta^m}{\partial x^j} - K_{ij}\frac{\partial\beta^m}{\partial x^m}, \tag{28}$$

where | means the covariant derivative with respect to γ_{ij}. In the left hand side of

equation (25), the transport term is treated numerically in the same way as that in the hydrodynamics equations.

D) Time Slice

Even for $t > 0$, we define the conformal factor ϕ as

$$\phi \equiv (det(\gamma_{ij}))^{\frac{1}{12}}. \tag{29}$$

We define α as

$$\alpha = \exp(-2(\tilde{\phi} + \frac{\tilde{\phi}^3}{3} + \frac{\tilde{\phi}^5}{5})), \tag{30}$$

and

$$\tilde{\phi} \equiv \phi - 1.$$

Shibata and Nakamura[9] called this time slice as conformal time slicing because α is determined by the conformal factor ϕ. The detailed discussions on the nature of the conformal time slicing is given in Shibata and Nakamura.[9] Here we just note that in the conformal time slice the space outside the central matter quickly approaches the Schwarzschild metric. At the same time, it has the singularity avoidance nature similar to the maximal slicing. The conformal factor ϕ is determined by either solving the evolution equation for ϕ or Hamiltonian constraint equations as

$$\frac{\partial \phi}{\partial t} = \frac{\phi}{12}(-2\alpha K + \frac{2}{\phi^6}\frac{\partial}{\partial x^l}(\phi^6 \beta^l)), \tag{31}$$

or

$$\tilde{\Delta}\phi = -2\pi\rho_H \phi^5 - \frac{\phi^5}{8}(K_{ij}K^{ij} - K^2 - \phi^{-4}\,{}^{(3)}\tilde{R}), \tag{32}$$

where $\tilde{\Delta}$ is the Laplacian with respect to

$$\tilde{\gamma}_{ij} = \gamma_{ij}/\phi^4.$$

E) Spatial Coordinate

We define conformal transformation as

$$\begin{gathered} \tilde{K}_{ij} \equiv \phi^{-4} K_{ij},\ \tilde{\beta}_i = \phi^{-4}\beta_i, \\ K = \tilde{K}, \tilde{K}^j_i = K^j_i \text{ and } \tilde{\beta}^i = \beta^i. \end{gathered} \tag{33}$$

Then the equation for metric becomes

$$\frac{\partial}{\partial t}\tilde{\gamma}_{ij} = (\tilde{\beta}_{i|j} + \tilde{\beta}_{j|i} - \frac{2}{3}\tilde{\gamma}_{ij}\tilde{\beta}^l_{|l}) - 2\alpha(\tilde{K}_{ij} - \frac{1}{3}\tilde{\gamma}_{ij}\tilde{K}) = A^T_{ij} \tag{34}$$

where | means the covariant derivative with respect to $\tilde{\gamma}_{ij}$. We demand that the usual

divergence of the right hand side of Eq.(34) to be zero, i. e.

$$\frac{\partial}{\partial x^j} A^T_{ij} = 0. \tag{35}$$

Then Eq.(35) becomes

$$\begin{aligned} \Delta_f \beta^i + \frac{1}{3}\frac{\partial}{\partial x^i}(\frac{\partial \beta^l}{\partial x^l}) = \frac{\partial}{\partial x^j}(2\alpha(\tilde{K}_{ij} - \frac{1}{3}\tilde{K}\tilde{\gamma}_{ij})) - \frac{\partial}{\partial x^j} \\ [(\tilde{\gamma}_{jl} - \delta_{jl})\frac{\partial \beta^l}{\partial x^i} + (\tilde{\gamma} - \delta_{il})\frac{\partial \beta^l}{\partial x^j} - \frac{2}{3}(\tilde{\gamma}_{ij} - \delta_{ij})\frac{\partial \beta^l}{\partial x^l} + \beta^l \frac{\partial}{\partial x^l}\tilde{\gamma}_{ij}] \end{aligned} \tag{36}$$

Eq.(36) is the similar to Eq.(8) in the initial value equations but in general Eq.(36) is the coupled equation for β^i. Instead of Eq.(35), if we demand

$$A^{Tj}_{i|j} = 0, \tag{37}$$

we have the minimal shear condition by York and Smarr.[10] In this sense we call Eq.(35) as "pseudo" minimal shear condition. Note here that we perform the same conformal transformation in the source terms of the evolution equations of extrinsic curvatures.

3. Numerical Methods

Although one can use any equation of state, for simplicity, we use a simple equation of state in this paper to express the equation of state for neutron stars as

$$P = \rho\epsilon \ , \tag{38}$$

For hydrodynamics equations we use a certain kind of TVD(Total Variation Diminishing) method adopted in Oohara and Nakamura.[4] The hydrodynamic code has passed various checking problems which are shown in Oohara and Nakamura.[4] For the evolution equation of metric all the equations are written as

$$\frac{\partial Q}{\partial t} - \frac{\partial (Q\beta^l)}{\partial x^l} = S \ , \tag{39}$$

where S is the source term. We use a leap frog method for the time derivative with second order spatial derivatives in the source terms. As for the second term in the left hand side of Eq.(39), we use the same procedure as the hydrodynamics equations regarding $-\beta^l$ as V^l. We use Cartesian equal spacing grids of $(80)^3$. For the elliptic equations we use ICCG method shown in Oohara and Nakamura[11] in details. The size of source program is about 6000 lines in FORTRAN. The typical CPU time by VP2600 (5GFLOPS, 500Mbyte Machine) in the present test simulations is three hours.

At present to make Eq.(36) simple, we use β^i at the previous step in r.h.s of Eq.(36). We rewrite Eq.(32) as

$$\Delta_f\phi = \Delta_f\phi - \tilde{\Delta}\phi - 2\pi\rho_H\phi^5 - \frac{\phi^5}{8}(K_{ij}K^{ij} - K^2 - {}^{(3)}\tilde{R}).$$

We use ϕ at the previous step in r.h.s of the above equation. By this treatment we do not need the iteration to solve β^i and ϕ. Moreover we can use the same subroutine in the initial value equations. To increase the accuracy of β^i and ϕ we need iterations or different numerical techniques in future simulations. However the above treatment seems to be enough for the present test simulations to know the global behavior of the numerical schemes and the coordinate conditions. We use the units of

$$M = M_\odot\ , L = \frac{GM_\odot}{c^2} \text{ and } T = \frac{GM_\odot}{c^3}\ . \tag{40}$$

4. Numerical Results

A)Coalescing Binary Neutron Stars

We put two spherical neutron stars of mass 1.0 and radius r_0=6 with density distribution (ρ_N) of $n = 1$ polytrope at $x = r_0$ and $x = -r_0$. This means that two neutron stars just touch with each other. We add the rigid rotation with angular velocity Ω as well as the approaching velocity to this system such that v_x^N and v_y^N are give as

$$v_x^N = -\Omega y - sgn(x)\Omega r_0,$$

$$v_y^N = \Omega x.$$

We solved three Models BI1, BI2 and BI3 with different value of Ω. Values of the total angular momentum divided by the square of the gravitational mass are 0.71, 1.43 and 1.01 for BI1, BI2 and BI3, respectively. The absolute value of outermost grid in each direction is 40. The total number of grids is $(80)^3$ and we use equal spacing grids with grid spacing 1 in our units. In Fig.1-a) to d), we show the time evolution of density (left) and "energy density of gravitational wave" (right) defined by $\rho_{GW} \equiv (A_{ij}^{TT})^2 r^2/(32\pi)$ (right) for Model BI3. Strictly speaking, energy density of the gravitational waves can not be defined locally. So by "gravitational wave energy" I mean the above definition using numerical data. In each figure we show density contours in $x-y, y-z$ and $x-z$ plane. The maximum and minimum value of density are shown as MAX and MIN. Each level of density contour is set as equal spacing in linear scale from MAX to MIN. In density contour (left), arrows mean the velocity vector V^ℓ. We see that two neutron stars rotate about 90° as well as they coalesce. The final object will be a rotating black hole although I have not tried to determine apparent horizon yet. The evolution of "gravitational wave energy" (right) shows an interesting feature of generation and

propagation of the wave. We see the spiral wave pattern in x-y plane while in x-z and z-y planes we see different pattern with main peak around z-direction. Naively quadrupole wave pattern given as

$$\rho_{GW} = (A_{ij}^{TT})^2 r^2/(32\pi) \propto \cos^2\theta + \sin^2\theta \sin^2(2\Omega(t-r) - 2\varphi)/4,$$

can explain this behavior. In x-y plane since $\theta = \pi/2, \rho_{GW}$ is constant along the spiral of $r = -\varphi/\Omega + const$, while near $\theta \sim 0$(z-directions) $\rho_{GW} \propto \cos^2\theta$

In the outermost grid point I put outgoing wave condition to $\tilde{\gamma}_{ij}$ and K_{ij}. However in the present simulation, $x_{\max}(= y_{\max} = z_{\max})$ is comparable to the wave length of the expected gravitational wave ~ 40. I tried various boundary conditions ($\sim$10 different types) but none works well. So adopting a simple extrapolation at the numerical boundary, I stopped simulations when the gravitational wave reaches the outermost grid point. A method to overcome this boundary problem is to increase $x_{\max}$ so that the outgoing wave boundary condition becomes appropriate. For this we need more powerful computers.

We computed the total gravitational wave energy E_{GW} by

$$E_{GW} = \int dt \int \rho_{GW} d\Omega \Big|_{r=20}$$

At $t = 35$, the total energy amounts to 3×10^{-3} for Model BI3. In other Models the results are qualitatively the same as those of BI3.

B)Spherically Symmetric Dust Collapse

To check whether A_{ij}^{TT} shows the gravitational waves' degree of freedom, I performed a spherically symmetric dust collapse using the same 3D code with $(80)^3$ grids. We put a dust sphere of radius $r_0 = 6$ and the total mass 1 with density distribution proportional to $\sin(\pi r/r_0)/r$. In Fig.2 we show density contours and "gravitational wave energy density". Although A_{ij}^{TT} has the value at the center, it does not propagate outward, and its value is small compared with that in Fig.1. Since the meaning of transverse traceless is clear only in an asymptotically flat region, the result of Fig.2 is consistent with the idea that A_{ij}^{TT} represents gravitational waves. The integration of ρ_{GW} gives us $E_{GW} \sim 10^{-7}$ at t=30 observed at r=20. This value is much smaller than the previous case, which is also consistent with being A_{ij}^{TT} gravitational energy.

C)Formation of a rotating black hole

Stark and Piran[12)] first showed axially symmetric numerical simulations of formation of rotating black holes. Although our coordinate conditions are different from theirs, we set similar initial conditions. We use a simple equation of state as Eq.(38) which is the same as Stark and Piran. We put a spherically symmetric density distribution (ρ_N) of $n = 1$ polytrope with internal energy necessary for Newtonian equilibrium. For this system we add the rotation velocity with constant Ω. We solved four models ROT1, ROT2, ROT3 and ROT4. Each model is characterized by the value of a/M_g where a

is the angular momentum per unit gravitational mass M_g. The value of a/M_g is 0.3 , 0.5, 0.8 and 1. for ROT1, ROT2, ROT3 and ROT4, respectively. We show the density contours and " gravitational energy" of ROT3 in Fig.3-a) to d). In the density contour, due to the centrifugal force, collapse in the direction perpendicular to the rotation axis is slowed. So we see the oblate spheroid. The gravitational wave generated by this motion has pattern shown in right figures. In x-y plane it is almost axially symmetric with two or three peaks. Since I am using the Cartesian coordinates, deviations from axial symmetry can be seen. But they are not so large. In x-z and y-z plane the wave pattern looks like quadrupole emission ($\propto \sin^4\theta$) which is also the case in Stark and Piran. The total energy radiated at t=30 observed at r=20 are $5.7 \times 10^{-7}, 3.8 \times 10^{-6}, 1.5 \times 10^{-5}$, and 3.6×10^{-5} for ROT1, ROT2, ROT3 and ROT4, respectively. Stark and Piran found for low a, the total energy is proportional to a^4 and it levels off at $a \sim M_g$. This same dependence can be seen also in our case. That is, the total energy is expressed approximately

$$E_{GW} = 5 \times 10^{-5}(a/M_g)^4.$$

Corresponding case in Stark and Piran to ROT1, the total energy is $\sim 1.5 \times 10^{-5}$ which is ~ 20 times larger than our case. But this is consistent. Stark and Piran evolve the initial data up to t=100 while we do only up to t=30. So the total energy we observed is just expected from the results of Stark and Piran.

D)Collision of Two Dust Sphere

Recently Anninos et al.[13] performed numerical simulations of two black hole collision which was first done by Smarr. To mimic the collision of two black hole we have performed collision of two dust sphere. We put two dust sphere of mass 0.5 and radius 3 just contact each other. Each dust sphere collapses to black hole and coalesce to a single black hole. Fig. 4 shows an example of such simulations. We see the quadrupole like wave pattern which is the dominant multipole in two black hole collision.

5. Summary

One of the goals in numerical relativity is to perform simulations of general space times for any initial data. For this, construction of 3D code is essential. In this article I showed what I have been done for this purpose. At present my code is on a way of construction. I made some approximations to the solution of pseudo minimal shear condition (Eq.(36)) and conformal factor ϕ (Eq.(32)). The number of grids is not enough for the application of the outgoing wave boundary conditions at the numerical outermost boundary. Although all the results shown in §4 should be considered preliminary, qualitatively the code works well without serious difficulties. I think that the completion of the present 3D code will be done near future.

This work is supported by the Grant-in-Aid for Scientific Research on Priority Area of Ministry Education (04234104).

References

1) A. Brillet, this volume.

2) C. Cutler et al., Phys. Rev. Lett. **70** (1993), 2984.
C. Cutler and E.E. Flanagen, Phys. Rev. **D49** (1994), 2658.

3) M. Sasaki, this volume.

4) K. Oohara and T. Nakamura, Prog. Theor. Phys. **81** (1989), 360; **821** (1989), 535; **82** (1989) 1060; **83** (1990), 906; **86** (1881), 73; **88** (1992), 307.
M. Shibata, K. Oohara and T. Nakamura, Prog. Theor. Phys. **88** (1992), 1079; **89** (1993), 809.
F. Rasio and S. L. Shapiro, Astrophys. J. **401** (1992), 226.
J. Centrella and S. McMillan, Astrophys. J. **416** (1993), 719.
M. B. Davies, W. Benz, T. Piran and F. K. Thielman, Astrophys. J. **431** (1994), 742.

5) J. Wilson, this volume.

6) E. Seidel, this volume.

7) H. Kurki-Suonio, P. Laguna and R. A. Matzner, Phys. Rev. **D48** (1993), 3611.

8) T. Nakamura and K. Oohara, in "Frontiers of Numerical Relativity" ed. C. Evans (Cambridge Univ. Press 1989), 254.
T. Nakamura, in Proceedings of GR13 ed. N. Ashby (Cambridge Univ. Press 1989), 61.

9) M. Shibata and T. Nakamura, Prog. Theor. Phys. **88** (1992), 317.

10) J. York and L. Smarr, Phys. Rev. **D17** (1978), 1945.

11) K. Oohara and T. Nakamura, in "Frontiers of Numerical Relativity" ed. C. Evans (Cambridge Univ. Press 1989), 74 .

12) R. Stark and T. Piran, Phys. Rev. Lett. **55** (1985), 891, in Dynamical Spacetimes and Numerical Relativity, ed. J. Centrella Cambridge Univ. Press 1985, P40.

13) P. Anninos et al., Phy. Rev. Lett. **71** (1993), 2851.

Fig.1-a

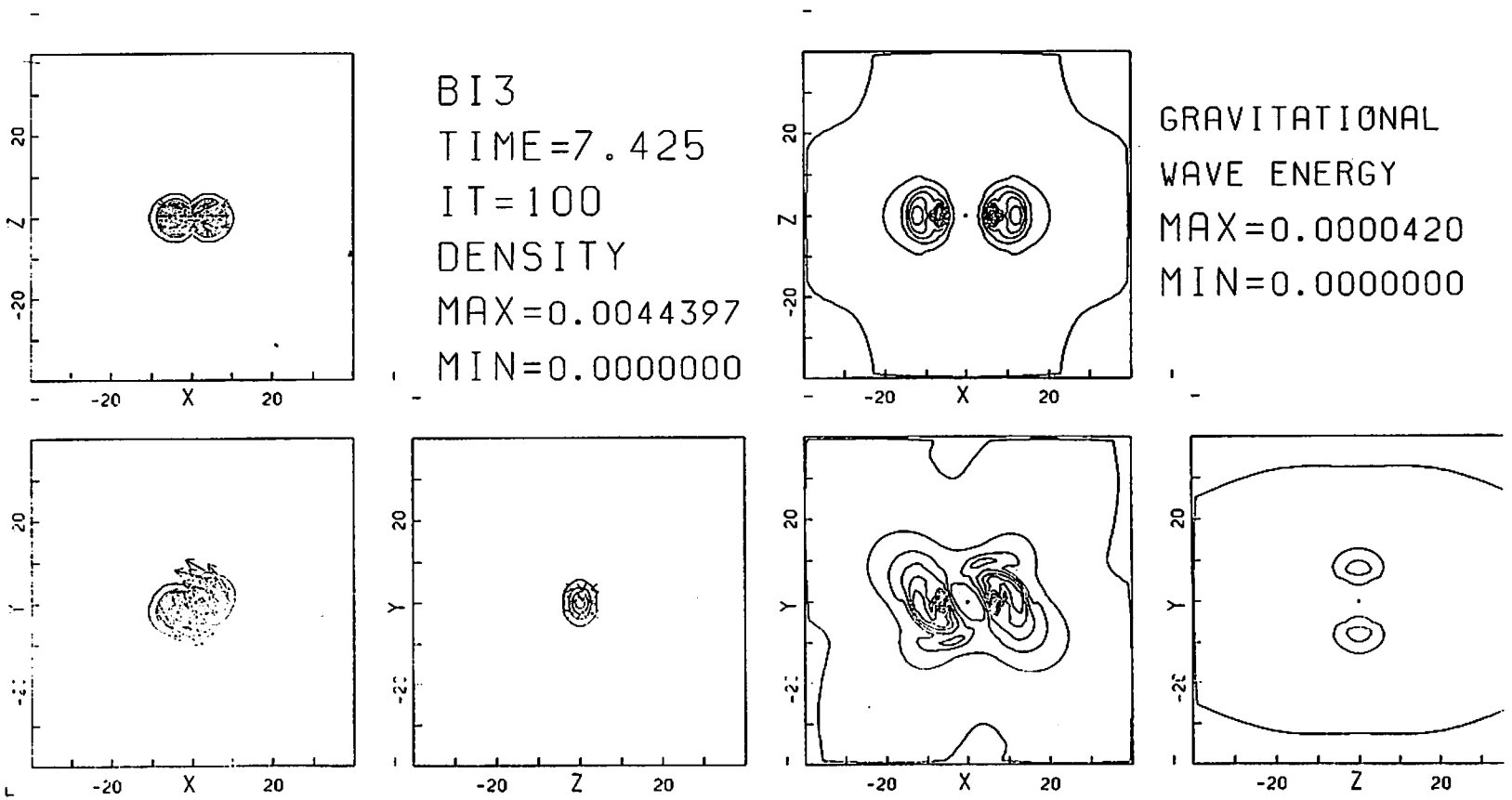
BI3
TIME=7.425
IT=100
DENSITY
MAX=0.0044397
MIN=0.0000000
GRAVITATIONAL
WAVE ENERGY
MAX=0.0000420
MIN=0.0000000
-20
X
20
Z
Y

Fig.1-b

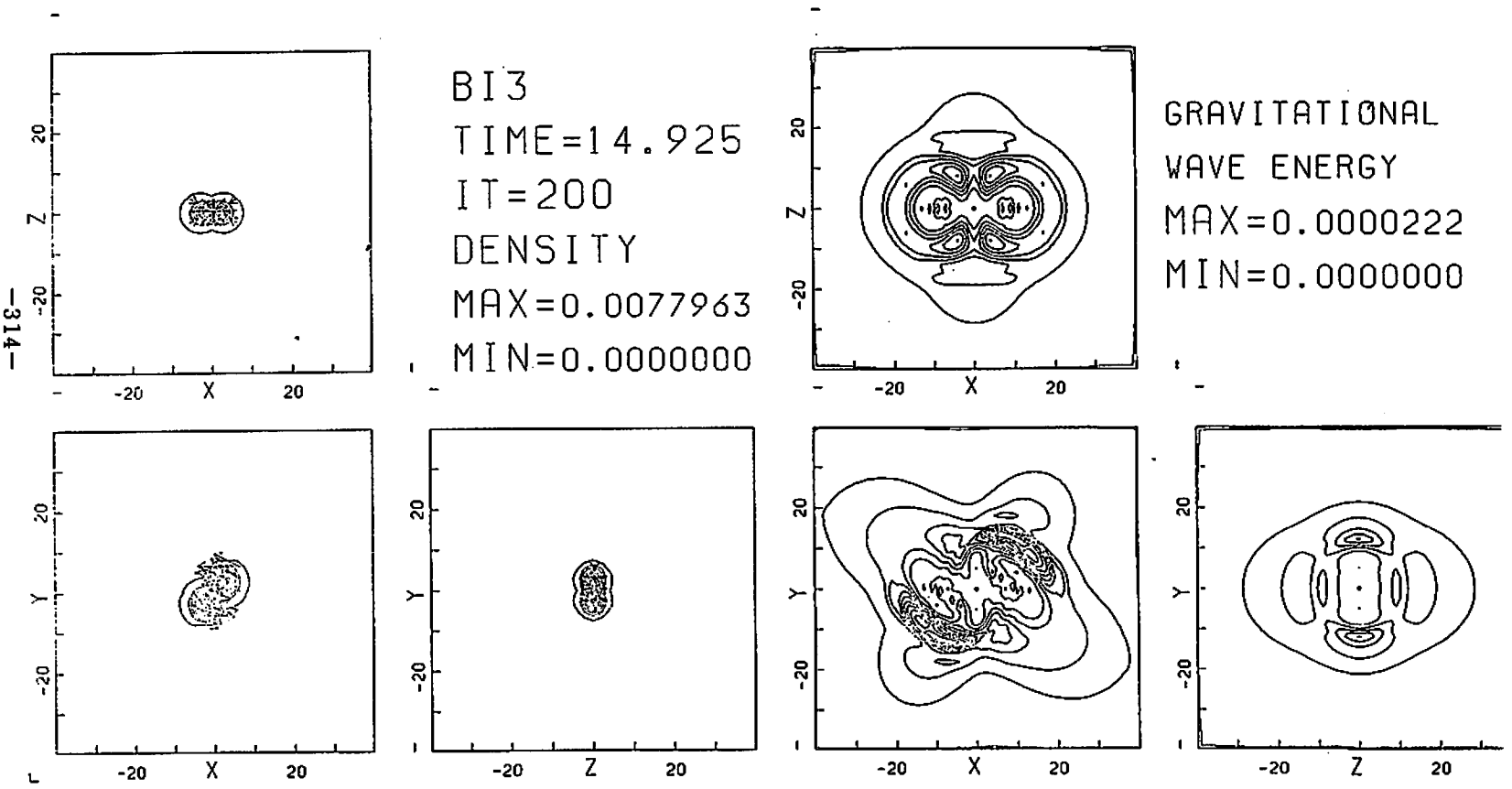
BI3
TIME=14.925
IT=200
DENSITY
MAX=0.0077963
MIN=0.0000000
GRAVITATIONAL
WAVE ENERGY
MAX=0.0000222
MIN=0.0000000
Z
X
Y
-20
20

Fig.1-c

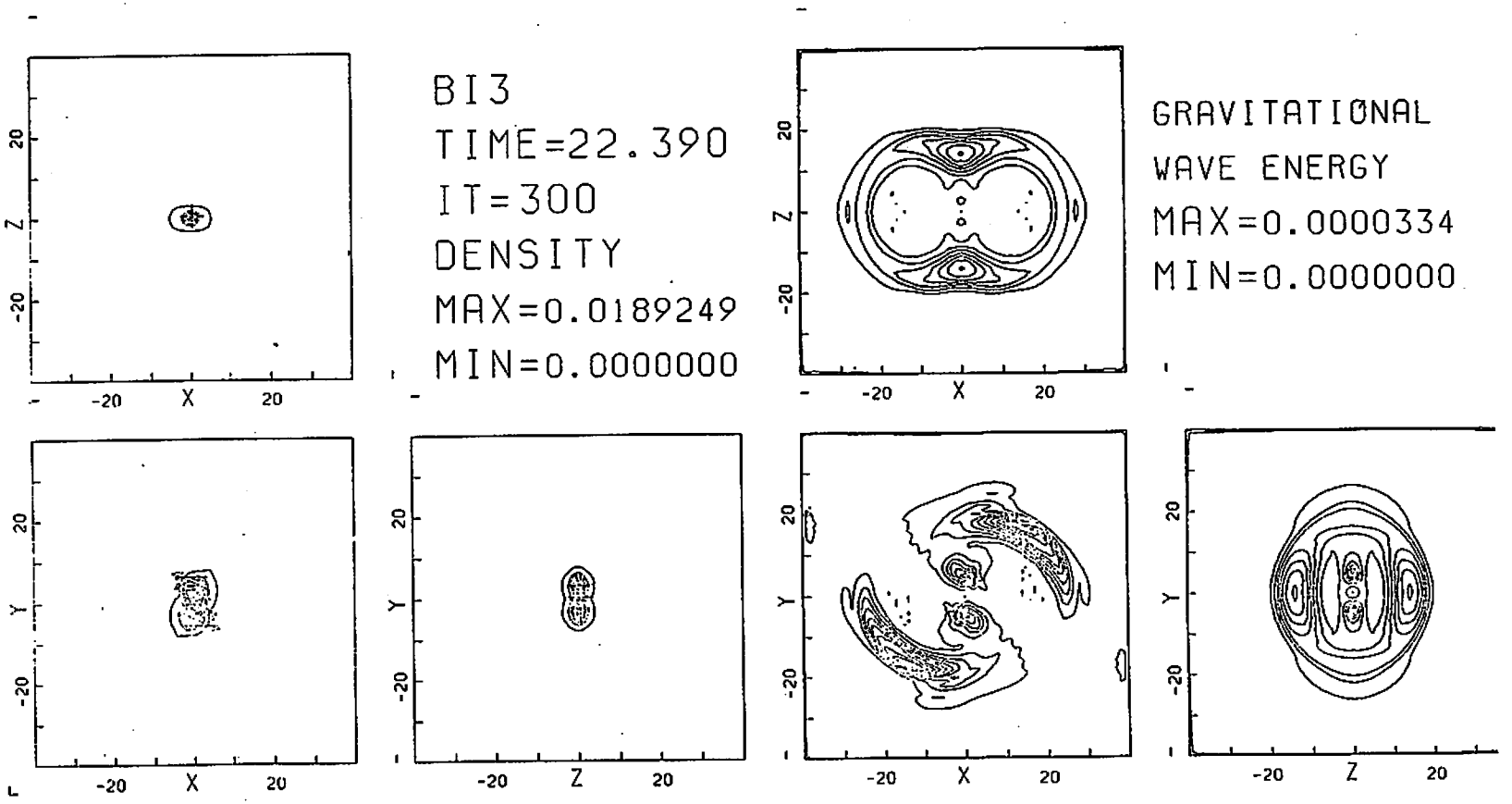
BI3
TIME=22.390
IT=300
DENSITY
MAX=0.0189249
MIN=0.0000000
GRAVITATIONAL
WAVE ENERGY
MAX=0.0000334
MIN=0.0000000
-20
X
20
Z
Y

Fig.1-d

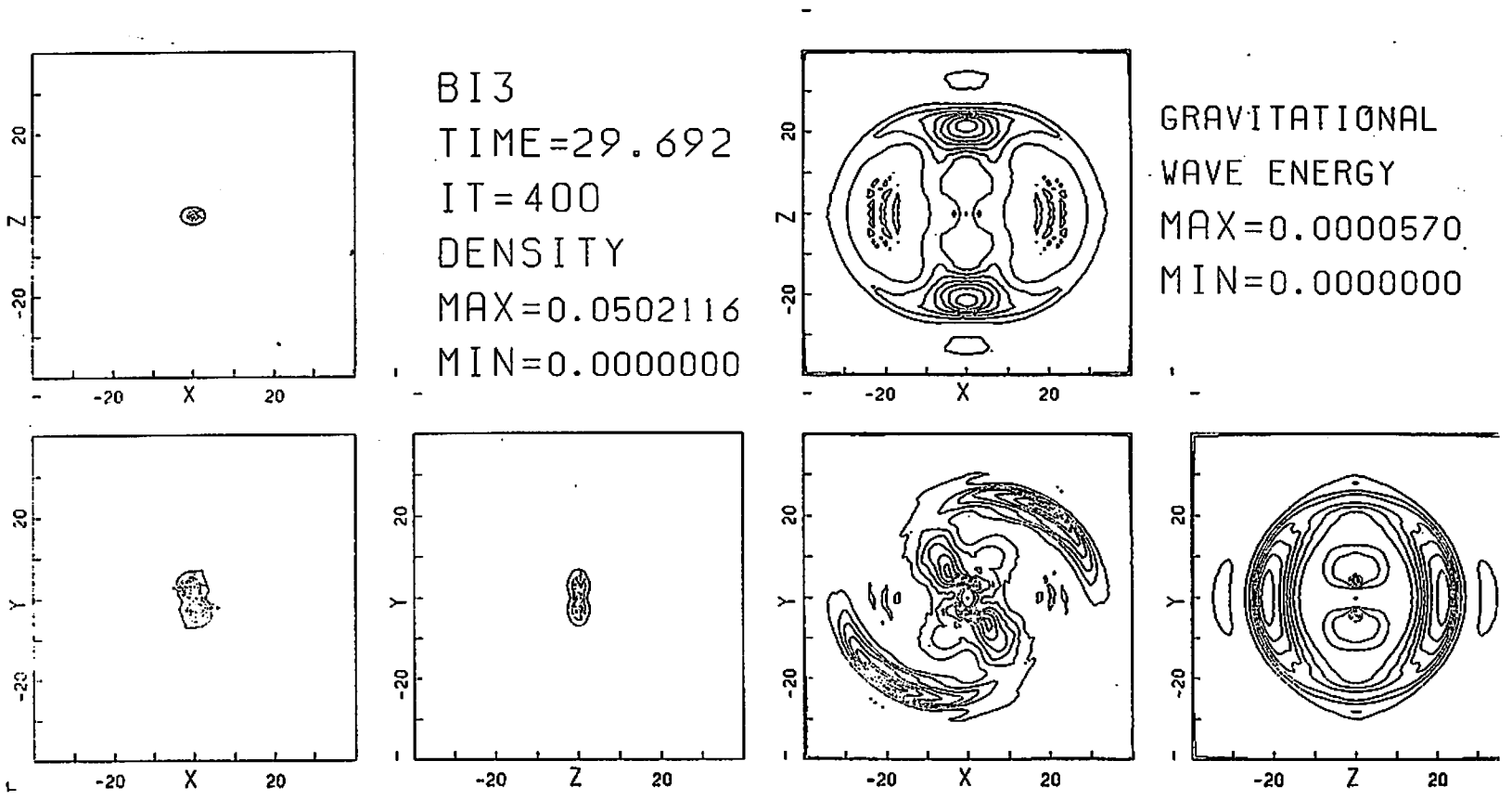
BI3
TIME=29.692
IT=400
DENSITY
MAX=0.0502116
MIN=0.0000000
GRAVITATIONAL
WAVE ENERGY
MAX=0.0000570
MIN=0.0000000
-20
X
20
Z
Y

Fig.2

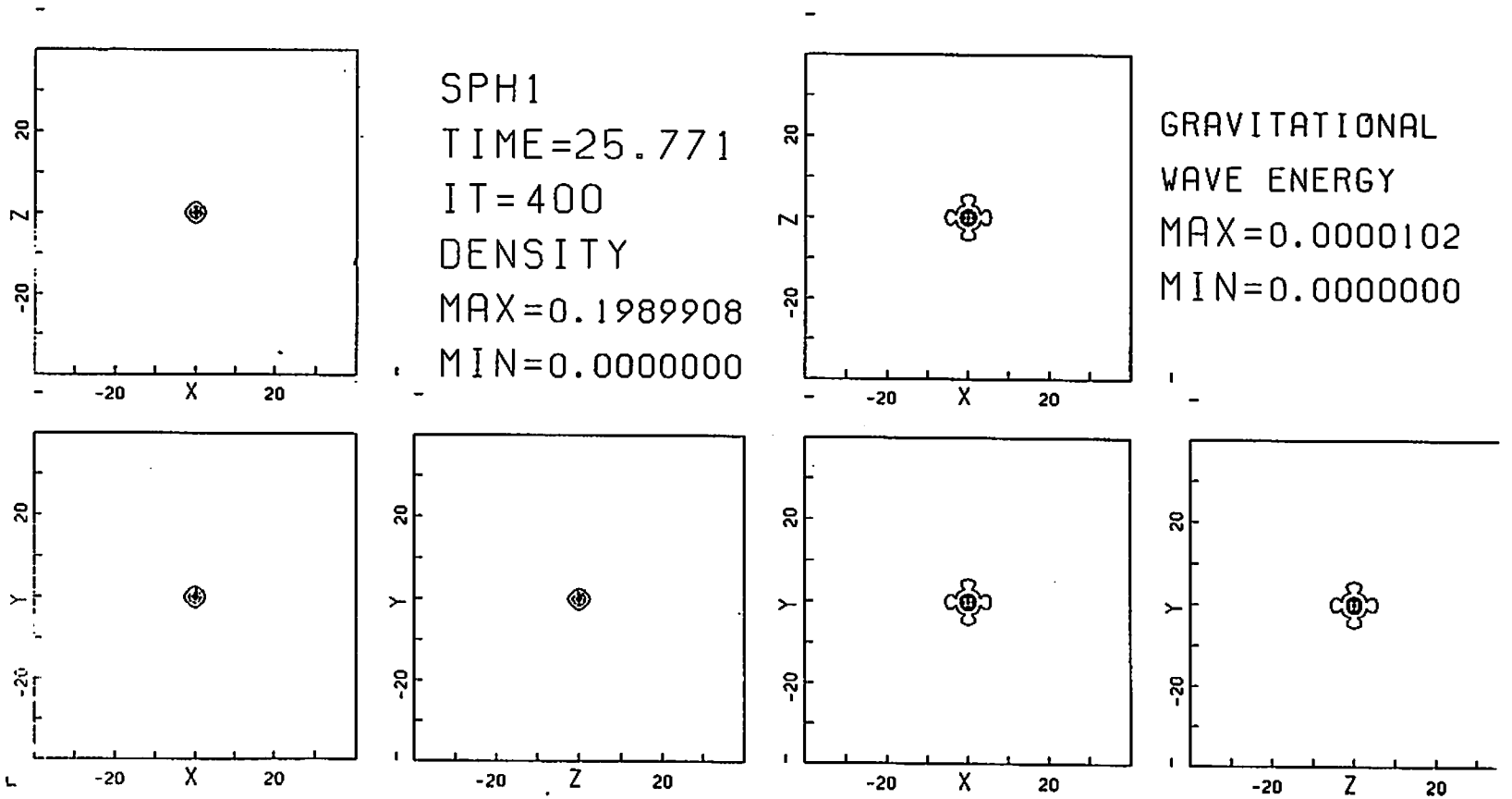
SPH1
TIME=25.771
IT=400
DENSITY
MAX=0.1989908
MIN=0.0000000
GRAVITATIONAL
WAVE ENERGY
MAX=0.0000102
MIN=0.0000000
-20
X
20
Z
Y

Fig.3-a

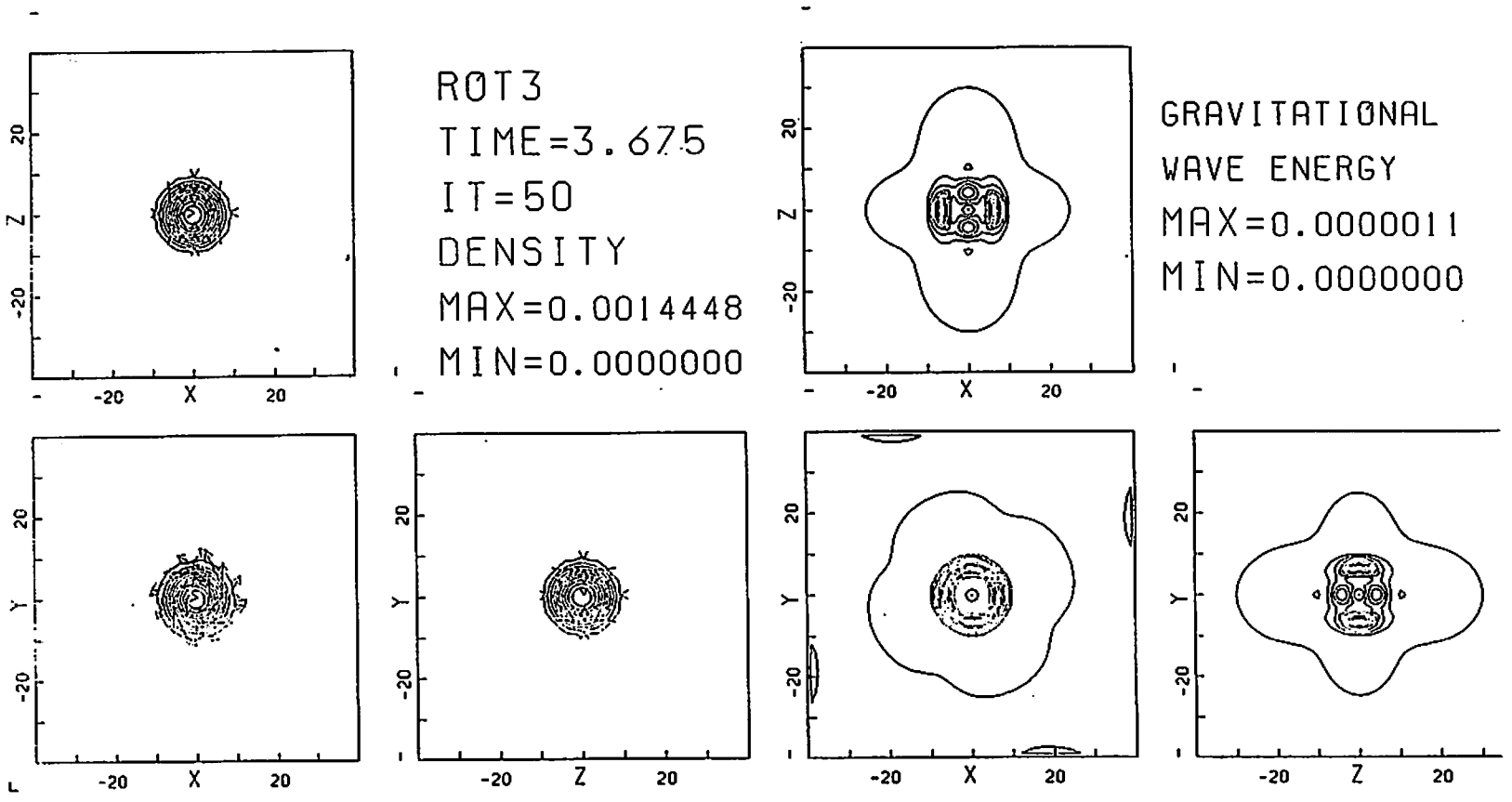
ROT3
TIME=3.675
IT=50
DENSITY
MAX=0.0014448
MIN=0.0000000
GRAVITATIONAL
WAVE ENERGY
MAX=0.0000011
MIN=0.0000000
-20
X
20
Z
Y

Fig.3-b

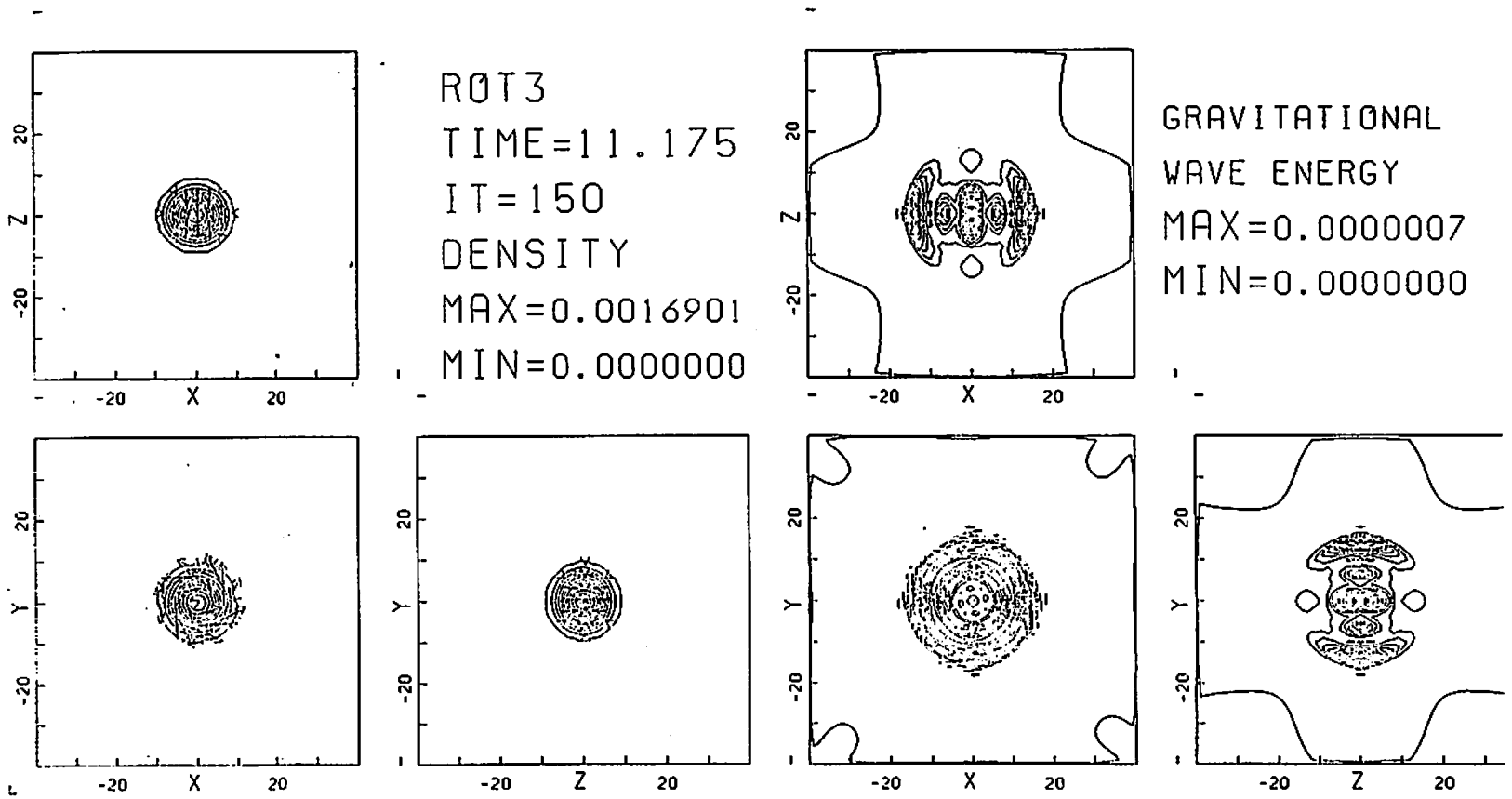
ROT3
TIME=11.175
IT=150
DENSITY
MAX=0.0016901
MIN=0.0000000
GRAVITATIONAL
WAVE ENERGY
MAX=0.0000007
MIN=0.0000000
Z
X
Y
20
-20

Fig.3-c

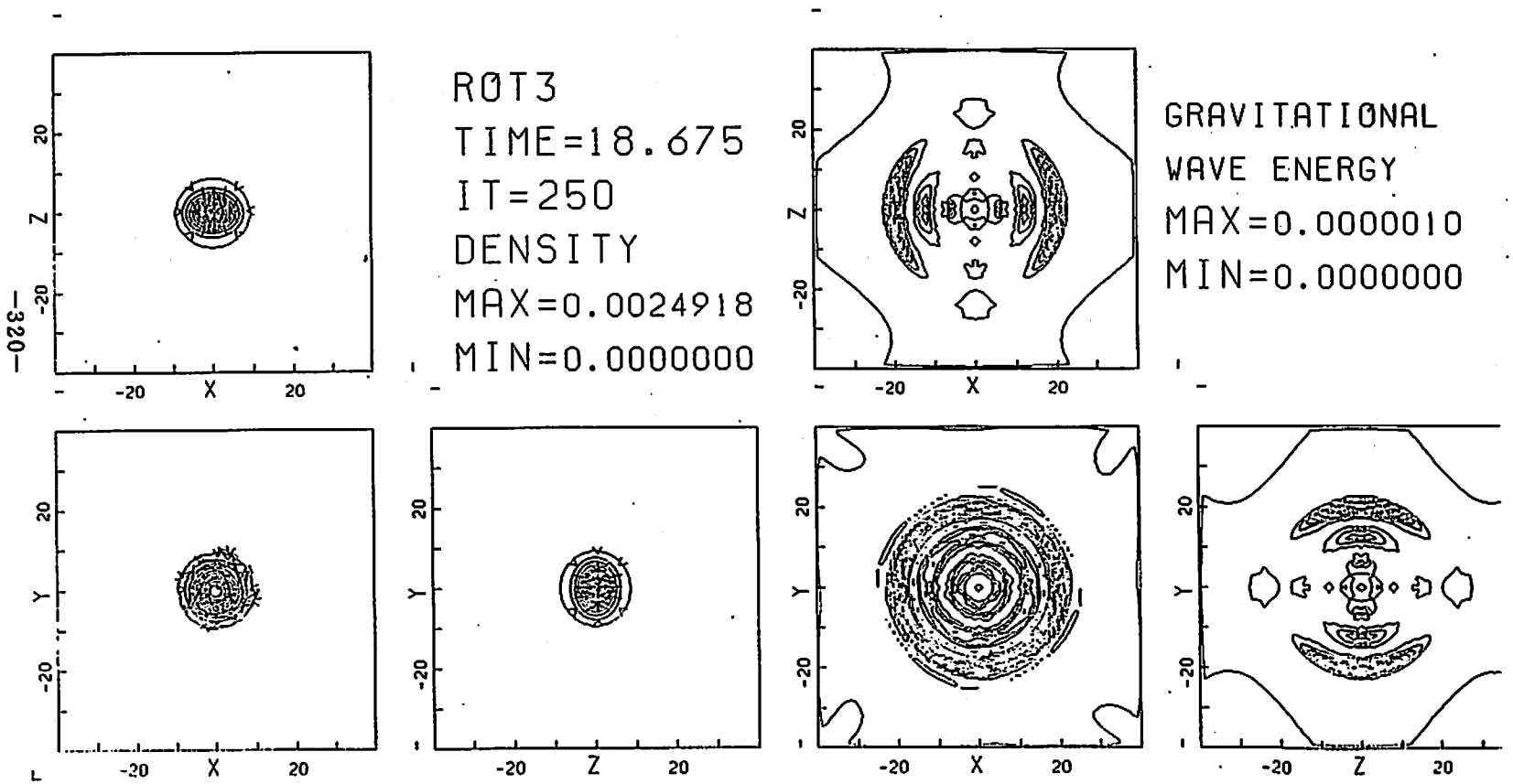
ROT3
TIME=18.675
IT=250
DENSITY
MAX=0.0024918
MIN=0.0000000
GRAVITATIONAL
WAVE ENERGY
MAX=0.0000010
MIN=0.0000000
X
Y
Z
-20
20

Fig.3-d

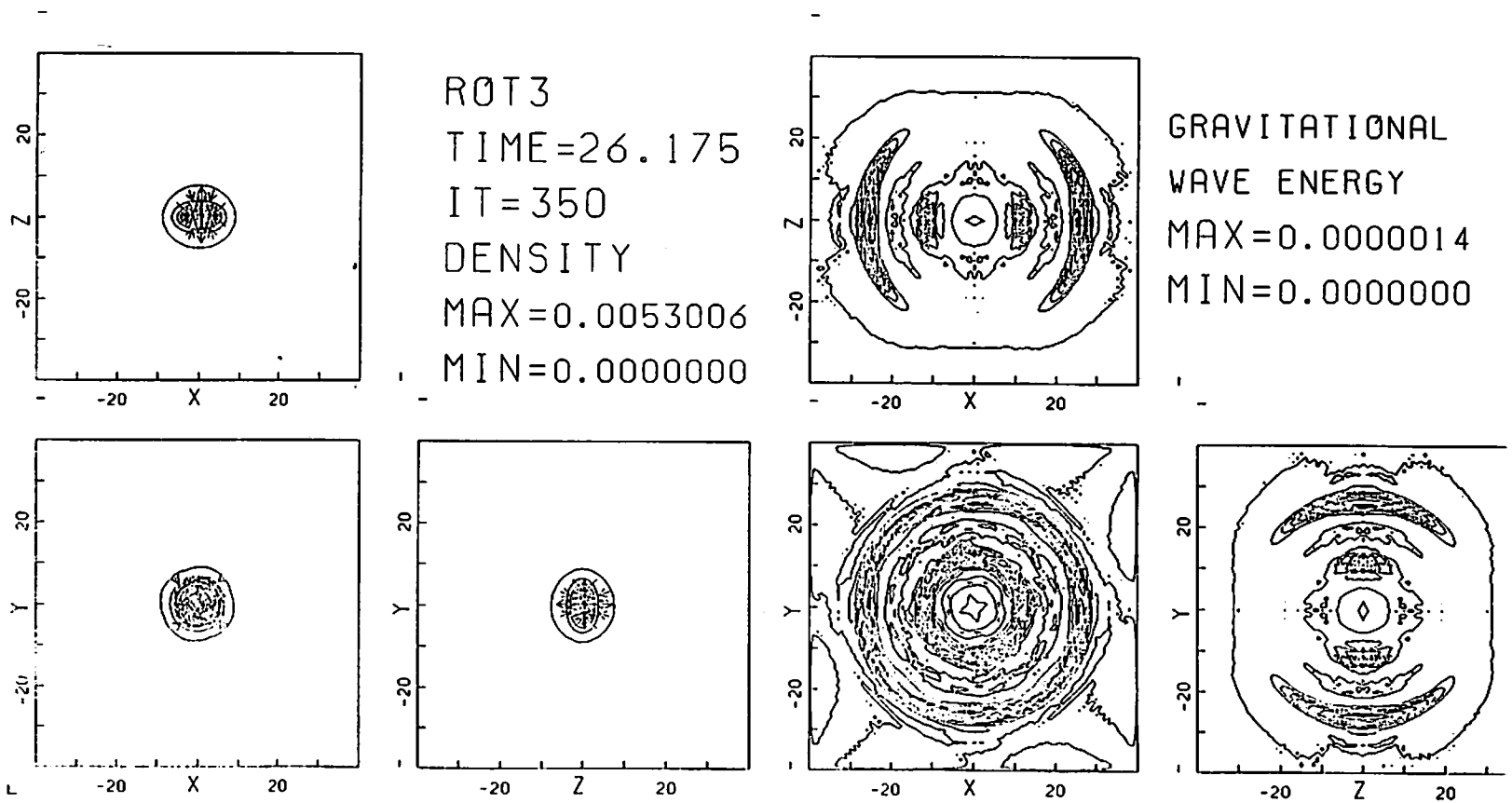
ROT3
TIME=26.175
IT=350
DENSITY
MAX=0.0053006
MIN=0.0000000
GRAVITATIONAL
WAVE ENERGY
MAX=0.0000014
MIN=0.0000000
-20
X
20
Z
Y

Fig.4

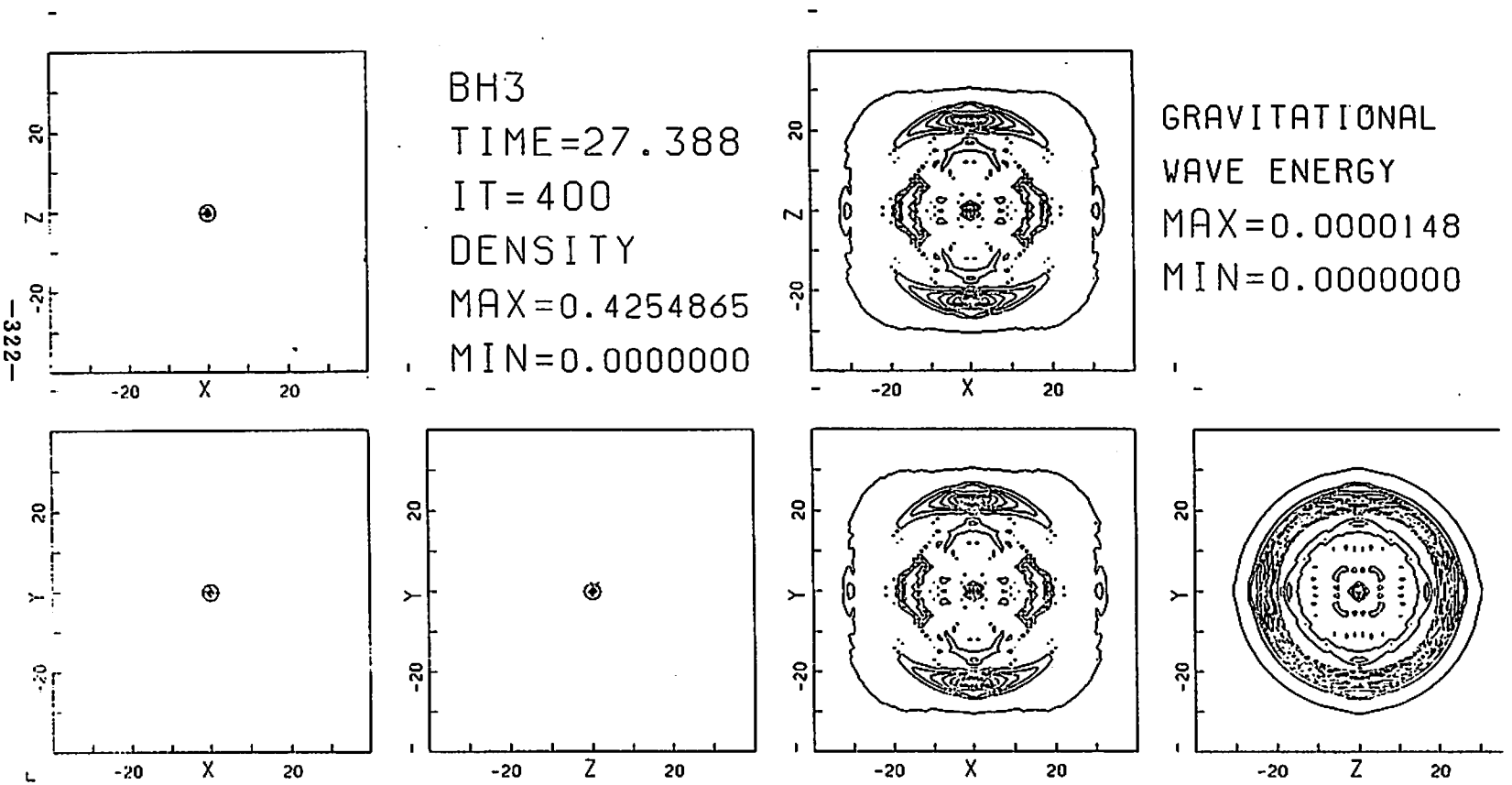
BH3
TIME=27.388
IT=400
DENSITY
MAX=0.4254865
MIN=0.0000000
GRAVITATIONAL
WAVE ENERGY
MAX=0.0000148
MIN=0.0000000
-20
X
20
Z
Y

Numerical relativity with help of Ashtekar's formulation

HISA-AKI SHINKAI† and GEN YONEDA‡

†*Dept. of Physics, Waseda University, Okubo 3-4-1, Shinjuku, Tokyo 169, Japan*
‡*Dept. of Mathematics, Waseda University, Okubo 3-4-1, Shinjuku, Tokyo 169, Japan*

Abstract

We apply Ashtekar's variables and Capovilla-Dell-Jacobson's connection formulation to classical numerical relativity and introduce a new procedure to follow time evolution based on the ADM formalism for a vacuum spacetime. In this formulation, the Hamiltonian and momentum constraint equations become trivial and only the gauge equation is the only non-trivial constraint. We anticipate that it might be useful to combine the connection approach with conventional methods by choosing one technique for evolution and the other for constraints.

1 Introduction

One of the most important features in general relativity is the non-linear nature of gravity. For highly dynamical phenomena, such as the collapse of matter, emission of the gravitational waves or the formation of a singularity, we expect that numerical simulations will provide the final answers. The research field of 'numerical relativity' is now actively developing because of the need for templates of gravitational wave forms by observations to be made in the near future.

So far, numerical relativity has achieved many results by using the Arnowitt-Deser-Misner (ADM) formalism [1]. In the ADM formalism, spacetime is decomposed into a 3-dimensional hypersurface, Σ, and one timelike coordinate. Since this Hamilton formulation fits our natural understandings of space and time, and also gives many insights to the Cauchy treatment of general relativity, most numerical simulations use this '3+1' formalism. however, we need to solve Hamiltonian and momentum constraint equations when we set the initial data or set proper coordinate condition, which is a time-consuming to compute. That is, we can not avoid an iterative procedures to solve elliptical partial differential equations numerically, which needs much computation time.

On the other hand, Ashtekar's new formulation of general relativity [2] reduces the Hamiltonian constraint equation, $\mathcal{C}_H$, and momentum constraint equations, $\mathcal{C}_M$, to polynomials, with a new set of additional gauge constraint equations, $\mathcal{C}_G$. Although there is a reality condition problem when the theory comes back to Einstein gravity, this formulation is attractive since it enables us to treat a quantum description of the theory

†Electronic address: shinkai@cfi.waseda.ac.jp
‡Electronic address: 61m511@cfi.waseda.ac.jp

non-perturbatively. Many applications are proposed in the field of quantum gravity, and applications to the classical Einstein theory is also expected. Later, Capovilla, Jacobson and Dell (CDJ) [4] discovered that, in the vacuum spacetime, the introduction of an arbitrary traceless and symmetric SO(3) tensor M_{ab} makes two constraints $\mathcal{C}_H$ and $\mathcal{C}_M$ trivial, leaving only the third constraint equations $\mathcal{C}_G$ to be solved. Recently, Salisbury *et al.* [5] proposed the use of the Ashtekar's and the CDJ's formulation in the numerical treatment of general relativity. They showed a full set of equations using Ashtekar's connection and Newman-Penrose's Weyl scalar as dynamical variables. Their formulation is based on Ashtekar's variables and has merit of showing the evolution of the Weyl scalar directly. However, it is not convenient for general numerical relativists, because the evolution of Ashtekar's connection does not give us a direct geometrical understanding and a way to set an initial value is not clear.

Here, we propose a new procedure to follow time evolutions in numerical relativity. We use Ashtekar's variables and CDJ's connection formulation together with the ADM formalism. Our main strategy is that we focus upon the ADM variables and use connection variables only when we have to solve the constraint equations. In this article, we present equations for vacuum spacetime.

The contents of this article are as follows. We will review Ashtekar's formulation and the CDJ approach briefly in §2. We will also comment on the work by Salisbury *el al.* Our procedure is shown in §3. Section 4 is devoted for discussions.

We use greek letters $(\mu, \nu, \rho, \cdots)$, which range over the four spacetime coordinates moving $0, \cdots, 3$, while upper latin letters from the middle of the alphabet $(I, J, K, \cdots)$ range over the four internal SO(1,3) indices moving $(0), \cdots, (3)$. The SO(1,3) indices are raised and lowered with the Minkowski metric, which we take to be $\eta_{IJ} = diag(-1, 1, 1, 1)$. Lower case latin indices from the middle of the alphabet $(i, j, k, ...)$ range over the three spatial indices moving $1, \cdots, 3$, while lower case latin indices from the beginning of the alphabet $(a, b, c, ...)$ range over the three internal SO(3) indices moving $(1), \cdots, (3)$. We use volume forms $\epsilon_{\mu\nu\rho\sigma}, \epsilon_{abc}$; $\epsilon_{\mu\nu\rho\sigma}\epsilon^{\mu\nu\rho\sigma} = -4!$, and $\epsilon_{abc}\epsilon^{abc} = 3!$.

2 Brief review of the formulations

2.1 The Ashtekar's formulation

The key feature of Ashtekar's formulation of general relativity [2] is the introduction of a self-dual connection as one of the basic dynamical variables. Let us write metric $g_{\mu\nu}$ by tetrad e^I_μ and define its inverse E^μ_I by

$$g_{\mu\nu} = e^I_\mu e^J_\nu \eta_{IJ}, \tag{1}$$

$$E^\mu_I := e^J_\nu g^{\mu\nu} \eta_{IJ}. \tag{2}$$

We define a SO(3,C) self-dual connection

$$^{\pm}\mathcal{A}^a_\mu := \omega^{0a}_\mu \mp \frac{i}{2}\epsilon^a{}_{bc}\omega^{bc}_\mu, \tag{3}$$

where $\omega^I{}_{J\mu}$ is a spin connection 1-form (Ricci connection)

$$\omega^I{}_{J\mu} := (e^I)_\nu \nabla_\mu (E_J)^\nu. \tag{4}$$

A self-duality of connection means that the self-duality is with respect to internal indices, which satisfies the eigen equations $^*(^{\pm}A^{ab}) = \pm i^{\pm}A^{ab}$ for any antisymmetric tensor A_{ab} and its dual $^*A^{ab} = \frac{1}{2}\epsilon^{abcd}A_{cd}$. Ashtekar's plan is to use only a self-dual part of connection $^+\mathcal{A}^a{}_\mu$ and to use its spatial part $^+\mathcal{A}^a{}_i$ as a dynamical variable. Note that the extrinsic curvature $K_{ij} = -(\delta_i{}^l + n_i n^l)\nabla_l n_j$ in the ADM formalism, where ∇ is a covariant derivative on Σ, satisfies the relation $K_{ij}E^{ja} = \omega^{0a}{}_i$, when the gauge condition $E^0_a = 0$ is fixed. So $^+\mathcal{A}^a_i$ is also expressed by

$$^+\mathcal{A}^a_i = K_{ij}E^{ja} - \frac{i}{2}\epsilon^a{}_{bc}\omega^{bc}_i. \tag{5}$$

For later convenience, we now define 2-forms related $e^I_\mu, \omega^I{}_{J\mu}$ and $^+\mathcal{A}^a_\mu$ as

$$F^a_{\mu\nu} := (d\,^+\mathcal{A}^a)_{\mu\nu} - \frac{i}{2}\epsilon^a{}_{bc}(\,^+\mathcal{A}^b \wedge \,^+\mathcal{A}^c)_{\mu\nu}, \tag{6}$$

$$R^{ab}_{\mu\nu} := (d\omega^{ab})_{\mu\nu} + (\omega^a{}_c \wedge \omega^{cb})_{\mu\nu}, \tag{7}$$

$$\Sigma^a := e^0 \wedge e^a - \frac{i}{2}\epsilon^a{}_{bc}e^b \wedge e^c, \tag{8}$$

those we denote curvature 2-form, Riemann tensor and complex 2-form, respectively.

Ashtekar fixes the gauge condition $E^0_a = 0$ and denote $E^\mu_0 = (\frac{1}{N}, -\frac{N^i}{N})$, where N and N^i are lapse function and shift vector, respectively. This allows us to think of E^μ_0 as a normal vector field to Σ spanned by the condition $t = x^0$ =const., which plays the same role as that of ADM.

Ashtekar [2] introduced the set $(^+\mathcal{A}^a{}_i, \tilde{E}^i{}_a)$ as basic dynamical variables, where $\tilde{E}^i{}_a$ is an inverse of the (densitized) triad defined by

$$\tilde{E}^i{}_a := tE^i{}_a. \tag{9}$$

where $t := \det e^a_i$ is a density. This pair forms the canonical relation

$$\{^+\mathcal{A}^a{}_i(x), \tilde{E}^j{}_b(y)\} = i\delta^j{}_i\delta^a{}_b\delta(x-y). \tag{10}$$

Then the half of the Hilbert action takes the form

$$S = \int d^4x[\,^+\dot{\mathcal{A}}^a{}_i\tilde{E}^i{}_a + \frac{i}{2}\underset{\sim}{N}\tilde{E}^i_a\tilde{E}^j_b F^c_{ij}\epsilon^{ab}{}_c - N^i F^a_{ij}\tilde{E}^j_a + \,^+\mathcal{A}^a{}_0\mathcal{D}_i\tilde{E}^i_a], \tag{11}$$

where $\underset{\sim}{N} := t^{-1}N$ and $\mathcal{D}_i\tilde{E}^i_a := \partial_i\tilde{E}^i_a - i\epsilon_{ab}{}^c\,^+\mathcal{A}^b_j\tilde{E}^j_c$. Non-dynamical variables $\underset{\sim}{N}$, N^i and $\mathcal{A}^a{}_0$ reduce the constraint equations, respectively,

$$\mathcal{C}_H = \epsilon^{ab}{}_c\tilde{E}^i_a\tilde{E}^j_b F^c_{ij} \approx 0, \tag{12a}$$

$$\mathcal{C}_{Mi} = F^a_{ij}\tilde{E}^j_a \approx 0, \tag{12b}$$

$$\mathcal{C}_{Ga} = \mathcal{D}_i\tilde{E}^i_a. \approx 0. \tag{12c}$$

The Hamiltonian constraint C_H and momentum constraint C_{Mi} are polynomial, while a new set of additional gauge constraint equations C_{Ga} are first order in the derivatives. These reductions are some of the advantages of the Ashtekar's formulation. And the dynamical variables ${}^+\mathcal{A}^a_i$ and $\tilde{E}^i_a$ reduce the equations of motion,

$$
\begin{aligned}
{}^+\dot{\mathcal{A}}^a{}_i &= -i\epsilon^{ab}{}_c \underset{\sim}{N} \tilde{E}^j_b F^c_{ij} + N^j F^a_{ji} + \mathcal{D}_i\, {}^+\mathcal{A}^a{}_0 && \text{(13a)}\\
\dot{\tilde{E}}^i{}_a &= -i\mathcal{D}_j(\epsilon^{cb}{}_a \underset{\sim}{N} \tilde{E}^j_c \tilde{E}^i_b) + 2\mathcal{D}_j(N^{[j}\tilde{E}^{i]}_a) + i\, {}^+\mathcal{A}^b{}_0 \epsilon_{ba}{}^c \tilde{E}^i_c && \text{(13b)}
\end{aligned}
$$

where $\mathcal{D}_j T^{ji}_a := \partial_j T^{ji}_a - i\epsilon^{abc}\, {}^+A^b_j T^{ji}_c$, for $T^{ij}_a + T^{ji}_a = 0$.

Next we put the variables $({}^+\mathcal{A}^a_i, \tilde{E}^i_a, \underset{\sim}{N}, N^i)$ into metric variables. Tetrad E^μ_I is obtained as

$$
\begin{aligned}
E^0_0 &= 1/\underset{\sim}{N}, && \text{(14a)}\\
E^i_0 &= -N^i/\underset{\sim}{N}, && \text{(14b)}\\
E^0_a &= 0, && \text{(14c)}\\
E^i_a &= \tilde{E}^i_a. && \text{(14d)}
\end{aligned}
$$

And we obtain metric $g^{\mu\nu}$ such that

$$
g^{\mu\nu} := E^\mu_I E^\nu_J \eta^{IJ}. \tag{15}
$$

If the constraint (12a), (12b), (12c) and the evolution equations (13a), (13b) are satisfied, the metric is Ricci flat since we start from the Hilbert action for vacuum spacetime. But notice that in general this metric is not real. Thus we must impose the reality conditions:

$$
\begin{aligned}
\Im(\underset{\sim}{N}) &= 0 && \text{(16a)}\\
\Im(N^i) &= 0 && \text{(16b)}\\
\Im(\tilde{E}^i_a \tilde{E}^{ja}) &= 0. && \text{(16c)}
\end{aligned}
$$

In total we have 36 real (18 complex) dynamical variables $({}^+\mathcal{A}^a_i, \tilde{E}^i_a)$. They are restricted by 14 real number constraint equations (12a), (12b), (12c) and by 6 real number equations for the gauge fixing condition (14c) and by 10 real number of equations for reality conditions (16a), (16b), (16c). Thus 6 real number degrees of dynamical freedom remain. This corresponds to the gauge freedom (4 real) and gravitational waves (2 real).

2.2 The CDJ approach

Capovilla, Jacobson and Dell (CDJ) [4] discovered how to obtain the free data in the vacuum spacetime, i.e. solutions to the constraint equations of C_H and C^i_M. A brief summary is given here. Choose any connection ${}^+\mathcal{A}^a{}_i$ such that its magnetic field

$$
B^{ia} := \epsilon^{ijk} F^a_{jk}, \tag{17}
$$

regarded as a matrix, is non-degenerate. Now, we can expand out $\tilde{E}^i{}_a$ as

$$\tilde{E}^i{}_a = M_{ab}B^{ib} \tag{18}$$

for some matrix M_{ab}. The pair $({}^+\mathcal{A}^a{}_i, \tilde{E}^i{}_a)$ then satisfies the Hamiltonian constraint $\mathcal{C}_H$ and momentum constraint $\mathcal{C}_{Mi}$ *if and only if* M_{ab} is of the form $M_{ab} = [\phi^2 - \frac{1}{2}\mathrm{tr}\,\phi^2]_{ab}$, where ϕ_{ab} is an arbitrary trace-free, symmetric field on Σ. Thus, as far as these four constraints are concerned, the free data consists of ${}^+\mathcal{A}^a{}_i$ and ϕ_{ab}. It remains to solve only the gauge constraint equations $\mathcal{C}_{Ga}$ which simply reduces to

$$\mathcal{C}_{Ga} = \mathcal{D}_i(B^{ib}M_{ba}) = B^{ib}\mathcal{D}_iM_{ba} = 0, \tag{19}$$

where in the last equality, the Bianchi identity $\mathcal{D}_iB^{ia} = 0$ has been used. The assumption of non-degeneracy is not too restrictive, because a "generic" connection will satisfy this condition.

2.3 Salisbury's approach

Recently, Salisbury *el al.* [5] proposed the use of the Ashtekar's formulation and the CDJ formulation in the numerical treatment of general relativity. They use the fact that a matrix Ψ_{ab}, which is constructed from Newman-Penrose's Weyl scalar Ψ_i as [6]

$$\Psi_{ab} = \begin{bmatrix} \frac{1}{2}(-\Psi_0 + 2\Psi_2 - \Psi_4) & -i\frac{1}{2}(\Psi_0 - \Psi_4) & \Psi_1 - \Psi_3 \\ & \frac{1}{2}(\Psi_0 + 2\Psi_2 + \Psi_4) & i(\Psi_1 + \Psi_3) \\ & & -2\Psi_2 \end{bmatrix}, \tag{20}$$

satisfies the traceless and symmetric conditions, which is supposed to a character of $M_{ab} = \Psi_{ab}^{-1}$ in the CDJ approach. The requirement of non-degeneracy of M_{ab} becomes as $\det\Psi \neq 0$, i.e. the Petrov type of the spacetime is not $\{31\}, \{4\}$ nor $\{\text{-}\}$. So the algebraically general spacetime (type $\{1111\}$) is applicable. Setting Ashtekar's connection ${}^+\mathcal{A}^a{}_i$ and Newman-Penrose's Weyl scalar Ψ_i as dynamical variables, they showed a full set of equations to follow the time evolution. As for restricting to a real metric, they require two conditions; the first condition is that the doubly densitized contravariant metric $\tilde{\tilde{g}}^{ij} := t^2g^{ij}$ be real

$$\Im(\tilde{E}^i_a\tilde{E}^j_a) = 0, \tag{21}$$

and the second condition is that the time derivative of $\tilde{\tilde{g}}^{ij}$ be real [7]

$$\dot{\tilde{\tilde{g}}}^{ij} = 2i\underset{\sim}{N}\epsilon_{abc}\mathcal{D}_k(\tilde{E}^k{}_b\tilde{E}^{(i}{}_c)\tilde{E}^{j)}_a, \tag{22}$$

which reduce the condition to

$$\Re(\epsilon_{abc}\mathcal{D}_k(\tilde{E}^k{}_b\tilde{E}^{(i}{}_c)\tilde{E}^{j)}_a) = 0. \tag{23}$$

Their formulation is based on Ashtekar's variables and has a merit of showing the evolution of Weyl scalar directly. It is, however, not convenient for numerical general

relativists, because a way to set an initial value is not clear and the evolution of Ashtekar's connection does not have a direct geometrical meaning. Moreover, it is not clear whether it has advantage over the original Newman-Penrose formalism when we follow the dynamics of Weyl scalar.

3 Our procedures

3.1 Our strategy

In this section, we show a new approach to follow time evolutions in numerical relativity. We hope to follow the procedure of solving initial conditions and evolving them by equations of motion. As for the constraint equations, the equations of motion ensure that the constraints are preserved under time evolution, so we can treat the constraints as an initial condition. However, the reality conditions must be imposed at all time, in general. Ashtekar[3] discovered that, with the second reality condition

$$\Im \frac{d}{dt}(\tilde{E}^i_a \tilde{E}^{jb}) = 0, \tag{24}$$

the reality of the metric are automatically preserved under time evolution owing to equations of motion. We think that this second reality condition is complicated and difficult to solve directly because it needs information from equations of motion. Therefore, we propose the following procedure.

We use the ADM variables (3-metric γ_{ij} and extrinsic curvature K_{ij}) basically to express the 3-hypersurface Σ. When we have to solve the constraint equations, i.e. when we set initial data and when we set proper coordinate conditions, we also prepare connection variables and solve the equations within the Ashtekar-CDJ's formulation. To execute this program, we need to transform variables between ADM and Ashtekar-CDJ formalisms. In the following subsections, we present our procedures, which are constructed from the following steps. [I] Setting initial data by solving gauge constraint equations $\mathcal{C}_{Ga}$ and reality conditions, and transform the variables $({}^+\mathcal{A}^a{}_i, \Psi_{ab})$ into the ADM variables (γ_{ij}, K_{ij}). [II] Evolve (γ_{ij}, K_{ij}) by the dynamical equations in the ADM formalism. [III] If we need to solve the gauge condition for N and/or N^i using the Hamiltonian and momentum constraint equation, then we transform trial variables $(\tilde{\gamma}_{ij}, \tilde{K}_{ij})$ to $({}^+\mathcal{A}^a{}_i, \Psi_{ab})$, and solve the condition within the Ashtekar-CDJ's formulation, then transform again back to the ADM's (γ_{ij}, K_{ij}). The appropriate condition may also transform into the gauge constraint equations $\mathcal{C}_{Ga}$.

Since we evolve the variables by dynamical equations in the ADM formulation, we think the reality condition will be preserved automatically except when setting the initial data.

3.2 Transform variables from ADM to Ashtekar-CDJ

Here, we present how to transform trial variables from the ADM 3-metric and extrinsic curvature $(\tilde{\gamma}_{ij}, \tilde{K}_{ij})$ to the Ashtekar-CDJ's $({}^{+}\mathcal{A}^{a}{}_{i}, \Psi_{ab})$. As for the Ashtekar connection ${}^{+}\mathcal{A}^{a}{}_{i}$, we can compute them directly from $\tilde{\gamma}_{ij}$ and $\tilde{K}_{ij}$ through the definition of spin connection (4) and Ashtekar connection (5) if we fix a tetrad e^{I}_{μ}. As for the traceless symmetric SO(3,C) matrix Ψ_{ab}, we follow (20), which needs to prepare Newman-Penrose Weyl scalar Ψ_i defined by

$$\begin{aligned}
\Psi_0 &\equiv C_{\mu\nu\rho\sigma} l^{\mu} m^{\nu} l^{\rho} m^{\sigma} \\
\Psi_1 &\equiv C_{\mu\nu\rho\sigma} l^{\mu} n^{\nu} l^{\rho} m^{\sigma} \\
\Psi_2 &\equiv C_{\mu\nu\rho\sigma} l^{\mu} m^{\nu} \bar{m}^{\rho} n^{\sigma} \\
\Psi_3 &\equiv C_{\mu\nu\rho\sigma} l^{\mu} n^{\nu} \bar{m}^{\rho} n^{\sigma} \\
\Psi_4 &\equiv C_{\mu\nu\rho\sigma} n^{\mu} \bar{m}^{\nu} n^{\rho} \bar{m}^{\sigma}
\end{aligned} \tag{25}$$

where $C_{\mu\nu\rho\sigma}$ is Weyl tensor and $l^{\mu} = \frac{1}{\sqrt{2}}(E^{\mu}_{0} + E^{\mu}_{3})$, $n^{\mu} = \frac{1}{\sqrt{2}}(E^{\mu}_{0} - E^{\mu}_{3})$, $m^{\mu} = \frac{1}{\sqrt{2}}(E^{\mu}_{1} - iE^{\mu}_{2})$ and $\bar{m}^{\mu} = \frac{1}{\sqrt{2}}(E^{\mu}_{1} + iE^{\mu}_{2})$ are null tetrad. Instead of using (25) directly, it is convenient to use the representation of Ψ_i by the decomposition of the Weyl tensor, electric part $\mathcal{E}_{ij}$ and magnetic part $\mathcal{B}_{ij}$;

$$\mathcal{E}_{ij} \equiv - \; C_{i\mu j\nu} E^{\mu}_{0} E^{\nu}_{0}, \quad \mathcal{B}_{ij} \equiv - \; {}^{*}C_{i\mu j\nu} E^{\mu}_{0} E^{\nu}_{0}, \tag{26}$$

where ${}^{*}C_{\mu\nu\rho\sigma} = \frac{1}{2}\varepsilon_{\mu\nu}{}^{\eta\lambda} C_{\eta\lambda\rho\sigma}$ is a dual of the Weyl tensor. The reason is that these decomposed elements $\mathcal{E}_{ij}$ and $\mathcal{B}_{ij}$ are also represented by the 3-metric γ_{ij} and the extrinsic curvature K_{ij} as [8]

$$\mathcal{E}_{ij} = {}^{(3)}R_{ij} - K_{i}{}^{m} K_{jm} + K K_{ij} - \frac{2}{3}\Lambda \gamma_{ij}, \tag{27}$$

$$\mathcal{B}_{ij} = \varepsilon_{i}{}^{kl} D_{l} K_{kj}. \tag{28}$$

The final form of this representation is as follows [9];

$$\Psi_0 = -(e_{\mu\nu} - J_{\mu}{}^{\rho} b_{\nu\rho}) m^{\mu} m^{\nu}, \tag{29a}$$

$$\Psi_1 = \frac{1}{\sqrt{2}}(e_{\mu} + J_{\mu}{}^{\rho} b_{\nu\rho}) m^{\mu}, \tag{29b}$$

$$\Psi_2 = \frac{1}{2}(-e + ib), \tag{29c}$$

$$\Psi_3 = \frac{1}{\sqrt{2}}(e_{\mu} - J_{\mu}{}^{\rho} b_{\nu\rho}) \bar{m}^{\mu}, \tag{29d}$$

$$\Psi_4 = -(e_{\mu\nu} + J_{\mu}{}^{\rho} b_{\nu\rho}) \bar{m}^{\mu} \bar{m}^{\nu}, \tag{29e}$$

where we set

$$e = \mathcal{E}_{\mu\nu} E^{\mu}_{3} E^{\nu}_{3}, \tag{30a}$$

$$
\begin{aligned}
e_\mu &= \mathcal{E}_{\nu\rho} E_3^\nu (\delta_\mu{}^\rho - e_\mu^3 E_3^\rho), && (30b)\\
e_{\mu\nu} &= \mathcal{E}_{\rho\sigma}(\delta_\mu{}^\rho - e_\mu^3 E_3^\rho)(\delta_\nu{}^\sigma - e_\nu^3 E_3^\sigma) + \frac{1}{2} e s_{\mu\nu}, && (30c)\\
b &= \mathcal{B}_{\mu\nu} E_3^\mu E_3^\nu, && (30d)\\
b_\mu &= \mathcal{B}_{\nu\rho} E_3^\nu (\delta_\mu{}^\rho - e_\mu^3 E_3^\rho), && (30e)\\
b_{\mu\nu} &= \mathcal{B}_{\rho\sigma}(\delta_\mu{}^\rho - e_\mu^3 E_3^\rho)(\delta_\nu{}^\sigma - e_\nu^3 E_3^\sigma) + \frac{1}{2} b s_{\mu\nu}, && (30f)
\end{aligned}
$$

where $s_{\mu\nu} = \gamma_{\mu\nu} - e_\mu^3 e_\nu^3$ and

$$
J_\mu{}^\nu \equiv \varepsilon_\mu{}^{\nu\rho\sigma} e_\rho^3 e_\sigma^0. \tag{31}
$$

3.3 Transform variables from Ashtekar-CDJ to ADM

Conversely, we describe a way to return to a metric $g_{\mu\nu}$.

The spatial part of curvature 2-from F_{ij}^a is derived from ${}^+\mathcal{A}^a{}_i$ and (6), and its magnetic part B^{ia} is obtained from (17). By definition, (18), we get a triad $\tilde{E}^i{}_a$,

$$
\tilde{E}^i{}_a = B^{ib}\Psi_{ba}^{-1}, \tag{32}
$$

and the related spatial components of a metric g_{ij} are calculated directly from

$$
\gamma^{ij} = \tilde{E}_a^i \tilde{E}^{ja}. \tag{33a}
$$

In order to get the extrinsic curvature K_{ij} from derived γ_{ij}, we need to impose $\underset{\sim}{N}$ and N^i. If we fix $(\underset{\sim}{N}, N^i)$ by hand [e.g. geodesic slicing condition $\underset{\sim}{N} = 1, N^i = 0$], then the rest of the metric will be obtained by imposing

$$
\begin{aligned}
g^{00} &= -1/\underset{\sim}{N}^2, && (33b)\\
g^{0i} = g^{i0} &= -N^i/\underset{\sim}{N}^2. && (33c)
\end{aligned}
$$

If we impose some condition to deside a gauge [e.g. constant-mean-curvature slicing condition], we need to solve $(\underset{\sim}{N}, N^i)$ from constraints. In Ashtekar's variables, the non-spatial part of connection, ${}^+\mathcal{A}^a{}_0$, operates to decide a gauge condition. If we assume that the way to choose tetrad on each time slice is definite, then we can construct a set of $(\gamma_{ij}, K_{ij}, \underset{\sim}{N}, N^i)$ naturally from a set of $({}^+\mathcal{A}^a{}_\mu, \tilde{E}_a^i)$. We note a method for deriving $(\underset{\sim}{N}, N^i)$ from $({}^+\mathcal{A}^a{}_\mu, \tilde{E}_a^i)$ in the Appendix.

3.4 The equations in the Ashtekar-CDJ

Now the variables $({}^+\mathcal{A}^a{}_i, \Psi_{ab}, \underset{\sim}{N}, N^i)$ are restricted as follows. The gauge constraint equation (19) becomes

$$
B^{ib}\mathcal{D}_i \Psi_{ba}^{-1} = 0, \tag{34}
$$

and the equations of motions are obtained by (13a) and (13b) by substitution $B^{ib}\Psi_{ba}^{-1}$ for $\tilde{E}_a^i$. The reality conditions (16a), (16b) and (16c) must be imposed at every time step.

Therefore, in order to set the initial condition, the equations we have to solve are the constraint (34) and the first and second reality conditions (16a), (16b), (16c) and (24). In order to solve the constraint equations during time evolution, the equations we have to solve are the constraint and the first reality conditions (16a), (16b), (16c). If we evolve the variables by dynamical equations in the ADM formulation, we think that the reality condition will be preserved automatically, so that only the gauge constraint remains to be solved.

4 Discussions

We apply Ashtekar's variables and Capovilla-Dell-Jacobson's connection formulation to classical numerical relativity and develop a new procedure to follow time evolution based on the ADM formalism for a vacuum spacetime. In this formulation, the Hamiltonian and momentum constraint equations become trivial and only the gauge equation is left to be a constraint.

In this article, we restrict our attention to vacuum spacetimes. However, applications such as including a cosmological constant or with a scalar field are also available [11]. We are now planning to execute finite-differencing these relations for numerical application to a plane-symmetric spacetime to investigate the dynamics of gravitational waves. We are now deriving coordinate conditions in the Ashtekar-CDJ frame, which are related to useful conditions on the lapse and shift function in the ADM frame. These will be presented elsewhere.

We hope that this approach allows us to make rapid progress toward the final goal of the numerical relativity: to integrate the Einstein field equations for an arbitrary spacetime with an arbitrary initial data.

Appendix
A method for deriving N and N^i from Ashtekar-CDJ variables

We note a method for deriving lapse and shift function (N, N^i) from a pair of $({}^+\mathcal{A}^a_\mu, \tilde{E}^i_a)$. We put 2-form [4]

$$\Sigma^a_{\mu\nu} := F^b_{\mu\nu} M_{ba}. \tag{35}$$

Since we use the Hilbert action, we have

$$(\Sigma^a \wedge \Sigma^b)_{\mu\nu} = \frac{1}{3}\delta^{ab}(\Sigma^c \wedge \Sigma_c)_{\mu\nu} \tag{36a}$$

$$(\Sigma^c \wedge \Sigma_c)_{\mu\nu} \neq 0 \tag{36b}$$

$$(\mathcal{D}\Sigma^a)_{\mu\nu\rho}[:= (d\Sigma^a)_{\mu\nu\rho} + \epsilon^{abc}(A^b \wedge \Sigma^c)_{\mu\nu\rho}] = 0 \tag{36c}$$

From (36a), there exist θ^I_μ such that

$$\Sigma^a_{\mu\nu} = (\theta^0 \wedge \theta^a)_{\mu\nu} - \frac{i}{2}\epsilon^a{}_{bc}(\theta^b \wedge \theta^c)_{\mu\nu}, \tag{37}$$

where we impose the gauge fixing condition

$$\theta^0_i = 0. \tag{38}$$

Therefore, if we put

$$g_{\mu\nu} := \theta^I_\mu \theta^J_\nu \eta_{IJ}, \tag{39}$$

then, from (35),(36a),(36b) and (36c), we see that this metric satisfies vacuum Einstein equation. Thus the gauge functions are determined by

$$g_{00} = -N^2 + N_i N^i, \tag{40a}$$

$$g_{0i} = N_i. \tag{40b}$$

Acknowledgments

One of the authors (H.S) would like to thank Prof. K. Maeda for suggesting the present subject. We also thank Dr. R. Easther for a careful reading of our manuscript.

References

[1] R. Arnowitt, S. Deser, C.W. Misner, "The Dynamics of General Relativity", in *Gravitation: An Introduction to Current Research*, ed. by L.Witten, (Wiley, New York,1962).

[2] A. Ashtekar, Phys. Rev. Lett. **57**, 2244 (1986); Phys. Rev. D **36**, 1587 (1987).

[3] A. Ashtekar, *Lectures on Non-Perturbative Canonical Gravity* (Singapore, World Scientific, 1991).

[4] R. Capovilla, T. Jacobson, and J. Dell, Phys. Rev. Lett. **63**, 2325 (1989); Class. Quantum Grav. **8**, 59 (1991).

[5] D.C Salisbury, L.C. Shepley, A. Adams, D. Mann, L.Turvan and B. Turner, Class. Quantum Grav. **11**, 2789 (1994).

[6] R. Penrose and W. Rindler, *Spinors and Space-time*, vol.1 and 2, (Cambridge University Press, 1984, 1986).

[7] A. Ashtekar, J.D. Romano, and R.S. Tate Phys. Rev. **D40**, 2572 (1989).

[8] L. Smarr, Ann. N.Y. Acad. of Sci. **302**, 569 (1977).

[9] L. Gunnarsen, H. Shinkai and K. Maeda, Class. Quantum. Grav. **12**, 133 (1995).

[10] N. O'Murchadha and J.W. York, Jr., Phys. Rev. **D 10**, 428 (1974).

[11] R. Capovilla, T. Jacobson, and J. Dell, *gr-qc/9302020.*

Ashtekar Variables and Matter Coupling

MOTOMU TSUDA, TAKESHI SHIRAFUJI AND HONG-JUN XIE
Physics Department, Saitama University
Urawa, Saitama 338, Japan

Abstract

It has been shown for low-spin fields that the use of only the self-dual part of the connection as basic variable does not lead to spurious equations or inconsistencies. We slightly generalize the form of the chiral Lagrangian of half-integer spin fields and express its imaginary part in a simple form. If the imaginary part is non-vanishing, it will lead to spurious equations. As an example, for (Majorana) Rarita-Schwinger fields the equations of motion of the torsion is solved and it is shown that it vanishes owing to the Fierz identity.

1. Introduction

In the mid-1980s Ashtekar has presented a new formulation of general relativity from a non-perturbutive point of view, in terms of which all the constraints of the gravity become simple polynomials of the canonical variables [1]-[4]. This formulation can be extended to include matter sources. In particular, in the cases of spin-1/2 fields [4,5] and $N = 1$ supergravity [3,6], the constraints are again polynomials of the canonical variables. On the other hand, the Ashtekar formulation of $N = 1$ supergravity was reformulated in the method of the two-form gravity [7]. The progress of the Ashtekar formalism can be traced from the references compiled in [8].

Here the complex chiral action using the self-dual connection and the tetrads e^i_μ is

$$S^{(+)} = \int d^4x\, e R^{(+)} + [\text{matter terms}], \tag{1.1}$$

where $e = \det(e^i_\mu)$ and

$$R^{(+)} := \frac{1}{2}\left(R - \frac{i}{2}\epsilon^{ij}{}_{kl} R^{kl}{}_{\mu\nu} e^\mu_i e^\nu_j\right). \tag{1.2}$$

Greek letters $\mu, \nu, \cdots$ are space-time indices, and Latin letters i, j, $\cdots$ are local Lorentz indices. Using the Bianchi identity, the chiral action (1.1) is reexpressed as

$$S^{(+)} = \frac{1}{2}\int d^4x\, eR(e) + [\text{quadratic terms of torsion}] + [\text{matter terms}]. \tag{1.3}$$

The first term of (1.3) is the Einstein-Hilbert action. Since the torsion equals zero in the source-free case, the complex chiral action is equivalent to the Einstein-Hilbert action. In this paper we shall take the form of matter terms to be slightly general, and analyze the consistency of the field equations.

In Sec.2 we will contemplate the half-integer spin fields minimally coupled to gravity, and introduce a slightly general form of the complex chiral Lagrangian of matter fields. In Sec.3 we will argue if the field equations are influenced by the imaginary part of the chiral Lagrangian. In the final section our result is summarized.

2. Lagrangian of Matter Fields

In the source-free case, although the chiral gravitational Lagrangian is complex, the imaginary part of the Lagrangian turns out to be simply the Bianchi identity. Since the Lagrangian of integer spin fields (spin-0,1) does not contain the Lorentz connection, the situation remains unaltered. Therefore, let us consider half-integer spin fields (ψ and ψ_μ for spin-1/2 and spin-3/2 fields, respectively) as matter fields.

Firstly, let us suppose that the matter Lagrangian is obtained by the minimal prescription; namely, by replacing ordinary derivatives by covariant derivatives,

$$\partial_i \to e_i^\mu D_\mu \tag{2.1}$$

with

$$D_\mu = \partial_\mu + \frac{i}{2}A_{ij\mu}S^{ij}. \tag{2.2}$$

Here e_i^μ is a tetrad field, $A_{ij\mu}$ means the Lorentz connection, and S_{ij} stands for the SL(2,C) generator. * The Lorentz connection $A_{ij\mu}$ is divided into the Ricci rotation

* In our convention $S_{ij} = \frac{i}{4}[\gamma_i, \gamma_j]$ and $\{\gamma_i, \gamma_j\} = -2\eta_{ij}$. We denote the Minkowski metric by $\eta_{ij} = \text{diag}(-1, +1, +1, +1)$. $\epsilon_{\mu\nu\rho\sigma}$ is the totally antisymmetric tensor normalized as $\epsilon_{0123} = +e$.

coefficients $A_{ij\mu}(e)$ and contorsion tensor $K_{ij\mu}$,

$$A_{ij\mu} = A_{ij\mu}(e) + K_{ij\mu}. \tag{2.3}$$

Secondly, we suppose that the chiral Lagrangian of matter fields is described by using the self-dual part of the Lorentz connection. According to the equation

$$A^{(+)}_{ij\mu} S^{ij} = A_{ij\mu} S^{ij} \frac{1+\gamma_5}{2}, \tag{2.4}$$

this demand that only the terms expressed by $D_\mu \psi_R$ and $\overline{\psi}_L \overleftarrow{D}_\mu$ should appear in the matter Lagrangian. ψ_R (ψ_L) is the right (left)-handed spinor field;

$$\begin{cases} \psi_R = \dfrac{1+\gamma_5}{2}\psi, \\ \psi_L = \dfrac{1-\gamma_5}{2}\psi. \end{cases} \tag{2.5}$$

Let us consider a (Majorana) Rarita-Schwinger field. (Spin-1/2 fields can be considered in the similar manner.) Its Lagrangian in Minkowski space is

$$L_{RS} = \frac{1}{2}\epsilon^{\mu\nu\rho\sigma}\overline{\psi}_\mu \gamma_5 \gamma_\rho \partial_\sigma \psi_\nu. \tag{2.6}$$

Applying the minimal prescription to (2.6), the Lagrangian density of a Rarita-Schwinger field becomes

$$\mathcal{L}_{RS} = \frac{1}{2} e \epsilon^{\mu\nu\rho\sigma}\overline{\psi}_\mu \gamma_5 \gamma_\rho D_\sigma \psi_\nu, \tag{2.7}$$

which is used in $N = 1$ supergravity [9]-[11].

On the other hand, the Lagrangian (2.6) can be rewritten as

$$L_{RS} = -\epsilon^{\mu\nu\rho\sigma}\overline{\psi}_{R\mu}\gamma_\rho \partial_\sigma \psi_{R\nu} + [\text{tot. div. term}]. \tag{2.8}$$

The minimal prescription applied to (2.8) leads to the chiral Lagrangian density,

$$\mathcal{L}^{(+)}_{RS} = -e\epsilon^{\mu\nu\rho\sigma}\overline{\psi}_{R\mu}\gamma_\rho D_\sigma \psi_{R\nu}. \tag{2.9}$$

Here the total divergence term in (2.8) is discarded. (The chiral Lagrangian density for the antiself-dual connection can be similarly defined by using the left-handed spinor field.)

The Lagrangian densities (2.7) and (2.9) can respectively be reexpressed as

$$\mathcal{L}_{RS} = \mathcal{L}_{RS}(e) + \frac{i}{4} e\epsilon^{\mu\nu\rho\sigma}\overline{\psi}_\mu \gamma_5 \gamma_\rho K_{ij\sigma} S^{ij} \psi_\nu, \tag{2.10}$$

$$\mathcal{L}_{RS}^{(+)} = \mathcal{L}_{RS}(e) + \frac{i}{2} e\epsilon^{\mu\nu\rho\sigma}\overline{\psi}_\mu \gamma_5 \gamma_\rho K_{ij\sigma}^{(+)} S^{ij} \psi_\nu, \tag{2.11}$$

where $K_{ij\mu}^{(+)}$ is the self-dual part of contorsion tensor $K_{ij\mu}$. In (2.11) a total divergence term has been omitted. We notice that the factor of the second term in (2.11) is twice that in (2.10).

Let us consider matter fields of which the real Lagrangian density is written as

$$\mathcal{L}_M = \mathcal{L}_M(e) + eX_{ijk}K^{ijk}, \tag{2.12}$$

where $X_{ijk} = X_{[ij]k}$ is a real tensor made of matter fields. Based on the case for spin-3/2 (and spin-1/2) fields, we assume that the complex chiral Lagrangian density of those matter fields is expressed as follows;

$$\mathcal{L}_M^{(+)} = \mathcal{L}_M(e) + 2eX_{ijk}K^{(+)ijk}. \tag{2.13}$$

It is noted that only the self-dual part $X_{ijk}^{(+)}$ contributes in (2.13).

In order to analyze the Lagrangian densities (2.12) and (2.13), it is convenient to decompose K_{ijk} into irreducible parts [12]; †

$$K_{ijk} = u_{ijk} - \frac{2}{3}\eta_{k[i}v_{j]} + \frac{1}{2}\epsilon_{ijkl}a^l, \tag{2.14}$$

where the tensor $u_{ijk} = u_{[ij]k}$ is traceless and

$$\epsilon^{ijkl}u_{jkl} = 0. \tag{2.15}$$

Here the vector v_i is

$$v_i = K_{ij}{}^j, \tag{2.16}$$

† The u_{ijk} of (2.14) is related to t_{ijk} of Ref. [12] by $u_{k(ij)} = t_{ijk}$.

and the axial vector a_i is

$$a_i = \frac{1}{3}\epsilon_{ijkl}K^{jkl}. \tag{2.17}$$

In the same way, $K^{(+)}_{ijk}$ is decomposed as

$$K^{(+)}_{ijk} = u^{(+)}_{ijk} - \frac{2}{3}\eta_{k[i}v^{(+)}_{j]} + \frac{1}{2}\epsilon_{ijkl}a^{(+)l}, \tag{2.18}$$

where $u^{(+)}_{ijk}$ is self-dual part of u_{ijk}, and

$$a^{(+)}_i = \frac{2}{3}iv^{(+)}_i = \frac{1}{2}\left(a_i + \frac{2}{3}iv_i\right). \tag{2.19}$$

Substituting (2.14) and (2.18) into (2.12) and (2.13), respectively, the matter Lagrangian densities can be represented as

$$\mathcal{L}_M = \mathcal{L}_M(e) + e(B_{ijk}u^{ijk} + C_iv^i + D_ia^i), \tag{2.20}$$

$$\mathcal{L}^{(+)}_M = \mathcal{L}_M(e) + 2e(B_{ijk}u^{(+)ijk} + C_iv^{(+)i} + D_ia^{(+)i}), \tag{2.21}$$

where $B_{ijk} = B_{[ij]k}, C_i$ and D_i are related to X_{ijk}. We notice that only the self-dual part $B^{(+)}_{ijk}$ contributes in (2.21).

3. Consistency of the field equations

Let us write the quadratic terms of the torsion in (1.3) explicitly. The gravitational Lagrangian density $\mathcal{L}_G = eR$ is represented as follows;

$$\mathcal{L}_G = \mathcal{L}_G(e) + \frac{e}{2}\left(\frac{1}{2}u^2 - \frac{2}{3}v^2 + \frac{3}{2}a^2\right), \tag{3.1}$$

where $u^2 = u^{ijk}u_{ijk}$, etc. We define the total Lagrangian density as the sum of (3.1) and (2.20);

$$\mathcal{L} = \mathcal{L}(e) + \frac{e}{2}\left(\frac{1}{2}u^2 - \frac{2}{3}v^2 + \frac{3}{2}a^2\right) + e(B_{ijk}u^{ijk} + C_iv^i + D_ia^i). \tag{3.2}$$

On the other hand, the chiral gravitational Lagrangian $\mathcal{L}_G^{(+)} = eR^{(+)}$ of (1.1) becomes

$$\mathcal{L}_G^{(+)} = \mathcal{L}_G(e) + e\left(\frac{1}{2}u^{(+)2} - \frac{2}{3}v^{(+)2} + \frac{3}{2}a^{(+)2}\right), \tag{3.3}$$

and the total chiral Lagrangian density is

$$\begin{aligned}\mathcal{L}^{(+)} &= \mathcal{L}^{(+)}(e) + e\left(\frac{1}{2}u^{(+)2} - \frac{2}{3}v^{(+)2} + \frac{3}{2}a^{(+)2}\right)\\ &\quad +2e(B_{ijk}u^{(+)ijk} + C_i v^{(+)i} + D_i a^{(+)i}),\end{aligned} \tag{3.4}$$

which is the sum of (3.3) and (2.21).

To begin with, let us consider the equations of motion for u_{ijk}, v_i and a_i. The equations of motion derived from (3.2) are

$$\begin{cases} u_{ijk} &= -2B_{ijk}, \\ v_i &= \dfrac{3}{2}C_i, \\ a_i &= -\dfrac{2}{3}D_i. \end{cases} \tag{3.5}$$

On the other hand, regarding $u_{ijk}^{(+)}$ and $v_i^{(+)}$ as independent variables in (3.4), we obtain the equations of motion as

$$\begin{cases} u_{ijk}^{(+)} &= -2B_{ijk}^{(+)}, \\ v_i^{(+)} &= \dfrac{3}{4}\left(C_i + \dfrac{2}{3}iD_i\right), \end{cases} \tag{3.6}$$

where $B_{ijk}^{(+)}$ is self-dual part of B_{ijk}. It can be shown that u_{ijk}, v_i and a_i derived from (3.6) coincide with (3.5). If u_{ijk}, v_i and a_i are regarded as independent variables in $\mathcal{L}^{(+)}$ of (3.4), both $\mathrm{Re}\mathcal{L}^{(+)}$ and $\mathrm{Im}\mathcal{L}^{(+)}$ give the same result as (3.5); namely, although $\mathcal{L}^{(+)}$ is complex, extra conditions do not appear.

Next, let us turn to investigate the detailed form of $\mathrm{Im}\mathcal{L}^{(+)}$. Using the solution (3.5) in (3.4), $\mathrm{Im}\mathcal{L}^{(+)}$ can be written in terms of u_{ijk}, v_i and a_i as

$$\mathrm{Im}\mathcal{L}^{(+)} = \frac{e}{8}(\epsilon_{ijmn}u^{ijk}u^{mn}{}_k - 8v_i a^i). \tag{3.7}$$

After a little calculation, we get

$$\mathrm{Im}\mathcal{L}^{(+)} = \frac{e}{8}\epsilon_{ijmn}T^{kij}T_k^{mn}, \tag{3.8}$$

where $T_{ijk} = K_{ijk} - K_{ikj}$ is the torsion tensor.

In the case of spin-1/2 fields,

$$\begin{cases} u_{ijk} &= 0, \\ v_i &= 0, \\ a_i &= \overline{\psi}\gamma_5\gamma_i\psi. \end{cases} \tag{3.9}$$

Substituting (3.9) into (3.7), we obtain $\mathrm{Im}\mathcal{L}^{(+)} = 0$. For a (Majorana) Rarita-Schwinger field, we have

$$\begin{cases} u_{ijk} &= -\frac{i}{4}\epsilon_{ij}{}^{rs}\epsilon_{mnkr}\overline{\psi}^m\gamma_s\psi^n \\ & \quad -[\text{trace part}] - [\text{tot. antisym. part}], \\ v_i &= \frac{i}{2}\overline{\psi}_i\gamma^j\psi_j, \\ a_i &= -\frac{i}{12}\epsilon_{ijkl}\overline{\psi}^j\gamma^l\psi^k. \end{cases} \tag{3.10}$$

Although u_{ijk} are considerably complicated, it can be shown after a little calculation that the torsion takes a simple form

$$T_{kij} = -\frac{i}{2}\overline{\psi}_i\gamma_k\psi_j, \tag{3.11}$$

which is the same result as $N = 1$ supergravity. With the help of the following identity

$$\epsilon^{ijkl}(\overline{\psi}_k\gamma_m\psi_l)\gamma^m\psi_j = 0, \tag{3.12}$$

which is valid because of the Fierz identity [13], substituting (3.11) into (3.8) shows that $\mathrm{Im}\mathcal{L}^{(+)}$ vanishes.

4. Summary

Based on the considerations of spin-1/2 fields and (Majorana) Rarita-Schwinger fields, we have generalized the chiral Lagrangian of half-integer spin fields a little. This generalized chiral Lagrangian of matter fields holds also in the case of $N = 2$

supergravity and (Dirac) Rarita-Schwinger fields, etc. For N-(Majorana) Rarita-Schwinger fields, we may merely replace ψ_μ in this paper by ψ_μ^I where I runs from 1 to N. We have seen that the field equations for the self-dual connection derived from the complex chiral Lagrangian is compatible with those derived from the real Lagrangian. Futhermore, we have shown that the imaginary part of the chiral Lagrangian takes a simple form in terms of the torsion tensor T_{ijk}.

For a (Majorana) Rarita-Schwinger field, $\mathrm{Im}\mathcal{L}^{(+)}$ vanishes owing to the identity (3.12). However, there is a possibility that $\mathrm{Im}\mathcal{L}^{(+)} \neq 0$ for $N = 2$ supergravity, because (3.12) does not hold for this case. If this is the case, $\mathrm{Im}\mathcal{L}^{(+)}$ will lead to spurious equations. (Dirac) Rarita-Schwinger fields are also under study.

References

[1] A. Ashtekar, *Phys. Rev. Lett.* **57**, 2244 (1986); *Phys. Rev.* **D36**, 1587 (1987).

[2] T. Jacobson and L. Smolin, *Phys. Lett.* **196B**, 39 (1987); *Class. Quantum Grav.* **5**, 583 (1988).

[3] A. Ashtekar, *New Perspectives on Canonical Gravity* (Bibliopolous, Naples, Italy, 1988).

[4] A. Ashtekar, *Lectures on Non-Perturbutive Canonical Gravity* (World Scientific, Singapore, 1991).

[5] A. Ashtekar, J. D. Romano and R. S. Tate, *Phys. Rev.* **D40**, 2572 (1989).

[6] T. Jacobson, *Class. Quantum Grav.* **5**, 923 (1988).

[7] R. Capovilla, J. Dell, T. Jacobson and L. Mason, *Class. Quantum Grav.* **8**, 41 (1991).

[8] Bibliography of Publications related to Classical and Quantum Gravity in terms of the Ashtekar Variables, updated by T. Schlling gr-qc 9409031.

[9] D. Z. Freedman, P. van Nieuwenhuizen and S. Ferrara, *Phys. Rev.* **D13**, 3214 (1976).

D. Z. Freedman and P. van Nieuwenhuizen *Phys. Rev.* **D14**, 912 (1976).

[10] S. Deser and B. Zumino, *Phys. Lett.* **62B**, 335 (1976).

[11] P. van Nieuwenhuizen, *Phys. Rep.* **68**, 189 (1981).

[12] K. Hayashi and T. Shirafuji, *Prog. Theor. Phys.* **64**, 866 (1980).

[13] See, for example, eq.(7) in p.365 of Ref.[11].

How to make an Open FRW Universe
~ One-Bubble Inflationary Model

Takahiro Tanaka[1], Kazuhiro Yamamoto[1] and Misao Sasaki[2]

[1] *Department of Physics, Kyoto University,*

Kyoto 606-01, Japan

[2] *Department of Earth and Space Science,*

Osaka University, Toyonaka 560, Japan

We consider an alternative scenario of inflation which predicts a spatially open universe. In this scenario the universe is created by the nucleation of a single bubble. The conditions to explain the homogeneity and isotropy of the universe and to solve the entropy problem is investigated. It should be emphasized that this scenario allows us to obtain definite prediction on the spectrum of the primordial density perturbations, which reflect the quantum fluctuations of the inflaton field. We describe the method to investigate the quantum state during and after the bubble nucleation based on multidimensional tunneling wave function.

I. INTRODUCTION

Inflationary cosmology has now become an integrated part of the standard model of the universe. However, predictions of inflationary cosmology do not always agree with observations. The standard models of inflation naturally predict $\Omega_0 = 1$ flat universe, though some observations favour a low density universe $\Omega_0 < 1$ [1]. If we take these observations serious, the cosmological constant is needed. In this paper, we do not assume the existence of the cosmological constant, instead, we pursue another possibility by constructing a consistent scenario of an open universe in the context of the inflationary cosmology.

Naively one might think that it is possible to realize an open universe by adjusting the period of inflation suitably. However, as discussed by Kashlinski *et.al.* [2], it is very difficult to realize a homogeneous and isotropic universe within the standard inflationary universe scenario. This is because the horizon and flatness problems, which are two different

problems in nature, happen to be closely related in the standard scenario, *i.e.*, they are explained simultaneously by means of the large e-foldings of the inflationary expansion. This difficulty can be overcome by solving the horizon problem and the flatness problem separately with different mechanism.

One-bubble inflationary model is a very attractive candidate to realize an open universe. Originally this idea was proposed by Gott III [3,4]. This scenario assumes a scalar field which has a new inflation type potential with a high potential barrier (see Figure 1). For such a potential, the first inflation in the false vacuum provides a coherently homogeneous scalar field due to the de Sitter expansion. Then bubble nucleation occurs due to the quantum tunneling in the sea of false vacuum.

The bubble nucleation process is described by an $O(4)$-symmetric bounce solution [5,6], which is a solution of the field equation in the Euclidean spacetime. The subsequent motion of a bubble after nucleation is given by the analytic continuation of the bounce solution to the Lorentzian spacetime. Hence the spacetime has the $O(3,1)$-invariance owing to the $O(4)$-symmetry of the bounce solution. In other words, the interior of the bubble can be regarded as an homogeneous and isotropic universe with negative spatial curvature, as long as the bubble collisions do not occur. Thus a high potential barrier must guarantees an exponentially small nucleation rate so that the bubble collisions can be neglected.

Then if the second inflation of slow rollover type occurs in the bubble for a suitable amount of time, the flatness of the universe with $\Omega_0 \sim 0.1$ can be explained without conflicting with the homogeneity and isotropy of the universe. The subsequent evolution of the universe after the second inflation is the same as that of the usual inflation scenarios.

Within the context of this scenario, the important issue to be addressed is the origin

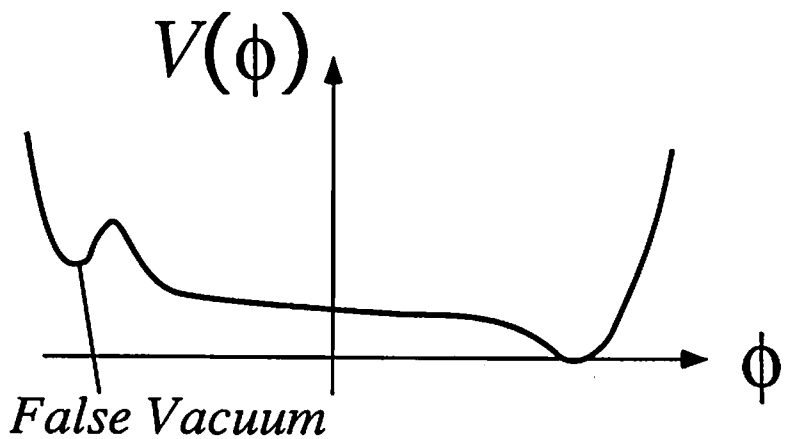

FIG. 1. The potential form of the scalar field which realize the open inflationary universe

of the density perturbations for the cosmic structure formation. According to the standard inflationary scenarios, the quantum fluctuations of the scalar field give rise to the cosmic density perturbations. There have been many papers devoted to the investigation of the perturbations in an open universe, however, most of them are always based on some *ad hoc* assumptions for the initial perturbation spectrum due to the lack of a definite scenario. In contrast, our scenario is definite enough to predict the initial perturbation spectrum in principle.

In this one-bubble inflationary scenario, the quantum fluctuations of the scalar field originate from two different parts. One is the fluctuations caused by the bubble nucleation process [23,24,7–12]. The other is the usual vacuum fluctuations which are imprinted during the first and second inflationary phases. In this paper, we are to cover the discussions on the former problem as widely as possible without details. The latter problem is discussed elsewhere [13–15].

This paper is organized as follows. In section 2, we first briefly review the difficulty to construct an open universe scenario in the context of the standard inflation, then describe the one-bubble inflationary model and examine the conditions for this model to be successful. To investigate the quantum fluctuations of a scalar field during and after the bubble nucleation, we review the method based on the multi-dimensional tunneling wave function in section 3. On the basis of this formalism, in section 4, we investigate the bubble nucleation which occurs in the Minkowski spacetime. The quantum state after the bubble nucleation is described in the language of a particle creation in the Milne universe. In section 5, we consider the extension of this consideration to the case with the effect of gravity. For this purpose, we consider the prescription to describe the Euclidean vacuum state of a scalar field in the open chart of the de Sitter spacetime. Section 6 is devoted to the summary and discussions.

II. STANDARD INFLATION AND ONE-BUBBLE INFLATION FOR AN OPEN UNIVERSE

The inflation scenario explains the homogeneity, isotropy and flatness of the universe elegantly, which is a part of reasons why inflation is attractive. You may think that the open universe, e.g. $\Omega_0 \sim 0.1$, can be realized easily by the fine tuning of the period of inflation in the standard inflationary scenario. However, we can show that it is difficult to realize an open universe in such a way [2]. This difficulty to nucleate an open universe in the standard inflation scenario originates from the fact that the homogeneity and isotropy of the universe and the entropy problem are solved at the same time by a large amount of expansion of the universe.

Writing the line element of the open Freedman-Robertson-Walker universe as

$$ds^2 = -dt^2 + a(t)^2(d\chi^2 + \sinh^2\chi d\Omega^2_{(2)}), \tag{2.1}$$

the Freedman equation is

$$\frac{1}{H^2(t)a^2(t)} = 1 - \Omega(t), \tag{2.2}$$

where $H(t) := \dot{a}(t)/a(t)$, the dot denotes t-differentiation and $\Omega(t)$ is the density parameter. From the above equation, we can write

$$(1 - \Omega_0)(H_0 a_0)^2 = (1 - \Omega_b)(H_b a_b)^2, \tag{2.3}$$

where the subscript '0' and 'b' denote the time at present and that at the beginning of inflation, respectively. In the standard inflation scenario, the region of horizon size, L_b, expands by inflation. As it is natural that the spatial curvature is not dominant at the beginning of inflation, we have $H_b L_b \sim O(1)$. Assuming the positive energy density of matter at the beginning of inflation, $\Omega_b > 0$, we can find the following constraint on the scale of homogeneous patch at present epoch $L_0 = (a_0/a_b)L_b$,

$$L_0 \lesssim \frac{1}{H_0}\sqrt{\frac{1}{1 - \Omega_0}}. \tag{2.4}$$

This implies that the homogeneous patch at present stretched by the inflation has a size comparable with the present horizon scale, *i.e.*, $L_0 \lesssim 1/H_0$, unless Ω_0 is precisely equal to unity.

Following the standard inflation scenario, the inflaton field shows stochastic behavior over the scale of horizon at the beginning of inflation. Thus it is expected that there exist fluctuations of $O(1)$ over that scale. Inflation produces coherence over the horizon scale, but the existence of the coherence over the horizon scale before inflation does not match with the spirit of inflation. Then, the density fluctuations of $O(1)$ must exist on the present horizon scale. In such case significant effect on the CMB anisotropy will appear. By analysing the Grishchuk-Zel'dovich effect [17], which is the contribution to the CMB anisotropy from the superhorizon scale perturbations, it is shown that only the value $|1 - \Omega_0| < 10^{-5}$ is allowed to match with the observed smoothness of CMB as long as we follow the standard inflation scenarios [2].

Now let us turn to the one-bubble inflation model. This model assumes a scalar field which has a potential of new inflation type but with rather high potential barrier (Fig. 1), and we consider a bubble nucleation from the state trapped in the false vacuum minimum. If the barrier of the field potential is high enough, the decay rate is small and the first de Sitter phase in the false vacuum minimum will lasts long. In this case, the bubble nucleation occurs in the coherently smooth background of the de Sitter spacetime. Because of the $O(4)$-symmetry of the bounce solution, the nucleated bubble has the $O(3,1)$-symmetry, which says that the inside of bubble can be regarded as an open universe [3,18], as long as bubble collision does not occur. Thus the rate of bubble collisions must be small not to disturb the homogeneity and isotropy of the universe. This condition have been analysed by Gott and Statler [4] essentially in a same way as will be presented here.

Let see the Fig. 2, which is the Penrose diagram of the de Sitter universe with one nucleated bubble. To make the situation definite, we assume that the inside of bubble is

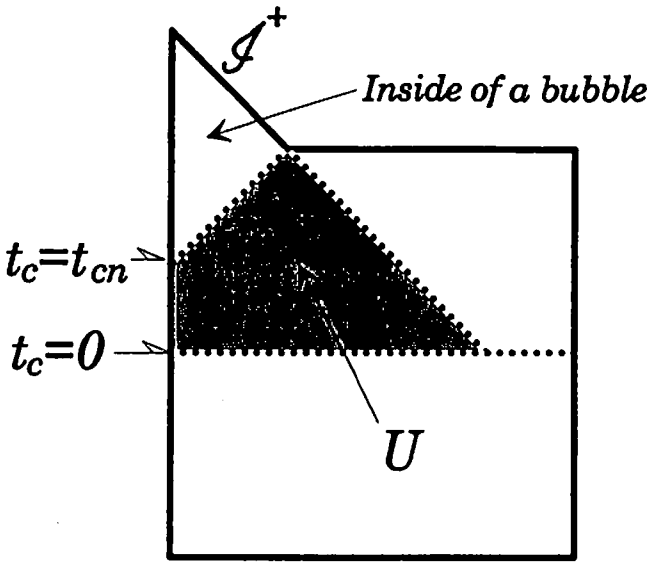

FIG. 2. Penrose diagram for the "one-bubble inflationary cosmology"

described by the de Sitter universe with vacuum energy V_i followed by a radiation dominant universe. The junction of these two eras is assumed to be instantaneous at $t = t_{ir}$. It is convenient to introduce a coordinate with the conformal time as

$$ds^2 = \bar{a}(\eta)^2(-d\eta^2 + d\chi^2 + \sinh^2\chi d\Omega^2_{(2)}), \tag{2.5}$$

where the cosmological time and the conformal time is related by the relation $\sinh(H_i t) = -1/\sinh\eta$.

Then the scale factor in the inflation era becomes $\bar{a}(\eta) = -1/H_i \sinh\eta$, where $H_i = \sqrt{8\pi G V_i/3}$. If the inflationary era lasts long enough, the scale factor in the radiation dominant era is given by $\bar{a}(\eta) = a_{ir}^2 H_i \sinh(\eta + c)$, where a_{ir} is the value of the scale factor at $t = t_{ir}$ and c is a small number of $O(\exp(-H_i t_{ir}))$. From the Eq.(2.2), we find

$$\tanh^2(\eta_0 + c) = 1 - \Omega_0. \tag{2.6}$$

Neglecting the small collection of c, this gives $e^{\eta_0} = (1 + \sqrt{1 - \Omega_0})/\sqrt{\Omega_0}$. The null geodesic terminating at $\chi = 0$ is trivially solved in the coordinate (2.5) as $\chi(\eta) = \eta_0 - \eta$. There is a sphere, S_0, where the past light cone of the present observer at $\eta = \eta_0$ and the future light cone of the nucleated bubble intersects. Denoting the circumference radius of this sphere as R, it is easy to see that $R = \lim_{\eta\to-\infty} -\sinh\chi(\eta)/H_i \sinh\eta = e^{\eta_0}/H_i$.

Since the past eternal inflation is impossible [19], we consider that a closed universe is first created by the quantum effect of the space time [20,21]. All scenarios of the creation of universe tell us that the nucleation occurs at the maximum surface. Introducing the closed chart of the de Sitter universe as

$$ds^2 = -dt_c^2 + a_c(\eta)^2(d\chi_c^2 + \sin^2\chi_c d\Omega_2^2), \tag{2.7}$$

we consider that the universe is born in the false vacuum at $t_c = 0$. Thus the bubble nucleation occurs at $t_c = t_{cn} > 0$. The point of bubble nucleation is denoted by p, and the point of the present observer is denoted by p_0. Using the notation $J^{+(-)}(p)$ which is the causal future (past) of the point p, we evaluate the volume of the region $U := \bar{J}^+(p) \cap J^-(p_0) \cap \bar{J}^-(p) \cap D$, where the over bar denotes the complimentary set and $D = \{p : p \text{ is a point with } t_c > 0\}$ (see Fig.2). The evaluation of this volume is tedious but straight forward. For simplicity, we assume that the sphere S is on one $t_c =$ constant surface. After the lengthy calculation, in the large t_{cn} limit, the volume of the region U is evaluated as

$$V = \frac{4\pi}{H^4}\left(\frac{2}{3}\log(1+R) + \frac{R^2}{3} + O(e^{-Ht_{cn}})\right). \tag{2.8}$$

As is expected, the volume stays finite in this limit. Since the probability that the present observer at p_0 sees bubble collisions in his past is given by V multiplied by the tunneling rate per unit space-time volume, which can be kept small by choosing the parameters of potential, it is easy to construct a model in which this probability is small enough that the present observer does not see bubble collisions. Thus we conclude that the second criterion can be satisfied in this context.

Next we consider the condition to explain the fact that the Ω-parameter is nearly unity at present, which is essentially the same as the condition to solve the entropy problem. In the following, before considering this condition, we first show the necessity of the inflation inside the bubble.

Assume that the potential of the field, ϕ, which causes the bubble nucleation, has only one mass scale, $\mathcal{M}$. The dynamics of the field is described by

$$\ddot{\phi} + 3\frac{\dot{a}}{a}\dot{\phi} + \frac{dV}{d\phi} = 0, \tag{2.9}$$

$$\dot{a}^2 = 1 + \frac{8\pi a^2}{3m_{Pl}^2}\left(\frac{1}{2}\dot{\phi}^2 + V\right), \tag{2.10}$$

where V is the potential and m_{Pl} is the Plank mass. The initial conditions of these equations at $t = 0$ are given by the one obtained by the analytic continuation of the bounce solution [6],

$$\begin{aligned} \dot{a} &= 1, \quad \dot{\phi} = 0, \\ a &= 0, \quad \phi = \phi_b, \end{aligned} \tag{2.11}$$

where ϕ_b is a constant of $O(\mathcal{M})$ by assumption. At the beginning, $t \sim 0$, we find the asymptotic solution, $a(t) \sim t$, from Eq.(2.10), which indicates that the universe behaves like Minkowski spacetime and is curvature dominant. In this case, the time scale of the evolution of ϕ is $\mathcal{M}^{-1}$. As $(\dot{\phi}^2/2 + V)$ is found to be a monotonically decreasing function, estimating $a \sim \mathcal{M}^{-1}$ at $t \sim \mathcal{M}^{-1}$, we find

$$\frac{8\pi a^2}{3m_{Pl}^2}\left(\frac{1}{2}\dot{\phi}^2 + V\right) \lesssim \frac{\mathcal{M}^2}{m_{Pl}^2} \ll 1, \tag{2.12}$$

where the last inequality comes from the condition that the phase transition is driven by the quantum tunneling. This means that the curvature term is still dominant at the time $t \sim \mathcal{M}^{-1}$. Then the scalar field oscillates around the true vacuum. It might transfer the energy to the other fields but the details are not important. Because the the total energy density of usual matter decreases faster than the curvature term, the universe can never be matter dominant. This contradicts with the Big Bang hot universe scenario.

We can conclude that the second inflation inside the bubble is required, which is the reason why we have assumed the potential with flat part outside the barrier as shown in Fig. 1. Here let us consider the restrictions on the inflation which occurs inside the bubble [22]. From the Freedman equation (2.2) or Eq.(2.3), we can write

$$(1-\Omega_0) = \frac{H_b^2 a_b^2}{H_e^2 a_e^2}\frac{H_e^2 a_e^2}{H_0^2 a_0^2}(1-\Omega_b), \tag{2.13}$$

where the subscript e denotes the 'end' of inflation. As the usual inflation scenario, the reheating of the universe must occur to produce the entropy after inflation. By using the facts that after reheating, $a \propto 1/T$, $H \propto T^2$, where T denotes the temperature of the universe, we find

$$(1-\Omega_0) \simeq 4e^{-2N}\frac{T_e^2}{T_0^2}(1-\Omega_b), \tag{2.14}$$

Here we have assumed that the inflation inside the bubble can be described by the open de Sitter spacetime, and N is the e-holding number of de Sitter expansion. Since $\Omega_b = 0$, we have

$$N \simeq \ln\left(\frac{T_e}{T_0}\right) - \ln\left(\frac{\sqrt{1-\Omega_0}}{2}\right). \tag{2.15}$$

For the case $T_e = 10^{15}$GeV and $\Omega_0 = 0.1$, we find $N \simeq 64$. Thus we need fine tuning for the relation between the reheating temperature and the duration of inflation. But this kind of fine tuning will be always necessary to realize an open universe with $\Omega_0 \sim 0.1$.

The one bubble inflation model might be just one of the scenarios which predict an open FRW universe, but it is also true that we do not know any alternatives unless the whole things to be explained are set as initial conditions. Therefore we concentrate on this model here. As was mentioned before, the comoving scale of our present horizon is comparable with that of the initial horizon. This means that the initial quantum fluctuations are not washed out by the expansion of the universe during the inflation. Then, it becomes important to determine the initial quantum state after the bubble nucleation. In the next section, we present the brief sketch of the technique to investigate the quantum state after tunneling.

III. MULTI-DIMENSIONAL TUNNELING WAVE FUNCTION

For the purpose of investigating the quantum fluctuations during and after the bubble nucleation, we here consider to describe the quantum state of a scalar field during and after

the tunneling process from the ground state in the false vacuum to the true vacuum state. Some different approaches were taken by Rubakov [23] and Vachaspati and Vilenkin [24]. Rubakov used the method of Bogoliubov transformation extensively on the background of the Euclidean solution of the field equation (instanton). His formal discussion is consistent with ours, but the derivation seems rigorous. The meaningful notion about the quantum state after $O(4)$-symmetric bubble nucleation is first obtained by Vachaspati and Vilenkin. They used the regularity of the wave function in the forbidden region to determine the quantum state after tunneling. They constructed the wave function by using the Rindler's time slicing in place of the Minkowski's one, which was not fully justified in their paper but we showed the correctness of their prescription.

On the other hand, we use the method of multi-dimensional tunneling wave function, which was initiated by de Vega, Gervais and Sakita [16] and developed to be applied to this problem by the present authors [7]. To explain the essential features of our approach, here we consider a simple system consisted of two degrees of freedom, X, and ϕ, whose the Lagrangian is given by,

$$\mathcal{L} = \frac{1}{2}\dot{X}^2 - V(X) + \frac{1}{2}\dot{\phi}^2 - \frac{1}{2}m^2(X)\phi^2, \tag{3.1}$$

where the potential $V(X)$ has the form as shown in Fig. 3. The quantum tunneling occurs in the direction of X and ϕ is a fluctuation degree of freedom coupling to X. Then we consider the quantum tunneling of a particle from the local potential minimum at $X = X_F$ to the right hand side of the potential barrier. This quantum tunneling process corresponds to the false vacuum decay. For simplicity, we have assumed that the fluctuation degree of

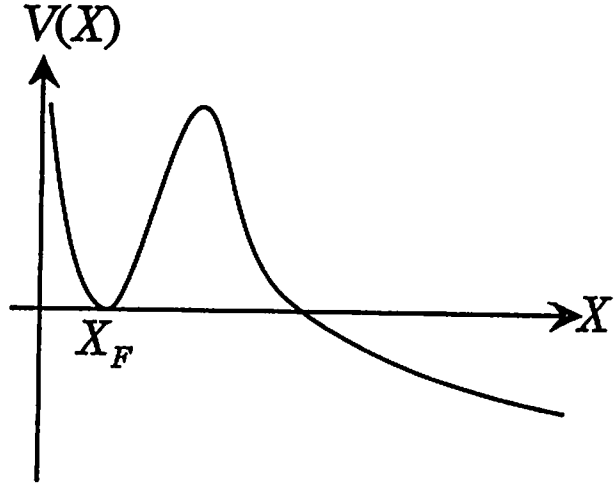

FIG. 3. The potential form of the tunneling degree of freedom, where X_F represents the values of X in the false vacuum.

freedom, ϕ, interacts with the tunneling degree of freedom only through the mass term. For the later convenience, we define $\omega^2 := m^2(X_F)$.

The Hamiltonian operator in the coordinate representation is obtained by replacing the conjugate momenta in the Hamiltonian with the corresponding differential operators as

$$\hat{H} = \hat{H}_X + \hat{H}_\phi, \tag{3.2}$$

where

$$\hat{H}_X = -\frac{\hbar^2}{2}\frac{\partial^2}{\partial X^2} + V(X), \quad \hat{H}_\phi = -\frac{\hbar^2}{2}\frac{\partial^2}{\partial \phi^2} + \frac{1}{2}m^2(X)\phi^2. \tag{3.3}$$

We construct a wave function which describes the quantum tunneling phenomena under the WKB approximation. We call it the *quasi-ground-state* wave function. It is the lowest eigenstate of the Hamiltonian which is sufficiently localized in the false vacuum. When the potential barrier is sufficiently high, we can approximately define the ground states localized in the false vacuum. Let us consider the situation in which the initial state is set in this ground-state in the false vacuum. As the tunneling rate Γ is exponentially small, after a long enough time but not too long compared with the time scale of the tunneling Γ^{-1}, the wave function is expected to become approximately time independent one, *i.e.*, an eigen state of the Hamiltonian. Therefore a *quasi-ground-state* wave function will describe the quantum tunneling from the ground state in the false vacuum. To obtain this wave function, we solve the time-independent Schrödinger equation,

$$\hat{H}\Psi^0 = E\Psi^0, \tag{3.4}$$

in the WKB approximation.

If we neglect the fluctuation degree of freedom, ϕ, the system reduces to that of the one-dimensional quantum mechanics of a particle. We impose the WKB ansatz on the wave function,

$$\Theta = e^{-\frac{1}{\hbar}(W^{(0)}(X)+\hbar W^{(1)}(X)+\cdots)}, \tag{3.5}$$

which should solve the time-independent Schrödinger equation,

$$\left[-\frac{\hbar^2}{2}\frac{\partial^2}{\partial X^2} + V(X)\right]\Theta(X) = E\Theta(X). \tag{3.6}$$

We solve this equation to the second lowest order with respect to $\hbar$. The energy eigen value E is formally divided into two parts, E_0 and E_1, of $O(\hbar^0)$ and $O(\hbar^1)$, respectively. The equation in the lowest order of $\hbar$ becomes the so-called Hamilton-Jacobi equation with the energy E_0,

$$-\frac{1}{2}\left(\frac{\partial W^{(0)}}{\partial X}\right)^2 + V(X) = E_0. \tag{3.7}$$

To obtain a solution of this equation, we introduce a function $\bar{X}(\tau)$ which satisfies the relation,

$$\frac{d\bar{X}}{d\tau} := \frac{\partial W^{(0)}}{\partial X}. \tag{3.8}$$

Then the Euclidean equation of motion for $\bar{X}(\tau)$,

$$\frac{d^2\bar{X}}{d\tau^2} = V'(\bar{X}), \tag{3.9}$$

is derived from the Eq. (3.7).

We take this solution to start from the false vacuum at $\tau = -\infty$ with the zero kinetic energy (*i.e.*, $E = E_0 := V(X_F)$) and to arrive at the turning point at $\tau = 0$ which is the boundary between the classically allowed and forbidden regions. It is a half of the so-called bounce solution. We also call it the dominant escape path (DEP). Using the definition (3.8), Eq. (3.7) gives

$$W^{(0)}(\bar{X}(\tau)) = \int_{-\infty}^{\tau} d\tau'\, 2\Big(U(\bar{X}(\tau')) - E_0\Big) + C', \tag{3.10}$$

where C' is a constant. Therefore, if $\bar{X}(\tau)$ is known, $W^{(0)}(X)$ can be calculated using this expression.

In the next order of $\hbar$, Eq. (3.6) gives

$$-\frac{dW^{(0)}}{dX}\frac{dW^{(1)}}{dX} + \frac{1}{2}\frac{d^2W^{(0)}}{dX^2} = \frac{E_1}{\hbar}. \tag{3.11}$$

As is well known, this equation can be formally integrated to give

$$W^{(1)}(\bar{X}(\tau)) = \frac{1}{4}\log\Big[2\Big(V(\bar{X}(\tau)) - E_0\Big)\Big] - \frac{E_1\tau}{\hbar}. \tag{3.12}$$

Combining Eqs. (3.5), (3.10) and (3.12), we obtain the second lowest WKB wave function as

$$\Theta(\bar{X}(\tau)) = \frac{Ce^{E_1\tau/\hbar}}{\Big[2\Big(V(\bar{X}(\tau)) - E_0\Big)\Big]^{1/4}} \exp\left(-\frac{1}{\hbar}\int_{-\infty}^{\tau} d\tau'\, 2\Big((V(\bar{X}(\tau')) - E_0\Big)\right). \tag{3.13}$$

To see that this has the property of the *quasi-ground-state* wave function, we examine the asymptotic behavior of this wave function near the false vacuum. There, since locally the potential $V(X)$ may be approximated by quadratic form as

$$V(X) = E_0 + \frac{1}{2}\omega_X^2 X^2 + \cdots, \tag{3.14}$$

with the definition, $\omega_X^2 := d^2V/dX^2|_{X=X_F}$, we can consider a ground state wave function normalized in the false vacuum as

$$\left(\frac{\omega_X}{\pi\hbar}\right)^{1/4} e^{-\frac{1}{2\hbar}\omega_X X^2} \tag{3.15}$$

Noting that the DEP is given by $\bar{X}(\tau) \sim Ae^{\omega_X \tau}$ at $\tau \to -\infty$, where A is a constant, the requirement that $\Theta(X)$ coincides with (3.15) near the false vacuum determines the unknown two parameters in (3.13) as

$$E_1 = \hbar\omega_X/2, \quad C = (\omega_X^3 A^2/\pi\hbar)^{1/4}. \tag{3.16}$$

The constant A is determined by the condition $\frac{d\bar{X}(\tau)}{d\tau} = 0$ at $\tau = 0$, which fixes the origin of time.

Thus we have constructed the wave function in the forbidden region. As is well known, the wave function in the allowed region is given by its analytic continuation. Replacing τ with it and $\bar{X}(\tau)$ with the solution of the equation of motion in the Lorentzian time t, $\bar{X}_L(t)$, which satisfies $\bar{X}_L(t) = \bar{X}(it)$, we obtain

$$\Theta(\bar{X}_L(t)) = \frac{Ce^{\frac{i}{2}\omega_X t}}{\left[2\left(V(\bar{X}_L(t)) - E_0\right)\right]^{1/4}} \exp\left(\frac{i}{\hbar}\int_{i\infty}^{t} dt' 2\left(V(\bar{X}_L(t')) - E_0\right)\right). \tag{3.17}$$

Here the path of t integration is shown in Fig. 4. To be more precise, it is necessary to add another term which is exponentially small in the forbidden region. However, as it does not change the discussions of the quantum state after tunneling, we will neglect it in the discussion below.

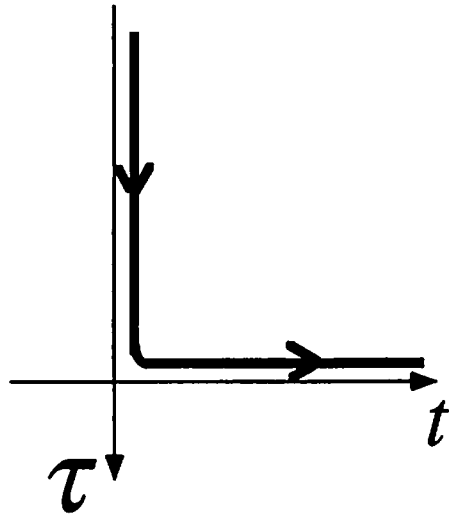

FIG. 4. A path of integration on the complex plane of time.

Next, let us consider the system including the fluctuation degree of freedom. We set an ansatz of the factorised wave function as

$$\Psi^0(X,\phi) = \Theta(X)\Phi^0(X,\phi). \tag{3.18}$$

Then we find that Eq. (3.4) gives

$$\left[\hbar\frac{\partial}{\partial\tau} + \hat{H}_\phi - E_{1\phi}\right]\Phi^0(\bar{X}(\tau),\phi) = 0, \tag{3.19}$$

where $\hat{H}_\phi$ is the Hamiltonian of ϕ defined in (3.3). To obtain a solution of this equation, we assume the Gaussian form of the wave function as

$$\Phi^0(\bar{X}(\tau),\phi) = \mathcal{N}(\tau)\exp\left(-\frac{1}{2\hbar}\Omega(\tau)\phi^2\right). \tag{3.20}$$

Then a solution of $\mathcal{N}(\tau)$ and $\Omega(\tau)$ are given by using one function, $g(\tau)$ as

$$\mathcal{N}(\tau) = \frac{(\omega/\pi)^{1/4}}{\sqrt{g(\tau)}}\exp\left(\frac{1}{\hbar}E_{1\phi}\tau\right), \tag{3.21}$$

$$\Omega(\tau) = \frac{dg}{d\tau}(\tau)g^{-1}(\tau), \tag{3.22}$$

and $g(\tau)$ satisfies the equation of motion with respect to ϕ on the background of $\bar{X}(\tau)$;

$$\frac{d^2g}{d\tau^2}(\tau) = m^2(\bar{X}(\tau))g(\tau). \tag{3.23}$$

We need to set an appropriate boundary condition for $g(\tau)$ at $\tau = -\infty$ to obtain the *quasi-ground-state* wave function. It is achieved by setting

$$g(\tau) \to e^{\omega\tau} \quad \text{for} \quad \tau \to -\infty. \tag{3.24}$$

In fact, if we choose $E_{1\phi} = \omega\hbar/2$, the wave function becomes

$$\Phi^0(\bar{X}(\tau),\phi) \to (\omega/\pi\hbar)^{1/4}\exp\left(-\frac{1}{2\hbar}\omega\phi^2\right) \quad \text{for} \quad \tau \to -\infty, \tag{3.25}$$

which coincides with the ground state wave function approximated by the harmonic potential in the false vacuum.

The wave function in the allowed region is expected to be given by its analytic continuation [25],

$$\Phi^0(\bar{X}_L(t),\phi_i) = \mathcal{N}_L(t)\exp\left(-\frac{1}{2\hbar}\Omega_L(t)\phi^2\right), \tag{3.26}$$

where

$$\mathcal{N}_L(t) = \mathcal{N}(it), \tag{3.27}$$

$$g_L(t) = g(it), \tag{3.28}$$

$$\Omega_L(t) = -ig_L^{-1}(t)\frac{dg_L}{dt}(t). \tag{3.29}$$

We must note the following fact. If we define

$$\bar{\Phi}^0(\bar{X}_L(t),\phi) = \exp(-iE_{1\phi}t/\hbar)\Phi^0(\bar{X}_L(t),\phi), \tag{3.30}$$

factoring out ϕ-independent phase, $\bar{\Phi}^0(\bar{X}_L(t),\phi)$ satisfies the Schrödinger equation,

$$\left[\frac{\hbar}{i}\frac{\partial}{\partial t} + \hat{H}_\phi\right]\bar{\Phi}^0(\bar{X}_L(t),\phi_i) = 0. \tag{3.31}$$

Thus $\bar{\Phi}^0(\bar{X}_L(t),\phi)$ represents the wave function of ϕ which evolves on a given background of $\bar{X}_L(t)$. *

Now we show that the quantum state described by $\bar{\Phi}^0(\bar{X}_L(t),\phi)$ is in a squeezed state. For this purpose, let us consider the way to represent a squeezed state in the language of wave function in general. A squeezed state is a vacuum state in the following sense. In the Heisenberg picture, the field operators and its conjugates are expanded as

$$\begin{aligned}\hat{\phi}(t) &= u(t)A + u^*(t)A^\dagger,\\ \hat{p}(t) &= \dot{u}(t)A + \dot{u}^*(t)A^\dagger,\end{aligned} \tag{3.32}$$

where $A^\dagger$ and A are the creation and the annihilation operator, respectively, and $u(\tau)$ is the mode function. The mode function satisfies the equation of motion,

$$-\frac{d^2u}{dt^2}(t) = m^2(\bar{X}_L(t))u(t), \tag{3.33}$$

and are orthonormalised with respect to the Klein-Gordon inner product,

$$(u,u) := -i(u\dot{u}^* - \dot{u}u^*) = \hbar. \tag{3.34}$$

Then the squeezed state specified by $u(t)$ is defined in the same manner as the usual vacuum state by

$$A|O\rangle = 0. \tag{3.35}$$

To move to the Schrödinger representation, we introduce time-dependent annihilation and creation operators $a(t)$ and $a^\dagger(t)$, respectively, as

$$a(t) = U(t)AU^\dagger(t), \quad a^\dagger(t) = U(t)A^\dagger U^\dagger(t), \tag{3.36}$$

and

---

*Here the WKB time t is only the coordinate parameter, and has nothing to do with the physical time. But it is treated as if it were the real physical time without giving any rigourous reason. The justification of this identification is discussed in [26].

$$U := e^{-\frac{i}{\hbar}\int^t dt \hat{H}_\phi}, \tag{3.37}$$

where $\hat{H}_\phi$ is a Hamiltonian operator for ϕ on the background $\bar{X}_L(t)$. The Schrödinger representations of the field operators $\hat{\phi}_S$ and $\hat{p}_S$ are given by

$$\begin{aligned}\hat{\phi}_S &= U(t)\hat{\phi}(t)U^\dagger(t) = u(t)a(t) + u^*(t)a^\dagger(t),\\ \hat{p}_S &= U(t)\hat{p}(t)U^\dagger(t) = \dot{u}(t)a(t) + \dot{u}^*(t)a^\dagger(t).\end{aligned} \tag{3.38}$$

Using these operators, the Schrödinger representation of the vacuum, *i.e.*, $|O(t)\rangle_S = U(t)|O\rangle$ is determined by the condition,

$$a(t)|O(t)\rangle_S = 0, \tag{3.39}$$

and $a(t)$ is expressed as

$$\hbar a(t) = i\Big(u^*(t)\hat{p}_S - \dot{u}^*(t)\hat{\phi}_S\Big). \tag{3.40}$$

Then, going over to the coordinate representation by the replacements,

$$\hat{p}_S \to -i\hbar\frac{\partial}{\partial\phi}, \quad \hat{\phi}_S \to \phi, \tag{3.41}$$

we find from Eq.(3.39) that

$$\langle\phi|O(t)\rangle_S = \mathcal{N}(t)\exp\left(-\frac{1}{2\hbar}\Omega(t)\phi^2\right), \tag{3.42}$$

where $\mathcal{N}(t)$ is a normalization factor and

$$\Omega(t) = \frac{1}{i}\dot{u}^*(t)u^{*-1}(t). \tag{3.43}$$

Now we are ready to show that $\bar{\Phi}^0(\bar{X}_L(t), \phi_i)$ describes a squeezed state. From Eqs. (3.26) and (3.42), we can read that $\bar{\Phi}^0(\bar{X}_L(t), \phi)$ is a squeezed state represented by the mode functions,

$$u^*(t) = c\sqrt{\frac{\hbar}{2\omega}}g_L(t), \tag{3.44}$$

where a constant c is chosen to satisfy the normalization condition (3.34).

As a result, the quantum state after tunneling from the *quasi-ground-state* in the false vacuum is described by a non-trivial vacuum state (squeezed state) whose mode functions are determined by solving Eq. (3.23) with the boundary condition (3.24). Their analytic continuations to the Lorentzian region gives the negative frequency functions after the renormalization to satisfy Eq. (3.34). If we notice that the boundary condition (3.24) is the analytic continuation to the Euclidean region of the negative frequency function in the false vacuum, we find that the mode function after tunneling is obtained by solving Eq.(3.23)

along the path given in Fig.5 with the initial condition, $g_L(t) = u_F^*(t)$, where $u_F^*(t)$ denotes the negative mode frequency function in the false vacuum state.

This statement allows natural extensions to many interesting situations. The same argument holds for the field theoretical problem on Minkowski spacetime [7]. The naive extension to the case with the effect of curved space, which will be explained briefly in section 5, also gives the correct answer [9]. Moreover, when the initial state is in the squeezed state in the false vacuum, the prescription presented above still holds [26].

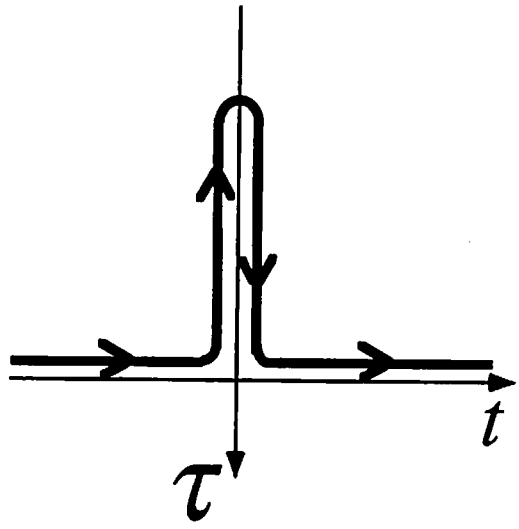

FIG. 5. A path on the complex plane of time, which represents a tunneling process.

IV. PARTICLE SPECTRUM AFTER BUBBLE NUCLEATION ON MINKOWSKI SPACETIME

In this section we apply the formalism explained in the previous section to the case of $O(4)$-symmetric bubble nucleation which occurs in the Minkowski space. The $O(3,1)$-symmetry of the system is just the same as that of the Milne universe, which is the hyperbolic time slicing of the future light cone in the Minkowski spacetime (see Fig.6). The quantum field theory in the Milne universe has been well investigated by many peoples as a simple example of the quantization of scalar fields in the curved space [27–30]. By using this, we develop the method to investigate the quantum state inside the bubble nucleation in terms of the particle creation in the Milne universe [10,11]. Here we focus on the case of four-dimensional spacetime.

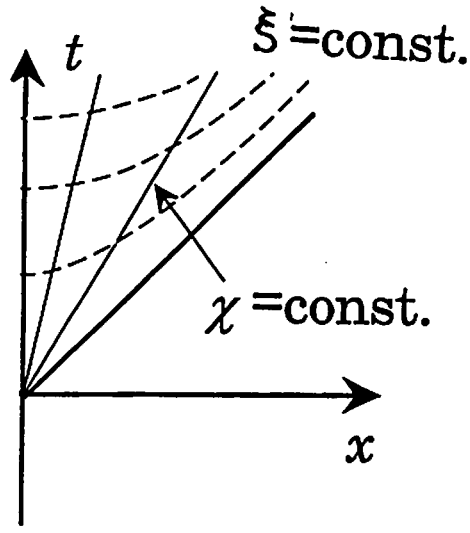

FIG. 6. A sketch of the coordinate describing the Milne universe.

The coordinate of the Milne universe is related to the Minkowski's one by

$$t = \xi \cosh \chi, \quad r = \xi \sinh \chi, \qquad (0 < \xi < \infty, \quad 0 < \chi < \infty) \tag{4.1}$$

the line element is written as

$$ds^2 = -d\xi^2 + \xi^2(d\chi^2 + \sinh^2 \chi d\Omega^2_{(2)}), \tag{4.2}$$

where $d\Omega^2_{(2)}$ is the line element of the unit two-sphere. In this coordinate, the Euclideanization is performed by

$$\xi_E = -i\xi, \quad \chi_E = i\chi, \tag{4.3}$$

which corresponds to the prescription, $\tau = it$, in the Minkowski coordinate. The region $\tau < 0$ is described by $0 < \chi_E < \pi/2$.

The field equation of a massive scalar field with mass M is

$$\left[\frac{\partial^2}{\partial \xi^2} + \frac{3}{\xi}\frac{\partial}{\partial \xi} - \frac{1}{\xi^2}\mathbf{L}^2 + M^2\right]\phi(\xi, \chi, \theta, \varphi) = 0, \tag{4.4}$$

where $\mathbf{L}^2$ is the Laplacian operator on the unit three-dimensional spatial hyperboloid,

$$\mathbf{L}^2 = \frac{1}{\sinh^2 \chi}\frac{\partial}{\partial \chi}\left(\sinh^2 \chi \frac{\partial}{\partial \chi}\right) + \frac{1}{\sinh^2 \chi}\mathbf{L}^2_\Omega, \tag{4.5}$$

and $\mathbf{L}^2_\Omega$ is the Laplacian on the unit two-sphere. We define the eigen functions Y_{plm} of $\mathbf{L}^2$ which satisfy

$$\mathbf{L}^2 Y_{plm}(\chi,\Omega) = -(1+p^2)Y_{plm}(\chi,\Omega), \tag{4.6}$$

as

$$Y_{plm}(\chi,\Omega) = f_{pl}(\chi)Y_{lm}(\Omega), \tag{4.7}$$

where

$$f_{pl}(\chi) = \frac{\Gamma(ip+l+1)}{\Gamma(ip)}\frac{1}{\sqrt{\sinh\chi}}P^{-l-1/2}_{ip-1/2}(\cosh\chi), \tag{4.8}$$

and $Y_{lm}(\Omega)$ is the spherical harmonics on the unit two-sphere, $\Gamma(z)$ is the Gamma function and $P^{-l-1/2}_{ip-1/2}(z)$ is the associated Legendre function of the first kind. The eigenfunctions Y_{plm} with $0 \le p < \infty$ form a complete orthonormal set for square-integrable functions on the unit hyperboloid.

With the aid of this harmonics, a complete set of the solutions of the field equation (4.4) is obtained as

$$\begin{aligned} u_{plm}(\xi,\chi,\Omega) &= F_{plm}(\xi)Y_{plm}(\chi,\Omega), \\ F_{plm}(\xi) &= \frac{\sqrt{\pi}}{2}e^{\pi p/2}\frac{H^{(2)}_{ip}(M\xi)}{\xi}, \end{aligned} \tag{4.9}$$

and its complex conjugate. This choice of the positive and negative frequency functions corresponds to the Minkowski vacuum, which is understood by considering the analytic continuation of $u^*_{plm}(\xi,\chi,\Omega)$ to the Euclidean region. The usual Minkowski negative frequency mode functions are regular on the upper half of the complex t plain ($\tau < 0$). If the Minkowski positive frequency function contributes, the negative frequency function does not show this behaviour. In fact, the negative frequency function $u^*_{plm}(\xi,\chi,\Omega)$ is continued to become

$$u^*_{plm} = \frac{1}{\sqrt{\pi}}\frac{K_{ip}(M\xi_E)}{\xi_E}\frac{\Gamma(-ip+l+1)}{\Gamma(-ip)}\frac{P^{-l-1/2}_{ip-1/2}(\cosh\chi_E)}{\sqrt{-i\sinh\chi_E}}Y^*_{lm}(\Omega), \tag{4.10}$$

where $K_\nu(z)$ is the Modified Bessel function, and is shown to be regular in the range where ξ_E is real and positive.

Now we consider the mode functions describing the quantum state after bubble nucleation. Following the general discussion given in the previous section, we first solve the field equation along the path given in Fig 5. Only the radial part of the mode function $F_p(\xi_E)$ is non-trivial and it obeys

$$\left[\frac{\partial^2}{\partial{\xi_E}^2} + \frac{3}{\xi_E}\frac{\partial}{\partial\xi_E} + \frac{p^2+1}{{\xi_E}^2} - m^2((\sigma_0({\xi_E}^2))\right]F_p(\xi_E) = 0. \tag{4.11}$$

In the limit $\xi_E \to \infty$, we have $\sigma_0 \to \sigma_F$. $F_p(\xi_E)$ must satisfy the boundary condition

$$F_p(\xi_E) = \frac{K_{ip}(M\xi_E)}{\sqrt{\pi}\xi_E}, \tag{4.12}$$

at $\xi_E \to \infty$. In order to obtain the mode function inside the future light cone, F_p must be continued to there. In a sufficiently small neighborhood of $\xi_E = 0$, we have $m^2(\xi_E) \simeq \mathcal{M}^2 =$ constant. Hence $F_p(\xi_E)$ can be expressed as

$$\begin{aligned} F_p(\xi_E) &= A_p K_{ip}(\mathcal{M}\xi_E) + B_p \left(I_{ip}(\mathcal{M}\xi_E) + I_{-ip}(\mathcal{M}\xi_E)\right)/2 \\ &= \tilde{A}_p K_{ip}(\mathcal{M}\xi_E) + B_p I_{ip}(\mathcal{M}\xi_E), \end{aligned} \tag{4.13}$$

where $\tilde{A}_p = A_p + \frac{i}{\pi}\sinh \pi p B_p$. Note that, since $F_p(\xi_E)$ is a real function, the coefficients A_p and B_p are real. Following the above prescription, the Modified Bessel functions in the above equation have been continued to the Lorentz region as

$$K_{ip}(\mathcal{M}\xi_E) \to \frac{\pi i}{2} e^{-\pi p/2} H^{(1)}_{ip}(\mathcal{M}\xi), \tag{4.14}$$

$$I_{ip}(\mathcal{M}\xi) \to \frac{1}{2} e^{\pi p/2}\left(H^{(1)}_{ip}(\mathcal{M}\xi) + H^{(2)}_{ip}(\mathcal{M}\xi)\right). \tag{4.15}$$

Therefore we have the following expression for the unnormalized negative frequency functions inside the future light cone at $\xi \simeq 0$,

$$g_{plm} = \left(c_p^* e^{-\pi p/2} \frac{H^{(1)}_{ip}(\mathcal{M}\xi)}{\xi} + d_p^* e^{\pi p/2} \frac{H^{(2)}_{ip}(\mathcal{M}\xi)}{\xi}\right) Y^*_{plm}(\chi, \Omega), \tag{4.16}$$

where

$$\begin{aligned} c_p &:= \frac{\pi}{2i} A_p + \frac{\cosh \pi p}{2} B_p, \\ d_p &:= \frac{1}{2} B_p. \end{aligned} \tag{4.17}$$

When the width of bubble wall cannot be neglected, the evolution of the classical background field inside the bubble also becomes important. This effect leads to time variation of the mass of the ϕ field, and additional particle creation may occur. In such a case, Eq.(4.16) gives the (asymptotic) initial condition of $g_{plm}(t, x)$ at $\xi \to 0$, and the subsequent field evolution is obtained by solving,

$$\left[\frac{\partial^2}{\partial \xi^2} + \frac{3}{\xi}\frac{\partial}{\partial \xi} + \frac{p^2+1}{\xi^2} + m^2((\sigma_0(\xi^2))\right] g_{plm} = 0. \tag{4.18}$$

Then the asymptotic solution at $\xi \to \infty$ takes the form,

$$g_{plm}(\xi, \chi) = \left(\tilde{c}_p^* e^{-\pi p/2} \frac{H^{(1)}_{ip}(\mu\xi)}{\xi} + \tilde{d}_p^* e^{\pi p/2} \frac{H^{(2)}_{ip}(\mu\xi)}{\xi}\right) Y^*_{plm}(\chi, \Omega), \tag{4.19}$$

where $\tilde{c}_p$ and $\tilde{d}_p$ depend on the evolutionary history of $m^2(\sigma_0(\xi^2))$,

In order to interpret the quantum state described by the mode functions obtained in Eq.(4.19) in the Heisenberg picture, we need to obtain the normalized mode functions with respect to the Klein-Gordon inner product. This is accomplished easily by the scaling as

$$\bar{u}_{plm} = \left[\alpha_p \frac{\sqrt{\pi}}{2} e^{\pi p/2} \frac{H^{(2)}_{ip}(\mu\xi)}{\xi} + \beta_p \frac{\sqrt{\pi}}{2} e^{-\pi p/2} \frac{H^{(1)}_{ip}(\mu\xi)}{\xi}\right] Y_{plm}(\chi, \Omega), \tag{4.20}$$

where

$$\alpha_p := \frac{\tilde{c}_p}{\sqrt{|\tilde{c}_p|^2 - |\tilde{d}_p|^2}}, \quad \beta_p := \frac{\tilde{d}_p}{\sqrt{|\tilde{c}_p|^2 - |\tilde{d}_p|^2}}. \tag{4.21}$$

One can easily check these mode functions satisfy the Klein-Gordon normalization on the $\xi =$ constant hypersurface in the Milne universe and the same is proved to be true on the $t = 0$ hypersurface. It seems a quite nontrivial fact but the function space which is consisted of the normalizable functions on the $\xi =$ constant hypersurface in the Milne universe with respect to the Klein-Gordon inner product does coincide with that on the $t =$ constant hypersurface for the massive scalar field. Since the coefficients α_p and β_p are the Bogoliubov coefficients with respect to the natural vacuum in the Milne universe which corresponds to the usual Minkowski vacuum, the spectrum of created particles with respect to this natural vacuum is

$$n_p = \left|\beta_p\right|^2 = \frac{1}{\left|\tilde{c}_p/\tilde{d}_p\right|^2 - 1}. \tag{4.22}$$

When the particle creation after the bubble nucleation can be neglected, as is the case in the thin wall approximation, we have $\tilde{c}_p = c_p$ and $\tilde{d}_p = d_p$. Then the spectrum of the particle can be expressed as

$$n_p = \frac{1}{\left(\pi A_p/B_p\right)^2 + \sinh^2 \pi p} = \left|\frac{B_p}{\pi \tilde{A}_p}\right|^2. \tag{4.23}$$

Now we consider a simple model of the particle creation through the tunneling process of bubble nucleation. We assume a thin-wall bubble so that the mass of the ϕ field is given by

$$m^2(\sigma_0({\xi_E}^2)) = \begin{cases} M^2; & R < \xi_E < \infty, \\ \mu^2; & 0 < \xi_E < R, \end{cases}$$

where R is the radius of the bubble when it nucleates.

The solution to Eq.(4.11) can be easily found by matching the solutions in both regions,

$$F_p(\xi_E) = \begin{cases} K_{ip}(M\xi_E); & R < \xi_E < \infty, \\ \tilde{A}_p K_{ip}(\mu\xi_E) + B_P I_{ip}(\mu\xi_E); & 0 < \xi_E < R, \end{cases}$$

where

$$\tilde{A}_p = \mu R I_{ip}'(\mu R) K_{ip}(MR) - MR I_{ip}(\mu R) K_{ip}'(MR), \tag{4.24}$$
$$B_p = -\mu R K_{ip}'(\mu R) K_{ip}(MR) + MR K_{ip}(\mu R) K_{ip}'(MR), \tag{4.25}$$

and a prime denotes differentiation with respect to the argument.

The particle spectrum is given by $n_p = \left|B_p/\pi\tilde{A}_p\right|^2$. Roughly, the Modified Bessel functions asymptotically behave as $K_{ip}(z) \propto e^{-\pi p/2}$ and $I_{ip}(z) \propto e^{\pi p/2}$ for $p \to \infty$. Hence the particle spectrum always decreases exponentially for large p as $n_p \propto e^{-2\pi p}$. This suppression of the spectrum at high momentum limit resembles that of a thermal state. The same feature has been found in a spatially homogeneous model of false vacuum decay, first discussed by Rubakov [23] and subsequently by us [7]. Note that the mode index p corresponds to a comoving wave number in the Milne universe and the scale $p = 1$ corresponds to the physical curvature scale on the hyperboloid. In what follows, we evaluate n_p for several limiting cases.

(1) $M \ll R^{-1}$ and $\mu \ll R^{-1}$:

In this case, we can use the following asymptotic formulae for the Modified Bessel functions at $z \ll 1$,

$$I_{ip}(z) \simeq \frac{(z/2)^{ip}}{\Gamma(ip+1)}, \quad K_{ip}(z) \simeq \frac{\pi}{2}\frac{1}{i\sinh\pi p}\left(\frac{(z/2)^{-ip}}{\Gamma(-ip+1)} - \frac{(z/2)^{ip}}{\Gamma(ip+1)}\right). \tag{4.26}$$

After some algebra, we find the following expression for the particle spectrum,

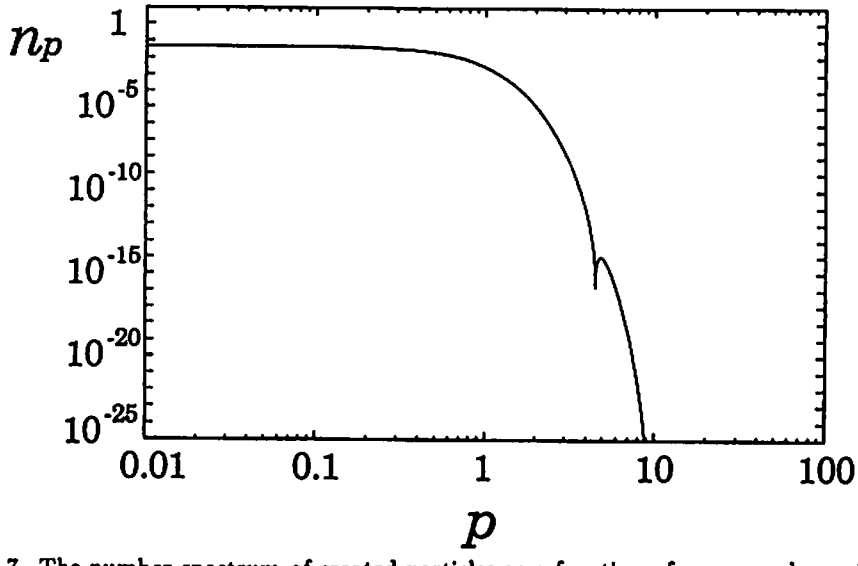

FIG. 7. The number spectrum of created particles as a function of wave number p for the case $MR = 0.02$ and $\mu R = 0.01$.

$$n_p \simeq \frac{\sin^2(p\log(\mu/M))}{\sinh^2 \pi p}. \tag{4.27}$$

We see that n_p decreases exponentially at large p, in accordance with the general discussion in the above. Due to the sinusoidal dependence, it has zeros in a period of $\pi/\log(\mu/M)$. In the limit $p \to 0$, n_p approaches a finite value, $n_p \to \left|\log(\mu/M)/\pi\right|^2$. Figure 7 shows the spectrum for the case $MR = 0.02$ and $\mu R = 0.01$.

(2) $M \gg R^{-1}$ and $\mu \ll R^{-1}$:

In this case, if we focus on the region $p \lesssim 1$, the asymptotic formulae for the Modified Bessel functions at $z \gg 1$ can be used,

$$I_{ip}(z) \simeq \frac{1}{\sqrt{2\pi z}} e^z, \quad K_{ip}(z) \simeq \sqrt{\frac{\pi}{2z}} e^{-z}, \qquad \text{for } z \gg 1. \tag{4.28}$$

Then n_p is evaluated as

$$n_p = \frac{1}{4\sinh^2 \pi p} \left| \frac{\Gamma(ip)}{\Gamma(-ip)} \left(\frac{\mu R}{2}\right)^{-2ip} + 1 \right|^2. \tag{4.29}$$

In the limit $p \to 0$, we find $n_p \to \left|(\gamma + \log(\mu R/2))/\pi\right|^2$, where $\gamma = 0.577\cdots$ is the Euler constant. Figure 8 shows n_p as a function of p for the case $MR = 20$ and $\mu R = 0.01$.

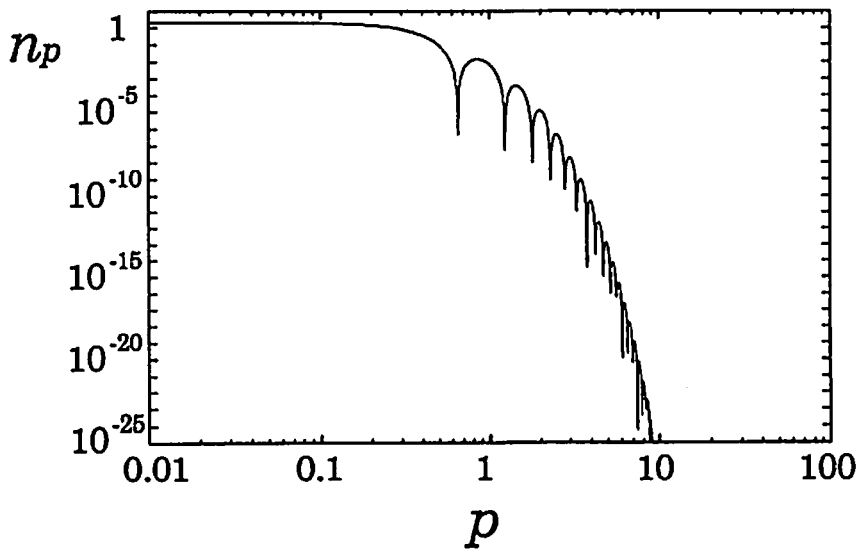

FIG. 8. The same figure as Fig.7, but for $MR = 20$ and $\mu R = 0.01$.

(3) $M \gg R^{-1}$ and $\mu \gg R^{-1}$:
Using the asymptotic formulae (4.28), we easily find n_p in the region $p \lesssim 1$,

$$n_p \simeq \left(\frac{\mu - M}{\mu + M}\right)^2 e^{-4\mu R}. \tag{4.30}$$

(4) $M \ll R^{-1}$ and $\mu \gg R^{-1}$:
In this case, using Eqs.(4.28) and (4.26), we obtain n_p at $p \lesssim 1$ as

$$n_p \simeq e^{-4\mu R}. \tag{4.31}$$

The first two cases for which $\mu R \ll 1$, the spectrum shows a similar feature, that is, it is constant of order unity at $p \lesssim 1$, and decreases exponentially at $p \gtrsim 1$. On the other hand, in the latter two cases when $\mu R \gg 1$, the particle creation is always suppressed exponentially by a factor of $O(e^{-4\mu R})$. This feature is the same as those obtained previously in the spatially homogeneous decay model of the false vacuum if we identify the Euclidean tunneling "time" in the homogeneous model with the radius of the bubble wall [23,7,31,32].

V. EXTENSION TO THE CASE WITH GRAVITY

In the previous section, we discussed the problem on the Minkowski spacetime. Here we consider the extension to the case with gravity. As in the usual inflation models, we expect that the quantum fluctuations of the scalar field give rise to the cosmic density fluctuations in the one-bubble inflationary scenario. Then we need investigate the quantum state of a field during and after the bubble nucleation which occurs in the de Sitter spacetime. In the case of flat spacetime, the description of the mode function in the Milne coordinate played a crucially important roll. It is required to know the expression of the mode function written in a coordinate which respects the symmetry of the system. Then we first consider the prescription to describe a quantized scalar field in the Euclidean vacuum state in the open chart of the de Sitter space.

Let us introduce the following coordinate system. The four-dimensional Euclidean de Sitter space is a four-sphere and can be embedded in the five-dimensional Euclidean space, $(\tilde{x}^0, x^i)$, as a hypersurface which satisfies $H^{-2} = (\tilde{x}^0)^2 + \sum (x^i)^2$, where H^{-1} is the Hubble radius of the de Sitter space. A fundamental coordinate system which we use in the Euclidean region is defined as

$$\tilde{x}^0 = \cos\xi \cos\rho, \quad x^1 = \sin\xi, \quad \begin{pmatrix} x^2 \\ x^3 \\ x^4 \end{pmatrix} = \cos\xi \sin\rho \begin{pmatrix} \cos\theta \\ \sin\theta\cos\varphi \\ \sin\theta\sin\varphi \end{pmatrix} \quad \begin{pmatrix} -\pi/2 \le \xi \le \pi/2 \\ 0 \le \rho \le \pi \end{pmatrix} \tag{5.1}$$

Then the metric is represented as

$$ds_E^2 = H^{-2}\left(d\xi^2 + \cos^2\xi(d\rho^2 + \sin^2\rho d\Omega^2)\right). \tag{5.2}$$

Coordinate systems in the Lorentzian region are obtained by the analytic continuation, $\tilde{x}^0 \to ix^0$. Performing this, we find that the Lorentzian region may be divided into three parts, which we call R, C, and L, whose coordinates are related to the fundamental ones by the relations,

$$\begin{cases} t_R = i(\xi - \pi/2), & (t_R \geq 0) \\ r_R = i\rho, & (r_R \geq 0) \end{cases}$$
$$\begin{cases} t_C = \xi, & (\pi/2 \geq t_C \geq -\pi/2) \\ r_C = i(\rho - \pi/2), & (\infty > r_C > -\infty) \end{cases}$$
$$\begin{cases} t_L = i(-\xi - \pi/2), & (t_L \geq 0) \\ r_L = i\rho, & (r_L \geq 0) \end{cases} \tag{5.3}$$

and their metrics are given respectively by

$$\begin{aligned} ds_R^2 &= H^{-2}\left(-dt_R^2 + \sinh^2 t_R(dr_R^2 + \sinh^2 r_R d\Omega^2)\right), \\ ds_C^2 &= H^{-2}\left(dt_C^2 + \cos^2 t_C(-dr_C^2 + \cosh^2 r_C d\Omega^2)\right), \\ ds_L^2 &= H^{-2}\left(-dt_L^2 + \sinh^2 t_L(dr_L^2 + \sinh^2 r_L d\Omega^2)\right). \end{aligned} \tag{5.4}$$

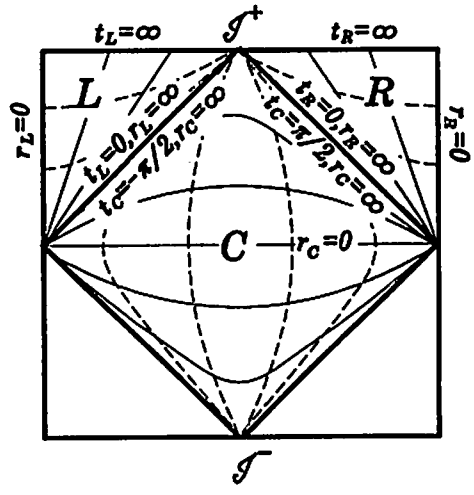

FIG. 9. Conformal diagram of de Sitter space.

In the above, the regions R and L are connected through $\xi \in (-\pi/2, \pi/2)$ along a path over the hemisphere $\Im x^0 < 0$ ($\bar{x}^0 > 0$), say along $\rho = 0$, and the region C is joined to this hemisphere at $\rho = \pi/2$. Note that one may connect the regions R and L in a different way by passing through the other hemisphere $\Im x^0 > 0$ ($\bar{x}^0 < 0$), say along $\rho = \pi$, but we take the former choice given by Eq. (5.3) for later convenience. A schematic picture of how these coordinates cover the spacetime is shown in a conformal diagram in Fig. 9. The regions R and L covered by the coordinates (t_R, r_R) and (t_L, r_L), respectively, are the two distinct spatially open charts of de Sitter space. We see that the whole Euclidean and Lorentzian de Sitter space is covered by complexifying the variables ξ and ρ.

Then we consider the mode functions of a scalar field with the mass M and the curvature coupling, ζ, in de Sitter space in the separated form with respect to these variables. To obtain these mode functions, we write down the field equation in terms of the coordinates in either of the regions R or L. Since these two regions are completely symmetric, we have

$$\left[\frac{1}{a^3(t)}\frac{\partial}{\partial t}a^3(t)\frac{\partial}{\partial t} - \frac{H^{-2}}{a^2(t)}\mathbf{L}^2 + \frac{9}{4} - \nu^2\right] u_{plm}(t, r, \Omega) = 0, \tag{5.5}$$

where $(t, r) = (t_R, r_R)$ or (t_L, r_L), $a(t) = H^{-1}\sinh t$ and $\nu := \sqrt{9/4 - M^2/H^2 - 12\zeta}$. We now take the harmonic expansion of the mode functions,

$$u_{plm}(t, r, \Omega) = \frac{1}{a(t)}\chi_{plm}(t)Y_{plm}(r, \Omega), \tag{5.6}$$

and look for a complete set of positive frequency functions $\{\chi_{plm}(t)\}$ for the Euclidean vacuum.

As well-known, the positive frequency functions of the Euclidean vacuum are characterized by their regularity on the $\Im x^0 < 0$ hemisphere of the Euclidean de Sitter space. To find such functions, let us first consider the mode functions in the region R. The general solution is expressed as a linear combination of the associated Legendre functions $P^{ip}_{\nu-1/2}(z_R)$ and $P^{-ip}_{\nu-1/2}(z_R)$, where $z_R = \cosh t_R$. However the function in R and in L are not independent of each other. Imposing the above regularity condition on χ_p, we find that the analytic continuation of it to the region L amounts to going through the branch cut $[-1, 1]$ of the associated Legendre function $P^{ip}_{\nu'}(z)$ from $\Im z < 0$ to $\Im z > 0$ and then to $z < -1$ on the real axis.

Then if $\Re\nu < 1/2$, the mode functions which is normalized with respect to the Klein-Gordon inner product is obtained as

$$\chi_{p,\sigma} = \begin{cases} \dfrac{N_{p\sigma}}{2\sinh\pi p}\left(\dfrac{e^{\pi p} - \sigma e^{-i\pi\nu'}}{\Gamma(\nu' + ip + 1)}P^{ip}_{\nu'}(z_R) - \dfrac{e^{-\pi p} - \sigma e^{-i\pi\nu'}}{\Gamma(\nu' - ip + 1)}P^{-ip}_{\nu'}(z_R)\right), \\[2ex] \dfrac{\sigma N_{p\sigma}}{2\sinh\pi p}\left(\dfrac{e^{\pi p} - \sigma e^{-i\pi\nu'}}{\Gamma(\nu' + ip + 1)}P^{ip}_{\nu'}(z_L) - \dfrac{e^{-\pi p} - \sigma e^{-i\pi\nu'}}{\Gamma(\nu' - ip + 1)}P^{-ip}_{\nu'}(z_L)\right), \end{cases} \tag{5.7}$$

where we have introduced $\nu' = \nu - 1/2$ for the notational simplicity and the normalization constant is given by

$$|N_{p\sigma}|^2 = \frac{4\left(\cosh \pi p - \sigma \cos \nu' \pi\right)}{\pi \left|\Gamma(\nu' + 1 + ip)\right|^2}. \tag{5.8}$$

In fact, the two point function obtained by calculating the summation of this mode functions over plm coincides with the so called Euclidean vacuum one [12]. The negative frequency function is given by taking their complex conjugate and is regular on the other hemisphere.

We must note that there appears the additional discrete modes in the case $0 < \nu' < 1$, which are given by

$$u_{(*)lm} = N_{(*)l} H(-i \cos t_C)^{\nu'-1} \frac{P^{-l-1/2}_{-\nu'-1/2}(i \sinh r_C)}{\sqrt{i \cosh r_C}} Y_{lm}(\Omega), \tag{5.9}$$

where

$$|N_{(*)l}|^2 = \frac{2\sqrt{\pi}\,\Gamma(\nu')}{\Gamma(\nu' + 1/2)\Gamma(-\nu' + l + 1)\Gamma(\nu' + l + 1)}. \tag{5.10}$$

These modes are unnormalizable on the hyperboloid but are nonsingular, which never appear in the usual harmonic analysis on the open universe. Then the quantized field in the Euclidean vacuum state is written in terms of the mode functions associated with an open chart as,

$$\hat{\phi}(x) = \int_0^\infty dp \sum_{\sigma,l,m} u_{p\sigma lm}(x) \hat{a}_{p\sigma lm} + \sum_{l,m} u_{(*)lm} \hat{a}_{(*)lm} + h.c.; \quad 0 < \nu' < 1. \tag{5.11}$$

As the notion of the Euclidean vacuum mode functions is obtained, we turn to the problem to find the mode functions after tunneling. As is discussed in the previous section, we consider the system which consists of two fields, i.e., the tunneling field σ and another field ϕ coupled to it. In order to include the effect of gravity, we consider the system whose Lagrangian is given by

$$\mathcal{L} = \mathcal{L}_{grav} + \mathcal{L}_\sigma + \mathcal{L}_\phi, \tag{5.12}$$

where

$$\mathcal{L}_{grav} = -\sqrt{-\mathcal{G}} \frac{1}{16\pi G} R,$$

$$\mathcal{L}_\sigma = \sqrt{-\mathcal{G}} \left[\frac{1}{2} \mathcal{G}^{\mu\nu} \nabla_\mu \sigma \nabla_\nu \sigma - V(\sigma)\right], \tag{5.13}$$

$$\mathcal{L}_\phi = \sqrt{-\mathcal{G}} \left[\frac{1}{2} \mathcal{G}^{\mu\nu} \nabla_\mu \phi \nabla_\nu \phi - \left(m^2(\sigma) + \zeta R\right) \phi^2\right]. \tag{5.14}$$

Here the spacetime metric is denoted by $\mathcal{G}_{\mu\nu}$.

First we need to construct a solution of the Euclidean equation of motion to obtain the lowest WKB order description. We also denote the instanton by $\sigma(x)$ and $\mathcal{G}_{\mu\nu}(x)$. As for the $O(4)$-symmetric bubble nucleation with the effect of gravity, the instanton is given in [6]. Consider the $O(4)$-symmetry metric and field:

$$ds^2 = d\eta^2 + a^2(\eta)(dr^2 + \sin^2 r d\Omega^2_{(2)})$$
$$\sigma(x) = \sigma(\eta), \qquad \phi(x) = 0. \tag{5.15}$$

The Euclidean field equation is

$$\ddot{\sigma} + 3\frac{\dot{a}}{a}\dot{\sigma} = \frac{dV}{d\sigma}, \tag{5.16}$$

where a dot means a derivative with respect to η. The constraint equation is

$$\dot{a}^2 - \frac{4\pi G}{3}a^2\dot{\sigma}^2 = 1 - \frac{8\pi G}{3}a^2 V(\sigma). \tag{5.17}$$

These equations are to be solved with the boundary condition, $\dot{\sigma} = 0$ when $a = 0$. A schematic picture of the solution is shown in Fig.10.

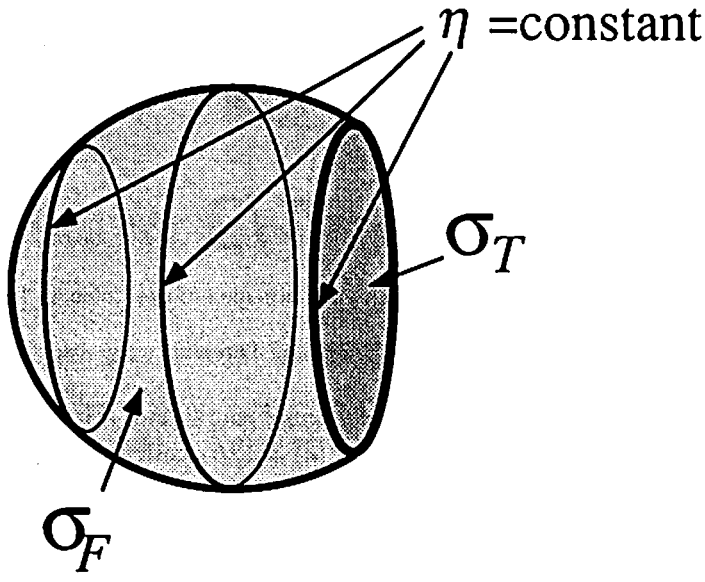

FIG. 10. A schematic picture of the Coleman DeLuccia in stanton solution

As was pointed out in [33], the coordinate η can not play the role of time in the sense of section 3 because when we see the tunneling solution as a sequence of the spatial configurations assigned by the time coordinate, it must connect the configuration at the false vacuum; $\sigma(\mathbf{x}; -\infty) = \sigma_{\mathbf{F}}$, and that with the nucleated bubble after tunneling. A relevant choice of it is obtained by the following coordinate transformation,

$$\sin T_E = -\frac{\cos r}{\sqrt{\cosh^2\eta - \sin^2 r}}; \quad -\pi \le T_E \le \pi, \tag{5.18}$$

$$R = \frac{\sin r}{\cosh\eta}; \quad 0 \le R \le 1, \tag{5.19}$$

Then we have

$$ds_E^2 = \cosh^2\eta\ a^2(\eta)\left\{(1-R^2)dT_E^2 + \frac{dR^2}{1-R^2} + R^2 d\Omega_{(2)}^2\right\}. \tag{5.20}$$

How this coordinate spans the Euclidean and the Lorentzian spacetime is schematically shown in Fig. 11.

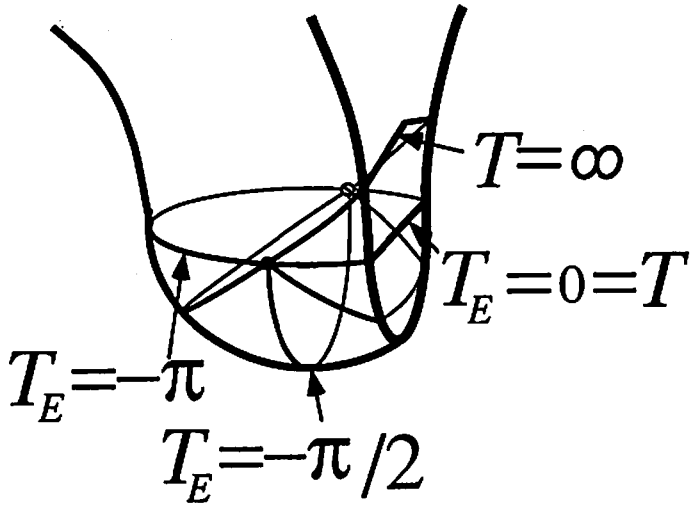

FIG. 11. The analytic continuation to the Lorentzian region of the Coleman DeLuccia instanton solution. The lower and upper halves are Euclidean and Lorentzian regions, respectively.

There are two main differences from the original coordinate. First, this coordinate reduces to the static de Sitter coordinate when $a(\eta) = 1/H_F \cosh\eta$. Therefore if we consider the thin wall case, at $T_E < -\pi/2$, the spatial metric and the background tunneling field configuration on each $T_E =$ constant surface are identical to those at the false vacuum origin and it is also possible to extend this solution beyond $T_E = -\pi$ to $T_E = -\infty$. Second, the configuration on the $T_E = 0$ surface corresponds to the turning point, where the solution can be analytically continued to the Lorentzian region by $T = -iT_E$ (> 0). Thus this time coordinate has the analogous feature to the Minkowski time coordinate in the flat case. Using this coordinate, our formalism of the multi-dimensional wave function can be extended naturally to the present case. Namely, the negative frequency mode functions which specify the quantum state after the tunneling must be chosen to coincide with that of the Euclidean vacuum at $T_E < -\pi/2$. The proof of this statement is given in [9]. This condition to determine the negative frequency functions after tunneling will be achieved by setting their regularity on the corresponding half of the instanton. However, the treatment of the discrete mode is still not so clear. We will discuss this topic in the future publication.

VI. SUMMARY AND DISCUSSIONS

In this paper we have considered the alternative inflation scenario which predicts an open universe. The open universe begins from the bubble nucleation in the de Sitter background in the false vacuum state. The conditions to solve the homogeneous and isotropy of the universe and the entropy problem have been examined. Within the context of this new scenario, the important issue to be addressed is the origin of the density perturbations for the cosmic structure formation. As in the standard inflation scenario, we expect the quantum fluctuation of the scalar field to give rise to the cosmic density perturbation. This scenario is definite enough to predict the initial perturbation spectrum as quantitatively as we please in principle.

In order to investigate the quantum state of a scalar field inside the bubble after the nucleation, we have developed the formalism based on the wave function in multi-dimensional tunneling systems. The wave function can be interpreted in the language of the second quantization, where the state is described by the mode functions. It is shown that the state of the field after the bubble nucleation is in the squeezed state in general.

For the bubble nucleation which occurs in the flat Minkowski spacetime, we have examined the quantum state of a scalar field after the bubble nucleation. Because the representation of a natural vacuum state in the Milne universe, which corresponds to the usual vacuum state in the Minkowski spacetime, is known, we could introduce the concept of particle in an unambiguous manner. Thus the quantum state after the bubble nucleation was described in terms of the particle creation in the Milne universe. The spectrum of created particle follows immediately by reading off the Bogoliubov coefficients from the mode functions. We have considered the simple model as an example and found the following results. (1) The spectrum of created particle is always suppressed exponentially at the large wavenumber compared with the characteristic scale of the spatial curvature on the hyperbolic time slicing. (2) If the mass of the field inside the bubble, μ, becomes larger than the inverse of the wall radius, R^{-1}, the particle creation is always suppressed by an exponential factor of $O(e^{-4\mu R})$. These results are consistent with the speculations obtained from the previous analyses [23,7,31].

To investigate the case with the effect of the curved space taking the gravity into consideration, we first developed the prescription to describe the field in the Euclidean vacuum state in the open chart of the de Sitter spacetime. We have found that there are additional modes, which are not expanded by the square-integrable harmonic functions on a hyperbolic time slice in an open chart but are normalizable with respect to the Klein-Gordon inner product, and their contribution can not be neglected in describing the Euclidean vacuum state. These modes never appeared in the traditional harmonic analysis of the open universe. We also obtained the method to find the mode functions which describe the quantum state after the bubble nucleation in the curved spacetime, although there remain some points to be discussed.

We could give the basic ideas to investigate the one-bubble inflationary model but there

are still many unanswered problems on this model. To investigate the quantum fluctuation of a inflaton field, we must consider the quantum state of the tunneling field which causes the bubble nucleation [11]. As described in the section 5, we must also examine the effect of gravity in detail, applying the formalism developed here. On the other hand, we need to compare the prediction of the one-bubble inflationary model with the observational results. As a rather direct comparison with the observational date, the anisotropy of the Cosmic Microwave Background should be considered [15]. As we have found that there appears the discrete modes, it is interesting problem whether the contribution from that mode to the CMB anisotropy is observable or not. This is now under study.

ACKNOWLEDGMENTS

We would like to thank B. Allen, R. Caldwell, T. Hamazaki, D. Lyth, and N. Turok for enlightening discussions. This work was supported in part by Monbusho Grant-in-Aid for Scientific Research Nos. 2010, 2841 and 05640342 and the Sumitomo Foundation.

---

[1] P. J. E. Peebles, *Principle of Physical Cosmology*, Princeton universe press (1993);
B. Rattra and P. J. E. Peebles, Astrophys. J. **432**, L5 (1994), references therein.

[2] A. Kashlinsky, I. I. Tkachev and J. Friedman, Phys. Rev. Lett., **73**, 1582 (1994).

[3] J.R. Gott III, Nature **295**, 304 (1982).

[4] J.R. Gott III and T.S. Statler, Phys. Lett. **136B**, 157 (1994).

[5] S. Coleman, Phys. Rev. **D15**, 2929 (1977);
C. Callan and S. Coleman, Phys. Rev. **D16**, 1763 (1977).

[6] S. Coleman and F. De Luccia, Phys. Rev.**D21** 3305 (1980).

[7] T. Tanaka, M. Sasaki, K. Yamamoto, Phys. Rev. **D49**, 1039 (1994).

[8] M. Sasaki, T. Tanaka, K. Yamamoto and J. Yokoyama, Prog. of Theor. Phys. **90**, 1019 (1993).

[9] T. Tanaka and M. Sasaki, Phys. Rev. **D50**, 6444 (1994).

[10] K. Yamamoto, T. Tanaka and M. Sasaki, preprint 1305, gr-qc/9412011.

[11] T. Hamazaki, M. Sasaki, T. Tanaka and K. Yamamoto, preprint in preparation;
T. Hamazaki, M. Sasaki, T. Tanaka and K. Yamamoto, This proceedings.

[12] M. Sasaki, T. Tanaka and K. Yamamoto, preprint KUNS 1308.

[13] M. Bucher, A. S. Goldhaber and N. Turok, PUTP-1507, hep-ph/9411206.

[14] B. Allen and R. Caldwell, preprint WISC-MILW-94-TH-21.

[15] K. Yamamoto, M. Sasaki and T.Tanaka, preprint KUNS1309.

[16] J. L. Gervais and B. Sakita, Phys. Rev. **D16**, 3507 (1977);
H. J. de Vega, J. L. Gervais and B. Sakita, Nucl. Phys. **B139** 435 (1978).

[17] L. P. Grishchuk and Ya. B. Zel'dovich, Sov. Astron. **22**, 125 (1978).

[18] M. Sasaki, T.Tanaka, K. Yamamoto and J. Yokoyama, Phys. Lett. **B317**, 510 (1993).

[19] A. Borde and A. Vilenkin Phys. Rev. Lett., **72**, 3305 (1994).

[20] J. B. Hartle and S. W. Hawking, Phys. Rev. **D28**, 2960 (1983).

[21] A. Vilenkin, Phys. Rev. **D33**, 3560 (1986); Phys. Rev. **D37**, 888 (1987).

[22] P. J. Steinhardt, Nature **345**, 47 (1990).

[23] V. A. Rubakov, Nucl. Phys. **B245**, 481 (1984).

[24] Vachaspati and Vilenkin, Phys. Rev. **D43**, 3846 (1991).

[25] T. Vachaspati and A. Vilenkin, . Rev. **D37** 898 (1988).

[26] T. Tanaka Prog. Theor., in press.

[27] N. D. Birrell and P. C. W. Davies, *Quantum fields in curved space*, (Cambridge University Press 1982);
T. S. Bunch and P. C. W. Davies, Proc. R. Soc. Lond. A. **360**, 117 (1978);
N. A. Chernicov and E. A. Tagirov, Ann. Inst. Henri Poincare, Sect A **9**, 43 (1968).

[28] A. diSessa, J. Math. Phys. **15**, 1892 (1974).

[29] C. M. Sommerfield, Ann. Phys. (N.Y.) **84**, 285 (1974).

[30] D. Gromes, H. J. Rothe and B. Stech, Nucl. Phys. **B75**, 313 (1973).

[31] H. E. Kandrup, Phys. Lett. **B225**, 222 (1989);
H. E. Kandrup, Phys. Rev. **D42**, 3401 (1990).

[32] K. Yamamoto, Prog. Theor. Phys. **91**, 437 (1994).

[33] T. Tanaka and M. Sasaki, Prog. Theor. Phys. **88** 503 (1992).

Excitation by the Self Interaction in the False Vacuum Decay

Takashi Hamazaki[1], Misao Sasaki[2]
Takahiro Tanaka[1] and Kazuhiro Yamamoto[1]

[1] *Department of Physics, Kyoto University*
Kyoto 606-01, Japan
and
[2] *Department of Earth and Space Science,*
Osaka University, Toyonaka 560, Japan

I. INTRODUCTION

Recently, receiving the observations which are thought to suggest that our universe is an open universe $\Omega_0 < 1$ (with negative spatial curvature), the possibility of revising the inflation scenario, keeping the advantage that it can explain the smoothness and horizon problems, so that it can make an open universe without significant fine tuning, has begun to be discussed [1]. This scenario realizes a homogeneous but a curvature dominant universe by considering the quantum nucleation of a bubble from the false vacuum sea. There, the homogeneous problem is solved by the existence of the de Sitter phase before tunneling and the entropy problem is solved by the existence of inflation era inside the nucleated bubble.

We think that it is important to investigate whether the false vacuum decay generates the density perturbations as much as the succeeding inflation era does, or equivalently, whether the quantum state after the false vacuum decay can be well described by the Euclidean vacuum (Bunch-Davies vacuum). So as a first step, we concentrate on the problem of the particle creation during and after the false vacuum decay in the Minkowski background dropping all the gravitational degrees of freedom, though it is important to take the full degrees of freedom of gravity into account.

Some of us investigated the particle creation of another scalar field coupled with the tunneling field, neglecting the fluctuations of the tunneling field itself [5]. They succeeded in calculating the particle spectrum on the basis of the spatially open foliation which is called Milne universe. But this model was so simple that it cannot be applied to the most interesting problem, i.e., the quantum state of the fluctuations of the tunneling field itself, on which we briefly report on the preliminary results in this paper. The paper which contains the detailed discussions is now under preparation [6].

This paper is organized as follows. In Sec.2, we show how the quantum state after the false vacuum decay can be understood on the basis of the quantum field theory in curved spacetime, and how the particle spectrum is obtained. In Sec.3, we present a potential model in which an analytic treatment is allowed. We investigate the particle creation under this potential model. By using this model, we can examine the dependence of the particle creation rate on the wall thickness and the radius. In Sec.4, the results of numerical calculations are presented. In Sec.5 a short discussion is provided.

Throughout this paper, the metric signature is $-+++$ for Lorentzian spacetime. We use the units $\hbar = 1$ and $c = 1$.

II. REVIEW OF FORMALISM

To begin with, we give the brief sketch of our formalism to investigate the change of the quantum state of the tunneling field itself in the false vacuum decay. We use a method to construct the WKB wave function of a system with many degrees of freedom, originally developed by Banks, Bender and Wu and de Vega, Gervais and Sakita [2], and recently elaborated by some of us [8]. We consider the following Lagrangian of a scalar field ϕ in the Minkowski spacetime,

$$\mathcal{L} = \int d^4x \left[-\frac{1}{2}\partial_\mu\phi\, \partial^\mu\phi - V(\phi) \right] \quad , \tag{2.1}$$

where $V(\phi)$ is a double-well type potential which triggers the quantum tunneling from the false vacuum $\phi = \phi_F$ to the true vacuum $\phi = \phi_T$.

In order to trace the time evolution of the quantum state during the false vacuum decay, it is not avoidable to start from the wave function. We consider the time independent Schrödinger equation

$$\hat{H}\Psi = E\Psi \quad ,$$
$$E = \int d^3\mathbf{x}\, V(\phi_F) + (\text{the zero point energy at the false vacuum}) \quad . \tag{2.2}$$

where

$$\Psi = \langle \phi(\cdot)|\Psi\rangle \quad ,$$
$$\hat{H} := \int d^3\mathbf{x}\left[\frac{1}{2}\left(\frac{1}{i}\frac{\delta}{\delta\phi(\mathbf{x})}\right)^2 + \frac{1}{2}\sum_{i=1}^{3}\left(\frac{\partial\phi(\mathbf{x})}{\partial x^i}\right)^2 + V(\phi)\right] \quad . \tag{2.3}$$

We solve Eq. (2.2) in the WKB approximation, where the field ϕ is decomposed into the classical background ϕ_B and the small fluctuations around the classical background φ.

$$\phi \longrightarrow \phi_B + \varphi \quad . \tag{2.4}$$

The lowest order WKB description is given by the classical background solution ϕ_B, which satisfies the equation of motion,

$$\frac{\partial^2\phi_B}{\partial T^2} + \sum_{i=1}^{3}\frac{\partial^2\phi_B}{\partial x^{i2}} - \frac{dV(\phi_B)}{d\phi_B} = 0 \quad , \tag{2.5}$$

where we introduced a complexified time variable $T = \tau = it$. When τ and T are used, we regard them as taking real values implicitly. As we consider the WKB wave function which describes the false vacuum decay, the classical background solution ϕ_B is taken as an $O(4)(O(3,1))$-symmetric bounce solution [3]. A schematic picture of this bounce solution is drawn in Fig. 1. Thus ϕ_B depends on $T^2 + \mathbf{x}^2$ only.

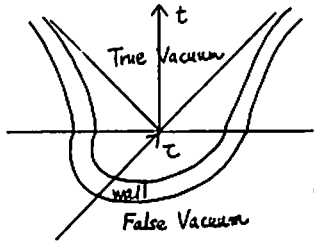

$T = \tau = it$

Fig.1. the classical background $\phi_B(T^2+\mathbf{x}^2)$ which describes the false vacuum decay

Following Gervais, Sakita [2], we construct the WKB wave function as,

$$\Psi = \mathcal{N}(T)\exp\left[-\int^T dT'\int d^3\mathbf{x}\left[\frac{1}{2}\left(\frac{\partial\phi_B}{\partial T'}\right)^2 + \frac{1}{2}\left(\frac{\partial\phi_B}{\partial\mathbf{x}}\right)^2 + V(\phi_B)\right]\right]$$
$$\times\exp\left[-\frac{1}{2}\int\int d^3\mathbf{x}d^3\mathbf{y}\varphi(\mathbf{x})\Omega(\mathbf{x},\mathbf{y};T)\varphi(\mathbf{y})\right] \quad , \tag{2.6}$$

where

$$\Omega(\mathbf{x},\mathbf{y};T) := \int d^3\mathbf{k}\frac{\partial g_{\mathbf{k}}(\mathbf{x},T)}{\partial T}g_{\mathbf{k}}^{-1}(\mathbf{y},T) \quad . \tag{2.7}$$

The "inverse matrix" $g_{\mathbf{k}}^{-1}$ is defined by

$$\int d^3\mathbf{x}\, g_{\mathbf{k}}(\mathbf{x},T)g_{\mathbf{k}'}^{-1}(\mathbf{x},T) = \delta^3(\mathbf{k}-\mathbf{k}') \quad . \tag{2.8}$$

¿From the Schrödinger equation, the equation to be satisfied by $g_k(x,t)$ is derived as,

$$\left[\frac{\partial^2}{\partial T^2}+\sum_{i=1}^{3}\frac{\partial^2}{\partial x^{i2}}-V''(\phi_B(T^2+x^2))\right]g_k(x,T)=0 \quad . \tag{2.9}$$

This is just the equation of motion of φ on the background ϕ_B. To solve Eq.(2.9), we need to set an appropriate boundary condition. If the quantum state at the false vacuum is supposed to be set in the ground state, the second line of the wave function (2.6) must coincide with that of the ground state at the false vacuum. This requirement determines the boundary condition at $T\to-\infty$,

$$g_k(x,T)\to e^{-ikx+\omega_k T} \tag{2.10}$$

where $\omega_k:=\sqrt{k^2+V''(\phi_F)}$ and $\phi_F=\phi_B(T\to-\infty)$. After all, the problem to construct the WKB wave function Ψ reduces to the problem to solve Eq.(2.5) and Eq.(2.9).

In the Lorentzian region, the second line in Eq.(2.6) can be interpreted in the second quantization picture. In the second quantization picture, the fluctuation of the field φ is represented as the field operator,

$$\varphi(x,t)=\int d^3k\left(u_k(x,t)b(k)+u_k^*(x,t)b^\dagger(k)\right) \quad , \tag{2.11}$$

where the mode function $u_k(x,t)$ satisfies the field equation and is normalized with respect to the Klein-Gordon inner product. In general, the 'vacuum' $|\tilde{0}\rangle$ annihilated by $b(k)$ is not the eigenstate of the Hamiltonian unlike the Minkowski vacuum $|0\rangle$. The former is excited from the latter, and the particle creation of the former from the latter is described by the Bogolubov coefficients. We know that the wave function of the 'vacuum' determined by $b(k)$ is written as

$$\langle\varphi(\cdot)|\tilde{0}\rangle\propto\exp\left[-\frac{1}{2}\int\int d^3xd^3y\varphi(x)\Omega(x,y;t)\varphi(y)\right] \quad . \tag{2.12}$$

where

$$\Omega(x,y;t):=\int d^3k\frac{1}{i}\frac{\partial u_k^*(x,t)}{\partial t}u_k^{*-1}(y,t) \quad . \tag{2.13}$$

This expression is nothing but the second line in Eq.(2.6) with $g_k(x,it)$ replaced by $u_k^*(x,t)$. Since the wave function given in Eq.(2.6) is invariant under the linear transformation of $g_k(x,it)$, i.e., $v_k^*(x,t)=\sum_{k'}c_{kk'}g_{k'}(x,it)$, where $v_k(x,t)$ is orthonormalized, we can understand the quantum state of φ after tunneling as the 'vacuum' determined by $v_k(x,t)$.

We consider the quantum state of the fluctuations of the tunneling field itself φ on the background of the $O(4)(O(3,1))$ -symmetric bubble in the Euclidean (Lorentzian) region. In order to calculate the mode function, it is desirable to use the coordinate known as Milne (Rindler) universe which respects the symmetry of the background ϕ_B. The coordinate of Milne universe is related to the usual Minkowski coordinate as follows.

In the Euclidean region, $\mathcal{E}$, the relation is

$$\begin{aligned} &r=\xi_E\sin\chi_E, \quad \tau=-\xi_E\cos\chi_E,\\ &0\le\chi_E\le\frac{\pi}{2}, \quad 0\le\xi_E<\infty \quad , \end{aligned} \tag{2.14}$$

and in the future light cone initiated from the origin in the Lorentzian region, $\mathcal{M}$,

$$\begin{aligned} &r=\xi\sinh\chi, \quad t=\xi\cosh\chi,\\ &0<\xi<\infty, \quad 0<\chi<\infty \quad . \end{aligned} \tag{2.15}$$

As the $O(4)$-symmetric bounce solution which has no angular dependence is considered as the classical background. , the equation of motion Eq.(2.5) reduces to

$$\left[\frac{d^2}{d\xi_E^2}+\frac{3}{\xi_E}\frac{d}{d\xi_E}\right]\phi_B(\xi_E)=V'(\phi_B(\xi_E)) \quad , \tag{2.16}$$

in $\mathcal{E}$, Using the harmonic expansion $g_{p\ell m}(\xi_E,\chi_E,\Omega) = \xi_E^{-1}F_p(\xi_E)Y_{p\ell m}(\chi_E,\Omega)$ where $Y_{p\ell m}(\chi_E,\Omega)$ is the analytical continuation into $\mathcal{E}$ of $Y_{p\ell m}(\chi,\Omega)$, which is the eigenfunction of the Laplacian operator on a unit three dimensional hyperboloid of $\mathcal{M}$ with eigenvalue $-(1+p^2)$, Eq.(2.9) is reduced to the equation of $F_p(\xi_E)$,

$$[\frac{\partial^2}{\partial\xi_E^2} + \frac{1}{\xi_E}\frac{\partial}{\partial\xi_E} + \frac{p^2}{\xi_E^2} - V''(\phi_B(\xi_E))]F_p(\xi_E) = 0 \quad , \tag{2.17}$$

with the boundary condition,

$$F_p(\xi_E) \to K_{ip}(m\xi_E) \;\; (\xi_E \to \infty) \quad . \tag{2.18}$$

Here we mention that p implies the comoving wave number in Milne universe. (In order to derive Eq.(2.18) from Eq.(2.10), the transformation formula between the Milne mode function and the Minkowski mode function is necessary. For the detail of it, see the paper by K. Yamamoto et al [5].) In $\mathcal{M}$, we solve Eq.(2.17) with ξ_E replaced with $-i\xi$ after the analytic continuation at $\xi_E = \xi = 0$. In the asymptotic region $\xi \to \infty$, the bounce solution $\phi_B(\xi)$ oscillates around the true vacuum ϕ_T. We assume that the mass of the fluctuations $V''(\phi_B)$ is M = constant in the asymptotic region. Then we obtain the expression of $F_p(\xi)$ in the asymptotic region is generally given by

$$F_p(\xi) = \frac{2}{\sqrt{\pi}}c_{1p}^* f_p^*(\xi) + \frac{2}{\sqrt{\pi}}c_{2p}^* f_p(\xi) \quad , \tag{2.19}$$

where

$$f_p(\xi) = \frac{\sqrt{\pi}}{2}e^{\pi p/2}H_{ip}^{(2)}(M\xi) \quad . \tag{2.20}$$

Thus in the second quantization picture, the fluctuations are expressed by the quantum field,

$$\begin{aligned}\varphi(\xi,\chi,\Omega) &= \int_0^\infty dp\sum_{\ell m}\left[\frac{f_p(\xi)}{\xi}Y_{p\ell m}(\chi,\Omega)a_{p\ell m} + \frac{f_p^*(\xi)}{\xi}Y_{p\ell -m}(\chi,\Omega)a_{p\ell m}^\dagger\right] \\ &= \int_0^\infty dp\sum_{\ell m}\left[\frac{\tilde{f}_p(\xi)}{\xi}Y_{p\ell m}(\chi,\Omega)b_{p\ell m} + \frac{\tilde{f}_p^*(\xi)}{\xi}Y_{p\ell -m}(\chi,\Omega)b_{p\ell m}^\dagger\right] \quad ,\end{aligned} \tag{2.21}$$

where the normalized mode function $\tilde{f}_p(\xi)$ is defined by $\tilde{f}_p^*(\xi) := \sqrt{\frac{\pi}{4(|c_{1p}|^2 - |c_{2p}|^2)}}F_p(\xi)$. The well-known Minkowski vacuum is defined as the vacuum annihilated by $a_{p\ell m}$ [5]. But the quantum state after the false vacuum decay is the 'vacuum' $|\tilde{0}\rangle$ annihilated by the annihilation operator $b_{p\ell m}$ Thus there exists excitation from the Minkowski vacuum. We can regard the coefficients in Eq.(2.19) as the Bogolubov coefficients between the two vacua. The particle creation is given by

$$n_p := \frac{\langle\tilde{0}|a_{p\ell m}^\dagger a_{p\ell m}|\tilde{0}\rangle}{\delta(0)} = \frac{1}{|c_{1p}/c_{2p}|^2 - 1}, \tag{2.22}$$

III. SOLVABLE MODEL

In this section, applying the formalism developed in the previous section, we examine the particle creation of the tunneling field ϕ itself. For this purpose, it is convenient to choose the tunneling potential so that both the equation of motion (2.16) and the equation of small fluctuations (2.17) can be solved analytically. So we consider the potential $V(\phi)$ consisted of three regions in each of which it is described by a quadratic function. We require that the first derivatives $V'(\phi)$ as well as the values of the potential $V(\phi)$ be continuous at the two junction points between adjacent regions so that the second derivatives $V''(\phi)$ do not have the delta function peaks there. Then provided that $V''(\phi)$ is fixed at m^2, μ^2, and M^2 in each region, and the junction points at ϕ_2, and ϕ_1, the potential $V(\phi)$ is determined uniquely as

$$
\begin{aligned}
\phi_1 \le \phi < \infty \quad &, \quad V(\phi) = \frac{M^2}{2}\phi^2 \quad , \\
\phi_2 \le \phi < \phi_1 \quad &, \quad V(\phi) = -\frac{\mu^2}{2}\phi^2 + a\phi + b \quad , \\
-\infty < \phi < \phi_2 \quad &, \quad V(\phi) = \frac{m^2}{2}\phi^2 + c\phi + d \quad ,
\end{aligned} \tag{3.1}
$$

where

$$
\begin{aligned}
a &= \phi_1(\mu^2 + M^2) \quad , \\
b &= -\frac{1}{2}\phi_1^2(\mu^2 + M^2) \quad , \\
c &= \phi_1(\mu^2 + M^2) - \phi_2(m^2 + \mu^2) \quad , \\
d &= -\frac{1}{2}\phi_1^2(\mu^2 + M^2) + \frac{1}{2}\phi_2^2(m^2 + \mu^2) \quad .
\end{aligned} \tag{3.2}
$$

A rough sketch of the potential is drawn in Fig. 2 for the convenience, We also require that the potential of the false vacuum $V(\phi_F = -c/m^2)$ is higher than that of the true vacuum $V(\phi_T = 0)$, and that the potential barrier exists between two vacua. These constraints lead to

$$
1 + \frac{M^2}{\mu^2} < \frac{\phi_2}{\phi_1} < 1 + \frac{M^2}{\mu^2} + \frac{mM}{\mu^2}\sqrt{\frac{\mu^2 + M^2}{m^2 + \mu^2}} \quad . \tag{3.3}
$$

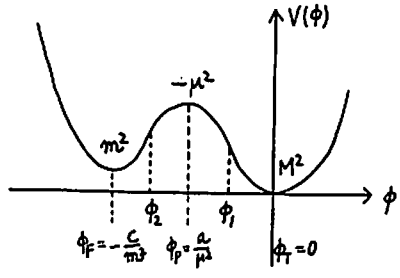

Fig.2. Our potential model

On this potential, Eq.(2.16) and Eq.(2.17) are reduced to the Bessel's differential equations. Thus the bounce solution $\phi_B(\xi_E)$ is given by using the Bessel function,

$$
\begin{aligned}
0 \le \xi_E < \xi_1 \quad &, \quad \phi_B(\xi_E) = A(M\xi_E)^{-1} I_1(M\xi_E) \quad , \\
\xi_1 \le \xi_E < \xi_2 \quad &, \quad \phi_B(\xi_E) = B_1(\mu\xi_E)^{-1} J_1(\mu\xi_E) + B_2(\mu\xi_E)^{-1} N_1(\mu\xi_E) + \frac{a}{\mu^2} \quad , \\
\xi_2 \le \xi_E < \infty \quad &, \quad \phi_B(\xi_E) = C_1(m\xi_E)^{-1} K_1(m\xi_E) - \frac{c}{m^2} \quad ,
\end{aligned} \tag{3.4}
$$

where ξ_1, ξ_2 are defined as solutions of $\phi_i = \phi_B(\xi_i)$ $(i = 1, 2)$. The general solution of the (modified) Bessel's differential equation is the linear combination of J and N (K and I). But in case that $0 \le \xi_E < \xi_1$ and $\xi_2 \le \xi_E < \infty$, one of the two independent function (I and K) is chosen by the boundary conditions to the bounce solution $\phi_B(\xi_E)$,

$$
\frac{d\phi_B(\xi_E)}{d\xi_E} = 0 \quad (\xi_E = 0) \quad , \tag{3.5}
$$

which guarantees the regularity of the bounce solution at the origin (the reality of the bounce solution) and

$$
\phi_B(\xi_E) = -\frac{c}{m^2} \quad (\xi_E \to \infty) \quad , \tag{3.6}
$$

which implies that the false vacuum realizes itself all over space at past infinity, respectively.

As stated above, we are considering the background field configuration where the false vacuum realizes itself outside the bubble, and so does the true vacuum inside the bubble. On the bubble wall the background field $\phi_B(\xi_E)$ varies connecting the false and the true vacua. In our potential model defined in Eq.(3.1), we can think that wall is roughly the spacetime region surrounded by the spheres labeled ξ_1 and ξ_2. So from now on,we call ξ_1 and ξ_2 the inner and the outer radius of the wall, respectively. In this definition, the wall is nothing but the negative mass region. Because of easiness of analytical treatments, what is called the thin wall case which corresponds to the case $\xi_1 = \xi_2$ in our model, have been discussed many times in terms of decay rate of the false vacuum [3], and quantum state of the fluctuations of the field [4] so far. In the present case, we can investigate the thick wall case freely by changing the separation between ξ_1 and ξ_2.

As we have found the background solution ϕ_B, we turn to solve the equation of small fluctuations Eq.(2.17). As in the previous case, $F_p(\xi_E)$ is solved to give

$$\begin{aligned} 0 \le \xi_E < \xi_1 \quad &, \quad F_p(\xi_E) = a_{1p}K_{ip}(M\xi_E) + a_{2p}I_{ip}(M\xi_E) \quad , \\ \xi_1 \le \xi_E < \xi_2 \quad &, \quad F_p(\xi_E) = b_{1p}J_{ip}(\mu\xi_E) + b_{2p}N_{ip}(\mu\xi_E) \quad , \\ \xi_2 \le \xi_E < \infty \quad &, \quad F_p(\xi_E) = K_{ip}(m\xi_E) \quad , \end{aligned} \tag{3.7}$$

where the reason why the only K appears in $\xi_2 \le \xi_E < \infty$ is that the quantum state of the fluctuations of the tunneling field itself φ is set in the ground state at $T \to -\infty$.

The bounce solution $\phi_B(\xi_E)$, and the radial part of the mode function $F_p(\xi_E)$ are the solutions of the differential equations of second rank with potential which has no delta function peak in the second derivative with respect to ϕ_B. So the functions and their first derivatives must be continuous everywhere. This leads to the junction conditions as follows:

$$\begin{aligned} \phi_B(\xi_i - \epsilon) = \phi_B(\xi_i + \epsilon) \quad &, \quad \frac{d\phi_B(\xi_i - \epsilon)}{d\xi_E} = \frac{d\phi_B(\xi_i + \epsilon)}{d\xi_E} \quad , \\ F_p(\xi_i - \epsilon) = F_p(\xi_i + \epsilon) \quad &, \quad \frac{dF_p(\xi_i - \epsilon)}{d\xi_E} = \frac{dF_p(\xi_i + \epsilon)}{d\xi_E} \; (i = 1, 2) \quad . \end{aligned} \tag{3.8}$$

Theoretically the coefficients appearing in Eqs.(3.4), (3.7) can be determined by solving the junction conditions above, which reduce to the simultaneous linear equations on these coefficients. But as these coefficients are written by using the products of the Bessel functions, it is difficult to obtain simple approximate expressions of these coefficients from them by hand, except for the extreme cases where the arguments of the Bessel's functions are near the origin or the infinity. In order to get over the difficulties, we appeal to the numerical calculation.

As for the mode function F_p, around the origin $\xi_E = \xi = 0$, We simply replace ξ_E by $-i\xi$, which corresponds to the replacement of τ with it. Following this prescription, for example, the modified Bessel functions are continued as follows,

$$\begin{aligned} K_{ip}(M\xi_E) \to K_{ip}(-iM\xi) &= \frac{\pi i}{2} e^{-\pi p/2} H^{(1)}_{ip}(M\xi) \quad , \\ I_{ip}(M\xi_E) \to I_{ip}(-iM\xi) &= \frac{1}{2} e^{\pi p/2} (H^{(1)}_{ip}(M\xi) + H^{(2)}_{ip}(M\xi)) \quad . \end{aligned} \tag{3.9}$$

In $\mathcal{M}$, the classical background ϕ_B oscillates around the true vacuum, but this oscillation only attenuates. In fact the classical background ϕ_B in $\mathcal{M}$ is

$$\phi_B(\xi) = A(M\xi)^{-1} J_1(M\xi) \quad . \tag{3.10}$$

Thus ϕ_B does not reach the junction point ϕ_1 any more, and ϕ_B is confined in the region $V''(\phi_B) = M$. Therefore we can regard that the Lorentzian mode function around the origin $\xi = 0$ also describes the quantum state of the fluctuations in the asymptotic region $\xi \to \infty$.

Hence in the case of Eq.(3.7), the Lorentzian mode function is written in the same form as given in Eq. (2.19) and the coefficients are determined by

$$\begin{aligned} c^*_{1p} &= \frac{\pi i}{2} a_{1p} + \frac{1}{2} e^{\pi p} a_{2p} \quad , \\ c^*_{2p} &= \frac{1}{2} a_{2p} \quad . \end{aligned} \tag{3.11}$$

From the discussion in the previous section, the spectrum of particles created through the bubble nucleation is given by

$$n_p = \frac{1}{\left|c_{1p}/c_{2p}\right|^2 - 1} = \frac{a_{2p}^2}{\pi^2 |a_{1p}|^2} \quad . \tag{3.12}$$

It is important to notice that $F_p(\xi_E)$ is determined by the five parameters m, μ, M, ξ_1, ξ_2, but they are not independent because both ξ_1,and ξ_2 are determined completely by $m, \mu, M, \phi_2/\phi_1$, inversely μ and ϕ_2/ϕ_1 are determined by m, M, ξ_1, ξ_2. Thus there are at least two ways of giving the independent parameters in calculating the mode function, or the spectrum of created particles. One is giving $m, \mu, M, \phi_2/\phi_1$ which characterize the form of the potential $V(\phi)$, and the other is giving m, M, ξ_1, ξ_2 which characterize the wall configuration in the spacetime. Note that μ is fixed in the latter case as will be understood from the fact that μ is necessarily of the order of $1/(\xi_2 - \xi_1)$.

Until now, we considered the case where the wall is in the Euclidean region only. But there is a case where the wall extends to the Lorentzian region from the Euclidean region. Since the scalar field ϕ_B jumps over the potential barrier only in $\mathcal{E}$, the outer surface of the wall ξ_2 must be in $\mathcal{E}$, while the inner surface of the wall ξ_1 can be in $\mathcal{M}$.

In this case the bounce solution ϕ_B is

$$\begin{aligned}
\infty > \xi > \xi_1 \quad &, \quad \phi_B(\xi) = A_1(M\xi)^{-1} J_1(M\xi) + A_2(M\xi)^{-1} N_1(M\xi) \quad , \\
\xi_1 \geq \xi > 0 \quad &, \quad \phi_B(\xi) = B(\mu\xi)^{-1} I_1(\mu\xi) + \frac{a}{\mu^2} \quad , \\
0 \leq \xi_E < \xi_2 \quad &, \quad \phi_B(\xi_E) = B(\mu\xi_E)^{-1} J_1(\mu\xi_E) + \frac{a}{\mu^2} \quad , \\
\xi_2 \leq \xi_E < \infty \quad &, \quad \phi_B(\xi_E) = C_1(m\xi_E)^{-1} K_1(m\xi_E) - \frac{c}{m^2} \quad .
\end{aligned} \tag{3.13}$$

The radial part of the mode function F_p is

$$\begin{aligned}
\infty > \xi > \xi_1 \quad &, \quad F_p(\xi) = c_{1p}^* e^{-\pi p/2} H_{ip}^{(1)}(M\xi) + c_{2p}^* e^{\pi p/2} H_{ip}^{(2)}(M\xi) \quad , \\
\xi_1 \geq \xi > 0 \quad &, \quad F_p(\xi) = B_{1p} I_{ip}(\mu\xi) + B_{2p} K_{ip}(\mu\xi) \quad , \\
0 \leq \xi_E < \xi_2 \quad &, \quad F_p(\xi_E) = b_{1p} J_{ip}(\mu\xi_E) + b_{2p} N_{ip}(\mu\xi_E) \quad , \\
\xi_2 \leq \xi_E < \infty \quad &, \quad F_p(\xi_E) = K_{ip}(m\xi_E), \quad .
\end{aligned} \tag{3.14}$$

Also in this case, all the coefficients are determined by the junction conditions and the particle creation n_p is given by Eq.(2.22). Around the origin, the Bessel functions are continued as follows in this case:

$$\begin{aligned}
J_{ip}(\mu\xi_E) - J_{ip}(-i\mu\xi) &= e^{\pi p/2} I_{ip}(\mu\xi) \quad , \\
N_{ip}(\mu\xi_E) - N_{ip}(-i\mu\xi) &= -ie^{\pi p/2} I_{ip}(\mu\xi) - \frac{2}{\pi} e^{-\pi p/2} K_{ip}(\mu\xi) \quad .
\end{aligned} \tag{3.15}$$

Therefore we get

$$\begin{aligned}
B_{1p} &= e^{\pi p/2}(b_{1p} - ib_{2p}) \quad , \\
B_{2p} &= -\frac{2}{\pi} e^{-\pi p/2} b_{2p} \quad .
\end{aligned} \tag{3.16}$$

We adopt as the independent parameters, m, M, ξ_1, ξ_2 which characterize the wall configuration in the spacetime. It is to be noticed that μ is determined completely by only m, ξ_2 in this case. In $\mathcal{E}$, the bounce solution is

$$\begin{aligned}
0 \leq \xi_E < \xi_2 \quad &, \quad \phi_B(\xi_E) + \frac{c}{m^2} = B(\mu\xi_E)^{-1} J_1(\mu\xi_E) - \left(1 + \frac{\mu^2}{m^2}\right) B(\mu\xi_2)^{-1} J_1(\mu\xi_2) \quad , \\
\xi_2 \leq \xi_E < \infty \quad &, \quad \phi_B(\xi_E) + \frac{c}{m^2} = C_1(m\xi_E)^{-1} K_1(m\xi_E) \quad .
\end{aligned} \tag{3.17}$$

Since μ is given by the junction condition of $\phi_B(\xi_E) + c/m^2$ at $\xi_E = \xi_2$, μ is the function of m, ξ_2.

IV. RESULTS OF THE NUMERICAL CALCULATIONS

As for many different cases which is characterized by the form of the potential $m, \mu, M, \phi_2/\phi_1$, or the wall configuration in the spacetime m, M, ξ_1, ξ_2, we investigated particle spectrums n_p. As a result,we found that the shapes of the particle spectrums n_p do not change so much, but the values of n_p depend on the cases. The typical form of n_p

is as follows. For $0 \leq p \lesssim p_c \sim O(1)$, n_p is constant, and for $p \gtrsim p_c$, n_p decreases very steeply. Thus we consider the value on the plateau to characterize the particle spectrum n_p of each case. For definiteness, we take $n_{p=0}$ as the value of the plateau.

In terms of the wall configuration in the spacetime, there are two cases as stated above. In the both cases the outer surface of the wall ξ_2 is in $\mathcal{E}$. On the other hand, the inner surface of the wall ξ_1 is in $\mathcal{E}$ in one case, and in $\mathcal{M}$ in the other case. As for many numerical calculations, we find that $n_{p=0}$ is approximated as follows considerably well on the level of the exponential behavior

$$n_{p=0} \propto \exp(-4M\xi_1) \quad , \tag{4.1}$$

in the former case, and

$$\begin{aligned} n_{p=0} &\propto \exp(2\mu\xi_1) \quad , \\ \mu &= \mu(m, \xi_2) \quad , \end{aligned} \tag{4.2}$$

in the latter case, when we regard as independent parameters, (m, M, ξ_1, ξ_2).

V. DISCUSSION

From many numerical calculations, we have found the rough impressions as follows. Under natural choice of parameters which characterize the wall configuration in the spacetime, when the wall is confined in $\mathcal{E}$, the particle creation is almost negligibly small, on the other hand when the wall extends through $\mathcal{E}$ and $\mathcal{M}$, the particle creation is significantly large. So we need investigate how the potential $V(\phi)$ which enhances the particle creation is. This point will be discussed in the forthcoming paper [6]

The next theme is to investigate the particle creation in the false vacuum decay with gravitational degrees of freedom taken into account. It has already been done to take the gravity into account as the classical background [8]. In this respect, it is left only to calculate the particle creation of the scalar field concretely. But the technical issues to get over exist in order to discuss change of the quantum state of the gravitational field. These problems has great importance in the scenario of the inflation with the false vacuum decay which creates the open universe in the true vacuum bubble [1].

ACKNOWLEDGMENTS

We would like to thank Prof. H. Sato for continuous encouragements. This work was supported by Monbusho Grant-in-Aid for Scientific Research Nos. 2841 and 2010 and 05640342, and in part by the Sumitomo Foundation.

---

[1] J.R. Gott III, Nature Vol.295, 304 (1982).
M. Bucher, A.S. Goldhaber and N. Turok, Preprint hep-ph/9411206 (1994).
B. Allen and R. Caldwell, preprint WISC-MILW-94-TH-21.
K. Yamamoto, M. Sasaki and T.Tanaka, preprint KUNS1309.
[2] T. Banks, C.M. Bender and T.T. Wu, Phys. Rev.D8, 3346 (1973).
T. Banks and C.M. Bender, Phys. Rev.D8, 3366 (1973).
J.L. Gervais and B. Sakita, Phys. Rev. D15, 3507 (1977).
H.J. de Vega, J.L. Gervais and B. Sakita, Nucl. Phys. B139, 20 (1978); B142, 125 (1978).
[3] S. Coleman, Phys. Rev.D15, 2929 (1977).
S. Coleman, Aspects of Symmetry (Cambridge Unv. Press, Cambridge, England, 1985).
C.G. Callan and S. Coleman, Phys.Rev. D16, 1762 (1977).
S. Coleman and F. De Luccia, Phys.Rev. D21, 3305 (1980)/
[4] M. Sasaki, T. Tanaka, K. Yamamoto and J. Yokoyama, Prog. Theor. Phys. 90 (1993), 1019.
[5] K. Yamamoto, T. Tanaka and M. Sasaki, Preprint KUNS1305, gr-qc/9412011 (1994).
[6] T. Hamazaki, M. Sasaki, T. Tanaka and K. Yamamoto, in preparation

[7] M. Sasaki, T. Tanaka and K. Yamamoto, Preprint KUNS1308, gr-qc/9412025 (1994).
[8] T. Tanaka and M. Sasaki, Phys.Rev. D50, 6444 (1994)

Density fluctuations in Brans-Dicke inflation *

Alexei A. STAROBINSKY[1,2] and Jun'ichi YOKOYAMA[1]

[1] *Yukawa Institute for Theoretical Physics, Kyoto University, Uji 611 (Japan)*
[2] *Landau Institute for Theoretical Physics, Kosygina St. 2, Moscow 117334 (Russia)*

Spectrum of density perturbations in the Universe generated from quantum-gravitational fluctuations in slow-roll-over inflationary scenarios with the Brans-Dicke gravity is calculated. It is shown that after inflation the isocurvature mode of perturbations may be neglected as compared to the adiabatic mode, and that an amplitude of the latter mode is not significantly different from that in the Einstein gravity. However, the account of the isocurvature mode is necessary to obtain the quantitatively correct spectrum of adiabatic perturbations.

I. INTRODUCTION

Inflationary expansion in the early Universe not only is able to explain the observed degree of homogeneity, isotropy and flatness of the present-day Universe [1] but can also account for the origin of small initial density perturbations which produce gravitationally bound objects (galaxies, quasars, etc.) and the large-scale structure of the Universe [2]. Historically, among models of inflation making use of a scalar field (called an inflaton), the original model or the first-order phase transition model [3] failed due to the graceful exit problem, which was taken over by the new [4] and the chaotic [5] inflation scenarios where the inflaton scalar field is slow rolling during the whole de Sitter (inflationary) stage. The latter property was shared by the alternative scenario with higher-derivative quantum gravity corrections [6] (where the role of an inflaton is played by the Ricci scalar R) just from the beginning. Note that a simplified version of this scenario - the $R + R^2$ model - was even shown to be mathematically equivalent to some specific version of the chaotic scenario [7] (see also a review in [8]). In order to obtain a small enough amplitude of density perturbations in all these slow-roll-over models, the inflaton should be extremely weakly coupled to other fields. It is therefore not easy to find sound motivations to have a such a scalar field in particle physics. (See, however, [9] for recent improvements along this line.)

Reflecting such a situation, the extended inflation [10] scenario was proposed several years ago to revive a GUT Higgs field as the inflaton by adopting non-Einstein gravity theories. Although the first version of the extended inflation model, which considers a first-order phase transition in the Brans-Dicke theory [11], resulted in failure again due to the graceful-exit problem [12], it triggered further study of more generic class of inflation models in non-Einstein theories, in particular extended chaotic inflation [13] where both the inflaton and the Brans-Dicke scalar fields are in the slow rolling regime during inflation. Note that the natural source of Brans-Dicke-like theories of gravity is the low-energy limit of the superstring theory [14,15] with the Brans-Dicke scalar being the dilaton.

Several analyses have been done on the density perturbations produced in extended new or chaotic inflation models [16–20], all of which made use of the constancy of the Bardeen's gauge-invariant quantity ζ [21] or its equivalent on super-horizon scales and match it directly to quantum field fluctuations at the moment of horizon crossing which would be the correct procedure in a single component inflationary model. However, such a treatment is not correct in the present case which contains two sources of quantum fluctuations, namely, the inflaton and the Brans-Dicke scalar field. In such a model not only adiabatic but also isocurvature perturbations are generated and ζ does not remain constant for all modes.

In the present article we analyze density perturbations generated in both new and chaotic inflationary models in the Brans-Dicke gravity. Keeping the above point in mind and extending the method used in [22,23] to find spectra of all modes of adiabatic and isocurvature fluctuations in the multiple inflationary scenario in the Einstein gravity (with scalar fields interacting with each other through gravity only), we separate adiabatic and isocurvature modes at the inflationary stage and carefully evaluate their final amplitude. As a result, we arrive at a formula which is apparently very different from that used previously but find that constraints on the model parameters in both models remain approximately the same as in Einstein gravity if we express them in terms of the values of coupling constants *at the end of inflation*, contrary to the analysis by Berkin and Maeda [16].

We make use of the conformal transformation which transforms the original or the Jordan frame to the Einstein frame in which equations are somewhat simpler. We calculate the spectrum of fluctuations in the Einstein frame and

---

*Presented by J. Yokoyama

then interpret the result to the Jordan frame.

The rest of the present article is organized as follows. In §2 we define the Lagrangian and perform conformal transformation to write down the equations of motion in the Einstein frame. Then in §3 solutions to these equations are given and they are interpreted in the Jordan frame. They are applied to both chaotic and new inflationary models in §4. Finally §5 is devoted to discussion and conclusion.

II. BASIC EQUATIONS

A. Conformal Transformation

It has been shown that with the help of a conformal transformation a wide class of non-Einstein gravity models can be recast in the action

$$S = \int \mathcal{L}\sqrt{-g}d^4x = \int \left[\frac{1}{2\kappa^2}\mathcal{R} + \frac{1}{2}g^{\mu\nu}\partial_\mu\chi\partial_\nu\chi - U(\chi) + \frac{1}{2}e^{-\gamma\kappa\chi}g^{\mu\nu}\partial_\mu\phi\partial_\nu\phi - e^{-\beta\kappa\chi}V(\phi)\right], \tag{1}$$

where $\kappa^2 = 8\pi G$, β and γ are constants, χ and ϕ are the dilaton and the inflaton fields, respectively [16]. For example, in the case of the Brans-Dicke theory [11], the original action in the Jordan frame

$$S = \int \left[\frac{\Phi_{\rm BD}}{16\pi}\hat{\mathcal{R}} + \frac{\omega^2}{16\pi\Phi_{\rm BD}}\hat{g}^{\mu\nu}\partial_\mu\Phi_{\rm BD}\partial_\nu\Phi_{\rm BD} + \frac{1}{2}\hat{g}^{\mu\nu}\partial_\mu\phi\partial_\nu\phi - V(\phi)\right]\sqrt{-\hat{g}}d^4x, \tag{2}$$

is transformed into (1) through the conformal transformation

$$g_{\mu\nu} = \Omega^2\hat{g}_{\mu\nu}, \qquad \Omega^2 \equiv \frac{\kappa^2}{8\pi}\Phi_{\rm BD} \equiv \exp\left(\frac{\kappa\chi}{\sqrt{\omega+3/2}}\right), \tag{3}$$

with $\beta = 2\gamma = \frac{2}{\sqrt{\omega+3/2}}$ and $U(\chi) = 0$. Observations constrain ω to be $\omega > 500$ [24], so that $\beta < 0.09 \ll 1$. Since the Brans-Dicke field $\Phi_{\rm BD}$ remains practically constant in the radiation or matter dominant stage (see below), χ must be equal to zero at the end of inflation in order to reproduce the correct value of the gravitational constant today. Although we focus on the original Brans-Dicke theory in the present paper, we will not put the explicit values for β and γ below until the very end of the calculation in order to sustain applicability of our analysis to other non-Einstein gravity theories.

B. Background equations in the Einstein frame

Since the analysis is much simpler in the Einstein frame (1), we first investigate equations of motion derived from (1) and then transform the results into the original frame. Taking the background as the spatially flat Friedmann-Robertson-Walker spacetime,

$$ds^2 = dt^2 - a(t)^2 d\mathbf{x}^2, \tag{4}$$

the scalar field equations for the homogeneous parts read

$$\ddot{\chi} + 3H\dot{\chi} + \frac{\gamma\kappa}{2}e^{-\gamma\kappa\chi}\dot{\phi}^2 - \beta\kappa e^{-\beta\kappa\chi}V(\phi) = 0, \tag{5}$$

$$\ddot{\phi} + 3H\dot{\phi} - \gamma\kappa\dot{\chi}\dot{\phi} + e^{(\gamma-\beta)\kappa\chi}V'(\phi) = 0, \tag{6}$$

with an overdot denoting time derivation. Because β, $\gamma \ll 1$ and $V(\phi)$, being the inflaton's potential, realizes slow roll over of ϕ, the above equations can be approximated as

$$3H\dot{\chi} = \beta\kappa e^{-\beta\kappa\chi}V(\phi), \tag{7}$$

$$3H\dot{\phi} = -e^{(\gamma-\beta)\kappa\chi}V'(\phi), \tag{8}$$

with

$$H^2 = \left(\frac{\dot{a}}{a}\right)^2 = \frac{\kappa^2}{3} e^{-\beta\kappa\chi} V(\phi), \tag{9}$$

during inflation. We note that the above approximation is valid provided that the following inequalities are satisfied.

$$\begin{aligned} \max\{e^{-\gamma\kappa\chi}\dot{\phi}^2, \dot{\chi}^2\} &\ll e^{-\beta\kappa\chi} V(\phi), \\ |V'(\phi)| &\ll 3\kappa e^{-\gamma\kappa\chi/2} V(\phi), \\ V''(\phi) e^{(\gamma-\beta)\kappa\chi} &\ll H^2. \end{aligned} \tag{10}$$

Then the system (7)–(9) admits a solution as a function of the scale factor as [13,16]

$$\chi = \frac{\beta}{\kappa} \ln a \equiv -\frac{\beta}{\kappa} z, \tag{11}$$

$$\kappa^2 \int_{\phi_f}^{\phi} \frac{V(\varphi)}{V'(\varphi)} d\varphi = \frac{1 - a^{\beta\gamma}}{\beta\gamma} = \frac{1 - e^{-\beta\gamma z}}{\beta\gamma}, \tag{12}$$

where a subscript f denotes the value of each quantity at the end of inflation and we have set $a_f = 1$.

In the case that ϕ changes slowly compared with χ and that $V(\phi)$ can be regarded as a constant, evolution of the scale factor and χ is given by

$$a(t) = a_0 t^{\frac{2}{\beta^2}}, \quad \chi(t) = \frac{1}{\kappa\beta} \ln\left(\frac{V(\phi)\kappa^2\beta^4 t^2}{12}\right). \tag{13}$$

We thus have a power-low inflation with an extremely large power exponent.

C. Linear perturbations

We now turn to linear perturbation, which is most easily taken into account in a gauge-invariant manner using the longitudinal gauge,

$$ds^2 = (1 + 2\Phi)dt^2 - a(t)^2(1 - 2\Psi)\delta_{ij} dx^i dx^j, \tag{14}$$

where Φ and Ψ are gauge-invariant variables related with Bardeen's Φ_A and Φ_H as $\Phi = \Phi_A$ and $\Psi = -\Phi_H$ [25]. Assuming an $e^{i\mathbf{k}\mathbf{x}}$ spatial dependence, each Fourier mode satisfies the following equations of motion which are derived from the perturbed Einstein equations.

$$\Phi = \Psi, \tag{15}$$

$$\dot{\Phi} + H\Phi = \frac{\kappa^2}{2}(\dot{\chi}\delta\chi + e^{-\gamma\kappa\chi}\dot{\phi}\delta\chi), \tag{16}$$

$$\begin{aligned} &\ddot{\delta\chi} + 3H\dot{\delta\chi} + \left(\frac{k^2}{a^2} - \frac{(\gamma\kappa)^2}{2} e^{-\gamma\kappa\chi}\dot{\phi}^2 + (\beta\kappa)^2 e^{-\beta\kappa\chi} V(\phi)\right)\delta\chi + \gamma\kappa e^{-\gamma\kappa\chi}\dot{\phi}\dot{\delta\phi} \\ &\quad -\beta\kappa e^{-\beta\kappa\chi} V'(\phi)\delta\phi = 2(\ddot{\chi} + 3H\dot{\chi})\Phi + \dot{\Phi}\dot{\chi} + 3\dot{\Psi}\dot{\chi} + \gamma\kappa e^{-\gamma\kappa\chi}\dot{\phi}^2\Phi, \end{aligned} \tag{17}$$

$$\begin{aligned} &\ddot{\delta\phi} + (3H - \gamma\kappa\dot{\chi})\dot{\delta\phi} + \left(\frac{k^2}{a^2} + e^{(\gamma-\beta)\kappa\chi} V''(\phi)\right)\delta\phi - \gamma\kappa\dot{\phi}\dot{\delta\chi} \\ &\quad +(\gamma - \beta)\kappa V'(\phi) e^{(\gamma-\beta)\kappa\chi}\delta\chi = 2(\ddot{\phi} + 3H\dot{\phi})\Phi + \dot{\Phi}\dot{\phi} + 3\dot{\Psi}\dot{\chi} - 2\gamma\kappa\dot{\phi}\dot{\chi}\Phi, \end{aligned} \tag{18}$$

where $\delta\chi$ and $\delta\phi$ are gauge invariant fluctuation variables of the respective fields and we have suppressed the argument $\mathbf{k}$. Under the slow-roll approximations (10) the last two equations read

$$\ddot{\delta\chi} + 3H\dot{\delta\chi} + \left(\frac{k^2}{a^2} + (\beta\kappa)^2 e^{-\beta\kappa\chi} V(\phi)\right)\delta\chi + \gamma\kappa e^{-\gamma\kappa\chi}\dot{\phi}\dot{\delta\phi} - \beta\kappa e^{-\beta\kappa\chi} V'(\phi)\delta\phi$$
$$= 2\beta\kappa e^{-\gamma\kappa\chi} V(\phi)\Phi + \dot{\Phi}\dot{\chi} + 3\dot{\Psi}\dot{\chi}, \tag{19}$$

$$\ddot{\delta\phi} + 3H\dot{\delta\phi} + \left(\frac{k^2}{a^2} + e^{(\gamma-\beta)\kappa\chi} V''(\phi)\right)\delta\phi - \gamma\kappa\dot{\phi}\dot{\delta\chi} + (\gamma-\beta)\kappa V'(\phi) e^{(\gamma-\beta)\kappa\chi}\delta\chi$$
$$= -2e^{(\gamma-\beta)\kappa\chi} V'(\phi)\Phi + \dot{\Phi}\dot{\phi} + 3\dot{\Psi}\dot{\chi}. \tag{20}$$

Since what we need are the non-decreasing adiabatic and isocurvature modes on large scale $k \ll aH$, which turn out to be weakly time-dependent as will be seen in the final result [23], we may consistently neglect $\dot{\Phi}$ and those terms containing two time derivatives. Then the equations of motion are greatly simplified to

$$\Phi = \frac{\kappa^2}{2H}(\dot{\chi}\delta\chi + e^{-\gamma\kappa\chi}\dot{\phi}\delta\phi) = \frac{\beta\kappa}{2}\delta\chi - \frac{V'(\phi)}{2V(\phi)}\delta\phi, \tag{21}$$

$$3H\dot{\delta\chi} + (\beta\kappa)^2 e^{-\beta\kappa\chi} V(\phi)\delta\chi - \beta\kappa e^{-\beta\kappa\chi} V'(\phi)\delta\phi = 2\beta\kappa e^{-\beta\kappa\chi} V(\phi)\Phi, \tag{22}$$

$$3H\dot{\delta\phi} + e^{(\gamma-\beta)\kappa\chi} V''(\phi)\delta\phi + (\gamma-\beta)\kappa V'(\phi) e^{(\gamma-\beta)\kappa\chi}\delta\chi = -2e^{(\gamma-\beta)\kappa\chi} V'(\phi)\Phi. \tag{23}$$

III. GENERATION OF PERTURBATIONS

A. Solution of non-decreasing modes

We shall now solve eqs. (21)-(23). Inserting (21) to (22) we easily find $3H\dot{\delta\chi} = 0$, or

$$\delta\chi = \frac{\beta}{\kappa} Q_1 = \text{const.} \tag{24}$$

Similarly (23) is transformed to

$$3H\dot{\delta\phi} + e^{(\gamma-\beta)\kappa\chi}\left(V''(\phi) - \frac{V'(\phi)^2}{V(\phi)}\right)\delta\phi + \beta\gamma e^{(\gamma-\beta)\kappa\chi} V'(\phi) Q_1 = 0. \tag{25}$$

The above equation can be solved taking ϕ as an independent variable instead of t. With the help of (8) we find

$$3H\frac{d}{dt} = 3H\dot{\phi}\frac{d}{d\phi} = -e^{(\gamma-\beta)\kappa\chi} V'(\phi)\frac{d}{d\phi}, \tag{26}$$

so that (25) reads

$$\frac{d}{d\phi}\delta\phi = \left(\frac{V''(\phi)}{V'(\phi)} - \frac{V'(\phi)}{V(\phi)}\right)\delta\phi + \beta\gamma Q_1. \tag{27}$$

Its solution is given by

$$\delta\phi = \frac{V'(\phi)}{V(\phi)}\left(\beta\gamma Q_1 \int_{\phi_f}^{\phi} \frac{V(\varphi)}{V'(\varphi)} d\varphi + \frac{Q_2 - Q_1}{\kappa^2}\right) = -\frac{V'(\phi)}{\kappa^2 V(\phi)}(Q_1 e^{\gamma\kappa\chi} - Q_2), \tag{28}$$

with Q_2 being another integration constant. We therefore find

$$\Phi = \frac{\beta^2}{2} Q_1 + \frac{1}{2\kappa^2}\left(\frac{V'(\phi)}{V(\phi)}\right)^2 (e^{\gamma\kappa\chi} Q_1 - Q_2). \tag{29}$$

Thus we have obtained a generic solution of the system (21)-(23) containing two undetermined constants.

In order to clarify physical meaning of the above solution, we should divide it to adiabatic and isocurvature modes. The latter mode is characterized by its vanishingly small contribution to the gravitational potential Φ, while the growing adiabatic mode can be described by the following universal expression.

$$\Phi = C_1\left(1 - \frac{H}{a}\int_0^t a(t')dt'\right) \cong -C_1\frac{\dot{H}}{H^2}, \tag{30}$$

$$\frac{\delta\chi}{\dot{\chi}} = \frac{\delta\phi}{\dot{\phi}} = \frac{C_1}{a}\int_0^t a(t')dt' \cong \frac{C_1}{H}, \tag{31}$$

where C_1 is a constant and the latter approximate equality in each expression is satisfied during the inflationary stage.
From (7)–(9) we find,

$$\dot{\chi} = \frac{\beta}{\kappa}H, \quad \dot{\phi} = -H\frac{e^{\gamma\kappa\chi}V'(\phi)}{\kappa^2 V(\phi)}, \quad \frac{\dot{H}}{H^2} = \frac{\beta^2}{2} + \frac{e^{\gamma\kappa\chi}}{2\kappa^2}\left(\frac{V'(\phi)}{V(\phi)}\right)^2, \tag{32}$$

and it turns out that defining new constants C_1 and C_3 by $Q_1 = C_1 - C_3$ and $Q_2 = -C_3$ discriminates between adiabatic and isocurvature modes in the final result. That is,

$$\frac{\delta\chi}{\dot{\chi}} = \frac{C_1}{H} - \frac{C_3}{H}, \tag{33}$$

$$\frac{\delta\phi}{\dot{\phi}} = \frac{C_1}{H} + \frac{C_3}{H}(e^{-\gamma\kappa\chi} - 1), \tag{34}$$

$$\Phi = -C_1\frac{\dot{H}}{H^2} + C_3\left[\frac{1}{2\kappa^2}(1 - e^{\gamma\kappa\chi})\left(\frac{V'(\phi)}{V(\phi)}\right)^2 - \frac{\beta^2}{2}\right]. \tag{35}$$

In the above expressions, terms in proportion to C_1 and C_3 represent adiabatic and isocurvature modes, respectively. The isocurvature nature of the C_3–terms is guaranteed by the fact that the second term in the right-hand-side of (35) is vanishingly small in the last stage of inflation when we have $\chi \cong 0$.

B. Quantum fluctuations

We shall next determine the constants C_1 and C_3 from amplitudes of quantum fluctuations of the scalar fields generated during the inflationary stage. Thanks to the inequalities (10), eqs. (19) and (20) can be approximated by equation of motion of a free massless scalar field in inflating background for $k \geq aH$ and even in the region $k < aH$ but with $H(t_k) \gg |\dot{H}(t_k)|(t - t_k)$ where t_k is the time k–mode leaves the Hubble horizon during inflation. The standard quantization gives the well-known result, that is, the Fourier components of the fields can be represented in the form

$$\delta\chi(\mathbf{k}) = \frac{H(t_k)}{\sqrt{2k^3}}\epsilon_\chi(\mathbf{k}), \quad \delta\phi(\mathbf{k}) = \frac{H(t_k)}{\sqrt{2k^3}}e^{\gamma\kappa\chi(t_k)/2}\epsilon_\phi(\mathbf{k}), \tag{36}$$

where the exponential factor in the latter equality is present because ϕ has a non-canonical kinetic term in the action in the Einstein frame. Here $\epsilon_\chi(\mathbf{k})$ and $\epsilon_\phi(\mathbf{k})$ are classical random Gaussian quantities with the following averages.

$$\langle\epsilon_\chi(\mathbf{k})\rangle = \langle\epsilon_\phi(\mathbf{k})\rangle = 0, \quad \langle\epsilon_i(\mathbf{k})\epsilon_j^*(\mathbf{k}')\rangle = \delta_{ij}\delta^{(3)}(\mathbf{k} - \mathbf{k}'), \quad i, j = \chi, \phi. \tag{37}$$

We thus find

$$C_1 = \left[e^{\gamma\kappa\chi}H\frac{\delta\phi}{\dot{\phi}} + (1 - e^{\gamma\kappa\chi})H\frac{\delta\chi}{\dot{\chi}}\right]_{t_k} = \frac{H^2(t_k)}{\sqrt{2k^3}}\left[\frac{e^{\frac{3}{2}\gamma\kappa\chi}}{\dot{\phi}}\epsilon_\phi(\mathbf{k}) + \frac{1 - e^{\gamma\kappa\chi}}{\dot{\chi}}\epsilon_\chi(\mathbf{k})\right]_{t_k}, \tag{38}$$

$$C_3 = \left[e^{\gamma\kappa\chi}H\left(\frac{\delta\phi}{\dot{\phi}} - \frac{\delta\chi}{\dot{\chi}}\right)\right]_{t_k} = \frac{H^2(t_k)}{\sqrt{2k^3}}\left[\frac{e^{\frac{3}{2}\gamma\kappa\chi}}{\dot{\phi}}\epsilon_\phi(\mathbf{k}) - \frac{\epsilon_\chi(\mathbf{k})}{\dot{\chi}}\right]_{t_k}. \tag{39}$$

Note the interesting fact that in the specific case of the "soft" inflation [26] ($\gamma \equiv 0$), the Brans-Dicke dilaton does not contribute to the adiabatic mode (C_1) at all.

C. Adiabatic modes

From (30) curvature perturbation due to primordially adiabatic fluctuation is given by

$$\Phi_{\rm ad} = \left[1 + \frac{2}{3(1+w)}\right]^{-1} C_1, \quad w \equiv \frac{\rho}{p}, \tag{40}$$

with p and ρ being total pressure and energy density, respectively. since Φ is related to the gauge-invariant density fluctuation $\delta\rho^{(c)}/\rho$, which reduces to $\delta\rho/\rho$ in the comoving gauge, as

$$\frac{\delta\rho^{(c)}}{\rho} = -\frac{2}{3}\left(\frac{k}{Ha}\right)^2 \Phi, \tag{41}$$

we find

$$\frac{\delta\rho^{(c)}}{\rho} = f\left[e^{\gamma\kappa\chi} H\frac{\delta\phi}{\dot\phi} + (1 - e^{\gamma\kappa\chi}) H\frac{\delta\chi}{\dot\chi}\right]_{t_h}, \tag{42}$$

at the horizon crossing ($k = aH$), where f is a constant equal to 4/9 during radiation domination and to 2/5 during matter domination (we omit the minus sign here because it may be absorbed into the stochastic variables $\delta\phi$ and $\delta\chi$).

The above formula is quite different from that used by the previous authors [16–20], who did not account for the isocurvature mode and its mixing with the adiabatic mode during inflation, and concluded that a density fluctuation at the second horizon crossing is approximately equal to $\delta\rho/(\rho + p)$ evaluated at the first horizon crossing during inflation. That is, up to a factor of order of unity,

$$\frac{\delta\rho}{\rho} \simeq \left.\frac{H(|\dot\chi|\delta\chi + e^{-\gamma\kappa\chi}|\dot\phi|\delta\phi)}{\dot\chi^2 + e^{-\gamma\kappa\chi}\dot\phi^2}\right|_{t_h} \text{(incorrect)}, \tag{43}$$

which gives

$$\frac{\delta\rho}{\rho} \simeq \begin{cases} \frac{H\delta\chi}{|\dot\chi|} & \text{for } |\dot\chi| > |\dot\phi|e^{-\gamma\kappa\chi/2} \\ \frac{H\delta\phi}{|\dot\phi|} & \text{for } |\dot\chi| < |\dot\phi|e^{-\gamma\kappa\chi/2} \end{cases} \quad \text{(incorrect)}. \tag{44}$$

Note also that we would have reached the above formula (43) or its analogue in the Jordan frame [20], had we put $C_3 = 0$ neglecting the isocurvature mode in (35). Clearly this is not justifiable because it results in imposing a redundant constraint between $\delta\chi$ and $\delta\phi$ in eqs. (33) and (34). The difference between the expressions (42) and (43) is especially large near the points where $V'(\phi) = 0$. Then Eq. (42) predicts much larger adiabatic perturbations than Eq. (43).

We are interested in the amplitude of density fluctuations about 40 ~ 60 e-folds before the end of inflation, or at $z \simeq 40 \sim 60$, corresponding to large-scale structures within the horizon scale today. From (11) the corresponding value of χ ranges $\kappa\chi = -40\beta \sim -60\beta$, for which we have $e^{\gamma\kappa\chi} \simeq 1.2$ with $\omega \simeq 500$. Thus the above incorrect formula and ours give practically opposite results with respect to the two cases $|\dot\chi| \gtrsim |\dot\phi|$ and $|\dot\chi| \lesssim |\dot\phi|$. In some models of inflation, unless β is too small, we find $|\dot\phi| < |\dot\chi|$, so that the adiabatic fluctuation is given by

$$\frac{\delta\rho}{\rho} \simeq e^{\gamma\kappa\chi}\frac{H\delta\phi}{|\dot\phi|}, \tag{45}$$

which gives practically the same result as in the Einstein gravity. On the other hand, in the limit $\omega \longrightarrow \infty$ or β, $\gamma \longrightarrow 0$, we find $e^{\gamma\kappa\chi} = 1$ so that the second term in (42) does not contribute to adiabatic fluctuation and we again find

$$\frac{\delta\rho}{\rho} \simeq \frac{H\delta\phi}{|\dot\phi|}, \tag{46}$$

in agreement with the result in the Einstein gravity.

D. Isocurvature modes

Isocurvature fluctuations can be significant if some ingredient of the model is essentially decoupled from the usual matter and constitutes a part of dark matter. In our model, the Brans-Dicke dilaton is a candidate of such an ingredient.

During inflation, its fractional comoving energy perturbation satisfies the inequality,

$$\frac{\delta\rho_\chi^{(c)}}{\rho_\chi} < \frac{2\delta\rho_\chi^{(c)}}{\rho_\chi + p_\chi} = 2\frac{\partial}{\partial t}\left(\frac{\delta\chi}{\dot{\chi}}\right) - 2\Phi = \frac{C_3}{\kappa^2}\left(\frac{V'(\phi)}{V(\phi)}\right)^2 < C_3. \tag{47}$$

Since C_3 is of the same order of C_1, which gives the amplitude of adiabatic perturbation at the second horizon crossing, fractional density fluctuation in χ is smaller than the adiabatic one. Furthermore, its contribution to the total energy density fluctuation, $\delta\rho_\chi^{(c)}/\rho$ turns out to be much smaller than the adiabatic counterpart, because we find $\rho_\chi = \mathcal{O}(\omega^{-1})\rho \ll \rho$ in the post inflationary universe as will be seen below. We, therefore, conclude that isocurvature fluctuations are negligible in this model.

E. Density fluctuations in the physical (Jordan) frame

We can relate the amplitude of density fluctuations in the Einstein frame with that in the Jordan frame using the conformal transformation [27]. First we note that gauge-invariant variables in both frames are related with each other as

$$\hat{\Phi} = \Phi - \frac{\delta\Omega}{\Omega}, \qquad \hat{\Psi} = \Psi + \frac{\delta\Omega}{\Omega}, \tag{48}$$

where $\delta\Omega = \frac{\sqrt{\kappa}}{2}\delta\chi\Omega$ is gauge-invariant perturbation of Ω. Using the equalities

$$\hat{a} = \Omega^{-1}a, \quad d\hat{t} = \omega^{-1}dt, \quad \hat{H} = \frac{\dot{\hat{a}}}{\hat{a}} = \Omega\left(H - \frac{\dot{\Omega}}{\Omega}\right), \tag{49}$$

one can write (30) and (31) in terms of physical variables as

$$\Phi = C_1\left[1 - \left(\hat{H} + \frac{\Omega_{\hat{t}}}{\Omega}\right)\frac{1}{\hat{a}\Omega^2}\int^{\hat{t}}\hat{a}\Omega^2 d\hat{t}'\right] \tag{50}$$

$$\frac{\delta\chi}{\dot{\chi}} = \Omega\frac{\delta\chi}{\chi_{\hat{t}}} = \frac{C_1}{\hat{a}\Omega}\int^{\hat{t}}\hat{a}\Omega^2 d\hat{t}'. \tag{51}$$

We, therefore, find

$$\hat{\Phi} = C_1\left[1 - \left(\hat{H} + 2\frac{\Omega_{\hat{t}}}{\Omega}\right)\frac{1}{\hat{a}\Omega^2}\int^{\hat{t}}\hat{a}\Omega^2 d\hat{t}'\right], \tag{52}$$

$$\hat{\Psi} = C_1\left[1 - \frac{\hat{H}}{\hat{a}\Omega^2}\int^{\hat{t}}\hat{a}\Omega^2 d\hat{t}'\right]. \tag{53}$$

The above two equations are the desired formula to relate density fluctuations in the Einstein frame and those in the Jordan frame through C_1. In practice, however, since the Brans-Dicke field varies extremely slowly in the post-inflationary universe, one can regard Ω as a constant in these equations. For example, in the matter dominated stage, we find [11]

$$\Phi_{\rm BD}(\hat{t}) = \Phi_{\rm BD0}\left(\frac{\hat{t}}{\hat{t}_0}\right)^{\frac{2}{3\omega+4}}, \tag{54}$$

$$\hat{a}(\hat{t}) = \hat{a}_0\left(\frac{\hat{t}}{\hat{t}_0}\right)^{\frac{2+2\omega^{-1}}{3+4\omega^{-1}}}, \tag{55}$$

Hence $\Omega_{\hat{t}}/\Omega$ is smaller than $\hat{H}$ by a factor less than 1/500. Thus we may simply conclude that the adiabatic fluctuations are described by the same formula in both frames.

Using (54), we can estimate energy density of χ in the Einstein frame in this stage as

$$\rho_\chi = \frac{1}{2}\dot{\chi}^2 = \frac{2\omega+3}{(3\omega+5)^2}\frac{1}{\kappa^2 t^2} \cong \frac{1}{6\omega}\rho. \tag{56}$$

Thus we may conclude the isocurvature perturbation due to χ is not important as stated in the previous subsection.

IV. APPLICATION TO SPECIFIC INFLATIONARY MODELS

Having developed general considerations, we now apply the above results to two specific inflation models, namely chaotic inflation [5] and new inflation [4], and examine constraints on their model parameters as well as the spectral shape.

A. Chaotic Inflation

Here we consider two different potentials $V(\phi) = \frac{1}{2}m^2\phi^2$ and $V(\phi) = \frac{\lambda_4}{4}\phi^4$ which are denoted collectively as $V(\phi) = \frac{\lambda_n}{n}\phi^n$. In this model, inflation occurs at large ϕ and it is terminated when $|\dot{\phi}/\phi|$ becomes as large as H at $\phi = \phi_f = \sqrt{n}/\kappa$. Since we are interested in the last 60 e-foldings in the inflationary stage, we may approximate (12) as

$$\kappa^2 \int_{\phi_f}^{\phi} \frac{V(\varphi)}{V'(\varphi)} d\varphi = \frac{\kappa^2}{2n}\left(\phi^2 - \frac{n}{\kappa^2}\right) \simeq z. \tag{57}$$

The error in the last expression is only about 12% with $z = 60$, $\beta = 2\gamma = 0.09$. The e-folding number, z_k, when the comoving wave-number k leaves the Hubble radius during inflation satisfies

$$\frac{k}{k_f} = e^{\left(1-\frac{\beta^2}{2}\right)z_k}(2z_k)^{\frac{n}{4}}, \qquad \text{for } 1 \ll z_k \lesssim 60. \tag{58}$$

We can express the amplitude of curvature perturbation on scale $l = \frac{2\pi}{k}$ as

$$\begin{aligned}\hat{\Phi}(l) &= \left[1+\frac{2}{3(1+w)}\right]^{-1}\frac{\sqrt{2k^3\langle|C_1|^2\rangle}}{2\pi} \\ &= \left[1+\frac{2}{3(1+w)}\right]^{-1}\frac{\kappa^2}{2\pi}\sqrt{\frac{\lambda_n}{3n}\left(\frac{2nz_k}{\kappa^2}\right)^{\frac{n}{2}}}\left[e^{\frac{1}{2}\beta(\gamma-\beta)z_k}\sqrt{\frac{2z_k}{n}} + \frac{e^{-\frac{\beta^2}{2}z_k}}{\beta}(e^{\beta\gamma z_k}-1)\right],\end{aligned} \tag{59}$$

again for $1 \ll z_k \lesssim 60$.

Since the large-angular-scale anisotropy of background radiation due to the Sachs-Wolfe effect is given by $\delta T/T = \hat{\Phi}/3$, we can normalize the value of λ_n by the COBE observation [28]. For $\beta = 2\gamma = 0.09$, we find

$$\frac{\delta T}{T} = \frac{1}{3}\hat{\Phi}(z_k \simeq 60) \simeq \begin{cases} 9\frac{m}{M_{Pl}} & \text{for } n=2 \\ 32\sqrt{\lambda_4} & \text{for } n=4 \end{cases} \tag{60}$$

$$= 1.1\times 10^{-5} \tag{61}$$

Note that our normalization of the background solution $a_f = 1$, $\chi_f = 0$ (see Eqs. (11,12)) means that m and λ_4 are values of physical parameters ("coupling constants") at the end of inflation. However, since χ generally grows only as logarithm of t after inflation and is even constant during the whole radiation-dominated stage in the Brans-Dicke case $\beta = 2\gamma$, their present values are not significantly different from those at the end of inflation. So, it is natural to use just the latter values when comparing non-Einstein gravity models having variable coupling constants with models based on the Einstein gravity. We find

$$m = 1\times 10^{13}\text{GeV}, \qquad n=2, \tag{62}$$

$$\lambda_4 = 1\times 10^{-13}, \qquad n=4 \tag{63}$$

which is no different from the values obtained assuming the Einstein gravity [29]. Since the behavior of the system approaches to that in the Einstein gravity as we increase ω, we can conclude that in Brans-Dicke theory, model parameters of the inflaton's potential should take the same value as in the Einstein gravity.

B. New Inflation

Next we consider new inflation with a potential

$$V(\phi) = V_0 - \frac{\lambda}{4}\phi^4, \tag{64}$$

for which we find, from (12),

$$\kappa^2 \int_{\phi_f}^{\phi} \frac{V(\varphi)}{V'(\varphi)} d\varphi \cong \frac{\kappa^2 V_0}{2\lambda}\left(\frac{1}{\phi^2} - \frac{1}{\phi_f^2}\right) \cong \frac{\kappa^2}{2\lambda\phi^2} \simeq z. \tag{65}$$

We can again express the amplitude of curvature fluctuation as a function of z_k, which is now related with k as,

$$\frac{k}{k_f} = e^{\left(1-\frac{\beta^2}{2}\right)z_k} H_f. \tag{66}$$

$$\hat{\Phi}(l) = \left[1 + \frac{2}{3(1+w)}\right]^{-1} \left[e^{-\frac{1}{2}\beta(\beta-\gamma)z_k}\sqrt{\frac{\lambda}{3}}(2z_k)^{\frac{3}{2}} + \kappa H_f \frac{e^{-\frac{\beta^2}{2}z_k}}{\beta}(e^{\beta\gamma z_k} - 1)\right], \tag{67}$$

with $H_f \equiv \sqrt{\frac{\kappa^2}{3}V_0}$. Taking $\beta = 2\gamma = 0.09$ again, it predicts the amplitude of $\delta T/T$ to be compared with COBE data as

$$\frac{\delta T}{T}(z_k \simeq 60) \simeq 21\sqrt{\lambda} + 0.4\frac{H_f}{M_{Pl}}. \tag{68}$$

Since H_f should also satisfy

$$\frac{H_f}{M_{Pl}} \lesssim 10^{-5} \tag{69}$$

to suppress long-wave gravitational radiation of quantum origin [30], we find

$$\lambda \lesssim 2 \times 10^{-13} \tag{70}$$

from (68). Again its amplitude is practically no different from the case of the Einstein gravity.

V. CONCLUSION

In the present paper we have investigated density perturbations generated during inflation in the Brans-Dicke theory, paying attention to the fact that quantum fluctuations of both the inflaton and the Brans-Dicke dilaton fields contribute to them. This implies that not only adiabatic (curvature) but also isocurvature perturbations exist and that the simple conservation formula of a perturbation outside the Hubble radius cannot be used.

Working in the Einstein frame, which is connected with the original frame through a conformal transformation, we have obtained expressions for growing adiabatic and isocurvature modes and have shown that only the former is important after inflation. Then we have corrected the previously used formula based on the use of incorrect matching of super-horizon perturbations with quantum fluctuations at horizon (Hubble radius) crossing. Since both the inflaton and the dilaton turn out to contribute to the perturbation with the same order of magnitude, the amplitude itself is not significantly altered compared with the case of inflation in the Einstein gravity.

However, our constraints on the model parameters turned out to be more severe than those obtained by Berkin and Maeda [16]. This is because they have taken the initial value of χ rather arbitrary, which might be appropriate to the case of original soft inflation model in which inflaton's potential is multiplied by an exponential potential by hand [26]. On the other hand, we, concentrating on the Brans-Dicke model, had to normalize its value to be zero after inflation to reproduce the correct gravitational constant today.

In conclusion, values of inflaton's coupling parameters in the Brans-Dicke gravity (if taken at the end of inflation) which are required to produce the correct amplitude of present adiabatic perturbations are practically no different from those in the Einstein gravity in the case of both chaotic and new inflationary models.

ACKNOWLEDGMENTS

A. S. is grateful to Profs. Y. Nagaoka and J. Yokoyama for their hospitality at the Yukawa Institute for Theoretical Physics, Kyoto University where this project was started. A. S. was supported in part by the Russian Foundation for Basic Research, Project Code 93-02-3631, and by Russian Research Project "Cosmomicrophysics". J. Y. acknowledges support by the Japanese Grant-in-Aid for Scientific Research Fund of Ministry of Education, Science, and Culture, No. 06740216.

---

[1] For a review of inflation see, *e.g.* A.D. Linde, Particle Physics and Inflationary Cosmology (Harwood, 1990).
[2] S.W. Hawking, Phys. Lett. **115B**, 295 (1982); A.A. Starobinsky, Phys. Lett. **117B**, 175 (1982); A.H. Guth and S-Y. Pi, Phys. Rev. Lett. **49**, 1110 (1982).
[3] A.H. Guth, Phys. Rev. **D23**, 347 (1981); K. Sato, Mon. Not. R. astr. Soc. **195**, 467 (1981).
[4] A.D. Linde, Phys. Lett. **108B**, 389 (1982); A. Albrecht and P.J. Steinhardt, Phys. Rev. Lett. **48**, 1220 (1982).
[5] A.D. Linde, Phys. Lett. **129B**, 177 (1983).
[6] A.A. Starobinsky, Phys. Lett. **91B**, 99 (1980).
[7] B. Whitt, Phys. Lett. **145B**, 176 (1984).
[8] S. Gottlöber, V. Müller, H.-J. Schmidt and A.A. Starobinsky, Int. J. Mod. Phys. **D1**, 257 (1992).
[9] H. Murayama, H. Suzuki, T. Yanagida, and J. Yokoyama, Phys. Rev. Lett. **70**, 1912 (1993); Phys. Rev. **D50**, R2356 (1994).
[10] D. La and P.J. Steinhardt, Phys. Rev. Lett. **62**, 376 (1989).
[11] C. Brans and R.H. Dicke, Phys. Rev. **24**, 925 (1961).
[12] D. La, P.J. Steinhardt, and E.W. Bertschinger, Phys. Lett. B **231**, 231 (1989); E. Weinberg, Phys. Rev. **D40**, 3950 (1989).
[13] A.D. Linde, Phys. Lett. **238B**, 160 (1990).
[14] E.S. Fradkin and A.A. Tseytlin, Phys. Lett. **158B**, 316 (1985); Nucl. Phys. **B261**, 1 (1985).
[15] C.G. Callan, D. Friedan, E.J. Martinec and M.J. Perry, Nucl. Phys. **B262**, 593 (1985); C.G. Callan, I.R. Klebanov and M.J. Perry, Nucl. Phys. **B278**, 78 (1986).
[16] A.L. Berkin and K. Maeda, Phys. Rev. **D44**, 1691 (1991).
[17] J. McDonald, Phys. Rev. **D44**, 2314 (1991).
[18] S. Mollerach and S. Matarrese, Phys. Rev. **D45**, 1961 (1992).
[19] N. Deruelle, C. Gundlach and D. Langlois, Phys. Rev. **D46**, 5337 (1992).
[20] J. García-Bellido, A.D. Linde and D.A. Linde, Phys. Rev. **D50**, 730 (1994); J. García-Bellido, Nucl. Phys. **B423**, 221 (1994).
[21] J.M. Bardeen, P.J. Steinhardt, and M.S. Turner, Phys. Rev. **D28**, 679 (1983).
[22] A.A. Starobinsky, JETP Lett. **42**, 152 (1985).
[23] D. Polarski and A.A. Starobinsky, Nucl. Phys. **B385**, 623 (1992); Phys. Rev. **D51**, 6123 (1994).
[24] R.D. Reasenberg *et al.* Astrophys. J. Lett. **234**, L219 (1979).
[25] J.M. Bardeen, Phys. Rev. **D22**, 1882 (1980).
[26] A.L. Berkin, K. Maeda and J. Jokoyama, Phys. Rev. Lett. **65**, 141 (1990).
[27] J. Hwang, Class. Quant. Grav. **7**, 1613 (1990).
[28] G.F. Smoot, *et al.* Astrophys. J. Lett. **396**, L1 (1992).
[29] D.S. Salopek, Phys. Rev. Lett. **69**, 3602 (1992).
[30] V.A. Rubakov, M.V. Sazhin, and A.V. Veryaskin, Phys. Lett. **115B**, 189 (1982).

Numerical Analysis of Topological Inflation

NOBUYUKI SAKAI[1], HISA-AKI SHINKAI[2], TAKASHI TACHIZAWA[3]
and KEI-ICHI MAEDA[4]

Department of Physics, Waseda University, 3-4-1 Okubo, Shinjuku-ku, Tokyo 169

Abstract

We study the dynamics of topological defects in the context of topological inflation. Analysing the time evolutions of planar domain walls and of global monopoles, we find that the defects undergo inflationary expansion if the vacuum expectation value of the Higgs field η is comparable to the Planck mass m_{Pl}, which confirms the results of Vilenkin and Linde. We also examine the effect of gauge field for static monopole solutions and find that gauge field changes the nature of spacetime around a monopole. It suggests that the effect of gauge fields cannot be negligible.

1 Introduction

Recently, Vilenkin [1] and Linde [2] independently pointed out that topological defects can be seeds for inflation. The basic idea of topological inflation is as follows. Suppose we have the Higgs field Φ^a $(a = 1, \cdots, N)$, whose potential is

$$V(\Phi) = \frac{1}{4}\lambda(\Phi^2 - \eta^2)^2, \quad \Phi \equiv \sqrt{\Phi^a \Phi^a}. \tag{1.1}$$

This model gives rise to different types of topological defects, *i.e.*, domain walls for $N = 1$, cosmic strings for $N = 2$ and monopoles for $N = 3$. Because the center of a defect must be in the false vacuum state ($\Phi = 0$), there is a possibility that inflation occurs near $\Phi = 0$. Vilenkin and Linde claimed that topological defects expand exponentially if

$$\eta \gtrsim m_{Pl} \tag{1.2}$$

for the following reasons.

1. If the size of the false vacuum region is greater than the horizon size, it is natural to assume that this region undergoes inflationary expansion. The thickness of a domain wall in a flat spacetime is given by $\delta_0 = \sqrt{2}/\sqrt{\lambda}\eta$, and the horizon size corresponding to the vacuum energy $V(0)$ is $H_0^{-1} = \sqrt{3/2\pi\lambda}(m_{Pl}/\eta^2)$. Then the condition $\delta_0 > H_0^{-1}$ implies $\eta \gtrsim m_{Pl}$ [1].

[1-4]electronic mail: [1]sakai@cfi.waseda.ac.jp, [2]shinkai@cfi.waseda.ac.jp,
[3]63L507@cfi.waseda.ac.jp, [4]maeda@cfi.waseda.ac.jp

2. New inflation or chaotic inflation occurs in Friedmann-Robertson-Walker spacetime if slow-rolling condition, $|\ddot{\Phi}| \ll 3H|\dot{\Phi}|$, $\dot{\Phi}^2/2 \ll V(\Phi)$, is satisfied. In the model (1.1) this condition leads to $\eta \gg m_{Pl}/\sqrt{6\pi}$ [1, 2].

3. Gravitational effect cannot be neglected if the Schwarzschild radius $r_g = 2M/m_{Pl}^2$ is comparable to δ_0, where $M \approx (4\pi/3)\delta_0^3 V(0)$. This condition is reduced to $\eta \gtrsim \sqrt{3/8\pi} m_{Pl}$ [1, 2].

4. In the case of a global string (monopole) there is a deficit angle in the static solution. This exceeds 2π (4π) for $\eta > m_{Pl}$, which indicates no static solution with an external asymptotically flat region [1].

5. Linde referred the previous papers [4] of gauged monopoles to verify the condition (1.2). It was shown in [4] and [5] that nonsingular monopole solutions exit only if $\eta \lesssim m_{Pl}$; otherwise, the monopole becomes Reissner-Nordström black hole.

6. Bass and Vilenkin [3] studied a related problem of static defect solutions in de Sitter spacetime, disregarding the gravitational backreaction of the defects on the background spacetime. They showed that static solutions exist only if $\delta_0 < H^{-1}/2$, where H^{-1} is de Sitter horizon.

In this paper we study topological inflation in detail in numerical relativity. On this subject, we need to clarify the following points.

First, although the condition for inflation to occur, (1.2), looks plausible, it is based on the naive discussions, which did not show that the defects really inflate. It is important to verify their arguments by numerical analysis which includes the gravitational effect completely.

Secondly, Vilenkin and Linde assumed the initial size of defects to be δ_0, which stems from the static solution without gravity. We expect that δ_0 expresses the typical size of the defects which remain stable. In the beginning of phase transition, however, the scalar field takes its phase randomly and the global distribution may be chaotic. Therefore, it is worth while studying the dynamics of the defects with various initial sizes.

Thirdly, the effect of gauge fields is unclear. Linde suggested that gauge fields do not affect inflation of strings nor monopoles, because the field exponentially decreases during inflation. Although we agree that, once inflation occurs, their effect gets smaller and smaller, it remains an unsettled question whether or not gauge fields affect the onset of inflation.

In order to answer the first and the second questions, we investigate the evolution of planar domain walls in §2 and global monopoles in §3. As to the third question, we discuss static monopole solutions in §4.

2 Evolution of Planar Domain Walls

To begin with, we shall investigate evolution of domain walls ($N = 1$) in a planar symmetric spacetime. We assume that the metric has a form,

$$ds^2 = -dt^2 + e^{F(t,x)}dx^2 + e^{Q(t,x)}dy^2 + e^{U(t,x)}dz^2, \tag{2.1}$$

and use the ADM formalism to pursue its dynamics. The basic numerical scheme was shown in [6]. By analogy with the static solution in a flat spacetime, we tentatively assume an initial configuration of the scalar field to be

$$\Phi(t = 0, x) = \eta \tanh(\frac{x}{\delta}), \quad \dot{\Phi}(t = 0, x) = 0, \tag{2.2}$$

where a dot denotes derivative with respect to t, and δ is a parameter of the initial width of the domain wall. (δ is a coordinate length, and later we will introduce a proper length of the initial width, Δ.) We adopt the periodic boundary condition and the constant-mean-curvature slicing condition on the initial hypersurface:

$$\text{(volume expansion rate)} \equiv \frac{\dot{F} + \dot{Q} + \dot{U}}{2} = 3\sqrt{\frac{8\pi}{3m_{Pl}^2}V(0)}\tilde{K}, \tag{2.3}$$

where $\tilde{K}$ is a positive constant. By solving the constraint equations of the Einstein equations, we obtain $\tilde{K}$ and the initial values of F, Q and U. The range of the parameters is $10^{-4} \leq \lambda \leq 10$, $0.25m_{Pl} \leq \eta \leq 2.5m_{Pl}$ (in (1.1)) and $0.5 \leq \delta/\delta_0 \leq 2$.

In Fig.1 we show two typical examples of the time evolutions: the case of $\eta = 0.5m_{Pl}$ and that of $\eta = 2m_{Pl}$. We see the latter is expanding exponentially while the former is not. Pursuing the time evolution until $t = 10H_0^{-1}$, we classify spacetimes into two groups: the ones which expands exponentially and the ones which do not. We summarize in Fig.2 which parameters allow inflation. From Fig.2(a) we confirm whether inflation occurs or not is determined mainly on η, but has little dependence on λ. If $\eta \gtrsim m_{Pl}$, the domain wall expands exponentially. In Fig.2(b) we see dependence of the dynamics of the spacetime on the initial width of the domain wall. Here we define the initial width of the domain wall Δ by the proper distance between the positions of $\Phi(x_1) = -\eta/2$ and of $\Phi(x_2) = \eta/2$. We also find that if $\Delta > 0.5H_0^{-1}$, the spacetime enters an inflationary phase.

3 Evolution of Global Monopoles

Next, we turn to the case of global monopoles ($N = 3$). We assume a spherically symmetric spacetime:

$$ds^2 = -dt^2 + A^2(t,r)dr^2 + B^2(t,r)r^2(d\theta^2 + \sin^2\theta d\varphi^2). \tag{3.1}$$

For the scalar field, we adopt the hedgehog ansatz:

$$\Phi^a = \Phi(t,r)\hat{\Phi}^a, \quad \hat{\Phi}^a = \omega^a_i \hat{r}^i, \tag{3.2}$$

where $\hat{\Phi}^a$ and $\hat{r}^i$ are a unit radial vector in the internal space and in the real space, respectively, and ω^a_i is a triad. As an initial configuration of the scalar field, we suppose

$$\Phi(t=0,r) = \Phi_{flat}\Big(\frac{r}{c}\Big), \quad \dot{\Phi}(t=0,r) = 0 \tag{3.3}$$

where $\Phi_{flat}(r)$ is the static solution in a flat spacetime, which is obtained only numerically, and c is a parameter of the initial size of monopole normalized by that of the static solution. We set $A = B = 1$ at the initial time and solve the constraint equations of Einstein equations to obtain $\dot{A}$ and $\dot{B}$. As a result, the volume expansion rate has the following approximate form:

$$\text{(volume expansion rate)} \equiv \frac{\dot{A}}{A} + \frac{2\dot{B}}{B} \approx 3\sqrt{\frac{8\pi}{3m_{Pl}^2}\rho(r)}, \tag{3.4}$$

where $\rho(r)$ is the initial distribution of the energy density. The range of the parameters is $10^{-10} \leq \lambda \leq 10$, $0.1m_{Pl} \leq \eta \leq m_{Pl}$ and $0.1 \leq c \leq 100$.

In Fig.3 we show examples of the time evolution of the scalar field, which correspond to a stable monopole ((a) $\eta = 0.2m_{Pl}$) and an inflating monopole ((b) $\eta = 0.6m_{Pl}$), respectively. In the case of (b) we find that the bottle-neck structure appears. Fig.4(a) shows trajectories of the boundary of a monopole. Here we define the boundary as $R_b(t) = Br$ at the position of $\Phi = \eta/2$. We find that a monopole expands if $\eta \gtrsim 0.4m_{Pl}$. This result also supports that of Vilenkin and Linde. We also investigate how the initial size influences the dynamics of a monopole, by varying c. Fig.4(b,c) indicates that whether a monopole expands or not is determined only by η. Even if the initial size is much larger than H_0^{-1}, the configuration eventually approaches to $\Phi_{flat}(r)$. This result contradicts that in the case of domain walls, for which reasons will be discussed in §5.

4 Effect of Gauge Fields for Static Monopole Solutions

Finally we shall discuss the effect of gauge fields for static monopole solutions. We consider the Einstein-Yang-Mills-Higgs system. A static and spherically symmetric spacetime is described as

$$ds^2 = \Big(1 - \frac{2Gm(r)}{r}\Big)e^{-2\delta(r)}dt^2 + \Big(1 - \frac{2Gm(r)}{r}\Big)^{-1}dr^2 + r^2(d\theta^2 + \sin^2\theta d\varphi^2). \tag{4.1}$$

Under the hedgehog ansatz, the Yang-Mills potential is written as

$$A^a_i = \omega^c_i \epsilon^{cab}\hat{r}^b \frac{1-w(r)}{er}, \quad A^a_0 = 0, \tag{4.2}$$

where e is a gauge coupling constant. We search numerically a monopole solution such that the spacetime has a regular origin and become asymptotically flat at infinity. The numerical scheme was shown in [5].

In Fig.5 we present the parameter plane of λ/e^2 and η. The triangle denotes that a static solution exists, while there is no static solution for those parameter values at the cross mark. This indicates that there exists no static solution for $\eta \gtrsim 0.4 m_{Pl}$, where the spacetime may be time-dependent. However, only from this result, we cannot conclude that a monopole inflates. It needs further analysis. Here we investigate how gauge fields affect the character of a static spacetime with a monopole. We pay attention to acceleration of test particles, which is governed by the geodesic equation in the coordinate system (4.1):

$$\frac{d^2r}{d\tau^2} = -\frac{e^{2\delta(r)}}{2}\frac{d}{dr}\left[e^{-2\delta(r)}\left(1 - \frac{2Gm(r)}{r}\right)\right], \tag{4.3}$$

where τ is the proper time and we have assumed $dr/d\tau = d\theta/d\tau = d\varphi/d\tau = 0$. In Fig.6 we present examples for the spacetime with a global monopole and with a gauged monopole. The figures tell us that the spacetime with a global monopole has repulsive nature [7], while the spacetime with a gauged monopole has attractive nature. Both the signs of acceleration do not change even for large η. Therefore, the effect of gauge fields on the spacetime with a monopole may not be able to be ignored.

5 Discussions

We have studied topological inflation in numerical relativity. We have considered three questions on topological inflation and found the following results.

The first subject is just to verify the arguments of Vilenkin and Linde. Our results support their discussions completely: if $\eta \gtrsim m_{Pl}$ is satisfied, planar domain walls and global monopoles inflate. We may extend this result to the case of global strings.

The second is to examine the dynamics of defects with various initial size. Our results indicate that in the case of domain walls (§2), if the initial width of a wall is greater than the horizon scale, the wall causes inflation even for small η. On the other hand, in the case of global monopoles (§3), only η determines whether a monopole expands or not. Even if the initial size of the monopole is much larger than the horizon scale, the monopole shrinks and approaches the stable configuration. The two results look contradictory to each other. We guess this difference stems from the difference in way of giving initial data of the volume expansion rate: (2.3) and (3.4). The former (domain wall) expresses a situation where the external region also has as much volume expansion rate as the region inside the wall does,

since we assume periodic boundary conditions. While the latter (monopole) expresses a situation where the external region has small volume expansion. We speculate, therefore, that the homogeneous initial expansion helps the whole spacetime start inflationary expansion in our analysis of domain walls, although we do not assume an additional scalar field. Hence, we need further investigation about domain walls, by setting different initial conditions.

The final subject we have investigated is the effect of gauge fields. We found that there exists no static solution for $\eta \gtrsim 0.4 m_{Pl}$, where the spacetime may be time-dependent. Comparing the gauged monopole static solution with the global monopole one, we find that those spacetimes have different characters: one is attractive and the other is repulsive. Hence, the effect of gauge fields may not be able to be ignored.

Acknowledgements

We would like to thank Dr K. Nakao for valuable advice about numerical procedure. This work was supported partially by the Grant-in-Aid for Scientific Research Fund of the Ministry of Education, Science and Culture (No.06302021 and No.06640412), by the Grant-in-Aid for JSPS Fellow (No. 053769), and by a Waseda University Grant for Special Research Projects.

References

[1] A. Vilenkin, Phys. Rev. Lett. **72**, 3137 (1994).

[2] A.D. Linde, Phys. Lett. **B327**, 208 (1994);
A. Linde and D. Linde, Phys. Rev. **D50**, 2456 (1994).

[3] R. Basu and A. Vilenkin, Phys. Rev. **D50**, 7150 (1994).

[4] K. Lee, V.P. Nair and E.J. Weinberg, Phys. Rev. **D45**, 2751 (1992);
P. Britenlohner, P. Forgàcs and D. Maison, Nucl. Phys. **B383**, 357 (1992).

[5] T. Tachizawa, K. Maeda and T. Torii, Phys. Rev. **D**, (to be published).

[6] H. Shinkai and K. Maeda, Phys. Rev. **D49**, 6367 (1994).

[7] D. Harari and C. Lousto, Phys. Rev. **D42**, 2626 (1990).

Figure Captions

Fig.1: Examples of the evolution of the spacetime with a domain wall. The ordinate is the volume element of the spacetime, $\gamma(t) \equiv e^{\frac{F+Q+U}{2}}$, and the abscissa is the proper length along the x-axis. We set $\eta = 0.5m_{Pl}$ in (a) and $\eta = 2m_{Pl}$ in (b). $\lambda = 0.01$ and $\delta = \delta_0$ in both the cases. We see that the spacetime goes into an inflationary phase in the case of (b).

Fig.2: We classify spacetimes into two groups: the ones which expand exponentially and the ones which do not. We have three parameters: η, λ and Δ. (a) is a λ-η plane and (b) is a Δ-η plane. The circle denotes a spacetime which goes into an exponentially expansion phase, while the cross denotes a spacetime which does not.

Fig.3: Examples of the evolution of a global monopole. We set $\eta = 0.2m_{Pl}$ in (a) and $\eta = 0.6m_{Pl}$ in (b). $c = 1$ and $\lambda = 0.1$ in both the cases. The case (a) expresses a stable monopole and the case (b) expresses an inflating monopole. In the latter we find that the bottle-neck structure appears.

Fig.4: Dynamics of a global monopole: trajectories of the positions of $\Phi = \eta/2$. $\lambda = 0.1$ in all cases. The case (a) shows the dependence on η ($c = 1$). A global monopole expands if $\eta \gtrsim 0.4m_{Pl}$. The cases (b) and (c) show the dependence on the initial size, c. We set $\eta = 0.2m_{Pl}$ in (b) and $\eta = 0.6m_{Pl}$ in (c). Only η determines whether or not inflation occurs, regardless of the initial size.

Fig.5: Parameter range for a static monopole solution to exist in the Einstein-Yang-Mills-Higgs system. $\lambda/e^2 = 0.1$. The triangle denotes that a static solution exists, while there is no static solution for those parameter values at the cross mark. We find that there exists no static solution for $\eta \gtrsim 0.4m_{Pl}$.

Fig.6: Acceleration of test particles in spacetimes with (a) a global monopole and with (b) a gauged monopole. We set $\lambda = 0.1$ and $\lambda/e^2 = 0.1$, respectively. $\eta = 0.05m_{Pl}$ in both the cases. We find that the spacetime with a global monopole has repulsive nature, while the spacetime with a gauged monopole has attractive nature.

Fig.1(a)

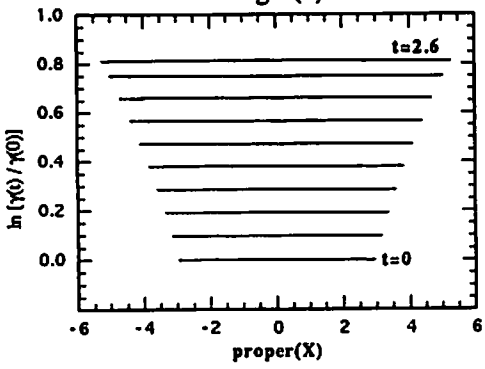

Fig.1(b)

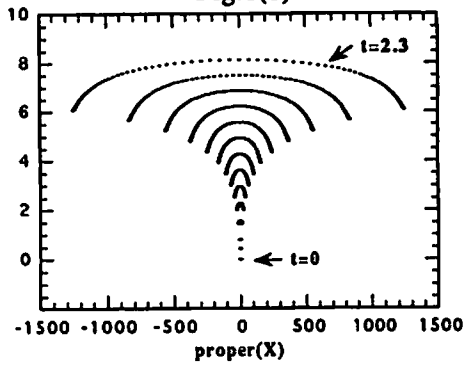

Fig.2(a)

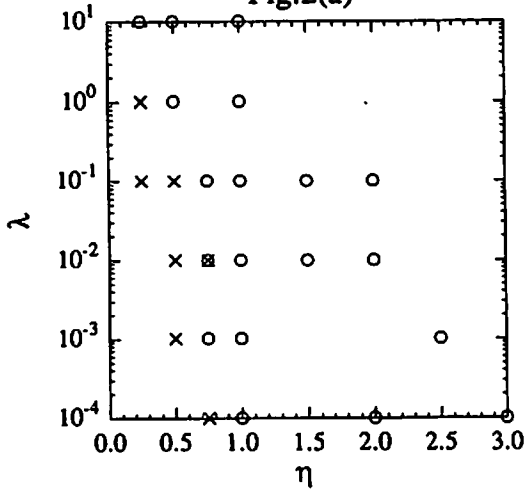

Fig.2(b)

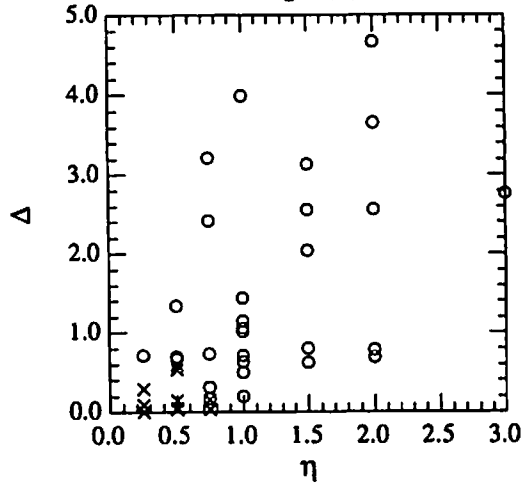

Fig.3(a)

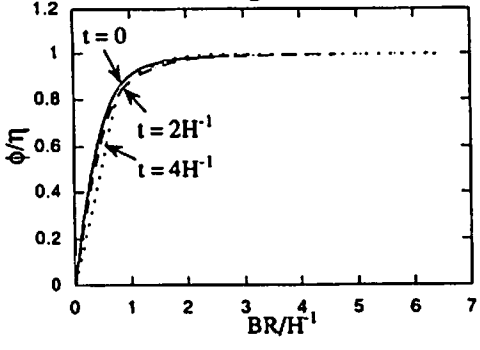

Fig.3(b)

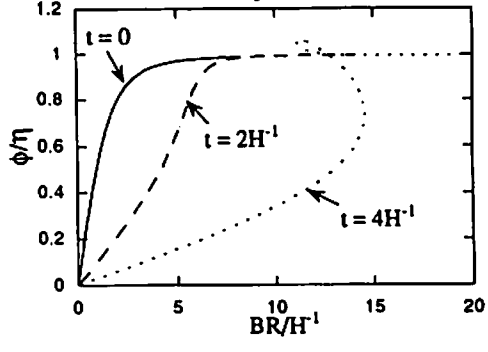

Fig.4(a)

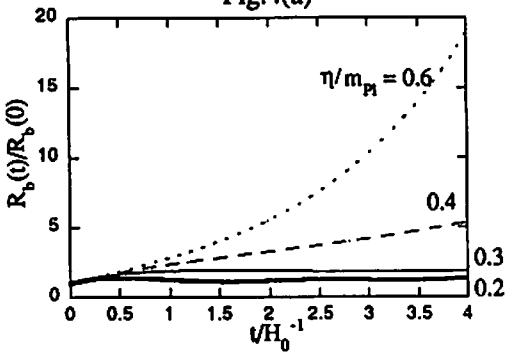

Fig.4(b)

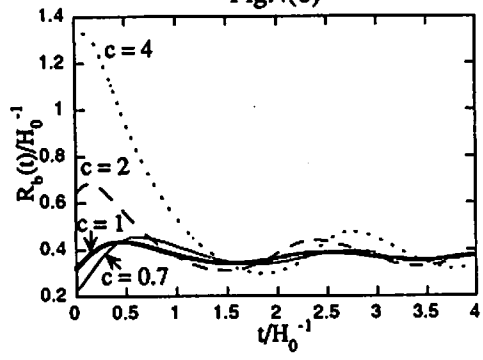

Fig.4(c)

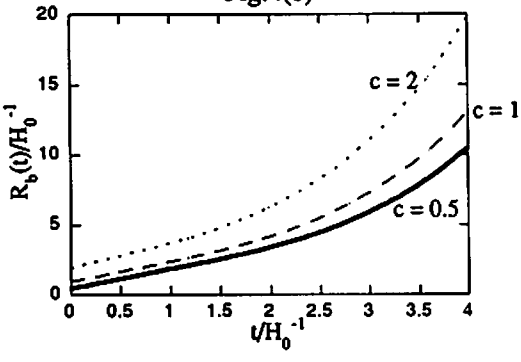

Fig.5

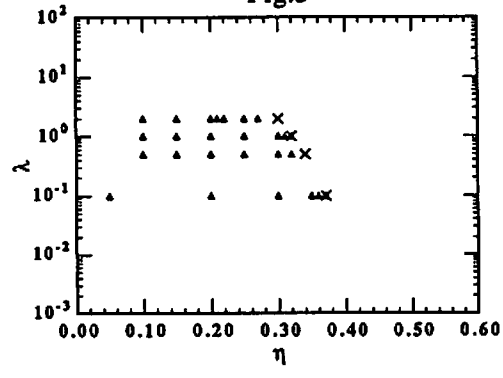

Fig.6(a)

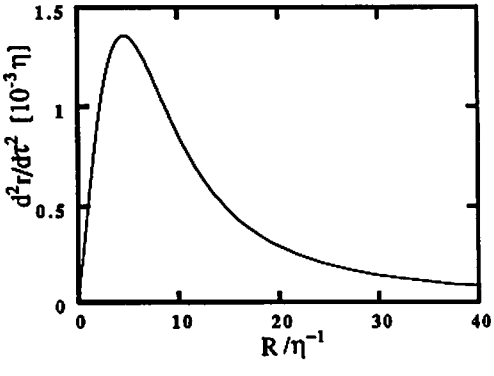

Fig.6(b)

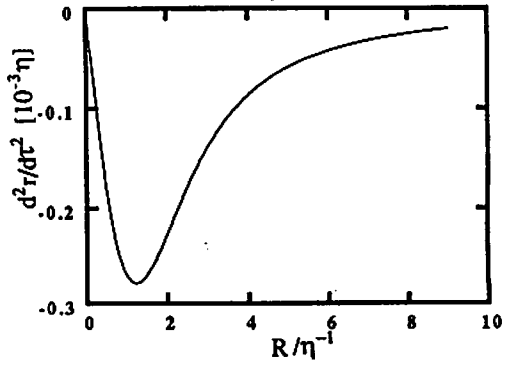

Exponential Potentials and Scalar Field Inflation

Richard Easther[1]
Department of Physics, School of Science and Technology, Waseda University,
3-4-1 Okubo, Shinjuku-ku, Tokyo-to, Japan.

Abstract

We consider the spectrum of primordial fluctuations produced by inflationary models where the inflaton potential is the sum of two exponential terms. A wide range of spectra result, with the only constraint being that the scalar spectrum must have more tilt than the tensor spectrum. This model can mimic the spectra of most inflationary models, as well as producing combinations of scalar and tensor perturbations not found in common varieties of slow-rolling inflation.

1 Introduction

Inflationary models based on exponential potentials have received wide attention. Potentials with exponential terms are associated with superstrings [1, 2, 3], supergravity [4, 5, 6] and theories with an extended gravitational sector [7, 8, 9]. The generic feature of these models is their use of a conformal transformation [10] to move into the Einstein frame, which typically introduces a scalar field with an exponential potential.

A potential consisting of a single exponential term produces power-law inflation [11, 12, 13, 14] which is interesting both as an inflationary model in its own right, and because the inflationary growth [15] and perturbation spectra [12, 16] are known

[1]email: easther@cfi.waseda.ac.jp

exactly. In many instances, however, the potential, $V(\phi)$, may contain more than one exponential term and in this paper we examine models based upon

$$V(\phi) = A \exp\left[-\xi\sqrt{\frac{8\pi}{m_p^2}}\phi\right] - B \exp\left[-\xi m\sqrt{\frac{8\pi}{m_p^2}}\phi\right], \tag{1}$$

with $A, B, \xi > 0$ and $m > 1$. Any specific theory will predict some or all of these parameters. However, by considering inflation driven by a potential with the generic form of equation (1) we can investigate the cosmological constraints upon the model parameters.

The potential, equation (1), produces a rich variety of inflationary behaviour. The essential feature of the model is that $V(\phi)$ has a maximum, near which it is approximately flat, but is dominated by a single exponential term at large ϕ. The two term potential discussed in this paper is recommended by its simplicity, but a large number of models have similar observational consequences. For instance, the potential $V(\phi) \propto \cosh(c\phi)^{-2}$ has a maximum at $\phi = 0$ and reduces to a single exponential at large ϕ. Copeland *et. al.* [17] discuss the inflationary perturbations produced by this potential, which are similar to those found here for equation (1). Exact solutions for potentials consisting of three exponential terms have been presented by the author [18], and the perturbation spectra for these models are also similar to that produced by the two term potential, equation (1).[2]

As in power-law and intermediate [19, 20, 21] inflation there is no natural end to the inflationary era in this model. We adopt the usual approach of specifying a value of ϕ at which inflation ends. The mechanism that ends inflation must not produce unacceptably large inhomogeneities in the microwave background, and must reheat the universe to a high enough temperature to allow baryogenesis. For large negative values of ϕ the potential is not bounded below, so we assume that ϕ does not enter this region. Physically, an unbounded potential often signals the breakdown of some perturbation expansion.

2 The Perturbation Spectrum

The Einstein field equations, when applied to a spatially flat, homogeneous and isotropic universe dominated by a scalar field, give [22, 23]

$$H^2 = \frac{8\pi}{3m_p^2}\left(\frac{\dot{\phi}^2}{2} + V(\phi)\right), \tag{2}$$

$$\ddot{\phi} + 3H\dot{\phi} + V(\phi)' = 0. \tag{3}$$

The Hubble parameter is defined by $H = \dot{a}/a$, where $a(t)$ is the scale factor. The dot and dash denote differentiation with respect to the time, t, and the field, ϕ,

[2]The spectra for the solutions in [18] can be found by the methods used in this paper.

respectively. In the slow rolling approximation these equations reduce to

$$H^2 = \frac{8\pi}{3m_p^2}V(\phi), \tag{4}$$

$$\dot{\phi} = -\frac{V(\phi)'}{3H}. \tag{5}$$

It is convenient to make the change of variables,

$$C = \frac{B}{A}, \tag{6}$$

$$\frac{1-y}{mC} = \exp\left[-(m-1)\xi\sqrt{\frac{8\pi}{m_p^2}}\phi\right]. \tag{7}$$

The potential, equation (1), has its global maximum at $y = 0$, and $y = 1$ corresponds to $\phi \to \infty$. We restrict attention to models where ϕ is monotonically increasing and $y \geq 0$.

Adopting the nomenclature of Liddle and Lyth [24], the perturbation spectra are described in terms of the parameters ϵ and η, where

$$\epsilon = \frac{m_p^2}{16\pi}\left[\frac{V(\phi)'}{V(\phi)}\right]^2, \tag{8}$$

$$\eta = \frac{m_p^2}{8\pi}\frac{V(\phi)''}{V(\phi)}. \tag{9}$$

The scalar (density) perturbation index, n, and the tensor (gravitational) perturbation index, n_g, are

$$n = 1 + 2\eta - 6\epsilon, \tag{10}$$

$$n_g = -2\epsilon. \tag{11}$$

It will be useful to define n in terms of n_d, where $n_d = n - 1$. If n_d and n_g are zero, then the corresponding spectrum is flat, or scale-free. Conversely, if the indices are non-zero, then the spectra are tilted. For high order terms in the multipole expansion the ratio of the tensor and scalar perturbation amplitudes, R, is [32]

$$R = 12.4\epsilon. \tag{12}$$

The above relationships apply to all inflationary models driven by a slowly rolling scalar field. From these expressions alone we see that the scalar and tensor perturbation spectra produced by inflation cannot be specified arbitrarily. In particular, if the spectrum of primordial gravitational waves is flat ($\epsilon \lll 1$), then it will also be of negligible amplitude compared to the scalar perturbations.

Expressed in terms of y, the parameters ϵ and η derived from $V(\phi)$, equation (1), are

$$\epsilon = \frac{m^2\xi^2}{2}\left[\frac{y}{m-1+y}\right]^2, \tag{13}$$

$$\eta = m\xi^2\frac{1-m+my}{m-1+y}, \tag{14}$$

leading to

$$n_d = \frac{m\xi^2}{(m-1+y)^2}\left[2(1-m)^2(y-1)-my^2\right], \tag{15}$$

$$n_g = -m^2\xi^2\left[\frac{y}{m-1+y}\right]^2. \tag{16}$$

These expressions depend only on m and ξ, and the field value ϕ (or y) at which the perturbations are produced.

The indices n_d and n_g can have a wide variety of values. Since $\epsilon \geq 0$ by definition, all slowly rolling inflationary models predict $n_g \leq 0$. From equations (15) and (16) we deduce $n_d \leq n_g$, with the equality holding only when $y = 1$. Hence for this model we have the relationship

$$n_d \leq n_g \leq 0. \tag{17}$$

This constraint is satisfied by almost all inflationary models, with the exceptions of false vacuum or hybrid inflation [25, 26] and intermediate inflation which may have $n_d > 0$. Thus inflation driven by the potential, $V(\phi)$, can mimic most of the usual models of inflation (tabulated by Liddle and Lyth [24], for instance). Furthermore, many combinations of n_g and n_d which satisfy equation (17) are not found in common inflationary models.

Consider the limiting cases $y \approx 0$ and $y \approx 1$ separately. When $y \approx 0$, the field point is rolling off the global maximum of the potential. In this case the tensor perturbations are of negligible amplitude, since $\epsilon \approx 0$, but the scalar perturbations may be sharply tilted, with

$$n_d(y=0) = -2m\xi^2. \tag{18}$$

This spectrum is identical to that produced by natural inflation [27, 28], where the field rolls off the maximum of a potential, $V(\phi) \propto 1 - \cos(\phi/f)$.

When $y \approx 1$, ϕ is large and the potential is dominated by the first term in equation (1), since it is assumed that $m > 1$. This limiting case then reduces to power-law inflation driven by a single exponential potential. The perturbation spectra for power-law inflation are known exactly [12, 16] but if the slow-rolling approximation is valid then

$$n_d(y=1) = n_g(y=1) = -\xi^2. \tag{19}$$

3 Observational Constraints

The strongest observational constraints on inflationary models are derived from the primordial perturbation spectrum. At large scales, COBE [29] and the Tenerife experiment [30] have been combined to give the 1σ lower bound, $n \geq 0.9$, although this bound will weaken considerably at the 2σ level. Adams *et. al.* [28] review the limits on n derived from a variety of sources. They conclude that the COBE results, combined with the requirement that galaxies form sufficiently early, requires $n \geq 0.6 - 0.7$, and that these bounds are raised if tensor perturbations make a significant contribution to the COBE signal. On the other hand, the APM survey [31] together with standard Cold Dark Matter (CDM) requires a sharply tilted scalar index, with $n \leq 0.6$. Liddle and Lyth [32] combine the COBE data with the QDOT survey [33] to obtain $n > 0.7$ for a purely scalar perturbation, rising to $n > 0.84$ for power-law inflation, which has a significant contribution from tensor perturbations.

Clearly, not all of these bounds can be satisfied simultaneously. However, constraints at shorter scales are sensitive to the composition of the dark matter, the baryon content of the universe, a non-zero cosmological constant and scale dependent biasing. Microwave background experiments at angular scales above one degree (such as COBE and Tenerife) probe the primordial spectrum directly as the inhomogeneities they observe have not evolved significantly since they re-entered the horizon. The latter experiments, often in conjunction with galaxy surveys at smaller scales, typically put a lower limit on n. Consequently, we will assume that the lower bounds on n described above are more robust, and fit the model discussed in this paper to them. This is a more stringent constraint than fitting to the APM data, since the model here has no difficulty producing large amounts of tilt.

For definiteness we take the bounds derived by Liddle and Lyth [32]. They give the following constraints from QDOT (with CDM) and the One Year COBE DMR anisotropy, respectively:

$$0.8\left(\frac{2.9-n}{1.9}\right)^{2/3} < b_8 < 1.4\left(\frac{2.9-n}{1.9}\right)^{2/3} \tag{20}$$

$$0.7\sqrt{1+R}\exp\left[2.62(1-n)\right] < b_8 < 1.5\sqrt{1+R}\exp\left[2.62(1-n)\right] \tag{21}$$

where b_8 is the bias factor and the uncertainties are taken at the 2σ level. The COBE limit increases if there is a significant component of tensor perturbations, whose relative amplitude is given by R.

Treating y_* (the value of value of y at which presently observable perturbations are generated) as adjustable, the spectra are determined by ξ, m and y_*. The region of parameter space where the constraints of equations (20) and (21) are both satisfied is plotted in Figure 1. While the numerical bounds adopted here are generous, the shape of the allowed region of parameter space is relatively insensitive to them, but shrinks as the bounds are tightened.

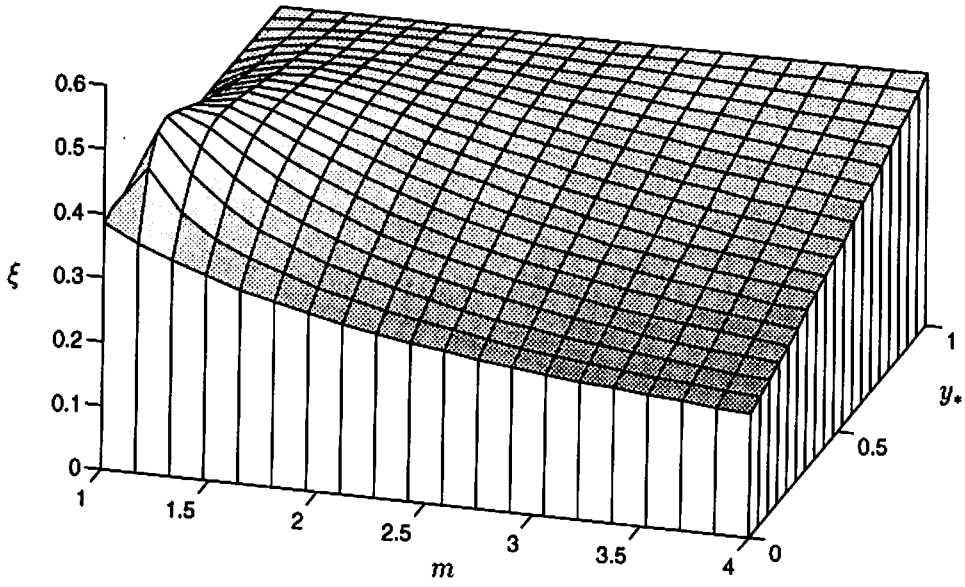

Figure 1: The region of parameter space where the constraints on b_8 from QDOT and COBE are both satisfied by the inflationary perturbation spectrum produced by $V(\phi)$, equation (1).

The limiting values of $y_* = 0$ and $y_* = 1$ correspond to the spectra produced by natural and power-law inflation, respectively. For $y_* = 0$, the constraints on b_8 require $n \geq 0.7$, or $2m\xi^2 \leq 0.3$. When $y_* = 1$ the added contribution from tensor perturbations tightens this limit to $n \geq 0.85$, or $\xi^2 \leq 0.15$. If $m\xi^2 \leq 0.15$ (remembering $m > 1$) the resulting spectrum satisfies the constraint of equations (20) and (21) at all values of y_*. Conversely, if $\xi \gtrsim 0.5$ there are no values of m and ξ which produce a viable perturbation spectrum. However, while $\xi \lesssim 0.5$, the co-efficient in the second exponential in $V(\phi)$, $m\xi$, may be of order unity.

The dominant second order corrections to the spectral indices [16] are proportional to $m^2\xi^4$. If $m \lesssim 5$, then the first order expressions for n and n_g, equations (10) and (11), are valid whenever the inequalities of equations (20) and (21) are satisfied. At larger values of m the second order corrections may be large, even when the spectral indices calculated from the first order expressions satisfy the constraints from COBE and QDOT.

Since $\xi \lesssim 0.5$ to satisfy the constraints on the perturbations, the model has no difficulty providing sufficient inflation to solve the usual cosmological problems. For given values of m and ξ, the perturbation spectra seen in the sky depend on the value of ϕ (or, equivalently, y) at which inflation ceases, and less strongly on the exact mechanism that brings about the transition from inflationary to ordinary expansion.

The matching equation [34] then determines the value of ϕ roughly sixty e-foldings before the end of inflation when the presently observable perturbations were formed. If inflation finishes at $y = y_{end}$, then y_* can be calculated from the matching equation and

$$N_* = \frac{8\pi}{m_p^2} \int_{\phi_{end}}^{\phi_*} \frac{V}{V'} d\phi, \tag{22}$$

where N is the number of e-foldings before inflation ceases. In terms of y,

$$\frac{(y_{end} - 1)^m}{y_{end}^{m-1}} \exp\left[m(m-1)\xi^2 N_*\right] = \frac{(y_* - 1)^m}{y_*^{m-1}}. \tag{23}$$

If y_{end} is not close to 1 and m is large, then $y_* \ll 1$, corresponding to the field point starting at a value of ϕ close to the maximum of the potential, $V(\phi)$. However, for smaller values of m or $\xi \ll 1$, this condition implies that y_* and y_{end} have similar values. While this constraint is expressed in terms of y, physical constraints are applied to ϕ. From equation (7), we see that a condition on y will be satisfied over a larger range of ϕ if ξ or $(m-1)$ is small, weakening any fine-tuning problems.

Finally, the amplitude of the perturbations will fix one of the parameters A and B, or alternatively A and C. From the COBE detection, we have the final constraint [24]

$$\left[\frac{V(\phi_*)}{\epsilon(\phi_*)}\right]^{1/4} = 6.2 \times 10^{16}\text{GeV}. \tag{24}$$

which will fix A in terms of C, y_*, m and ξ. If gravitational waves make a significant contribution then this value will be lowered.

4 Discussion

We have seen that slow-rolling inflation driven by a potential, $V(\phi)$, that consists of two exponential terms, produces a wide variety of inflationary perturbations. The versatility of this model is a consequence of the different inflationary regimes near the maximum of $V(\phi)$ and at large values of ϕ. The observed perturbation spectrum depends on the portion of the potential which the field "saw" when the perturbations that seeded the observable structure in the universe were formed. This is determined by the value of ϕ at which inflation ceases.

Clearly, the presence of several free parameters in $V(\phi)$ is necessary for an inflationary model to be able to produce a wide range of values of n and n_g. However, this is not a sufficient condition. Changing the sign of B in equation (1) does not alter the number of free parameters, but the resulting perturbation spectrum is always approximately similar to that found in a power-law model.

Recently, there has been considerable interest in reconstructing the potential of a slowly rolling scalar field that is hypothesised to have produced the primordial perturbation spectrum [17, 35, 36]. The model developed in this paper can mimic

most varieties of inflation, underlining the point that reconstructions of inflation do not unambiguously identify the inflaton potential, as they do not sample a large enough piece of $V(\phi)$. This is especially relevant while the available experimental data is not sufficiently sensitive to probe the scale dependence of n and n_g.

Inflation driven by a potential composed of two exponential terms, such as equation (1), produces combinations of scalar and tensor perturbations not found in any common slow-rolling model. In particular, a tilted spectrum of scalar perturbations, which is one of the possible solutions to the excess small scale structure in standard CDM, is predicted by both natural and power-law inflation. The tensor perturbations are either negligible (natural inflation) or have the same tilt as the scalar perturbations (power-law inflation). The model developed in this paper may also have a tilted scalar spectrum. The only constraint on the tensor spectrum, however, is that it has less tilt than than the scalar one, which extends the range of possibilities open to the inflationary model builder. Furthermore, exponential potentials are typically associated with power-law inflation, with its characteristic perturbation spectrum. As the model developed here demonstrates, a potential with more than one exponential term may produce a broad range of perturbations, significantly increasing the types of inflationary behaviour that can be associated with exponential potentials.

Acknowledgements

The author is supported by a JSPS Postdoctoral Fellowship.

References

[1] C. G. Callan, I. R. Klebanov, and M. J. Perry, Nuc. Phys. B 278 (1986) 78.

[2] B. A. Campbell, A. Linde, and K. A. Olive, Nuc. Phys. B 355 (1991) 146.

[3] E. S. Fradkin and A. A. Tseytlin, Phys. Lett. B 158 (1985) 316.

[4] A. Salam and E. Sezgin, Phys. Lett. B 147 (1984) 47.

[5] J. J. Halliwell, Nuc. Phys. B 286 (1987) 729.

[6] G. L. Cardoso and B. A. Ovrut, Phys. Lett. B 298 (1993) 292.

[7] G. Magnano and L. M. Sokołowski, Phys. Rev. D 50 (1994) 5039.

[8] S. Mignemi and D. L. Wiltshire, Phys. Rev. D 46 (1992) 1475.

[9] D. Wands, Class. Quantum Grav. 11 (1993) 269.

[10] S. Kalara, N. Kaloper, and K. Olive, Nuc. Phys. B 341 (1990) 252.

[11] L. F. Abbott and M. B. Wise, Nuc. Phys. B 244 (1984) 541.

[12] F. Lucchin and S. Matarrese, Phys. Rev. D 32 (1985) 1316.

[13] F. Lucchin and S. Matarrese, Phys.Lett. B 164 (1985) 282.

[14] B. Ratra, Phys. Rev. D 45 (1992) 1913.

[15] D. S. Salopek and J. R. Bond, Phys. Rev. D 42 (1990) 3936.

[16] E. D. Stewart and D. H. Lyth, Phys. Lett. B 302 (1993) 171.

[17] E. J. Copeland, E. W. Kolb, A. R. Liddle, and J. E. Lidsey, Phys. Rev. D 48 (1993) 2529.

[18] R. J. M. Easther, Class. Quantum Grav. 10 (1993) 2203.

[19] J. D. Barrow, Phys. Lett. B 235 (1990) 40.

[20] J. D. Barrow and P. Saich, Phys. Lett. B 249 (1990) 406.

[21] J. D. Barrow and A. R. Liddle, Phys. Rev. D 47 (1993) R5219.

[22] E. W. Kolb and M. S. Turner, *The Early Universe*, volume 69 of *Frontiers in Physics*, Addison Wesley, Redwood City, California, 1990.

[23] A. D. Linde, *Particle Physics and Inflationary Cosmology*, volume 5 of *Contemporary Concepts in Physics*, Harwood Academic Publishers, Chur, Switzerland, 1990.

[24] A. R. Liddle and D. H. Lyth, Phys. Rep. 231 (1993) 1.

[25] E. J. Copeland, A. R. Liddle, D. H. Lyth, E. D. Stewart, and D. Wands, SUSSEX-AST 94/1-1, astro-ph@babbage.sissa.it 9401011 (1994).

[26] A. Linde, Phys. Rev. D 49 (1994) 748.

[27] K. Freese, J. A. Frieman, and A. V. Olinto, Phys. Rev. Lett. 65 (1990) 3233.

[28] F. C. Adams, J. R. Bond, K. Freese, J. A. Frieman, and A. Olinto, Phys. Rev. D 47 (1993) 426.

[29] G. F. Smoot et al., Ap. J 396 (1992) L1.

[30] S. Hancock et al., Nature 367 (1994) 333.

[31] S. J. Maddox, G. Efstathiou, and W. J. Sutherland, Mon. Not. R. astr. Soc. 246 (1990) 433.

[32] A. R. Liddle and D. H. Lyth, Phys. Lett. B 291 (1992) 391.

[33] W. Saunders et al., Nature 349 (1991) 32.

[34] M. S. Turner, Phys. Rev. D 48 (1993) 3502.

[35] E. J. Copeland, E. W. Kolb, A. R. Liddle, and J. E. Lidsey, Phys. Rev. Lett. 71 (1993) 219.

[36] E. J. Copeland, E. W. Kolb, A. R. Liddle, and J. E. Lidsey, Phys. Rev. D 49 (1994) 1840.

Lorentzian Topology Changing Cosmology

A. Ishibashi* , T. Koike† and M. Siino‡

Department of Physics
Tokyo Institute of Technology
Oh-Okayama, Meguro-ku, Tokyo 152
Japan

January 18, 1995

Abstract

A spatially compact hyperbolic Friedmann-Robertson-Walker universe is investigated. It is assumed that an inflation occurred at the beginning which makes it possible that a initial curvature singularity does not appear and spacetime is extended beyond the past horizon. In addition, compact universe is constructed by the identifications of points of spacetime. Then, it is shown that the topology change classically takes place due to the analytic extension and compactifications. The fundamental region of compact universe is investigated. It is found that closed timelike curves appear in the extended regions. A cosmological implication for the topology change is given in which the compact universe is born from the causality violated regions and evolves as the inflationary universe.

1 Introduction

Big-bang universe has a initial singularity. If the universe was born from a singular point where present physical theory breaks down, one has to resign classical physics at there or have a wish to the quantum gravitational theory as an alternative theory of physics. As one of such trial, for example, A. Vilenkin (1983) proposed a cosmological model in which the universe was created by quantum tunneling from "nothing" into a deSitter space[1]. In the model above, he treats a closed Friedmann-Robertson-Walker universe with deSitter expansion of which closed spatial section has a finite minimal size at the beginning and the initial expansion velocity is zero. A. Vilenkin gave the quantum tunneling solution as the Euclidean four-sphere S^4 joined across an equator to the Lorentzian deSitter universe at its minimal size.

Current observations indicate the density parameter $\Omega_0 \simeq 0.1$ and normalized cosmological constant $\lambda_0 \simeq 0.9$, assuming flatness; namely the normalized spatial curvature constant $k_0 = 0$ [2].However there are no direct evidences which support existence of cosmological constant and it does not seems to be exactly $k_0 = 0$. These suggest that the curvature constant k_0 should have a little negative value, that is, the universe is hyperbolic. In addition to the expectation above, the observations of

*e-mail:akihiro@phys.titech.ac.jp
†e-mail:bartok@phys.titech.ac.jp, JSPS fellow
‡e-mail:msiino@phys.titech.ac.jp, JSPS fellow

isotropy of temperature fluctuations of the microwave background support that an inflation happened in the early stage of the universe. So far, an inflation scenario is the only theory which gives a possible solution to the cosmological problems; flatness problem, horizon problem, monopole problem [3], [4]. During an inflation epoch, the universe is approximated to the deSitter spacetime. If an inflation occurred initially in the hyperbolic universe then we notice that the scalar polynomials of curvature do not necessarily diverge on the initial surface where, even though, spatial volume becomes zero. In other words, there is a possibility that there is no initial curvature singularity. In such case, it is natural to extend space-time beyond past null infinity $\mathcal{I}^-$ and we can argue the structure of the spacetime beyond the beginning of the universe without quantum gravitational theory.

Now we are going to discuss the cosmology without initial curvature singularity. Especially, we investigate the case that our universe is spatially compact, in which case we show that the topology change classically occurs. Topology changes are prosperously investigated in quantum theory(semi-classical theory) as the quantum tunneling solutions of the Einstein equation which consist of compact Euclidean geometries joined to Lorentzian geometries [5]. Various topology changes are presented as quantum tunneling solutions in the (2+1)-dimensional spacetime with negative cosmological constant [6]. There are some works on the topology change in classical gravity [7]. M. Siino(1994) investigated in the case of (2+1)-dimensional compact black hole in which the topology change occurs due to the compactifications and the analytic extensions in the (2+1)-dimensional anti-deSitter spacetime. This suggests that topology change can take place in the compactified (3+1)-dim deSitter universe with hyperbolic chart and there appear closed timelike curves in the spacetime. In this paper, we are trying to study the topology change in the hyperbolic Friedmann-Robertson-Walker spacetime with the deSitter like expansion phase and give a cosmological implication.

2 Hyperbolic Friedmann-Robertson-Walker universe

As we discussed in the preceding section, we are going to treat a hyperbolic FRW(Friedmann-Robertson-Walker) universe in the inflationary expansion phase. The metric is given by

$$ds^2 = -dt^2 + a(t)^2[d\xi^2 + sinh^2 t(d\theta^2 + \sin^2\theta d\psi^2)]. \tag{1}$$

In addition, we assume that an inflation occurred in the early stage of the universe by the homogeneous scalar field $\phi(t)$ which energy-momentum tensor is described as

$$T_{ab} = \nabla_a\phi\nabla_b\phi - \frac{1}{2}g_{ab}\left(\nabla^c\phi\nabla_c\phi + V(\phi)\right). \tag{2}$$

Then the Einstein equation and the conservation law $\nabla_c T^c{}_a = 0$ are written as follows

$$3\left(\frac{\dot{a}}{a}\right)^2 - \frac{3}{a^2} = \frac{1}{2}\dot{\phi}^2 + V(\phi), \tag{3}$$

$$2\frac{\ddot{a}}{a} + \left(\frac{\dot{a}}{a}\right)^2 - \frac{1}{a^2} = -\frac{1}{2}\dot{\phi}^2 + V(\phi), \tag{4}$$

$$\ddot{\phi} + 3\frac{\dot{a}}{a}\dot{\phi} + V'(\phi) = 0, \tag{5}$$

where " t " is taken such that $a = 0$ for $t = 0$ and we normalize $8\pi G = 1$. We assume that the scale factor $a(t)$ and scalar field $\phi(t)$ are analytic functions around $t = 0$. We can see that if the sale factor forms

$$a(t) = t + t^3 S(t), \tag{6}$$

where $S(t)$ is an arbitrary function such that $t\dot{S}(t)$ becomes regular at $t = 0$, then the scalar polynomials of curvature : R, $R_{ab}R^{ab}$, $R_{abcd}R^{abcd}$ do not diverge at $a = 0$, since these scalar polynomials of curvature consist of two parts below

$$\frac{\ddot{a}}{a} = \frac{6S(t) + 6t\dot{S}(t) + t^2\ddot{S}(t)}{1 + t^2 S(t)}, \tag{7}$$

$$\left(\frac{\dot{a}}{a}\right)^2 - \frac{1}{a^2} = \frac{6S(t) + 2t\dot{S}(t) + \{3tS(t) + t^2\dot{S}(t)\}^2}{\{1 + t^2 S(t)\}^2}, \tag{8}$$

both of which are regular at $t = 0$. $S(t)$ is determined by solving the Einstein equation. We know the exact solutions satisfying conditions above, Minkowski spacetime with hyperbolic chart, which is called Milne universe, and deSitter spacetime with hyperbolic chart. The both of them correspond to the case of constant $\phi(t)$. From the Einstein equation, it is proved that the scale factor $a(t)$ is an odd function of t (The proof is given in [9]). It means that the universe is born with initial expansion velocity $\dot{a}(t = 0)$. It is also proved that the scalar field $\phi(t)$ is an even function from the conservation law [9]. It means that the initial velocity of $\phi(t)$ is zero. Therefore the Einstein equation approximately forms

$$\dot{a}^2 - 1 = H^2 a^2, \tag{9}$$

at about $t = 0$, and the solution is the deSitter space

$$a(t) = H^{-1}\sinh(Ht), \tag{10}$$

where $H := \frac{1}{3}V(\phi)$.

3 Analytic Extension

In the previous section, we see that if our universe is the hyperbolic FRW universe and expanded inflationary at the beginning, i.e., $a(t) = t + t^3 S(t)$ near the initial time, we see that the affine length of each past directed geodesic curve is finite and the scalar polynomials of curvature are bounded. Assuming that one can find such solution, all these curves can be extended analytically beyond the past null infinity $\mathcal{I}^-$. To see this we define new coordinates (U, V, θ, ψ) [10] which behave well around hypersurfaces $\mathcal{I}^-$ as follows

$$UV := -\exp\left[2\int \frac{dt}{a(t)}\right] \quad ; \quad \frac{V}{U} := -\exp[2\xi] \quad . \tag{11}$$

In this coordinates the metric is

$$ds^2 = -\frac{a^2}{UV}[dUdV + \frac{(U+V)^2}{4}(d\theta^2 + \sin^2\theta d\psi^2)] \quad . \tag{12}$$

Then we obtain the maximally extended FRW space-time which are composed of four inequivalent regions

$$\begin{array}{ll} I & \{V > 0,\, U < 0\}\,, \\ II & \{V > 0,\, U > 0\}\,, \\ III & \{V < 0,\, U < 0\}\,, \end{array}$$

$$IV \qquad \{V < 0, U > 0\}\,.$$

The region I is the original FRW universe and region IV is the same spacetime as the region I but takes inverse time evolution. In the extended regions II and III , one can take static chart $(\tau, \chi, \theta, \psi)$ defined as follows

$$UV =: \exp\left[2\int \frac{d\tau}{b(\tau)}\right] \quad , \qquad \frac{V}{U} =: \exp[2\chi]\,, \tag{13}$$

$$ib(\tau) := a(i\tau) \tag{14}$$

The metric takes the form

$$ds^2 = d\tau^2 + b(\tau)^2[-d\chi^2 + \cosh^2\chi d\Omega^2] \tag{15}$$

and the Einstein equation and the conservation law are described below

$$3\left(\frac{\dot{b}}{b}\right)^2 - \frac{3}{b^2} = \frac{1}{2}\dot{\phi}^2 - V(\phi)\,, \tag{16}$$

$$2\frac{\ddot{b}}{b} + \left(\frac{\dot{b}}{b}\right)^2 - \frac{1}{b^2} = -\frac{1}{2}\dot{\phi}^2 - V(\phi)\,, \tag{17}$$

$$\ddot{\phi} + 3\frac{\dot{b}}{b}\dot{\phi} - V'(\phi) = 0\,, \tag{18}$$

where '$\cdot$' means 'τ' derivative.

We can also confirm that $b(\tau)$ is an odd function and $\phi(\tau)$ is an even function of τ . Therefore these equations above can be obtained by changing $t \longrightarrow -i\tau$, as the Euclidean versions of equations (3), (4), (5). At about $\tau = 0$, equation (9) approximately forms

$$-\dot{b}^2 - 1 = H^2 b^2\,, \tag{19}$$

and the solution is

$$ib(\tau) = H^{-1}\sin(H\tau)\,. \tag{20}$$

However, 'τ' does not express a time and these equations do not describe evolutions of $b(\tau)$ and $\phi(\tau)$ because the homogeneous slices are time like hypersurfaces in the extended regions. When we compare the Einstein and the conservation equations in the extended regions with those in the original universe, we notice that the difference between them is the only signature of potential $V(\phi)$. The behaviors of scalar field are qualitatively argued in the figure(1).

4 The Lorentzian topology change

Now we consider the case that the universe is spatially compact. Of course, no one knows whether the universe is spatially compact or not. But intuitively the compactness seems to be acceptable notion rather than spreading infinitely since the compact universe has finite volume. We construct the compact spacetime by identifications of points of spacetime, which is the same procedure constructing Misner space in the (1+1)-dimensional case and the compactified 3-dim black hole [8], in the case of (2+1)-dimensional spacetime. We are going to try to construct the case of (3+1)-dimensional spacetime.

The compact hyperbolic FRW spacetime is given as the quotient space of the region I by the discrete subgroup Γ of isometry of spacetime. The orbits of the isometry $SO(3,1)$ are H^3 which can be embedded in the 4-dim Minkowski spacetime $E^{3,1}$ as follows

$$-(y^0)^2 + (y^1)^2 + (y^2)^2 + (y^3)^2 = -1 \tag{21}$$

Then the concrete representation of Γ is given as the following six matrices $\{T_{i=1\sim 6}\}$ in the $E^{3,1}$;

$$T_1 := B_{0-3}(\alpha) \circ R_3\left(\frac{3}{5}\pi\right), \tag{22}$$

$$T_2 := R_2(2\psi) \circ T_1 \circ R_2(-2\psi), \tag{23}$$

$$T_3 := R_3\left(\frac{2}{5}\pi\right) \circ T_2 \circ R_3\left(-\frac{2}{5}\pi\right), \tag{24}$$

$$T_4 := R_3\left(\frac{4}{5}\pi\right) \circ T_2 \circ R_3\left(-\frac{4}{5}\pi\right), \tag{25}$$

$$T_5 := R_3\left(-\frac{4}{5}\pi\right) \circ T_2 \circ R_3\left(\frac{4}{5}\pi\right), \tag{26}$$

$$T_6 := R_3\left(-\frac{2}{5}\pi\right) \circ T_2 \circ R_3\left(\frac{2}{5}\pi\right), \tag{27}$$

where

$$B_{0-3}(\alpha) := \begin{pmatrix} \cosh\alpha & 0 & 0 & \sinh\alpha \\ 0 & 1 & 0 & 0 \\ 0 & 0 & 1 & 0 \\ \sinh\alpha & 0 & 0 & \cosh\alpha \end{pmatrix}, \tag{28}$$

$$R_2(2\psi) := \begin{pmatrix} 1 & 0 & 0 & 0 \\ 0 & \cos 2\psi & 0 & \sin 2\psi \\ 0 & 0 & 1 & 0 \\ 0 & -\sin 2\psi & 0 & \cos 2\psi \end{pmatrix}, \tag{29}$$

$$R_3(\gamma) := \begin{pmatrix} 1 & 0 & 0 & 0 \\ 0 & \cos\gamma & -\sin\gamma & 0 \\ 0 & \sin\gamma & \cos\gamma & 0 \\ 0 & 0 & 0 & 1 \end{pmatrix}, \tag{30}$$

$$\tanh\frac{\alpha}{2} := \frac{\sqrt{40\sqrt{5}-75}}{5}, \quad \cos 2\psi = \frac{\sqrt{5}}{5}, \quad \sin 2\psi = \frac{2\sqrt{5}}{5}. \tag{31}$$

The compact hypersurfaces H^3/Γ are constructed by the identifications

$$y^a \overset{identify}{\longleftrightarrow} y'^b = (T_i)^a{}_b y^b. \tag{32}$$

The rotation $R_3(3\pi/5)$ is necessary so that the quotient space becomes manifold and the value of the boost angle α is determined such that the quotient space H^3/Γ becomes regular (no conical singularity) compact manifold [8], [11]. The physical distance of periodicity is given by multiplying the scale factor $a(t)$ to the α [12]. The fundamental region of H^3/Γ is a hyperbolic dodecahedron [13]. Each of the T_i transforms each surface of a dodecahedron to opposite side after rotating by $\frac{3}{5}\pi$ as illustrated in figure (2).

In the previous section, we see that FRW universe can be extended under suitable situations. When the FRW universe, namely region I , is extended maximally, then the actions of Γ continue on the extended regions. The orbits of the isometry become dS^3 in the regions II , III . Therefore, the compactified hypersurfaces are given as the quotient space dS^3/Γ .

Each quotient space I/Γ , II/Γ , III/Γ , IV/Γ is a Hausdorff manifold, but the quotient space of the maximally extended FRW spacetime by Γ is non-Hausdorff non-manifold. The quotient space; $\{I+II+III+IV\}/\Gamma$ becomes non-Hausdorff manifold if we remove the point $V=U=0$ from the spacetime, because of the same reasons for Misner space [14].

The fundamental region of dS^3/Γ is a domain between two polyhedra, each polyhedron is made up of twelve pentagonal pyramids and twenty

triangular pyramids, and each of the six circles on one polyhedron is identified with a corresponding circle on the other one as illustrated in figure (3). However, we have not confirmed how to identify each surface of pyramids is, i.e. we do not know what the topology of dS^3/Γ is, yet.

The covering manifold dS^3 is a Lorentzian manifold and timelikely separated two points are identified by the compactification above. Hence, closed timelike curves appear in the extended regions. The simplest example is transforming the point $(0,0,0,1)$ on the dS^3 to the point $(\sinh\alpha, 0, 0, \cosh\alpha)$ by T_1 and identifying each other. The points $(0,0,0,1)$ and $(\sinh\alpha, 0, 0, \cosh\alpha)$ are timelikely separated, thus all curves which through these two points are closed timelike curves. Therefore causality is violated in the extended regions and it is meaningless for us to consider further past times of the spacetime. The null surface between the original region and the extended regions, i.e. the causality violated regions, is called chronology horizon. The non-trivial topology change takes place from the extended regions to the original region across the chronology horizon by rearrangement of the homogeneous hypersurfaces from dS^3 to H^3 on the covering manifold, as illustrated in figure(4). This is called Lorentzian topology change which consists of Lorentzian geometries joined to a Lorentzian geometry across a null surface.

5 Summary

We consider the case that the universe has no initial curvature singularity and is spatially compact. We assume that the universe is hyperbolic FRW universe and an inflation had occurred at the beginning which means the violation of the strong energy condition. Then it is possible that the universe has no initial curvature singularity, even though spatial volume becomes zero at the beginning, and is extendible. In addition we construct the compact universe by the identification of points of spacetime. In such case we showed the Lorentzian topology change has occurred with appearing closed timelike curves [7]. We can give a implication that the compact hyperbolic universe has been born in the inflationary phase from the causality violated regions beyond the chronology horizon. The fundamental region of the compact homogeneous hypersurface in the universe is a dodecahedron and that of in the causality violated regions is a region or are regions between two polyhedra. Each of the polyhedra is composed of twelve pentagonal pyramids and twenty triangular pyramids, and each of the six circles on one polyhedron coincides with a corresponding circle on the other one. However, we do not confirm how to identify the boundary of the fundamental region of dS^3/Γ is, namely what the topology of dS^3/Γ is, yet.

The problem of the instability of the chronology horizon arises. In the chronology protection conjecture [15], Hawking(1992) asserted that the expectation value of the energy-momentum tensor of quantum fields would diverge on the chronology horizon and of which back reaction would prevent the chronology horizon from being formed. However, there are some counter results. For example, Sushkov(1994) calculated the energy-momentum tensor of quantum complex scalar field in $(1+1)$ dimensional model of spacetime with the chronology horizon [16]. It is shown that the expectation value of the energy-momentum tensor becomes finite on the chronology horizon for some values of parameters. This problem is not settled down yet.

6 Acknowledgment

T. K. and M. S. thank the Japan Society for the Promotion of Science for financial support.

References

[1] Vilenkin, A. : Phys. Rev. D,**27**, 2848 (1983)

[2] Fukugita, M. et al. : Astrophys. J.,**361**, L1 (1990)

[3] Guth, A. H., Phys. Rev. D,**23**, 347 (1981) ;

[4] Sato, K. M. N. R. A. S. **195**, 467 (1981)

[5] Gibbons, G. W. and Hartle, J. B. : Phys. Rev. D, *42*, 2458 (1990)

[6] Fujiwara, Y., Higuchi, S., Hosoya, A., Mishima, T., and Siino, M. : Phys. Rev. D, *44*, 1756 (1991), Phys. Rev. D, *44*, 1763 (1991), Class. Quantum Grav., 7, 163 (1992)

[7] Geroch, R. P. : J. Math. Phys., **8**, 782 (1967)

[8] Siino, M. : Class. Quantum Grav., **11**, 1995 (1994)

[9] Ishibashi, A. in Master thesis

[10] Sato, H. and Kodama, H. : *General Theory of Relativity* (Iwanami, 1992, in Japanese)

[11] Hitotsumatsu, S. : *High Dimensional Regular Polyhedron* (Nihon-hyouron-sya, 1983, in Japanese)

[12] Nakano, M. : *Introduction to The Hyperbolic geometry* (Sience-sya, 1993, in Japanese)

[13] Weber, C. and Seifert, H., : Die beiden Dodekaederräume, Math. Z. 37, 237-253, (1933)

[14] Hawking, S. W. and Ellis, G. F. R. :*The Large Scale Structure Of Space-Time* (Cambridge University Press, 1973)

[15] Hawking, S. W. : Phys. Rev. D, **46**, 603 (1992)

[16] Sushkov, S. V. : *Quantum Complex Scalar Field In The Two-Dimensional Space-time With Closed Timelike Curves And A Time Machine Problem* (gr-qc/9410008)

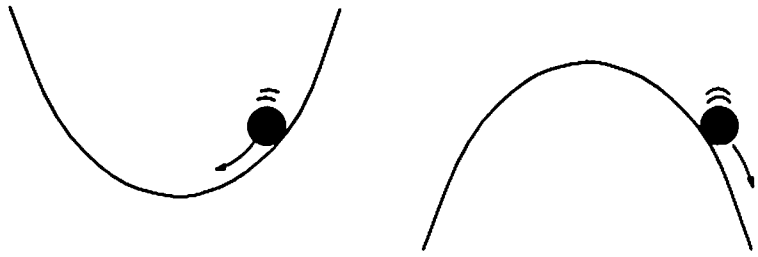

The region I Extended region II, III

Figure 1: The case of $V(\phi) = \frac{1}{2}\mu\phi^2$, which causes the chaotic inflation, is depicted. The universe inflates while the scalar field ϕ slopes down on the gentle slope of the potential in the original region I . In the extended regions I , II , the scalar field is rolling down on the potential slope which goes to be steep because of reversing the signature of the potential. Therefore the potential shape of $\phi(t=0) \leq \phi$ has effect on the behavior of scalar field in the extended regions. This is easily confirmed by numerical investigations.

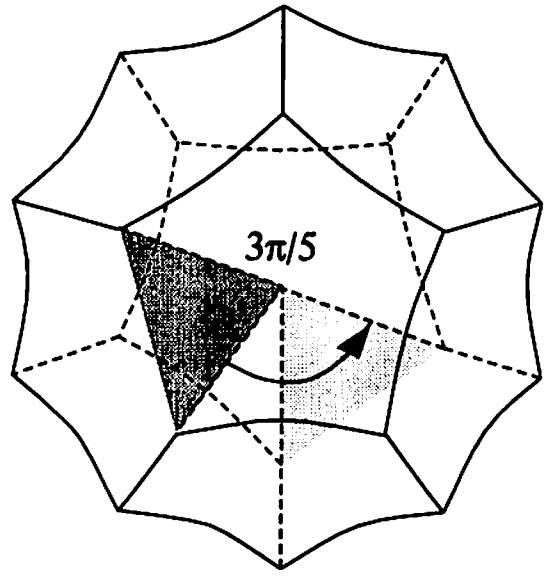

Figure 2: Hyperbolic dodecahedron. A boundary surface of the hyperbolic dodecahedron is rotated by $\frac{3\pi}{5}$ and transformed to the opposite side by T_i .

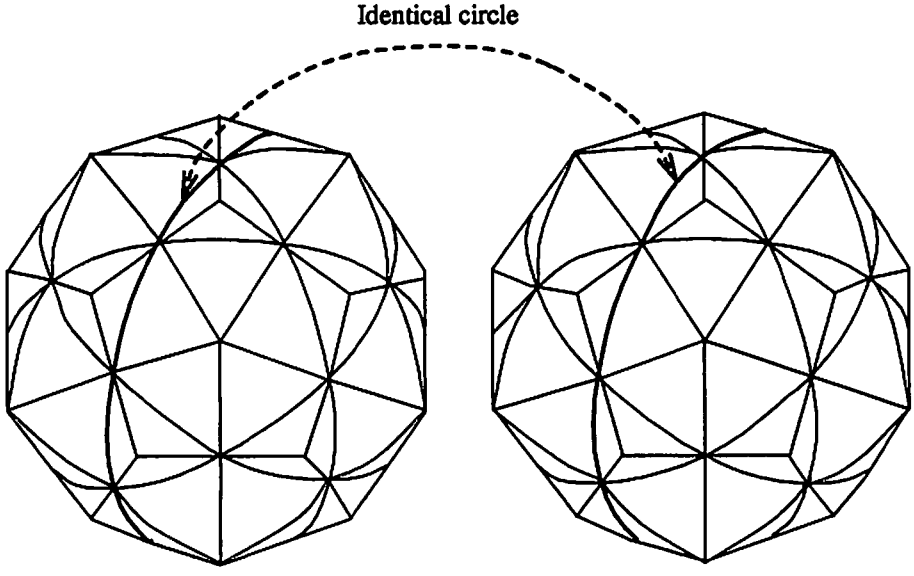

Figure 3: The fundamental region of dS^3/Γ .

CAN QUANTUM MATTER BE AN ENERGY SOURCE TO MAKE A VISIBLE CHANGE IN THE CLASSICAL GEOMETRY?

Shigeru KONNO

Department of Physics, Faculty of Science, Nagoya University, Furoutyou Chikusa-ku Nagoya, Aichi, JAPAN

1. Introduction

It is well known that a negative energy called Casimir energy can be realized to cause visible effects in the laboratory (e.g. Birrell & Davies 1982). According to the theory of general relativity, this quantum originating energy can be, in principle, a source of the classical gravity to cause geometrical effects. It has been long thought that, however, its geometrical effects would be too small to be visible in the laboratory. While, in the modern picture of cosmology, it is believed that there once was a quantum matter dominant epoch called inflationary era. When one discussed dynamics of the spacetime in the inflationary era, the quantum field driving an exponentially rapid expansion of the universe has often been treated as if it were classical matter. However, justification of this picture of the inflationary scenario has not yet proved. One can never be back to the past without *Time Machine* to directly see how the quantum field could affects the classical geometry.

Usual relativists and cosmologists may think that it takes very long time that one can succeed in constructing a complete theory of quantum gravity and, moreover, that it will take further longer time to have its application to quantum cosmology, while, in comparatively near future, one may succeed in obtaining super advanced technology beyond our present imagination. It seems, at least, for the author that it is quite uncertain at present whether progress of the science will be more rapid than that of the technology or vice versa. Therefore, some people may also recognize that researches of possibility of the experimental tests to detect quantum effects on the geometry is as meaningful as researches of quantum theory of gravity, which may die without any experimental prediction in vain.

In this article, believing significant progress of the future technology instead of that of the future quantum theory of gravity, the author would like to propose an example of the experimental test for the possible detection of the *quantum geometrical* effects with a simple toy model. Reality and limitation of this kind of experiment are also briefly discussed in order to derive necessary conditions for the success in detecting the having never been directly seen quantum effects in general relativity because its future success will bring us a key to open a door of the inflationary era in the past.

2. An experimental proposal with a spherical toy model

One of the well known general relativistic effects is a time delay due to gravitational fields. However, the delay is not a proper effect in general relativity but is owing to positivity of the classical energy. In particular, in a static and spherically symmetrical spacetime, namely Schwarzschild's inner and outer solutions, one necessarily has a positive definite time delay when the weak energy condition (e.g. Hawking & Ellis 1973) is imposed on the matter fields. Therefore, it is impossible to have a *negative* time delay in the *classical* Schwarzschild spacetime.

However, when one considers the quantum field theoretical effects, the weak energy condition can be *locally* violated to cause visible phenomena in the laboratory known as the Casimir effects. Here, the term, locally, means that one may believe positivity of the total energy of the whole experimental system to realize a locally negative energy. Keeping this constraint in mind, a simple toy model will be proposed in the below in order to examine possibility of the detection of negative time delay, a quantum effect on the classical geometry, in the laboratory.

A toy model is a Schwarzschild spacetime made by matching the inner and outer solutions. Since the spacetime is spherically symmetric, the positivity of the total energy is trivial if one has a positive definite Schwarzschild mass in the outer solution region. It is the only requirement for the present model, however, since a boundary between the inner and outer solutions usually consists of classical matter, a stronger condition is imposed on the matter field. That is, the dominant energy condition should be satisfied, at least, in the neighborhood of the boundary.

A spacetime metric of the Schwarzschild solution is given in a standard form,

$$ds^2 = -e^{2f(r)}dt^2 + \frac{dr^2}{1-2m(r)/r} + r^2 d\Omega^2, \tag{1}$$

in the c=G=1 unit, and the energy-momentum tensor in the inner region is assumed to have a following form,

$$T_\mu{}^\nu = \mathrm{diag}[-\rho(r), 0, P(r), P(r)]. \tag{2}$$

The form of the energy-momentum tensor is partially motivated by Candelas (1986), in which field theoretical origin of the vacuum energy in the bag model is discussed. However, the present model should be regarded as just a toy model because any scales appearing in the QCD phenomenology are too small to be relevant with the classical geometry. Basic equations derived from the Einstein equation are

$$m' = 4\pi r^2 \rho, \quad f' = \frac{m}{r(r-m)}, \quad P = \frac{m}{2(r-2m)}\rho, \tag{3}$$

where a prime means a derivative with respect to r.

In order to solve the basic equations, one needs, for example, a supplemental equation of state for the matter. Instead of imposing the equation of state, one may

first specify the matter density profile, $\rho(r)$, and the other field variables are then solved. In this article, the later procedure is taken for simplicity. The inner solution region ($0 < r < r_2$) is assumed to consist of two zones. The inner part ($0 < r < r_1$) is a quantum matter region, where the energy density, ρ takes a constant negative value such that the mass function is given by

$$m(r) = \frac{1}{2}ar^3, \quad a \equiv \frac{8}{3}\pi\rho < 0. \tag{4}$$

The outer part ($r_1 < r < r_2$) is a positive density region,

$$\rho(r) = \frac{b}{4\pi r^2} > 0, \tag{5}$$

and the mass function is given by

$$m(r) = \bar{m} + br, \quad \bar{m} \equiv \frac{1}{2}a{r_1}^3 - br_1 < 0. \tag{6}$$

As described before, the positivity of the total mass should be satisfied. Let M be a Schwarzschild mass in the outer solution region. Then the constant parameter, b is given in terms of a, r_1, r_2, and M as

$$b = \frac{M + \mu}{r_2 - r_1}, \quad \mu \equiv -\frac{1}{2}a{r_1}^3 > 0. \tag{7}$$

Since both $\rho(r)$ and $m(r)$ were given, the pressure, $P(r)$, is easily obtained. However, it should be noted that $P(r)$ shows slightly peculiar behavior. In the negative density region ($0 < r < r_1$), $\rho(r)$ and $m(r)$ are negative definite, and, therefore, $P(r)$ is a positive definite function of r, which plays a role of bag pressure in the QCD phenomenology. In the positive density region ($r_1 < r < r_2$), though $\rho(r)$ becomes positive, $m(r)$ remains negative when $r < -\bar{m}/b$. That is, in the region, $r_1 < r < -\bar{m}/b$, $P(r)$ should be interpreted as rather tension than pressure although it will be hard to give justification of the existence of such matter. Instead of justifying the peculiar nature of the matter field, it is better to regard it as the limitation of the present toy model. For $r > -\bar{m}/b$, $\rho(r)$, and $m(r)$ are positive definite if there is no black hole region, where $r < 2m(r)$, and the matter fields behave classically.

Finally, the remaining metric function, $f(r)$, can be solved such that $f(r)$ is continuous everywhere and that the spacetime becomes Schwarzschild's outer solution. In the below, a functional form of $f(r)$ in each region is summarized for $b \neq 1/2$:

$$e^{2f(r)} = \begin{cases} k_2/\sqrt{1 - ar^2} & 0 < r < r_1 \\ (k_1/r)[r - 2(\bar{m} + br)]^{1/(1-2b)} & r_1 < r < r_2 \\ 1 - 2M/r & r_2 < r \end{cases}, \tag{8}$$

where

$$\begin{aligned} k_1 &= (r_2 - 2M)^{-2b/(1-2b)}, \\ k_2 &= k_1 {r_1}^{-3/2}(r_1 - a{r_1}^3)^{(1/(1-2b)+1/2)}. \end{aligned} \tag{9}$$

Now, a simple method to detect a quantum effect on the geometry is proposed. As described before, the noticeable geometrical effect is an occurrence of the negative time delay due to the locally violated weak energy condition. For simplicity, suppose that light rays are emitted from an observer at $r = r_0(> r_2 > r_1)$, $\theta = 0$ such that they pass a center of the (spherically symmetric) experimental machine whose geometry has already been examined and that the light rays are reflected by a test mirror put at $r = r_0$, $\theta = \pi$ such that they return to the observer. If there were not the experimental machine such that the geometry would be described by the Minkowski spacetime, it would take $4r_0 \equiv t_M$ till the observer would receive the light rays. However, it is not the case due to presence of the experimental machine, and the observer will detect time difference between the actual arrival time and t_M. Let the time difference be Δt. Since the gravitational field due to the experimental machine is expected to be comparatively weak, Δt is calculated as

$$\begin{aligned}\Delta t &= 4\int_0^{r_0} \frac{\exp\left(f(r_0) - f(r)\right) dr}{\sqrt{1 - \frac{2m(r)}{r}}} - t_M \\ &\approx 8\left(1 - \frac{r_1}{r_2 - r_1}\log\frac{r_2}{r_1} + \log\frac{r_0}{r_2}\right) M + \left(\frac{20}{3} - \frac{8r_2}{r_2 - r_1}\log\frac{r_2}{r_1}\right)\mu.\end{aligned} \tag{10}$$

The term proportional to M is positive definite and a decreasing function of r_2/r_1, while the term proportional to μ is negative definite and a decreasing function of r_2/r_1. Therefore, if it is possible for r_2/r_1 to take a large value such that the later term is dominant, the negative time delay can be realized in the laboratory. However, it should be noted that one cannot give arbitrary values for M, μ, r_1, and r_2. For example, a vacuum energy, μ, is related with r_1 as $\mu \sim \hbar/r_1$. Moreover, one should impose a further condition on the matter fields that energy density of the quantum matter should not dominate over that of the classical matter. Combining these conditions, a possible way to have a negative time delay is letting r_1 be as small as possible, while r_1 should remain in the *classical* scales. Another way to have a negative time delay is that r_1, r_2, and r_0 are chosen such that $r_1 \sim r_2 \sim r_0$. However, it may need a bit of fine tuning in the *Negative Time Delay Machine.* Further detailed analyses are being examined, especially a case that the negative Casimir energy induced by parallel conducting plates is a gravitational source.

The author thanks Prof. Hosoya and his colleagues for their hospitality.

References

Birrell, N.D. & Davies, P.C.W. Quantum fields in curved space, (Cambridge University Press, Cambridge, 1982) p.96.
Candelas, P. 1986, Ann Phys, 167, 257.
Hawking, S.W., & Ellis, G.F.R, The large scale structure of space-time, (Cambridge University Press, Cambridge, 1973) p.96.

Subcritical Bubbles and Electroweak Phase Transition *

Tetsuya Shiromizu
Department of Physics, Kyoto University, Kyoto 606-01, Japan

Masahiro Morikawa
Department of Physics, Ochanomizu University, Tokyo 112, Japan

Jun'ichi Yokoyama
Uji Research Center, Yukawa Institute for Theoretical Physics
Kyoto University, Uji, Kyoto 611, Japan

We estimate the amplitude of thermal fluctuations by calculating the typical size of subcritical bubbles in cosmological electroweak phase transition and show that this thermal fluctuation effect drastically changes dynamics of the phase transition from the ordinary first order type with supercooling. From this fact, we conclude that the standard electroweak baryogenesis scenario associated with such a first order transition does not work in the minimal standard model in certain conditions.

Recently electroweak baryogenesis scenario has been actively investigated [2] [3]. In this scenario the phase transition must be of first order with supercooling in order to attain a non-equilibrium state for baryon number non-conserving processes. In one-loop appoxmation, the finite temperature effective potential always yields a barrier between the false and the true vacua, *i.e.*, a first order phase transition [4]. However, if thermal fluctuation is too large, the perturbation scheme breaks down and its prediction of a first-order phase transition becomes suspect. Although the dynamics of the phase transition is of primary importance in such a cosmological context, the analyses so far done have mainly been confined in other aspects, namely, spontaneous baryon-number generation in thick walls [2] and charge transport mechanism in thin walls [3]. In fact, if the transition is not of first order with supercooling, then these mechanisms do not work, invalidating the entire scenario. In the present paper we consider effects of thermal fluctuations on the electroweak phase transition paying attention to the role of subcritical bubbles.

So far Gleiser et al. [5] and Dine et al. [6] have estimated the amplitude of thermal fluctuations and obtained the result that they are dominant if $m_H > 80$GeV [5] and therefore the critical bubble cannot be borne due to inhomogeneities of background fields. As the experimental constraint is $m_H > 60$GeV [7], the parameter range allowing electroweak baryogenesis is still open. However, in their analyses, they assumed that the spatial scale of the thermal fluctuation is equal to the correlation length, that is, the inverse mass scale. In the microscopic level, the true nature of the dominant thermal fluctuation would be a perpetual creation and annihilation of spherical subcritical bubbles. Thus one should identify the typical size of the bubbles with that estimated by the statistical ensemble averaging. What we would like to claim here is that the amplitude of the thermal fluctuation sensitively depends on the size of the subcritical bubble. A small change of the size results in a drastic change of the phase transition.

To derive the characteristic scale of a subcritical bubble we shall construct effective Lagrangian for the size of the bubble $R(t)$. In high temperature phase, the motion for the wall of asymmetric subcritical bubble is bounded from the above and then one can obtain the finite thermal average scale $\overline{R}$ of $R(t)$. On the other hand, in the low temperature phase, symmetric subcritical bubble is bounded from the above also and the size is almost the same as the above $\overline{R}$. The correlation length is the maximum scale of thermal correlation and dose not necessarily coincide with the size of the subcritical bubble in general. This means that $\overline{R}$ is smaller than the correlation length and that the amplitude of thermal fluctuation will increase, invalidating perturbation analysis. Intuitively, this means that one cannot find the distinction between symmetric vacuum and asymmetric vacuum and that the spontaneous critical bubble nucleation out of the homogeneous symmetric state, which is usually assumed, cannot happen.

In this paper we concentrate on the minimal standard model. The effective potential with one-loop and finite temperature correction [4] is given by

$$V_T(\phi) = D(T^2 - T_2^2)\phi^2 - ET\phi^3 + \frac{1}{4}\lambda_T\phi^4, \tag{1}$$

where

---

*See Ref.[1] also.

$$D = \frac{1}{24}\left[6(\frac{m_W}{\sigma})^2 + 3(\frac{m_Z}{\sigma})^2 + 6(\frac{m_t}{\sigma})^2\right] \sim 0.169, \tag{2}$$

$$E = \frac{1}{12\pi}\left[6(\frac{m_W}{\sigma})^3 + 3(\frac{m_Z}{\sigma})^3\right] \sim 0.00965, \tag{3}$$

and

$$\lambda_T = \lambda - \frac{1}{16\pi^2}\left[\sum_B g_B(\frac{m_B}{\sigma})^4 \ln(\frac{m_B^2}{c_B T^2}) - \sum_F g_F(\frac{m_F}{\sigma})^4 \ln(\frac{m_F^2}{c_F T^2})\right] \sim 0.0350, \tag{4}$$

where we have taken $m_W = 80.6$GeV, $m_Z = 91.2$GeV, $m_t = 174$GeV and $\sigma = 246$GeV [8]. In this case $T_2 = \sqrt{(m_H^2 - 8B\sigma^2)/4D} \sim 92.69$GeV and the critical temperature at which the hight of the potential at two local minima, $\phi_- := 0$ and $\phi_+ := \frac{3ET}{2\lambda_T}[1 + \sqrt{1 - \frac{8\lambda_T D}{9E^2T^2}(T^2 - T_2^2)}]$, degenerates is $T_c = T_2/\sqrt{1 - E^2/\lambda_T D} \sim 93.43$GeV, where

$$B = \frac{1}{64\pi^2}\left[6(\frac{m_W}{\sigma})^4 + 3(\frac{m_Z}{\sigma})^4 - 12(\frac{m_t}{\sigma})^4\right] \sim -0.00456. \tag{5}$$

The temperature at which the global minimum appears is $T_1 = T_2/\sqrt{1 - 9E^2/8\lambda_T D} \sim 93.52$GeV.

We have also chosen the minimal value $m_H = 60$GeV for Higgs mass permitted from experimental constraint. As the thermal fluctuation is an increasing function of the Higgs mass, it is sufficient for our purpose if thermal fluctuation is shown to be too large with $m_H = 60$GeV. On the other hand, in order to avoid baryon number destruction due to sphaleron-mediated processes after the phase transition, we need $m_H < 55$GeV in one-loop perturbation theory [9]. Further, Shaposhnikov has obtained the result $m_H < 100$GeV in lattice calculation [10]. Recently, the loop correction for the sphaleron transition rate have been estimated and in this case $m_H < 63$GeV [11]. Thus, the possibility for the explanation of the present net baryon-number remains at present time.

As we have already mentioned, the typical size of thermal fluctuation is a calculable quantity. Since one cannot use the instanton method for them, we must invent new method. The subcritical bubble which minimizes the free energy would have the $O(3)$ symmetry. Hence in the Lagrangian,

$$L = \int d^3x\left[\frac{1}{2}\dot{\phi}^2 - \frac{1}{2}(\nabla\phi)^2 - V_T(\phi)\right], \tag{6}$$

we adopt the following ansatz for the bubble configuration:

$$\phi = \phi_+ \exp\left[-\frac{r^2}{R(t)^2}\right], \qquad r := |\mathbf{x}|, \tag{7}$$

where $R(t)$ is the size of subcritical bubble and is time dependent. Without any definite argument, previous authors have chosen the correlation length $\ell(T) = 1/\sqrt{2D(T^2 - T_2^2)}$ as the typical size $R(t)$. However, in the microscopic level, the bubble has dynamics. Inserting (7) into the above Lagrangian (6) yields an effective Lagrangian for $R(t)$:

$$L_{eff} = \frac{15\pi^{3/2}}{16\sqrt{2}}\phi_+^2 R\dot{R}^2 - \frac{3\pi^{3/2}}{4\sqrt{2}}\phi_+^2 R - \frac{\pi^{3/2}}{2\sqrt{2}}D(T^2 - T_2^2)\phi_+^2 R^3 + \frac{\pi^{3/2}}{3\sqrt{3}}ET\phi_+^3 R^3 - \frac{\pi^{3/2}}{32}\lambda_T\phi_+^4 R^3. \tag{8}$$

Applying the variational principle on $R(t)$ we obtain the equation of motion for $R(t)$:

$$\frac{d^2R}{dt^2} + \frac{1}{2R}(\frac{dR}{dt})^2 + \frac{2}{5}\frac{1}{R} + \frac{4}{5}D(T^2 - T_2^2)R - \frac{8\sqrt{2}}{15\sqrt{3}}ET\phi_+ R + \frac{1}{10\sqrt{2}}\phi_+^2\lambda_T R = 0. \tag{9}$$

In the vicinity of the turning point $|dR/dt| \ll 1$, one can omit the second term of the left-hand-side and then we get an energy equation by multiplying dR/dt and integrating over t, which reads

$$\frac{1}{2}\left(\frac{dR}{dt}\right)^2 + \mathcal{U}(R, \phi_+, T) = E_0, \tag{10}$$

with

$$\mathcal{U}(R, \phi_+, T) := \frac{2}{5}\ln\frac{R}{R_c} + \left[\frac{2}{5}D(T^2 - T_2^2) - \frac{4\sqrt{2}}{15\sqrt{3}}ET\phi_+ + \frac{1}{20\sqrt{2}}\lambda_T\phi_+^2\right]R^2 \tag{11}$$

where E_0 is a constant of motion and $R_c := \sqrt{E_0/U(\phi_+,T)}$ is the turning radius. The potential $U(R,\phi,T)$ is a monotonically increasing function of R and therefore the wall motion is restricted from the above in the high temperature phase($T > T_c$). The existence of the upper limit will give the typical size of the subcritical bubble.

What we would like to obtain is the typical size of a subcritical bubble. In order to estimate it we must construct the Hamiltonian which describes the dynamics for $R(t)$. The canonical momentum is defined by

$$P := \frac{\partial L_{eff}}{\partial \dot{R}} = \frac{15\pi^{3/2}}{8\sqrt{2}}\phi_+^2 \dot{R}R. \tag{12}$$

The effective Hamiltonian then becomes

$$\begin{aligned} H_{eff}(R,P) &:= P\dot{R} - L_{eff} \\ &= \frac{4\sqrt{2}}{15\pi^{3/2}\phi_+^2}\frac{P^2}{R} + \frac{3\pi^{3/2}}{4\sqrt{2}}\phi_+^2 R + \left[\frac{\pi^{3/2}}{2\sqrt{2}}D(T^2 - T_2^2)\phi_+^2 - \frac{\pi^{3/2}}{3\sqrt{3}}ET\phi_+^3 + \frac{\pi^{3/2}}{32}\lambda_T\phi_+^4\right]R^3 \\ &=: \frac{4\sqrt{2}}{15\pi^{3/2}\phi_+^2}\frac{P^2}{R} + W(R) \\ &=: \frac{4\sqrt{2}}{15\pi^{3/2}\phi_+^2}\frac{P^2}{R} + \frac{R}{\alpha} + \frac{R^3}{\beta}. \end{aligned} \tag{13}$$

Thus the thermal average of R is given by

$$\begin{aligned} \overline{R} &:= \frac{\int \frac{dPdR}{2\pi} R\exp\left[-\frac{H_{eff}}{T}\right]}{\int \frac{dPdR}{2\pi}\exp\left[-\frac{H_{eff}}{T}\right]} \\ &= \frac{\int_0^\infty dRR^{3/2}\exp\left[-\frac{W(R)}{T}\right]}{\int_0^\infty dRR^{1/2}\exp\left[-\frac{W(R)}{T}\right]} \\ &\sim \frac{\int_0^\infty dRR^{3/2}\exp\left[-\frac{R}{\alpha}\right]}{\int_0^\infty dRR^{1/2}\exp\left[-\frac{R}{\alpha}\right]} \\ &\sim \frac{3}{2}\alpha. \end{aligned} \tag{14}$$

As $\alpha \sim 0.015 \ll 1$ and $\alpha^3/\beta \sim 0.5$, the last appoxmation is certainly justified. Further, one must treat carefully the measure. As

$$d\phi = \frac{2\phi_+ r^2}{R^3}e^{-\frac{r^2}{R^2}}dR \tag{15}$$

and

$$dp_\phi = -\frac{32\sqrt{2}r^2}{15\pi^{3/2}R^5\phi_+}e^{-\frac{r^2}{R^2}}PdR + \frac{16\sqrt{2}r^2}{15\pi^{3/2}R^4\phi_+}e^{-\frac{r^2}{R^2}}dP, \tag{16}$$

the original measure becomes

$$\int d^3x d\phi dp_\phi = dRdP\int d^3x\frac{\partial(\phi,p_\phi)}{\partial(R,P)} = dRdP. \tag{17}$$

Thus, naively used measure in eq.(14) is justified. Moreover, since the three-dimensional volume integral is done in eq. (17), weight associated with three volume has already been taken into account. The temperature dependence of eq.(14) is depicted in Fig.1. As one can easily see, the above result gives an *upper* bound for $\overline{R}$. In fact, at $T = T_c$ and $T = T_1$, we numerically obtain the more accurate result that $\overline{R}(T = T_c) = 0.012\text{GeV}^{-1}$ and $\overline{R}(T = T_1) = 0.0202\text{GeV}^{-1}$, respectively. In Fig. 1, we can easily find $\overline{R}(T) < \ell(T)$ as expected.

Next, let us estimate the amplitude of the thermal fluctuation on the scale $\overline{R}$, adopting the trial function

$$\phi = \phi_A \exp\left[-\frac{r^2}{\overline{R}^2}\right]. \tag{18}$$

Then the free energy becomes

$$F_0(\phi_A,T)=\Big[\frac{3\pi^{3/2}}{4\sqrt{2}}\overline{R}+\frac{\pi^{3/2}}{2\sqrt{2}}D(T^2-T_2^2)\overline{R}^3\Big]\phi_A^2-\frac{\pi^{3/2}}{3\sqrt{3}}ET\phi_A^3\overline{R}^3+\frac{\pi^{3/2}}{32}\lambda_T\phi_A^4\overline{R}^3. \tag{19}$$

Thus the RMS amplitude of ϕ at the symmetric vacuum is

$$\sqrt{\overline{\phi^2}}=\sqrt{\frac{\int d\phi_A\phi_A^2e^{-\frac{F_0(\phi_A,T)}{T}}}{\int d\phi_A e^{-\frac{F_0(\phi_A,T)}{T}}}}\sim\frac{\phi_+}{\sqrt{3+\frac{16D(T^2-T_2^2)T^2}{\pi^3\phi_+^4}}}. \tag{20}$$

Its temperature dependence is depicted in Fig.2. In the same way as in the case of $\overline{R}$, the above approximation result gives the *lower* bound for $\sqrt{\overline{\phi^2}}$. At $T=T_c$ and $T=T_1$, one obtains numerically $\sqrt{\overline{\phi^2}}(T=T_c)=36.2$GeV and $\sqrt{\overline{\phi^2}}(T=T_1)=28.2$GeV, respectively. This exceeds the first reflection point $\phi_*=\frac{ET}{\lambda_T}-\sqrt{\frac{E^2T^2}{\lambda_T^2}-\frac{2D(T^2-T_2^2)}{3\lambda_T}}$, which implies that the perturbation theory breaks down and that one can no longer conclude that electroweak phase transition is of first order. For the comparison we calculate the RMS by the same treatment as Dine et al [6]. According to their analysis, it becomes

$$\langle\phi^2\rangle_{k<1/\overline{R}}\sim\frac{T}{2\pi^2\overline{R}}\sim\frac{\phi_+^2}{4\sqrt{2}\pi^{1/2}} \tag{21}$$

and then $\sqrt{\langle\phi^2\rangle}\sim\phi_+/3$. This value is slightly smaller than eq. (20), but exceeds ϕ_* in the most range of temperature as one can see in Fig. 2.

To obtain the general view of the phase transition we must examine the dynamics of the symmetric subcritical bubbles. In the low temperature, symmetric bubbles are also always bounded, and this gives the typical scale of the subcritical bubble. We adopt the trial function for a symmetric bubble in the asymmetric phase as follows:

$$\phi=\phi_+\Big[1-\exp\big[-\frac{r^2}{R(t)^2}\big]\Big]. \tag{22}$$

The same procedure as the above discussion yields the energy equation near the turning point R_c:

$$\frac{1}{2}\Big(\frac{dR}{dt}\Big)^2+\tilde{U}(R,\phi_+,T)=E_0, \tag{23}$$

where

$$\begin{aligned}\tilde{U}(R,\phi_+,T):=&\frac{2}{5}\ln\frac{R}{R_c}-\Big[\frac{4\sqrt{2}}{5}(2-\frac{1}{2\sqrt{2}})D(T^2-T_2^2)-\frac{4\sqrt{2}}{5}(3-\frac{3}{2\sqrt{2}}-\frac{1}{3\sqrt{3}})ET\phi_+\\&+\frac{2\sqrt{2}}{5}(4-\frac{1}{8}-\frac{3}{\sqrt{2}}+\frac{4}{3\sqrt{3}})\lambda_T\phi_+^2\Big]R^2,\end{aligned} \tag{24}$$

and E_0 is the constant of motion. Note that the above energy equation holds in the case in which turning point exists. In the low temperature phase($T<T_c$), the potential $\tilde{U}(R,\phi_+,T)$ is a monotonically increasing function of R. To estimate the typical size we construct the effective Hamiltonian for the variable $R(t)$ and its canonically conjugate momentum $P(t)$:

$$\begin{aligned}H_{eff}(R,P)=&\frac{4\sqrt{2}}{15\pi^{3/2}\phi_+^2}\frac{P^2}{R}+\frac{3\pi^{3/2}}{4\sqrt{2}}\phi_+^2R-\pi^{3/2}(2-\frac{1}{2\sqrt{2}})D(T^2-T_2^2)\phi_+^2R^3+\pi^{3/2}(3-\frac{3}{2\sqrt{2}}+\frac{1}{3\sqrt{3}})ET\phi_+^3R^3\\&-\pi^{3/2}(1-\frac{1}{32}-\frac{3}{4\sqrt{2}}+\frac{1}{3\sqrt{3}})\lambda_T\phi_+^4R^3.\end{aligned} \tag{25}$$

We obtain the same result

$$\overline{R}\sim\frac{2\sqrt{2}T}{\pi^{3/2}\phi_+^2} \tag{26}$$

as the asymmetric bubble in the same approximation level. By the same argument with the asymmetric bubbles, this gives an upper bound for numerical results.

Let us clarify the total dynamics of electroweak phase transition. The following argument is based on the work in ref. [12]. Although it is a rough estimate, the results give us qualitative picture which is necessary for understanding the phase transition. Then transition rate becomes

$$\Gamma_{[0\to+]} = m(T)\exp\left[-\frac{F_0(\phi_+)}{T}\right], \tag{27}$$

and

$$\Gamma_{[+\to0]} = m(T)\exp\left[-\frac{F_+(\phi_+)}{T}\right], \tag{28}$$

with $m(T) = \sqrt{2D(T^2 - T_2^2)}$, where

$$F_0(\phi_+) = \frac{3}{2}T + \frac{1}{\pi^3}\left[8D(T^2 - T_2^2)\phi_+^{-4} - \frac{16\sqrt{2}}{3\sqrt{3}}ET\phi_+^{-3} + \frac{1}{\sqrt{2}}\lambda_T\phi_+^{-2}\right]T^3, \tag{29}$$

and

$$F_+(\phi_+) = \frac{3}{2}T - \frac{16\sqrt{2}}{\pi^3}\left[(2 - \frac{1}{2\sqrt{2}})D(T^2 - T_2^2)\phi_+^{-4} + \pi^{3/2}(3 - \frac{3}{2\sqrt{2}} - \frac{1}{3\sqrt{3}})ET\phi_+^{-3}\right.$$
$$\left. - \pi^{3/2}(1 - \frac{1}{32} - \frac{3}{4\sqrt{2}} + \frac{1}{3\sqrt{3}})\lambda_T\phi_+^{-2}\right]T^3. \tag{30}$$

For the more detailed analysis of phase transition the above formulae are not sufficient. In particular, note that the prefactor $m(T)$ is determined from the dimensional argument although this term is important when we determine the freeze out temperature T_{fo}. The master equations for the number density of the symmetric (asymmetric) state, N_0 (N_+), are

$$\frac{dN_0}{dt} = -\Gamma_0 N_0 + \Gamma_+ N_+, \tag{31}$$

and

$$\frac{dN_+}{dt} = -\Gamma_+ N_+ + \Gamma_0 N_0, \tag{32}$$

respectively. The behaviour of the both transition rates can be seen in Fig.3, where we can find that T_{fo} is barely larger than T_2. However, this results is mainly due to the prefactor $m(T)$. As the both transition rates are much larger than $H = \dot{a}/a$ during the phase transition, T_{fo} is probably lower than T_2 if one can calculate the exact transition rate. For example, if we substitute $m(T)$ by T, T_{fo} becomes lower than T_2. Thus the fraction of false vacuum for true vacuum $Y = N_0/N_+$ has the equilibrium value at $T = T_2$:

$$Y = Y^{eq} = \frac{N_0^{eq}}{N_+^{eq}} = \frac{\Gamma_+}{\Gamma_0} = \exp\left[-\frac{F_+ - F_0}{T}\right], \tag{33}$$

Its temperature dependence is seen in Fig.4. When the temperature becomes T_1, the asymmetric vacuum appears. The fraction which the asymmetric vacuum occupies will be almost zero at this moment. The transition rate from asymmetric to symmetric vacuum exceeds during a small temperature difference from $T = T_1$. When the temperature becomes the critical temperature, the fraction Y becomes unity. If the freeze-out temperature is higher than T_2, after the temperature becomes the freeze-out temperature the symmetric region will collapse by surface tension. The phase transition cannot be accomplished by critical bubbles. If the freeze out temperature is lower than T_2, the phase transition becomes of the second order type. Here we remark that the last attempt exists and some new aspect have been obtained in the case with light Higgs mass($m_H \leq 53$GeV) by considering the kinematics of the subcritical bubble [13]. For such a case, destruction of symmetric bubble by thermal noise becomes dominant.

In this paper, we investigated the strength of the thermal fluctuation and the structure of the phase transition. Our main focus is the estimation of the size of sub-critical bubbles. According to our calculation, the typical size is smaller than the correlation length and the amplitude of thermal fluctuation increases compared with the previous estimation. For experimentally allowed values of Higgs mass, the amplitude of thermal fluctuation always exceeds the first reflection point and then perturbation scheme is not guaranteed. At the critical temperature, the fraction which symmetric and asymmetric vacua occupy is almost the same and therefore the critical bubble cannot be nucleated.

Note that Borrill and Gleiser have obtained the results that the two phase mixing is completely attained in numerical experiment [14] and our discussion might be supported by this.

When we obtain effective Lagrangian for the size $R(t)$ we used the thick wall ansatz. In this case, one can easily confirm that the typical size $\overline{R}$ of subcritical bubble is comparable with the thickness of the wall. Thus, the thin wall is not suitable for subcritical bubbles.

In the microscopic level, the subcritical bubble expands and then collapses and any departure from thermal equilibrium is not provided. Thus, the baryon number cannot be generated in minimal standard model. We conclude that the baryogenesis is quite difficult in the minimal standard model, even apart from the fact that CP-violation source is in Kobayashi-Maskawa phase only which is quite small. Thus, we need to investigate "beyond the standard model" and this work will be reported in the near future.

Acknowledgement

We would like to thank H. Sato and M. Sasaki for their useful comments. TS thanks T. Tanaka for discussions. MM thanks Kurata foundation for financial support. This work was partly supported by Grant-in-Aid for Scientific Research Fellowship, No. 2925 (TS) and by the Scientific Research Fund of Ministry of Education, Science, and Culture, No. 06740216 (JY).

---

[1] T. Shiromizu, M. Morikawa and J. Yokoyama, "Thermal fluctuation in electroweak phase transition", Kyoto Preprint KUNS-1297, OCHA-PP-51, YITP/U-95-1(Submitted to Phys. Lett. B)
[2] M. Dine, Nucl. Phys. B(Proc. Suppl.)37A, 127(1994); and references therein
[3] A. G. Cohen, D. B. Kaplan and A. E. Nelson, Ann. Rev. and Part. Sci., 43, 27(1993);
M. Shaposhnikov, Nucl. Phys. B(Proc. Suppl.)37A, 117(1994);
A. G. Cohen, D. B. Kaplan and A. E. Nelson, Phys. Lett., B336 41(1994);
G. R. Farrar and M. Shaposhnikov, Phys. Rev. D50,744(1994)
[4] G. W. Anderson and L. J. Hall, Phys. Rev. D45, 2685(1992);
M. Sher, Phys. Rep. 179, 273(1989);
M. Dine, R. G. Leigh, P. Huet, A. Linde and D. Linde, Phys. Rev. D46, 550(1992)
[5] M. Gleiser and R. O. Ramos, Phys. Lett. B300, 271(1993)
[6] M. Dine, R. G. Leigh, P. Huet, A. Linde and D. Linde, Phys. Rev. D46, 550(1992)
[7] Particle Data Group, Phys. Rev. D50, 1173(1994)
[8] F. Abe et al(CDF Collaboration), Phys. Rev. Lett., 73, 225(1994); Phys. Rev. D50, 2966(1994);
Particle Data Group, Phys. Rev. D50, 1173(1994)
[9] M. Shaposhnikov, Nucl. Phys. B287, 757(1987); B299, 797 (1988)
[10] M. Shaposhnikov, Phys. Lett. B316, 112(1993)
[11] D. Diakonov, M. Polyakov, P. Pobylista, P. Sieber, J. Schaldach and K. Goeke, Phys. Lett. B366, 457(1994)
[12] M. Gleiser, E. W. Kolb and R. Watkins, Nucl. Phys. B364, 411(1991);
M. Gleiser and E. W. Kolb, Phys. Lett. 69, 1304(1992);
M. Gleiser and E. W. Kolb, Phys. Rev. D48,1560(1993)
[13] G. Gelmini and M. Gleiser, Nucl. Phys. B410,129(1994)
[14] J. Borrill and M. Gleiser, preprint IMPERIAL/IP/93-94/58, DART-HEP-94/06(hep-ph/9410235)

Figure Captions

1. Fig.1: The thermal correlation length ℓ and the typical size $\overline{R}$ of subcritical bubbles. The unit of the vertical axis is GeV^{-1}.

2. Fig.2: The RMS of thermal fluctuations. The unit of the the vertical axis is GeV.

3. Fig.3: Transition rates. Both rates degenerate in this figure.

4. Fig.4: The fraction of the symmetric phase.

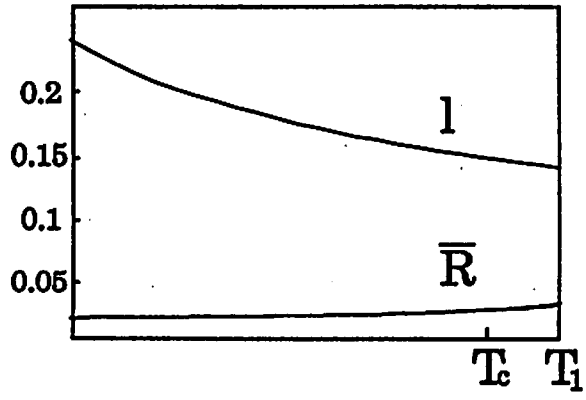
0.2
0.15
0.1
0.05
l
$\overline{R}$
T_c
T_1

Fig. 1

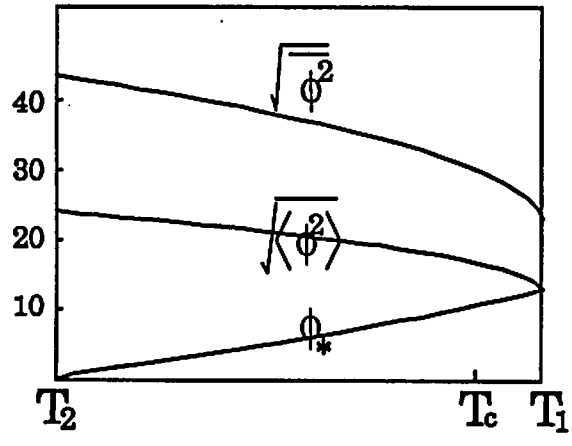
40
30
20
10
$\sqrt{\overline{\phi^2}}$
$\sqrt{\overline{\langle\phi^2\rangle}}$
ϕ_*
T_2
T_c
T_1

Fig. 2

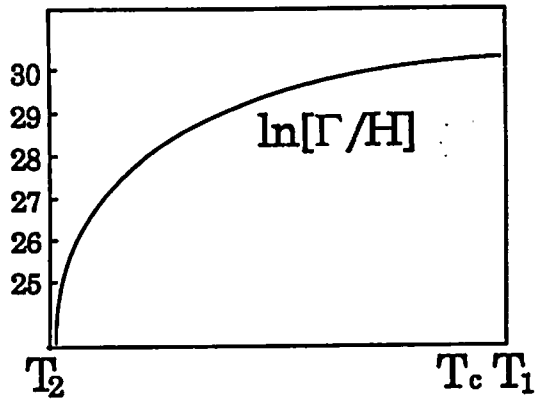
30
29
28
27
26
25
ln[Γ/H]
T2
Tc T1

Fig. 3

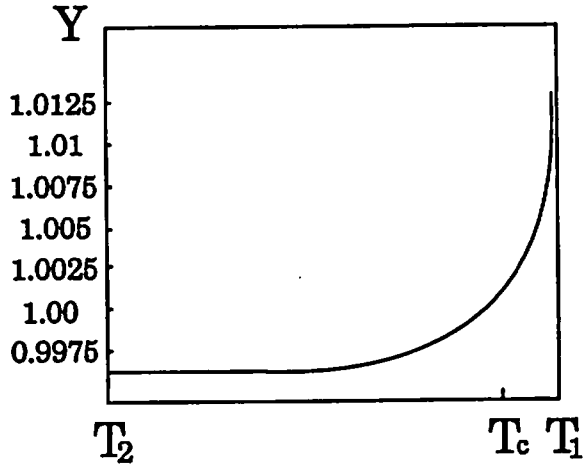
Y
1.0125
1.01
1.0075
1.005
1.0025
1.00
0.9975
T2
Tc T1

Fig. 4

GENERAL-RELATIVISTIC SECOND-ORDER GRAVITATIONAL INSTABILITY AND INHOMOGENEOUS COSMOLOGICAL MODELS

KENJI TOMITA
Yukawa Institute for Theoretical Physics
Kyoto University, Uji, 611, Japan

ABSTRACT

First we briefly review various treatments for inhomogeneous cosmological models, and next show the evolution of inhomogeneities in the second-order gravitational instability theory and in the anti-Newtonian approximation.

1. Introduction

Inhomogeneous cosmological models which describe the large-scale structure of the universe have so far been studied in various formalisms. In the following we classify them into three types and show their connection with our theories which will be used in the next section.

1.1. Newtonian treatment

In this treatment, the equations of continuity, motion and gravitational field in the expanding universe are derived under the condition that the gravitational potential ϕ/c^2, the square of velocity v^2/c^2, and L (the characteristic size) / L_h (the horizon size of the universe) are much small, compared with unity[1]. Nowadays these equations are solved in the semi-analytic treatments in the Zeldovich approximation, the adhesive approximation, and so on, and in the numerical methods such as the N body simulation[2].

Recently the Newtonian equations in the Lagrangian formalism have been solved to study the density and velocity fields in the large-scale structure and the Ω parameter of the Universe.[3] Moreover the role of the Weyl tensor ($C_{\alpha\beta\gamma\delta}$) in the Newtonian situation was examined by Bertschinger et al.[4], who showed that the magnetic part does not vanish in general and the Lagrangian evolution of the fluid is not purely local. This may mean that the post-Newtonian effect is not negligible in the Lagrangian treatment.

In the post-Newtonian treatment, the next-order terms with respect to $\phi/c^2, v^2/c^2$, and L/L_h are considered into account, and the dynamical equations and their behaviors were studied by Tomita[5] and Futamase[6]. In the latter work the spatial averaging was introduced and a more rigorous treatment of it was given by Kasai[7].

1.2. Relativistic perturbation theories

The linear perturbation theory was first derived by Lifshitz[8] in the synchronous coordinate system. In his theory there remained a gauge problem that unphysical perturbations were included as the solutions. This problem was solved by Bardeen[9] in the gauge-invariant formalism and his theory was extended by Kodama and Sasaki[10] and by other workers[11] to that for many fluids system in more general situations. This formalism was also applied to the instability of collisionless gas by Kasai and Tomita[12] and the instability in the Bianchi type I anisotropic background by Tomita and Den[13].

Moreover, second-order perturbations were treated by Tomita[14] and recently also by Materrase et al.[15] Their treatment in the synchronous condition has no gauge problem for the pressureless (dust) matter.

1.3. Relativistic inhomogeneous models

Under special spatial symmetries such as spherical symmetry and plane symmetry, several exact solutions have been derived. Representative two of them are the Lemaitre-Tolman-Bondi solution[16] and the Ellis-Szekeres solution[17] in the irrotational dust matter. Eardley et al. discussed the velocity-dominated character of their solutions[18].

Lifshitz and Khalatnikov[19], and other russian workers[20] derived the approximate solutions for inhomogeneous cosmological models near the singularity, including quasi-isotropic solutions[21].

The solutions in the anti-Newtonian approximation were derived by Tomita[22],[23], noticing the inhomogeneities with the characteristic length much larger than the horizon size. The similar treatment (the long wavelength approximation) was developed by Salopek et al.[24] in the Hamilton-Jacobi theory. These treatments have recently been revived and extended by Comer et al.[25] and Tomita and Deruelle.[26]

As one of the other approaches, the solutions in the case of vanishing magnetic Weyl tensor were studied by Materrase et al.[27] for the irrotational dust matter. This seems to be an extension of Lemaitre-Tolman-Bondi solution and Ellis-Szekeres solution.

2. Second-order gravitational instability

First in the Lifshitz formalism we show the density perturbations in the flat, dust case. In this formalism the synchronous coordinate condition is used.

For the background (Einstein-de Sitter) spacetime

$$ds^2 = a^2(\eta)[-d\eta^2 + d\mathbf{x}^2] \tag{1}$$

with $a = a_0\eta^2$, we have the first-order perturbations in the growing mode :

$$a^{-2}\delta_1 g_{ij} \equiv h_i^j = \delta_i^j F(\mathbf{x}) + \frac{1}{10}\eta^2 F_{|i}^{|j}, \tag{2}$$

$$\delta_1\epsilon/\epsilon = -\frac{1}{20}\eta^2\Delta F, \tag{3}$$

$$\delta_1 u^i = 0, \tag{4}$$

where $F(\mathbf{x})$ is an arbitrary function of the spatial variable $\mathbf{x} = (x^1, x^2, x^3), \Delta F = F_{|l}^{|l}$, and $F_{|i}, F^{|i}(= \gamma^{ij}F_{|j})$ are covariant derivatives of F in the three dimensional Euclidean space ($ds^2_{(3)} = \gamma_{ij}dx^i dx^j$). The corresponding second-order perturbations are expressed as[14)]

$$a^{-2}\delta_2 g_{ij} \equiv l_i^j = \frac{1}{20}\{-3(F_{|i}f^{|j}) - 2FF_{|i}^{|j} + \frac{1}{2}\delta_i^j F_{|l}f^{|l}\}$$
$$+\frac{1}{2800}\eta^4\{19F_{|il}F^{|jl} - 12F_{|i}^{|j}\Delta F - \delta_i^j[F_{|lm}F^{|lm} - (\Delta F)^2]\} + C_i^j, \tag{5}$$

$$\delta_2\epsilon/\epsilon = \frac{1}{2800}\eta^4[2F_{|lm}F^{|lm} - 5(\Delta F)^2], \tag{6}$$

$$\delta_2 u^i = 0, \tag{7}$$

where C_i^j represents the gravitational waves emitted by the first-order density perturbations. It satisfies

$$\Box C_i^j (\equiv C_{i\ ;\mu}^{j\ ;\mu}) = \frac{3}{1400}a_0{}^{-2}G_i^j, \tag{8}$$

where $;\mu$ means the four dimensional covariant derivative and

$$G_i^j \equiv \Delta(F_{|i}^{|j}\Delta F - F_{|il}F^{|jl}) + (F_{|i}^{|j}F_{|l}^{|m} - F_{|i}^{|m}F_{|l}^{|j})_{|m}^{|l} - \frac{1}{2}\delta_i^j\Delta[(\Delta F)^2 - F_{|lm}F^{|lm}]. \tag{9}$$

Here G_i^j satisfies the relations $G_l^l = 0$ (traceless) and $G_{i|l}^l = 0$ (transverse), so that C_i^j as the solution of the above equation is also traceless and transverse. Because $\delta_1 u^i = \delta_2 u^i = 0$, the density perturbations are given in the comoving system.

Recently we have studied the second-order perturbations in the gauge-invariant formalism. Corresponding to the first-order invariant variables $\Phi_{1H}, \Phi_{1A}, E_{1m}, V_{1s}$, etc, we introduce the second-order variables $\Phi_{2H}, \Phi_{2A}, E_{2m}, V_{2s}$, etc, which are invariant for the second-order gauge-invariant transformations in the background space-time. An example of equations for them to be derived from the Einstein equations are

$$(\epsilon a^3 E_{2m})'' + (1+3w)\frac{a'}{a}(\epsilon a^3 E_{2m})' - [w\Delta + \frac{1}{2}(1+w)\epsilon a^2](\epsilon a^3 E_{2m})$$
$$= (1+w)\epsilon a^2[\frac{1}{4}a(h_i^j)'(h_j^i)' + \frac{3}{2}(1+w)\epsilon a^3(\delta_1 v^i)^2 + ...], \tag{10}$$

where $w = c_s{}^2 = p/\epsilon =$ const. In the (flat) dust case we obtain the growing solution :

$$E_{2m} = \frac{1}{2800}\eta^4[2F_{|lm}F^{|lm} - 5(\Delta F)^2]. \tag{11}$$

This solution is consistent with the corresponding one in the above-mentioned Lifshits formalism.

3. Homogenization in the anti-Newtonian approximation

In this section we show the inhomogeneous models with a positive cosmological constant in the anti-Newtonian approximation, which was derived in our recent paper.[26] The spacetime is described in the synchronous condition with the line-element

$$ds^2 = -dt^2 + \gamma_{ij}dx^i dx^j, \tag{12}$$

where we use the units $c = 8\pi G = 1$, and the Einstein equations for two perfect fluids are expressed as

$$\frac{1}{2}\dot{\kappa}^i_i + \frac{1}{4}\kappa^j_i\kappa^i_j = -\sum_a\{\frac{1}{2}(\epsilon_a + 3p_a) + (\epsilon_a + p_a)[({u_{(a)}}^0)^2 - 1]\}, \tag{13}$$

$$\kappa^j_{j;i} - \kappa^j_{i;j} = 2\sum_a(\epsilon_a + p_a){u_{(a)}}^0 u_{(a)_i}, \tag{14}$$

$$2P^j_i + \frac{1}{\sqrt{\gamma}}(\sqrt{\gamma}\kappa^j_i)^{\cdot} = \sum_a\{2(\epsilon_a + p_a)u_{(a)_i}{u_{(a)}}^j + \delta^j_i(\epsilon_a - p_a)\}, \tag{15}$$

where P^j_i are components of the Ricci tensor in the three-dimensional space with metric $dl^2 = \gamma_{ij}dx^i dx^j$, κ^j_i is defined by $\gamma^{jl}\dot{\gamma}_{li}$, a dot denotes the derivative with respect to t, and γ is the determinant $|\gamma_{ij}|$. Here the cosmological constant is regarded as a fluid, and the total energy and pressure as the sums of the ordinary ones (ϵ_s, p_s) and the cosmological-constant ones $(\epsilon_\Lambda, p_\Lambda)$ are given by ϵ and p : $\epsilon = \epsilon_s + \epsilon_\Lambda$, $p = p_s + p_\Lambda$. Their equations of state are $p_s/\epsilon_s = w_s$ $(= \Gamma_s - 1)$, $p_\Lambda/\epsilon_\Lambda = -1$, where $1 > w_s \geq -1/3$ $(2 > \Gamma_s \geq 2/3)$.

When we neglect the spatial curvature P_{ij} and the square of spatial velocities $({u_{(a)}}^i)^2$, we obtain from the Einstein equations (13) and (15)

$$\kappa^j_i = (\dot{X}/X)\delta^j_i + A^j_i X^{-3/2}, \tag{16}$$

$$\epsilon - p = \ddot{X}/X + \frac{1}{2}(\dot{X}/X)^2, \tag{17}$$

$$\epsilon + 3p = -3\ddot{X}/X + \frac{3}{2}(\dot{X}/X)^2 - 6\xi/X^3, \tag{18}$$

where $X \equiv \gamma^{1/3}$, $\gamma = \det(\gamma_{ij})$, and A^j_i is an arbitrary traceless function of only spatial variables with $\xi \equiv A^j_i A^i_j/12$. From Eqs.(17) and (18) we obtain

$$\ddot{Y} + \frac{9}{8}(1 - {w_s}^2)\xi Y^{(w_s-3)/(w_s+1)} - \frac{3}{4}(1 + w_s)^2\epsilon_\Lambda Y = 0, \tag{19}$$

where $Y \equiv X^{3(1+w_s)/4} = \gamma^{(1+w_s)/4}$.

In the quasi-isotropic case $A^j_i = 0$ where we consider in the following, the solution Y is expressed as

$$Y = X^{\frac{3}{4}(1+w_s)} = Y_0(\mathrm{x})\ \sinh(Ht), \tag{20}$$

where $H \equiv (1+w_s)(\frac{3}{4}\epsilon_\Lambda)^{1/2}$. Then the energy density and velocity are

$$\epsilon_s = \epsilon_\Lambda / \sinh^2(Ht), \quad u_{(s)_i} = 0. \tag{21}$$

and the metric components are

$$\gamma_{ij} = A_0 h_{ij}, \quad A_0{}^{\frac{3}{4}(1+w_s)} = \sinh(Ht). \tag{22}$$

When we treat higher-order solutions with respect to the spatial curvature, the above solution is regarded as the first-order solution ${}^{(1)}\gamma_{ij}$, ${}^{(1)}\epsilon_s$ and ${}^{(1)}u_{(s)_i}$. Let us derive the next third-order solution in Comer et al.'s procedure[24] :

$${}^{(3)}\gamma_{ij} = A_0\{f_2(t)R_{ij} + \frac{1}{3}[g_2(t) - f_2(t)]Rh_{ij}\}, \tag{23}$$

where $R_{ij} = P_{ij}, R_i^j \equiv h^{ik}R_{kj}$ and $R = R_i^i$, and the independence of functions R_{ij} and Rh_{ij} is used for the derivation of separate equations dependent only on time. Thus the Einstein equations (13) and (15) for the metric $\gamma_{ij} = {}^{(1)}\gamma_{ij} + {}^{(3)}\gamma_{ij}$ lead to

$$\ddot{f}_2 + \frac{3}{2}\frac{\dot{A}_0}{A_0}\dot{f}_2 + 2A_0^{-1} = 0, \quad \ddot{g}_2 + \frac{3}{2}(1+w_s)\frac{\dot{A}_0}{A_0}\dot{g}_2 + \frac{1}{2}(1+3w_s)A_0^{-1} = 0. \tag{24}$$

Their solutions are

$$f_2 = -2\int dt A_0^{-3/2}\int dt' A_0^{1/2}, \tag{25}$$

$$g_2 = -\frac{1}{2}(1+3w_s)\int dt A_0^{-3(1+w_s)/2}\int dt' A_0^{(1+3w_s)/2}. \tag{26}$$

The energy density derived from Eqs.(17) and (18) is

$${}^{(3)}\epsilon_s = \delta\epsilon_s = \frac{1}{2}(\dot{g}_2\frac{\dot{A}_0}{A_0} + A_0{}^{-1})R. \tag{27}$$

By the use of Eq.(26) we can rewrite as

$${}^{(3)}\epsilon_s = \frac{1}{2}A_0{}^{-3(1+w_s)/2}\frac{\dot{A}_0}{A_0}R\int dt(1 - A_0\ddot{A}_0/\dot{A}_0^2)A_0{}^{(1+3w_s)/2}. \tag{28}$$

The general behaviors of f_2 and g_2 are found by solving numerically Eq.(24) in various initial conditions. Homogeneous part of solutions f_2 and g_2 show the components being constant or decaying with time always, and the constant terms can be included in h_{ij} with the factors R_{ij} and Rh_{ij}. This means that the changes in h_{ij} and R_{ij} are brought by the dynamical evolution of fluids. Next we pay attention to the special solutions which may bring growing components. They are shown in the following two extreme cases $Ht << 1$ and $Ht >> 1$.

(a) $Ht << 1$

As $A_0 \propto t^{4/[3(1+w_s)]}$, we have

$$f_2 \propto g_2 \propto t^{2(1+3w_s)/[3(1+w_s)]}. \tag{29}$$

The energy density is

$$^{(3)}\epsilon_s = \delta\epsilon_s \propto t^{-4/[3(1+w_s)]}, \tag{30}$$

so that the contrast is

$$\delta\epsilon_s/\epsilon \propto t^{2(1+3w_s)/[3(1+w_s)]}. \tag{31}$$

Therefore the inhomogeneities grow with time.
(b) $Ht >> 1$
As $A_0 \simeq (\frac{1}{2}e^{Ht})^{4/[3(1+w_s)]}[1 - \frac{4}{3(1+w_s)}e^{-2Ht} + 0(e^{-4Ht})]$, we have

$$f_2 \propto g_2 \propto e^{-4Ht/[3(1+w_s)]}, \tag{32}$$

and

$$^{(3)}\epsilon_s = \delta\epsilon_s = e^{-\{2+4/[3(1+w_s)]\}Ht}, \tag{33}$$

where it is noted that the density in the special solution decays more rapidly than that ($\propto e^{-2Ht}$) in the homogeneous solution, because of the factor $(1 - A_0\ddot{A}_0/\dot{A}_0^2)$ in Eq.(28). Since ϵ is constant at this stage, the density contrast is proportional to $^{(3)}\epsilon_s$, and so the inhomogeneities including an ordinary fluid decay with time. The case when A_0 is exactly exponential, i.e., $A_0 = (\frac{1}{2}e^{Ht})^{4/[3(1+w_s)]}$ was treated by Starobinskii[21].

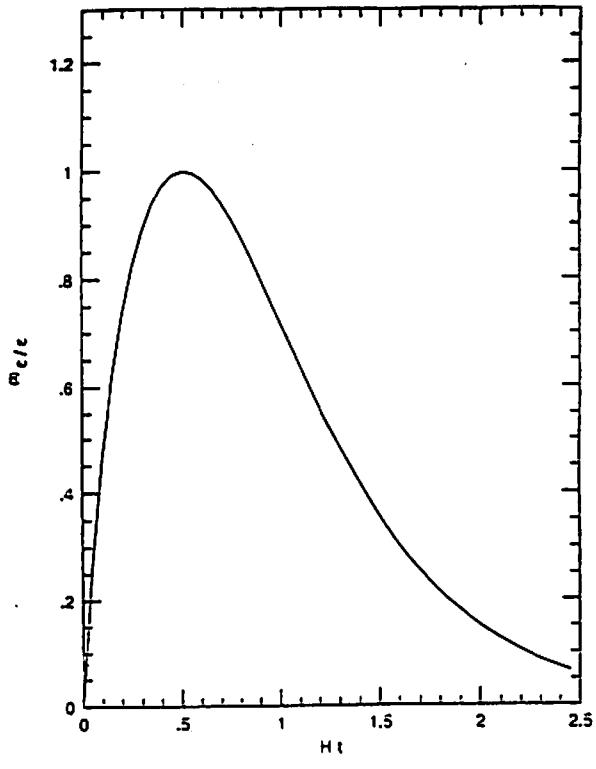

The third-order velocity ${}^{(3)}u_i$ is derived using Eq.(14), where the third-order components of κ_i^j consist of terms R_i^j and Rh_i^j. Because of the identity $R_{i;j}^j = R_{,j}$, the left-hand side of Eq.(14) vanishes, so that we obtain ${}^{(3)}u_{(s)_i} = 0$.

For higher-order terms, more separate equations dependent only on time are derived similarly. It is found that the $(2n+1)-$th metric components are in proportion to $t^{2n(1+3w_s)/[3(1+w_s)]}$ or $e^{-4nHt/[3(1+w_s)]}$ for $Ht << $ or $Ht >> 1$, respectively. In the intermediate case $Ht \sim 1$ the analysis is rather complicated.

From the above two cases, we can conclude that the inhomogeneities can grow at the early stage such as $Ht < 1$, the growth is prevented gradually at $Ht \sim 1$, and decay finally, when the exponential inflation becomes dominant. Accordingly gravitational collapse can occur only at the stage $Ht < 1$. The behavior of density perturbations is shown in the figure.

References

1. H. Nariai and Y. Ueno, Prog. Theor. Phys. **23**(1960) 305.
2. Y. Suto, Prog. Theor. Phys. **90**(1993) 1173.
3. A. Nusser and A. Dekel, Astrophys. J. **379**(1991) 6, **405**(1993) 437; T. Buchert, MNRAS **254**(1992), 729; M. Gramann, Astrophys. J. **405**(1993) L47, 449.
4. E. Bertschinger and A.J.S. Hamilton, Astrophys. J. **435**(1994) 1; E. Bertschinger and B. Jain, Astrophys. J. **431**(1994) 486.
5. K. Tomita, Prog. Theor. Phys. **79**(1988) 258 ; **85**(1991) 1041.
6. T. Futamase, Prog. Theor. Phys. **89**(1993) 581.
7. M. Kasai, Phys. Rev. Lett. **69**(1992) 2330; Phys. Rev. **D47**(1993) 3214.
8. E.M. Lifshitz, J. Phys. (Moscow) **10**(1946) 116.
9. J.M. Bardeen, Phys. Rev. **D23**(1980) 1882 .
10. H. Kodama and M. Sasaki, Prog. Theor. Phys. Suppl. **78**(1984) 1.
11. J. Hwang and E.T. Vishniac, Astrophys. J. **353**(1990) 1; D.H. Lyth, Phys. Rev. **D31**(1985) 1792; D.H. Lyth and M. Mukherjee, *ibid.* **38**(1988) 485; T. Hirai and K. Maeda, Astrophys. J. **431**(1994) 16.
12. M. Kasai and K. Tomita, *ibid.* **33**(1986) 1576.
13. K. Tomita and M. Den, Phys. Rev. **D34**(1986) 3570; Prog. Theor. Phys. **77**(1987) 653
14. K. Tomita, Prog. Theor. Phys. **37**(1967) 831; *ibid.* **45**(1971) 1747; *ibid.* **47** (1972) 416.
15. S. Materrase, O. Pantano, and D. Saez, MNRAS in press (1994).
16. R.C. Tolman, Proc. Natl. Acad. Sci. **20**(1934) 169; H. Bondi, MNRAS **410** (1947) 107.
17. G.F.R. Ellis, J. Math. Phys. **8**(1967) 1171; P. Szekeres, Comm. Math. Phys. **41** (1975) 55.

18. D. Eardley, E. Liang and R. Sachs, J. Math. Phys. **13**(1972) 99.
19. E.M. Lifshitz and L.M. Khalatnikov, Adv. Phys. **121963**) 185.
20. V.A. Belinski, I.M. Khalatnikov and E.M. Lifshitz, Adv. Phys. **19**(1970) 525.
21. A.A. Starobinskii, JETP Lett. **37**(1983) 66.
22. K. Tomita, Prog. Theor. Phys. **48**(1972) 1503; *ibid.***50**(1973) 1285; *ibid.* **54** (1975) 730; *ibid.***67**(1982) 1076.
23. K. Tomita, Phys. Rev. D**48**(1993) 5634.
24. D.S. Salopek, and J.R. Bond, Phys. Rev. D**42**(1990) 3936; D.S. Salopek, J.M. Stewart, and J. Parry, Phys. Rev. D**48**(1993) 719; J. Parry, D.S. Salopek, and J.M. Stewart, *ibid.* D**49**(1994) 2872.
25. G.L. Comer, N. Deruelle, D. Langlois, and J. Parry, Phys. Rev. D**49**(1994) 2759.
26. K. Tomita and N. Deruelle, Phys. Rev. **D50**(1994) No. 12.
27. S. Materrase, O. Pantano, and D. Saez, Phys. Rev. **D47**(1993) 1311; Phys. Rev. Lett. **72**(1994) 320.

Gradient Expansion in Ashtekar Formalism

Akika Nakamichi* and Hideki Ishihara†

* *Uji Research Center*
Yukawa Institute for Theoretical Physics
Kyoto University, Gokashou, Uji-shi, Kyoto 611, Japan

† *Department of Fundamental Sciences, FIHS*
Kyoto University, Kyoto 606-01, Japan

Abstract

We develop gradient expansion method in Ashtekar formalism for vacuum Universe. The non-linear solutions describe inhomogeneous Universe. The 1st-class constraints and evolution equations are solved at the lowest order in case of vanishing structure functions and non-vanishing $C^a{}_{bc} = \epsilon^a{}_{bc}$ case.

1 Introduction

There is a long history of "gradient expansion"[1], which is the perturbation scheme, so called "long wavelength approximation" or "anti-Newtonian". This scheme has been applied to inhomogeneous Universe. We emphasize that 0th order solution is not necessarily homogeneous, but only requirement is that this 0th order solution is analytically expressed. So far the gradient expansion scheme has been studied using traditional metric variables. In this paper, we shall use Ashtekar variables[2] instead of the traditional metric variables in the gradient expansion. We hope that solving Einstein's equations becomes remarkably simple. In fact, as far as we investigated, it becomes apparently simple compared to the traditional method. We shall consider almost Bianchi I case (with long wavelength inhomogeneity) and also IX case in vacuum geometry. Firstly we define gradient expansion scheme in Ashtekar formalism. Next we solve 1st-class constraints and evolution equations to obtain the metric.

2 Brief Review of Ashtekar Formalism

Ashtekar formalism is based on canonical formalism [2]. One considers that general relativity is a dynamically constrained system. In the Ashtekar formalism, the gravitational phase space is extended to have the internal triad coordinates. The dynamical variables are $(\tilde{e}^i_I, A_i{}^I)$, a densitized triad on a 3-manifold Σ , and an $SL(2,C)$ connection $A_i{}^I$. Here the tilde over $e^i{}_I$ means densitized: $\tilde{e}^i_I = \sqrt{\det \gamma_{ij}}\, e^i{}_I$, γ_{ij} is 3-dimensional metric.

There is the local triad invariance, in addition to the diffeomorphism invariance. As a result we have the Gauge constraint noted below. Three 1st-class constraints are as follows:

Hamiltonian constraint:

$$C_H = Tr(\tilde{e}^i \tilde{e}^j F_{ij}) \approx 0\,. \tag{1}$$

Momentum constraint:

$$C_{M_j} = Tr(\tilde{e}^i F_{ij}) \approx 0\,. \tag{2}$$

Gauge constraint:

$$C_{G_I} = D_i \tilde{e}^i_I \approx 0\,. \tag{3}$$

The Poisson brackets among these three constraints are closed.

3 Ashtekar Variable Approach to Gradient Expansion Method

First we introduce an invariant 1-form E^a : $\mathcal{L}_{\xi_a} E^a = 0$, where a denotes components of group G, which acts on 3-dimensional manifold simply transitive. It is satisfied the following Mauer-Cartan relation:

$$dE^a = \frac{1}{2}\, C^a{}_{bc}(x) E^b \wedge E^c\,. \tag{4}$$

Here $C^a{}_{bc}(x)$ is structure function of the group G.

Next we expand Ashtekar's connection 1-form using the invariant 1-form E^a :

$$\mathbf{A}^I = A^I{}_a(x)\, E^a\,. \tag{5}$$

The canonical conjugate variable $\tilde{e}^i_I$ is expanded using the basis χ_a, which is dual to the invariant basis E^a:

$$\tilde{\mathbf{e}}_I = \tilde{e}^a_I(x)\, \chi_a\,. \tag{6}$$

The spatial dependences of $A^I{}_a$, $C^a{}_{bc}$, and of $\tilde{e}^a_I$ represent inhomogeneity of the Universe.

From now on we consider the gradient expansion method at the lowest order. Recall that in the usual metric variable approach to the gradient expansion at the lowest order, we neglect second order spatial gradients and keep only time derivative and linear terms in the spatial gradients. On the other hand in the Ashtekar variable approach, we have only first order spatial gradients in the 1st-class constraints. Therefore we decide to ignore spatial derivatives $dA^I{}_a$ and $d\tilde{e}^a_I$ in the constraints, however we keep dE^a by virtue of the Mauer-Cartan relation eq.(4).

Then the field strength 2-form is expanded at the lowest order as the following:

$$F_{ab}{}^I = -A^I{}_c C^c{}_{ab} + i\,\epsilon^I{}_{MN}\, A^M{}_a A^N{}_b\,. \tag{7}$$

Using the group components indices, the 1st-class constraints are expressed as:

$$\begin{aligned} C_H &= \epsilon_K{}^{IJ}\, \tilde{e}^a_I\, \tilde{e}^b_J\, F_{ab}{}^K \approx 0\,, \\ C_{M_j} &= \tilde{e}^a_I\, F_{ab}{}^I \approx 0\,, \\ C_{GI} &= -\tilde{e}^a_I\, C^b{}_{ba} + \epsilon_{IJ}{}^K\, A_a{}^J\, \tilde{e}^a_K \approx 0\,. \end{aligned} \tag{8}$$

From the next section, we will solve these lowest 1st-class constraints and also evolution equations, to obtain metric. We will adopt synchronous reference frame:

$$ds^2 = -\,dt^2 + \gamma_{ab}(x,t)\, E^a\, E^b\,. \tag{9}$$

4 In case of $C^a{}_{bc} = 0$

First we consider the simple case, vanishing the structure function $C^a{}_{bc} = 0$. In this case we can use coordinate basis without complexities. The 1st-class constraints becomes at the lowest order:

$$\begin{aligned} C_H &= i\,\epsilon_K{}^{IJ}\, \epsilon^K{}_{MN}\, \tilde{e}^i_I\, \tilde{e}^j_J\, A_i{}^M\, A_j{}^N \approx 0\,, \\ C_{M_j} &= i\,\epsilon^K{}_{IJ}\, \tilde{e}^i_K\, A_i{}^I\, A_j{}^J \approx 0\,, \\ C_{GI} &= \epsilon_{IJ}{}^K\, A_i{}^J\, \tilde{e}^i_K \approx 0\,. \end{aligned} \tag{10}$$

Here we observe that $C_G \approx 0$ means $C_{M_j} \approx 0$ automatically. Note that this degeneracy in the constraints disappears in the next order of the gradient expansion. However at the lowest order, we still need an information from the momentum constraint. Therefore we add the first order derivative terms to the momentum constraint in order to the constraint be non-trivial:

$$C_{M_j} = \tilde{e}^i_K\, (\partial_i A_j{}^K - \partial_j A_i{}^K + i\,\epsilon_K{}^{IJ} A_i{}^I A_j{}^J) \approx 0\,. \tag{11}$$

We will use the triad invariance to make the densitized triad be diagonal:

$$\tilde{e}^i_I = diag\,[e_1(x),\, e_2(x),\, e_3(x)]\,. \tag{12}$$

Then the 3-metric is expressed as:

$$\gamma_{ij} = diag\,[\frac{e_2 e_3}{e_1}, \frac{e_3 e_1}{e_2}, \frac{e_1 e_2}{e_3}]\,. \tag{13}$$

Moreover we assume that $SL(2,C)$ connection is diagonal for simplicity:

$$A_i{}^I = diag\,[k_1(x),\, k_2(x),\, k_3(x)]\,. \tag{14}$$

Using these diagonal variables, Hamiltonian constraint becomes:

$$C_H = 2\,i\,(e_1 e_2 k_1 k_2 + e_1 e_3 k_1 k_3 + e_2 e_3 k_2 k_3) \approx 0\,. \tag{15}$$

Momentum constraint becomes:

$$\begin{aligned} C_{M_1} &= e_2\,(\partial_1\,k_2 - \partial_2\,k_1) + e_3\,(\partial_1\,k_3 - \partial_3\,k_1) \approx 0\,, \\ C_{M_2} &= e_3\,(\partial_2\,k_3 - \partial_3\,k_2) + e_1\,(\partial_2\,k_1 - \partial_1\,k_2) \approx 0\,, \\ C_{M_3} &= e_1\,(\partial_3\,k_1 - \partial_1\,k_3) + e_2\,(\partial_3\,k_2 - \partial_2\,k_3) \approx 0\,. \end{aligned} \tag{16}$$

Gauge constraint is automatically satisfied because we have already fixed internal $SL(2,C)$ rotation:

$$C_G = 0\,. \tag{17}$$

The lapse function is chosen to be $\underline{N} = 1$ for simplicity. Then evolution equations become as follows:

$$\begin{aligned} \dot{e}_1 &= -\frac{\partial C_H}{\partial k_1} = 2\,i\,e_1\,(\,e_2 k_2 + e_3 k_3\,)\,, \\ &\quad \text{cyclic permutation}\,, \\ \dot{k}_1 &= \frac{\partial C_H}{\partial e_1} = -\,2\,i\,k_1\,(\,e_2 k_2 + e_3 k_3\,)\,, \\ &\quad \text{cyclic permutation}\,. \end{aligned} \tag{18}$$

Here we have the following relation: $\frac{\dot{k}_1}{k_1} + \frac{\dot{e}_1}{e_1} = 0$, cyclic permutation. We can observe that the product $e_1 k_1$ does not depend on time:

$$e_1 k_1 \equiv \frac{1}{2}\,i\,p_1(x)\,, \quad \text{cyclic permutation}\,. \tag{19}$$

Using these relations we can solve the evolution equations as:

$$e_1 = [e_1]_0\,\exp[\,p_2 + p_3\,](x)\,t\,, \quad \text{cyclic permutation}\,. \tag{20}$$

where $[e_1]_0$ expresses the initial value of e_1 at the time $t = 0$.

If we define physical time τ as $d\tau \equiv N dt = \underline{N}\sqrt{\gamma}dt$, and re-define physical time as $\bar{\tau} \equiv \frac{p_1+p_2+p_3}{[e_1 e_2 e_3]_0^{\frac{1}{2}}}\,\tau$, then 3-metric is solved as follows:

$$\gamma_{ij} = [\gamma_{ij}]_0(x)\,diag[\,\bar{\tau}^{2P_1(x)},\, \bar{\tau}^{2P_2(x)},\, \bar{\tau}^{2P_3(x)}\,]\,. \tag{21}$$

Here $P_i(x)$ are defined as

$$P_i(x) \equiv \frac{p_i}{p_1 + p_2 + p_3} . \tag{22}$$

These parameters satisfy following relations:

$$\begin{aligned} P_1(x) + P_2(x) + P_3(x) &= 1 , \\ {P_1}^2(x) + {P_2}^2(x) + {P_3}^2(x) &\approx 1 . \end{aligned} \tag{23}$$

The second equation of eq.(23) is satisfied if and only if Hamiltonian constraint eq.(15) is satisfied. We also have constraints on the above parameters due to the momentum constraints eq.(16). This solution describes inhomogeneous anisotropic *locally* Kasner Universe. If we set e_i be pure real and k_i be pure imaginary, the reality of this metric is satisfied and consistent with its time evolution.

5 In case of $C^a{}_{bc} = \epsilon^a{}_{bc}$

In this section we consider the case $C^a{}_{bc} = \epsilon^a{}_{bc}$.

Even if in the homogeneous case, the general analytic solutions are not founded for this type of structure function. Therefore we will look for special solutions. Especially we will obtain the solutions satisfy

$$F^I{}_{ab} = - A^I{}_c C^c{}_{ab} + i\, \epsilon^I{}_{MN} A^M{}_a A^N{}_b = 0 . \tag{24}$$

One of the simple configurations satisfying this assumption eq.(24) is:

$$A^I{}_a = - i\, \delta_a{}^I . \tag{25}$$

The evolution equations become in the form:

$$\dot{A}^I_a = 2\underline{N}\, \epsilon_{KIJ}\, \tilde{e}^{bJ}\, F_{ab}{}^K , \tag{26}$$

$$\dot{\tilde{e}}^a_I = - 2\, i\, \underline{N}(\tilde{e}^a_I \tilde{e}^b_J A_b{}^J - \tilde{e}^a_J A_b{}^J \tilde{e}^b_I) + \underline{N} C^a{}_{bc} \epsilon_I{}^{JK}\, \tilde{e}^b_J \tilde{e}^c_K . \tag{27}$$

From eq.(26), we observe that on the constraint surface $F_{ab}{}^K = 0$, the Ashtekar's connection $A^I{}_a$ does not depend on time.

In this section we also use the triad invariance to make the densitized triad be diagonal:

$$\tilde{e}^a_I = diag[X, Y, Z] . \tag{28}$$

Then 3-dimensional metric is expressed as the same as in the previous section:

$$\gamma_{ab} = diag[\frac{YZ}{X}, \frac{ZX}{Y}, \frac{XY}{Z}] . \tag{29}$$

The momentum constraint becomes:

$$\begin{aligned} C_{M_1} &= e_2(\chi_1 k_2 - \chi_2 k_1) + e_3(\chi_1 k_3 - \chi_3 k_1) \approx 0, \\ C_{M_2} &= e_3(\chi_2 k_3 - \chi_3 k_2) + e_1(\chi_2 k_1 - \chi_1 k_2) \approx 0, \\ C_{M_3} &= e_1(\chi_3 k_1 - \chi_1 k_3) + e_2(\chi_3 k_2 - \chi_2 k_3) \approx 0. \end{aligned} \tag{30}$$

The evolution equations of the densitized triad are:

$$\begin{aligned} \dot{X} &= -2\underline{N}[-YZ + X(Y+Z)], \\ \dot{Y} &= -2\underline{N}[-ZX + Y(Z+X)], \\ \dot{Z} &= -2\underline{N}[-XY + Z(X+Y)]. \end{aligned} \tag{31}$$

From now on we assume Taub-NUT type symmetry $\gamma_{22} = \gamma_{33}$ to search special analytic solution. This symmetry is expressed in terms of diagonal densitized triad: $Y^2 = Z^2$. In this section we request a little stronger relation: $Y = Z$. Then the evolution equations becomes:

$$\begin{aligned} \dot{X} &= -2\underline{N}[-Y^2 + 2XY], \\ \dot{Y} &= -2\underline{N}Y^2. \end{aligned} \tag{32}$$

We will choose lapse function $\underline{N} = \frac{l}{2a(x)Y}$, where a depends only on x, not on time. Using this lapse function, we can solve evolution equations on the constraint surfaces as follows:

$$\begin{aligned} X &= Y_0(x)\exp(-\frac{1}{a}t)[1 + \frac{\{X_0(x) - Y_0(x)\}}{Y_0(x)}\exp(-\frac{1}{a}t)], \\ Y &= Y_0(x)\exp(-\frac{1}{a}t). \end{aligned} \tag{33}$$

Using the expression of the lapse function: $N^2 = \underline{N}^2 X Y^2 = (\frac{1}{2a})^2 X$, we obtain metric from eq.(29) as follows:

$$\begin{aligned} ds^2 = Y_0\exp(-\frac{1}{a}t) \quad [\quad & \{1 + \frac{X_0 - Y_0}{Y_0}\exp(-\frac{1}{a}t)\}(\frac{dt}{2a})^2 \\ + \quad & \frac{1}{1 + \frac{X_0 - Y_0}{Y_0}\exp(-\frac{1}{a}t)}(E^1)^2 \\ + \quad & \{1 + \frac{X_0 - Y_0}{Y_0}\exp(-\frac{1}{a}t)\}\{(E^2)^2 + (E^3)^2\}]. \end{aligned} \tag{34}$$

Here the parameters X_0, Y_0, and a must satisfy the constraints from eq.(30). If we consider special case: X_0, Y_0 and a are constants, then we can obtain Taub-NUT Universe:

$$ds^2 = -\frac{1}{4}\frac{r \pm M}{r \mp M}dr^2 + 4M^2\frac{r \mp M}{r \pm M}(E^1)^2 + (r^2 - M^2)[(E^2)^2 + (E^3)^2], \tag{35}$$

by using coordinate transformation:

$$r^2 - M^2 = Y_0 \exp(-\frac{1}{a}t) \{ 1 + \frac{X_0 - Y_0}{Y_0} \exp(-\frac{1}{a}t) \} . \tag{36}$$

Therefore the solution eq.(34) is the generalized *locally* Taub-NUT metric.

The reality of this metric is also satisfied and consistent with its time evolution.

6 Summary

We developed expansion method in Ashtekar formalism. We solved 1st-class constraints and evolution equations in case of almost Bianchi I case and almost Bianchi IX case. In case of almost Bianchi I, we obtained locally Kasner metric. In case of almost Bianchi IX, we assume an extra Taub-NUT type symmetry and obtain locally Taub-NUT metric. These observation lead us to infer that the gradient expansion method can be applicable to almost Bianchi type Universe. In future work, we would like to apply this method to just a bit wider class than familiar homogeneous Universe classified by Bianchi type, and clarify limitation of the gradient expansion.

Acknowledgment

We would like to thank Professor T. Fukuyama, Professor H. Kodama, Professor J. Soda, Professor K. Tomita and Dr. Y. Fujiwara for useful discussions.

References

[1] E. M. Lifschitz and I. M. Khalatnikov, Adv. Phys. **12** (1963) 185.

K. Tomita, Prog. Theor. Phys. **54** (1975) 730.

D. S. Salopek and J. M. Stewart, Class. Quantum Grav. **9** (1992) 1943.

G. L. Comer, N. Deruelle, D. Langlois, J. Parry, Phys. Rev. D**49** (1994) 2759.

[2] A. Ashtekar, Phys. Rev. Lett. **57** (1986) 2244.

A. Ashtekar, *Lectures on Non-perturbative Canonical Gravity* (World Scientific, Singapore, 1991).

The Relation of the Gradient Expansion Method to the Linear Perturbation Theory

Osamu Iguchi*, Hideki Ishihara† and Jiro Soda†

* *Graduate School of Human and Environmental Studies, Kyoto University, Kyoto 606-01, Japan*

† *Department of Fundamental Sciences Faculty of Integrated Human Studies, Kyoto University, Kyoto 606-01, Japan*

1 Introduction

The most popular tool to study the evolution of inhomogeneities of the Universe is the linear perturbation theory [1, 2, 3]. An alternative method, the long-wavelength approximation (gradient expansion), is proposed [4, 5], and recently, the higher order terms of the expansion in the gradient expansion is calculated [6, 7]. It is difficult to deal with the inhomogeneities of short wave length in this formalism, however, non-linear effects may be taken into account. In this point of view, this method is interesting as a complemental approach against the linear perturbation theory.

In general relativity, a solution of the Einstein equation may have unphysical modes whose origin is the covariance of the theory. The solution in the gradient expansion method might contain the unphysical modes. If so, we must select the physical modes to get physical information.

In the linearized theory of perturbation, how to treat the gauge modes is well understood. Thus, we compare the gradient expansion method to the linear perturbation theory and clarify whether the solution in the gradient expansion method has the unphysical modes or not.

2 The gradient expansion method

We briefly review the gradient expansion method in the Einstein equation. The metric in a synchronous coordinate take the form

$$\begin{aligned} ds^2 &= g_{\mu\nu}dx^\mu dx^\nu \\ &= -dt^2 + \gamma_{ij}(t, x^k)dx^i dx^j. \end{aligned}$$

Throughout this paper Latin letters denote spatial indices and Greek letters spacetime indices. It is crucial to choose the synchronous coordinate system in the gradient expansion formalism. At each point in the spacetime a local scale factor a and a local Hubble parameter H can be defined by

$$\begin{aligned} a(t,x) &\equiv \gamma^{\frac{1}{6}}, \quad (\gamma \equiv \det \gamma_{ij}), \\ H(t,x) &\equiv \frac{\dot{a}}{a}. \end{aligned}$$

As a matter, we shall consider a prefect fluid which is characterized by the energy-momentum tensor

$$T_{\mu\nu} = (\rho + p)u_\mu u_\nu + p g_{\mu\nu},$$

where p, ρ and u_μ are pressure, energy density and four velocity, respectively. We also assume the equation of state $p/\rho \equiv \Gamma - 1$ $(= constant)$. The Einstein equations become

$$ {}^3R_i^j + \frac{1}{2\sqrt{\gamma}}\partial_t(\sqrt{\gamma}K_i^j) = \frac{2\dot{K} + K_l^m K_m^l}{4(2-3\Gamma-2\Gamma u_l u^l)}[2\Gamma u_i u^j + \delta_i^j(2-\Gamma)], \tag{2.1}$$

$$\kappa\rho(1+\Gamma u_l u^l) = \frac{1}{2}{}^3R + \frac{1}{8}(K^2 - K_l^m K_m^l), \tag{2.2}$$

$$\kappa\Gamma\rho u_i = -\frac{1}{2\sqrt{1+u_l u^l}}(K_{i;j}^j - K_{,i}), \tag{2.3}$$

where $K_{ij} \equiv \dot{\gamma}_{ij}$, $\kappa \equiv 8\pi G$ and ${}^3R_i^j$ is the Ricci tensor for the three-dimensional space. The dot denotes the derivative with respect to t and the semicolon denotes the covariant derivative with respect to γ_{ij}.

We now consider the situation that the spatial derivative of γ_{ij} is much smaller than the time derivative. First, we neglect ${}^3R_{ij}$ and $u_l u^l$ in Eq.(2.1), and get the lowest-order (0th-order) solution.

The traceless part and trace part of Eq.(2.1) become

$$\frac{1}{2\sqrt{\gamma}}\partial_t\left[\sqrt{\gamma}(K_i^j - \frac{1}{3}K\delta_i^j)\right] = 0, \tag{2.4}$$

$$\frac{1}{2\sqrt{\gamma}}\partial_t(\sqrt{\gamma}K) = \frac{3(2-\Gamma)}{4(2-3\Gamma)}(2\dot{K} + k_l^m K_m^l). \tag{2.5}$$

Equation (2.4) is integrated into

$$K_i^j = \frac{1}{3}K\delta_i^j + a^{-3}S_i^j(x), \tag{2.6}$$

where $S_i^j(x)$ is an arbitrary traceless function of spatial coordinates. Substituting Eq.(2.6) into Eq.(2.5), we obtain

$$\partial_t\left(\frac{\dot{a}}{a}\right)+\frac{3\Gamma}{2}\left(\frac{\dot{a}}{a}\right)^2+\frac{2-\Gamma}{16}S_l^m S_m^l a^{-6} = 0. \tag{2.7}$$

In the quasi-isotropic case ($S_i^j(x)=0$), we obtain

$$\gamma_{ij} = a^2 h_{ij}(x) \tag{2.8}$$

$$a(t,x) = (t-t_0(x))^{\frac{2}{3\Gamma}} \tag{2.9}$$

where the symmetric matrix $h_{ij}(x)$ and $t_0(x)$ are arbitrary functions of only spatial coordinates. The matrix $h_{ij}(x)$ is called "seed metric". At sufficiently late time, $t_0(x)$ can be neglected because it is a time-independent function, and hereafter we ignore it.

When we neglect $S_i^j(x)$ and $t_0(x)$, we obtain the 0th-order solution:

$$\overset{(0)}{\gamma}_{ij} = a(t)^2 h_{ij}(x), \qquad a(t)=t^{\frac{2}{3\Gamma}}, \tag{2.10}$$

$$\overset{(0)}{\rho} = \frac{4}{3\kappa\Gamma^2}t^{-2}, \tag{2.11}$$

$$\overset{(0)}{u}_i = 0. \tag{2.12}$$

The next order (1st-order) solution is obtained by taking into account the terms neglected previously. Here, we consider the terms with the second order in the spatial derivative. Thus, we take the Ricci tensor of $\overset{(0)}{\gamma}_{ij}$ in place of ${}^3R_{ij}$ in Eq.(2.1). We will look for corrections in the form

$$\overset{(1)}{\gamma}_{ij} = a(t)^2[\tfrac{1}{3}g_1(t)R(h)h_{ij}+f_1(t)\{R_{ij}(h)-\tfrac{1}{3}R(h)h_{ij}\}], \tag{2.13}$$

$$\overset{(1)}{\rho} = \rho_1(t)R(h), \tag{2.14}$$

$$\overset{(1)}{u}_i = u_1(t)\partial_i R(h), \tag{2.15}$$

where $R_{ij}(h)$ is the Ricci tensor of h_{ij}.

From Eq.(2.1) we get ordinary differential equations

$$\ddot{f}_1+3\frac{\dot{a}}{a}\dot{f}_1 = -\frac{2}{a^2}, \tag{2.16}$$

$$\ddot{g}_1+3\Gamma\frac{\dot{a}}{a}\dot{g}_1 = \frac{2-3\Gamma}{2a^2}. \tag{2.17}$$

Using the solutions of these equations we get

$$\begin{aligned}\overset{(1)}{\gamma}_{ij} = a(t)^2\Bigg[&\left\{-\frac{9\Gamma^2}{4(9\Gamma-4)}t^{2-\frac{4}{3\Gamma}}+\alpha t^{-1}\right\}\frac{1}{3}R(h)h_{ij}\\ &+\left\{-\frac{9\Gamma^2}{(9\Gamma^2-4)}t^{2-\frac{4}{3\Gamma}}+\beta t^{1-\frac{2}{\Gamma}}\right\}\left(R_{ij}(h)-\tfrac{1}{3}Rh_{ij}\right)\Bigg],\end{aligned} \tag{2.18}$$

where α and β are arbitrary constants. Here, we discard constant terms which can be absorbed by redefinition of the seed metric. From Eqs.(2.2), (2.3) and (2.18), we get

$$\overset{(1)}{\rho} = \left[\frac{3\Gamma}{2(9\Gamma-4)\kappa}t^{-\frac{4}{3\Gamma}} - \frac{2}{3\Gamma}\alpha t^{-3}\right]R(h), \tag{2.19}$$

$$\overset{(1)}{u_i} = \left[\frac{27\Gamma^3(1-\Gamma)}{8(3\Gamma+2)(9\Gamma-4)}t^{3-\frac{4}{3\Gamma}} + \frac{2-\Gamma}{16}\beta t^{2-2/\Gamma} - \frac{\Gamma}{4}\alpha\right]\partial_i R(h), \tag{2.20}$$

Similarly, we can calculate the higher order solution, iteratively.

3 Gauge problem

The aim of this section is to clarify the following points: Is the solution in gradient expansion method gauge invariant? If so, what is the coordinate condition?

To see the relation between the gradient expansion and the linear perturbation method on the flat Friedmann universe, we take $h_{ij}(x) = \delta_{ij} + \delta h_{ij}(x)$ ($\delta h_{ij} \ll \delta_{ij}$) as a seed metric. The inverse metric tensor h^{ij} contains all order in δh_{ij} as follows:

$$\begin{aligned} h^{ij} &= \delta^{ij} - \delta h_{lm}\delta^{il}\delta^{jm} + \delta h_{lm}\delta h_{nk}\delta^{nl}\delta^{ik}\delta^{jm} + \cdots \\ &\sim O\left[(\delta h)^0\right] + O\left[(\delta h)^1\right] + O\left[(\delta h)^2\right] + \cdots. \end{aligned}$$

In the gradient expansion method, the metric is symbolically expanded in the form

$$\gamma_{ij} = A(t)h_{ij} + B(t)R_{ij} + C(t)R_{ij}^2 + \cdots \tag{3.1}$$

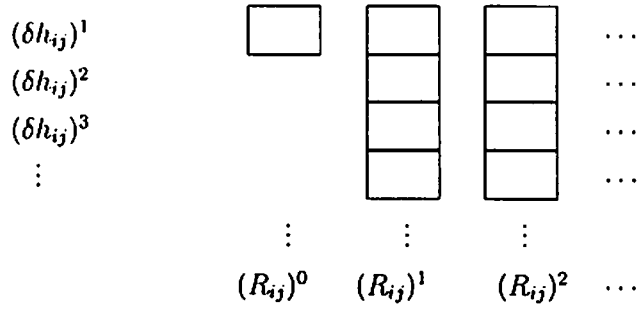

Fig. 1

Noting $R_{ij}(h)$ has the form

$$R_{ij}(h) \sim \partial_j\left(h^{lm}\partial_m h_{il}\right) + h^{ln}\left(\partial_n h_{im}\right)h^{mk}\left(\partial_k h_{jl}\right) + \cdots, \tag{3.2}$$

it also contains all order in h^{ij}. Then each curvature term in the gradient expansion (3.1) contains all order in δh_{ij}. Taking this fact into account, the expansion schemes are schematically represented in Fig.1.

Gathering all linear terms in δh_{ij} (e.g. $\delta h, \partial\delta h, \partial^2\delta h, \cdots$) which are contained in curvature terms in Eq.(3.1), we should get the solution of linearized Einstein equation.

We examine the relation of the solutions in the gradient expansion to the one in the linear perturbation theory. It is impossible to sum all terms in Eq.(3.1). In this paper, we calculate up to the 2nd-order solution, which includes 4th-order in spatial derivative, and sum the linear terms in δh_{ij}. We compare it to the solution in the linear perturbation theory.

In the gradient expansion method, the synchronous frame is adopted. However, in the linear perturbation theory this frame admits residual gauge freedom. Therefore, we impose a coordinate condition $h_{0i} = 0, \delta u^i = 0$ in the linear perturbation theory. This condition fixes the gauge completely. If there is one-to-one correspondence between the solutions in the linear perturbation in this gauge and the solutions in the gradient expansion via a gauge transformation, the unphysical solution is not contained in the latter solution.

In the linear perturbation theory, the perturbation is decomposed in tensor, vector, and scalar modes. As far as we consider the linear perturbation, we can assume spatial dependence of δh_{ij} is $\exp(ik_jx^j)$ without loss of generality. In this case, we replace the spatial derivative by ik_j.

The tensor mode contains no gauge solution, thus solutions for two formalisms coincide. In the gradient expansion method, the spatial dependence of the solution comes through $R_{ij}(h)$. For the seed metric of vector mode, $R_{ij}(h)$ is vanishing. Thus, there is no solution corresponding to the vector mode solution in the linear perturbation theory.

The growing solution of the density perturbation in the gradient expansion formalism up to the 2nd-order is

$$\frac{\overset{(1)}{\rho} + \overset{(2)}{\rho}}{\overset{(0)}{\rho}} = \left[\frac{\Gamma(3\Gamma-2)^2}{12(9\Gamma-4)}(k\eta)^2 - \frac{\Gamma(\Gamma-1)(3\Gamma-2)^3}{24(3\Gamma+2)(15\Gamma-8)}(k\eta)^4\right]\exp(ikx), \tag{3.3}$$

where $\eta \equiv \frac{3\Gamma}{3\Gamma-2}t^{1-\frac{2}{3\Gamma}}$. On the other hand, the growing solution in the linear perturbation theory is

$$\frac{\delta\rho}{\rho} = \left[\frac{\Gamma(3\Gamma-2)^2}{12(3\Gamma+2)}(k\eta)^2 - \frac{\Gamma(\Gamma-1)(3\Gamma-2)^3}{24(3\Gamma+2)(9\Gamma-2)}(k\eta)^4\right]\exp(ikx). \tag{3.4}$$

We can find a unique gauge transformation which connects these two solutions. The gauge transformation is in the following form:

$$\begin{aligned} \eta &\longrightarrow \eta + \delta\eta(\eta)\exp(ikx), \\ x^i &\longrightarrow x^i + \delta r(\eta)\frac{ik^i}{k^2}\exp(ikx), \end{aligned}$$

where $\delta\eta, \delta r$ is

$$\begin{aligned}\delta\eta &= \frac{1}{k^2}\partial_\eta \delta r, \\ \delta r &= \frac{(1-\Gamma)(3\Gamma-2)^3}{48(3\Gamma+2)(9\Gamma-4)}(k\eta)^4 - \frac{(1-\Gamma)^2(3\Gamma-2)^2}{144(3\Gamma+2)(9\Gamma-2)(15\Gamma-8)}(k\eta)^6.\end{aligned}$$

The one-to-one correspondence between Eq.(3.3) and Eq.(3.4) guarantees that the solution Eq.(3.3) is physical.

4 Conclusion

To examine whether the gauge modes exist in a solution in the gradient expansion method, we compare the solution in this method to the one in the linear perturbation theory.

We assume that the 0th-order solution takes the form of Eq.(2.10) ($t_0 = 0, S_i^j = 0$) and obtain the 2nd-order solution (including 4th-order spatial derivative) for the perfect fluid in the gradient expansion method. On the other hand, we consider the solution in the linear perturbation theory with a gauge condition $h_{0i} = 0, \delta u^i = 0$. As a result, the solution in the gradient expansion method is related to the gauge-fixed solution in the linear perturbation theory by a unique gauge transformation. Thus, the solution in the gradient expansion method has no unphysical mode.

For future works, we will study the relation of the gradient expansion method to the second order perturbation theory.

References

[1] E.M.Lifshitz and I.M.Khalatnikov, Adv. Phys. **12**, 185 (1963).

[2] J.M.Bardeen, Phys.Rev. D **23**, 1882 (1980).
H.Kodama and M.Sasaki, Prog. theor. Phys. Suppl. **78**, 1 (1984).

[3] K.Tomita, Prog. theor. Phys. **37**, 831 (1967).
K.Tomita, Prog. theor. Phys. **47**, 416 (1972).

[4] V.A.Belinski, I.M.Khalatnikov and E.M.Lifshitz Adv. Phys. **19**, 525 (1970).

[5] K.Tomita, Prog. theor. Phys. **48**, 1503 (1972).
K.Tomita, Prog. theor. Phys. **54**, 730 (1975).

[6] G.L.Comer, D.Deruuelle, D.Langlois and J.Parry, Phys. Rev. D **49**, 2759 (1994).

[7] J.Parry and D.S.Salopek,J.M.Stewart, Phys. Rev. D **49**, 2872 (1994).

December 1994

Solving the Hamilton-Jacobi equation for General Relativity with Perfect Fluid

TAKESHI CHIBA

Department of Physics, Kyoto University, Kyoto 606-01 Japan

ABSTRACT

We solve the Hamilton-Jacobi equation for general relativity with perfect fluid by the gradient expansion method. Solving higher order Hamiltonian reduces to a recursion relation and the solution is immediately given similar to dust or scalar field. The three-metric is found up to the third order. The expression for the three-metric is in agreement with that of Comer et al.(1994) but the numerical coefficient is slightly different because of the different choice of coordinate condition. It is found that if a perfect fluid violates the strong energy condition (i.e. condition for inflation), then longwave nonlinear inhomogeneities decay, while grow otherwise. The Hamilton -Jacobi theory is again poweful in deriving the higher order solutions which describe inhomogeneous spacetime.

1. Introduction

Recent redshift surveys of galaxies show that sheets and clusters are quite common in the universe. CfA survey[1]suggests that the universe is made up of lots of cells each with a scale of 100 h^{-1}Mpc. A pencil beam survey[2]is consistent with this picture up to the redshift $z \lesssim 0.5$. Relativistic linear perturbation theory is inadequate to describe these clumpy structures. We need an alternative method to study nonlinear inhomogeneities in the universe.

The gradient expansion method for the Hamilton-Jacobi equation[3][4]is one way to treat longwave inhomogeneities. It solves the Hamilton-Jacobi equation for general relativity by simply expanding the generating functional in a series of terms according to the number of spatial gradients they contain.

Recently, it has been shown how to solve systematically the Hamilton-Jacobi equation for general relativity with the inclusion of matter fields by Parry et al.[4]They considered an irrotational dust and a scalar field as a matter field. In this paper we attempt two generalization; irrotational perfect fluid (generalization from dust fluid) and irrotational dust in n-dimensional space (generalization in spacial dimension).

There is another scheme of approximation treat inhomogeneities larger than the Hubble radius called anti-Newton mathod.[5]In this method, the three-metric is expanded under the assumption that the characteristic comoving length for the metric variation is greater than the comoving Hubble radius and the approximate solution is obtained by solving the Einstein equations iteratively. Recently, the three-metric with perfect fluid up to fifth-order is obtained by anti-Newton mathod.[6]These two schemes (Hamilton-Jacobi method and anti-Newton method) are apparently different in the way of getting approximate solutions of the Einstein equation. Therefore, comparison of the results with each other is important, which is the subject of the present paper.

This paper is organized as follows. In Sec.2, we solve the Hamilton-Jacobi equation for general relativity interacting with a perfect fluid. In Sec.3, we derive the three-metric for perfect fluid up to the third order and compare it with the three-metric by anti-Newton method and then comment on the role of the velocity potential as a time variable. Finally Sec.4 is devoted to conclusions.

We use units $8\pi G = c = 1$.

2. Action for Perfect Fluid

The Hamilton -Jacobi equation of order zero for a perfect fluid was solved by Salopek and Stewart(1993),[7] however, neither higher order term nor the 3-metric was obtained. We will derive these in this section and Sec.4.

The action for general relativity interacting with an irrotational perfect fluid is

$$I = \int d^4x\sqrt{-g}(\frac{1}{2}\,{}^{(4)}R + p - \frac{n}{2\epsilon}(\epsilon^2 + g^{\mu\nu}\chi_{,\mu}\chi_{,\nu})). \tag{2.1}$$

Here p, n, ϵ and χ are the pressure, the number density, the specific enthalpy, and the velocity potential of the fluid, respectively. ϵ is written in terms of the energy density ρ and the pressure p as

$$\epsilon = \frac{\rho + p}{n}. \tag{2.2}$$

n and ϵ are Lagrange multipliers; variation of the action with respect to n implies that the 4-velocity

$$U_\mu = -\chi_{,\mu}/\epsilon \tag{2.3}$$

satisfies the normalization $U^\mu U_\mu = -1$, and variation with respect to ϵ yields the first law of thermodynamics $n = (\partial p/\partial\epsilon)_s$. As for the equation of state, we take

$$p = A\epsilon^{\Gamma/(\Gamma-1)}, \tag{2.4}$$

or in terms of ρ

$$p = (\Gamma - 1)\rho, \tag{2.5}$$

where A is a constant depending on the specific entropy.

In the ADM formalism the line element is written as

$$ds^2 = (-N^2 + \gamma^{ij}N_iN_j)dt^2 + 2N_idtdx^i + \gamma_{ij}dx^idx^j, \tag{2.6}$$

where N and N_i are the lapse and shift functions respectively. We can then rewrite the action in the Hamiltonian form,[7]

$$I = \int d^4x(\pi^{ij}\dot{\gamma}_{ij} + \pi^\chi\dot{\chi} - N\mathcal{H} - N^i\mathcal{H}_i). \tag{2.7}$$

Here π^{ij} and π^χ are the conjugate momenta to γ_{ij} and χ, respectively.

Variations of the action with respect to the lapse and shift functions yield the Hamiltonian and momentum constraints:

$$\mathcal{H} = \gamma^{-1/2}\pi^{ij}\pi^{kl}(2\gamma_{il}\gamma_{jk} - \gamma_{ij}\gamma_{kl}) + \pi^{\chi}(\epsilon^2 + \gamma^{ij}\chi_{,i}\chi_{,j})^{1/2} - \gamma^{1/2}p - \frac{1}{2}\gamma^{1/2}\,{}^{(3)}R = 0, \quad (2.8)$$

$$\mathcal{H}_i = -2(\gamma_{ik}\pi^{kl})_{,l} + \pi^{kl}\gamma_{kl,i} + \pi^{\chi}\chi_{,i} = 0. \quad (2.9)$$

Variations with respect to the momenta give the evolution equations for the field variables:

$$(\dot{\gamma}_{ij} - N_{i|j} - N_{j|i})/N = 2\gamma^{-1/2}\pi^{kl}(2\gamma_{il}\gamma_{jk} - \gamma_{ij}\gamma_{kl}), \quad (2.10)$$

$$(\dot{\chi} - N^i\chi_{,i})/N = (\epsilon^2 + \gamma^{ij}\chi_{,i}\chi_{,j})^{\frac{1}{2}} \equiv D, \quad (2.11)$$

where vertical line denotes covariant derivative with respect to the three-mteric.

Now we eliminate the Lagrange multiplier ϵ from the Hamiltonian. From the variation of the action with respect to ϵ gives

$$\gamma^{-1/2}\pi^{\chi} = \frac{\partial p}{\partial \epsilon}\frac{D}{\epsilon} = \frac{\Gamma}{\Gamma - 1}DA\epsilon^{(2-\Gamma)/(\Gamma-1)}. \quad (2.12)$$

In order to apply the gradient expansion in solving the Hamilton-Jacobi equation, we must also solve ϵ by the spatial gradient expansion. We have

$$\epsilon = \epsilon_0 + \epsilon_2 + \cdots, \quad (2.13)$$

where

$$\epsilon_0 = (\frac{(\Gamma - 1)\pi^{\chi}}{\Gamma A\gamma^{1/2}})^{\Gamma-1} \quad (2.14)$$

and

$$\epsilon_2 = -\frac{(\Gamma - 1)}{2\epsilon_0}\gamma^{ij}\chi_{,i}\chi_{,j}. \quad (2.15)$$

From Eq.(2.4) and Eq.(2.12), we can eliminate the pressure from the Hamiltonian;

$$\mathcal{H} = \gamma^{-1/2}\pi^{ij}\pi^{kl}(2\gamma_{il}\gamma_{jk} - \gamma_{ij}\gamma_{kl}) + \pi^{\chi}(D - \frac{\Gamma - 1}{\Gamma}\frac{\epsilon^2}{D}) - \frac{1}{2}\gamma^{1/2}\,{}^{(3)}R. \quad (2.16)$$

Then for the zeroth order Hamiltonian, the field χ evolves as

$$(\dot{\chi} - N^i\chi_{,i})/N = \epsilon_0. \quad (2.17)$$

Next we derive the Hamilton-Jacobi equation. We constract a canonical transformation in which the new Hamiltonian vanishes. By functional differentiation of the generating

functional $\mathcal{S}$ governing the transformation, we obtain the canonical momenta;

$$\pi^{ij} = \frac{\delta \mathcal{S}}{\delta \gamma_{ij}}, \pi^{\chi} = \frac{\delta \mathcal{S}}{\delta \chi}. \tag{2.18}$$

In terms of the generating functional, the Hamiltonian constraint Eq.(2.8) becomes the Hamilton-Jacobi (HJ) equation:

$$\mathcal{H} = \gamma^{-1/2} \frac{\delta \mathcal{S}}{\delta \gamma_{ij}} \frac{\delta \mathcal{S}}{\delta \gamma_{kl}} (2\gamma_{il}\gamma_{jk} - \gamma_{ij}\gamma_{kl}) + \frac{\delta \mathcal{S}}{\delta \chi}(D - \frac{\Gamma - 1}{\Gamma}\frac{\epsilon^2}{D}) - \frac{1}{2}\gamma^{1/2(3)}R = 0, \tag{2.19}$$

while the momentum constraint Eq.(2.9) demands $\mathcal{S}$ be diffeomorphism invariant.

Now we solve the HJ equation by the gradient expansion method. It is simply to expand the generating functional in a series of terms according to the number of spatial gradients they contain:

$$\mathcal{S} = \mathcal{S}^{(0)} + \mathcal{S}^{(2)} + \dots. \tag{2.20}$$

Here from the demand of the diffeomorphism invariance, $\mathcal{S}^{(0)}$ can be written as

$$\mathcal{S}^{(0)} = -2 \int d^3x \gamma^{1/2} H(\chi), \tag{2.21}$$

Substituting this into the HJ equation Eq.(2.19), we find that H satisfies the following equation:

$$H^2 = \frac{2}{3\Gamma}(\frac{2(\Gamma - 1)}{\Gamma A})^{\Gamma - 1}(-\frac{\partial H}{\partial \chi})^{\Gamma} \tag{2.22}$$

Then the solution is:

$$H = H_0 \chi^{-\Gamma/(2-\Gamma)}, \tag{2.23}$$

where

$$H_0 = (\frac{1}{2-\Gamma})^{\Gamma/(2-\Gamma)}(\frac{2}{3})^{1/(2-\Gamma)}(\frac{2(\Gamma - 1)}{A})^{(\Gamma-1)/(2-\Gamma)}. \tag{2.24}$$

2.1. SOLVING THE HIGHER ORDER HJ EQUATION

In this section we will show that even for a perfect fluid we can find a recursion relation for the generating functional.

For simplicity we take the comoving coordinate($\chi_{,i} = 0$). Then the Hamiltonian of order $2m$ is:

$$\mathcal{H}^{(2m)} = 2H\gamma_{ij}\frac{\delta\mathcal{S}^{(2m)}}{\delta\gamma_{ij}} + \frac{\delta\mathcal{S}^{(2m)}}{\delta\chi}\frac{\epsilon_0}{\Gamma} + \mathcal{R}^{(2m)} = 0. \tag{2.25}$$

Here $\mathcal{R}^{(2m)}$ is written by previous order terms:

$$\mathcal{R}^{(2m)} = \gamma^{-1/2}\sum_{p=1}^{n-1}\frac{\delta\mathcal{S}^{(2p)}}{\delta\gamma_{ij}}\frac{\delta\mathcal{S}^{(2m-2p)}}{\delta\gamma_{kl}}(2\gamma_{jk}\gamma_{il} - \gamma_{ij}\gamma_{kl}) + \mathcal{V}^{(2m)}, \tag{2.26}$$

where $\mathcal{V}^{(2m)}$ is defined as

$$\mathcal{V}^{(2m)} = \begin{cases} -\frac{1}{2}\gamma^{1/2}\,{}^{(3)}R & \text{for } m{=}1, \\ 0 & \text{otherwise.} \end{cases} \tag{2.27}$$

ϵ_0 can be evaluated by Eq.(2.14) by the use of $S^{(0)}$ and Eq.(2.25) is rewritten as

$$2H\gamma_{ij}\frac{\delta\mathcal{S}^{(2m)}}{\delta\gamma_{ij}} + \frac{\delta\mathcal{S}^{(2m)}}{\delta\chi}\frac{3(2-\Gamma)}{2\Gamma}H\chi + \mathcal{R}^{(2m)} = 0. \tag{2.28}$$

Now we consider the conformal transformation

$$\gamma_{ij} = \Omega^2(u)f_{ij}, \tag{2.29}$$

such that

$$\frac{\partial\Omega}{\partial u} = H\Omega, \tag{2.30}$$

where u is defined by

$$u = \int\frac{2\Gamma d\chi}{3(2-\Gamma)H\chi} = \frac{2}{3H_0}\chi^{\Gamma/(2-\Gamma)} \tag{2.31}$$

and thus

$$\Omega(u) = u^{2/3}. \tag{2.32}$$

Then the HJ equation Eq.(2.28) reduces to

$$\frac{\delta\mathcal{S}^{(2m)}}{\delta u}|_{f_{ij}} + \mathcal{R}^{(2m)} = 0. \tag{2.33}$$

The solution is immediate. For example, the second-order and the fourth-order solutions

are:

$$\mathcal{S}^{(2)} = \int d^3x\gamma^{1/2}\frac{1}{5H_0}\chi^{\Gamma/(2-\Gamma)}\,{}^{(3)}R,$$
$$\mathcal{S}^{(4)} = \int d^3x\gamma^{1/2}(\frac{9}{700}\,{}^{(3)}R^2 - \frac{6}{175}\,{}^{(3)}R_{ij}\,{}^{(3)}R^{ij})\frac{\chi^{3\Gamma/(2-\Gamma)}}{H_0^2}. \tag{2.34}$$

Thus we have obtained the generating functional up to the second order which will be used in Sec.4 to solve the evolution equation for the three-metric Eq.(2.10).

RANGE OF VALIDITY

Perturbative expansion Eq.(2.20) is valid up to second order if $\mathcal{S}^{(0)} > \mathcal{S}^{(2)}$, or from Eqs.(2.21,34)

$$10H^2 > {}^{(3)}R. \tag{2.35}$$

If the characteristic scale length of inhomogeneity is ℓ, then above condition is equivalent to $\ell \gtrsim H^{-1}$. In this sence, this scheme of perturbation is longwave approximation and is equivalent to anti-Newton method.

3. Evolution of three-metric for Perfect Fluid

In this section we solve the evolution equation (2.10) and investigate the dynamics of inhomogeneous spacetime for perfect fluid.

We take the comoving coordinate ($\chi_{,i} = 0$) and set the shift $N_i = 0$. Then by taking χ as time variable, from Eq.(2.17) the lapse function is written as $N = 1/\epsilon_0$. Then the evolution equation of the three-metric Eq.(2.10) at the first order is

$$\frac{\partial\gamma_{ij}^{(1)}}{\partial\chi} = \frac{4}{3(2-\Gamma)}\frac{\gamma_{ij}^{(1)}}{\chi}. \tag{3.1}$$

The first order expression for the three-metric is then

$$\gamma_{ij}^{(1)} = \chi^{4/3(2-\Gamma)}k_{ij}, \tag{3.2}$$

where k_{ij} is an arbitrary function of the spatial coordinates and is called the "seed metric". We can caluculate the third order metric

$$\gamma_{ij}^{(3)} = \chi^{4/3(2-\Gamma)}k_{ij} + \frac{J_0}{(3\Gamma-2)H_0}\chi^{2\Gamma/(2-\Gamma)}(k_{ij}\widehat{R} - 4\widehat{R}_{ij}), \tag{3.3}$$

where $\widehat{R}_{ij}$ refers to the Ricci tensor of the seed metric.

COMPARISON WITH ANTI-NEWTONIAN RESULTS

Recently, Comer et al.[6] have derived the nonlinear solution of Einstein equations for a perfect fluid in the synchronous gauge which describes an inhomogeneous universe at scales larger than the Hubble radius. They expand the three-metric under the assumption that the characteristic comoving length for the metric variation L is greater than the comoving Hubble radius $(aH)^{-1}$:

$$aL > H^{-1} \tag{3.4}$$

This approximation is also called "anti-Newtonian"[5] in the sence that the characteristic velocity of the problem $v \equiv aL/H^{-1}$ is much bigger than the light velocity. Their result up to the third-order is

$$\gamma_{ij}^{(3)} = t^{4/3\Gamma} k_{ij} + \frac{9\Gamma^2}{4(9\Gamma^2 - 4)} t^2 (k_{ij}\widehat{R} - 4\widehat{R}_{ij}). \tag{3.5}$$

Let's make direct comparison of our result Eq.(3.3) with Eq.(3.5). From Eq.(2.17), we find that the lapse function behaves as

$$N = 1/\epsilon_0 = \left(\frac{(\Gamma - 1)}{\Gamma A \gamma^{1/2}} \frac{\delta S}{\delta \chi}\right) \propto \chi^{(2\Gamma-2)/(2-\Gamma)}. \tag{3.6}$$

So if we take $N = \chi^{(2\Gamma-2)/(2-\Gamma)}$, the numerical coefficient H_0 defined in Eq.(2.24) is fixed as

$$H_0 = \frac{2}{3(2-\Gamma)}. \tag{3.7}$$

Then the numerical coefficient in front of the second term in Eq.(4.3) becomes

$$\frac{J_0}{(3\Gamma - 2)H_0} = \frac{1}{5(3\Gamma - 2)H_0^2} = \frac{9(2-\Gamma)^2}{20(3\Gamma - 2)}. \tag{3.8}$$

Now introduce the cosmic time t by $dt = N d\chi$, or

$$t = \frac{2-\Gamma}{\Gamma} \chi^{\Gamma/(2-\Gamma)}. \tag{3.9}$$

Then the third-order three-metric becomes

$$\gamma_{ij}^{(3)} = \left(\frac{\Gamma}{2-\Gamma}\right)^{4/3\Gamma} t^{4/3\Gamma} k_{ij} + \frac{9\Gamma^2}{20(3\Gamma - 2)} t^2 (k_{ij}\widehat{R} - 4\widehat{R}_{ij}). \tag{3.10}$$

By redefining k_{ij} as

$$\left(\frac{\Gamma}{2-\Gamma}\right)^{4/3\Gamma} k_{ij} \to k_{ij}, \tag{3.11}$$

we finally have

$$\gamma_{ij}^{(3)} = t^{4/3\Gamma} k_{ij} + \frac{9\Gamma^2}{20(3\Gamma - 2)} t^2 (k_{ij}\widehat{R} - 4\widehat{R}_{ij}). \tag{3.12}$$

Comparing Eq.(3.12) with Eq.(3.5), we find that the time dependence in Eq.(3.12) is in

perfect agreement with that in Eq.(3.5). Therefore we again conclude in accordance with their result that if a perfect fluid violates the strong energy condition ($\Gamma < 2/3$), then nonlinear inhomogeneities larger than the Hubble radius decay, while grows if a perfect fluid satisfies the strong energy condition. This result has implications for the behaviour of inhomogeneities during an inflationary stage. However, both numerical coefficients are slightly different. This difference ascribes to the difference in the gauge condition taken; we take comoving time orthogonal gauge condition($N_i = 0, U_i \propto \chi_{,i} = 0$), while Comer et al. adopts synchronous gauge condition($N = 1, N_i = 0$). For dust fluid the comoving condition necessarily implies the synchronous condition, and thus two expressions are the same, while for general perfect fluid this is not the case and the difference arises.

Finally we comment on the role of χ as 'time variable'. From Eq.(3.2) and Eq.(3.6), we see that χ field corresponds to the proper time for dust fluid and the conformal time for radiation fluid. This is in agreement with the previous analysis.[4][7]

4. Conclusions

In this paper we have solved the Hamilton-Jacobi equation for general relativity interacting with a perfect fluid up to fourth order. Then we have obtained the respective three-metric. It is indeed possible to apply the gradient expansion to the Hamilton-Jacobi equation for general relativity with a perfect fluid. Solving higher order Hamiltonian reduces to a recursion relation and the solution is immediately given, and it is easy to generalize to higher dimension. We assumed the perfect fluid is irrotational and took comoving coordinate. First condition can be loosened, but taking coordinate other than comoving one is difficult because counting the order of spatial gradient in Eq.(2.13) would be difficult.

We found that if a perfect fluid violates the strong energy condition, which is necessary for inflation to occur, then longwave nonlinear inhomogeneities decay, while they grow otherwise and the same conclusion is drawn for scalar field with an exponential potential in arbitral dimension.

As for the comparison between the two schemes (HJ method and anti-Newton(AN) method), previous and our analysis show that for a quasi-isotropic spacetime (in the sence that zeroth order generating functional neglects the degree of freedom of shear) HJ method is more poweful in deriving higher order solution for a dust, a scalar field and a perfct fluid. And for generalization to higher dimension, HJ method is simpler and much more

straightforward. Moreover, in HJ method different gauge choice is easy to be implemented because deriving the generating functional does not require the lapse function. However, in that sheme the inclusion of the degree of freedom of shear is not easy to handle, while AN method can handle the shear at least up to third-order.[8] Hence, we may say that the roles of two schemes are complementary.

Acknowledgements: The author would like to thank Misao Sasaki for suggesting this problem and a critical reading of the manuscript, and Takashi Nakamura and Yasufumi Kojima for useful discussions and comments, and Yasusada Nambu for drawing his attention to the HJ method. He also wishes to thank Professor H.Sato for continuous encouragement.

REFERENCES

1. V.De Lapparent, M.J.Gellar, and J.P.Huchra, Ap. J. **302**, L1 (1986).
2. T.J.Broadhurst, R.S.Ellis, D.C.Koo, and A.S.Szalay, Nature **343** 726 (1990).
3. D.S. Salopek and J.R. Bond, Phys. Rev.**D42**, 3936 (1990); Phys. Rev.**D43**, 1005 (1991); D.S. Salopek, Phys. Rev.**D43**, 3214 (1991); D.S. Salopek and J.M. Stewart, Class. Quant. Grav.**9**, 1943 (1992) .
4. J. Parry, D.S. Salopek, and J.M. Stewart, Phys. Rev.**D49**, 2872 (1994).
5. K. Tomita, Prog. Theor. Phys. **54**, 730 (1975).
6. G. L. Comer, N. Deruelle, D. Langlois, and J. Parry, Phys. Rev.**D49**, 2759 (1994).
7. D. S. Salopek and J. M. Stewart, Phys. Rev.**D47**, 3235 (1993).
8. D. Langlois and N. Deruelle, preprint gr-qc/9411040.

Silent Universe Damaged by Gravito-Magnetic Part [1]

Yasufumi Kojima

Department of Physics, Tokyo Metropolitan University,
Hachioji, Tokyo 192-03, Japan

Abstract

Evolution of collisionless matter in the expanding universe is studied within general relativity. An approximate solution, whose perturbation scale is comparable to or larger than the Hubble radius, is obtained by the series expansion with respect to the background scale factor. The solution represents that the early density contrast is controlled by the initial data at each Lagrangian position and the subsequent growth is modified by the presence of the magnetic part of the Weyl curvature, which is produced by the non-linear coupling, even if it vanishes in the initial condition. Therefore, the adaptability of the "silent universe" recently proposed is limited to the early phase or the modes with large wavelength beyond the horizon scale.

1 Introduction

Zel'dovich [1] examined the dynamics of irrotational dust flow as a model of large-scale structure of the Universe. He formulated the motion under the Newtonian potential in the expanding universe in terms of the Lagrangian coordinate. The model is valid before the pressure force becomes important, and can be used to connect the results of the linear stage to the non-linear regime regarding the density contrast. The Lagrangian formalism is extended to include higher order corrections [2,3].

Recently, Matarrese et al. [4] proposed an approximate method to calculate the dynamics of dust in the expanding universe within the relativistic framework. If the so-called "magnetic" part of the Weyl curvature can be neglected, the dynamics can be described by the sixth-order ordinary differential equations. The motion of the dust is geodesic and the dynamics of the system can be determined only by the initial data at each Lagrangian position. That is, there is no force exerted to change the motion. The flow never communicates with neighbors, and the model is therefore called as "silent universe". They subsequently estimated the effect of the gravito-magnetic part in a qualitative way [5]. Croudace et al. [6] showed that nearly one-dimensional dust collapse is numerically unstable in the system where the gravito-magnetic part is approximately neglected. They also suggested that the instability is attributed to the neglect of the gravito-magnetic part. It is therefore important to clarify the role of the gravito-magnetic part to the dynamics. The post-Newtonian formalism is used and the relation between the Newtonian and the general relativistic dynamics is examined in Ref. [7,8]. The approximation is useful if the characteristic scale of the spatial variation is smaller than the Hubble radius. The opposite limit is also sometimes drawing attention, i.e., "the long wavelength limit" or "anti-Newtonian approximation" [9]. The relevant physical situation is as follows. Due to the large expansion during the inflationary epoch, the perturbation scale has been stretched out beyond

[1] This is based on Y. Kojima(1994), Phys. Rev. D50, 6110, *Early Growth of Cosmological Inhomogeneity at the Horizon Scale*

the horizon. The perturbation subsequently has re-entered the horizon and has started to form the Zel'dovich's pancake.

In this paper, the role of the gravito-magnetic part to the dynamics is examined in such a situation. It is adequate to approximate the fluid as collisionless dust, because the pressure force is negligible there. If the initial data are given by a scalar function, then the density perturbation can be determined by the function. The tensor modes corresponding to the degree of the gravitational wave vanish for the initial condition. The non-linear coupling however produces the modes at the later time, which subsequently affect the density growth. This picture is general, but when and how this occurs depend on the initial data. We will consider a simple model and demonstrate the effect. In Section 2, the basic equations governing the dynamics of the collisionless dust in the expanding universe are summarized. We consider spatially flat universe, i.e., Einstein-de Sitter universe, as the background. An approximate solution is obtained by the power series of the scale factor in Section 3. The solution is valid until the mildly non-linear stage. The solution describes how the gravito-magnetic part is produced and affects the density evolution. The result is applied to a simple case in Sections 4. Finally, conclusion is given in Section 5.

2 Relativistic dynamics of dust

In this section, we shall summarize the basic equations which describe the evolution of dust. (See e.g., Ref.[5].) Following Ellis [10], equations can be written in terms of the observable fluid and geometric quantities: the mass density ρ, the volume expansion θ, the shear tensor σ_{ij}, and the electric and magnetic parts of the Weyl tensor, E_{ij}, H_{ij}. These tensors, σ_{ij}, E_{ij} and H_{ij} are symmetric traceless tensors. We shall use the normalized quantities, Δ, ϑ, s^i_j, e^i_j, $\mathcal{H}^i_j$, which vanish in the background, as

$$\Delta = (\rho/\rho_0 - 1)/a, \quad \vartheta = (3t/2a)(\theta - \theta_0), \quad s^i_j = (3t/2a)\sigma^i_j,$$
$$e^i_j = (3t^2/2a)E^i_j, \quad \mathcal{H}^i_j = (3t^2/2a)H^i_j, \tag{1}$$

where ρ_0, θ_0 are the background density and volume expansion, and a is the scale factor in the Einstein-de Sitter universe. They are given by

$$\rho_0 = 1/(6\pi G t^2), \quad \theta_0 = 2/t, \quad a = a_0(t/t_0)^{2/3} = B^{-1/3}t^{2/3}, \tag{2}$$

where $B = t_0^2/a_0^3$. Throughout this paper, we use the comoving synchronous coordinate,

$$ds^2 = -dt^2 + a^2 h_{ij} dq^i dq^j. \tag{3}$$

The metric tensor, h_{ij} evolves as

$$h'_{ij} = s^k_j h_{ik} + s^k_i h_{kj} + \frac{2}{3}\vartheta h_{ij}, \tag{4}$$

where the prime means a derivative with respect to a.

The full set of equations for the variables in equation (1) consists of two different kinds: propagation equations and constraint equations. The propagation equations are

$$\Delta' + \frac{1}{a}(\Delta + \vartheta) + \Delta\vartheta = 0, \tag{5}$$

$$\vartheta' + \frac{3}{2a}(\Delta + \vartheta) + \frac{1}{3}\vartheta^2 + s^i_j s^j_i = 0, \tag{6}$$

$$s^{i\prime}_j + \frac{3}{2a}(s^i_j + e^i_j) + \frac{2}{3}\vartheta s^i_j + s^i_k s^k_j - \frac{1}{3}\delta^i_j s^k_l s^l_k = 0, \tag{7}$$

$$\begin{aligned} &e^{i\prime}_j + \frac{1}{a}(s^i_j + e^i_j) + \vartheta e^i_j + \Delta s^i_j - \frac{5}{2}e^i_k s^k_j - \frac{1}{2}s^i_k e^k_j + \delta^i_j e^k_l s^l_k \\ &-\frac{3t}{4a^2}h_{jk}(\epsilon^{kpq}\mathcal{H}^i_{p;q} + \epsilon^{ipq}\mathcal{H}^k_{p;q}) = 0, \end{aligned} \tag{8}$$

$$\begin{aligned} &\mathcal{H}^{i\prime}_j + \frac{1}{a}\mathcal{H}^i_j + \vartheta\mathcal{H}^i_j - \frac{5}{2}\mathcal{H}^i_k s^k_j - \frac{1}{2}s^i_k\mathcal{H}^k_j + \delta^i_j\mathcal{H}^k_l s^l_k \\ &+\frac{3t}{4a^2}h_{jk}(\epsilon^{kpq}e^i_{p;q} + \epsilon^{ipq}e^k_{p;q}) = 0, \end{aligned} \tag{9}$$

where ϵ^{ijk} is the Levi-Civita tensor. The quantities in equation (1) have to satisfy the following constraint equations,

$$\mathcal{H}^i_j = \frac{t}{2a}h_{jk}(\epsilon^{kpq}s^i_{p;q} + \epsilon^{ipq}s^k_{p;q}), \tag{10}$$

$$s^i_{j;i} = \frac{2}{3}\vartheta_{,j}, \tag{11}$$

$$\mathcal{H}^i_{j;i} = \frac{2a^2}{3t}h_{jk}h_{lm}\epsilon^{kpq}s^l_p e^m_q, \tag{12}$$

$$e^i_{j;i} = \frac{2}{3}\Delta_{,j} - \frac{2a^2}{3t}h_{jk}h_{lm}\epsilon^{kpq}s^l_p\mathcal{H}^m_q. \tag{13}$$

If $\mathcal{H}^i_j = 0$, s^i_j and e^i_j can be diagonalized at the same time. The dynamical system is reduced to the six-order ordinary differential equations for the six variables, $\Delta, \vartheta, s^1_1, s^2_2, e^1_1, e^2_2$, and $s^3_3 = -s^1_1 - s^2_2$, $e^3_3 = -e^1_1 - e^2_2$.

3 Approximate solution

In the linear regime, the metric for the scalar perturbations is given by a single gauge-invariant potential, Φ_H [11]. In the comoving synchronous gauge, we have

$$h_{ij} = (1 + \frac{10}{3}\Phi_H)\delta_{ij} + \frac{3t_0^2 a}{a_0^3}\Phi_{H,ij}. \tag{14}$$

We may neglect the potential itself in practical problem, but not the spatial derivative of it [6,7]. With the definition, $\varphi(q^i) = -(3t_0^2/2a_0^3)\Phi_H$, we take as the initial condition,

$$h_{ij} = \delta_{ij} - 2a\varphi_{ij}. \tag{15}$$

The indices of φ mean the derivative with respect to q^i and can be raised and lowered by η_{ij}, η^{ij}, where η_{ij} and η^{ij} are the metrics of three dimensional Euclidian space, e.g., $\varphi^i_{jk} = \eta^{il}\partial_l\partial_j\partial_k\varphi$, which will be used later. Equations (5)-(13) admit the following solution by the expansion series near $a \sim 0$,

$$\begin{aligned} &\Delta = \sum_{n=1}\Delta_{(n)}a^{n-1}, \quad \vartheta = \sum_{n=1}\vartheta_{(n)}a^{n-1}, \quad s^i_j = \sum_{n=1}s^i_{(n)j}a^{n-1}, \\ &e^i_j = \sum_{n=1}e^i_{(n)j}a^{n-1}, \quad \mathcal{H}^i_j = \frac{t}{2a}\sum_{n=1}\mathcal{H}^i_{(n)j}a^{n-1}, \end{aligned} \tag{16}$$

where the expansion coefficients such as $\Delta_{(n)}$ are functions of q^i. The growing and decaying solutions in the linear regime are given by e.g., $\Delta \propto$ const., and $\Delta \propto a^{-5/2}$ in our convention (1). The only growing mode solutions are examined here. The order n in this paper does not refer to $n-$fold multiplication of φ, i.e., perturbation amplitude. The number n is related to the order of the gradient expansion method [12], i.e., the order n means $2n-$times spatial derivatives of the expansion coefficient. Equations are grouped into the terms with the same number of spatial derivatives in the gradient expansion method. The range of the validity of the expansion series will be discussed later.

Corresponding to the initial condition given by the scalar function $\varphi(q^i)$, the growing solution of the linearized equations can be given by

$$\Delta_{(1)} = -\vartheta_{(1)} = K, \quad -s^i_{(1)j} = e^i_{(1)j} = \varphi^i_j - \frac{1}{3}K\delta^i_j, \quad \mathcal{H}^i_{(1)j} = 0, \tag{17}$$

where $K = \mathrm{tr}[\varphi^i_j]$. The magnetic part of the Weyl tensor vanishes for the initial condition as expected, because the tensor perturbations are decoupled with the density contrast within the linearized equations. See, e.g., standard textbooks or Ref.[13] for the linearized equations of (5)-(13).

Now we proceed the expansion to examine the effect of gravito-magnetic part to the density contrast. The gravito-magnetic part at the second-order level, $\mathcal{H}^i_{(2)j}$ does not vanish in general. It affects the shear and the gravito-electric part at the third-order level, $s^i_{(3)j}, e^i_{(3)j}$, and the density and the expansion at the fourth-order level, $\Delta_{(4)}, \vartheta_{(4)}$. See the following diagram.

$$\begin{array}{ccccccc}
\Delta_{(1)}, \vartheta_{(1)} & \rightarrow & \Delta_{(2)}, \vartheta_{(2)} & \rightarrow & \Delta_{(3)}, \vartheta_{(3)} & \rightarrow & \Delta_{(4)}, \vartheta_{(4)} \\
 & \times & & \times & & \nearrow & \\
s^i_{(1)j}, e^i_{(1)j} & \rightarrow & s^i_{(2)j}, e^i_{(2)j} & \rightarrow & s^i_{(3)j}, e^i_{(3)j} & & \\
 & \searrow & & \nearrow & & & \\
\mathcal{H}^i_{(1)j} = 0 & & \mathcal{H}^i_{(2)j} & & & &
\end{array}$$

We calculate these quantities influenced by the presence of gravito-magnetic part. The results are

$$\Delta_{(2)} = K^2 - \frac{4}{7}M, \tag{18}$$

$$\vartheta_{(2)} = -K^2 + \frac{8}{7}M, \tag{19}$$

$$s^i_{(2)j} = (\frac{1}{3}K^2 + \frac{10}{21}M)\delta^i_j - \frac{12}{7}K\varphi^i_j + \frac{5}{7}\varphi^i_k\varphi^k_j, \tag{20}$$

$$e^i_{(2)j} = -(\frac{1}{3}K^2 + \frac{26}{21}M)\delta^i_j + \frac{20}{7}K\varphi^i_j - \frac{13}{7}\varphi^i_k\varphi^k_j, \tag{21}$$

$$\mathcal{H}^i_{(2)j} = \frac{12}{7}[\bar{\epsilon}^{ipq}(\varphi^m_{mp}\varphi_{qj} + \varphi^q_{jm}\varphi^m_p) + \bar{\epsilon}_{jpq}(\varphi^{mp}_m\varphi^{iq} + \varphi^{iq}_m\varphi^{mp})], \tag{22}$$

$$\Delta_{(3)} = K^3 - \frac{8}{7}KM - \frac{10}{21}P, \tag{23}$$

$$\vartheta_{(3)} = -K^3 + \frac{12}{7}KM + \frac{10}{7}P, \tag{24}$$

$$
\begin{aligned}
s^i_{(3)j} &= -\frac{1}{16}Bw^i_j + (\frac{1}{3}K^3 + \frac{11}{21}MK + \frac{92}{21}P)\delta^i_j - (\frac{46}{21}K^2 + \frac{25}{7}M)\varphi^i_j \\
&\quad + \frac{39}{7}K\varphi^i_k\varphi^k_j - \frac{92}{21}\varphi^i_k\varphi^k_l\varphi^l_j,
\end{aligned} \tag{25}
$$

$$
\begin{aligned}
e^i_{(3)j} &= \frac{7}{48}Bw^i_j - (\frac{1}{3}K^3 + \frac{137}{63}KM + \frac{92}{9}P)\delta^i_j + (\frac{46}{9}K^2 + \frac{179}{21}M)\varphi^i_j \\
&\quad - \frac{43}{3}K\varphi^i_k\varphi^k_j + \frac{92}{9}\varphi^i_k\varphi^k_l\varphi^l_j,
\end{aligned} \tag{26}
$$

$$
\Delta_{(4)} = K^4 - \frac{12}{7}K^2M + \frac{292}{693}M^2 - \frac{6460}{4851}PK + \frac{2}{77}BQ, \tag{27}
$$

$$
\vartheta_{(4)} = -K^4 + \frac{16}{7}K^2M - \frac{5008}{4851}M^2 + \frac{16600}{4851}PK - \frac{8}{77}BQ, \tag{28}
$$

where $\bar{\epsilon}^{ijk}$ and $\bar{\epsilon}_{ijk}$ are the Levi-Civita tensor in the Euclidian space, and

$$
M = (\varphi^i_i\varphi^j_j - \varphi^i_j\varphi^j_i)/2, \tag{29}
$$

$$
P = \det[\varphi^i_j], \tag{30}
$$

$$
\begin{aligned}
Q &= \varphi^i_j(\varphi^k_l\varphi^{jl}_{ik} - 4\varphi^j_k\varphi^{kl}_{il} + 4\varphi^j_{ik}\varphi^{kl}_l - 3\varphi^{kl}_i\varphi^j_{kl} - \varphi^k_{ik}\varphi^{jl}_l) \\
&\quad + K(2\varphi^i_j\varphi^{jk}_{ik} - \varphi^j_{ij}\varphi^{ik}_k + \varphi^i_{jk}\varphi^{jk}_i) + (K^2 - 4M)\varphi^{ij}_{ij},
\end{aligned} \tag{31}
$$

$$
w^i_j = [\bar{\epsilon}^{ipq}\mathcal{H}_{(2)jp,q} + \bar{\epsilon}_{jpq}\mathcal{H}^{ip,q}_{(2)}]. \tag{32}
$$

We can easily discriminate the terms come from the gravito-magnetic part in these expressions. They contain the third- or fourth-order derivatives of φ. In the other words, the system can be determined only by the initial deformation tensor, φ^i_j, if the gravito-magnetic term is neglected. The typical ratio of the gravito-magnetic term to other terms is $(B\partial^2_q\varphi_{ij})/(\varphi_{ij})^2 \sim t^2/(l^2 a\varphi_{ij})$, where l is perturbation scale of φ_{ij}. The ratio of the wavelength of the perturbation to the horizon is therefore determined by the constant B in the approximate solution. Small values of B correspond to the perturbations beyond the horizon scale. In the limit of $B \to 0$, we can eliminate the gravito-magnetic terms in $s^i_{(3)j}, e^i_{(3)j}, \Delta_{(4)}, \vartheta_{(4)}$. As pointed in Ref. [5], this limit corresponds to the physical situation in which the perturbation scale is much larger than the Hubble radius, $l^2 \gg t^2$, even though $a\varphi_{ij}$ is small. Spatial gradients play no role in this case. However, the dynamical role is not negligible for the perturbations with the subhorizon scale. For such perturbations, i.e., large B, a is limited to sufficiently small value for the convergence of the expansion series (16). That is, such perturbations behave as wave, so that our approximation breaks down soon and different treatment is necessary. We therefore assume that the perturbation scale is not so smaller than the Hubble radius, and that B is smaller than a critical value.

4 Effect of the magnetic part

Different degrees of freedom, i.e., information about higher derivatives of φ, are necessary to evaluate the gravito-magnetic term. We can not evaluate the effect of the term unless the function is specified. One trivial example is $\varphi_{ijk} = \varphi_{ijkl} = 0$, in which the contribution from the gravito-magnetic part vanishes in $s^i_{(3)j}, e^i_{(3)j}, \Delta_{(4)}, \vartheta_{(4)}$. In order to demonstrate the effect of the gravito-magnetic term, we adopt a simple function near the origin;

$$\varphi = -X_1(q^1)X_2(q^2)X_3(q^3), \tag{33}$$

where $X_i(q^i) = 1 - \lambda_i(q^i)^2/2 + \lambda_i^2 d(q^i)^4/8 + \cdots$, and λ_i and d are positive constants. This potential gives the local density maximum at the origin and the matter near the origin collapses anisotropically with the rate λ_i along the axis q^i. The function X_i is the approximation of the cosine type, $\cos\sqrt{\lambda_i}q^i$ for $d = 1/3$, and of the Gaussian type, $\exp[-\frac{1}{2}\lambda_i(q^i)^2]$ for $d = 1$, near the origin. In this way, a class of the potential can be described in the form (33) near the density peak. Although it is possible to calculate the evolution at every Lagrangian points, the motion at the density peak is the most interesting. Therefore, we concentrate on the behavior at the Lagrangian coordinate $q^i = 0$ from now on. The evolution at the linear stage is given as

$$\Delta_{(1)} = -\vartheta_{(1)} = \lambda_1 + \lambda_2 + \lambda_3 > 0,$$

$$-s^i_{(1)j} = e^i_{(1)j} = \frac{1}{3}\mathrm{diag}(2\lambda_1 - \lambda_2 - \lambda_3, -\lambda_1 + 2\lambda_2 - \lambda_3, -\lambda_1 - \lambda_2 + 2\lambda_3). \tag{34}$$

If the distortion is one dimensional, the solution of equations (5)-(13) can be written as the Szekeres solution [15],

$$\Delta = -\vartheta = 3s^1_1 = 3s^2_2 = -\frac{3}{2}s^3_3 = -3e^1_1 = -3e^2_2 = \frac{3}{2}e^3_3 = \frac{f}{1-af}, \tag{35}$$

where f is a constant given at each Lagrangian position and the other components vanish. The caustic, i.e., the shell-crossing singularity, corresponds to $af = 1$. Croudace et al. [6] showed that the Szekeres solution is unstable in the system without the gravito-magnetic part. They showed that the deviation from the exact solution goes to minus infinity in one component of the electric part, e^1_1, and to plus infinity in e^2_2, as the solution approaches the singularity. They also conjectured that the gravito-magnetic part might suppress the instability. We will consider this problem in terms of the expansion solution. For small af, the function in (35) can be written as $\frac{f}{1-af} = f(1 + af + (af)^2 + \cdots)$, and we compare the analytic form with the expansion one. If completely planar initial condition is imposed, i.e., $\lambda_1 = \lambda_2 = 0$, then the gravito-magnetic part term always vanishes and equations (18) - (28) reduce to the Szekeres solution with $f = \lambda_3$. The initial condition is relaxed to include the small deviation from the symmetric case, i.e., nearly one-dimensional collapse, $f = \lambda_3 \gg \lambda_1 > \lambda_2 = 0$. Keeping the lowest order of $\xi = \lambda_1/\lambda_3$, we have the approximate solution as

$$\begin{aligned}
s^1_{(1)1} &= \frac{f}{3}(1 - 2\xi), \quad s^2_{(1)2} = \frac{f}{3}(1 + \xi),\\
s^1_{(2)1} &= \frac{f^2}{3}(1 - \frac{12}{7}\xi), \quad s^2_{(2)2} = \frac{f^2}{3}(1 + \frac{24}{7}\xi),\\
s^1_{(3)1} &= \frac{f^3}{3}[1 - 2\xi + \frac{9}{14}(1 + 3d)B\xi],\\
s^2_{(3)2} &= \frac{f^3}{3}[1 + \frac{32}{7}\xi - \frac{9}{14}(1 + 3d)B\xi],\\
e^1_{(1)1} &= -\frac{f}{3}(1 - 2\xi), \quad e^2_{(1)2} = -\frac{f}{3}(1 + \xi),\\
e^1_{(2)1} &= -\frac{f^2}{3}(1 - \frac{20}{7}\xi), \quad e^2_{(2)2} = -\frac{f^2}{3}(1 + \frac{40}{7}\xi),\\
e^1_{(3)1} &= -\frac{f^3}{3}[1 - \frac{122}{21}\xi + \frac{3}{2}(1 + 3d)B\xi],\\
e^2_{(3)2} &= -\frac{f^3}{3}[1 + \frac{200}{21}\xi - \frac{3}{2}(1 + 3d)B\xi].
\end{aligned} \tag{36}$$

The shear and electric part tensors can be diagonalized in this model up to this order, and $e^3_{(n)3} = -e^1_{(n)1} - e^2_{(n)2}$, $s^3_{(n)3} = -s^1_{(n)1} - s^2_{(n)2}$. If small ξ is allowed, the numerical coefficients in front of ξ increase with the order n and have definite sign in each series. When summing up the series, the terms with ξ can not be ignored for later time. This tendency is significant in the electric part terms. The sign in front of ξ is opposite in $e^1_{(n)1}$ and $e^2_{(n)2}$, so that the deviation in these components increases toward different direction, i.e., to minus infinity and to plus infinity. In this way, we can understand the reason why the deviation from the planar symmetric case increases as a increases. The expansion solution up to the third-order suggests that the planar collapse solution is unstable in the system without the gravito-magnetic part. One interesting thing is that the gravito-magnetic term has the opposite sign in $s^1_{(3)1}, s^2_{(3)2}, e^1_{(3)1}, e^2_{(3)2}$. Hence, the gravito-magnetic part will cancel or weaken the instability somewhat. This is true in the third-order level, but it is necessary to extend to the higher order or to simulate numerically in order to address this problem completely.

Next we consider the effect of the gravito-magnetic part on the evolution of density contrast. For the initial condition (33), the solutions at the origin are given by

$$
\begin{aligned}
\Delta_{(2)} &= \lambda_1^2 + \lambda_2^2 + \lambda_3^2 + \frac{10}{7}(\lambda_1\lambda_2 + \lambda_2\lambda_3 + \lambda_3\lambda_1), \\
\Delta_{(3)} &= \lambda_1^3 + \lambda_2^3 + \lambda_3^3 + \frac{13}{7}[(\lambda_1 + \lambda_2)\lambda_3^2 + (\lambda_2 + \lambda_3)\lambda_1^2 + (\lambda_3 + \lambda_1)\lambda_2^2] \\
&\quad + \frac{44}{21}\lambda_1\lambda_2\lambda_3, \\
\Delta_{(4)} &= \lambda_1^4 + \lambda_2^4 + \lambda_3^4 + \frac{16}{7}[(\lambda_1 + \lambda_2)\lambda_3^3 + (\lambda_2 + \lambda_3)\lambda_1^3 + (\lambda_3 + \lambda_1)\lambda_2^3] \\
&\quad + [\frac{2074}{693} + \frac{12}{77}B(1-d)](\lambda_1^2\lambda_2^2 + \lambda_2^2\lambda_3^2 + \lambda_3^2\lambda_1^2) \\
&\quad + [\frac{14260}{4851} - \frac{12}{77}B(1-d)](\lambda_1 + \lambda_2 + \lambda_3)\lambda_1\lambda_2\lambda_3 \\
&\quad - \frac{8}{77}B[\lambda_1^2(\lambda_2 - \lambda_3)^2 + \lambda_2^2(\lambda_3 - \lambda_1)^2 + \lambda_3^2(\lambda_1 - \lambda_2)^2].
\end{aligned}
\tag{37}
$$

All terms except the terms proportional to B in $\Delta_{(4)}$ are positive. As mentioned before, there is no force to stop the collapse in the system without the gravito-magnetic part. The gravito-magnetic part terms affect the evolution of $\Delta_{(4)}$ except spherically symmetric case, $\lambda_1 = \lambda_2 = \lambda_3$, and planar symmetric case, $\lambda_1 = \lambda_2 = 0$. The terms are not definite sign, but the terms become negative and hence suppress the collapse in the Gaussian peak, $d = 1$. In this way, the gravito-magnetic parts in general affect the density contrast in the fourth-order level and the effect is significant for the perturbation with subhorizon scale, which corresponds to larger B.

5 Discussion

In this paper, the dynamical role of the magnetic part of the Weyl tensor was examined in the model of expanding universe. We assumed that the density perturbation with long wavelength is given and the gravito-magnetic part vanishes at the linear stage. The gravito-magnetic part is produced in general, and affects the shear and gravito-electric part at the third-order level, and the density contrast at the fourth-order level in the expansion series solution. The effect of the gravito-magnetic part is therefore crucial for the late stage.

We evaluated the effect at the Lagrangian position corresponding to the local density peak. The model shows that the planar collapse is unstable in the approximate system without the gravito-magnetic term, but that the gravito-magnetic term suppresses the growth of the instability at the lowest order. In this way, nearly planar collapse may be realized if the gravito-magnetic

part is correctly taken into account. We have to pay attention to avoiding spurious solutions, if the gravito-magnetic part is approximately ignored.

Bertschinger and Jain [15] numerically calculated the relativistic collapse without the magnetic part. They found that the growth rate of the spindle-like collapse is larger than that of the planer collapse. This is contrast to the Newtonian case. Therefore, it is necessary to include the magnetic part and to reexamine which is more generic, spindle-like or planar collapse in the relativistic system.

References

[1] Ya.B. Zel'dovich, Astron. Astrophys. **5**, 84(1970).

[2] T. Buchert, Astron. Astrophys. **267**, L51(1993).

[3] M. Lachièze-Rey, Astrophys. J. **408**, 403(1993).

[4] S. Matarrese, O. Pantano, and D. Saez, Phys. Rev. D**47**, 1311 (1993).

[5] S. Matarrese, O. Pantano, and D. Saez, Phys. Rev. Lett. **72**, 320 (1994), Mon. Not. R. Astron. Soc. **271**, 513(1994).

[6] K.M. Croudace, J. Parry, D.S. Salopek, and J.M. Stewart, Astrophys. J. **423**, 22(1994).

[7] L. Kofman, and D. Pogsyan, preprint, IfA-94/22 (1994).

[8] E. Bertschinger, and A.J.S., Hamilton, Astrophys. J. **435**, 1(1994).

[9] K. Tomita, Prog. Theor. Phys. **54**, 730(1975).

[10] G.F.R. Ellis, in *General Relativity and Cosmology* edited by R.K. Sachs (Academic, New York, 1971)

[11] J.M. Bardeen, Phys. Rev. D**22**, 1882(1980).

[12] J. Parry, D.S. Salopek, and J.M. Stewart, Phys. Rev. D**49**, 2872(1994).

[13] M. Bruni, P.K.S. Dunsby, and G.F.R. Ellis, Astrophys. J. **395**, 34(1992).

[14] P. Szekeres, Commun. Math. Phys., **41**, 55(1975).

[15] E. Bertschinger, and B. Jain, Astrophys. J. **431**, 486(1994).

Gradient Expansion in Brans-Dicke Theory

Jiro SODA

Department of Fundamental Sciences
FIHS
Kyoto University, 606, Japan

Abstract

The non-linear time evolution of the inhomogeneities of the gravitational constant is investigated in the context of the Brans-Dicke theory. It is shown that the variation rate is surpressed in the case of the negative curvature. On the contrary, in the case of the positive curvature the competition between the curvature inhomogenieties and that of the Brans-Dicke field determines the rate of the change of the gravitational constant.

1 Introduction

It is Dirac who first takes smallness of the following number seriously:

$$\frac{Gm_p m_e}{e^2} \sim 10^{-40} , \tag{1}$$

where G, e, m_p and m_e are the gravitational constant, the charge of the electron, the proton mass and the electron mass. Dirac' idea is simple; The gravitational constant varies with time like as

$$G \propto \frac{1}{t} . \tag{2}$$

The smallness of the number merely indicates our Universe is old!!

As a concrete model that realizes Dirac's idea, it is known that Brans-Dicke theory [1] is most permissible in the sense that it appears as a low energy theory of superstring theory naturally and it passed the classical tests such as the equivalence principle. The action for Brans-Dicke theory with dust matter is

$$I = \int d^4x\sqrt{-g}[\phi R^{(4)} - \frac{\omega}{\phi}g^{\mu\nu}\partial_\mu\phi\partial_\nu\phi - \frac{n}{2m}(g^{\mu\nu}\partial_\mu\chi\partial_\nu\chi + m^2)] , \tag{3}$$

where ω is the Brans-Dicke parameter and χ is the velocity potential for the dust fluid. In the isotropic and homogeneous flat Universe, the time variation of the gravitational constant becomes

$$\frac{\dot{G}}{G} = -\frac{H(t)}{\omega+1} \propto \frac{1}{t} , \tag{4}$$

where H is the Hubble parameter. Experimental constraint is not so severe,

$$\frac{\dot{G}}{G} < 10^{-11}/\text{year}. \tag{5}$$

The homogeneous results give us some feeling, however our universe is not homogeneous in reality. Hence we study the effects of the non-linear inhomogeneties on the variation of the gravitational constant in this paper. As a method to treat the inhomogeneities, we use the gradient expansion method which has old history. [2, 3, 4, 5, 6]

2 Hamilton-Jacobi Equation for Brans-Dicke Theory

Let us begin to write down the Hamiltonian form of the action for the Brans-Dicke theory. In the ADM formalism, the metric is parametrized as

$$ds^2 = -N^2dt^2 + \gamma_{ij}(dx^i + N^i dt)(dx^j + N^j dt) , \tag{6}$$

where N and N^i are the lapse and shift functions respectively, and γ_{ij} is the 3-metric. Using the above metric, we obtain the Hamiltonian form of the action (3) as

$$I = \int d^4x\{\pi^{ij}\dot{\gamma}_{ij} + \pi^\phi\dot{\phi} + \pi^\chi\dot{\chi} - NH - N^iH_i\} , \tag{7}$$

where

$$\begin{aligned} H &= \frac{1}{\phi\sqrt{\gamma}}\pi^{ij}\pi^{kl}[\gamma_{ik}\gamma_{jl} - \frac{\omega+1}{2\omega+3}\gamma_{ij}\gamma_{kl}] \\ &+ \frac{1}{2(2\omega+3)}\frac{\phi}{\sqrt{\gamma}}\pi_\phi^2 - \frac{1}{2\omega+3}\frac{1}{\sqrt{\gamma}}\pi\pi_\phi + \sqrt{1+\gamma^{ij}\chi_i\chi_j}\,\pi^\chi \\ &- \sqrt{\gamma}\phi R + \omega\frac{\sqrt{\gamma}}{\phi}\gamma^{ij}\partial_i\phi\partial_j\phi + 2\sqrt{\gamma}\Delta\phi , \end{aligned} \tag{8}$$

$$H_i = -2(\gamma_{ik}\pi^{kj})_{,j} + \pi^{lk}\gamma_{lk,i}\pi^\phi\phi_{,i} + \pi^\chi\chi_{,i} . \tag{9}$$

Here π^{ij}, π^ϕ and π^χ are conjugate to γ_{ij}, ϕ and χ, respectively, and R denotes the 3-dimensional scalar curvature. Variation with respect to the momentum yields the

equations of motion

$$\frac{1}{N}(\dot{\phi} - N^i\phi_{,i}) = \frac{1}{2\omega+3}\frac{1}{\sqrt{\gamma}}[\phi\pi_\phi - \pi] , \tag{10}$$

$$\frac{1}{N}(\dot{\chi} - N^i\chi_{,i}) = \sqrt{1+\gamma^{ij}\chi_i\chi_j} , \tag{11}$$

$$\begin{aligned}\frac{1}{N}(\dot{\gamma}_{ij} - N_{i\bar{j}} - N_{j\bar{i}}) &= \frac{2}{\phi\sqrt{\gamma}}\pi^{kl}[\gamma_{ik}\gamma_{jl} - \frac{\omega+1}{2\omega+3}\gamma_{ij}\gamma_{kl}] \\ &\quad -\frac{1}{2\omega+3}\frac{1}{\sqrt{\gamma}}\gamma_{ij}\pi_\phi . \end{aligned} \tag{12}$$

Hamilton-Jacobi equation is convenient for our purpose,

$$\begin{aligned}&\frac{1}{\phi\sqrt{\gamma}}\frac{\delta S}{\delta\gamma_{ij}}\frac{\delta S}{\delta\gamma_{kl}}[\gamma_{ik}\gamma_{jl} - \frac{\omega+1}{2\omega+3}\gamma_{ij}\gamma_{kl}] \\ &+\frac{1}{2(2\omega+3)}\frac{\phi}{\sqrt{\gamma}}(\frac{\delta S}{\delta\phi})^2 - \frac{1}{2\omega+3}\frac{1}{\sqrt{\gamma}}\gamma_{ij}\frac{\delta S}{\delta\gamma_{ij}}\frac{\delta S}{\delta\phi} \\ &+\sqrt{1+\gamma^{ij}\chi_{,i}\chi_{,j}}\frac{\delta S}{\delta\chi} - \sqrt{\gamma}\phi R + \omega\frac{\sqrt{\gamma}}{\phi}\gamma^{ij}\partial_i\phi\partial_j\phi + 2\sqrt{\gamma}\Delta\phi = 0 .\end{aligned} \tag{13}$$

The momentum constraint is rather trivial condition which states that the generating functional is invariant under the spatial coordinate transformation.

3 Gradient Expansion

At this point, we need some approximation procedure. We adopt the long wavelength approximation to treat the nonlinear inhomogeneities beyond the horizen scale. In particular, let us follow the method developed by Salopek and the coorthors. [5, 6] They expand the generating functional in a series of terms according to the number of spatial gradients they contain:

$$S = S^{(0)} + S^{(2)} + S^{(4)} + S^{(6)} + \cdots . \tag{14}$$

After solving the Hamilton-Jacobi equation perturbatively, the metric is obtained from the equations of motion. At this point, we must choose the gauge; we take the synchronous gauge $N = 1, N^i = 0$. Furthermore, the comoving gauge is also taken to fix the gauge freedom completely. Then the velocity potential field bocomes equivalent with the proper time. Then, eqs.(10), (11) and (12) reduce to

$$\dot{\phi} = \frac{1}{2\omega+3}\frac{1}{\sqrt{\gamma}}[\phi\frac{\delta S}{\delta\phi} - \gamma_{ij}\frac{\delta S}{\delta\gamma_{ij}}] , \tag{15}$$

$$\dot{\gamma}_{ij} = \frac{2}{\phi\sqrt{\gamma}}\frac{\delta S}{\delta\gamma_{kl}}[\gamma_{ik}\gamma_{jl} - \frac{\omega+1}{2\omega+3}\gamma_{ij}\gamma_{kl}] - \frac{1}{2\omega+3}\frac{1}{\sqrt{\gamma}}\gamma_{ij}\frac{\delta S}{\delta\phi} . \tag{16}$$

3.1 The lowest order Hamilton-Jacobi equation

Now we shall solve the lowest Hamilton-Jacobi equation:

$$\frac{1}{\phi\sqrt{\gamma}}\frac{\delta S^{(0)}}{\delta\gamma_{ij}}\frac{\delta S^{(0)}}{\delta\gamma_{kl}}[\gamma_{ik}\gamma_{jl}-\frac{\omega+1}{2\omega+3}\gamma_{ij}\gamma_{kl}]+\frac{1}{2(2\omega+3)}\frac{\phi}{\sqrt{\gamma}}(\frac{\delta S^{(0)}}{\delta\phi})^2$$
$$-\frac{1}{2\omega+3}\frac{1}{\sqrt{\gamma}}\gamma_{ij}\frac{\delta S^{(0)}}{\delta\gamma_{ij}}\frac{\delta S^{(0)}}{\delta\phi}+\frac{\delta S^{(0)}}{\delta\chi}=0\ . \tag{17}$$

It is difficult to obtain the complete solutions of the Hamilton-Jacobi equation. Fortunately, we need only the growing mode in the late stage or inflationary stage. Hence, we put the quasi-isotropic ansatz:

$$S^{(0)}=-2\int d^3x\sqrt{\gamma}\phi H(\chi)\ . \tag{18}$$

Substituting the ansatz (18) into eq.(17), we obtain

$$H(\chi)=\frac{4\omega+6}{3\omega+4}\ \frac{1}{\chi}\ . \tag{19}$$

Equations of motion is given by

$$\dot{\phi} = \frac{H}{2\omega+3}\phi\ , \tag{20}$$
$$\dot{\gamma}_{ij} = \frac{2\omega+2}{2\omega+3}\ H\gamma_{ij}\ . \tag{21}$$

Their solutions are

$$\phi = \chi^{\frac{2}{3\omega+4}}\ \tilde{\phi}(x)\ , \tag{22}$$
$$\gamma_{ij} = \chi^{\frac{4\omega+4}{3\omega+4}}\ h_{ij}(x)\ , \tag{23}$$

where $\tilde{\phi}(x)$ and h_{ij} are arbitrary functions, which we call seed scalar and seed metric, respectively.

3.2 The second order Hamilton-Jacobi equation

The second order equation is written as

$$\frac{2\omega+2}{2\omega+3}\gamma_{ij}\frac{\delta S^{(2)}}{\delta\gamma_{ij}}+\frac{H}{2\omega+3}\phi\frac{\delta S^{(2)}}{\delta\phi}+\frac{\delta S}{\delta\chi}$$
$$-\sqrt{\gamma}\phi R+\omega\frac{\sqrt{\gamma}}{\phi}\gamma^{ij}\partial_i\phi\partial_j\phi+2\sqrt{\gamma}\Delta\phi=0\ . \tag{24}$$

Simple integration procedure gives

$$S^{(2)}=\frac{3\omega+4}{5\omega+8}\chi\int d^3x\sqrt{\gamma}[\phi R(\gamma)-\frac{\omega}{\phi}\gamma^{ij}\partial_i\phi\partial_j\phi]\quad . \tag{25}$$

Iteratively we solve the following equations:

$$\begin{aligned}
\dot{\phi} &= \frac{1}{2\omega+3}\frac{1}{\sqrt{\gamma}}[\phi\frac{\delta S}{\delta\phi}-\gamma_{ij}\frac{\delta S}{\delta\gamma_{ij}}] \\
&= \frac{H}{2\omega+3}\phi+\frac{1}{2\omega+3}\frac{1}{\sqrt{\gamma}}[\phi\frac{\delta S^{(2)}}{\delta\phi}-\gamma_{ij}\frac{\delta S^{(2)}}{\delta\gamma_{ij}}] , \qquad (26) \\
\dot{\gamma}_{ij} &= \frac{2}{\phi\sqrt{\gamma}}\frac{\delta S}{\delta\gamma_{kl}}[\gamma_{ik}\gamma_{jl}-\frac{\omega+1}{2\omega+3}\gamma_{ij}\gamma_{kl}]-\frac{1}{2\omega+3}\frac{1}{\sqrt{\gamma}}\gamma_{ij}\frac{\delta S}{\delta\phi} \\
&= \frac{2\omega+2}{2\omega+3}H\gamma_{ij} \\
&\quad +\frac{2}{\phi\sqrt{\gamma}}\frac{\delta S^{(2)}}{\delta\gamma_{kl}}[\gamma_{ik}\gamma_{jl}-\frac{\omega+1}{2\omega+3}\gamma_{ij}\gamma_{kl}]-\frac{1}{2\omega+3}\frac{1}{\sqrt{\gamma}}\gamma_{ij}\frac{\delta S^{(2)}}{\delta\phi} . \qquad (27)
\end{aligned}$$

Some calculations give the second order solution:

$$\phi = \chi^{\frac{2}{3\omega+4}}\tilde{\phi}+\frac{(3\omega+4)^2}{(5\omega+8)(2\omega+3)(2\omega+4)}\chi^{\frac{2\omega+6}{3\omega+4}}F(h,\tilde{\phi}) , \qquad (28)$$

$$\gamma_{ij} = \chi^{\frac{4\omega+4}{3\omega+4}}h_{ij}+\frac{(3\omega+4)^2}{(5\omega+8)(2\omega+4)}\chi^2 P(h,\tilde{\phi}) , \qquad (29)$$

where

$$F(h,\tilde{\phi}) = \frac{1}{2}\tilde{\phi}R(h)-\frac{1}{2}\frac{\omega}{\tilde{\phi}}h^{ij}\partial_i\phi\partial_j\phi+(2\omega+2)h^{ij}\tilde{\phi}_{;ij} , \qquad (30)$$

$$\begin{aligned}
P(h,\tilde{\phi}) &= \frac{\omega+1}{2\omega+3}h_{ij}R(h)-2R_{ij}(h)-\frac{\omega+1}{2\omega+3}h_{ij}\frac{\omega}{\tilde{\phi}^2}\partial_k\tilde{\phi}\partial_l\tilde{\phi}h^{kl} \\
&\quad +\frac{2\omega}{\tilde{\phi}^2}\partial_i\tilde{\phi}\partial_j\tilde{\phi}-\frac{2\omega+2}{2\omega+3}h_{ij}\frac{1}{\tilde{\phi}}h^{kl}\tilde{\phi}_{;kl}+\frac{2}{\tilde{\phi}}\tilde{\phi}_{;ij} . \qquad (31)
\end{aligned}$$

In principle, we can continue this procedure to obtain higher order corrections. Especially, the recursion relation for the generating functional exists.

4 Results

Let us define the local Hubble as $\tilde{H}=\frac{1}{6}\gamma^{ij}\dot{\gamma}_{ij}$. Then, the variation of gravitational constant is given by

$$\frac{\dot{G}}{G}=-\frac{\tilde{H}}{\omega+1}[1+\frac{(3\omega+4)^2}{6(5\omega+8)(\omega+1)}\chi^{\frac{2\omega+2}{3\omega+4}}Q(h,\tilde{\phi})] , \qquad (32)$$

where

$$Q(h,\tilde{\phi})=R(h)-\frac{\omega}{\tilde{\phi}^2}h^{ij}\partial_i\tilde{\phi}\partial_j\tilde{\phi}+\frac{6\omega^2+13\omega+6}{(2\omega+3)\tilde{\phi}}h^{ij}\tilde{\phi}_{;ij} . \qquad (33)$$

In the case of negative curvature space, the variation rate of the gravitational constant is surpressed. On the other hand, we could not give the definite answer from the information of the curvature only, in the case of the positive curvature. Indeed, the competition between the inhomogeneities of the metric and that of Brans-Dicke field determines the rate of the change of the gravitational constant.

Acknowledgments

The author would like to thank H.Ishihara for useful discussions. This work was supported in part by Monbusho Grant-in-Aid for Scientific Research No.06740222.

References

[1] C. Brans and R. H. Dicke,, *Phys. Rev.* **124** (1961) 925.

[2] E. M. Lifschitz and I. M. Khalatnikov, *Adv. Phys.* **12** (1963) 185.

[3] K. Tomita, *Prog. Theor. Phys.* **54** (1975) 730.

[4] G. L. Comer, N. Deruelle, D. Langlois and J. Parry, *Phys. Rev.* **D49** (1994) 2759.

[5] J. Parry, D. S. Salopek and J. M. Stewart, *Phys. Rev.* **D49** (1994) 2872.

[6] K. M. Croudace, J. Parry, D. S. Salopek and J. M. Stewart, *Ap. J.* **423** (1994) 22.